FUNCTIONAL AND STRUCTURAL ANNOTATION OF *PSEUDOMONAS* CHEMORECEPTORS

Doctoral Thesis
Granada, 2019

Programa de Doctorado de Biología Fundamental y de Sistemas
Doctorate Program of Fundamental and Systems Biology
Universidad de Granada

UNIVERSIDAD DE GRANADA

Doctoral Candidate
David Martín Mora

Thesis Supervisor
Dr. Tino Krell
Scientific Researcher of CSIC

Estación Experimental del Zaidín
Consejo Superior de Investigaciones Científicas
Spanish National Research Council

MINISTERIO DE CIENCIA, INNOVACIÓN Y UNIVERSIDADES

CSIC Consejo Superior de Investigaciones Científicas

eez Estación Experimental del Zaidín

KRELL LABORATORY

Editor: Universidad de Granada. Tesis Doctorales
Autor: David Martín Mora
ISBN: 978-84-1306-309-6
URI: http://hdl.handle.net/10481/57192

Editorial de la Universidad de Granada
Autor: David Martín Mora
Imagen: *Detail of the binding site of McpN ligand binding domain with nitrate bound*
Edita portada: Josemydiseño (Graphic Designer)
Impreso en junio de 2019

This doctoral thesis was carried out in the Environmental Microbiology and Biodegradation research group of the Department of Environmental Protection of the Estación Experimental del Zaidín (Spanish National Research Council). The funds that have made possible this work has been thanks to the FPI grant 2014 (BES-2014-068355), and to the funds granted to Dr. Tino Krell through the projects of the Ministry Economy and Competitiveness (BIO2013-42297-P and BIO2016-76779-P).

Esta tesis doctoral ha sido realizada en el grupo de investigación de Microbiología Ambiental y Biodegradación del departamento de Protección Ambiental de la Estación Experimental del Zaidín (Consejo Superior de Investigaciones Científicas). La financiación que ha posibilitado su desarrollo ha sido gracias a la ayuda para contratos predoctorales para la formación de doctores 2014 (FPI) (BES-2014-068355), y a los fondos concedidos al Dr. Tino Krell a través de los proyectos del Ministerio de Economía y Competitividad (BIO2013-42297-P y BIO2016-76779-P).

"Todo lo que no se da, se pierde"

Proverbio hindú

"¿Cómo sabes que esto es bueno para mí?
¿Cómo sabes que esto es malo para mí?"

El granjero, parábola china

"La suerte está ahí, pero hay que trabajarla"

Tino Krell

"Los grandes actos se componen de pequeñas obras"

Lao-Tse

"Haz todo lo que puedas, lo demás déjaselo al destino"

Proverbio japonés

"Obras son amores, y no buenas razones"

Refrán español

"Si en lugar de quejarte tanto te hubieras puesto a ello, ya estaría hecho"

Manuel Martín e Isabel Mora

Petti Fyri Petti

AGRADECIMIENTOS

Permítame el lector de esta tesis tomarme la licencia de escribir los agradecimientos en lengua castellana, pues así llegarán a la mayoría de personas a quienes la deuda acumulada durante estos años, me exige gustosamente corresponder con estas palabras.

En primer lugar, quisiera realizar un recuerdo general a la Estación Experimental del Zaidín y a quienes allí trabajan. Empezando desde la directora Matilde Barón y el gerente José Luís Sánchez, a quienes agradezco el permiso y gestiones para realizar mi tesis doctoral. También pasando por cada departamento administrativo, técnico, mantenimiento e incluyendo a la limpieza. Un agradecimiento de tal magnitud como la voluntad y la ayuda recibidas cuando lo he necesitado.

Al departamento de Protección Ambiental, en especial al grupo de investigación de Microbiología Ambiental y Biodegradación, quienes me han acogido desde el principio de manera tan cercana. Su dedicación, su trabajo y sus recursos científicos han facilitado mi labor llegara. A Juan Luís y Estrella quienes, a pesar de que el tiempo compartido ha sido breve, siempre han tenido unas palabras interesantes y amables. A Silvia, Regina, Marian, Ana, Manolo, Pieter y Maribel. Muchas gracias por vuestros consejos, vuestras indicaciones, vuestras respuestas y la ayuda recibida durante estos años.

Quiero continuar mis agradecimientos por las personas que se han convertido en mi familia en la EEZ: El laboratorio de Tino Krell. A Tino, mi mentor y guía en esta carrera de fondo para la que me confió un lugar en la línea de salida. Su comprensión, sus charlas, sus consejos maestros, su visión y su ayuda han sido y son inestimables. A Miguel, compañero de fatigas y esfuerzos; abrazo y oído amigo, quien me ha regalado consejos expertos y buenos momentos. A Mati, el brioso tacón del laboratorio; guardo en buen recuerdo sus consejos y sus ánimos que siempre han sido de ayuda. A Félix, última incorporación, buen compañero siempre dispuesto a ayudar, de mirada capaz, con una energía y unas ganas que auguran una prometedora senda. Muchas gracias.

No quiero olvidarme a quienes me acompañaron en nuestro laboratorio durante estos años. A José Antonio, carismático canario, enemigo de los despertadores; quien me acompañó con paciencia en mis primeros pasos en este laboratorio, y que siempre ha tenido un momento para charlar y aconsejarme. A Míriam, por su intuición amiga y su generoso abrazo, por sus consejos y su apoyo. A Álvaro, resuelto y capaz compañero de silencios, de buen consejo y versada ayuda, de quien guardo con afecto el tiempo que compartimos. A Diana, quien con la amabilidad dulce y su sonrisa me ayudó y aconsejó cuando lo necesité. A Andrés, por la simpatía mexicana con la que me recibió, y las palabras de consejo que me brindó que siempre recordaré. Bertrand, compañero de risa alegre y genio galo, cuya ayuda y respuestas expertas siempre estaba dispuesto a darme. A Ali, maura decidido y capaz, de consejo rápido, de quien podías aprender sólo observándolo, y que me enseñó a qué sabe una pelota de pádel. A Noel, compañero de nervio afable, cuyos consejos siempre estaba dispuesto a escuchar. A Georg, simpático maestro de la lógica computada, de quien guardo un recuerdo alegre. Muchas gracias.

Continuaré agradeciendo otros compañeros quienes me han ayudado, animado y aconsejado, y cuya compañía he tenido la fortuna de compartir. A Pacheco, por el saber llano con el que acompaña a sus palabras bienhumoradas. A Sophie por su güera alegría y por su interés compañero. A Patri por la simpatía de su sonrisa añil siempre dispuesta a ayudarme. Gracias.

A Alicia con su expresión amable, y a Lázaro con su nervio y su buen hacer. Gracias.

A Josemi, amable compañero y buena persona, por su cercana y desinteresada ayuda, sus consejos y sus palabras de ánimo. A Joaquín, socarrón y pillo compañero, con las anécdotas de las noches liverpulianas que me dejó para el recuerdo. A Cristina, que siempre tenía un momento para contagiar su alegría y regalar las palabras de ánimo que ha compartido conmigo. Gracias.

A Óscar, por la pasión inquieta de su potente carcajada rubicunda, sus consejos y sus ánimos. A Laura, por compartir conmigo su risa sincera, su franqueza y sus ánimos, y por el recuerdo de cuando jugamos al "¡aventureros al tren!" versión inglesa y ganamos. A Nené, por su amable ayuda siempre que lo he necesitado. Gracias.

A Inés, compañera de promoción FPI, por su alegría hispalense. A Jesús, por sus palabras de interés y sus ánimos. A Silvia B., quien con sus palabras me mantenía despierto. Gracias.

A María, agradable y paciente, por su presta disposición a ayudarme. A Víctor, albaceteño llano y cercano, portador de la navaja de adamantium, siempre presto a ayudar y dar ánimos, además de otro buen jugador de "¡aventureros al tren" versión inglesa. Gracias.

A María Angustias, que siempre me recibía con una sonrisa alegre, por sus palabras cariñosas de ánimo y las conversaciones en la cocina. Gracias.

Sin olvidarme de agradecer las palabras y el tiempo compartido con Patri B., Carlos, Verónica, Saray y Ana Isabel. Y si me olvido de alguien, ruego que me perdone pues es un fallo sin intención.

A Victor Sourjik, por acogerme en su laboratorio y brindarme la oportunidad y la ayuda de aprender allí. A Shuangyu y a Remy, por sus pacientes explicaciones y sus conversaciones científicas. A Silvia G., por tanta alegría y ayuda desinteresada desde que salí de la estación de tren. Ojalá la nueva estrella en tu cielo guíe el regreso de la sonrisa a tus labios. A Melissa, con su talante jubiloso y enérgico, con la mano tendida cuando hacía falta. A Nicolas y a Judita, por sus amables palabras y su interés. A Claudia, por el guiño sonriente y simpático que acompañaba a sus amables palabras. Gracias

Finalmente, como el esperado postre que culmina una buena velada, quisiera escribir unas palabras para la familia Martín Mora, quienes han compartido mis pasos desde que calzaba patucos hasta que supe como atarme unas botas de montaña. A mi padre y a mi madre, Manolo e Isabel, los culpables de que yo haya llegado hasta aquí, cuyas humildes y sabias enseñanzas y cuyo ejemplo han sido, son y serán luces guía en el firmamento de mi memoria. A Eugenia, por ser el agua que nutre mis campos, que deja su huella profunda junto a la mía a lo largo de este camino. A Manolo y Eva, a Mónica y a José Miguel, y a Cristina y Rodri, pilares del templo invisible que nos hermana, por su compañía sincera, sus oídos pacientes y sus apoyos firmes, haciéndome sentir su cariño en la cercanía y en la distancia. A la trovadora blanca y a la trepadora azul, energía incansable de brisa fresca que me arrancan risas y lágrimas desde el corazón. Mil gracias.

A la que es mi vieja guardia, por las misiones rescate, por tantos momentos de soles y lunas, de cambios estáticos y calmas trepidantes. Mil gracias.

A todos, ¡GRACIAS!

TABLE OF CONTENT

FIGURE INDEX

TABLE INDEX

SUPPLEMENTARY FIGURE INDEX

SUPPLEMENTARY TABLE INDEX

LIST OF ABBREVIATIONS

4HB	four-helix bundle
AI-2	auto-inducer 2
AUC	analytical ultracentrifugation
Cache	calcium channels and chemotaxis receptors
cAMP	cyclic adenosine monophosphate
CD	circular dichroism
c-di-GMP	cyclic diguanosine monophosphate
CF	cystic fibrosis
CFU	colony-forming unit
CH	chemoreceptor
CRP	cAMP Receptor Protein
CZB	chemoreceptor zinc-binding
DNA	deoxyribonucleic acid
DSF	differential scanning fluorimetry
EDTA	ethylenediaminetetraacetic acid
GABA	gamma-amino butyric acid
GAF	found in cGMP-specific phosphodiesterases, adenylyl cyclases and FhlA
HAMP	present in histidine kinases, adenylate cyclases, methyl-accepting proteins and phosphatases
HBM	helical bimodular
HK	histidine kinase
HTH	Helix-Turn-Helix
ID	identification
IPTG	Isopropyl-β-D-1-thiogalactopyranoside
ITC	isothermal titration calorimetry
K_D	dissociation constant
LB	lysogeny broth
LBD	ligand binding domain
LBP	ligand binding protein
MA	methyl-accepting
MCP	methyl-accepting chemotaxis protein
NANA	N-acetyl neuroaminic acid
NIT	nitrate- and nitrite sensing
OCS	one-component system
OD_n	optical density
PAS	found in Per-Arnt-Sim
PCR	polymerase chain reaction
PDB	protein data bank
PDC	found in PhoQ/DcuS/CitA
PTS	phosphotransferase system
RNA	ribonucleic acid
RR	response regulator

SAXS	small-angle X-ray scattering
SMART	simple modular architecture research tool
T4P	type-IV pili
TCA	tricarboxylic acid
TCS	two-component system
Tlp	transducer like protein
TM	transmembrane
T_m	denaturation midpoint temperature
WHO	World Health Organization
wt	wild-type
αKG	alpha-ketoglutaric acid

GENERAL ABSTRACT

Bacteria possess different systems to sense and respond to environmental signals. Most abundant are one-component systems, two-component systems and chemosensory pathways . While one- and two-component systems mainly control gene expression, chemosensory pathways mediate chemotaxis or are associated with alternative functions.

The analysis of the increasing number of bacterial genomes shows that about half of bacteria have genes encoding chemosensory pathways.

The central element of a chemosensory pathway is the ternary complex formed by chemoreceptors, the CheA autokinase and the CheW coupling proteins . Ligand mediated stimulation of the chemoreceptor causes an alteration of CheA activity that in turn modulates transphosphorylation to CheY that in its phosphorylated form binds to the flagellar motor causing ultimately chemotaxis.

The chemoreceptor typically is composed by a periplasmic ligand binding domain, a transmembrane module and a cytoplasmic signaling domain. The function and signals recognized of most chemoreceptors are unknown. Casting light into this issue is essential to understand the forces that have led to the evolution of chemoreceptors in bacteria that inhabit different ecological niches.

In this thesis I report the functional annotation of a number of chemoreceptors of *Pseudomonas putida* KT2440 and *Pseudomonas aeruginosa* PAO1, which are important models to study chemotaxis and chemoreceptors. Approaches are multidisciplinary and include experimentation in the fields of biochemistry, biophysics, microbiology, bioinformatics and structural biology. Chemoreceptors annotated were found to recognize organic acids (McpP, McpQ, McpK and CtpM), polyamines (McpU and TlpQ) or nitrate (McpN).

McpP is the major chemoreceptor that mediates chemotaxis toward the C2- and C3-carboxylic acids acetate, pyruvate, propionate, and L-lactate. Its sCACHE-type ligand binding domain recognizes theses ligands as monomer. McpQ has a HBM ligand binding domain which recognizes citrate and citrate in complex with metal ions and complements the broad ligand range homologue McpS that is little sensitive to citrate. These organic acids serve as carbon sources for *P. putida* KT2440 growth and are abundantly present in root exudates. Since *P. putida* KT2440 efficiently colonizes plant roots, chemotaxis to organic acids is likely to drive root colonization.

McpK of *P. aeruginosa* PAO1 was identified as a specific chemoreceptor for α-ketoglutaric acid. This receptor has an HBM-type ligand binding domain that recognizes α-ketoglutaric acid with positive cooperativity. α-ketoglutaric acid is a key metabolite and is a signal molecule that controls the carbon and nitrogen balance. Another organic acid chemoreceptor studied is CtpM, which mediates chemotaxis toward the C4-dicarboxylic acids L-malic, D,L-bromosuccinic and D,L-citramalic acids . L-malic acid is a central metabolic molecule, and D,L-bromosuccinic and D,L-critramalic acids are present naturally in the environment. The ligand binding domain of CtpM is a sCACHE domain. It recognizes not only L-malic, D,L-bromosuccinic and D,L-critramalic acids, but also D.L-methylsuccinic and D,L-citraconic acids. However, methylsuccinic and citraconic acids do not generate a chemotactic response. Interestingly, methylsuccinic and citraconic acids act as antagonists, competing with malic, bromosuccinic and citramalic acids for binding at CtpM, decreasing the chemotactic response toward malate.

McpU and TlpQ are two homologous chemoreceptors from *P. putida* KT2440 and *P. aeruginosa* PAO1, respectively. Their ligand binding domains recognize and mediate chemotaxis toward histamine and polyamines (spermidine, putrescine, cadaverine, agmatine, ethylenediamine) . The ligand affinities of TlpQ are in the nanomolar range and correspond to the highest affinities ever measured for chemoreceptors. The three-dimensional structures of the ligand binding domains of both chemoreceptors has been resolved during these thesis and site-directed mutagenesis was

employed to study the role of individual amino acids in ligand recognition. Polyamines were found to support bacterial growth as carbon and nitrogen sources.

Lastly, the McpN chemoreceptor from *P. aeruginosa* PAO1 was found to possess a PilJ-type ligand binding domain that recognizes and mediates chemotaxis specifically towards nitrate. The three-dimensional structure of McpN revealed that nitrate is recognized by a single site on the symmetry axis of the McpN-LBD dimer. Sequence alignments with McpN homologues identified a conserved sequence motif around the nitrate binding site, termed N-box, that may help to identify nitrate binding PilJ domains. Nitrate is of central physiological relevance in bacteria. In P. aeruginosa, it was found to serve as nitrogen source for growth and final electron acceptor for anaerobic respiration.

The results presented in this thesis increase the knowledge about the chemotactic chemosensory pathways, reveal the signals sensed and cast light into the sensing mechanisms, which is important information to understand important physiological processes such as bacterial migration, colonization, infection and virulence. Future work will determine the potential application of this knowledge, for instance the determination of the role of these chemoreceptors in the promotion of plant root colonization or infection. The demonstration that chemoreceptors respond to chemoeffectors and structurally related antagonists may be a potential strategy to interfere specifically with chemotaxis and virulence.

This abstract has the approval of the thesis supervisor, Dr. Tino Krell.

INTRODUCTION

INTRODUCTION

Since life appeared on earth, all kinds of organisms had to adapt to changing environmental conditions. The appearance of systems capable of sensing these changes and creating an appropriate adaptive response, was a critical feature during evolution and have consequently become a common feature of living species.

Among the most important sensing systems in life are those in charge of detecting changes in the concentration of chemical signals in the environment. They are present in all domains of life, from bacteria to mammals (Wicher, 2012). The first systems appeared very early in life history, likely in a common ancestral microorganism (Croset *et al.*, 2010). Since then, they have been conserved, spread and specialized during evolution (Wicher, 2012, Chantranupong *et al.*, 2015). At present, estimations indicate that, among others, bacteria are the most abundant form of life with over ~10^{30} individuals worldwide (Schloss & Handelsman, 2004) and a biomass of ~70 gigatons of carbon (Bar-On *et al.*, 2018). However, from the accepted estimation of 10^{7} – 10^{12} bacterial species, less than ~11,000 of them have been classified so far (Yarza *et al.*, 2014). This is a dark abyss of unknown knowledge about bacteria and in particular about sensing and signaling systems.

BACTERIAL HABITATS AND LIFE CONDITIONS

Bacteria are ubiquitous. They are present in the "big five" habitats: deep oceanic subsurface, deep continental subsurface, upper oceanic sediment, oceans and soil, which together sum up approximately 11.5 x 10^{29} bacteria (Flemming & Wuertz, 2019)(Fig. 1). Other important minor habitats include ground water, microbiome of phyllosphere, cattle, termites, pigs and humans, sea surface layer and atmosphere, with around 5.2 x 10^{27}bacteria (Flemming & Wuertz, 2019)(Fig. 1). In these habitats, bacteria are particularly exposed to these changesdue to their unicellular

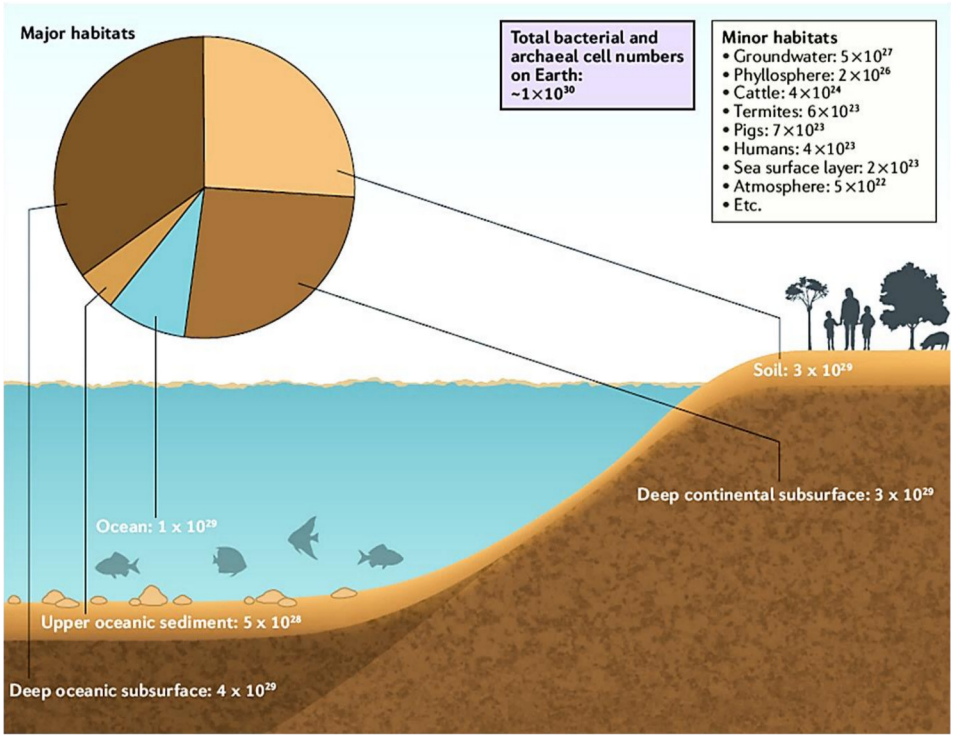

Figure 1. Abundance and distribution of bacteria and archaea among the main habitats on earth. Figure from Flemming & Wuertz, 2019.

organization and their microscopic size (from 0.5 to 5 μm). It has been described that the complexity of sensing and signaling systems depends on bacterial lifestyle (Alexandre *et al.*, 2004).

In general, these environmental changes involve variations in abiotic and/or biotic factors. Abiotic factors include changes in air composition, temperature, humidity, pressure, radiation, nutrients and chemical elements concentration. Meanwhile, biotic factors are associated with the presence of other living beings in the habitat, such as microorganisms from the same or other species, plants and animals, that interact and influence each other (Flemming & Wuertz, 2019).

Altogether, changing habitat conditions are a powerful evolutionary pressure for bacteria which, over time, have led to the emergence of adaptive systems, referred to as signal transduction pathways, to permanently sense and perform adaptive responses that allow bacteria to survive.

SIGNAL TRANSDUCTION PATHWAYS

Bacteria present several systems to sense the environmental conditions and generate a specific response. Twelve different types of signal transduction machineries have been reported that sense environmental changes (Galperin, 2018), and their concerted actions permits to respond to key physicochemical parameters as well as nutrients or toxic compounds (Galperin, 2018). These systems are responsible for key phenotypic choices such as for example growth or persistence, motility or sessility, planktonic or biofilm state, virulence or avirulence (Galperin, 2018). Among the most abundant signal transduction mechanisms are one-component systems (OCS) (Ulrich *et al.*, 2005), two-component systems (TCS) (Stock *et al.*, 2000) and chemosensory pathways (Wadhams & Armitage, 2004, Porter *et al.*, 2011).

ONE-COMPONENT SYSTEMS

The simplicity of design in signal transduction systems is represented by the OCSs. A typical OCS is a single protein composed of an input domain and an output domain (Ulrich *et al.*, 2005). The input domain is in charge of signal sensing, which in turn alters the activity of the output domain (Fig, 2). The main function of the input domains is the direct recognition of small molecules (93 %)(Ulrich *et al.*, 2005). It is known that OCSs typically have the physiological role of sensing signals in the cytoplasm that act as activators or repressors of gene expression regulation, as 87 % of output domains are DNA-binding domains containing the Helix-Turn-Helix (HTH) motif, and typically lack transmembrane regions (97 %). However, the output domain repertoire also includes enzymes that regulate, for example, the level of second messengers or protein phosphorylation (Ulrich *et al.*, 2005).

OCSs are very abundant in bacteria (Ulrich *et al.*, 2005) and representative examples are the LacI and CRP regulators of *Escherichia coli*. The LacI lactose operon repressor is bound to its cognate operator and, when the input domain recognizes lactose or isopropyl-β-D-1-thiogalactopyranoside, a conformational change occurs and the repressor is released from DNA (Kercher *et al.*, 1997), enabling in turn transcription In contrast, the cAMP Receptor Protein (CRP) acts in the opposite way. In the absence of bound signal molecule it is DNA-unbound (or bound to non-specific DNA), whereas cAMP binding promotes CRP binding to is target DNA, which in turn regulates gene expression (Kolb *et al.*, 1993).

There is evidence which suggests that OCSs appeared before other more complex systems, such as TCSs (Ulrich *et al.*, 2005). This notion is based on the fact that the design of OCSs is relatively simple, that the domain repertoire of OCS is more diverse than TCS and that OCSs are more widely distributed among prokaryotes than TCSs (Ulrich *et al.*, 2005).

TWO-COMPONENT SYSTEMS

This kind of signal transduction system shows a broad phylogenetic distribution; it is abundant in Eubacteria, and present to a lower degree in Archaea and Eukarya (Stock *et al.*, 2000). With respect to Eubacteria, genome analyses have shown that TCSs are present in almost all bacteria, with an average of 52 TCS per genome (Krell *et al.*, 2010). The prototypical system is composed by a histidine sensor kinase (HK) bound to the membrane, consisting of at least a ligand

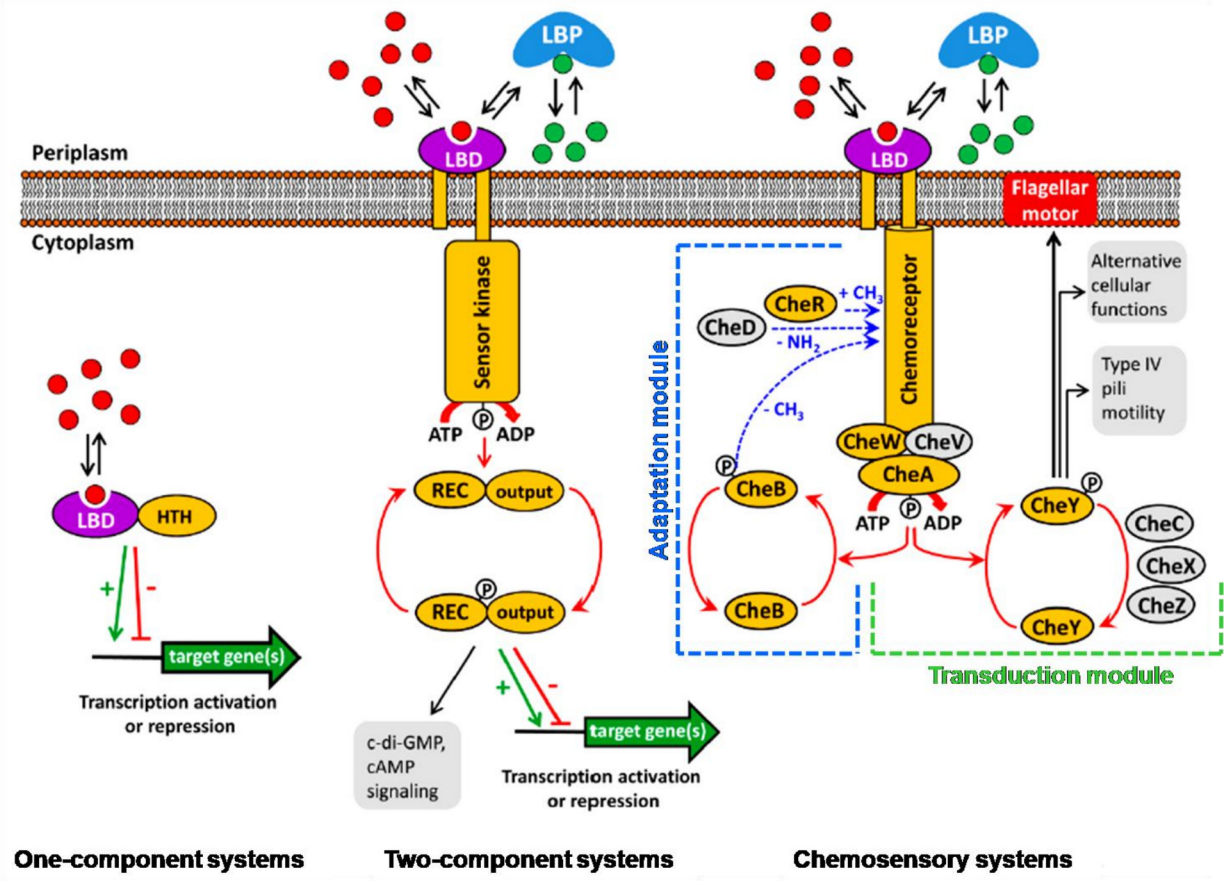

Figure 2. Major bacterial signal transduction systems. Ligand binding domains (LBD) in purple, ligand binding proteins (LBP) in blue, core chemosensory proteins in yellow, alternative chemosensory proteins in grey. HTH: DNA binding domain containing helix-turn-helix motif. Red and green dots represent signal molecules. Red arrows: phosphorylation/dephosphorylation reactions; blue arrows: methylation/demethylation and deamidation reactions; black arrows: pathway output; red T-lines and green arrows indicate transcriptional repression or activation, respectively. Marked in dashed blue lines is the adaptation module and in dashed green lines, the transduction module. Modified from Martín-Mora *et al.*, 2018.

binding domain (LBD) (input) and an autokinase domain, and a response regulator (RR), composed of a phosphorylatable receiver domain and an output domain. In most of the cases, the RR interacts with DNA promoter regions enabling for transcriptional regulation, but in other cases possess enzymatic activities or interact with other proteins (Krell *et al.*, 2010)(Fig 2).

Typically, extracellular signals are sensed by the HK, modulating the activity of its autokinase domain, which in turn alters the transphosphorylation activity towards the RR. RR phosphorylation changes the functional properties of its output domain, leading to the manifestation of the ultimate signaling response. Both, the HK and RR, undergo dephosphorylation reactions, which together define the reactivity and immediacy of responses mediated by a given TCS (Stock *et al.*, 2000).

The PhoQ/PhoP TCS of *Salmonella typhimurium* illustrates this prototypical process. Cationic antimicrobial peptides are recognized by the periplasmic PAS (Per-Arnt-Sim) sensor domain (Bader *et al.*, 2005), which creates a molecular stimulus that is transduced across the membrane where it stimulates the autokinase domain. Subsequently, the phosphotransfer to the RR receiver domain induces its binding to a set of promoters causing the regulation of DNA expression (Krell *et al.*, 2010, Zwir *et al.*, 2012). Next to the canonical systems are hybrid TCSs that involve multiple phosphotransfer reactions, termed *phosphorelays,* of which an example is the TodS/TodT TCS of *Pseudomonas putida* DOT-T1E. The sensor kinase TodS is composed of two sensor and autokinase domains as well as an internal receiver domain. The binding of toluene to the N-terminal sensor domain of TodS stimulates its vicinal autokinase domain. Subsequently, the phosphoryl group is transferred to the Asp residue of the internal receiver domain, and then to the His of the C-terminal autokinase domain, from which the phosphoryl group parts to be transferred to TodT receiver domain, activating ultimately the transcription from the P_{todX} promoter(Busch *et al.*, 2009).

The fact that TCSs are present in almost all Eubacteria, but are present to a lesser degree in Archaea and Eukarya (Stock *et al.*, 2000), suggests that they appeared after OCSs. The similarities between the OCSs and TCSs repertoire of input and output domains suggest that they detect similar stimuli and carry out similar functions. However, a major difference between both families is the site of signal sensing: where OCSs sense intracellular signals, TCSs typically respond to extracellular signals (Ulrich *et al.*, 2005).

CHEMOSENSORY PATHWAYS

GENERAL INSIGHTS

Chemosensory pathways are signaling circuits that are stimulated by chemoreceptors (Wadhams & Armitage, 2004). These pathways can be understood as sophisticated versions of TCSs (Martín-Mora *et al.*, 2018). The *E. coli* chemosensory pathway has been extensively studied and has served as a model to elucidate pathway function (Parkinson *et al.*, 2015). Chemosensory pathways are considered to be among the most complex signal transduction systems in prokaryotes (Wuichet & Zhulin, 2010)(Fig. 2). Pathways are formed by core signaling proteins that are present in almost all pathways, such as chemoreceptors, the CheA autokinase, the CheW coupling protein, the CheR methyltransferase and the CheB methylesterase as well as by auxiliary proteins that are present in only some pathways. These proteins include the CheD deamidase and the CheC, CheX and CheZ phosphatases (Wuichet & Zhulin, 2010)(Fig. 2).

CHEMOSENSORY PATHWAYS INVOLVED IN CHEMOTAXIS

Chemotaxis is biased flagella-mediated swimming in chemoeffector gradients. Taxis occurs either toward or away from chemoeffectors, referred to as chemoattractants or repellents, respectively (Wadhams & Armitage, 2004). The anticlockwise rotation of *E. coli* flagella creates a flagellar bundle that propels the bacterium. Switching the rotation direction to clockwise, disrupts the bundle and causes cell tumbling and reorientation (Turner *et al.*, 2000). The function of a chemosensory pathway consists basically in controlling the switch between both directions of flagellar rotation (Parkinson *et al.*, 2015). Chemosensory pathway function is based on the concerted action of the signal transduction module and the adaptation module (Colin & Sourjik, 2017).

The Signal Transduction Module

This module is composed of a ternary protein complex involving the chemoreceptor, CheA and CheW (Wadhams & Armitage, 2004)(Fig. 2). *E. coli* has five chemoreceptors, namely Tar, Tsr, Trg, Tap and Aer (Parkinson *et al.*, 2015). Tar, Tsr, Tap and Trg have a periplasmic 4-helix bundle (4HB) LBD, whereas the LBD of Aer is a cytoplasmic PAS domain (Ortega *et al.*, 2017a). Tar mediates attractant responses toward aspartate (Springer *et al.*, 1977) and maltose (Milburn *et al.*, 1991), and repellence to metal ions (Tso & Adler, 1974). Tsr is in charge of mediating attraction toward serine, the quorum autoinducer 2 (AI-2), norepinephrine (Pasupuleti *et al.*, 2014), oxygen (Bibikov *et al.*, 1997) and redox and oxidizable substrates (Greer-Phillips *et al.*, 2003). The chemotactic role of Tap is to mediate attraction to dipeptides (Manson *et al.*, 1986) and pyrimidines (Liu & Parales, 2008), whereas Trg mediates chemoattractant responses toward ribose and galactose (Harayama *et al.*, 1979). In contrast, Aer has a FAD containing, redox-sensitive PAS LBD and mediates responses to oxygen and was also found to be associated with energy taxis (Greer-Phillips *et al.*, 2003). All chemoreceptors are anchored to the cytoplasmic membrane by two transmembrane regions (TM). The MA (methyl-accepting) domain of the cytoplasmic part of chemoreceptors interacts with CheA and CheW (Parkinson *et al.*, 2015).

At low signal concentration, CheA autokinase is in the ON state, leading to CheA autophosphorylation and CheY transphosphorylation (Parkinson *et al.*, 2015). CheY is an atypical RR as it lacks an output domain (Kofoid & Parkinson, 1988). The function of CheY~P is to reverse the direction of the flagellar motor rotation by interacting with the switch protein FliM of the flagellar motor (Welch *et al.*, 1993, Toker & Macnab, 1997)(Fig. 2). This changes flagellar rotation from anticlockwise to clockwise rotation, which disperses the flagellar bundle to provoke cell reorientation (Turner *et al.*, 2000). The activity of CheY~P is controlled by the dedicated phosphatase CheZ (McEvoy *et al.*, 1999). In the ON state, *E. coli* alternates between short swims with frequent tumbling reorientations.

Signal binding to the chemoreceptor LBD creates a molecular stimulus that is transmitted across the membrane to the MA domain, inhibiting CheA autophosphorylation and CheY transphosphorylation. The resulting drop in CheY~P makes that flagellar bundle is maintained for a longer stretch of time causing a more extensive swim movement that is interrupted less frequently by tumbling (Turner *et al.*, 2000).

The Adaptation Module

The capacity of chemosensory pathways to respond to signal gradients (and not to the presence of uniformly distributed signal) is based on the action of adaptational mechanisms that adjust the system sensitivity to the signal concentration present in the bacterial environment. The canonical adaptation mechanism is based on the methylation of the chemoreceptor MA domain (Sourjik & Wingreen, 2012). To avoid saturation and loss of sensitivity, the adaptation module performs a sensory adaptation using a negative feedback, with the ability to reset the signal transduction module to pre-stimulus levels (Parkinson *et al.*, 2015).

The adaption module consists of two proteins: the CheR methyltransferase and the CheB methylesterase (Fig. 2) that act on several glutamyl residues in the MA domain of the chemoreceptor. CheR catalyzes glutamyl methylation reactions in the OFF-state of the chemoreceptor, shifting the equilibrium to the ON state (Parkinson *et al.*, 2015). CheB is a RR composed of a receiver domain (that is phosphorylated by CheA) and the catalytic domain (Djordjevic *et al.*, 1998). CheB demethylates glutamyl groups to glutamic acid, shifting the equilibrium to the OFF state (Parkinson *et al.*, 2015). The preferred substrate for CheB is the MA domain in its ON state, while CheR preferentially acts on the OFF state of the MA domain. Chemoeffector binding to the LBD turns CheA OFF, reducing in turn CheB~P causing a drop in methylesterase activity and CheR mediated methylation shifts the CheA equilibrium to the ON state.

The rate of CheR/CheB activity of the sensory adaptation process is controlled by CheA. When CheA is ON, the regulatory domain of CheB is phosphorylated, and a conformational change increases the methylesterase activity of the catalytic domain (Anand *et al.*, 1998). With this adaption process, *E. coli* achieves a fine-tuning of the swimming mechanism, including the extent of cell reorientation during a tumble (Vladimirov *et al.*, 2010, Saragosti *et al.*, 2011).

BACTERIAL CHEMORECEPTORS: METHYL-ACCEPTING CHEMOTAXIS PROTEINS

Signal integration into chemosensory pathways is achieved by the action of chemoreceptors. They are also termed methyl-accepting chemotaxis proteins (MCP) or transducer-like proteins (Tlp). The specificity of signal recognition at chemoreceptors determines the specificity of the resulting response (Porter *et al.*, 2011, Parkinson *et al.*, 2015).

The domain composition of a typical chemoreceptor is shown in Fig. 3. It is composed of a periplasmic LBD for sensing, that is flanked by two TM regions. The cytosolic fragment is composed of an MA domain and a HAMP domain (histidine kinases, adenylyl cyclases, methyl-accepting chemotaxis proteins and phosphatases) containing several structural and functions segments that will be discussed below (Hazelbauer *et al.*, 2008). These structural regions can be functionally group into different modules: transmembrane sensing module, signal conversion module and kinase control module (Hazelbauer *et al.*, 2008)(Fig. 3).

TRANSMEMBRANE SENSING MODULE

This module is composed of the periplasmic LBD and the transmembrane region (Hazelbauer *et al.*, 2008).

- **Periplasmic LBD**: This domain is responsible for signal sensing that in turn creates a molecular stimulus. The Tar homodimer contains two symmetric 4HB LBDs, each composed of two long and two short helixes (Milburn *et al.*, 1991, Chi *et al.*, 1997). The homodimer interface of Tar-LBDs forms two binding sites for the direct recognition of aspartate that binds with very strong negative cooperativity (Milburn *et al.*, 1991, Milligan & Koshland, 1993)(Fig. 3A).
- **Transmembrane region**: Helixes α1 and α4 of the LBD span the membrane to form transmembrane regions TM1 and TM2, respectively (Parkinson *et al.*, 2015). TM2 has one or more aromatic residues near the cytoplasmic end that probably interact with the lipid-water interface and regulate transmembrane signaling (Miller & Falke, 2004, Draheim *et al.*, 2005, Adase *et al.*, 2012). TM2 has an extension of several residues at the cytosolic side, called control cable, that connect the transmembrane sensing module to the signal conversion module (Parkinson, 2010, Kitanovic *et al.*, 2011)(Fig. 3B).

The binding of one aspartate molecule to the Tar-LBD homodimer creates a conformational asymmetry in the receptor dimer that initiates the response. Different mechanisms have been proposed to be responsible for the transmembrane signal transduction (Bi & Lai, 2015):

a) **Piston displacement:** Ligand binding generates a downward piston-like displacement of the α4-TM2 helix with respect to the α1-TM1 helix within a LBD monomer. This small conformational change is transmitted across the membrane into the cytoplasm (Ottemann *et al.*, 1999, Falke & Erbse, 2009).
b) **Scissoring motions:** Ligand binding causes a rotation of one monomer with respect to the other (Lowe *et al.*, 2012, Falke, 2014).
c) **Rotation of helices:** The binding of the ligand causes a counter-clockwise rotation of the α4-TM2/α4'-TM2' helices along an axis perpendicular to the membrane (Maruyama *et al.*, 1995).
d) **Supercoil unwinding:** The binding of the ligand generates a partial unwinding of supercoiled chemoreceptor monomers, changing the orientation of the cytoplasmic domains (Kim, 1994).

Recently, a significant body of evidence supports the notion that the piston-like displacement is the key mechanism for signaling (Falke & Erbse, 2009, Hall *et al.*, 2011, Falke, 2014). However, due to the large amount of LBD types the existence of alternative mechanisms cannot be excluded (see section "Diversity of Chemoreceptors and Chemosensory Pathways: Type of Ligand Binding Domain"). For example, the transducer protein NpH-trII in *Natronomonas pharaonis*, which is activated by the phototaxis receptor NpSRII, suffers on stimulation a 15° clockwise rotation and a lateral 0.9 Å displacement of TM2 (Moukhametzianov *et al.*, 2006). In addition, the McpB chemoreceptor of *Bacillus subtilis* experiences a counter-clockwise rotation of TM1 and TM1', triggering chemotactic signaling (Szurmant *et al.*, 2004b). However, further investigation is required to fully characterize and understand alternative signaling mechanisms.

SIGNAL CONVERSION MODULE

This module is composed of the HAMP domain, which is widely distributed among transmembrane signaling proteins (Parkinson, 2010). This domain plays an important role in signal transduction between the transmembrane signal module and the kinase control module (Hazelbauer *et al.*, 2008)(Fig. 3).

HAMP domains are composed of two amphiphilic helices (AS1 and AS2), linked by a non-helical connector. TM2 is connected with AS1 by the helical control cable (Zhou *et al.*, 2011, Lai & Parkinson, 2014), which modulates the stability of the HAMP domain (Kitanovic *et al.*, 2011). In the homodimer, both HAMPs form a parallel four-helix coiled coil bundle, as reported for the Tar and Aer2 (McpB) chemoreceptors from *E. coli* and *Pseudomonas aeruginosa*, respectively (Hulko *et al.*, 2006, Airola *et al.*, 2010, Airola *et al.*, 2013a, Airola *et al.*, 2013b). The molecular mechanism of HAMP signal transduction, which receives the signal input from TM2 and modulates the kinase control module to control kinase-ON and kinase-OFF states, remains controversial (Stewart, 2014). Several hypotheses have been proposed:

a) **The dynamic-bundle model:** The downward piston displacement of TM2, caused by the ligand binding, modulates the helicity of the control cable, relaxing it, relieving thereby the structural strain on HAMP domain (Zhou *et al.*, 2009, Kitanovic *et al.*, 2011, Wright *et al.*, 2011). This enhances the packing stability of the HAMP domain, which in turn provoke the kinase-OFF output through the kinase control module (99)(Fig 3C).
b) **Alternative output states:** The HAMP domain switches between compact and dynamic conformations, that can be associated with kinase-ON and kinase-OFF states, respectively (Doebber *et al.*, 2008, Klare *et al.*, 2011).
c) **Scissor-like model:** Signaling from the Tar-LBD was reported to cause a scissor-type displacement of the C-terminal AS2 and AS2' (Swain & Falke, 2007). A scissor-open conformation was found to be related to kinase-OFF state, while a scissor-closed conformation is related to kinase-ON state (Swain & Falke, 2007, Swain *et al.*, 2009).
d) **Helix rearrangement model:** This model suggests that the HAMP domain can switch between two conformations, according to the X-ray structures from tandem HAMP domains of the McpB chemoreceptor from *P. aeruginosa* (Airola *et al.*, 2010).
e) **Cogwheel model:** It was proposed that by a 26° rotation of all four HAMP helixes, the HAMP domains would interconvert between discrete *x-da* and a *knobs-into-holes* packing conformations (Hulko *et al.*, 2006). Both states are associated with kinase-ON and kinase-OFF outputs in *Archaeoglobus fulgidus* HAMP domain (Hulko *et al.*, 2006).

Although it is still a controversial topic, some models have been suggested to be more probable in transmembrane chemoreceptors (Parkinson *et al.*, 2015). However, the mechanisms of signal input into HAMP domains and the output to the methylation helix bundle of the kinase control module might be different for chemoreceptors from different chemosensory pathways. Therefore, it is possible that different HAMP domains utilize different conformational signaling mechanisms (Stewart, 2014).

KINASE CONTROL MODULE

The methylation helix bundle, the flexible bundle and the protein interaction region form this module (Hazelbauer *et al.*, 2008). The kinase control module structure is a continuous four-helix, anti-parallel coiled-coil (Hazelbauer *et al.*, 2008), where each monomer contributes with two helixes containing a hairpin turn at the membrane-distal end (Kim *et al.*, 1999)(Fig. 3A).

- **Methylation helix bundle:** This element has a parallel helical structure and contains the adaptation sites, where 1 – 4 glutamyl residues can be amidated or methylated to glutaminyl or glutamyl methyl ester residues, respectively (Starrett & Falke, 2005, Swain *et al.*, 2009)(Fig 3A and Fig 3C). In some chemoreceptors, the four-helix bundle of the kinase control module contains an unstructured linker harbouring a terminal pentapeptide at the C-terminal extension of each monomer. The linker and the pentapeptide have an adaptive role, as they provide an

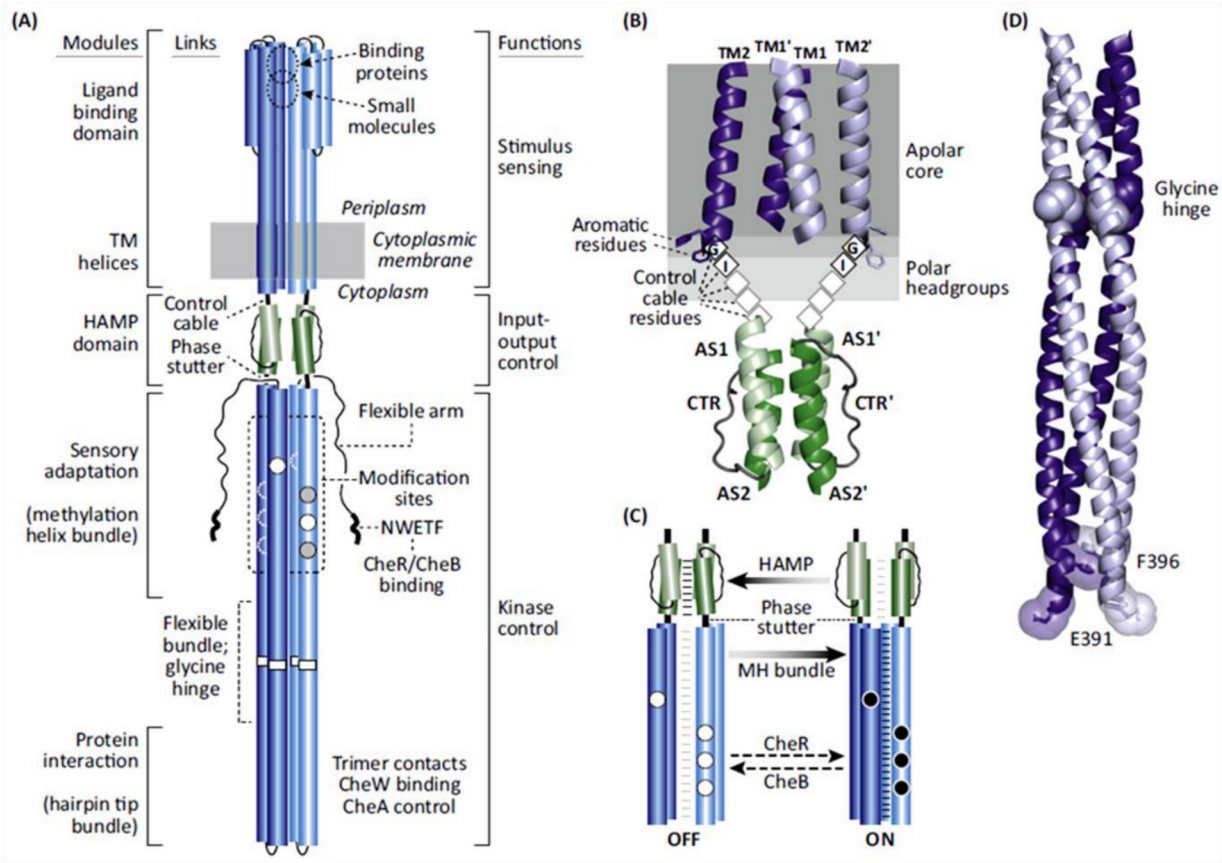

Figure 3. Structural and functional modules of a canonical chemoreceptor. A: Monomers are in dark blue and light blue, whereas HAMP domains are in green. Adaptational sites: in grey, Gln residues; in white, Glu residues. B: The arrangement of transmembrane regions (TM), control-cable and HAMP domain. C: Dynamic-bundle model of the signaling between the HAMP domain and the methylation helix bundle. Grey arrows: weak opposing packing forces. Dashed arrows: strong packing forces by the sensory adaptation system. Light-gray horizontal lines represent weak inter-helix packing forces; black lines represent strong bundle-packing forces. Black circles: Methylated sites. D: Flexible bundle and protein interaction region. Solid spheres: glycine hinge residues. Image from Parkinson *et al.*, 2015.

additional binding site for CheR and CheB (Lai *et al.*, 2006b, Garcia-Fontana *et al.*, 2014)(Fig 3A).

- **Flexible bundle:** This is a flexible region (Alexander & Zhulin, 2007) that joins the methylation helix bundles and the protein interaction module. This region contains six conserved glycine residues at its midpoint (Coleman *et al.*, 2005) that might serve as a structural hinge, enabling the bundle to bend (Kim *et al.*, 1999, Coleman *et al.*, 2005)(Fig. 3A). Importantly, in the Tsr flexible bundle, mutations in Gly340 locked the chemoreceptor in kinase-ON state, and same substitutions in Gly341 or Gly439 inhibited CheA docking or activation, suggesting an important role in ON-OFF switching and kinase docking (Coleman *et al.*, 2005)(Fig 3D).

- **Protein interaction region:** This module comprises the hairpin turn and a region of elevated sequence conservation that brackets the hairpin. This region contains the CheA and CheW binding sites (Piasta *et al.*, 2013, Pedetta *et al.*, 2014)(Fig. 3A and 3D).

Overall, the mechanism of signaling in this module is not entirely clear, which is likely due to its dynamic nature (Hazelbauer *et al.*, 2008).

CONFORMATIONAL AND MOLECULAR SIGNAL TRANSDUCTION MECHANISM

According to the piston-like displacement and the dynamic-bundle signaling model, the LBD-TM2 piston displacement acts, through the control cable, on AS1 helixes of HAMP, changing their packing to a tight state (Fig. 3B). This change is transmitted to the methylation helix bundle by a "phase stutter" connection, which produces a four-residue shift between AS2 and methylation helix region (Danielson *et al.*, 1997, Stewart & Chen, 2010)(Fig. 3C). The coupling between HAMP and methylation helix bundles probably occurs in opposition (Zhou *et al.*, 2009, Zhou *et al.*, 2011): tight packing of the HAMP domain weakens methylation helix bundle packing and, on the contrary, loose packing of HAMP permits tight methylation helix bundle packing (Fig. 4).

These packing changes of methylation helix bundles are transmitted to the protein interaction region by the flexible bundle, although the corresponding molecular detail is unknown. However, "yin – yang" opposite rearrangements of helix-helix contacts at the monomer interface of the receptor tip were observed (Swain *et al.*, 2009), changing between tight and loose packing states, which in turn controls the CheA-OFF and –ON switch, respectively (Mowery *et al.*, 2008, Piasta *et al.*, 2013, Pedetta *et al.*, 2014).

Changes in the methylation helix bundles also acts on the adaptive feedback, since a loose packing state of the methylation helix bundles may favour CheR recognition of methylation sites (Ames *et al.*, 2014). The adaptation sites of Tar and Tsr lie on solvent-exposed faces in regions of high negative charge density, which provokes destabilization in helix packing by charge of vicinal Glu residues (Starrett & Falke, 2005, Lai *et al.*, 2006a). These changes are neutralized by CheR-mediated methylation, which might enhance the stability of the methylation helix bundle (Lai *et al.*, 2006a). On the contrary, a tight packing state of the methylation helix bundles may favour CheB recognition (Ames *et al.*, 2014), and as a consequence the CheB-mediated demethylation decreases methylation helix bundle stability. Importantly, it has been suggested that conformational changes caused by methylation/demethylation in the adaptation region can also reverse the conformational change in the transmembrane sensing module that is induced by ligand recognition (Lai *et al.*, 2006a, Hazelbauer *et al.*, 2008). Ligand binding and covalent modifications in the methylation helix bundle apparently drive opposite helix piston movements, decreasing the ligand affinity, preventing

chemoeffector recognition in the kinase-OFF state (Lai *et al.*, 2006a)(Fig. 4). This implies that the signal conversion module converts signals bi-directionally.

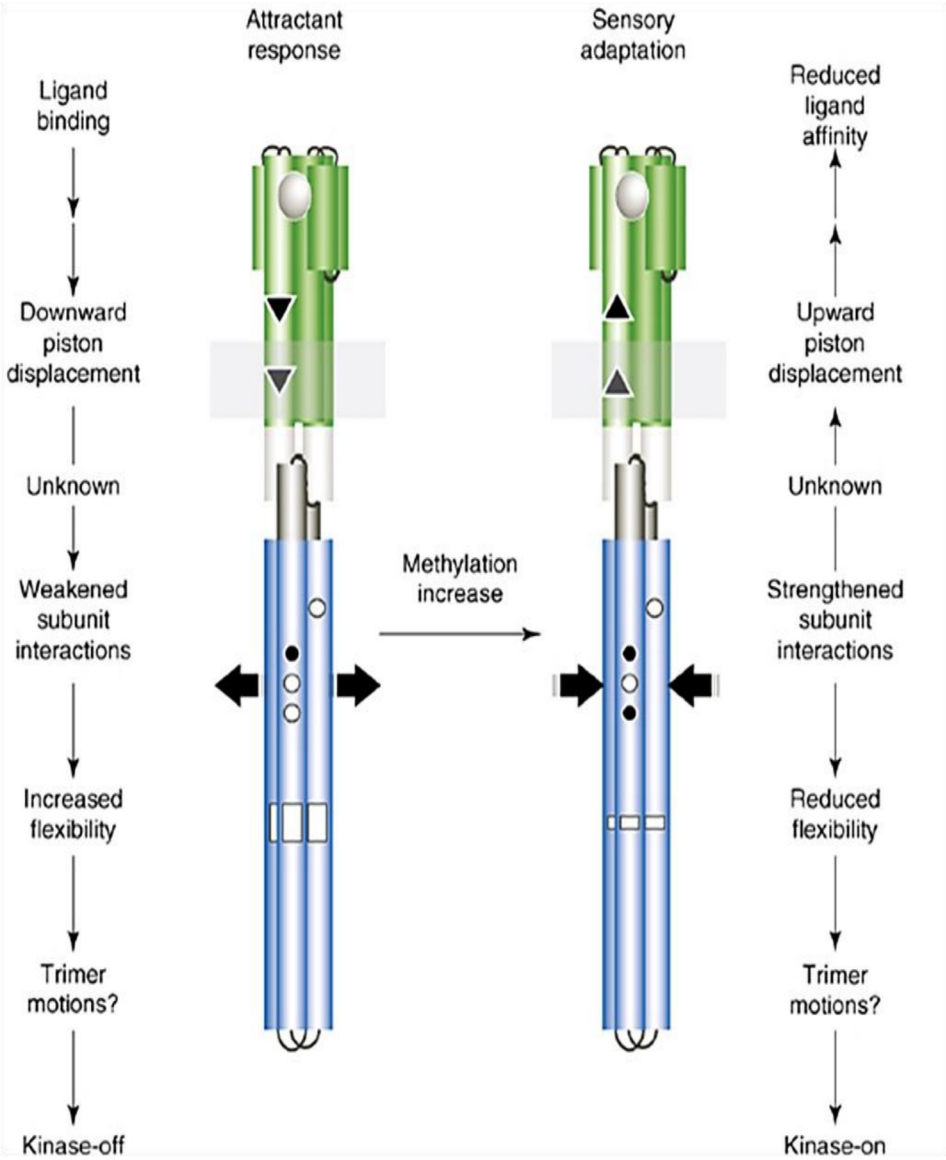

Figure 4. Summary of the conformational changes during signal transduction and adaptation. On the left, conformational changes and downward signal transduction caused by attractant recognition by the LBD. On the right, conformational changes produced during sensory adaptation. In green: transmembrane sensing module. Grey: signal conversion module. Blue: kinase control module. Black triangles: signaling helix displacement. Thick horizontal arrows: demethylation/methylation driven forces. Black circles: methylated sites. White circles: demethylated sites. Thin vertical arrows: transmission of the conformations changes during signal recognition (left) and sensory adaptation (right). Modified from Hazelbauer *et al.*, 2008.

DIVERSITY OF CHEMORECEPTORS AND CHEMOSENSORY PATHWAYS

During the last years, the availability of new genome sequences and new experimental efforts have increased the knowledge of the genetic basis of chemotaxis, chemoreceptors and chemosensory pathways (Ortega *et al.*, 2017a). Nowadays we know that the chemosensory pathways can be rather different among bacteria (Bardy *et al.*, 2017), as many other bacteria possess more complex chemosensory pathways (Lacal *et al.*, 2010b, Porter *et al.*, 2011). Variations can be found at different levels that are detailed below.

NUMBER OF CHEMORECEPTORS PER GENOME

There are very important differences in the number of chemoreceptor genes found in bacteria that range from 1 in the plant pathogen *Xylella fastidiosa* to 88 in the human pathogen *Vibrio parahaemolyticus* (Bardy *et al.*, 2017), with an average of 14 chemoreceptor genes per genome (Lacal *et al.*, 2010b). There is a correlation between the number of chemoreceptors and the bacterial lifestyle (Alexandre *et al.*, 2004) and species that inhabit multiple and variable environments encode around five times more chemoreceptors than species that live in a specific ecological niche (Lacal *et al.*, 2010b).

CHEMORECEPTOR TOPOLOGY

Chemoreceptors can adapt different topologies (Lacal *et al.*, 2010b) that are detailed below (Wuichet *et al.*, 2007)(Fig. 5):

1. **Division I** is composed of chemoreceptors with an extracytoplasmic N-terminal LBD. It can have one or two TM regions (topologies Ia and Ib, respectively). This is the most abundant topology and represents almost three quarters of bacterial chemoreceptors. The *E. coli* receptors Tar, Tsr, Tap and Trg belong to this family.
2. **Division II** is formed by receptors that possess two TM regions and a cytosolic LBD. A representative example is the *E. coli* Aer receptor.
3. **Division III** includes receptors that lack any dedicated LBD. The function of receptors with this topology remains unclear.
4. **Division IV** corresponds to chemoreceptors that lack TM regions and that are consequently entirely located in the cytosol. Receptors of topology IVa possess an LBD, whereas topology IVb are devoid of LBD. However, some IVb receptors were found to interact with individual LBDs forming a non-covalently linked protein complex that appears to carry out chemoreceptor function (Ortega *et al.*, 2017a).

Despite the fact that the majority of chemoreceptors have an N-terminal LBD, some species contain chemoreceptors with the LBD in the C-terminal region. In fact, it has been predicted bioinformatically that about 5 % of LBDs in microbial chemoreceptors are located at the C-terminal extension (Ortega *et al.*, 2017a).

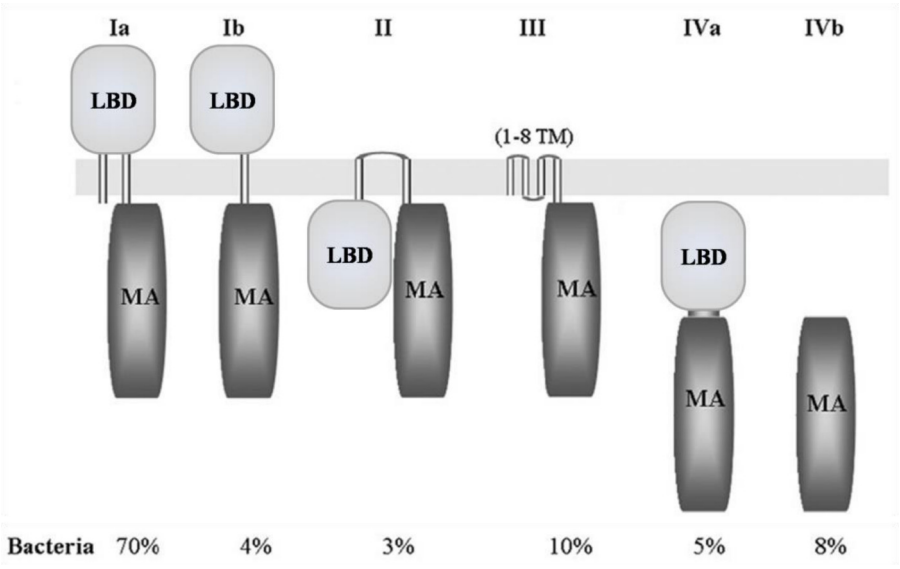

Figure 5. Classification of the chemoreceptor topologies. Shown is the relative abundance of each topology in bacteria. Modified from Lacal *et al.*, 2010.

TYPE OF LIGAND BINDING DOMAIN

Large differences were observed for the size and type of chemoreceptor LDBs. A recent sequence analysis (Ortega *et al.*, 2017a) indicated that chemoreceptors employ more than 80 different LBD types that differ in their size between approximately 120 to 340 amino acids (Lacal *et al.*, 2010b). This diversity is likely to be the key determinant that allows chemoreceptors to recognize a structurally very diverse range of ligands (Fig. 6).

- **Size:** Chemoreceptors and its LBDs were classified into two clusters depending on the LBD size (Lacal *et al.*, 2010b). Cluster I includes chemoreceptors with a LBD size between 120 and 210 amino acids. The 4HB domain of the *E. coli* chemoreceptors are included in this group. Cluster II LBDs have sizes between 220 and 340 amino acids. Almost 40 % of chemoreceptors belong to cluster II that are not found in *E. coli*.
- **LBD families:** In contrast to the conserved MA domain (Alexander & Zhulin, 2007), the LBDs are characterised by a very important sequence divergence (Ulrich & Zhulin, 2005, Upadhyay *et al.*, 2016). LBD types that are relevant for this PhD thesis are (Fig. 6):

  - **Four-helix bundle domains (4HB)**: This is the most abundant family representing 31 % of chemoreceptors (Ortega *et al.*, 2017a) (Fig. 6 top). Representatives of this family are described in the "Bacterial chemoreceptor: Methyl-accepting Chemotaxis Proteins" section.
  - **PAS domains**: Per-Arnt-Sim family represents the third most abundant LBD family (Fig. 6 top) and contains a significant number of different subfamilies as defined by sequences signatures (Upadhyay *et al.*, 2016). PAS domains are universally present in different bacterial signal transduction systems, and are also widely distributed in eukaryotes (Henry & Crosson, 2011). These domains typically sense ligands in the cytosol, and were found to be associated with heme, FAD or FMN cofactors (Taylor & Zhulin, 1999), permitting the sensing of different gases or redox changes.

– **Cache domains**: The Ca^{2+} channels and chemotaxis (CACHE) LBDs include single Cache (sCache) and double Cache (dCache) domains. sCache domains are less abundant than dCache, and possess a PAS-like fold (Upadhyay *et al.*, 2016). dCache

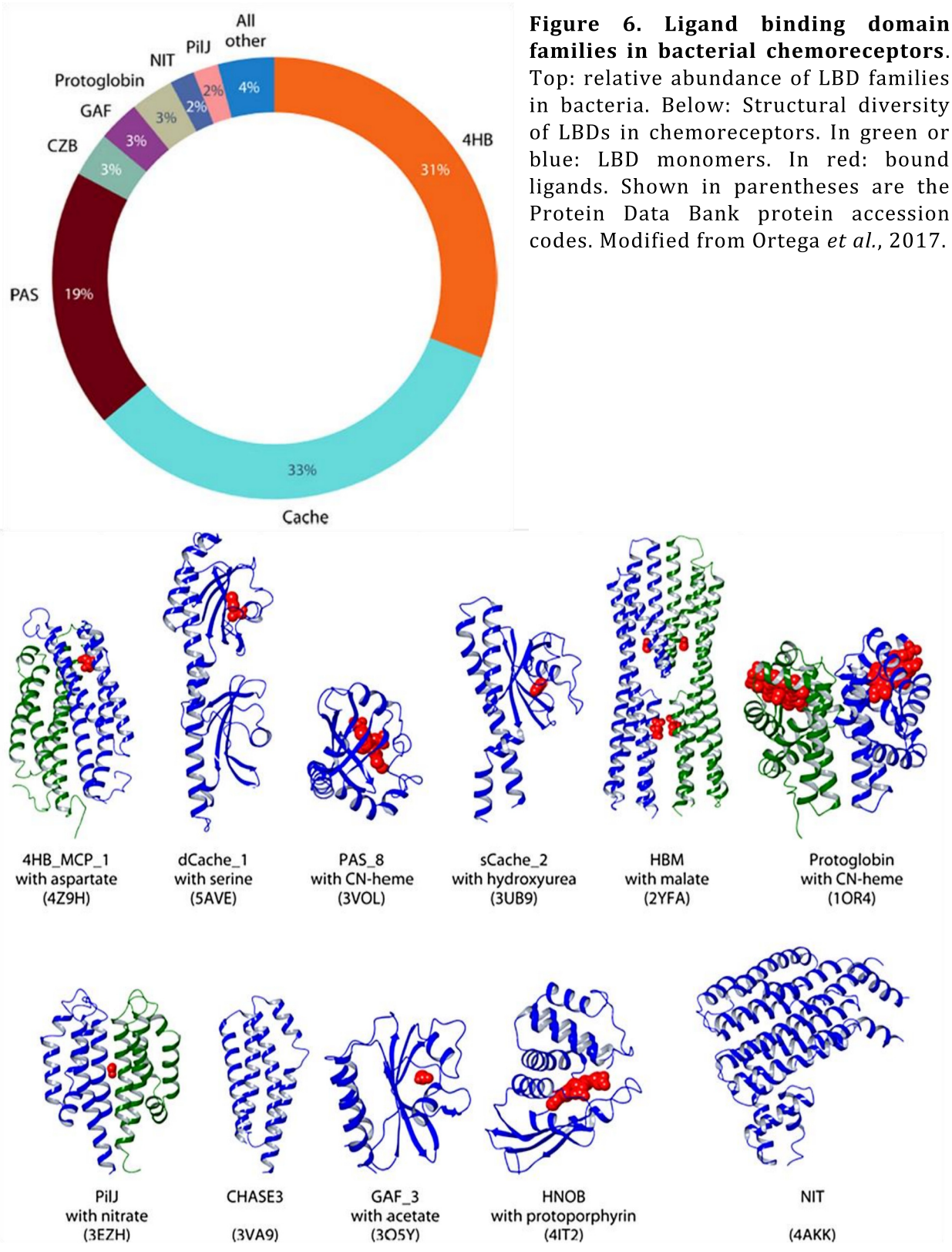

Figure 6. Ligand binding domain families in bacterial chemoreceptors. Top: relative abundance of LBD families in bacteria. Below: Structural diversity of LBDs in chemoreceptors. In green or blue: LBD monomers. In red: bound ligands. Shown in parentheses are the Protein Data Bank protein accession codes. Modified from Ortega *et al.*, 2017.

domains are the second most abundant LBD family and is one of the two known LBDs with a bimodular arrangement (Ortega *et al.*, 2017a), where ligand binding occurs typically in the distal module (Rico-Jimenez *et al.*, 2013b). dCACHE domains have originated from sCache domains by gene duplication (Upadhyay *et al.*, 2016). Together, sCache and dCache domains represent one third of all LBDs (Ortega *et al.*, 2017a) (Fig. 6 top).

- **HBM:** The helical bimodular domain is the second characterized domain that shows a bimodular conformation. Studies of the McpS chemoreceptor of *P. putida* KT2440 have shown that both modules bind ligands and that molecular stimuli additively mediate chemotaxis to both ligands (Gavira *et al.*, 2012).
- **Other families:** Taken together, 4HB, Cache and PAS domains account for more than 80 % of known LBDs in chemoreceptors (Ortega *et al.*, 2017a). However, there are further families of which the most abundant are CZB, (chemoreceptor zinc-binding), GAF (cGMP-specific phosphodiesterases, adenylyl cyclases and FhlA), PilJ (type IV Pili methyl-accepting chemotaxis transducer) and NIT domains (predicted nitrate- and nitrite sensing domain) (Ortega *et al.*, 2017a)(Fig 6 top).

- **Structural classification of chemoreceptor LBDs:** Although many different LBD families can be identified using sequence based classification (see above)(Ortega *et al.*, 2017a) emerging structural information appear to suggest that they adopt two major folds which are (Fig. 6):

  - **Antiparallel α-helix bundle:** This group is represented by domains that are present in the mono-modular (4HB, PilJ, CHASE and NIT) and bimodular arrangement (HBM).
  - **PAS-like α/β-fold:** PAS, GAF, Cache domains belongs to this group and are also found in the mono- and bimodular arrangement.

AUXILIARY SIGNALING PROTEINS

Studies on the chemosensory pathways from other species have shown that frequently multiple copies of paralogous core signaling proteins (chemoreceptors, CheA, CheW, CheB, CheR, CheY) are present in a cell. In some species, more than ten copies of both CheW and CheY were detected (Hamer *et al.*, 2010). Moreover, additional signaling proteins have been detected that are referred to as auxiliary signaling proteins. These alternative proteins have been reported to form alternative adaptation circuits, for example in *B. subtilis* or *Thermotoga maritime* (Porter *et al.*, 2011). Most characterized of these auxiliary proteins are those of the CheC/CheX-CheD and CheV circuits that are discussed below (Rao *et al.*, 2008)(Fig. 2).

- **CheC/CheX-CheD circuit**: Genome analyses suggest that this circuit may be present in more than 40 % of chemotactic bacteria (Wuichet & Zhulin, 2010). CheC and CheX are CheY~P phosphatases (Park *et al.*, 2004a, Szurmant *et al.*, 2004a), whereas CheD is a deamidase that acts on the chemoreceptor MA domain to convert glutamine to methylatable glutamate residues (Kristich & Ordal, 2002). CheD can either bind to chemoreceptors or to the CheC-CheY~P complex. The binding of CheD to chemoreceptors was found to stimulate CheA autophosphorylation when CheY~P levels are low. On the contrary, when the CheY~P levels

are high, CheD forms the ternary complex with CheC-CheY~P, stimulating CheC and reducing the CheA activity (Kristich & Ordal, 2002, Chao *et al.*, 2006)(Fig. 2).

- **CheV circuit**: The CheV protein is composed of a N-terminal CheW domain and a C-terminal receiver domain (Ortega & Zhulin, 2016) that can be phosphorylated by CheA (Alexander *et al.*, 2010). It is considered as an alternative and phosphorylatable form of the CheW adaptor protein. Phosphorylated CheV was found to inhibit CheA kinase activity, which conduces to the adaptive feedback of CheA activity (Rao *et al.*, 2008)(Fig. 2).

NON-CHEMOTACTIC CHEMOSENSORY PATHWAYS

Most chemosensory pathways appear to control chemotaxis, but there is evidence for pathways that carry out other physiological functions (Kirby, 2009, Wuichet & Zhulin, 2010). Examples of species that harbour pathways for chemotaxis and alternative functions are the three chemosensory pathways of *Rhodobacter sphaeroides*, the four chemosensory pathways of *P. aeruginosa* or the eight chemosensory pathways of *Myxococcus xanthus*. In particular, *M. Xanthus* has the Che3 chemosensory pathway for cell differentiation (Kirby & Zusman, 2003, Zusman *et al.*, 2007), *Rhodospirillum centenum* has Che_3 CP for cyst formation (Berleman & Bauer, 2005), and *P. aeruginosa* has the Wsp and Chp chemosensory pathways. Whereas the *wsp* pathways controls c-di-GMP levels that in turn impacts on biofilm formation, the Chp pathways controls cAMP levels modulating in turn the biosynthesis of Type IV pili (T4P)(Whitchurch *et al.*, 2004, Hickman *et al.*, 2005). These pathways with non-chemotactic function appear to share the key features of chemotaxis pathways such as temporal sensing, memory and adaptation.

MECHANISMS FOR SENSING AND CHEMORECEPTOR STIMULATION

Sensing mechanisms

The exhaustive studies of *E. coli* chemoreceptors have identified the homodimer as structural unit. The Tar LBD structure showed that the binding of aspartate occurs at the dimer interface (Milburn *et al.*, 1991) with very strong negative cooperativity, where the binding of the first aspartate molecule reduces the affinity of the second aspartate to levels that are difficult to detect (Biemann & Koshland, 1994). Aspartate recognition not only induced the dimerization and stabilization of the LBD, but also mediated oligomerization of the core signaling complex (Milburn *et al.*, 1991, Boldog *et al.*, 2006). This sensing mechanism is shared by other LBDs, such as is the case of the McpS chemoreceptor that employs a HBM LBD (Pineda-Molina *et al.*, 2012).

However, this is not a general mechanism applicable to all LBD types. PAS, sCache and dCache domains were found to be monomeric when produced as individual protein and ligands bound to a single binding sites at the monomer (Goers Sweeney *et al.*, 2012, Rico-Jimenez *et al.*, 2013b, Nishiyama *et al.*, 2016). In addition, no changes in oligomeric state was noted upon ligand binding (Rico-Jimenez *et al.*, 2013a).

Chemoreceptor stimulation

A variety of molecular mechanisms have been reported that lead to chemoreceptor stimulation (Fig. 7):

a) **Direct ligand binding:** This canonical mechanism has been most extensively studied. The signal molecule is recognized directly by the LBD and triggers the signaling process, causing adaptive responses in the presence of background ligand concentrations (Krembel *et al.*, 2015).
b) **Indirect binding:** Receptors are stimulated by the binding of signal molecule loaded ligand binding proteins (LBP) to the chemoreceptor LBD (Fig. 2). This indirect mode is characterised by a narrower dynamic response range, because the adaptation system is not influenced by LBP binding (Neumann *et al.*, 2010). Sugar and dipeptide chemotaxis in *E. coli* or inorganic phosphate taxis in *P. aeruginosa* are examples for this mechanism (Manson *et al.*, 1986, Zhang *et al.*, 1999, Rico-Jimenez *et al.*, 2016).
c) **Unconventional sensing:** Other ways of stimulation involve ligand induced perturbations in different chemoreceptor regions, causing changes in the structural stability or the position of the TM helixes, the LBD or the MA regions. However, the detailed molecular mechanisms are little understood. Examples are repellence responses from phenol, (Pham & Parkinson, 2011), or taxis in response to pH (Goers Sweeney *et al.*, 2012), osmolarity (Vaknin & Berg, 2006) and temperature (Aguilar *et al.*, 2001, Inda *et al.*, 2014), that appear to be initiated by the signal induced alteration of the TM regions.
d) **Receptor-independent signaling:** A link between chemotactic responses and sugar uptake through the phosphotransferase system (PTS) was reported in *B. subtilis* and *E. coli* (Garrity *et al.*, 1998, Kristich *et al.*, 2003, Neumann *et al.*, 2012, Somavanshi *et al.*, 2016). The influx of

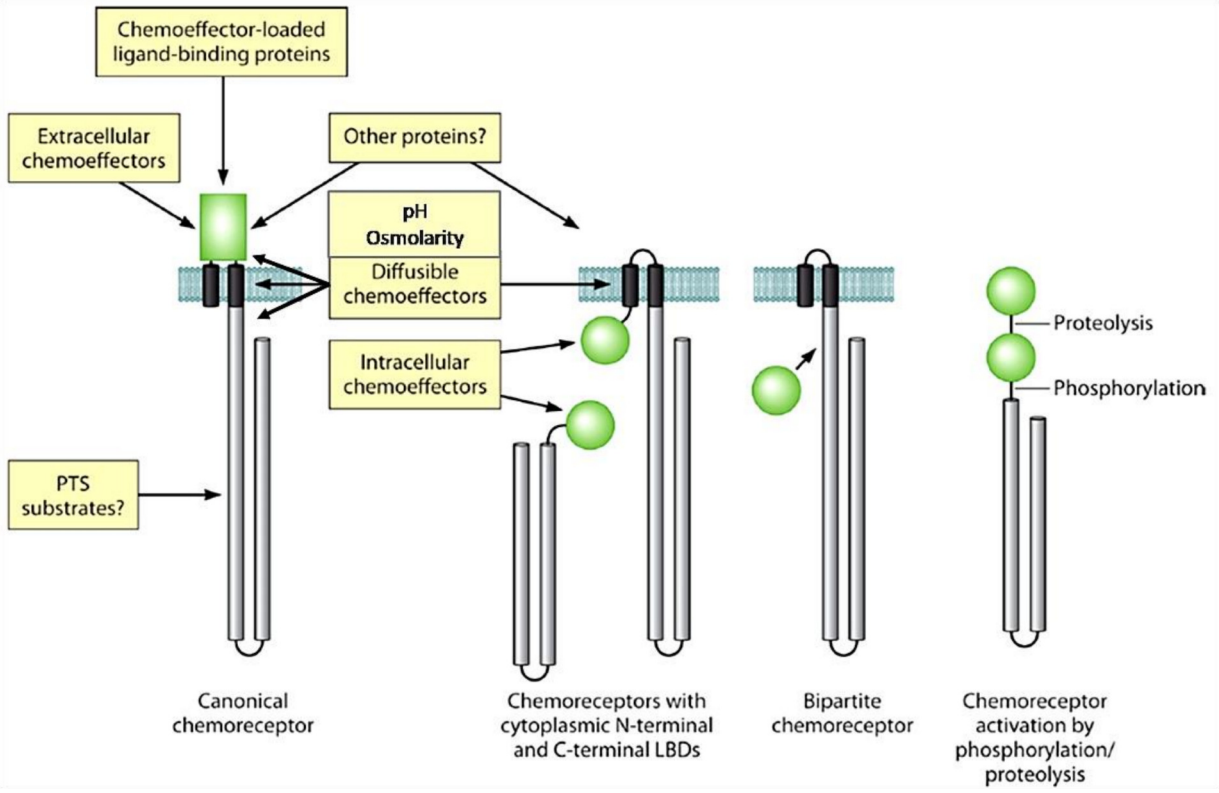

Figure 7. Different mechanisms for ligand recognition and chemoreceptor stimulation. In green: ligand binding domain. In black: transmembrane region. In grey: cytosolic signaling domain. Modified from Ortega *et al.*, 2017.

PTS substrates lowers the phosphorylation state of the PTS proteins which is a molecular stimulus that is transmitted to CheA, modulating its activity. This response seems to propagate to the chemoreceptor causing an adaptation of the methylation region (Neumann *et al.*, 2012).

e) **Chemoreceptor processing:** Another unorthodox chemoreceptor stimulation mode might be case of the BdlA chemoreceptor of *P. aeruginosa*. BdlA requires phosphorylation and a consecutive proteolytic cleavage of one of its sensor domains prior to its activity (Petrova & Sauer, 2012).

f) **Bipartite chemoreceptors:** Some chemoreceptors that lack sensor domains (Lacal *et al.*, 2010b) were found to interact with individual LBDs forming a fully functional chemoreceptor formed by two non-covalently associated proteins, also referred to as bipartite receptors. Representative examples are the bipartite chemoreceptors CetA/CetB and Tlp7 of *Campylobacter jejuni* (Elliott & Dirita, 2008, Elliott *et al.*, 2009, Tareen *et al.*, 2010).

However, most chemoreceptors are functionally un-annotated, which implies that the signal molecules sensed as well as their sensing/signaling mechanisms are unknown. Future research, such as that presented in this PhD thesis, is therefore required to cast further light into these issues.

THE CHEMOSENSORY SIGNALING COMPLEX: TRIMERS OF DIMERS

The *E. coli* chemoreceptors were found to form dimers of some ~300 Å length and to associate with CheA and CheW to form a ternary complex (Weis *et al.*, 2003). This protein complex is capable of performing ligand recognition, transmembrane signaling and adaptational covalent modifications; processes that do not require any additional interactions (Boldog *et al.*, 2006). However, *in vitro* reconstructions using nano-discs showed that a dimer alone is ineffective in CheA activation, and at least the formation of a complex harboring a trimer of chemoreceptor dimers was required for CheA activation (Li *et al.*, 2011). Trimer of dimers comprises the smallest arrangement of chemosensory proteins with the ability to perform all central chemosensory functions, referred to as core chemosensory complex (Li & Hazelbauer, 2011). Recent electron-cryotomography and X-ray crystallographic studies have provided an integrative view of the architecture and organization of bacterial chemoreceptors in trimers of dimers arrays (Liu *et al.*, 2012, Briegel *et al.*, 2013, Briegel *et al.*, 2014a).

Organization of the core chemosensory signaling complex

The CheA kinase is a large protein composed of five domains, connected by flexible linkers (Fig. 8). The P1 domain contains the histidine substrate for autophosphorylation, whereas P2 forms the docking site for CheY and CheB and subsequent transphosphorylation. P3 is the dimerization domain, P4is the catalytic domain, containing the P1 and ATP binding site, whereas the P5domain is a CheW paralog and mediates the control of the kinase activity (Bilwes *et al.*, 1999, Park *et al.*, 2004b, Liu *et al.*, 2012, Briegel *et al.*, 2013).

A model of the arrangement of the core signaling complex is shown in Fig. 8A and B. The central CheA dimer connects two different trimers of chemoreceptor dimers. In this arrangement the regulatory P5 domain is in contact with the chemoreceptor tip, and the dimerization of domains

P3/P3'positionsthe catalytic P4 domain close to P5 regulatory domain. The phosphoryl group accepting domain P1 is in vicinity of the catalytic P4 domain as well as in proximity of the P2 domain for CheY and CheB binding.

Core signaling complex arrays and signal transmission

Core complexes are assembled forming a hexagonal lattice (Briegel *et al.*, 2012)(Fig. 8C). One chemoreceptor of each of the six trimers of dimers is connected to a hexagonal 3CheW-3CheA-P5 ring, and P3 dimers link neighboring hexagons to form extended and stable arrays (Briegel *et al.*, 2012). Through the chemoreceptor, these chemosensory signaling complex arrays can modulate CheA autophosphorylation more than a 100-fold (Parkinson *et al.*, 2015). Ligand recognition causes conformational changes or dynamic motions transmitted to CheA, involving the allosteric regulation in P1-P4 interactions and/or in the active site (Briegel *et al.*, 2013). The structural features of core complexes are consistent with an allosteric mechanism in which alterations in P3-P4 and P4-P5 linkers by chemoreceptors, through CheW and P5 contacts, impose conformational changes on the P4 domain, modulating its autophosphorylation activity and/or its binding interactions with the P1 domain (Wang *et al.*, 2012, Nishiyama *et al.*, 2014, Wang *et al.*, 2014b).

Another important feature that arises from the signaling complex array is the cooperativity. Ligand binding by a single chemoreceptor can regulate the activity of approximately 35 CheA proteins (Sourjik & Berg, 2002). This causes the amplification of the signal within the array (Goldman *et al.*, 2009, Briegel *et al.*, 2012). The cooperative signal amplification model correlates with the structural hexagonal array model (Briegel *et al.*, 2012), which implies that ligand recognition switches a core complex from a dynamic ON state to a more static OFF state, and that those dynamic shifts propagate to neighboring complexes through the rings (Frank & Vaknin, 2013, Parkinson *et al.*, 2015). Finally, the structure of stable chemosensory complex arrays is an important adaptive feature conserved in bacteria and in Archaea and were observed in both membrane-bound and cytoplasmic arrays (Briegel *et al.*, 2009, Briegel *et al.*, 2014b). Specifically, the chemosensory pathways appeared in ancient bacteria and were transferred to ancestral Archaea via lateral gene transfer, likely before the diversification of Euryarchaeota more than 3.5 billion years ago (Briegel *et al.*, 2015), which explains why these chemosensory pathways are not found in Eukarya (Briegel *et al.*, 2015).

THE PHYSIOLOGICAL RELEVANCE OF CHEMOTAXIS AND CHEMOSENSORY PATHWAYS

Approximately half of all bacteria contain genes for chemosensory pathways (Wuichet & Zhulin, 2010). The chemotaxis chemosensory pathways are structurally and functionally conserved and show a wide distribution among bacteria and archaea (Briegel *et al.*, 2009, Briegel *et al.*, 2015). Chemotaxis provides a selective advantage, especially in non-homogeneous environments containing nutrient gradients and toxins, that permit bacteria to find favorable ecological niches or to flee from adverse environmental conditions (Wadhams & Armitage, 2004).

Beyond getting access to nutrients and optimal conditions for life, chemotaxis is an important part of many biological processes such as:

- **Autoaggregation and biofilm formation:** The first stages of autoaggregation and biofilm formation involves a chemotactic response toward extracellular signals, such as quorum-sensing signals. For example, chemotaxis toward autoinducer-2 (AI-2) causes a strong attractant response in *E. coli*, mediating autoaggregation (Alexandre, 2015, Laganenka *et al.*, 2016) and microcolony formation (Laganenka & Sourjik, 2018). Alternatively, AI-2 causes repellent response in *Helicobacter pylori* (Rader *et al.*, 2011), which may be related to

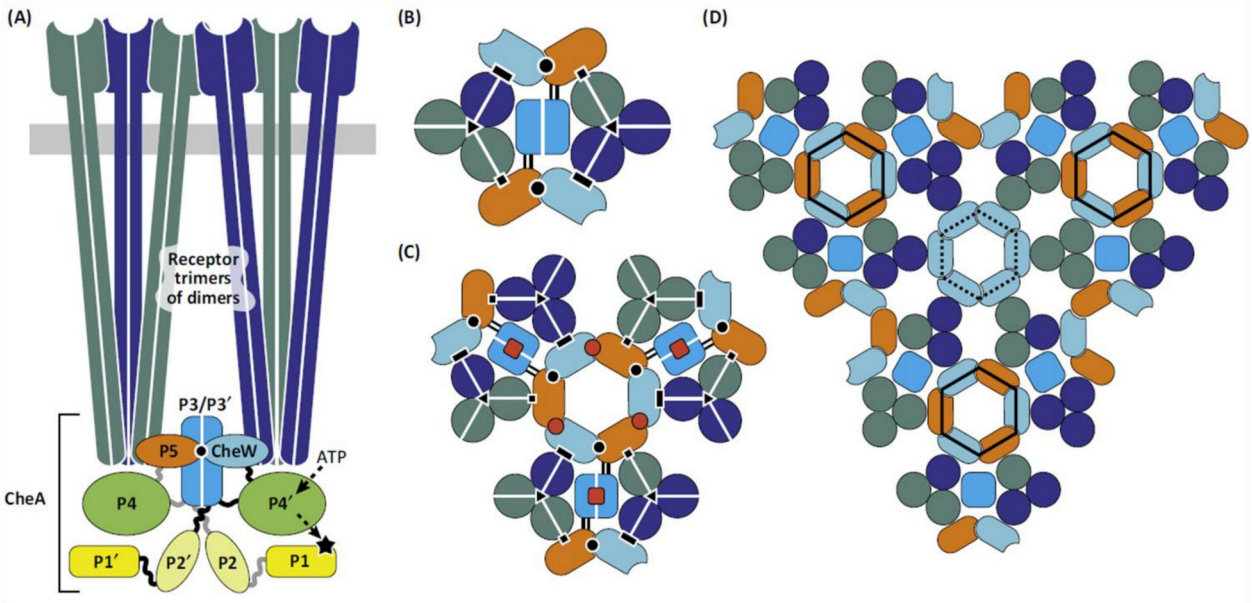

Figure 8. The chemosensory signaling core complex and array. In dark blue and dark green: chemoreceptor homodimers. In light blue: CheW. The CheA subdomains are highlighted in: yellow, P1 (phosphorylation site); ocher, P2 (CheB/CheY binding sites); blue, P3 (dimerization domain); green, P4 (catalysis, P1 and ATP binding sites); brown, P5 (receptor and CheW coupling subdomain). Black symbols (circle, triangle, square, rectangle): protein-protein contacts. A: Two chemoreceptor trimers of dimers. Shown are the CheA subdomains and their protein interactions. B: Cross section of the core complex at the CheA-P5/CheW level. C: CheA-CheW hexagonal ring and signaling connections between the core complexes array. Red squares: P3-P3' dimerization. Red circles: P5-CheW interface interactions. D: Receptor core complex array. Black line: CheA-P5-CheW rings. Dashed black line: hexagonal CheW ring. Image taken from Parkinson *et al.,* 2015.

biofilm dispersal (Anderson *et al.*, 2015). Signaling by chemoreceptors also modulates biofilm formation in *P. putida* (Corral-Lugo *et al.*, 2016), although the corresponding mechanisms are not well understood yet. A recent study in *Comamonas testosteroni* has reported evidence for cross-talk between chemosensory pathways involved in chemotaxis and biofilm formation, which may explain why some chemoreceptors, like in the above cited example of *P. putida*, have a dual role and are involved in chemotaxis and biofilm formation (Huang *et al.*, 2019).

- **Plant root colonization and symbiotic associations:** Signals in plant root exudates are sensed by free-living bacteria, and a positive chemotactic response is essential for efficient root colonization (Scharf *et al.*, 2016). This is a mutualism in which bacteria promote plant growth, fix nitrogen, induce the systemic resistance to pathogens and obtain resources from root exudates. These processes are of significant interest in agrobiology (Souza *et al.*, 2015). Rhizobacteria were found to possess chemoreceptors to sense root exudate components, which serve bacteria as nitrogen and carbon sources such as amino acids, organic acids, polyamines (Li *et al.*, 2013). Well studied examples of chemoreceptors that play an important role in sensing root exudate components and consequently root colonization are the McpU and McpX chemoreceptors of *Sinorhizobium melitoti* (Webb *et al.*, 2014, Webb *et al.*, 2017a, Webb *et al.*, 2017b), mediating responses to amino acids and quaternary ammonium compounds, respectively, or multiple chemoreceptors of *Pseudomonas fluorescens* (Oku *et al.*, 2012) for amino acid sensing.

  Other symbiotic processes occur between bacteria and animals, of which the squid *Euprymna scolopes* and *Vibrio fischeri* (Millikan & Ruby, 2003) are a representative example. In *V. fischeri*, it has been reported that chemotaxis to sugars N-acetyl neuroaminic acid (NANA) and N-acetylglucosamine mono- and disaccharide (GlcNA and $(GlcNA)_2$) mediates the successful colonization of the squid light organ (Norsworthy & Visick, 2013). NANA is present in the mucus around the pores of the light organ channels, and a gradient of GlcNA and $(GlcNA)_2$ is formed inside these channels, which has been suggested as the mechanism by which the squid may guide *V. fischeri* to the crypts inside the light organs (Norsworthy & Visick, 2013). Once in the crypts, bacteria survive in a favorable niche, and bioluminescence emitted from bacteria is used by the squid to confuse predators (Norsworthy & Visick, 2013).
- **Pathogenicity:** Chemotaxis is required for many plant and animal pathogenic bacteria for effective host invasion and infection (Matilla & Krell, 2018). For example, the sensing of specific host signals by the TlpA, TlpB, TlpC and TlpD chemoreceptors of *H. pylori* drives stomach colonization and infection by guiding the bacteria to the mucus layer (Johnson & Ottemann, 2018). In *Borrelia burgdorferi*, it has been shown that chemotaxis is essential for dissemination and viability, both in the transition between hosts and during infection within the hosts (Sze *et al.*, 2012). The plant pathogen *Agrobacterium tumefaciens* detects and swims toward amino acids, organic acids and sugars released from plant wounds, leading to cell attachment and subsequent establishment of infection (Escobar & Dandekar, 2003, Merritt *et al.*, 2007).
- **Bioremediation:** Pollution is one of the main problems of human activity. In some environmental bacteria, such as *P. putida* DOT-T1E, *Burkholderia cepacia* and *Rhizobium* sp., exist chemosensory pathways and chemoreceptors that mediate chemoattraction to degradable environmental pollutants such as toluene, benzene or naphthalene (Lacal *et al.*,

2013). The resulting increase in pollutant bioavailability enhances the biodegradation efficiency, which has the potential to optimize biodegradation processes (Lacal *et al.*, 2013).

PSEUDOMONAS AS ALTERNATIVE MODELS TO STUDY CHEMOTAXIS

As detailed above, *E. coli* is the reference model organism to study chemosensory signaling processes, which has 4 chemoreceptors that feed into a single chemosensory pathway mediating chemotaxis. Bacterial genome analyses have shown that many species contain an elevated number of chemoreceptors such as on average 33 for plant pathogens (Matilla & Krell, 2018) and multiple copies of signaling protein suggesting the existence of parallel chemosensory pathways with potentially different functions. This complexity of signaling requires novel bacterial models and the Krell laboratory has chosen *P. putida* KT2440 and *P. aeruginosa* PAO1 as model to study chemosensory signaling a decade ago.

Pseudomonas aeruginosa PAO1

The strain PAO1 is a spontaneous chloramphenicol-resistant mutant of the original PAO strain, isolated from a wound in Melbourne, Australia in 1954 (Klockgether *et al.*, 2010). This bacterium can survive in many environments (Moradali *et al.*, 2017), and can infect animals and plants, being one of the most serious causes of nosocomial infections, especially in cystic fibrosis (CF), immunocompromised, cancer and burn patients (Juhas, 2015). It is the main cause of death in CF patients by causing chronic lung infections (Driscoll *et al.*, 2007). It has been placed second on the WHO priority list for research on the development of new antibiotics (WHO, 2017).

P. aeruginosa has become an important model to study chemosensory pathways with differing functions (Kato *et al.*, 2008). The bacterium has four chemosensory pathways encoded by five gene clusters (Sampedro *et al.*, 2015) as well as26 chemoreceptors (Ortega *et al.*, 2017a). The *che1* pathway is required for flagellum-mediated chemotaxis, whereas the *che2* pathway is required for virulence and required for optimal chemotactic responses (Ferrandez *et al.*, 2002, Garvis *et al.*, 2009). The *wsp* pathway mediates changes in c-di-GMP levels (Hickman *et al.*, 2005) whereas the *chp* pathway controls T4P mediated motility and modulates c-AMP levels (Fulcher *et al.*, 2010). A bioinformatic study supports a model by which 23 chemoreceptors feed into the *che1* pathway, whereas a single chemoreceptor feeds into each of the remaining three pathways (Ortega *et al.*, 2017b).

Of the 26 chemoreceptors, twenty are of the canonical topology containing a periplasmic LBD that belong to the families 4HB, sCache, PAS, PilJ, HBM, dCache and NIT (Ortega *et al.*, 2017a)(Fig. 6). Three chemoreceptors are entirely cytosolic, whereas three other receptors are membrane bound but lack periplasmic LBDs.

At the time of the beginning of this thesis in 2015 chemoreceptors PctA, PctB and PctC had been identified to mediate chemoattraction to different proteinogenic amino acids and GABA (Taguchi *et al.*, 1997, Rico-Jimenez *et al.*, 2013a), to_high and low concentrations of inorganic phosphate (CtpH and CtpL) (Wu *et al.*, 2000), to malate (chemoreceptor PA2652)(Alvarez-Ortega & Harwood, 2007) and ethylene (TlpQ)(Kim & Tokura, 2007)(Fig. 9 (top), Table 1). The soluble chemoreceptor McpB/Aer2 was found to be involved in gas sensing but its final output remained unclear (Airola *et al.*, 2013a). The Aer receptor has been identified to mediate aerotaxis (Hong *et al.*,

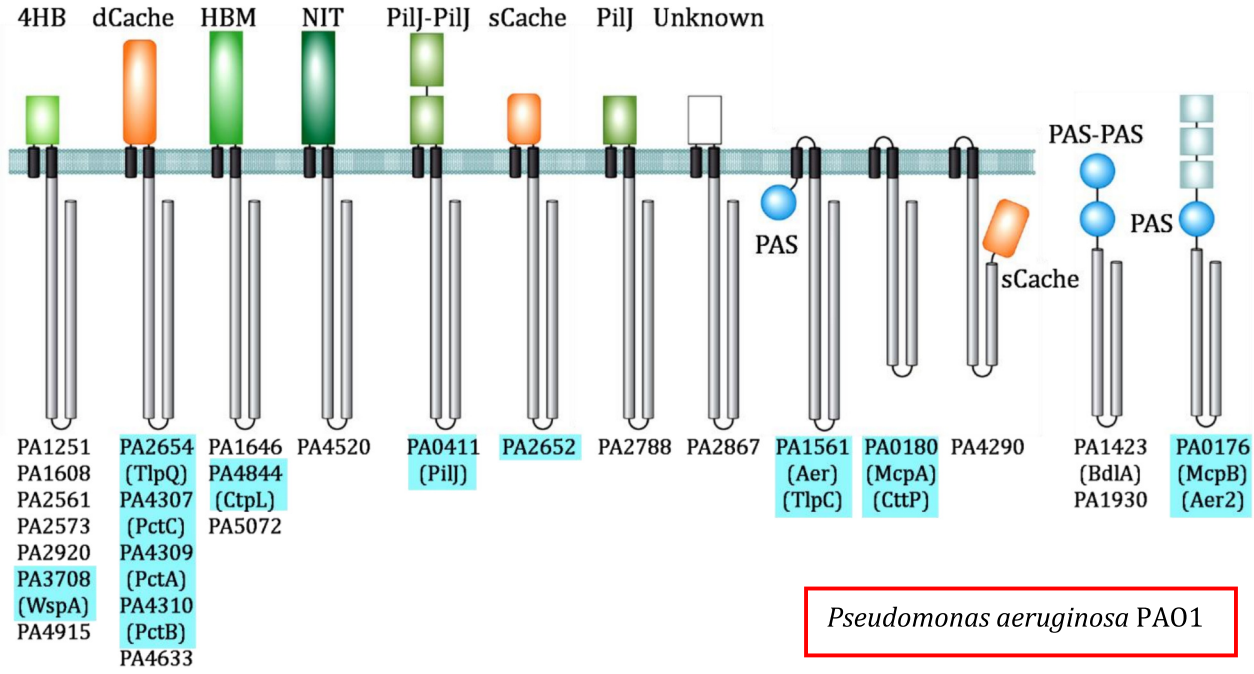

Figure 9. Chemoreceptor repertoire of *P. aeruginosa* PAO1 and *P. putida* KT2440. The LBD type is indicated. Chemoreceptors that were functionally characterized at the beginning of this thesis are shaded in blue. Modified from Ortega *et al.*, 2017.

2004b). However, the signal molecules recognized and function of the remaining chemoreceptors was unknown.

Pseudomonas putida KT2440

P. putida KT2440 is a derivative of *P. putida* mt-2, curated of the TOL plasmid, that was isolated from Japanese soil in 1961 by Hosakawa (Nakazawa, 2002). It can survive in many different soil and water environments and is also known for its metabolic versatility and its potential to degrade aromatic and xenobiotic compounds (Moreno & Rojo, 2013). Moreover, it is able to promote plant growth by colonizing plant roots (Colauto *et al.*, 2016). These features make it an interesting candidate strain for biotechnological applications (Nikel & de Lorenzo, 2014), bioremediation processes (Nikel *et al.*, 2014) as well as for agricultural uses (Kertesz & Mirleau, 2004).

P. putida KT2440 has three paralogues of each core signaling protein suggesting that this strain has 3 chemosensory pathways (Garcia-Fontana *et al.*, 2013). Experimental data showed that this strain has a chemosensory pathway for chemotaxis as well as a pathway that is homologous to the *wsp* pathway of *P. aeruginosa* that controls c-di-GMP levels, whereas the function of a potential third pathway is unknown (Garcia-Fontana *et al.*, 2013, Ortega *et al.*, 2017a).

The chemoreceptor repertoire of *P. putida* KT2440 is comparable to that of *P. aeruginosa* PAO1. Of the 27 chemoreceptors, 22 are of the canonical topology harboring a periplasmic LBD (Ortega *et al.*, 2017a). Similar to *P. aeruginosa*, LBD types of *P. putida* chemoreceptors include 4HB, sCache, PAS, PilJ, HBM, and dCache (Ortega *et al.*, 2017a). At the beginning of this thesis there was scarce information as to the function of KT2440 chemoreceptors. The McpS receptor had been identified by the Krell laboratory to mediate chemotaxis to Krebs cycle intermediates and acetate (Lacal *et al.*, 2010a, Lacal *et al.*, 2011b, Pineda-Molina *et al.*, 2012) and two receptors, Aer and Aer2, had been identified to be responsible for energy taxis (Nichols & Harwood, 2000, Sarand *et al.*, 2008) (Figure 9 (bottom), Table 1). Information on the remaining chemoreceptors was lacking which clearly defined the research need that formed the basis for this thesis.

Several issues defined the strategy pursued in the functional annotation of the *Pseudomonas* chemoreceptors:

1. The 4HB domain is the most abundant LBD in bacterial chemoreceptors. However, the second most abundant LBD type in the chemoreceptor repertoire of both strains are dCACHE domains (Fig. 9). Since little information was available on these receptors, the study of chemoreceptors with this particular LBD had been prioritized.
2. So far only one member of the HBM domain family had been identified (McpS) and, therefore, attempts had been made to identify other chemoreceptors with this LBD to define this chemoreceptor family.
3. Receptors with a PilJ type of LBD had so far not been characterized and, therefore, attempts were made to identify the ligands and function of this chemoreceptor sub-family.

Table 1. Functionally characterized chemoreceptors of *P. aeruginosa* PAO1 and *P. putida* KT2440 at the beginning of 2015.

Chemoreceptor Locus	Name	LBD type	Effector(s)	Binding mode	Reference
P. aeruginosa PAO1					
PA0176	Aer2, McpB	PAS	O_2, NO, CO, cyanide	Direct	(Hong *et al.*, 2004a, Hong *et al.*, 2004b, Sawai *et al.*, 2012, Airola *et al.*, 2013a)
PA0180	CttP, McpA	None	Chloroethylenes	Unknown	(Kim *et al.*, 2006)
PA0411	PilJ	PilJ	Phosphatidylethanolamine	Unknown	(Kearns *et al.*, 2001)
PA1561	Aer, TlpC	PAS	Aerotaxis	Unknown	(Hong *et al.*, 2004a, Hong *et al.*, 2004b)
PA2561	CtpH	4HB	Inorganic phosphate	Direct	(Wu *et al.*, 2000)
PA2652	CtpM	sCache	Malate	Unknown	(Alvarez-Ortega & Harwood, 2007)
PA2654	TlpQ	dCache	Ethylene	Unknown	(Kim & Tokura, 2007)
PA3708	WspA	4HB	Growth on solid surfaces, ethanol	Unknown	(O'Connor *et al.*, 2012, Chen *et al.*, 2014)
PA4307	PctC	dCache	GABA, histidine, proline chloroethylenes	Direct Unknown	(Kuroda *et al.*, 1995, Taguchi *et al.*, 1997, Rico-Jimenez *et al.*, 2013a, Reyes-Darias *et al.*, 2015b) (Shitashiro *et al.*, 2005)
PA4309	PctA	dCache	17 amino acids, chloroethylenes	Direct Unknown	(Kuroda *et al.*, 1995, Taguchi *et al.*, 1997, Rico-Jimenez *et al.*, 2013a) (Shitashiro *et al.*, 2005)
PA4310	PctB	dCache	5 amino acids, chloroethylenes	Direct Unknown	(Kuroda *et al.*, 1995, Taguchi *et al.*, 1997, Rico-Jimenez *et al.*, 2013a) (Shitashiro *et al.*, 2005)
PA4844	CtpL	HBM	Inorganic phosphate, chloroaniline, catechol	Indirect Unknown	(Wu *et al.*, 2000) (Vangnai *et al.*, 2013)
P. putida KT2440					
PP_2111	Aer2	PAS	Aerotaxis, methylphenols, phenylaceticacid	Unknown Unknown	(Sarand *et al.*, 2008) (Luu *et al.*, 2013)
PP_2257	Aer1	PAS	Aerotaxis	Unknown	(Nichols & Harwood, 2000)
PP_4658	McpS	HBM	TCA intermediates, acetate, butyrate	Direct	(Lacal *et al.*, 2010a)

OBJECTIVES

OBJECTIVES

The objectives of this thesis are:

- Chapter 1: Identification of chemoreceptors that mediate chemotaxis to organic acids.
    - Chapter 1.1.: Identification of a chemoreceptor for C2 and C3 carboxylic acids in *P. putida* KT2440.
    - Chapter 1.2.: Identification of a citrate chemoreceptor in *P. putida* KT2440.
    - Chapter 1.3.: Identification of a α-ketoglutarate specific chemoreceptor in *P. aeruginosa* PAO1.
    - Chapter 1.4.: Identification of a chemoreceptor in *P. aeruginosa* PAO1 specific for . C4-dicarboxylic acids and assessment of the role of chemoeffectors and signal antagonists.
- Chapter2: Identification of chemoreceptors that mediate chemotaxis to polyamines.
    - Chapter 2.1.: Structural basis of polyamine recognition at dCache containing chemoreceptor in *P. putida* KT2440.
    - Chapter 2.2: Molecular basis of *P. aeruginosa* PAO1 taxis to histamine and polyamines.
- Chapter 3: Identification of the molecular mechanism for nitrate chemotaxis in *P. aeruginosa* PAO1.

METHODOLOGY

METHODOLOGY

This section contains general information about the experimental procedures that have been employed during this thesis. The detailed protocols are found in the methodology section of each chapter.

MICROBIOLOGICAL PROCEDURES

Bacterial strains, culture media and growth conditions

Bacterial strains used in this thesis were *P. aeruginosa* PAO1 and *P. putida* KT2440 as well as their derivative mutant strains. Cloning procedures were generally carried out in *E. coli* DH5α and protein overexpression in *E. coli* BL21 (DE3). Other particular strains are specified in each chapter. Unless otherwise is stated, general culture media used were lysogeny broth (LB) and M9 or MS minimal media, supplemented with 10 – 20 mM of succinic acid or D-glucose. Growth temperatures were 37 °C for *P. aeruginosa* and 30 °C for *P. putida*. Full information about bacterial strains can be found in Tables 2, 4, 7, 12 and Supp. Table 5.

Growth experiments

The assessment of different compounds as potential carbon and nitrogen sources was carried out on a Bioscreen Microbiological Growth Analyser (Oy Growth Curves Ab Ltd, Helsinki, Finland). The assays were conducted in a 100-well polystyrene plates containing 200 µl of bacterial suspension at an OD_{600} of 0.02 – 0.05 as well as 0.5 - 10 mM of the compound to be tested. Typically, growth was followed over a time of 24 hours and growth rates were calculated from three independent experiments conducted at least in triplicate.

BIOMOLECULAR PROCEDURES

Plasmid construction for LBD overexpression

The DNA fragments encoding each LBD of the chemoreceptors studied were amplified by polymerase chain reaction (PCR) using *P. aeruginosa* PAO1 or *P. putida* KT2440 genomic DNA as template. The resulting products were then cloned into the expression plasmid pET28(b). The resulting plasmids were verified by sequencing the insert and flanking regions and transformed into *E. coli* DH5α for storage at -80 °C.

Site-directed mutagenesis

Plasmids containing site-directed mutants were either purchased from Genescript (Piscataway, NJ,) or were generated using the overlapping PCR method (Ho *et al.*, 1989). To this end the DNA fragment was cloned into pCR2.1-TOPO (Invitrogen) that was then used for the PCR reactions using oligonucleotides containing the desired mutation. The mutant plasmid was verified by DNA sequencing, and then transformed into *E. coli* DH5α for storage at -80 °C.

Construction of *Pseudomonas* mutant strains

A modified version of the unmarked non-polar deletion mutant procedure was used for the replacement of wild type genes in the chromosome (Schweizer, 1992). The plasmids for the construction of these mutants were generated by amplifying the DNA fragments comprising 200-500 bp of the upstream and downstream regions of each chemoreceptor to be deleted. The resulting PCR products were digested with enzymes specified in each chapter and cloned into pUC18NotI (Herrero *et al.*, 1990). The resulting plasmids were then digested with NotI and then the fusion of both fragments was subcloned into the marker exchange suicide vector pKNG101 (Kaniga *et al.*, 1991). Subsequently, plasmids for mutagenesis were transferred into *Pseudomonas* strains by three-partner conjugation using *E. coli* CC118λ*pirm* and *E. coli* HB101 (pRK600) as helper strain. Selection for plasmid cointegration in *Pseudomonas* strains was performed using M9 minimal medium supplemented 0.2% (w/v) glucose and 400 µg/ml streptomycin. For the construction of the final mutant, sucrose was added to a final concentration of 10% (w/v) to select derivatives that had undergone a second cross-over event during marker exchange mutagenesis. Streptomycin sensitive colonies were screened by PCR analyses and the resulting mutants were confirmed by DNA sequencing.

For the construction of the kanamycin-resistant *P. aeruginosa* mutant strain, a derivative plasmid of pKNG101 was constructed. This plasmid contains the intergenic region of genes *pa5548* and *pa5549* (*glmS*) with the kanamycin cassette from p34S-Km3 (Dennis & Zylstra, 1998) inserted into a neutral position downstream of *glmS* (Koch *et al.*, 2001). Then, the steps detailed above for deletion mutant generation were followed. The kanamycin resistant strain was confirmed by PCR and sequencing.

Plasmids construction for mutant complementation

For the construction of plasmids to be used for mutant complementation, the coding sequences of the chemoreceptors were amplified by PCR and cloned into pBBR1MCS-based plasmids (Kovach *et al.*, 1995, Obranic *et al.*, 2013). The insertions were confirmed by PCR and sequencing. Plasmids were electroporated into the corresponding mutant strain for phenotypic analyses.

PROTEIN OVEREXPRESSION AND PURIFICATION

Protein overexpression

E. coli BL21 (DE3) was transformed with each of the expression plasmids. The resulting strains were cultured at 30 °C in LB supplemented with kanamycin under continuous shaking. At an OD_{600} of 0.5 – 0.6 protein overexpression was induced by the addition of 0.1 mM isopropyl-β-D-1-thiogalactopyranoside (IPTG). After 14 – 16 h of further growth at 16 °C and continuous shaking, cells were harvested by centrifugation at 10000g and 4°C for 30 min.

Protein purification

Cells pellets containing overexpressed polyHis-tagged protein, were resuspended in buffer and broken by French press treatment at a gauge pressure of 62.5 lb/in. After centrifugation at 20000 g and 4 °C for 1 h, the supernatant was filtered and loaded onto an immobilized metal ion affinity chromatography column (HisTrap, Amersham Bioscience), connected to a ÄKTA P-920/UPC-900 fast liquid protein chromatography instrument. After a wash step with buffer containing 35 mM imidazole, the protein was eluted by a gradient of buffer containing 35 – 500 mM

imidazole. Protein-containing fractions were pooled and dialysed into analysis buffer for immediate analysis.

BIOPHYSICAL PROTEIN CHARACTERIZATION

Differential scanning fluorimetry based high throughput ligand screening

High-throughput ligand screening was performed by Differential Scanning Fluorimetry based thermal shift assays, using commercially available compound arrays (Biolog, Hayward, CA, USA). Each well of a 96-well plate was filled with a 25 µl aliquot containing 10 – 50 µM of protein, 5x SYPRO Orange (Life Technologies) and 1 – 2 mM of the compound to be tested. One of the wells (control) contained only the protein and 5 x SYPRO. Plates were inserted into a MyIQ2 Real-Time PCR instrument (Bio-Rad) and heated from 23 °C to 85 °C at a scan rate of 1 °C/min, during which time fluorescence changes were monitored. T_m values were calculated analyzing the minima of the first derivatives of the raw data.

Isothermal titration calorimetry

Experiments were carried out on a VP microcalorimeter (Microcal, Amherst, MA, USA) at a temperature of 15 – 35 °C. Protein solutions, typically between 10 – 100 µM, were placed into the sample cell and titrated with 6.4 – 19.2 µl aliquots of ligand solutions at a concentration of 0.25 – 20 mM. The mean enthalpy changes arising from the titration of buffer with ligand solution were subtracted from the protein raw titration data prior to data analysis. Unless otherwise is stated, data analysis was performed with the "One binding site model" of the MicroCal version of ORIGIN.

Analytical ultracentrifugation

Experiments were performed on a Beckman Coulter Optima XL-I analytical ultracentrifuge (Beckman-Coulter, Palo Alto, CA, USA) equipped with UV-visible light absorbance and interference optics detection systems, and using an AnT50Ti 8-hole rotor and 12-mm-path-length charcoal-filled epon double-sector centrepieces.

Sedimentation velocity (SV) runs were carried out with 400 µl of sample at a rotor speed of 48000 – 128796 x g. Laser wavelength was 236 nm in the absorbance optics mode. The temperature was set at 7 – 10 °C, and 5 – 50 µM of protein were used (with and without ligand). Least-squares boundary modeling of the SV data was used to calculate sedimentation coefficient distributions with SEDFIT software (Schuck, 2000). Buffer density, viscosity and the partial specific volume were estimated using the SEDNTERP software from buffer components (Laue *et al.*, 1992).

Sedimentation equilibrium (SE) experiments were conducted measuring absorbance at 280 nm as a function of radius. Protein at three different concentrations was loaded, in the absence or in the presence of ligand. A multi-speed of 9740, 20606 and 185462 g run was used. The data were analyzed globally by the SEDPHAT "species analysis with mass conservation constraints" model (Vistica *et al.*, 2004). The quality of the fit was evaluated on the basis of the residuals, expressed as the difference between the experimental data and the theoretical curve.

Intrinsic tryptophan fluorescence spectroscopy

Fluorescence measurements were performed on a PTI QM-2003 spectrofluorimeter (Photon Technology International, Law-renceville, NJ). Proteins were excited at a wavelength of 290 – 295 nm and emission spectra were recorded between 300 and 500 nm at a scan speed of 1 – 2 nm/s. Collected spectra data were corrected with the buffer emission spectra.

Circular dichroism spectroscopy

Measurements were made using a Jasco J-715 (Tokyo, Japan) spectropolarimeter equipped with a thermostatized cell holder. For each dialyzed protein, five far-UV CD spectra were recorded with a 1-mm-path-length quartz cuvette using a bandwidth of 1 – 2 nm, a response time of 1 – 4 s, a scan rate of 100 nm/min. Each spectrum was corrected by baseline subtraction using the buffer spectrum. The CD signal was normalized to mean residue molar ellipticity.

Differential scanning calorimetry

Experiments were carried out on a VP-DSC capillary-cell microcalorimeter (MicroCal, Northampton, MA, USA) at a scan rate of 180 °C/h from 5 to 95 °C. Calorimetric cells of 134 µl were kept under a pressure of 60 psi to prevent sample degassing. After several buffer-buffer baselines were obtained, protein sample runs were conducted, in the absence or presence of ligand. The calorimetric enthalpies were estimated by data integration of the transition peaks, and the peak width at half-height was determined using ORIGIN 7.5 (OriginLab Corporation, Northampton, MA, USA).

PROTEIN CRYSTALLIZATION AND STRUCTURE RESOLUTION

Protein crystallization

Optimal conditions for protein crystallization were screened using the capillary counter-diffusion technique using the commercially available crystallization kits GCB-CSK, PEG448-49 and AS-49 (Triana Science & Technology, Granada, Spain). Purified protein was incubated with saturating ligand concentrations at 4 – 25 °C and the excess of ligand was removed by centrifugation using 3 kDa cutoff Amicon concentrators. The apo-protein and protein-ligand complex were loaded into capillaries with an inner diameter of 0.2-mm. Crystals were extracted from the capillaries, flash cooled in liquid nitrogen and stored until data collection.

Structure resolution

Crystals were diffracted at the European Synchotron Radiation Facility or the Spanish Synchrotron ALBA. Data were indexed and integrated with XDS (Kabsch, 2010) and scaled with SCALA (Evans, 2006). Initially, attempts to solve the phase problem were undertaken using molecular replacement techniques and homology models. When the attempts failed, other approaches were applied which have been specified in each chapter.

GENE EXPRESSION STUDIES

RNA extraction

Flasks containing 20 ml minimal media were inoculated with overnight bacterial culture to an initial OD_{600} of 0.05. Unless otherwise is indicated, at mid-exponential phase, 1 mM of cognate ligand was added to the cultures, whereas sterile water was added to control flasks. At regular time intervals,500 µl samples were taken and total RNA was extracted using the High Pure RNA Isolation Kit (Roche Diagnostics) and treated with Turbo DNAse (Ambion). The quality and quantity of isolated RNA was determined spectrophotometrically and by agarose-gel electrophoresis.

Quantitative real-time PCR analyses (RT-qPCR)

Complementary DNA (cDNA) was synthesized from 500 ng RNA using SuperScript II reverse transcriptase (Invitrogen) and200 ng of random hexaprimers (Roche) following manufacturers' instructions. Quantitative PCRs were performed using a MyiQ2 thermal cycler (Bio-Rad) with a 96-well plate containing7.5 µl of 2× iQ SYBR green supermix (Bio-Rad), 500 nM of each primer and 1 µl of cDNA in a final reaction volume of 15 µl. The temperature protocol as well as the primers and the reference genes used are specified in each chapter. Gene expression data were normalized to the expression of the reference genesusing the BIO-RAD iQ5 software.

PHENOTYPICAL ASSESSMENTS

Swimming plate motility assay

Overnight cultures from single colonies of bacteria were grown at the appropriate temperature. Two-microliter aliquots of bacterial suspension were transferred to the center of swim agar plates (0.25 % (w/v) agar in minimal medium supplemented with 10 % (w/v) LB. Plates were inspected after growth for 14-18 h.

Gradient plate chemotaxis assay

Overnight cultures were grown in minimal medium supplemented with 10 mM succinic acid or D-glucose. Bacterial suspensions were washed twice by centrifugation at 3750 g for 3 min followed by re-suspension in minimal medium. Aliquots of 10 µl chemoeffector solution (10 – 250 mM) were placed along the vertical central line of square Petri dishes containing 80 ml of soft agar minimal medium (0.25 % (w/v) agar supplemented with 25 mM glycerol). After an incubation at 4 °C for 12 – 16 h, which permitted the formation of a chemoeffector gradient, 2µl aliquots of washed bacterial suspension were placed along a line parallel to the central line (distance between both lines 1 – 2.5 cm). Plates were inspected for chemotaxis after incubation at 30 °C for 14 -20 h. The chemotaxis index (RI) was calculated as the ratio between the distances from the inoculation point to the closest (D1) and furthest (D2) fringes of the spread bacteria with respect to the site of chemoeffector deposition (RI = D1 / (D1 + D2)).

Quantitative capillary chemotaxis assay

Bacterial chemotaxis was quantified in a modified version of the capillary assay (Adler, 1973). Unless otherwise indicated, flasks containing 20 ml minimal medium were inoculated with overnight cultures grown in minimal medium to an initial $OD_{600}$of 0.05-0.075. The cultures were grown until an OD_{600} of 0.5 – 0.6 and washed twice by a 5 minute centrifugation at 1667 x g and 4 °C, followed by resuspension in chemotaxis buffer (50 mM potassium phosphate, 20 µM EDTA, 0.05 % (v/v) glycerol, pH 7.0) and dilution with the same buffer to an OD_{600} of 0.08 – 0.1. The wells of 96-well plates were filled with 230 µl of the resulting bacterial suspension. Capillaries (Microcaps, Drummond Scientific) were heat-sealed on one end and filled by heating the capillary over a flame and subsequent placement of the open end of the capillary into buffer or chemoeffector solution. The open end of the capillaries were submerged into the bacterial suspension for 30 min, after which time the capillary content was emptied into Eppendorf tubes containing 1 ml of chemotaxis medium (see chemotaxis media composition details in "Methodology" section of each chapter). Serial dilutions were plated on LB or M9 minimal medium plates supplemented with10 – 20 mM D-glucose or succinic acid. Colonies were counted after overnight incubation.

Competitive root colonization assay

A slightly modified version of the colonization assay (Matilla *et al.*, 2007) was used. Sterile maize seeds were incubated at 30 °C for 1 h with a total bacterial concentration of 10^6 CFU/ml 1:1 mixture of wild-type and mutant strains. Thereafter, seeds were rinsed with sterile deionized water and planted in 50 ml Sterilin tubes containing 40 g of sterile washed silica sand and 10 % (v/w) plant nutrient solution (2.5 mM $Ca(NO_3)_2$, 2.5 mM KNO_3, 1 mM $MgSO_4$, 0.5 mM KH_2PO_4) supplemented with Fe-EDTA and micronutrients (Goodies A9). After 6 – 7 days of culture at 24 °C, with a light period of 16 h, bacterial cells were recovered from the rhizosphere and serial dilutions were plated on LB and LB plates supplemented with the appropriate antibiotic for selection.

RESULTS

RESULTS

CHAPTER 1
FUNCTIONAL ANNOTATION OF CHEMORECEPTORS THAT MEDIATE CHEMOTAXIS TO ORGANIC ACIDS IN *P. AERUGINOSA* PAO1 AND *P. PUTIDA* KT2440

CHAPTER 1.1: IDENTIFICATION OF A CHEMORECEPTOR FOR C2 AND C3 CARBOXYLIC ACIDS IN *P. PUTIDA* KT2440

Published article

Identification of a chemoreceptor for C2- and C3-carboxylic acids.

Vanina García, Jose-Antonio Reyes-Darias, **David Martín-Mora**, Bertrand Morel, Miguel A. Matilla and Tino Krell.

Dept. of Environmental Protection, Estación Experimental del Zaidín, Consejo Superior de Investigaciones Científicas

Applied and Environmental Microbiology (Published online 15 June 2015); 81(16):5449-57.
doi: 10.1128/AEM.01529-15

ABSTRACT

Chemoreceptors are at the beginning of chemosensory signaling cascades that mediate chemotaxis. Most bacterial chemoreceptors are functionally un-annotated and are characterized by a diversity in the structure of their ligand binding domains (LBDs). Data available indicate that there are two major chemoreceptor families at the functional level, namely those that respond to amino acids or Krebs cycle intermediates. Since Pseudomonads show chemotaxis to many different compounds and possess different types of chemoreceptors, they are model organisms to establish relationships between chemoreceptor structure and function. Here, we identify PP2861 (termed McpP) of *Pseudomonas putida* KT2440 as chemoreceptor with a novel ligand profile. We show that the recombinant McpP-LBD recognizes acetate, pyruvate, propionate and L-lactate with K_D values ranging from 34 to 107 μM. Deletion of the *mcpP* gene resulted in a dramatic reduction in chemotaxis towards these ligands and complementation restored a native-like phenotype, indicating that McpP is the major chemoreceptor for these compounds. McpP has a CACHE type LBD and we present data indicating that CACHE containing chemoreceptors of other species also mediate taxis to C2- and C3-carboxylic acids. In addition, the LBD of NbaY of *P. fluorescens*, a McpP homologue mediating chemotaxis to 2-nitrobenzoate, did neither bind nitrobenzoates nor the McpP ligands. This work provides further insight into receptor structure-function relationships and will be helpful to annotate chemoreceptors of other bacteria.

AEM
Journals.ASM.org

Identification of a Chemoreceptor for C_2 and C_3 Carboxylic Acids

Vanina García, Jose-Antonio Reyes-Darias, David Martín-Mora, Bertrand Morel, Miguel A. Matilla, Tino Krell
Department of Environmental Protection, Estación Experimental del Zaidín, Consejo Superior de Investigaciones Científicas, Granada, Spain

Chemoreceptors are at the beginnings of chemosensory signaling cascades that mediate chemotaxis. Most bacterial chemoreceptors are functionally unannotated and are characterized by a diversity in the structure of their ligand binding domains (LBDs). The data available indicate that there are two major chemoreceptor families at the functional level, namely, those that respond to amino acids or to Krebs cycle intermediates. Since pseudomonads show chemotaxis to many different compounds and possess different types of chemoreceptors, they are model organisms to establish relationships between chemoreceptor structure and function. Here, we identify PP2861 (termed McpP) of *Pseudomonas putida* KT2440 as a chemoreceptor with a novel ligand profile. We show that the recombinant McpP LBD recognizes acetate, pyruvate, propionate, and L-lactate, with K_D (equilibrium dissociation constant) values ranging from 34 to 107 μM. Deletion of the *mcpP* gene resulted in a dramatic reduction in chemotaxis toward these ligands, and complementation restored a native-like phenotype, indicating that McpP is the major chemoreceptor for these compounds. McpP has a CACHE-type LBD, and we present data indicating that CACHE-containing chemoreceptors of other species also mediate taxis to C_2 and C_3 carboxylic acids. In addition, the LBD of NbaY of *Pseudomonas fluorescens*, an McpP homologue mediating chemotaxis to 2-nitrobenzoate, bound neither nitrobenzoates nor the McpP ligands. This work provides further insight into receptor structure-function relationships and will be helpful to annotate chemoreceptors of other bacteria.

Many microorganisms have developed chemotactic mechanisms that allow them to rapidly respond to environmental changes by actively moving toward more favorable environments. Data suggest that the access to compounds that are required for growth is a major reason for chemotaxis, and chemotactic movement was observed, for instance, toward sugars, amino acids, organic acids, or inorganic phosphate (1–5). In addition, chemotaxis has been observed for other classes of compounds, such as neurotransmitters, plant hormones, or quorum-sensing signals (6–10). The specificity of a chemotactic response is determined by the chemoreceptor that is at the beginning of the chemosensory signaling cascade.

Chemoreceptors are typically composed of a cytosolic methyl-accepting signaling domain and a ligand binding domain (LBD) that is frequently located in the extracytoplasmic space. Ligand recognition at the LBD generates a molecular stimulus that is transmitted to the other extension of the chemoreceptor, where it modulates CheA autokinase activity. Phosphoryl groups are then transferred to the CheY response regulator, which in turn permits its interaction with the flagellar motor to ultimately mediate chemotaxis (1).

In contrast to the conserved methyl-accepting signaling domain, chemoreceptor LBDs show a high degree of diversity. The very large majority of chemoreceptor LBDs are unannotated in the SMART database (11). However, LBDs can be classified according to their size into cluster I domains (120 to 210 amino acids) and cluster II domains (220 to 300 amino acids) (11). Cluster I domains include the 4-helix bundle, GAF, PAS, CHASE, and CACHE domains (12–16). So far, two cluster II domain types have been identified, which are the helical bimodular (HBM) (17) and the double PDC (PhoQ/DcuS/CitA) domains (18, 19).

Pseudomonads are ubiquitously present in different ecological niches, and many strains are characterized by a metabolic diversity, as evidenced by the fact that some *Pseudomonas putida* strains can use more than 100 different compounds for growth (20). This metabolic versatility appears to be reflected in a chemotactic versatility, and so far 140 compounds have been identified to induce chemotaxis in *Pseudomonas* strains (21), including organic acids, amino acids, differently substituted aromatic hydrocarbons, biphenols, nucleotide bases, sugars, inorganic phosphate, metal ions, or peptides. *P. putida* KT2440, the model organism of this study, has 27 chemoreceptors that differ in their topologies and LBD types (Fig. 1). So far only the McpS, McpQ, McpR, and McpG receptors have been annotated with a function, and they mediate chemotaxis toward different organic and amino acids (3, 10, 19, 22). The diversity in the type of chemoreceptors and chemoattractants makes pseudomonads ideal model organisms to address a central question in the field (2), namely, to establish chemoreceptor structure-function relationships.

As shown in Fig. 1, most chemoreceptors of *P. putida* KT2440 form paralogous groups. One of the exceptions is the receptor encoded by the open reading frame PP2861, which is predicted to have a CACHE-type LBD. CACHE domains are ubiquitously present in bacterial signal transduction systems and also form parts of one- and two-component systems (23). PP2861 is paralo-

Received 8 May 2015 **Accepted** 27 May 2015
Accepted manuscript posted online 5 June 2015
Citation García V, Reyes-Darias J-A, Martín-Mora D, Morel B, Matilla MA, Krell T. 2015. Identification of a chemoreceptor for C_2 and C_3 carboxylic acids. Appl Environ Microbiol 81:5449–5457. doi:10.1128/AEM.01529-15.
Editor: M. Kivisaar
Address correspondence to Tino Krell, tino.krell@eez.csic.es.
V.G. and J.-A.R.-D. contributed equally to this article.
Supplemental material for this article may be found at http://dx.doi.org/10.1128/AEM.01529-15.

doi:10.1128/AEM.01529-15

INTRODUCTION

Many microorganisms have developed chemotactic mechanisms that allow them to rapidly respond to environmental changes by actively moving towards more favorable environments. Data suggest that the access to compounds that are required for growth is a major reason for chemotaxis and chemotactic movement was observed for instance towards sugars, amino acids, organic acids or inorganic phosphate (Adler, 1966, Mesibov & Adler, 1972, Kato *et al.*, 2008, Lacal *et al.*, 2010a, Sourjik & Wingreen, 2012). In addition, chemotaxis has been observed for other classes of compounds like neurotransmitters, plant hormones or quorum sensing signals (Bansal *et al.*, 2007, Antunez-Lamas *et al.*, 2009, Hegde *et al.*, 2011, Rader *et al.*, 2011, Reyes-Darias *et al.*, 2015b). The specificity of a chemotactic response is determined by the chemoreceptor that is at the beginning of the chemosensory signaling cascade.

Chemoreceptors are typically composed of a cytosolic MA domain and a LBD that is frequently located in the extra-cytoplasmic space. Ligand recognition at the LBD generates a molecular stimulus that is transmitted to the other extension of the chemoreceptor where it modulates CheA autokinase activity. Phosphoryl groups are then transferred to the CheY response regulator, which in turn permits its interaction with the flagellar motor to ultimately mediate chemotaxis (Sourjik & Wingreen, 2012).

In contrast to the conserved MA domain, chemoreceptor LBDs show a high degree of diversity. The very large majority of chemoreceptor LBDs are un-annotated in the SMART database (Lacal *et al.*, 2010b). However, LBDs can be classified according to their size into cluster I (120 to 210 amino acids) and cluster II (220-300 amino acids) domains (Lacal *et al.*, 2010b). Cluster I domains include the 4-helix bundle, GAF, PAS, CHASE and CACHE domains (Anantharaman & Aravind, 2000, Mougel & Zhulin, 2001, Martinez *et al.*, 2002, Ulrich & Zhulin, 2005, Moglich *et al.*, 2009). So far two cluster II domain types have been identified, which are the HBM (Ortega & Krell, 2014) and double PDC (PhoQ/DcuS/CitA) domain (Zhang & Hendrickson, 2010, Pineda-Molina *et al.*, 2012).

Pseudomonads are ubiquitously present in different ecological niches and many strains are characterized by a metabolic diversity as evidenced by the fact that some *P. putida* strains can use more than 100 different compounds for growth (Timmis, 2002). This metabolic versatility appears to be reflected in a chemotactic versatility and so far 140 compounds were identified to induce chemotaxis in *Pseudomonas* strains (Sampedro *et al.*, 2015), including organic acids, amino acids, differently substituted aromatic hydrocarbons, biphenols, nucleotide bases, sugars, inorganic phosphate, metal ions or peptides. *P. putida* KT2440, the model organism of this study, has 27 chemoreceptors that differ in their topology and LBD type (Fig. 10). So far only the McpS, McpQ, McpR and McpG receptors have been annotated with a function and mediate chemotaxis towards different organic and amino acids (Lacal *et al.*, 2010a, Pineda-Molina *et al.*, 2012, Parales *et al.*, 2013, Reyes-Darias *et al.*, 2015b). The diversity in the type of chemoreceptors and chemoattractants make Pseudomonads ideal model organisms to address a central question in the field (Kato *et al.*, 2008), namely to establish chemoreceptor structure-function relationships.

As shown in Fig. 10 most chemoreceptors of *P. putida* KT2440 form paralogous groups. One of the exceptions is the receptor encoded by the open reading frame PP2861, which is predicted to have a sCACHE type LBD. sCACHE domains are ubiquitously present in bacterial signal transduction systems and form also part of one-and two-component systems (Ulrich *et al.*, 2005). PP2861 is paralogous (58 % sequence identity) to the also sCACHE domain containing NbaY receptor from *P. fluorescens*, which was shown to mediate chemotaxis towards 2-nitrobenzoate (Iwaki *et al.*, 2007). Since *P. putida* shows chemotaxis to benzoate (Harwood *et al.*, 1984, Harwood, 1989) and substituted benzoates including nitro-derivatives (Parales, 2004), we hypothesized that PP2861 may be the corresponding chemoreceptor. Here we report the functional annotation of PP2861 that

we term McpP. We show that it recognizes and responds specifically to some C2- and C3- carboxylic acids, representing thus a novel chemoreceptor type.

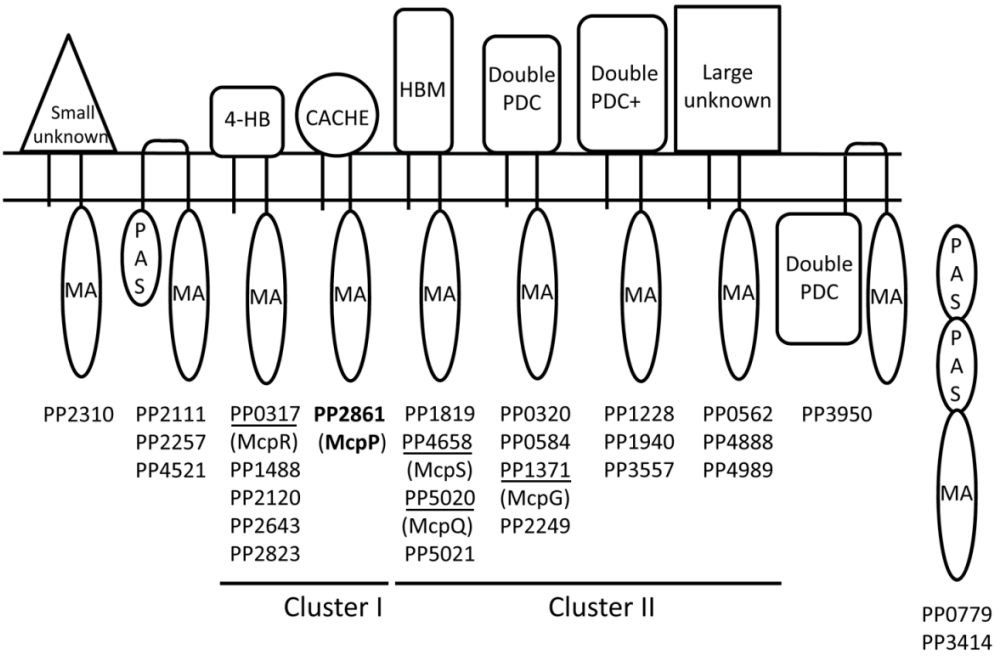

Figure 10. Predicted topologies and ligand binding domains of *P. putida* KT2440 chemoreceptors. Annotation is based on the fold recognition by the Phyre[2] algorithm (Kelley & Sternberg, 2009) and consensus secondary structure predictions (Deleage *et al.*, 1997). Topologies are based on the prediction of transmembrane regions using the DAS algorithm (Cserzo *et al.*, 1997). MA, methylaccepting domain;4-HB, 4-helix bundle domain; HBM, helical bimodular domain; double PDC, repeat of PhoQ/DcuS/CitA–domain (Zhang & Hendrickson, 2010); double PDC+, double PDC domain containing a 40-50 amino acid insert into double PDC domains. Functionally annotated receptors are underlined. HAMP domains have been omitted and classification is based on receptor topology and LBD type.

METHODOLOGY

Strains and plasmids: The strains and plasmids used are listed in Table 2.

Table 2. Bacterial strains and plasmids used.

Strains or plasmids	Relevant genotype and/or description	Source or ref.
Strains		
Escherichia coli		
BL21 (DE3)	F⁻, *ompI*, *hsdSB* (r^-_B m^-_B) *gal*, *dam*, *met*	(Studier & Moffatt, 1986)
DH5α	F-*endA*1 *glnV*44 *thi*-1 *recA*1 *relA*1 *gyrA*96 *deoR nupG* Φ80d*lacZ*ΔM15 Δ(*lacZYA-argF*)*U169*, *hsdR*17(r_K^- m_K^+), *phoA supE44* λ⁻; host for DNA manipulations	(Woodcock *et al.*, 1989)
TK1132	Ap^r; *E. coli* DH5α derivative carrying pJRG1 plasmid	This work
CC118 λ*pir*	Rif^r ;Δ(*ara-leu*) *araD* Δ*lacX74 galE galK phoA20 thi-1 rpsE rpoB argE*(Am) *recA1* Tn*7*λpir	(Herrero *et al.*, 1990)
TK1133	Rif^r Sm^r; *E. coli* CC118 λ*pir* derivative carrying pJRG2	This work
Pseudomonas putida		(Espinosa-Urgel & Ramos, 2004)
KT2440R	Rif^r derivative of *P. putida* KT2440, wild type	
TK1134	Rif^r Ap^r; *P. putida* KT2440R *Δpp2861*	This work
HB101	Sm^r; K-12/B hybrid; *recA thi pro leuhsdR⁻M⁺* with pRK600	(Boyer & Roulland-Dussoix, 1969, Kessler *et al.*, 1992)
*P. fluorescens*KU-7	Wild type, grows on 2-nitrobenzoate, chemotactic to 2-nitrobenzoate	(Hasegawa *et al.*, 2000)
Plasmids		
pGEMT	Ap^r;cloning vector	Promega
pUC18NotI	Apr; similar to pUC18 but with NotI sites flanking the MCS;	(Herrero *et al.*, 1990)
pJRG1	pUC18NotI derivative containing a 1-kb HindIII-EcoRI fragment from *P. putida KT2440R* genome (containing upsteam and downstream region of *pp2861*)	This work
pRK600	Cm^r; *ori* of ColE1; RK2-*mob*⁺; RK2-*tra*⁺; conjugational helper plasmid	(Kessler *et al.*, 1992)
pKNG101	Sm^r;suicide vector; MOB SAC	(Kaniga *et al.*, 1991)
pJRG2	Sm^r; pKNG101 derivative containing a 1.1 Kb *Not*I fragment from pJRG1 cloned into pKNG101	This work
pET28b	Km^r; protein expression plasmid	Novagen
pET28b-McpP-LBD	Km^r; pET28b containing McpP-LBD	This work
pET28b-NbaY-LBD	Km^r; pET28b containing NbaY-LBD	This work
pBBR1MCS2_START	Km^r; *oriRK2 mobRK2*	(Obranic *et al.*, 2013)
pMAMV240	Km^r; 2.1 Kb PCR fragment containing *mcpP* gene and its promoter region was cloned into HindIII/XbaI sites of pBBR1MCS2-START	This work

Ap, ampicillin; Cm, chloramphenicol; Km, kanamycin; Rif, rifampin; Sm, streptomycin

Construction of expression plasmids for McpP-LBD and NbaY-LBD: The DNA fragment of *mcpP* encoding amino acids Arg^{33}–Ser^{194} was amplified with the primers 5'-TGCATATGCGGCAGATCCATGG-3' and 5'-TACGGATCCCTACGAAGCGTCG-3' using genomic DNA of *P. putida* KT2440R. Similarly, the DNA fragment of *nbaY* encoding amino acids Met^{31}–Ala^{193} was amplified using the primers 5'-GGAATTCCATATGATGCTCAACCAAATCCGCAACGAT–3' and 5'–AAGAATTCTCACGCACTGATAACTTTTTCGCGGAACT–3' using genomic DNA of *Pseudomonas fluorescens* KU-7 as template. Both sets of primers contained restriction sites for NdeI and BamHI. The resulting PCR products were digested with these enzymes and then cloned into the expression plasmid pET28b(+) linearized with the same enzymes. The resulting plasmids, termed pET28-McpP-LBD and pET28-NbaY-LBD, were verified by DNA sequencing of the insert and flanking regions.

Overexpression and purification of McpP-LBD and NbaY-LBD: *E. coli* BL21 (DE3) containing pET28-McpP-LBD was grown in 2 L Erlenmeyer flasks containing 500 mL LB medium supplemented with 50 µg/mL kanamycin at 30 °C until an OD_{660} of 0.6. At this point, protein production was induced by adding 0.1 mM IPTG and the cultures were shifted to 18 °C. After overnight incubation, cells were harvested by centrifugation at 10000 x g for 30 min. Cell pellets were resuspended in buffer A (30 mM Tris/HCl, 300 mM NaCl, 10 mM imidazole and 5 % (v/v) glycerol, pH 8.0) and broken by French press at 1000 psi. After centrifugation at 20000 x g for 1 h, the supernatant was loaded onto a 5 mL HisTrap column (Amersham Bioscience), washed with five column volumes of buffer A and eluted with an imidazole gradient of 45–500 mM in buffer A.

A slightly modified protocol was used to purify NbaY-LBD*. E. coli* BL21 (DE3) containing pET28b-NbaY-LBD was grown in 2 L Erlenmeyer flasks containing 400 mL of 2xYT medium supplemented with 50 µg/mL kanamycin at 30 °C to an OD_{660} of 0.6, moment at which protein expression was induced by adding 0.1 mM IPTG. Growth was continued at 18 °C overnight before cells were harvested by centrifugation at 6000 x g during 30 min. Cell pellets were resuspended in buffer B (20 mM Tris/HCl, 500 mM NaCl, 10 mM imidazole, 0.1 mM EDTA, 5 % (v/v) glycerol, pH 7.8) and broken by French press at 1000 psi. After centrifugation at 20000 x g for 1 h, the supernatant was loaded onto a 5 mL HisTrap column (Amersham Bioscience), washed with five column volumes of buffer B and eluted with an imidazole gradient of 45–500 mM in buffer B.

Isothermal titration calorimetry: Experiments were conducted on a VP-microcalorimeter (Microcal, Amherst, MA) at 20 °C. Proteins were dialyzed overnight against polybuffer (5 mM Tris/HCl, 5 mM PIPES, 5 mM MES, 10 % glycerol (v/v), 150 mM NaCl, pH 8.0) and placed into the sample cell. Typically, 10 µM protein was introduced into the sample cell and titrated with 0.5- 5 mM ligand solutions that were prepared in dialysis buffer immediately before use. The mean enthalpies measured from the injection of ligands into the buffer were subtracted from raw titration data prior to data analysis with the MicroCal version of ORIGIN. Data were fitted with the 'One binding site model' of ORIGIN.

Circular Dichroism (CD) spectroscopy: CD experiments were performed using a Jasco J-715 (Tokyo, Japan) spectropolarimeter equipped with a thermostatically controlled cell holder. Far-UV CD spectra were recorded with a 1 mm path-length quartz cuvette using a bandwidth of 2 nm, a scan rate of 100 nm/min, a response time of 4 seconds and an average of 5 scans. NbaY-LBD was at 16.4 µM in 5 mM Tris/HCl, 5 mM Pipes, 5 mM MES pH 8.0. Spectra were corrected for buffer contributions to the signal. Analyses were performed at 25 °C, 50 °C and 85 °C.

Intrinsic tryptophan fluorescence spectroscopy: Fluorescence measurements were performed on a PTI spectrofluorimeter (Photon Technology International) equipped with the Photomultiplier Detection System 814. NbaY-LBD was dialyzed into 5 mM Tris/HCl, 5 mM Pipes, 5 mM MES pH 8.0, adjusted to 4 µM, loaded into a 3 mm quartz cuvette and placed into the cell holder thermostated at 25 °C. An excitation wavelength of 290 nm was used, and emission spectra were recorded between 300 and 500 nm in 2 nm steps. Slit widths of 4 nm were used for both excitation and emission.

Growth experiments: Overnight cultures were grown in M9 minimal medium (Abril *et al.*, 1989) supplemented with 10 mM glucose, which were then used to inoculate 20 ml of fresh M9 minimal media supplemented with the appropriate carbon source to an initial OD_{600} of 0.05. The cultures were then put into an orbital platform at 200 r.p.m. and allowed to grow at 30 °C. OD_{600} readings were taken every thirty minutes using the Lambda 20 UV/vis spectrophotometer (Perkin-Elmer). Cultures were maintained in the exponential phase by periodic dilutions with fresh prewarmed M9 medium supplemented with different carbon sources.

Construction of P. putida KT2440R mutant in pp_2861 (mcpP): Two 0.5-kb DNA fragments containing the upstream and downstream sequences of the *pp_2861* gene were amplified using the primer pairs 5'-ATAAAGCTTAATCTTGCTGCGAAACTCCC-3' and 5'-CTAGTCTAGACTAGCCATCAGCTCCCGCATTGTT-3' for the upstream region as well as 5'-CTAGTCTAGACTAGTGTTGCGGCAGTTCCGGGT-3' and 5'-AAGAATTCTGGGCGTGGCAGACGGGAG-3' for the downstream region. Primers contained sequences that introduced HindIII and XbaI as well as XbaI and EcoRI restriction sites (underlined) to the upstream and downstream fragments, respectively. Both fragments were cloned into pUC18NotI and transformed into *E. coli* DH5α giving rise to strain TK1132. The NotI fragment containing the upstream and downstream sequences was excised from pJRG1 and cloned into pKNG101 to produce pJRG2. The resulting plasmid, pJRG2 was transformed into *E. coli* CC118λ*pir* to generate *E. coli* TK1133 (Table 2). Plasmid pJRG2 was mobilized from *E. coli* TK1133 into *P. putida* KT2440R by triparental mating using *E. coli* HB101 (pRK600) as helper strain. In contrast to *E. coli, P. putida* KT2440R is able to grow on benzoate. Therefore, the selection of plasmid cointegrates of *P. putida* KT2440R was accomplished using M9 minimal medium (Abril *et al.*, 1989) supplemented with 10 mM benzoate and 100 μg/mL streptomycin. The Sm^r colonies were unable to grow on LB medium containing 5 % (w/v) sucrose, confirming that the plasmid pJRG2, with its *sacB* gene had integrated into these strains. The transconjugant was grown overnight in streptomycin-free LB medium, diluted 1000-fold, and following incubation for 12 h, serially diluted and plated on LB medium plates with or without 15 % (w/v) sucrose. PCR analysis of one of the Suc^rSm^s clones confirmed that gene deletion had occurred.

Motility and chemotaxis assays: Swim Plate Motility Assays. Bacteria from single colonies were grown overnight on LB medium supplemented with 10 μg/mL of rifampicin. Two-microliter aliquots of bacterial suspension were transferred to the center of swim agar plates (10 % LB, 0.25 % (w/v) agar). Plates were incubated at 30 °C overnight and motility monitored the following day. Plate Gradient Assays. Bacteria were grown overnight in minimal saline (MS) medium (Muraki *et al.*, 2003) supplemented with 10 mM succinate and diluted to an OD_{600} of 0.8–1 with fresh MS medium. Cells were then washed twice with MS medium by consecutive resuspension and centrifugation at 3750 g for 3 min. Square Petri dishes were filled with 80 mL MS-agar (0.25% agar, w/v) medium, containing 25 mM glycerol. Plates were cooled to room temperature for at least 30 min. Along the vertical central line of the plate, 10 μl aliquots of a 10 mM chemoattractant solution, dissolved in MS medium, were placed at regular distances. Plates were incubated at 4 °C for 12–16 h to allow the formation of the chemoattractant gradient. Two-microliter aliquots of bacterial suspension were then placed horizontally to each of the chemoattractant deposits with a distance of 2.5 cm to the vertical line. Plates were incubated at 30 °C for 16–20 h prior to the inspection of chemotaxis. Quantitative capillary chemotaxis assay. A modified version of the capillary assay was used (Adler, 1973). MS medium supplemented with 10 mM succinate was inoculated with *P. putida* KT2440R or KT2440RΔpp2861 and grown to early logarithmic phase. Cultures were then centrifuged at 1667 x g at 4 °C for 5 minutes and washed twice with 50 mM potassium phosphate, 20 μM EDTA, 0.05 % (w/v) glycerol, pH 7.0. Cells were resuspended in the same buffer to an OD_{600} of 0.08-0.1 and 230 μl aliquots of bacterial suspension were then placed into the wells of a 96-well plate. Capillaries (Microcaps, Drummond Scientific) were heat-sealed at one end, warmed over fire and the open end inserted into the chemoattractant solution for filling. The pH of the chemoattractant solution had been adjusted to that of the bacterial suspension. MS medium lacking chemoattractants was used as

a control. After an immersion of the open end of the capillaries in the bacterial suspension (for 30 min), capillaries were removed, the open end rinsed and placed into a microfuge tube containing 1 mL MS medium. The sealed end was broken and the content was emptied into the tube by short centrifugation. One hundred µl of the resulting cell suspension was plated out and incubated at 30 °C. Colonies were counted after growth on M9 medium supplemented with 10 mM succinate at 30 °C for 24 h.

Construction of mcpP containing plasmid for complementation: Primers 5´-ATAAAGCTTAATCTTGCTGCGAAACTCCC-3´ and 5´-CTAGTCTAGACTAGTCAGACCCGGAACTGCCGCAACA-3´ were used to amplify the *mcpP* gene and its promoter region. The resulting 2.1 kb PCR fragment was cloned into HindIII and XbaI sites of pBBR1MCS2-START. The insert was confirmed by PCR and sequencing. The resulting plasmid, pMAMV240, was transformed into *P. putida* TK1134 by electroporation.

RESULTS

PP2861-LBD recognizes C2- and C3-carboxylic acids

The DNA sequence encoding the fragment flanked by the two transmembrane regions of PP2861, harboring the LBD, was cloned into an expression vector, the protein expressed as his-tag fusion protein in *E. coli* and purified from the soluble fraction of the cell lysate. The purified protein was submitted to microcalorimetric binding studies (Krell, 2008) to identify its cognate ligands. Based on our hypothesis that this NbaY homologue may be involved in recognizing benzoates, McpP-LBD was titrated with benzoate and a number of its derivatives, including 2-nitrobenzoate (listed in Supp. Table 1). However, none of these compounds was found to bind.

Since the only other characterized chemoreceptor with a CACHE domain is the malate specific PA2652 of *P. aeruginosa* (Alvarez-Ortega & Harwood, 2007) we continued microcalorimetric ligand screening by titrations with malate and other dicarboxylates (Supp. Table 1), which, however, did not bind. We therefore extended the ligand screen to different monocarboxylic acids. Whereas glyoxylate did not bind, acetate was identified as PP2681-LBD ligand (Fig. 11) and data analysis revealed a K_D of 34 ± 5 µM (Table 3). Interestingly, the C3-carboxylic acid propionate bound with the same affinity but the C4 acid butyrate failed to bind (Fig. 11, Table 3). Further experiments showed that C3-acids pyruvate and L-lactate bound to PP2861-LBD with affinities of 39 ± 3 and 107 ± 11 µM, respectively (Fig. 11, Table 3). In contrast, D-lactate and phosphoenolpyruvate were unable to bind. In order to continue the assessment of the PP2861-LBD ligand spectrum, we tested different compounds like propanol, acetone or amino acids (Supp. Table 1) which, however, did not bind. We can therefore conclude that PP2861-LBD binds acetate, pyruvate, L-lactate and propionate and have renamed the receptor McpP.

The McpP ligands and nitrobenzoates do not bind to NbaY-LBD

Since McpP and NbaY are paralogous, we were also interested in identifying the compounds that are recognized by NbaY. To this end, we followed a similar strategy and submitted purified NbaY-LBD to microcalorimetric titrations with different nitrobenzoates. Since no binding was observed ITC experiments with the four McpP ligands and further compounds (listed in Supp. Table 1) were carried out. However, none of these compounds bound to NbaY-LBD.

Circular dichroism and intrinsic fluorescence spectroscopy experiments were conducted to determine whether NbaY-LBD corresponded to folded protein. As shown in Supp. Fig. 1A the maximum of the intrinsic tryptophan fluorescence emission spectrum was at 330 nm. This is consistent with a significant protection of the Trp residues from the solvent, which is a typical feature of proteins in its folded state (Righetti & Verzola, 2001).

As a control, the spectrum was recorded in the presence of the chaotropic agent guanidine hydrochloride (GdnHCl, Supp. Fig. 1A) that causes protein unfolding and exposure of Trp residues to the solvent. Under these conditions the maximum was shifted to 344 nM indicting that the presence of GdnHCl had induced protein unfolding. Supp. Fig. 1B shows a far UV circular dichroism spectrum of NbaY-LBD, from which α-helical and β-strand contents of 18 % and 30 %, respectively, were calculated using the procedure described by Bohm et al. (Bohm *et al.*, 1992). Supp. Fig. 1B also shows that the exposure of the protein to heat caused loss of the CD signal indicative of protein unfolding. The fact that both, high concentrations of GdnHCl and heat treatment, caused protein

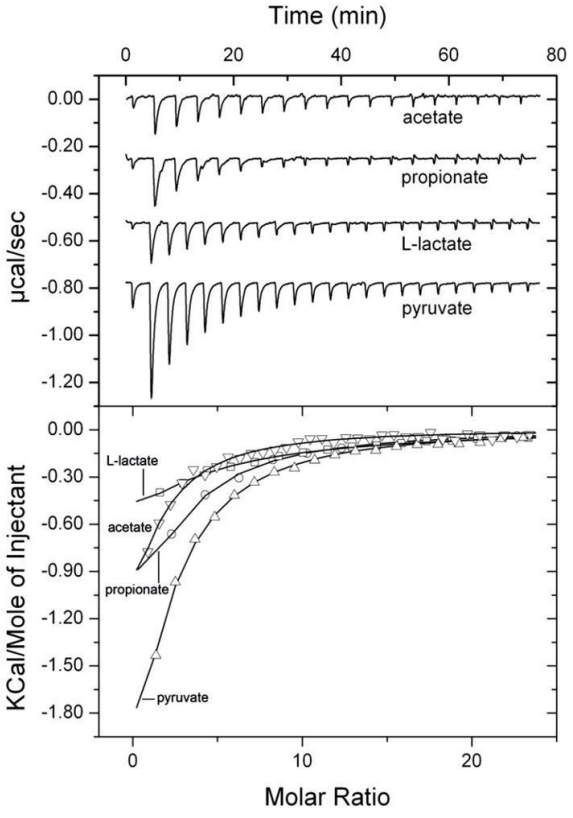

Figure 11. Microcalorimetric titration of McpP-LBD with different C2- and C3-carboxylic acids. Upper panel: Raw data for the titration of 10 µM protein with 2 mM ligand solutions. In all cases the first injection was of 1.6 µl, followed by a series of 9.6 µl injections. Lower panel: Dilution-corrected and concentration-normalized integrated peak areas of the raw data. Fitting was done using the "One binding site model" of the MicroCal version of ORIGIN. Shown are representative experiments and thermodynamic data presented in Table 2 are means and standard deviation from three independent experiments.

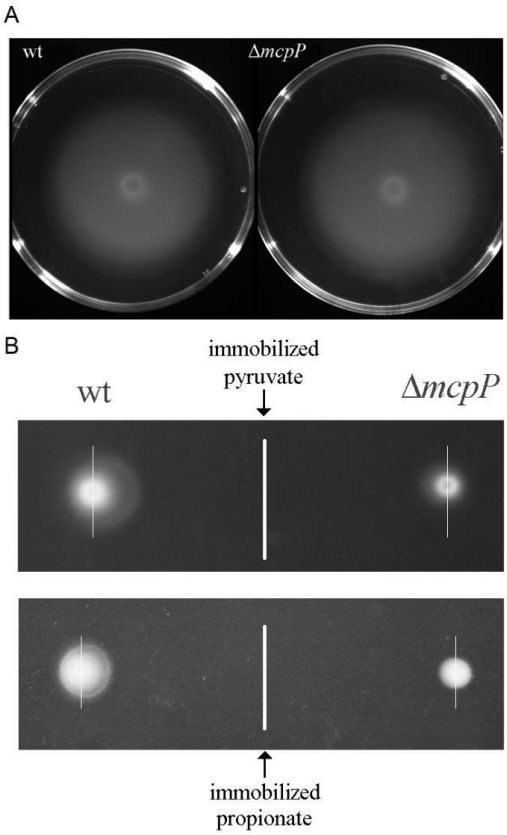

Figure 12. Mutation of the *mcpP* gene does not alter motility but reduces chemotaxis to pyruvate and propionate. A) Swim plate assays of *P. putida* KT2440R and its *mcpP* deficient mutant. Shown are representative images. B) Plate gradient chemotaxis assays in which 10 mM of pyruvate or propionate were deposited along a vertical line on MS-agar plates. After overnight incubation for gradient formation, suspensions of wt or *mcpP* mutant strains were deposited at either side. Plates were inspected the following day for chemotaxis. This assay was repeated 3 times and representative images are shown. To visualize the acentric spread thin vertical lines that go through the center of bacterial deposition are shown.

unfolding suggests that NbaY-LBD was present as a folded protein.

The four McpP ligands support growth of *P. putida* KT2440

Many chemoattractants serve as carbon sources for growth (Sampedro *et al.*, 2015). To verify whether *P. putida* KT2440 can use the identified McpP ligands as sole carbon source, growth experiments were conducted in minimal medium supplemented with 10 mM of the individual compounds. As shown in Supp. Fig. 2 all four McpP ligands supported growth of *P. putida* KT2440R. In contrast to L-lactate, acetate and pyruvate, a lag phase of more than 4 h was observed for propionate.

Mutation of the *mcpP* gene reduces largely chemotaxis to McpP ligands

It has been shown that chemoreceptors feed into signaling pathways that either mediate chemotaxis or carry out alternative cellular functions like controlling the levels of second messengers (Wuichet & Zhulin, 2010). In subsequent experiments we wanted to establish whether McpP is involved in chemotaxis and, if so, determine its contribution to the taxis of *P. putida* towards the four ligands identified. To this end we constructed a *mcpP* deletion mutant by homologous recombination. To assess any potential effect of this mutation on bacterial motility, the wild type (wt) and the mutant were analyzed on swim plate assays. As shown in Fig 12A, the motilities of the wt and *mcpP* mutant strain are comparable.

When then assessed the contribution of McpP to chemotaxis towards the four ligands identified using plate gradient assays. In this assay, a 10 mM ligand solution is immobilized on agar plates, which are then left overnight for gradient formation. At identical distances to the immobilized compounds, aliquots of the wt or mutant strain are placed. Using pyruvate and propionate as chemoattractant (Fig. 12B) an acentric spread of bacteria towards the immobilized compound was observed for the wt strain. The corresponding chemotaxis indices, as calculated according to Pham and Parkinson (Pham & Parkinson, 2011), were 0.70 ± 0.05 (n=8) for pyruvate and 0.60 ± 0.02 (n=8) for propionate, indicative of chemotaxis. The *mcpP* mutant cells showed a minor spread that was only slightly acentric and chemotaxis indices of 0.54 ± 0.02 (n=8) for pyruvate and 0.53 ± 0.05 (n=8) for propionate were obtained. Both values are close to 0.5 (observed in the absence of taxis) and are indicative of some residual chemotaxis towards these compounds.

Table 3. Thermodynamic parameters of ligand binding derived from the microcalorimetric titration of McpP-LBD with different ligands. Data are means and standard deviations from three experiments.

Ligand	K_A (M^{-1})	K_D (μM)	ΔH (kcal/mol)	n[1]
Acetate	(2.9 ± 0.4) x 10^4	34 ± 5	-5.11 ± 3.1	0.77 ± 0.4
Propionate	(2.9 ± 0.3) x 10^4	34 ± 4	-5.35 ± 3.3	1.37 ± 0.6
Pyruvate	(2.6 ± 0.2) x 10^4	39 ± 3	-9.94 ± 2.6	0.89 ± 0.2
L-lactate	(9.3 ± 1) x 10^3	107 ± 11	-5.20 ± 4.1	1.26 ± 0.8

[1] Stoichiometry of binding of ligands to McpP-LBD.

Assessment of the concentration dependence of McpP mediated taxis

We have then conducted quantitative capillary chemotaxis assays to determine the concentration dependence of response. Prior to the study of McpP ligands, a number of control experiments were conducted. As positive control we studied the chemotaxis to casamino acids, which is mediated by a different chemoreceptor. As shown in Fig. 13A, the responses of the wt and *mcpP* mutant strain were similar, confirming that *mcpP* mutation did not alter motility in a non-specific manner. Since the McpP ligands used were sodium salts, we also measured the response of the wt strain to sodium chloride (Fig. 13B). Very minor repellent responses towards NaCl were

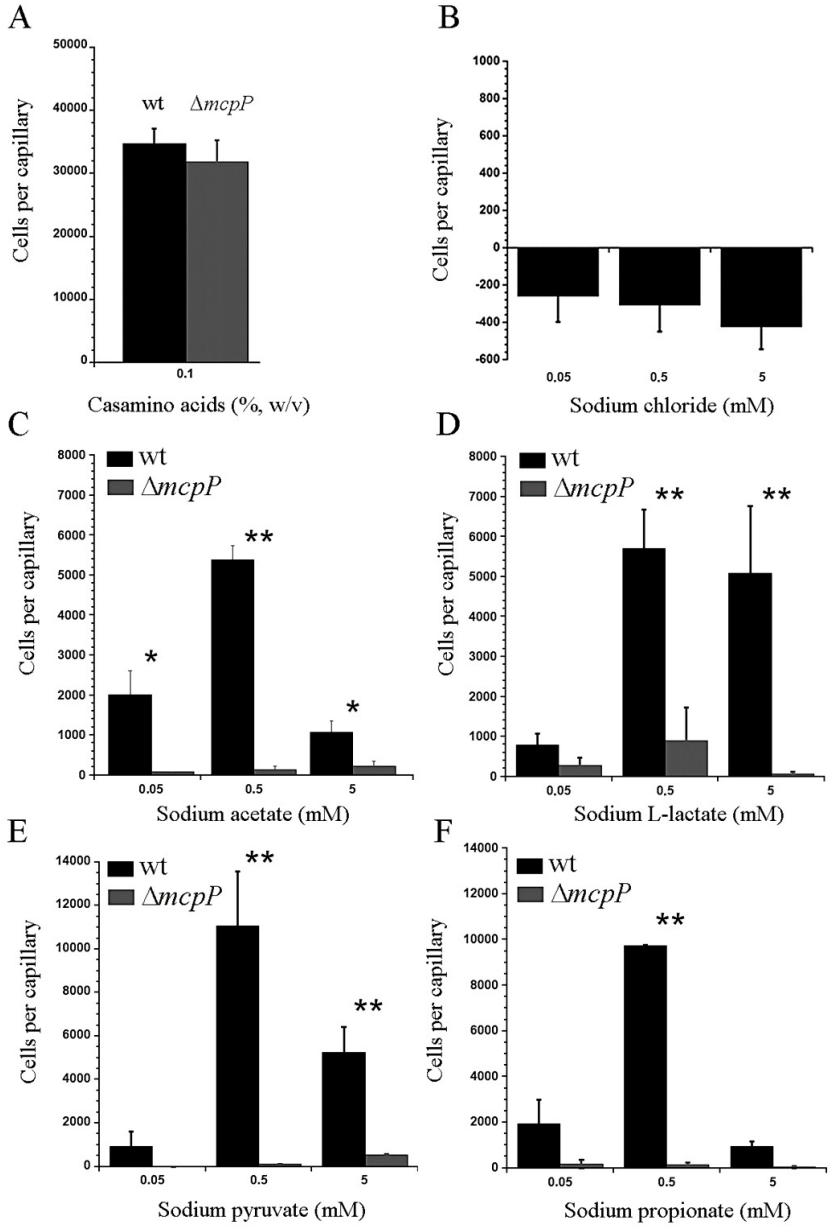

Figure 13. Quantitative capillary chemotaxis assays of *P. putida* KT2440R towards casamino acids (A, control), NaCl (B, control), sodium acetate (C), sodium L-lactate (D), sodium pyruvate (E) and sodium propionate (F). Data were corrected with the number of cells that migrated into buffer containing capillaries. Data are means and standard deviations from at least three independent experiments.* P<0.1, ** P<0.05 in student's t-test.

measured, which allowed the use of sodium salts for further experiments.

Quantitative capillary assays with the four McpP ligands were conducted over a ligand concentration range of 5 nM to 50 mM. Significant responses were only observed at the concentration range between 50 μM and 5 mM and replicate measurements at this range were carried out to determine the responses precisely. The wt strain showed for all four ligands optimal responses at a concentration of 0.5 mM (Fig. 13 C-F). At this concentration the magnitude of response towards pyruvate and propionate was around twice that of acetate and L-lactate. In all cases, chemotaxis responses at 50 μM and 5 mM were inferior to that at 0.5 mM. For all four ligands the mutation of *mcpP* reduced taxis to very low levels. For complementation assays we cloned the *mcpP* gene and its promoter region into vector pBBR1MCS2 and introduced the resulting plasmid (pMAMV240) into the *mcpP* mutant. As control, pBBRMCS2 was introduced into the wt and *mcpP* mutant strain. Chemotaxis assays of the resulting three strains towards 0.5 mM solutions of the four McpP ligands were conducted (Supp. Fig. 3). Statistical analysis of the resulting data revealed that the response of the complemented mutant was similar to the wt for three ligands whereas chemotaxis of the complemented mutant to L-lactate was superior to that of the wt strain. Taken together, these data show that McpP is the primary chemoreceptor of *P. putida* KT2440 for acetate, L-lactate, pyruvate and propionate.

DISCUSSION

A significant number of chemoreceptors have been identified that mediate chemotaxis towards organic acids of the Krebs cycle like McpS of *P. putida* KT2440 (Lacal *et al.*, 2010a, Lacal *et al.*, 2011b), its three homologues in *P. putida* F1 (Parales *et al.*, 2013), Mcp2201 of *Comamonas testosteroni* (Ni *et al.*, 2013), the citrate specific TCP of *Salmonella typhimurium* (Yamamoto & Imae, 1993, Iwama *et al.*, 2006) or the malate specific PA2652 of *P. aeruginosa* (Alvarez-Ortega & Harwood, 2007). Although chemotaxis to non-Krebs cycle organic acids has been reported for different species (Harwood *et al.*, 1984, Cuppels, 1988, Hugdahl *et al.*, 1988, Poole & Armitage, 1988, Lambert *et al.*, 2012), little information is available on the corresponding chemoreceptors. Here we report that McpP specifically responds to C2- and C3- carboxylic acids, which corresponds to a novel chemoreceptor ligand profile. Within *P. putida* KT2440, the receptors for Krebs cycle and non-Krebs cycle organic acids belong to different families. Whereas McpS is a cluster II receptor with a HBM LBD (Pineda-Molina *et al.*, 2012, Ortega & Krell, 2014), McpP forms part of cluster I and has a CACHE domain for ligand recognition. Pseudomonads are model organisms for the study of chemotaxis and a recent review contains a list of all known chemoeffectors of this genus (Sampedro *et al.*, 2015). So far there are no reports on the chemotaxis to pyruvate, propionate and L-lactate and our data thus expand the list of known chemoattractants for Pseudomonads.

We sought to determine whether CACHE domain containing chemoreceptors in other species may also respond to C2- and C3-carboxylic acids. To this end we conducted a BLAST search in the protein data bank using the McpP-LBD sequence. The domains with highest sequence similarity were CACHE type LBDs of chemoreceptors from *Anaeromyxobacter dehalogenans* (pdb ID: 4K08) and of *Vibrio parahaemolyticus* (Q87T87, pdb ID: 4EXO). These chemoreceptors are uncharacterized and the LBD structures unpublished. As shown in Fig. 14, both structures are similar to the homology model of McpP-LBD. Most interestingly, these structures contain in the ligand binding pocket of the CACHE domain either bound acetate (4K08) or pyruvate (4EXO), suggesting that they may be chemoattractants of the corresponding receptors (Fig. 14). Acetate was part of the crystallization buffer of the 4K08 structure, whereas pyruvate must have been co-purified with the protein of structure 4EXO.

Bacterial LDBs are characterized by a high degree of sequence divergence (Taylor & Zhulin, 1999, Anantharaman & Aravind, 2000, Ulrich & Zhulin, 2005) that hampers a functional annotation

based on sequence similarities. Although McpP-LBD and 4EX0 bind the same ligand, these domains show only 22 % sequence identity. The inspection of the 4EXO structure shows that pyruvate binding is accomplished by nine amino acids, of which four establish hydrogen bonds (Supp. Fig. 4A). Interestingly, eight of the nine amino acids involved in pyruvate recognition are conserved (5 identical, 3 strong similarity) in the alignment of the McpP-LBD and 4EXOB sequences (Supp. Fig. 4B), suggesting that pyruvate recognition at McpP-LBD occurs in a similar manner as in 4EXOB. Taken together, data suggest that CACHE LBD containing chemoreceptors function as C2- and C3-carboxylic acid chemoreceptors in different bacterial species.

An interesting feature of the McpP mediated chemotaxis is that optimal responses for all four ligands are observed at a concentration of 500 μM (Fig. 13). As mentioned above, the McpS chemoreceptor of *P. putida* KT2440 mediates chemotaxis towards Krebs cycle organic acids and, using quantitative capillary chemotaxis assays, we have previously reported the McpS dose-response ratios (Lacal *et al.*, 2010a). For the three primary McpS ligands, malate, succinate and fumarate, strong responses were obtained at a concentration of 1 μM, a concentration at which no significant responses were measured for McpP ligands. These data indicate a higher sensitivity of the bacterium to Krebs cycle intermediates as compared to the C2- and C3-carboxylic acids.

The NbaY chemoreceptor of *P. fluorescens* was shown to mediate chemotaxis to 2-nitrobenzoate (Iwaki *et al.*, 2007). This function is also supported by the fact that the *nbaY* gene is located next to a gene cluster encoding the proteins for 2-nitrobenzoate degradation. NbaY-LBD could be produced in large amounts as highly soluble protein and its analysis by CD and intrinsic fluorescence spectroscopy indicates that the protein is folded. As shown in the Supp. Fig. 5, the homology model of NbaY-LBD is similar to the structures/models of the other CACHE domains displayed in Fig. 14. However, microcalorimetric titrations of this protein with different benzoate derivatives and the McpP ligands did not reveal any binding. Data thus suggest that ligand recognition at NbaY may not occur directly but may require previous binding to a periplasmic ligand binding protein.

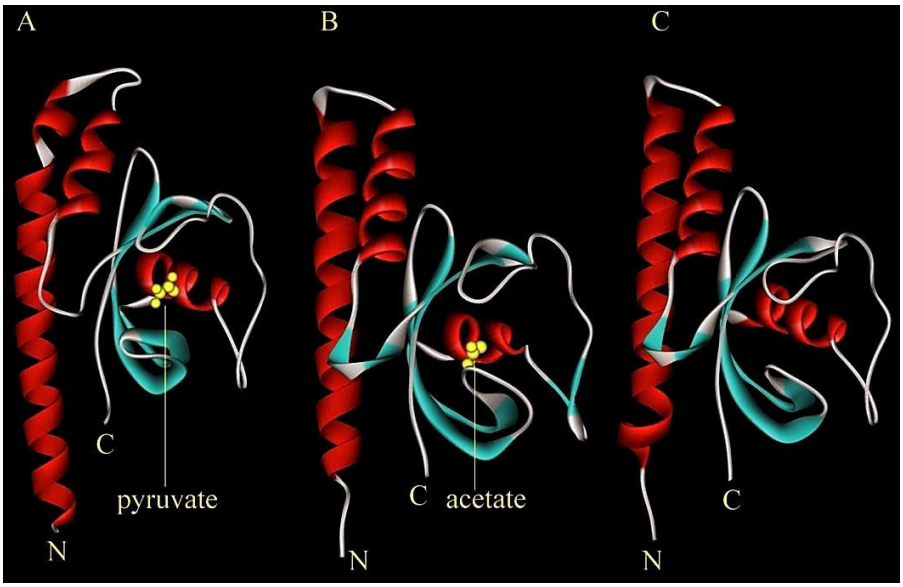

Figure 14. CACHE domains of chemoreceptors that recognize pyruvate and acetate. A) Structure of a CACHE type LBD of an uncharacterized chemoreceptor from *V. parahaemolyticus* (pdb ID: 4EXO) in complex with pyruvate. B) Structure of a CACHE type LBD of an uncharacterized chemoreceptor from *Anaeromyxobacter dehalogenans* in complex with acetate (pdb ID: 4K08). C) Homology model of McpP-LBD. The model was generated using Phyre[2](Kelley & Sternberg, 2009). Ninety one percent of the McpP-LBD residues were modelled at >90 % confidence.

Given the diversity of bacterial chemoreceptors, their functional annotation is a major research need in the field. Here we report a chemoreceptor with a novel ligand spectrum and present data suggesting that CACHE domain containing chemoreceptors of diverse species may be involved in the chemotaxis to C2- and C3-carboxylic acids, a finding that may facilitate the functional annotation of chemoreceptors.

SUPPLEMENTARY MATERIAL

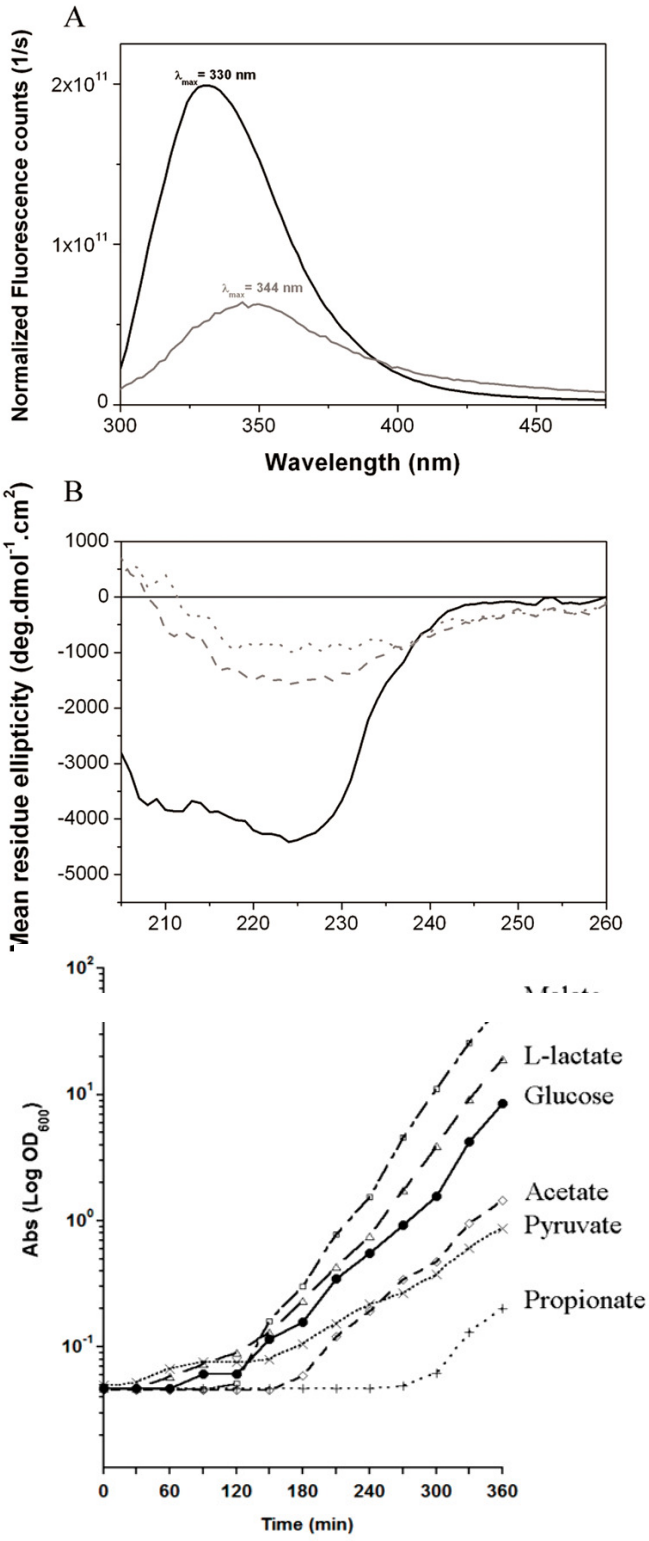

Supp. Fig 1. Analysis of NbaY-LBD by intrinsic tryptophan fluorescence and circular dichroism (CD) spectroscopy. A) Tryptophan fluorescence emission spectrum of 4 µM NbaY-LBD in polybuffer (black line) and in the presence of 3 M guanidine hydrochloride (grey line). The wavelengths of maximal fluorescence are indicated. B) Far UV CD spectra of 16.4 µM NbaY-LBD at 25 °C (black line), 50 °C (dashed grey line) and 85 °C (dotted grey line).

Supp. Fig 2. Growth curves of *P. putida* KT2440R in the presence of different compounds as carbon source. Assays were conducted in M9 minimal medium supplemented with 10 mM of each compound. Assays were conducted with the four McpP ligands and glucose and malate as references. Shown are representative curves. The doubling times calculated form three different experiments were as follows: malate 33 ± 2.51 min, L-lactate 36.47 ± 3.03 min, glucose 40.76 ± 2.13 min, acetate 46.47 ± 2.81 min, pyruvate 89 ± 8.53 min, propionate 46.2 ± 2.03 min.

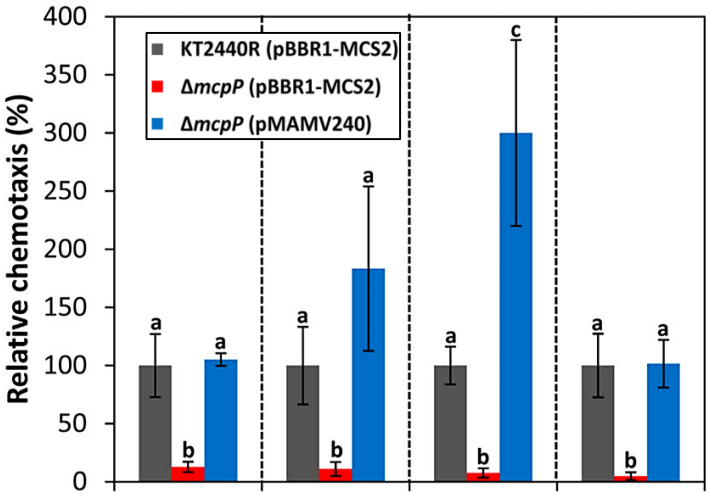

Supp. Fig 3. Genetic complementation of *P. putida* KT2440R Δ*mcpP* using quantitative capillary chemotaxis assays. Sodium pyruvate, sodium propionate, sodium L-lactate and sodium acetate were used at 0.5 mM (concentration for observed optimal chemotaxis). Data were corrected with the number of cells that migrated into the capillaries containing buffer and are expressed as the percentage of bacteria in the capillaries relative to the wild type strain. Data are means and standard deviations from at least three independent experiments. Data were statistically analyzed using the one-way analysis of variance. Bars with the same letter are not significantly different (P-value < 0.5), whereas different letters indicate statistically significant differences.

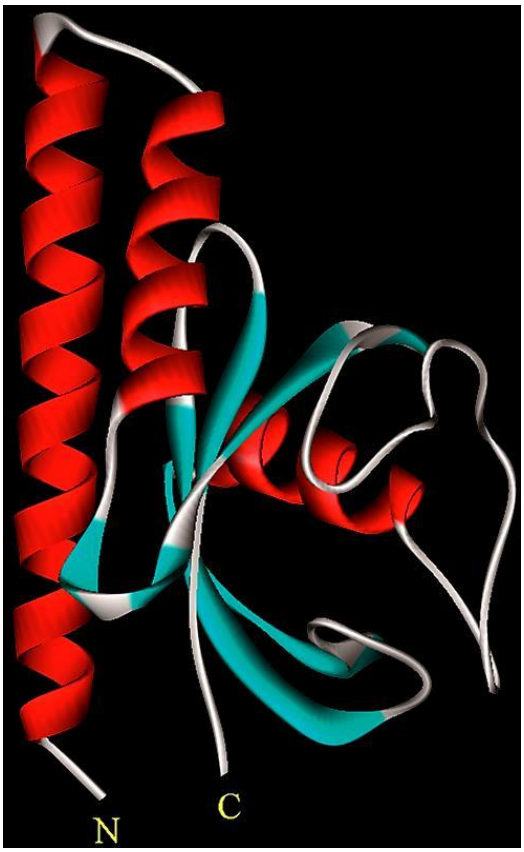

Supp. Fig 4. NbaY-LBD homology model generated using the Phyre2 server. Eighty nine percent of residues were modelled with a confidence above 90 %.

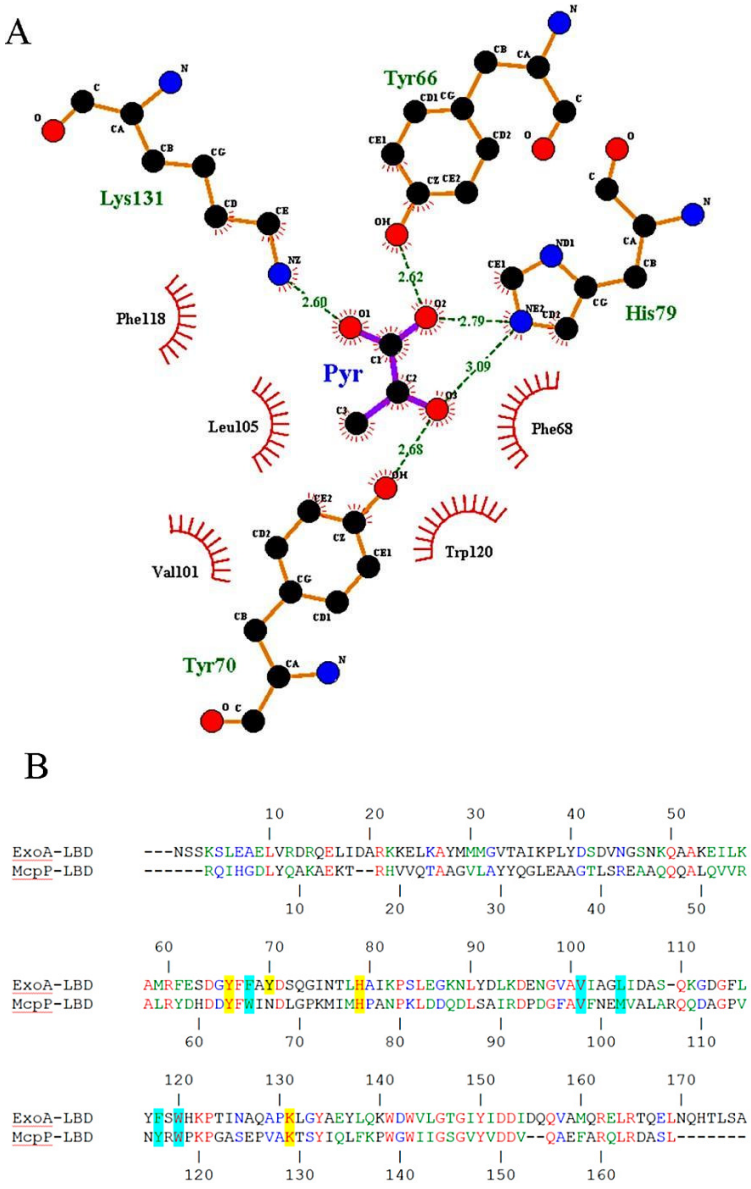

Supp. Fig 5. Conservation of amino acids involved in pyruvate recognition of CACHE sensor domains. A) Amino acids involved in pyruvate binding in the LBD of an uncharacterized chemoreceptor of *V. parahaemolyticus* (pdb ID 4EXO). The figure was generated using LigPlot+ (Laskowski & Swindells, 2011). (B) Alignment of the McpP-LBD and 4ExoA-LBD sequences. Amino acids in red are identical, in green highly similar and in blue weakly similar. Amino acids involved in pyruvate binding in the 4EXO structure as well as their conserved counterparts in McpP-LBDare shaded in yellow (hydrogen bonds) and cyan (hydrophobic interactions). The sequence alignment was done using the CLUSTALW algorithm (Thompson *et al.*, 1997) of the NPSA server (http://npsa-pbil.ibcp.fr/cgi-bin/npsa_automat.pl?page=/NPSA/npsa_clustalw.html) using a gap opening penalty of 10 and a gap extension penalty of 0.1.

Supp. Table 1. Compounds used for microcalorimetric binding studies to NbaY-LBD and McpP (PP2861)-LBD. Compounds that bound are underlined and the corresponding thermodynamic data are shown in Table 3.

McpS (PP2861)-LBD	NbaY-LBD
Benzoates	**Benzoates**
Benzoate	2-nitrobenzoate
2-nitrobenzoate	3-nitrobenzoate
3-nitrobenzoate	4-nitrobenzoate
4-nitrobenzoate	Sodium benzoate
3,5-dinitrobenzoate	**Monocarboxylic acids**
Dicarboxylic acids	Pyruvate
Malate	L-lactate
Succinate	Propionate
Fumarate	Acetate
Malonate	**Other aromatic compounds**
Monocarboxylic acids	Naphthalene
Glyoxylate	Benzene
Acetate	Toluene
Pyruvate	2-nitrotoluene
Propionate	**Other compounds**
L-lactate	Urea
D-lactate	
Phosphoenolpyruvate	
Butyrate	
Other C3 compounds	
Acetone	
1-propanol	
2-propanol	
Amino acids	
L-alanine	
L-glutamate	
Tricarboxylic acids	
Citrate	

CHAPTER 1.2: IDENTIFICATION OF A CITRATE CHEMORECEPTOR IN *P. putida* KT2440

Published article

McpQ is a specific citrate chemoreceptor that responds preferentially to citrate/metal ion complexes

David Martín-Mora*, José Antonio Reyes-Darias*, Álvaro Ortega, Andrés Corral-Lugo, Miguel Ángel Matilla, Tino Krell.

Dept. of Environmental Protection, Estación Experimental del Zaidín, Consejo Superior de Investigaciones Científicas.

Environmental Microbiology (Published online 15 August 2015); 18(10), 3284–3295.

doi: 10.1111/1462-2920.13030

*Authors contributed equally to this work

ABSTRACT

Chemoreceptors are at the beginning of chemosensory pathways that mediate chemotaxis. *P. putida* KT2440 is predicted to have 27 chemoreceptors, most of which uncharacterised. We have previously identified McpS as chemoreceptor for Krebs cycle intermediates. Citrate is primarily present in the environment as metal-complex, which, however, is not recognized by McpS. We show here that the McpS paralogue McpQ recognizes specifically citrate and citrate/metal^{2+} complexes. The McpQ ligand binding domain (McpQ-LBD) binds citrate/metal^{2+} complexes with higher affinity than citrate. McpQ-LBD is present in a monomer-dimer equilibrium and citrate and particularly citrate/Mg^{2+} binding stabilize the dimer. The bacterium showed much stronger responses to citrate/Mg^{2+} than to citrate and *mcpQ* inactivation caused a dramatic reduction in chemotaxis. Responses to Krebs cycle intermediates are thus mediated by the broad range McpS and McpQ that responds specifically to an intermediate not recognized by McpS. Interesting parallels exist to the paralogous amino acid chemoreceptors of *P. aeruginosa* and *B. subtilis*. Whereas one paralogue recognizes most amino acids, the remaining paralogue binds specifically one of the few acids not recognized by the broad range receptors. Therefore, chemotaxis to compound families by the concerted action of broad and narrow range receptors may represent a general mechanism.

environmental microbiology

Environmental Microbiology (2016) **18**(10), 3284–3295 doi:10.1111/1462-2920.13030

McpQ is a specific citrate chemoreceptor that responds preferentially to citrate/metal ion complexes

David Martín-Mora,† Jose-Antonio Reyes-Darias,† Álvaro Ortega, Andrés Corral-Lugo, Miguel A. Matilla and Tino Krell*

Department of Environmental Protection, Estación Experimental del Zaidín, Consejo Superior de Investigaciones Científicas, C/ Prof. Albareda, 1, 18008 Granada, Spain.

Summary

Chemoreceptors are at the beginning of chemosensory pathways that mediate chemotaxis. *Pseudomonas putida* KT2440 is predicted to have 27 chemoreceptors, most of which uncharacterized. We have previously identified McpS as chemoreceptor for Krebs cycle intermediates. Citrate is primarily present in the environment as metal complex, which, however, is not recognized by McpS. We show here that the McpS paralogue McpQ recognizes specifically citrate and citrate/metal^{2+} complexes. The McpQ ligand binding domain (McpQ-LBD) binds citrate/metal^{2+} complexes with higher affinity than citrate. McpQ-LBD is present in a monomer-dimer equilibrium and citrate and particularly citrate/Mg^{2+} binding stabilize the dimer. The bacterium showed much stronger responses to citrate/Mg^{2+} than to citrate and *mcpQ* inactivation caused a dramatic reduction in chemotaxis. Responses to Krebs cycle intermediates are thus mediated by the broad range McpS and McpQ that responds specifically to an intermediate not recognized by McpS. Interesting parallels exist to the paralogous amino acid chemoreceptors of *Pseudomonas aeruginosa* and *Bacillus subtilis*. Whereas one paralogue recognizes most amino acids, the remaining paralogue binds specifically one of the few acids not recognized by the broad range receptors. Therefore, chemotaxis to compound families by the concerted action of broad and narrow range receptors may represent a general mechanism.

Received 29 January, 2015; revised 11 August, 2015; accepted 15 August, 2015. *For correspondence. E-mail: tino.krell@eez.csic.es; Tel. (+34) 958 181600 (ext. 294); Fax. (+34) 958 135740. †Authors contributed equally to this work.

Introduction

Chemotaxis provides the bacterium with the capacity to approach or escape from different types of compounds. Taxis has been observed towards compounds that serve as carbon or energy sources like sugars, amino acids or organic acids (Mesibov and Adler, 1972; Adler *et al.*, 1973; Seymour and Doetsch, 1973; Moulton and Montie, 1979). In addition, chemotaxis has been reported for other classes of compounds like neurotransmitters, plant hormones or quorum sensing signals (Bansal *et al.*, 2007; Antunez-Lamas *et al.*, 2009; Hegde *et al.*, 2011; Rader *et al.*, 2011). Typically, the specificity of a chemotactic response is determined by the chemoreceptor that is at the beginning of the chemosensory signalling cascade.

Chemoreceptors are typically composed of a cytosolic methyl accepting signalling domain and a ligand binding domain (LBD) that is frequently located in the extracytoplasmic space. Ligand recognition at the LBD generates a molecular stimulus that modulates the CheA autokinase activity. Phosphoryl groups are subsequently transferred to the CheY response regulator, which in turn permits its interaction with the flagellar motor to control cell tumbling and to ultimately mediate chemotaxis (Sourjik and Wingreen, 2012).

A large number of different chemoreceptors have evolved that differ in the type of their LBD. Based on size differences, LBDs can be classified into cluster I (120 to 210 amino acids) and cluster II (220–299 amino acids) (Lacal *et al.*, 2010a). Compared with cluster I domains, relatively little information is available on cluster II domains that represent approximately 40% of all chemoreceptors (Lacal *et al.*, 2010a). *Pseudomonas putida* KT2440, the model organism for this study, has 27 predicted chemoreceptors of which most possess a cluster II LBD (Garcia *et al.*, 2015). So far, receptors McpS, McpR, McpP and McpG have been functionally annotated and shown to mediate chemotaxis to different organic and amino acids (Lacal *et al.*, 2010b; Pineda-Molina *et al.*, 2012; Parales *et al.*, 2013; Garcia *et al.*, 2015; Reyes-Darias *et al.*, 2015b).

The McpS receptor belongs to cluster II receptors. Its LBD is the first characterized member of the helical bimodular domain (HBM) family (Ortega and Krell, 2014). This receptor was found to mediate chemotaxis towards

INTRODUCTION

Chemotaxis provides the bacterium with the capacity to approach or escape from different types of compounds. Taxis has been observed towards compounds that serve as carbon or energy sources like sugars, amino acids or organic acids (Mesibov & Adler, 1972, Adler *et al.*, 1973, Seymour & Doetsch, 1973, Moulton & Montie, 1979). In addition, chemotaxis has been reported for other classes of compounds like neurotransmitters, plant hormones or quorum sensing signals (Bansal *et al.*, 2007, Antunez-Lamas *et al.*, 2009, Hegde *et al.*, 2011, Rader *et al.*, 2011). Typically, the specificity of a chemotactic response is determined by the chemoreceptor that is at the beginning of the chemosensory signaling cascade.

Chemoreceptors are typically composed of a cytosolic MA signaling domain and a LBD that is frequently located in the extra-cytoplasmic space. Ligand recognition at the LBD generates a molecular stimulus that modulates the CheA autokinase activity. Phosphorylgroups are subsequently transferred to the CheY response regulator, which in turn permits its interaction with the flagellar motor to control cell tumbling and to ultimately mediate chemotaxis (Sourjik & Wingreen, 2012).

A large number of different chemoreceptors have evolved that differ in the type of their LBD. Based on size differences, LBDs can be classified into cluster I (120 to 210 amino acids) and cluster II (220-299 amino acids) (Lacal *et al.*, 2010b). Compared to cluster I domains, relatively little information is available on cluster II domains that represent approximately 40 % of all chemoreceptors (Lacal *et al.*, 2010b). *P. putida* KT2440, the model organism for this study, has 27 predicted chemoreceptors of which most possess a cluster II LBD (Garcia *et al.*, 2015). So far, receptors McpS, McpR, McpP and McpG have been functionally annotated and shown to mediate chemotaxis to different organic and amino acids (Lacal *et al.*, 2010a, Pineda-Molina *et al.*, 2012, Parales *et al.*, 2013, Garcia *et al.*, 2015, Reyes-Darias *et al.*, 2015b).

The McpS receptor belongs to cluster II receptors. Its LBD is the first characterized member of the HBM family (Ortega & Krell, 2014). This receptor was found to mediate chemotaxis towards 6 different Krebs cycle intermediates as well as to butyrate and acetate. These compounds were found to bind directly to the recombinant LBD of the McpS receptor (Lacal *et al.*, 2010a, Pineda-Molina *et al.*, 2012). We have also reported 3D structures of McpS-LBD in the presence of different ligands (Pineda-Molina *et al.*, 2012). The domain is composed of two stacked helical modules that are each able to bind ligands. Structures reveal that malate and succinate bind to the same site at the membrane proximal module whereas acetate binds to the membrane distal module. Ligand binding to each of the modules was found to cause a chemotactic response (Pineda-Molina *et al.*, 2012). We have proposed that this novel receptor structure may be related to a novel mechanism where the final response is defined by the recognition of different signals by a same chemoreceptor (Pineda-Molina *et al.*, 2012).

One of the McpS ligands, citrate, forms complexes with metal ions like magnesium or calcium (Lacal *et al.*, 2011b). Interestingly, McpS bound citrate but not citrate/metal^{2+} complexes (Lacal *et al.*, 2011b). Chemotaxis towards root exudates was identified as an essential requisite for efficient root colonization (de Weert *et al.*, 2002). *P. putida* KT2440, the model strain of this study, is a nutritionally versatile, saprophytic and plant root-colonizing Gram-negative soil bacterium (Bagdasarian *et al.*, 1981, Espinosa-Urgel *et al.*, 2002, Regenhardt *et al.*, 2002). Several studies show that citrate is the most abundant organic acid in plant root exudates (Kuiper *et al.*, 2002, Kravchenko *et al.*, 2003, Kamilova *et al.*, 2006). Since exchangeable magnesium and calcium cations are also abundant in soil (Doi & Ranamukhaarachchi, 2009, Pestana & Gomes, 2014) and root exudates (Collins & Reilly, 1968), citrate is primarily present as metal complex in soil ecosystems. We therefore concluded that McpS does not play a role in the chemotactic response to citrate/metal^{2+} in the natural habitat of the strain (Lacal *et al.*, 2011b).

We have recently reported the domain signature of the HBM domain family (Ortega & Krell, 2014). These domains were found in bacteria and archaea and form part of chemoreceptors and histidine kinases. We have noted that most conserved amino acids of family members are located in the ligand binding sites of McpS-LBD. We have therefore suggested that the function of HBM family members consists in mediating responses to organic acids. This hypothesis was then supported by work of Parales *et al*. on the paralogous McpQ receptor (Parales *et al.*, 2013). The introduction of the *mcpQ* gene into a *Pseudomonas* mutant deficient in Krebs cycle intermediate taxis, conferred chemotaxis to citrate but not to succinate, malate and fumarate (Parales *et al.*, 2013). McpQ has an HBM type LBD that shares 27 % sequence identity with McpS-LBD (Supp. Fig. 6).

We show here that McpQ is a citrate specific receptor, which, in contrast to McpS, mediates preferentially chemotaxis towards citrate/metal^{2+}complexes. McpQ has thus evolved to recognize with high specificity one of the Krebs cycle intermediates that is not recognized by the broad ligand range McpS receptor. We show that a similar pattern is observed for other paralogous receptors, indicating that this may be a more general feature in chemoreceptor evolution.

METHODOLOGY

Strains and plasmids: The strains and plasmids used are provided in Table 4.

Generation of P. putida KT2440R mutant strains deficient in mcpQ and mcpQS: Generation of the *mcpQ* mutant strain: The mutant in *pp5020* (*mcpQ*) was constructed using a derivate plasmids of pCHESIΩKm. This plasmid, termed pCHESI-*pp5020*, was generated by amplifying a 0.6 Kb region of the gene to be mutated using the primers 5'-AA**GAATTC**TGACCGGCTGGCACGGCATG-3' and 5'-AA**GGATCC**CGCCCATGGCTGTGGCGGCA-3'. The PCR products were then cloned into pCHESIΩKm in the same transcriptional direction as the P_{lac} promoter. The resulting plasmid was transferred to *P. putida* KT2440R by electroporation or triparental conjugation (using *E. coli* HB101 (pRK600) as helper strain).

Construction of a double mutant deficient in mcpS (pp4658) and mcpQ (pp5020): The double mutant was constructed by homologous recombination using a derivative plasmid of the suicide vector pKNG101, as described previously (Ramos-Gonzalez & Molin, 1998). The plasmid for mutagenesis was transferred to *P. putida* KT2440R*mcpS* by triparental conjugation using *E. coli* CC118λ*pir* and *E. coli* HH26 (pNJ500) as helper. The plasmid for the in-frame deletion of *mcpQ* was generated by amplifying the up- and downstream flanking regions of *mcpQ* using primers PP5020-EcoRI-F (5´-TAATGAATTCCAGACCGTAGCCACGC-3´) and PP5020-KpnI-R (5´-TAATGGTACCCAAGCATCAGCTGCACCTGG-3´), and PP5020-KpnI-F (5´-TAATGGTACCTGCAAGGGTTGGTTGGGCG-3´) and PP5020-HindIII-R (5´-TAATAAGCTTCACGCAGGGCTACACGG-3´), respectively. The resulting PCR products were digested with EcoRI-KpnI and KpnI-HindIII and ligated in a three-way ligation into pUC18Not to be cloned into the marker exchange vector pKNG101. Plasmids were verified by PCR and DNA sequencing. For the construction of the final mutant, sucrose was added to a final concentration of 10% (w/v) to select derivatives that had undergone a second cross-over event during marker exchange mutagenesis. The resulting mutants were confirmed by PCR and DNA sequencing.

Construction of an expression plasmid for McpQ-LBD: The DNA fragment encoding the LBD of McpQ, Thr35 – Thr287, was amplified by PCR using genomic DNA of *P. putida* KT2440R and primers 5'-GGAATTCCATATGACCGGCTGGCACGGCATGGACA–3' and 5'–AAGAATTCTCATGTTTTGGCCTGCGCGGCA–3', which contained the restriction sites for NdeI and EcoRI (underlined), respectively. The resulting product was digested and cloned into the expression plasmid pET28b(+) linearized with the above enzymes. The insert and flanking region of the resulting plasmid, termed pET28b-McpQ-LBD, were verified by DNA sequencing.

Table 4. Strains and plasmids used in this study.

Strains	Characteristics[a]	References
E, coli BL21 (DE3)	F^-, *ompI*, *hsdSB* (r^-_B m^-_B) *gal*, *dam*, *met*	(Studier & Moffatt, 1986)
E. coli DH5α	F^-*endA*1 *glnV*44 *thi*-1 *recA*1 *relA*1 *gyrA*96 *deoRnupG* Φ80d*lacZ*ΔM15 Δ(*lacZYA-argF*)U169, *hsdR*17(r_K^- m_K^+), *phoA supE44*, λ– ; host for DNA manipulations	(Woodcock *et al.*, 1989)
E. coli HB101	F^- Δ*(gpt-proA)62 leuB6 supE44 ara-14 galK2 lacY1* Δ*(mcrC-mrr) rpsL20* (Sm^r) *xyl-5 mtl-1 recA13 thi-1*	(Boyer & Roulland-Dussoix, 1969)
E. coli CC118λ*pir*	Rif^R, λ*pir*	(Herrero *et al.*, 1990)
P. putida KT2440R	Rif^R derivative of *P. putida* KT2440, wild type	(Espinosa-Urgel & Ramos, 2004)
P. putida KT2440R *mcpQ*	*pp5020*::pCHESIΩKm;Rif^R, Km^R	This study
P. putida KT2440R *mcpS*	*pp4658*::mini-tn*5*-Km; Rif^R, Km^R	(Duque *et al.*, 2007)
P. putida KT2440R *mcpQS*	KT2440R *mcpS* in-frame Δ*pp5020* (1593 bp Δ); Rif^R, Km^R	This study
Plasmids		
pET28b	Km^R; protein expression plasmid	Novagen
pET28b-McpQ-LBD	Km^R; pET28b containing McpQ-LBD	This study
pRK600	Cm^R, *mob tra*	(Finan *et al.*, 1986)
pUC18NotI	Ap^R; identical to pUC18 but with two NotI sites flanking pUC18 polylinker	(Herrero *et al.*, 1990)
pKNG101	Sm^R; *oriR6K mob sacBR*	(Kaniga *et al.*, 1991)
pMAMV238	Ap^R; 1.5-kb PCR product containing a 1593 bp in frame deletion of *pp5020* (*mcpQ*) of KT2440R inserted into the EcoRI/HindIII sites of pUC18Not	This study

[a]Ap, ampicillin; Cm, chloramphenicol; Km, kanamycin; Rif, rifampin; Sm, streptomycin

Overexpression and purification of McpQ-LBD: E. coli BL21 (DE3) was transformed with pET28b-McpQ-LBD. The resulting strain was grown in 2 l Erlenmeyer flasks containing 400 ml of 2 x YT medium supplemented with 50 µg/ml kanamycin at 30 °C. At an OD_{660} of 0.5 the growth temperature was lowered to 18 °C and after another 30 min protein expression was induced by adding 0.1 mM isopropyl-β-D-1-thiogalactopyranoside. Growth was continued at 18 °C overnight prior to cells harvest by centrifugation at 6037 g. Cell pellets were resuspended in 30 ml buffer A (20 mM Tris/HCl, 0.1 mM EDTA, 500 mM NaCl, 10 mM imidazole, 5% (v/v) glycerol, pH 7.8) and broken by French press at 1000 psi. The resulting lysate was centrifuged at 20 000 g during 1 h, the supernatant passed through a 0.22 µm cut-off filter (Millipore) and loaded onto a 5-ml HisTrap HP column (Amersham Biosciences) equilibrated with buffer A. Protein was eluted by applying a 45 mM to 500 mM imidazole gradient in buffer A. Fractions were analysed by SDS-PAGE and McpQ-

LBD containing fractions were pooled. The protein concentration was determined by the Bradford assay.

Isothermal titration calorimetry (ITC): ITC measurements were done using a VP-microcalorimeter (MicroCal, Northampton, MA) at 25 and 15 °C. McpQ-LBD was dialyzed against polybuffer (5 mM Tris/HCl, 5 mM Pipes, 5 mM MES, pH 6.8). The ligand solutions were prepared in dialysis buffer at a concentration of 4 mM and placed into the injector syringe. Protein at 50-55 µM was placed into the sample cell and titrated with 3.2 µl ligand aliquots. The mean enthalpies measured from the injection of ligands into the buffer were subtracted from raw titration data prior to data analysis with the "One binding site model" of the MicroCal version of ORIGIN. Thermodynamic parameters provided are means and standard deviation from three independent experiments.

Analytical ultracentrifugation (AUC): AUC experiments were performed on a Beckman Coulter Optima XL-I analytical ultracentrifuge (Beckman-Coulter, Palo Alto, CA, USA) equipped with UV-visible absorbance as well as interference optics detection systems, using an An50Ti 8-hole rotor and 12 mm path-length charcoal-filled epon double-sector centrepieces. The experiments were carried out at 7°C. Like the ITC studies AUC experiments were conducted in polybuffer, pH 6.8. Sample concentrations ranged from 8.5 µM to 27 µM for McpQ-LBD protein as determined spectrophotometrically at 280 nm. Protein was analysed in the absence and presence of 1 mM sodium citrate and a mixture of 1 mM sodium citrate with 1 mM $MgCl_2$. The signal at 280 nm was followed in the absorbance optics mode. Sedimentation velocity (SV) runs were carried out at a rotor speed of 45 000 rpm using 400 µl samples with dialysis buffer as reference. A series of 150 scans without time intervals between successive scans were acquired for each sample. A least squares boundary modelling of the SV data was used to calculate sedimentation coefficient distributions with the size-distribution *c(s)* method and the non-interacting discrete species model (Schuck, 2000) implemented in the SEDFIT v14.1 software. The molecular weight was extracted from the sedimentation profiles, via the Lamm equation solution included in the *c(s)* model of SEDFIT (Schuck, 2000). The best fit values obtained for the sedimentation coefficient (*s*, in S or Svedbergs) and diffusion were used to estimate the molar mass of the molecule using the Svedberg equation. Buffer density (ρ= 1.0004 g/mL) and viscosity (η= 0.0143 Poise) at 7 °C were estimated by SEDNTERP software (Laue *et al.*, 1992) from the buffer components. The partial specific volume used was 0.723 ml/g as calculated from the amino acid sequence using the SEDNTERP software.

Growth experiments: The strain was grown overnight in M9 minimal medium (Abril *et al.*, 1989) supplemented with 10 mM succinate. Cultures were diluted into M9 medium supplemented with either 10 mM sodium citrate or a mixture of 10 mM sodium citrate with 10 mM magnesium chloride to an initial OD_{600} of 0.02. Cultures were grown in 100-well polystyrene plates and incubated at 30 °C in a Bioscreen Microbiological Growth Analyzer. Data shown are means and standard deviation from 3 individual experiments each conducted in triplicate.

Chemotaxis assays: Gradient plate assays: Bacteria were grown overnight in MS medium (MY medium (Hasegawa *et al.*, 2000) without yeast extract) supplemented with 10 mM succinate and diluted to an OD_{600} of 0.8–1 with MS medium. Cells were then washed twice with MS medium by consecutive resuspension and centrifugation at 3750 g for 3 min. Petri dishes were filled with 80 ml semisolid agar (0.25 %, w/v) in MS medium, containing 25 mM glycerol. Plates were cooled to room temperature for 30 min. Along the vertical central line of the plate, 10 µl aliquots of a 250 mM chemoattractant solution dissolved in MS medium were placed at regular distances. Plates were incubated at 4 °C for 12–16 h for chemoattractant gradient formation. Two-microliter aliquots of bacterial suspensions grown to an OD_{600} = 1.0 were then placed horizontally to each of the chemoattractant spots with a distance of 2 cm to the vertical line. Plates were incubated at 30 °C for 16–20 h prior to the inspection of chemotaxis. The chemotaxis index (RI) was calculated as described in (Pham & Parkinson, 2011). To calculate this index the distance from the site of

inoculation to the colony edges closest to (D1) and furthest from (D2) the citrate source was measured. RI corresponds to D1/(D1 + D2).

Quantitative capillary chemotaxis assay: A modified version of the capillary assay was used (Adler, 1973). MS medium supplemented with 10 mM succinate was inoculated with the wt and mutant strains and grown to early logarithmic phase (OD_{600} = 0.35-0.4). Cultures were then centrifuged at 1667 g at 4 °C for 5 minutes and washed twice with 50 mM potassium phosphate, 20 µM EDTA, 0.05 % (w/v) glycerol, pH 7.0. Cells were resuspended in the same buffer to an OD_{600} of 0.08-0.1 and 230 µl aliquots of bacterial suspension were then placed into the wells of a 96-well plate. For filling, capillaries (Microcaps, Drummond Scientific) were heat-sealed at one end, warmed over the flame and the open end inserted into the chemoattractant solution of which the pH had been adjusted to that measured for the bacterial suspension. MS medium lacking chemoattractants was used as a control. The capillaries were immersed into the cell suspension at its open end. After incubation for 30 min, the open end of the capillary was rinsed and placed into a microfuge tube containing 1 ml MS medium. The sealed end was broken and the content was emptied into the tube. A volume of 25 µl of the resulting cell suspension was plated out and incubated at 30 °C. Colonies were counted after growth on M9 medium supplemented with 10 mM succinate at 30 °C for 24 h.

RESULTS

The ligand binding domain of McpQ binds citrate with high specificity

To identify the potential LBD of McpQ, its sequence was submitted to the DAS algorithm (Cserzo *et al.*, 1997) that predicted two transmembrane regions comprising amino acids 18 to 34 and 288 to 307 (Supp. Fig. 6). The DNA sequence encoding the fragment flanked by the two transmembrane regions (Thr35 to Thr287), corresponding to the potential LBD, was cloned into an expression vector. The protein was produced in *E. coli* and purified McpQ-LBD was submitted to microcalorimetric titrations (Krell, 2008). Initial experiments involved the titration of McpQ-LBD with the Krebs cycle intermediates that bound to McpS, namely citrate, isocitrate, succinate, fumarate, malate, and oxalacetate. However, binding was exclusively detected for citrate (Fig. 15) whereas the other ligands failed to bind. Citrate binding was driven by favourable enthalpy (ΔH=-3.6 ± 0.7 kcal/mol) and entropy changes (2.4 ± 0.7 kcal/mol). Binding was characterized by a K_D of 39 ± 3 µM, which is lower than the K_D for citrate binding to McpS-LBD (109 µM) (Lacal *et al.*, 2010a). To further characterize ligand recognition by McpQ-LBD we analysed the binding of other di- and tricarboxylic acids like tricarballylate, cis-aconitate, oxalate, α-ketoglutarate, tartrate or itaconate, but no binding was observed. Microcalorimetric ligand screening was continued by testing recognition of monocarboxylic acids (pyruvate, propionate, L-lactate, valerate, 5-amino-valerate) and amino acids (L-glutamate, L-aspartate), which in all cases were not recognized by McpQ-LBD. Pineda *et al*. (2012) have shown that acetate bound to the membrane distal module of McpS-LBD. We conducted an analogous experiment and titrated McpQ-LBD with aliquots of 50 mM acetate, which, however, did not show binding. Similar results were obtained when the experiment was repeated at 15 °C (note: Change of the analysis temperature alters the ratio of exothermic to endothermic contributions to binding. This excludes the possibility that at 25 °C potential endothermic and exothermic contributions to binding cancel out each other). We therefore conclude that McpQ recognizes citrate with high specificity.

McpQ-LBD recognizes citrate/metal^{2+}complexes with higher affinity than free citrate

McpS does not recognize citrate in complex with physiologically relevant metal ions like magnesium or calcium (Lacal *et al.*, 2011b). To assess whether McpQ-LBD can bind citrate/metal^{2+} complexes, the experiment shown with free citrate (upper trace of Fig. 15) was repeated except that equimolar amounts of $MgCl_2$ or $CaCl_2$ (4 mM) were added to McpQ-LBD and citrate prior to the titration. As shown in the lower trace of Fig. 15, the titration of the protein with citrate/Mg^{2+} complexes resulted in much larger exothermic heat changes as compared to the titration with free citrate. As a consequence, the thermodynamic mode of ligand binding was altered dramatically. Binding was driven by very favourable enthalpy changes (ΔH= -15.7 ± 2 kcal/mol) and counterbalanced by large unfavourable entropy changes ($T\Delta S$=-9.5 ± 2 kcal/mol). Interestingly, the affinity of McpQ-LBD for the citrate/Mg^{2+} complex (K_D=27 ± 1 µM) was higher than that for free citrate. Very similar results were obtained for the titration of McpQ-LBD with citrate/Ca^{2+} complexes. Binding was also driven by large favourable enthalpy changes (Table 5) and the affinity

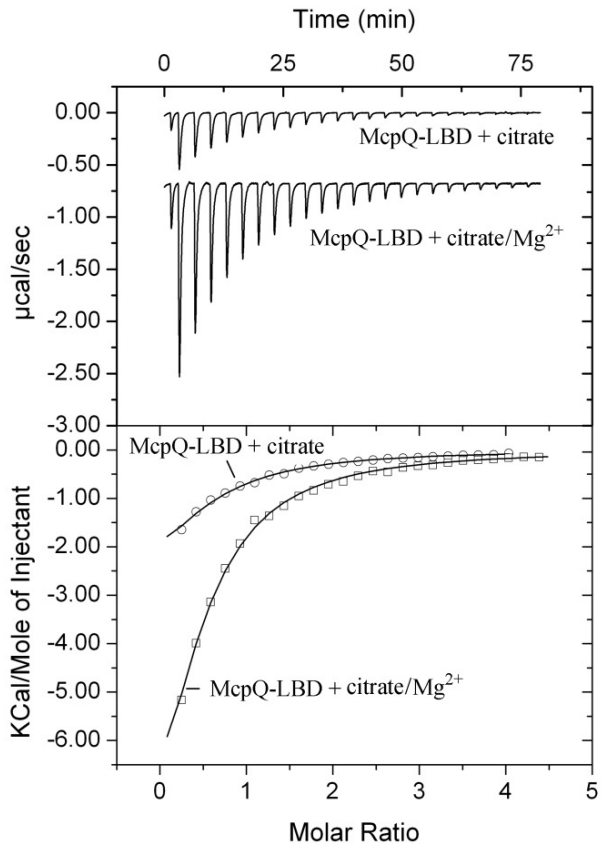

Figure 15. Microcalorimetric analysis of the binding of free or Mg^{2+} complexed citrate to McpQ-LBD. Upper panel: Raw titration data for the injection of a single 1.6 µl and a series of 3.2 µl aliquots of 4 mM citrate into 55 µM McpQ-LBD (upper trace). The lower trace is a repetition of this experiment except that 4 mM $MgCl_2$ had been added to the protein and citrate solution prior to the experiment. Lower panel: Integrated, dilution heat corrected and concentration normalized peak areas of the raw data that were fitted with the "One binding site" model of ORIGIN.

Table 5. Thermodynamic parameters for the titration of McpQ-LBD with different ligands. Shown are means and standard deviations from three independent experiments.

Ligand 1	Ligand 2	K_A M^{-1}	K_D µM	ΔH kcal/mol	$T\Delta S$ kcal/mol
McpQ-LBD	citrate	(2.67 ± 0.2) 10^4	39 ± 3	-3.6 ± 0.7	2.4 ± 0.7
McpQ-LBD/$MgCl_2$	citrate/$MgCl_2$	(3.67 ± 0.2) 10^4	27 ± 1	-15.7 ± 2	-9.5 ± 2
McpQ-LBD/$CaCl_2$	citrate/$CaCl_2$	(6.92 ± 0.9) 10^4	14 ± 2	-22.3 ± 3	-16.0 ± 3
McpQ-LBD	$MgCl_2$	No binding			
McpQ-LBD	$CaCl_2$	No binding			

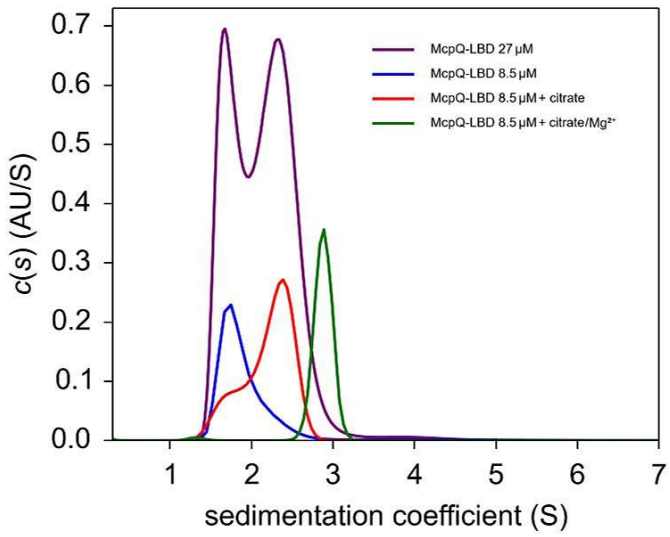

Figure 16. Analytical ultracentrifugation studies of McpQ-LBD in the absence and presence of citrate or citrate/Mg^{2+}. Shown are c(s) profiles corresponding to McpQ-LBD in the absence and presence of sodium citrate or sodium citrate/$MgCl_2$ (each at 1 mM). In the absence of ligands the protein was analysed at two different concentrations.

was even higher (K_D=14 ± 2 µM) than that for the citrate/Mg^{2+}complex. Control titrations of McpQ-LBD with either $MgCl_2$ or $CaCl_2$ did not reveal any binding. We can therefore conclude that McpQ has a higher affinity for citrate/metal^{2+}complexes as compared to free citrate.

Citrate/Mg^{2+} is superior to citrate in its capacity to stabilize the dimeric form of McpQ-LBD

Analytical ultracentrifugation studies were conducted to assess the effect of ligand binding to McpQ-LBD. Initial sedimentation velocity (SV) experiments were conducted at different protein concentrations in the absence of ligand (Fig. 16). At low concentrations (8.5 µM) the analysis of the profiles showed a single peak corresponding to a standard sedimentation coefficient of $s_{20,w}$= 2.6 S with tailing towards higher $s_{20,w}$ values. At higher concentrations (27 µM) two peaks at $s_{20,w}$= 2.5 S and$s_{20,w}$= 3.4 S were observed. When the experiments were repeated in the presence of 1 mM sodium citrate, the major peak had an$s_{20,w}$= 3.3 S, whereas a minor peak was observed at $s_{20,w}$= 2.5 S. In contrast, in the presence of citrate/Mg^{2+} a single peak at $s_{20,w}$= 4.2 S was detected.

The frictional ratio (*fr*) for the peak at 2.5 S is 1.5, indicative of a slightly elongated protein morphology. Based on this frictional ratio and using the diffusional scaling law used by SEDFIT and the Svedberg equation, the average molar mass of the protein was determined 34.4 kDa, which is very close to the sequence derived mass of the monomer (30.3 kDa). The peak at 3.3/3.4 S shows a similar *fr* corresponding to an elongated particle. The molar mass extracted was between 45 and 50 kDa (depending on the protein concentration), which may point to a virtual intermediate species resulting from the fast equilibrium between the monomers and dimers. The peak at 4.2 S observed in the presence of citrate/Mg^{2+} translates into a species of 58 kDa, which is very close to the mass of the sequence derived dimer (60.6 kDa).

We calculated the theoretical sedimentation coefficient for the monomer and the dimer of McpQ-LBD using the bead-model hydrodynamic properties predictor implemented in HYDROPRO as well as the McpS-based homology models of the monomer (Pineda-Molina *et al.*, 2012) and the virtual docked (using ClusPro 2.0 (Kozakov *et al.*, 2013) dimer. The theoretical sedimentation coefficient of the monomer was 2.5 S whereas that for the dimer was of 4.3 S.

Our results show that McpQ-LBD is monomeric at low concentrations and as the concentration is incremented the equilibrium shifts towards the dimer. In the presence of citrate the difference between the experimentally determined and the theoretical $s_{20,w}$of the fast sedimenting species, 3.4 S and 4.3 S respectively, are most likely due to a rapid interconversion of monomeric and dimeric species during the experiment, resulting in a virtual intermediate species. In marked

contrast, there is no evidence of virtual intermediate species in the presence citrate/Mg^{2+}. Instead, the $s_{20,w}$ value of the single peak observed corresponds to that of the protein dimer.

Taken together McpQ-LBD exists in monomer-dimer equilibrium in the absence of ligand. Citrate binding causes a partial shift to the protein dimer. In contrast, citrate/Mg^{2+} binding causes a complete and quantitative shift of protein molecules to the dimeric state.

Citrate and citrate/Mg^{2+} permit efficient growth of *P. putida* KT2440

To assess whether *P. putida* KT2440 can use citrate as sole carbon source, growth curves were recorded for *P. putida* KT2440R and its mutants in M9 minimal medium supplemented with either 10 mM citrate or citrate/Mg^{2+}. Data showed (Fig. 17) efficient growth of the wt and mutant strains under both conditions. The mean doubling times, calculated from three biological replicates conducted in triplicate (Supp. Table 2), were between 52 and 58 minutes. A statistical analysis of these data revealed no significant differences indicating that citrate and citrate/Mg^{2+} sustain growth of *P. putida* in a similar manner and that the mutation of citrate chemoreceptors did not alter growth properties under the conditions tested.

McpQ is the principal chemoreceptor for citrate and citrate/Mg^{2+} complexes

Experiments were conducted to assess the contribution of McpQ and McpS to citrate/$Mg^{2+}$and citrate chemotaxis. To this end we generated mutants in *mcpQ* and *mcpQS*, whereas the *mcpS* mutant was retrieved from the *Pseudomonas* mutant collection (Duque *et al.*, 2007).

Initial experiments involved gradient plate chemotaxis assays. In these assays a concentrated solution of citrate/Mg^{2+} was placed along a central vertical line on MS medium plates, which were then incubated overnight for gradient formation. At a distance of 2 cm to this central line aliquots of the wt or mutant strains were deposited and chemotaxis inspected the following day. As shown in Fig. 18, the wt strain showed an acentric spread towards the plate centre. Acentric spreads of minor extension were also observed for the *mcpS*, *mcpQ* and *mcpQS* mutant strains. For these experiments the chemotaxis indices were calculated as described in (Pham & Parkinson, 2011) (see also "Chapter 1.2: Methodology") and are presented in Table 6. The chemotaxis index of 0.67 indicates significant taxis of the wt strain. Mutation of either the *mcpQ* or *mcpS* gene resulted in a statistically relevant decrease in chemotaxis. The index of 0.53 for the *mcpQS* double mutant reveals only very weak taxis since values comprised between 0.48 to 0.52 indicate neutral behavior

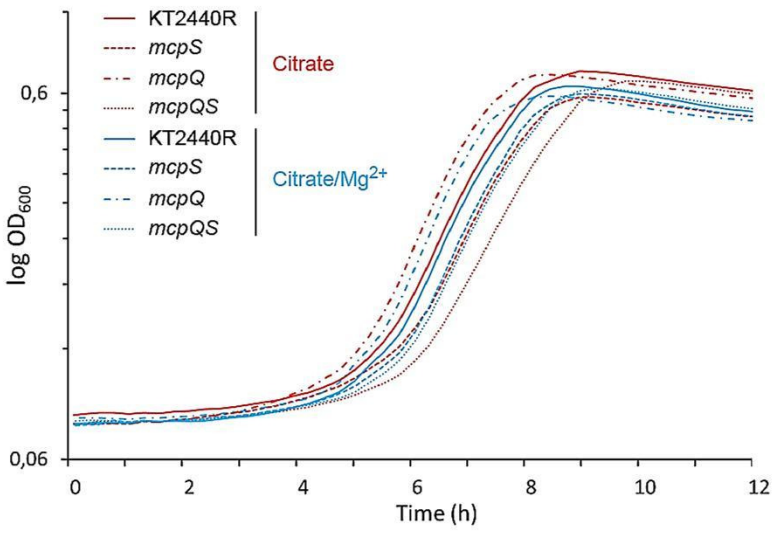

Figure 17. Growth curves of *P. putida* KT2440R and its *mcpQ*, *mcpS* and *mcpQS* mutants. Experiments were conducted in M9minimal medium supplemented with either 10 mM sodium citrate or a mixture of 10 mM sodium citrate with 10 mM magnesium chloride. The mean generation times and corresponding standard deviations derived from three experiments conducted in triplicate are provided in Supp. Table 1.

(Pham & Parkinson, 2011).

To assess the concentration dependence of chemotaxis, quantitative capillary assays of the wt and mutant strains were conducted (Fig. 19). Initial control experiments showed that the chemotaxis of the wt and mutant strains towards casamino acids are not significantly different (Fig. 19A). Since there is some free $MgCl_2$ in an equimolar $MgCl_2$ – citrate mixture, we assessed chemotaxis of the wt strain to different concentrations of $MgCl_2$. However, data in Supp. Fig. 7 show that taxis towards $MgCl_2$ is negligible. Figs. 19 B and C show quantitative capillary chemotaxis measurements of the wt strain as well as the *mcpQ*, *mcpS* and *mcpQS* mutants to different citrate and citrate/Mg^{2+} concentrations.

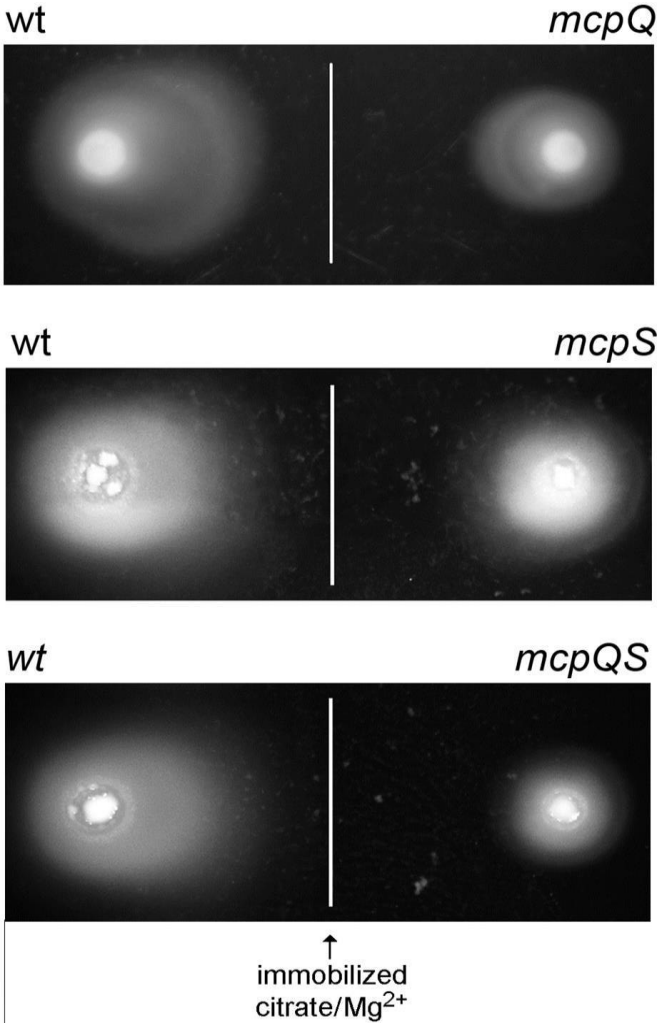

Figure 18. Gradient plate chemotaxis assays of *P. putida* KT2440R and its *mcpQ, mcpS and mcpQS* mutants towards citrate/Mg^{2+} complexes. Aliquots of a 250 mM citrate/Mg^{2+} solution were placed along the central vertical line. The plates were left overnight for gradient formation and bacterial suspensions were placed at a distance of 2 cm from this central line. The following day plates were inspected for chemotaxis.

Table 6. Chemotaxis indices of different strains derived from gradient plate chemotaxis assays towards citrate/Mg^{2+}. Representative images of these assays are shown in Fig. 18. Data shown are derived from three biological replicates each conducted in triplicate.

Strain	Means chemotaxis index	Standard deviation	t-student P value[1]
KT2440R	0,67	0,03	
mcpS	0,61	0,02	0.0015
mcpQ	0,56	0,04	< 0.0001
mcpQS	0,53	0,007	< 0.0001

[1]comparing the wt with mutant strains

Several conclusions can be drawn from these experiments: 1) As observed for the McpS ligands (Lacal *et al.*, 2010a), chemotaxis of the wt strain towards citrate and citrate/Mg^{2+} showed a slight biphasic behaviour. Measurable taxis was seen at 0.5 and 5 µM as well as at 5 to 50 mM, whereas no significant taxis was observed at 50 and 500 µM. 2). The magnitude of response towards high citrate/Mg^{2+}concentrations (5 and 50 mM) was approximately 6 times superior as compared to that towards citrate. 3). Mutation of *mcpQ* caused very strong reduction in the chemotaxis towards citrate/Mg^{2+} complexes, indicating that it is the primary chemoreceptor for this ligand.

The mutation of *mcpS* caused a modest reduction of citrate/Mg^{2+} taxis, which may be due to the presence of free citrate that is present in a citrate/Mg^{2+} mixture. 4) No measurable chemoattraction to citrate and citrate/Mg^{2+} was observed for the *mcpQS* double mutant, showing

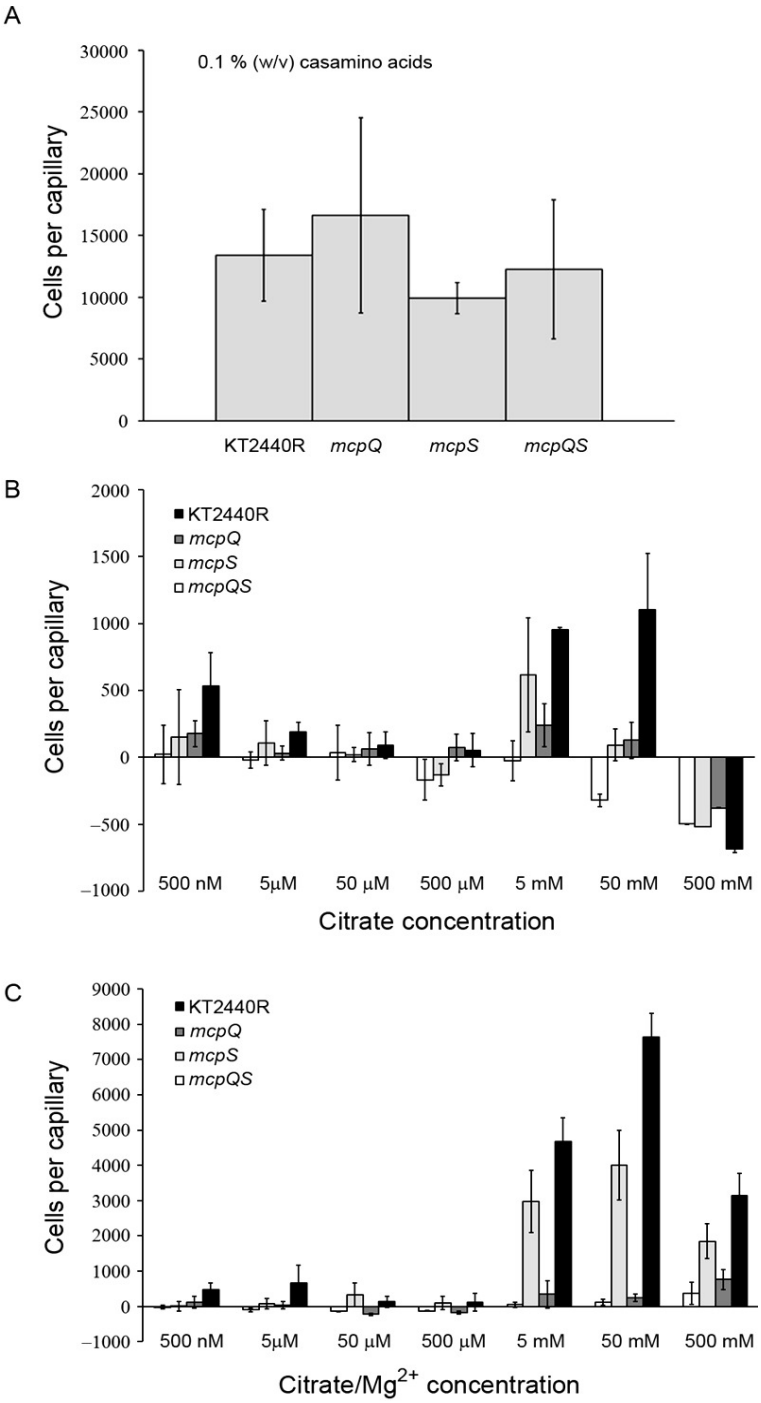

Figure 19. Quantitative capillary chemotaxis assays of *P. putida* KT2440R and its *mcpQ*, *mcpS* and *mcpQS* mutants towards casamino acids, citrate and citrate/Mg^{2+}. A) Chemotaxis towards 0.1 % (w/v) casamino acids (control). B) Chemotaxis of the four strains towards different citrate concentrations. C) Chemotaxis of the four strains towards different citrate/Mg^{2+} concentrations. Data were corrected with the number of cells that swam into buffer containing capillaries. Shown are means and standard deviations from three biological replicates each conducted in triplicate.

that taxis is mediated by these two receptors. Data indicate that responses by McpS and McpQ are additive. 5) At high concentrations free citrate caused a repellent response, whereas citrate/Mg^{2+} caused chemoattraction in all strains analysed.

DISCUSSION

P. putida strains are characterized by a metabolic versatility (Timmis, 2002) which appears to be reflected in the capacity to respond chemotactically to a wide range of different compounds (Sampedro *et al.*, 2015). *P. putida* KT2440 is a saprophytic soil bacterium able to colonize plant roots efficiently (Espinosa-Urgel *et al.*, 2002, Regenhardt *et al.*, 2002, Dos Santos *et al.*, 2004). Citrate is amongst the most abundant compounds in plant tissues and root exudates (Lipton *et al.*, 1987, Popova & Pinheiro de Carvalho, 1998, Kamilova *et al.*, 2006, Liao *et al.*, 2006, Qin *et al.*, 2007). Peñaloza and co-workers showed that citrate is present in different plant tissues at concentrations between approximately 7-23 mM depending on the plant part (Penaloza *et al.*, 2002). Experiments with sweet pepper and cucumber have shown that citrate represents 32 to 58 % of the total pool of organic acids and sugars in their root exudates (Kamilova *et al.*, 2006). These measurements also show that citrate is present at millimolar concentration in root exudates. We show here that maximal chemotactic responses occur to relatively high citrate concentrations of 5 to 50 mM. However, these concentrations agree with the abundance of citrate in the physiological habitat of a root-colonising saprophyte.

Citrate forms complexes with different metal cations (Lacal *et al.*, 2011b) and since they are abundantly present in the soil and root exudates (Lipton *et al.*, 1987, Qin *et al.*, 2007), citrate is predominantly present in complex with metal ions in the natural habitat of *P. putida*. The three dimensional structures of free and Mg^{2+} bound citrate have been solved (Johnson, 1965, Glusker *et al.*, 1969). As shown in Fig. 20A, the binding of Mg^{2+} to citrate causes major structural changes and induces significant rotation of both external carboxyl groups. Therefore, citrate and citrate/Mg^{2+} complexes should be regarded as two different ligands.

McpS is a broad ligand range receptor that recognizes citrate but not metal citrate complexes (Lacal *et al.*, 2011b). We show here that the McpS paralogue McpQ binds specifically citrate and that it mediates chemotaxis preferentially to citrate/$metal^{2+}$ complexes. The response of *P. putida* KT2440 to Krebs cycle intermediates is thus mediated by two paralogous receptors, of broad and narrow ligand specificity. Interestingly, one compound that is not recognized by the broad range receptor, citrate/$metal^{2+}$, binds with elevated specificity to the narrow range receptor McpQ. Interestingly, similar observations have been made for other chemoreceptors, like the paralogous amino acid receptors of *B. subtilis* and *P. aeruginosa*. These receptors possess a double PDC type of LBD (Zhang & Hendrickson, 2010). Chemotaxis to amino acids in *B. subtilis* is mediated by McpC and McpB. McpC was found to mediate chemotaxis to all proteinogenic amino acids except asparagine (Muller *et al.*, 1997). In turn McpB was identified as asparagine chemoreceptor and responds to this amino acid with high specificity (Hanlon & Ordal, 1994, Glekas *et al.*, 2010). In strong analogy, amino acid chemotaxis in *P. aeruginosa* is mediated by the PctA and PctB paralogues (Taguchi *et al.*, 1997, Reyes-Darias *et al.*, 2015a). The broad range receptor PctA is responsible for the chemotaxis towards 18 amino acids whereas PctB mediates with high specificity taxis to glutamine which is one of the two amino acids that is not recognized by PctA. The molecular recognition of different amino acids by the PctA-LBD and PctB-LBD has been assessed by titration calorimetry (Rico-Jimenez *et al.*, 2013a) and the corresponding responses were quantified (Reyes-Darias *et al.*, 2015a). Data show that PctB has a strong preference for asparagine, which in turn is not recognized by PctA. The existence of receptors dedicated to a specific compound may suggest a particular importance of this ligand. The abundance of citrate in the natural habitat of *Pseudomonas* together with citrate being a carbon source may have driven the evolution of McpQ.

Data indicate that the response magnitudes of McpQ to citrate/Mg^{2+} complexes are much larger than those to free citrate (Fig. 19). This may be surprising since citrate and citrate/Mg^{2+} bind with similar affinity to McpQ-LBD (Table 5). In this context, interesting parallels exist to McpS, where the binding affinities of different ligands did not correlate with the magnitude of the chemotactic response (Lacal *et al.*, 2010a). However, analytical ultracentrifugation and differential scanning calorimetry studies showed that the capacity of ligands to stabilize the dimeric form of McpS-LBD, and not their affinity, correlated with the magnitude of chemotaxis (Lacal *et al.*, 2010a). We have made here similar observations with McpQ-LBD. Ultracentrifugation studies have shown complete and quantitative McpQ-LBD dimer formation in the presence of citrate/Mg^{2+}. In the presence of citrate stabilization was observed to a lesser extent since, firstly, protein monomers were present and, secondly, the S value of the fast sedimenting species did not correspond to a dimer but to a virtual species corresponding to rapidly exchanging monomers and dimers. Taken together, ligand induced dimer formation of HBM containing receptors appears to be a necessary step for efficient transmembrane signaling. Ligand induced stabilization of the receptor LBD has also been observed for the Tar chemoreceptor (Milligan & Koshland, 1993).

McpQ is not the first specific citrate receptor reported. In contrast to *E. coli*, *S. typhimurium* is able to grow on citrate (Iwama *et al.*, 2006). This may be linked to the fact *S. typhimurium* shows chemoattraction towards citrate whereas *E. coli* is not attracted (Ingolia & Koshland, 1979). The difference in behaviour between both species can be linked to the presence of the Tcp chemoreceptor in *S. typhimurium* that mediates citrate chemotaxis (Yamamoto & Imae, 1993). Several parallels exist between Tcp and McpQ: firstly, they mediate attraction responses specific to citrate (Yamamoto & Imae, 1993), secondly, they respond to free as well as citrate/metal^{2+}

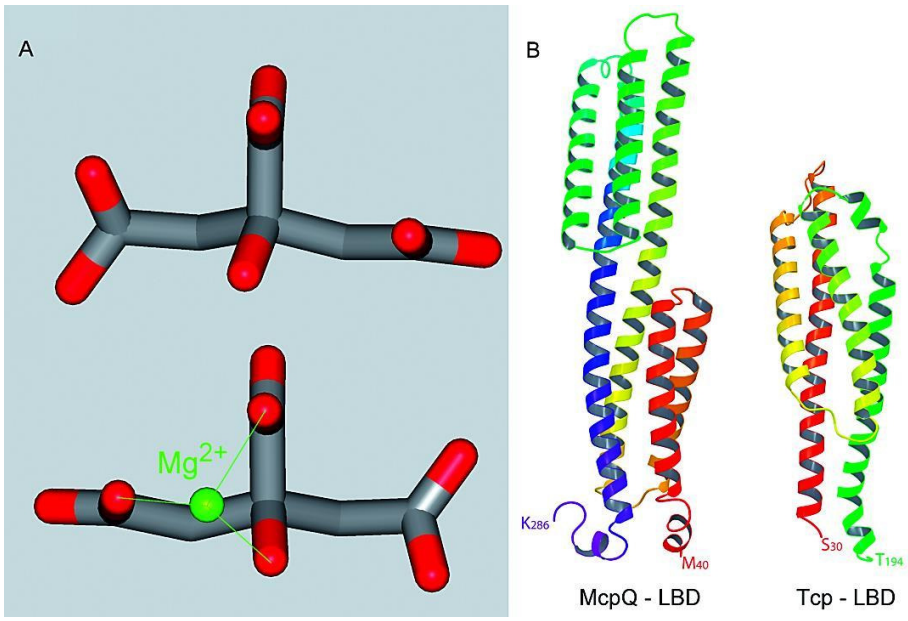

Figure 20. Structures of citrate and citrate receptor LBDs: A) Structures of free and Mg^{2+} bound citrate assolved by X-ray crystallography (Johnson, 1965, Glusker *et al.*, 1969). Files were retrieved form the Cambridge Structural Database (http://www.ccdc.cam.ac.uk/Solutions/CSDSystem/Pages/CSD.aspx). The figure was produced using the Web Lab Viewer software (http://accelrys.com/). B) Homology models of the LBDs of the citrate specific receptors McpQ of *P. putida* KT2440 and Tcp of *S. typhimurium*. Both models were created using the Phyre^2 algorithm (Kelley & Sternberg, 2009). Figures were prepared suing the Maestro 9.3. program of the Schrödinger suite (Suite 2012: Maestro, version 9.3, Schrödinger, LLC, New York, NY, 2012).

complexes (Iwama *et al.*, 2006) and, thirdly, they recognize their ligands directly (Iwama *et al.*, 2000). We have generated homology models of the LBDs of both receptors. As shown in Fig. 20B, domains differ in size and structure. The Tcp-LBD forms a 4-helix bundle and McpQ-LBD an HBM fold. These differences are also supported by the absence of any significant similarities in the alignment of their sequences (Supp. Fig. 8). There is thus evidence that two different receptor types have evolved that mediate specific taxis towards citrate and citrate/metal^{2+}complexes. The existence of two different receptor types that recognize specifically citrate underlines the physiological relevance of this compound. Further research will show to what extent specific citrate receptors are also found in other species.

SUPPLEMENTARY MATERIAL

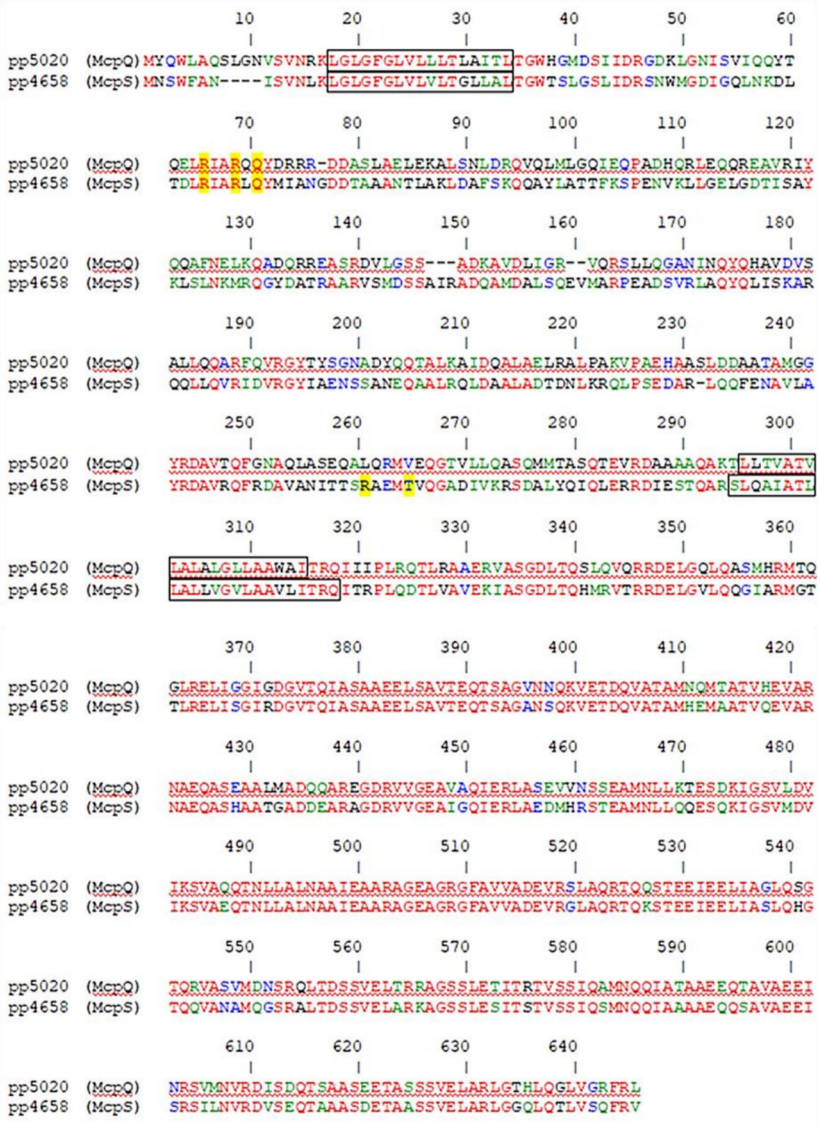

Supp. Fig 6. Sequence alignment of McpS with McpQ. Transmembrane regions as predicted by the DAS server (Cserzo *et al.*, 1997) are boxed. Amino acids that are involved in the binding of TCA cycle intermediates in McpS as well as their conserved counterparts in McpQ are shaded in yellow. The alignment was made using the CLUSTALW multiple alignment tool of the NPSA suite (https://npsa-prabi.ibcp.fr/cgi-bin/npsa_automat.pl?page=/NPSA/npsa_server.html) using GONNET weight matrix with gap opening and extension penalties of 10 and 0.1, respectively.

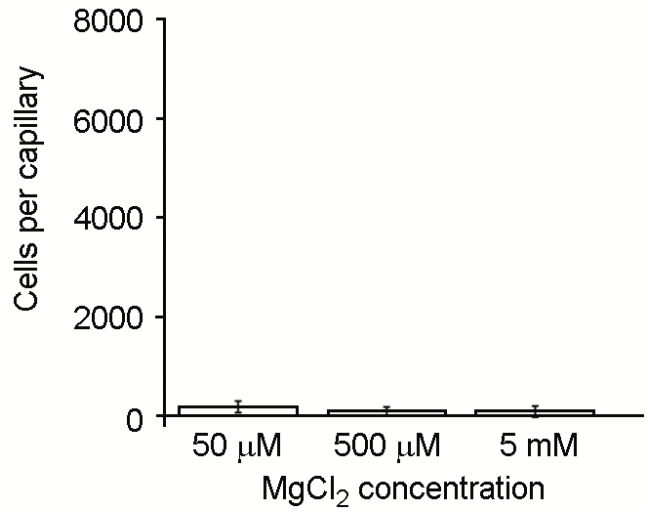

Supp. Fig 7. Quantitative capillary chemotaxis assays of *P. putida* KT2440R to different concentrations of $MgCl_2$. Data were corrected with the number of cells that swam into buffer containing capillaries. Shown are means and standard deviations of three biological replicates each conducted in triplicates.

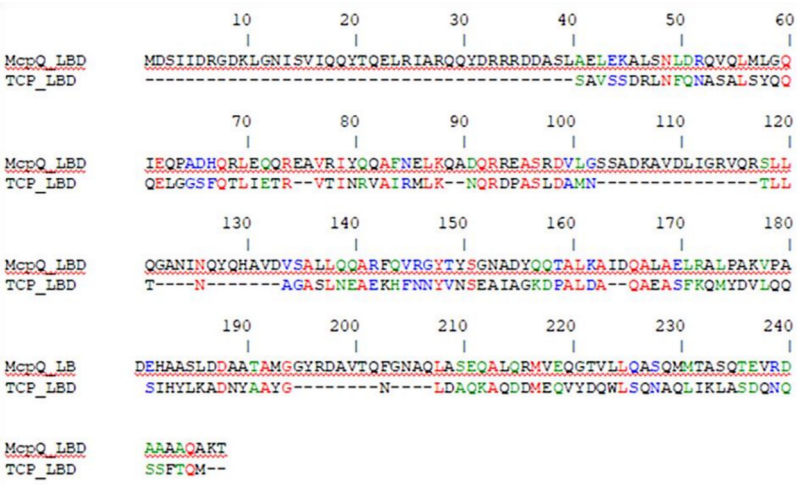

Supp. Fig 8. Alignment of the sequences of the citrate specific chemoreceptors Tcp of *S. typhimurium* and McpQ of *P. putida*. The alignment was made using the CLUSTALW multiple alignment tool of the NPSA suite (https://npsa-prabi.ibcp.fr/cgi-bin/npsa_automat.pl?page=/NPSA/npsa_server.html) using GONNET weight matrix with gap opening and extension penalties of 10 and 0.1 were used, respectively.

Supp. Table 2. Growth experiments of *Pseudomonas putida* KT2440R and its mutant deficient in *mcpQ*, *mcpS* or both genes in citrate or citrate/Mg^{2+}. The first part of the table shows the means of generation times and corresponding standard deviations calculated from three biological replicates each conducted in triplicate. The lower part of this figure shows statistical analysis of the data using the t-student test.

Strain	Growth medium	Mean Generation time	Standard deviation
KT2440R	M9 + Citrate	54,68	2,12
mcpQ	M9 + Citrate	54,52	6,62
mcpS	M9 + Citrate	56,96	0,82
mcpQS	M9 + Citrate	56,98	1,10
KT2440R	M9 + Citrate/Mg^{2+}	58,35	10,86
mcpQ	M9 + Citrate/Mg^{2+}	52,24	3,44
mcpS	M9 + Citrate/Mg^{2+}	54,07	2,78
mcpQS	M9 + Citrate/Mg^{2+}	55,78	2,25

Statistical analysis of data

Strains		Growth medium	t-student P-value
KT2440R	*mcpQ*	M9 + Citrate	0,97
KT2440R	*mcpS*		0,15
KT2440R	*mcpQS*		0,17
KT2440R	*mcpQ*	M9 + Citrate/Mg^{2+}	0,40
KT2440R	*mcpS*		0,54
KT2440R	*mcpQS*		0,70

Strains		t-student P-value
Citrate	Citrate/Mg^{2+}	
KT2440R	KT2440R	0,59
mcpQ	*mcpQ*	0,62
mcpS	*mcpS*	0,15
mcpQS	*mcpQS*	0,45

CHAPTER 1.3: IDENTIFICATION OF A α-KETOGLUTARATE SPECIFIC CHEMORECEPTOR IN *P. aeruginosa* PAO1

Published article

Identification of a Chemoreceptor in *Pseudomonas aeruginosa* that Specifically Mediates Chemotaxis Toward α-Ketoglutarate.

David Martín-Mora, Álvaro Ortega, José Antonio Reyes-Darias, Vanina García, Diana López-Farfán, Miguel Ángel Matilla, Tino Krell.

Dept. of Environmental Protection, Estación Experimental del Zaidín, Consejo Superior de Investigaciones Científicas

Frontiers in Microbiology (Published online 29 November 2016);18(10), 3284–3295.
doi: 10.3389/fmicb.2016.01937

ABSTRACT

P. aeruginosa is an ubiquitous pathogen able to infect humans, animals and plants. Chemotaxis was found to be associated with the virulence of this and other pathogens. Although established as a model for chemotaxis research, the majority of the 26 *P. aeruginosa* chemoreceptors remain functionally un-annotated. We report here the identification of PA5072 (named McpK) as chemoreceptor for α-ketoglutarate (αKG). High-throughput thermal shift assays and isothermal titration calorimetry studies (ITC) of the recombinant McpK LBD showed that it recognizes exclusively α-ketoglutarate. The ITC analysis indicated that the ligand bound with positive cooperativity (K_{d1}=301μM, K_{d2}=81 μM). McpK is predicted to possess a HBM type of LBD and this and other studies suggest that this domain type may be associated with the recognition of organic acids. Analytical ultracentrifugation studies revealed that McpK-LBD is present in a monomer-dimer equilibrium. αKG binding stabilized the dimer and dimer self-dissociation constants of 55 μM and 5.9 μM were derived for ligand-free and αKG-bound forms of McpK-LBD, respectively. Ligand-induced LBD dimer stabilization has been observed for other HBM domain containing receptors and may correspond to a general mechanism of this protein family. Quantitative capillary chemotaxis assays demonstrated that *P. aeruginosa* showed chemotaxis to a broad range of αKG concentrations with maximal responses at 500 μM. Deletion of the *mcpK* gene reduced chemotaxis over the entire concentration range to close to background levels and wild type like chemotaxis was recovered following complementation. Real-time PCR studies indicated that the presence of αKG does not modulate *mcpK* expression. Since αKG is present in plant root exudates it was investigated whether the deletion of *mcpK* altered maize root colonization. However, no significant changes with respect to the wild type strain were observed. The existence of a chemoreceptor specific for αKG may be due to its central metabolic role as well as to its function as signaling molecule. This work expands the range of known chemoreceptor types and underlines the important physiological role of chemotaxis towards tricarboxylic acid cycle intermediates.

frontiers in Microbiology

ORIGINAL RESEARCH
published: 29 November 2016
doi: 10.3389/fmicb.2016.01937

Identification of a Chemoreceptor in *Pseudomonas aeruginosa* That Specifically Mediates Chemotaxis Toward α-Ketoglutarate

*David Martín-Mora, Alvaro Ortega, José A. Reyes-Darias, Vanina García, Diana López-Farfán, Miguel A. Matilla and Tino Krell**

Department of Environmental Protection, Estación Experimental del Zaidín, Consejo Superior de Investigaciones Científicas, Granada, Spain

Pseudomonas aeruginosa is an ubiquitous pathogen able to infect humans, animals, and plants. Chemotaxis was found to be associated with the virulence of this and other pathogens. Although established as a model for chemotaxis research, the majority of the 26 *P. aeruginosa* chemoreceptors remain functionally un-annotated. We report here the identification of PA5072 (named McpK) as chemoreceptor for α-ketoglutarate (αKG). High-throughput thermal shift assays and isothermal titration calorimetry studies (ITC) of the recombinant McpK ligand binding domain (LBD) showed that it recognizes exclusively α-ketoglutarate. The ITC analysis indicated that the ligand bound with positive cooperativity (K_{d1} = 301 μM, K_{d2} = 81 μM). McpK is predicted to possess a helical bimodular (HBM) type of LBD and this and other studies suggest that this domain type may be associated with the recognition of organic acids. Analytical ultracentrifugation (AUC) studies revealed that McpK-LBD is present in monomer-dimer equilibrium. Alpha-KG binding stabilized the dimer and dimer self-dissociation constants of 55 μM and 5.9 μM were derived for ligand-free and αKG-bound forms of McpK-LBD, respectively. Ligand-induced LBD dimer stabilization has been observed for other HBM domain containing receptors and may correspond to a general mechanism of this protein family. Quantitative capillary chemotaxis assays demonstrated that *P. aeruginosa* showed chemotaxis to a broad range of αKG concentrations with maximal responses at 500 μM. Deletion of the *mcpK* gene reduced chemotaxis over the entire concentration range to close to background levels and wild type like chemotaxis was recovered following complementation. Real-time PCR studies indicated that the presence of αKG does not modulate *mcpK* expression. Since αKG is present in plant root exudates it was investigated whether the deletion of *mcpK* altered maize root colonization. However, no significant changes with respect to the wild type strain were observed. The existence of a chemoreceptor specific for αKG may be due to its central metabolic role as well as to its function as signaling molecule. This work expands the range of known chemoreceptor types and underlines the important physiological role of chemotaxis toward tricarboxylic acid cycle intermediates.

Keywords: chemotaxis, chemoreceptor, signal transduction, molecular recognition, *Pseudomonas aeruginosa*, α-ketoglutarate

OPEN ACCESS

Edited by:
Biswarup Mukhopadhyay, Virginia Tech, USA

Reviewed by:
Birgit Edeltraud Scharf, Virginia Tech, USA
Robert B. Bourret, University of North Carolina at Chapel Hill, USA

****Correspondence:***
Tino Krell
tino.krell@eez.csic.es

Specialty section:
This article was submitted to Microbial Physiology and Metabolism, a section of the journal Frontiers in Microbiology

Received: *19 September 2016*
Accepted: *17 November 2016*
Published: *29 November 2016*

Citation:
Martín-Mora D, Ortega A, Reyes-Darias JA, García V, López-Farfán D, Matilla MA and Krell T (2016) Identification of a Chemoreceptor in Pseudomonas aeruginosa That Specifically Mediates Chemotaxis Toward α-Ketoglutarate. Front. Microbiol. 7:1937. doi: 10.3389/fmicb.2016.01937

INTRODUCTION

Bacteria possess a variety of signal transduction systems that allow them to adapt their metabolism and behavior to different changes in environmental cues. One of the major signal transduction mechanisms is based on the action of chemosensory signaling pathways (Wuichet & Zhulin, 2010). Typically, signaling is initiated by the binding of signals to the chemoreceptor LBD, which in turn triggers a molecular stimulus that modulates autophosphorylation of the CheA histidine kinase and consequently transphosphorylation of the CheY response regulator (Hazelbauer *et al.*, 2008). Chemosensory systems carry out multiple functions such as mediating chemotaxis, type IV pili-based motility or alternative cellular processes (Hickman *et al.*, 2005, Zusman *et al.*, 2007, Wuichet & Zhulin, 2010).

E. coli is the traditional model to study chemoreceptor-based signaling processes (Parkinson *et al.*, 2015). This bacterium has 5 chemoreceptors, of which 4 contain a periplasmic 4-helix bundle ligand LBD. The fifth receptor, Aer, causes aerotaxis and has a cytosolic PAS type LBD. Signals bind either directly to the LBD or in complex with a periplasmic ligand binding protein. Chemoreceptors feed into a single chemosensory cascade that mediates chemotaxis towards compounds like sugars, amino acids or dipeptides.

The analysis of 450 bacterial genomes showed that approximately half of them possess genes encoding chemosensory signaling proteins (Wuichet & Zhulin, 2010). Frequently, chemosensory signaling is in many bacteria more complex than in *E. coli*. Bacteria that possess chemosensory signaling proteins have on average 14 chemoreceptor genes (Lacal *et al.*, 2010b) and for some species up to 60 chemoreceptors were identified (Matsunaga *et al.*, 2005). Genome analyses have furthermore demonstrated that other bacteria possess different types of chemoreceptors that differ in the type of LBD. Most chemoreceptors are functionally un-annotated but such knowledge is indispensable to identify the forces that have shaped the evolution of chemotactic behavior. Chemoreceptors can be classified according to the size of their LBD into cluster I (approx. 150 amino acids) or cluster II (approx. 250) (Lacal *et al.*, 2010b). Cluster II receptors are absent from *E. coli* but were estimated to correspond to 40% of all chemoreceptors (Lacal *et al.*, 2010b). The main representatives of cluster II LBDs are the dCACHE (Liu *et al.*, 2015, Upadhyay *et al.*, 2016) and helical bimodular domain (HBM) (Pineda-Molina *et al.*, 2012, Ortega & Krell, 2014) which, despite their abundance, remain poorly characterized.

The first receptor characterized with an HBM domain was McpS of *P. putida* KT2440 that mediated chemotactic responses to different Krebs cycle intermediates (Lacal *et al.*, 2010a, Lacal *et al.*, 2011b). The 3D structure of the cluster II LBD of McpS revealed that it corresponds to a novel bacterial sensor domain composed of two structural modules that each can bind directly signal molecules (Pineda-Molina *et al.*, 2012). Other HBM domain containing receptors are the citrate specific McpQ of *P. putida* KT2440 (Martin-Mora *et al.*, 2016b) as well as McfS (Parales *et al.*, 2013) of *P. putida* F1 and McpS of *P. fluorescens* Pf0-1 (Oku *et al.*, 2014) that mediate chemotaxis to organic acids. HBM domains were found to form part of chemoreceptors and sensor kinases and were found in bacteria and archaea (Ortega & Krell, 2014).

P. aeruginosa is a ubiquitously occurring microorganism that is capable of causing multiple human opportunistic infections (Gellatly & Hancock, 2013). As such, *P. aeruginosa* is the leading cause of nosocomial infections, particularly in immunocompromised, cancer, burn and cystic fibrosis patients (Juhas, 2015). This, combined with the emergence of strains resistant to all commercially available antibiotics, makes *P. aeruginosa* one of the most feared pathogens (Dorotkiewicz-Jach *et al.*, 2015). In addition, *P. aeruginosa* was found to colonize (Walker *et al.*, 2004) and infect different plants (Cao *et al.*, 2001). A number of reports show that *P. aeruginosa* chemotaxis is necessary for efficient host colonization and virulence (Garvis *et al.*, 2009, McLaughlin

et al., 2012, Kamath *et al.*, 2016, Schwarzer *et al.*, 2016) and the interference with the motility and chemotaxis was proposed as an alternative strategy to block this pathogen (Erhardt, 2016).

P. aeruginosa is a model organism to study chemotaxis (Kato *et al.*, 2008, Sampedro *et al.*, 2015). In particular its responses to amino acids by the three paralogous receptors PctA, PctB and PctC (Kuroda *et al.*, 1995, Taguchi *et al.*, 1997, Rico-Jimenez *et al.*, 2013a, McKellar *et al.*, 2015, Reyes-Darias *et al.*, 2015b, Reyes-Darias *et al.*, 2015a) as well as its response to inorganic phosphate (Wu *et al.*, 2000, Rico-Jimenez *et al.*, 2016) by the CtpL and CtpH receptors have been studied in some depth. In addition, the cytosolic and atypical receptor McpB (also named Aer2)(Watts *et al.*, 2011, Airola *et al.*, 2013a, Garcia-Fontana *et al.*, 2014, Garcia *et al.*, 2016) was subject to many studies and is amongst the best studied members of the chemoreceptor sub-family with cytoplasmic location. Chemoreceptor PA2652 was identified as a specific malate chemoreceptor (Alvarez-Ortega & Harwood, 2007) and TlpQ responsible for the chemotaxis towards the plant hormone ethylene (Kim & Tokura, 2007). Two other chemoreceptors, WspA and BdlA, play important roles in biofilm formation and dispersion (Hickman *et al.*, 2005, Morgan *et al.*, 2006, O'Connor *et al.*, 2012, Petrova & Sauer, 2012). However, of the 26 *P. aeruginosa* chemoreceptors more than half remain of unknown function. This knowledge however is indispensable to understand the forces that have driven the evolution of chemotaxis in this ubiquitous pathogen.

P. aeruginosa PAO1 has three receptors with an HBM domain. One of them, CtpL, was found to mediate specifically chemotaxis to low Pi concentrations (Wu *et al.*, 2000). However, CtpL does not bind Pi directly but recognizes the Pi loaded periplasmic binding protein PstS (Rico-Jimenez *et al.*, 2016). The remaining two receptors, PA1646 and PA5072, are of unknown function. We report here the functional annotation of one of them, PA5072, that binds and mediates chemotaxis exclusively to αKG. This receptor, termed McpK, expands the range of known chemoreceptor types.

METHODOLOGY

Bacterial strains, plasmids and primers

The strains and plasmids used in this study are listed in Table 7. Different primers for molecular biology manipulations are provided in Supp. Table 3.

Construction of expression plasmid for McpK-LBD

The DNA fragment of *mcpK* encoding amino acids Arg^{38}–Ser^{293} was amplified using primers McpK-LBD_fw and McpK-LBD_rv and genomic DNA of *P. aeruginosa* PAO1. The resulting PCR product was cloned into pGEM-T and digested with NdeI and BamHI and then subcloned into the expression plasmid pET28b(+) linearized with the same enzymes. The resulting plasmid, termed pET28-McpK-LBD, was verified by DNA sequencing of the insert and flanking regions.

Overexpression and purification of McpK-LBD

E. coli BL21 (DE3) containing pET28-McpK-LBD was grown in 2 L Erlenmeyer flasks containing 500 ml LB medium supplemented with 50 μg ml^{-1} kanamycin at 30°C until an OD_{660} of 0.6, at which point protein production was induced by adding 0.1 mM IPTG. Growth was continued at 18 °C overnight before cell harvest by centrifugation at 10 000 *g* for 30 min. All subsequent manipulations were carried out at 4°C. Cell pellets were resuspended in buffer A (20 mMTris/HCl, 200 mM NaCl, 10 mM imidazole, 5% (vol/vol) glycerol, pH 8.0) and broken by French press treatment at 1000 psi. After centrifugation at 20,000 g for 1 h, the supernatant was loaded onto a 5 ml HisTrap column (Amersham Bioscience), washed with five column volumes of buffer A and eluted with a 30–300 mM imidazole gradient in buffer A. Protein-containing fractions were pooled.

Thermal Shift Assays

Thermal shift assays were performed using a BioRad MyIQ2 Real-Time PCR instrument. Ligands were prepared by dissolving Biolog Phenotype Microarray compounds in 50 µl of MilliQ water to obtain a final concentration of around 10-20 mM (as indicated by the manufacturer). Screening was performed with plates PM1, PM2A, PM3B, PM4A and PM5. Each plate contains 95 compounds and a control (the composition of these arrays is provided in http://208.106.130.253/pdf/pm_lit/PM1-PM10.pdf). Each 25 µl assay mixture contained 40 µM protein in 5 mM Tris, 5 mM Pipes, 5 mM Mes, pH 8.0 and SYPRO orange (Life Technologies) at 5 x concentration. Aliquots of 2.5 µl of the resuspended Biolog compounds were added to each well. Samples were heated from 23 °C to 85 °C at a scan rate of 1 °C/min. The protein unfolding curves were monitored by detecting changes in SYPRO Orange fluorescence. Melting temperatures were determined using the first derivative values from the raw fluorescence data.

Isothermal titration calorimetry

Experiments were conducted on a VP-microcalorimeter (Microcal, Amherst, MA) at 20 °C or 10 °C. McpK-LBD was dialyzed overnight against 5 mM Tris, 5 mM PIPES, 5 mM MES, pH 8.0 and placed into the sample cell. Typically, protein at 20-100 µM was introduced into the sample cell and titrated with 1-3 mM ligand solutions that were prepared in dialysis buffer immediately before use. For fitting, data were integrated using NITPIC (Keller *et al.*, 2012) before global fitting to a two symmetric-site binding model in SEDPHAT (Houtman *et al.*, 2007). The binding constants expressed are corrected as $K_d1 = 2*K_d1'$ and $K_d2 = 0.5*K_d2'$ in order to express an estimation of the microscopic constants for the two binding sites model, where Kx' are the macroscopic constants measured. The cooperativity factor α is expressed as $\alpha=K_d1/K_d2$. Statistical uncertainties for best-fit estimates of K_d and ΔH were calculated using standard error surface projection methods built into SEDPHAT.

Analytical ultracentrifugation

Experiments were performed in a Beckman Coulter Optima XL-I analytical ultracentrifuge (Beckman-Coulter, Palo Alto, CA, USA) equipped with UV-visible absorbance as well as interference optics detection systems, using an An50Ti 8-hole rotor and 12 mm path-length charcoal-filled epon double-sector centrepieces. The experiments were carried out at 7 °C with at least 1 h stabilizing after reaching 7 °C in the rotor chamber, using 5 mM Tris, 5 mM PIPES, 5 mM MES, pH 8.0. Samples of 10 µM to 50 µM for McpK-LBD were analyzed in the presence and absence of 1 mM αKG.

Sedimentation velocity (SV) runs were carried out at a rotor speed of 128,793x g using 400 µL samples with McpK-LBD dialysis buffer as reference. A series of 180 scans without time intervals between successive scans were acquired for each sample. Laser at a wavelength of 236 nm was used in the absorbance optics mode. A least squares boundary modeling of the SV data was used to calculate sedimentation coefficient distributions with the size-distribution *c(s)* method and the non-interacting discrete species model (Schuck, 2000) implemented in the SEDFIT v14.1 software. The molecular weight was extracted from the sedimentation profiles, via the Lamm equation solution included in the *c(s)* model of SEDFIT (Schuck, 2000). The best fit values obtained for the sedimentation coefficient (*s*, in S or Svedbergs) and diffusion were used to estimate the molar mass of the molecule using the Svedberg equation. Buffer density (ρ = 1.00036 g/ml) and viscosity (η= 0.01433 Poise) at 7 °C were estimated by SEDNTERP software (Laue *et al.*, 1992) from the buffer components. The partial specific volume used was 0.71274 ml/g as calculated from the amino acid sequence also using SEDNTERP software.

Sedimentation equilibrium (SE) experiments were performed at 7 °C, measuring absorbance at 280 nm as a function of radius. Three different concentrations of McpK-LBD (40 µM, 50 µM and

60 µM) both in the absence or in the presence of 1mM αKG were loaded with the dialysis buffer as reference and a multi-speed (9,740, 20,606 and 185,462 x g) run was used. The data were analyzed globally by the SEDPHAT (Vistica *et al.*, 2004) "species analysis with mass conservation constraints" model. The goodness of fit was evaluated on the basis of the residuals, expressed as the difference between the experimental data and the theoretical curve.

Construction of *P. aeruginosa* PAO1 Δ*pa5072* (Δ*mcpK*)

An unmarked non-polar deletion of *pa5072* was created by allelic exchange as described (Schweizer, 1992) with the following modifications: two DNA fragments comprising the 234 bp upstream and 336 bp downstream regions of *pp5072* were obtained by PCR amplification of genomic DNA using primers PA5072UpF-HindIII and PA5072UpR-XbaI (upstream region) and primers PA5072DownF-XbaI and PA5072DownR-EcoRI (downstream region). The upstream DNA fragment was digested with HindIII and XbaI and cloned into pUC18NotI digested with the same restriction enzymes, resulting in pUC18NotI-5072Up, whereas the downstream DNA fragment was digested with XbaI and EcoRI and cloned into pUC18NotI-5072Up digested with the same restriction enzymes, resulting in pUC18NotI-5072UpDw. The 570 bp 5072UpDw DNA fragment was digested from pUC18NotI-5072UpDw using NotI and subcloned into the suicide vector pKNG101 a mobilizable suicide vector, hosted routinely in the permissive *E. coli* strain CC118λ*pir* bearing the positive counter selection marker *sacB* and conferring resistance to streptomycin. The resulting plasmid, pKNG101-PA5072UpDw was transformed into *E. coli* CC118 λ*pir*. The pKNG101-PA5072UpDw plasmid was mobilized from this strain into *P. aeruginosa* PAO1 by three-partner conjugation using the *E. coli* HB101 (pRK600) helper strain. Selection for plasmid cointegration in *P. aeruginosa* PAO1 was accomplished using M9 minimal medium supplemented with 10 mM succinate and 2000 µg/ml streptomycin (Sm). The Sm^r colonies were unable to grow on LB medium containing 10% sucrose (Suc), confirming that the plasmid pKNG101-PA5072UpDw with its *sacB* gene had integrated into *P. aeruginosa* PAO1. Transconjugants were plated on LB plates and incubated for 48 hours at room temperature. PCR analysis of the Suc^rSm^s colonies confirmed that gene replacement had occurred.

Construction of plasmid for complementation

The DNA fragment corresponding to the *mcpK* gene and the 607 bp upstream region was amplified by PCR using primers McpK-comp_fw and McpK-comp_rv and genomic DNA of *P. aeruginosa* PAO1. The resulting fragment was digested with KpnI and XbaI and cloned into pBBR1MCS-2, linearized with the same enzymes. The resulting plasmid pBBR1MCS-2-McpK was verified by DNA sequencing of the insert and flanking regions. The mutant strain was transformed with pBBR1MCS-2-McpK by electroporation (2800 V). Transformed colonies were selected on LB agar plates containing 300 µg/ml kanamycin and verified by colony PCR.

Quantitative capillarity chemotaxis assays

Assays were carried out at a temperature of 25 °C. Bacterial cultures were grown to an OD_{600} of 0.35-0.4 in MS medium, washed and resuspended in chemotaxis buffer (30 mM K_2HPO_4, 19 mM KH_2PO_4, 20 µM EDTA and 0.05 % (v/v) glycerol, pH 7.0) to an OD_{600} of 0.08-0.1. Polystyrene multi-well plates were filled with 230 µl of the resulting bacterial suspension. For filling with chemoeffector solutions, capillaries (Microcaps, Drummond Scientific, USA) were heat-sealed at one end, warmed over the flame and the open end inserted into the chemoattractant solution.

Table 7. Bacterial strains and plasmids used in this study.

Strain or plasmid	Relevant characteristics	Reference or source
Strains		
E. coli BL21 (DE3)	F–, *ompI, hsdS*$_B$(r^-_B m^-_B) *gal*, *dam*, *met*	(Jeong *et al.*, 2009)
E. coli DH5α	*supE44 lacU169* (*Ø80lacZ*ΔM15) *hsdR17* ($r_k^-m_k^-$), *recA1 endA1 gyrA96 thi-1 relA1*	(Woodcock *et al.*, 1989)
E. coli HB101	F- Δ*(gpt-proA)62 leuB6 supE44 ara-14 galK2 lacY1* Δ*(mcrC-mrr) rpsL20* (Sm^r) *xyl-5 mtl-1 recA13 thi-1*	(Boyer & Roulland-Dussoix, 1969, Kessler *et al.*, 1992)
E. coli CC118λ*pir*	Rif^r;Δ(*ara-leu*) *araD*Δ*lacX74 galEgalK phoA20 thi-1 rpsE rpoB argE*(Am) *recA1* Tn*7*λpir	(Herrero *et al.*, 1990)
P. aeruginosa PAO1	Reference strain	(Stover *et al.*, 2000)
*P. aeruginosa*PAO1-Km	Km^r; wild type PAO1 with a Km cassette inserted in a neutral position downstream of *glmS*	This study
P. aeruginosa PAO1 Δ*mcpK*	*P. aeruginosa*PAO1 deletion mutant of Δ*mcpK* gene	This study
Plasmids		
pGEM-T	Ap^r; TA-cloning vector	Promega
pET28b(+)	Km^r; Protein expression plasmid	Novagen
p34S-Km3	Km^r, Ap^r; Km3 antibiotic cassette	(Dennis & Zylstra, 1998)
pET28-McpK-LBD	Km^r;pET28b(+) derivative containing DNA fragment encoding McpK-LBD	This study
pUC18NotI	Ap^r; *ori* pMB1, similar to pUC18 but with NotI sites flanking the MCS; cloning vector	Purchased from Biomedal
pUC18NotI-5072Up	Ap^r; pUC18NotI derivative containing a 0.3-kb HindIII-XbaI fragment of upsteam region of *pa5072*	This study
pMAMV257	Ap^r; 1.4-kb PCR product containing the intergenic region between genes *pa5548* and *pa5549* (*glmS*) of *P. aeruginosa* PAO1 was inserted into the EcoRI/HindIII sites of pUC18NotI. A BamHI site was inserted into this intergenic region by PCR.	This study
pMAMV258	Ap^r, Km^r; 0.96-kb BamHI fragment containing *km3* cassette of p34S-Km3 was inserted into the BamHI downstream of *glmS* in pMAMV257	This study
pUC18NotI-5072UpDw	Ap^r; pUC18NotI derivative containing a 1-kb HindIII-EcoRI fragment containing upstream and downstream region of *pa5072*	This study
pKNG101	Sm^r; oriR6K, mob, sac; suicide vector	(Kaniga *et al.*, 1991)
pKNG101-PA5072UpDw	Sm^r; pKNG101derivative containing a 0.6 Kb NotI fragment from pUC18NotI-5072UpDw cloned into pKNG101	This study
pMAMV261	Sm^r, Km^r; 2.4-kb NotI fragment of pMAMV258 was cloned at the same site in pKNG101	This study
pRK600	Cm^r; *oriColE1*, RK2 *mob*$^+$, *tra*$^+$;helper plasmid	(de Lorenzo *et al.*, 1990)
pBBR1MCS-2	Km^r; broad-host-range cloning plasmid pBB1MCS derivative containing Km^r cassette, *mob*$^+$, *rep*$^+$	(Kovach *et al.*, 1995)
pBBR1MCS-2-McpK	Km^r; pBBR1MCS-2 derivative containing *mcpK* gene and its 607 bp upstream region	This study

The following abbreviations were used for antibiotics: kanamycin, km; chloramphenicol, cm; ampicillin, ap; rifampicin, rif; streptomycin, sm

The capillary was immersed into the cell suspension at its open end. After incubation for 30 min, the capillary was removed from the cell suspension, rinsed with water and emptied into an Eppendorf tube containing 1 ml M9 medium. Serial dilutions were made and 20 µl aliquots of the resulting cell suspension were plated onto agar plates containing M9 minimal medium supplemented with 15 mM succinate and incubated at 30 °C. Colonies were counted after growth for 24 hours. Positive (casamino acids) and negative (buffer only) controls were included in each experiment. Data shown are means from three independent experiments conducted in triplicate.

RNA extraction and RT-qPCR analysis

Two flasks with 20 ml of minimal medium M9 containing 10mM glucose were inoculated with an overnight culture to an OD_{600} of 0.05. At mid-exponential phase, 1 mM of αKG was added to one of the flasks and 0.5 ml samples were taken after 0, 15, 30 and 45 minutes. Total RNA was extracted using the High Pure RNA Isolation Kit (Roche Diagnostics) according to the manufacturer´s instructions. RNA was treated with Turbo DNAse (Ambion) and the RNA quality and quantity was analyzed by NanoDrop Spectophotometer and agarose gel electrophoresis. cDNA was synthesized from 500 ng of RNA using the SuperScript II Reverse Transcriptase (Invitrogene) and 200 ng of random primers following manufacturers' instructions. Quantitative PCR was performed using the iQ SYBR green supermix (BIO-RAD) in a MyiQ™2 thermocycler (BIO-RAD). The PCR protocol used was 95 °C for 5 min followed by 35 cycles of 95 °C (10 sec) and 60 °C (30 sec) and melting curve analysis from 55 to 95 °C, with increment of 0.5 °C/10 sec. Gene expression data were normalized to the expression of the reference gene *rpoD* and reported as normalized fold expression. The primers for *mcpK* and *rpoD* were designed using the Primer3 Plus software.

Construction of the strain PAO1-Km

The kamanycin-resistant strain *P. aeruginosa* PAO1-Km was constructed by homologous recombination using a derivative plasmid of the suicide vector pKNG101. The initial plasmid pMAMV257 was generated by separately amplifying the 5´ ends of the convergently-transcribed genes *pa5548* and *pa5549* (*glmS*) of *P. aeruginosa* PAO1. These PCR products were obtained using primers glmS-EcoRI_fw and gmlS-BamHI_rv (for amplifying 5´ end of *glmS*) and glmS-BamHI_fw and glmS-HindIII_rv (for amplifying 5´ end of *pa5548*). Subsequently, the PCR products were digested with EcoRI and BamHI (5´ end of *glmS*) or BamHI and HindIII (5´ end of *pa5548*) and ligated in a three-way ligation into pUC18Not. For the generation of the final PAO1-Km strain, the suicide plasmid pMAMV261 was transferred to *P. aeruginosa*PAO1by triparental conjugation using *E. coli* CC118λ*pir* and *E. coli* HB101 (pRK600) as helper. PAO1 cells, in which pMAMV261 has integrated into the chromosome, were selected on minimal medium containing 400 µg/ml streptomycin and 200 µg/ml kanamycin. To select derivatives that had undergone a second crossover event, sucrose was added to a final concentration of 10% (w/v). The final PAO1-Km strain was confirmed by PCR and sequencing.

Competitive root colonization assays

Sterilization, germination and inoculation of maize seeds was carried out as described previously, with minor modifications (Matilla *et al.*, 2007). Briefly, sterile seeds were incubated for 1 h at 30 °C with a 10^7 CFU/ml 1:1 mixture of PAO1-Km and Δ*mcpK*. Thereafter, seeds were rinsed with sterile deionized water and planted in 50 ml Sterilin tubes containing 40 g of sterile washed silica sand and 10% (v/w) plant nutrient solution supplemented with Fe-EDTA and micronutrients. Plants were maintained at 24 °C with a daily light period of 16 h. After 7 days, bacterial cells were recovered from the rhizosphere or from 1 mm of the main root apex, as described previously

(Matilla *et al.*, 2007). Serial dilutions were plated in LB-agar and LB-agar medium supplemented with 400 µg/ml of kanamycin, to select the wild type strain PAO1-Km.

RESULTS

Alpha-ketoglutarate causes the most pronounced increase in thermal stability of the PA5072-LBD

To identify the putative LBD of chemoreceptor PA5072, its sequence was analyzed using the DAS transmembrane prediction algorithm (Cserzo *et al.*, 1997). Two transmembrane regions were identified that flank the segment of amino acids 38 to 293, which likely corresponds to the periplasmic LBD (Supp. Fig. 9). The DNA fragment encoding the PA5072-LBD was cloned into an expression vector, the protein overexpressed in *E. coli* and purified from the soluble fraction of the *E. coli* lysate.

To identify whether and which ligand bind may bind to this domain, we carried out thermal shift assays in high throughput screening format as reported by McKellar and coworkers (McKellar *et al.*, 2015). In this assay, a temperature gradient is applied to a mixture of the purified protein and a fluorescent compound. During protein unfolding buried hydrophobic parts of the protein will be exposed leading to additional dye binding, causing fluorescent changes, which is the signal recorded. Consequently, this assay permits the calculation of the Tm value, which corresponds to the temperature at which half of the protein is in its native form and half is in the unfolded form (Krell, 2015). Ligand binding to a protein causes typically Tm changes, which gives useful initial information as to the identification of potential ligands. This assay has been essential to gain initial insight into the specificity of several chemoreceptors (McKellar *et al.*, 2015, Corral-Lugo *et al.*, 2016, Fernandez *et al.*, 2016).

The thermal shift assays of ligand-free PA5072-LBD resulted in a Tm of 38.7 °C. Ligands tested included different bacterial carbon-, nitrogen-, phosphorous- and sulfur sources as well as to

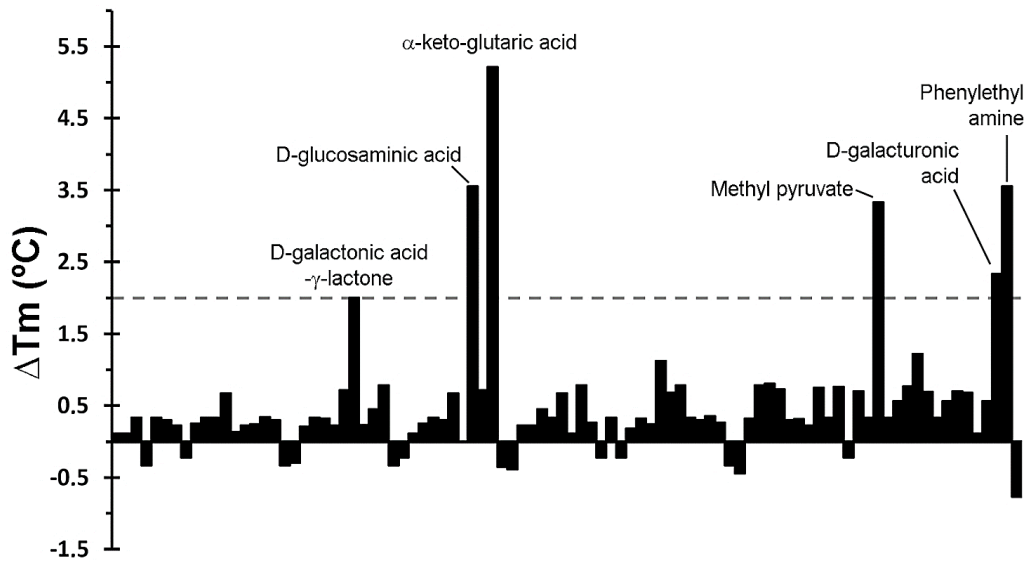

Figure 21. Thermal shift assays of the recombinant ligand binding domain of the PA5072/McpK chemoreceptor in the presence of bacterial carbon sources from the Biolog screen plate PM1. Shown are changes in Tm respective to the protein without ligand (38.7 °C). A list of the individual compounds in this screen is provided in Supp. Fig. 9. Compounds that caused Tm shifts of at least 2 °C are annotated.

nutrient supplements (http://208.106.130.253/pdf/pm_lit/PM1-PM10.pdf). As a representative example, the Tm changes induced by compounds of plate PM1 are shown in Fig. 1. A total of 13 compounds were identified that increased or decreased the Tm by at least 2 °C (Supp. Table 4), which is the generally accepted threshold for a relevant ligand-induced change in protein stability. This analysis showed also that α-KG acid caused with 5.2 °C the most pronounced Tm increase.

α-ketoglutarate binds with positive cooperativity to PA5072-LBD

Thermal shift assays provide initial information on ligands that bind but represent no evidence of binding. A valid criterion to ascertain binding are isothermal titration calorimetry (ITC)(Krell, 2008) binding experiments. PA5072-LBD was titrated with all compounds that caused Tm changes of at least 2 °C (Supp. Table 4). In these experiments αKG was the only compound that showed binding and the corresponding titration data are shown in Fig. 22. The titration caused exothermic heat changes (down going peaks), but the biphasic titration curve indicates that the reaction is more complex than the binding of a ligand to a single site at a macromolecule. Data analysis was carried out with several models for the dependent or independent binding of ligands to multiple sites. A very satisfactory curve fit was obtained using a model for the cooperative binding of a molecule to two sites. The initial binding event was characterized by a K_{d1} of 301.4 ± 0.2 μM ($\Delta H1$=-0.16 ± 0.05 kcal/mol), whereas the second event had a K_{d2} of 80.90 ± 0.05 μM (ΔH_2=-2.99 ± 0.15 kcal/mol). The cooperativity factor μ was of 4.41 (with μ of 1 for a non-cooperative process), indicating an approximately 4-fold increase in binding affinity of the second binding event as compared to the initial event. Alpha-KG binds thus with positive cooperativity to PA5072-LBD.

The criterion to establish that a given compound does not bind is the absence of binding heats in experiments conducted at two different analysis temperatures to exclude the possibility

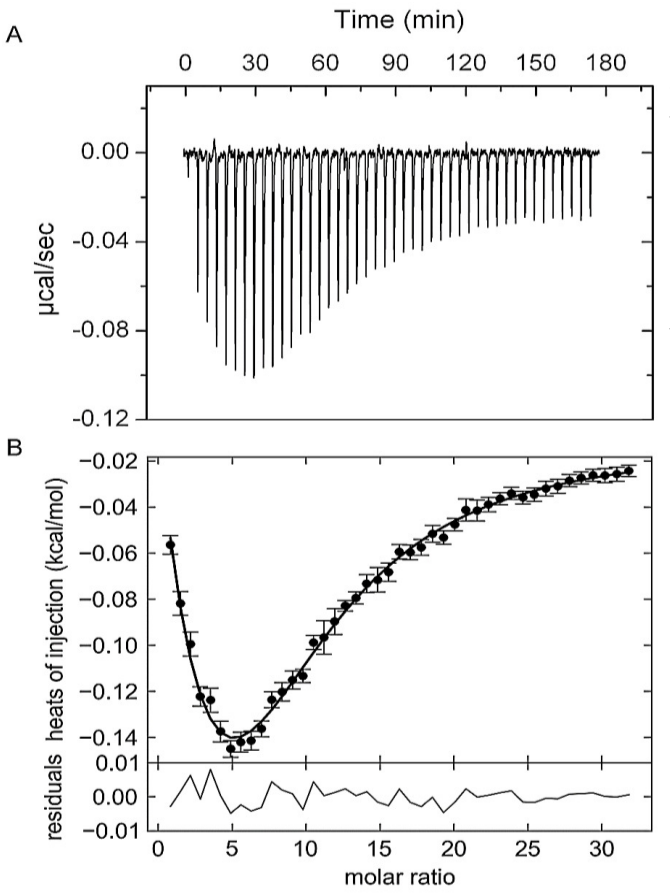

Figure 22. Isothermal titration calorimetry data for the binding of αKG to the ligand binding domain of the McpK chemoreceptor. A) Heat changes caused by the injection of 3 mM αKG into 20 μM McpK-LBD. B) Dilution heat-corrected and concentration-normalized integrated peak areas of raw data. The solid line shows the best fit with "the two symmetric-site binding model" of the SEDPHAT program. The residual of the curve fit are shown in the lower part of the figure.

that exothermic and endothermic contributions to binding cancel out each other at a given analysis temperature. Therefore, binding of compounds that failed to bind at 20 °C were also analyzed at 10 °C, which in all cases confirmed the absence of binding. As additional control experiment, αKG was titrated into mixtures of protein with ligands that did not cause binding heats to verify protein integrity. In summary, of the compounds that caused significant Tm shifts, only αKG was confirmed as PA5072 ligand.

We then explored by ITC whether other compounds that are structurally similar to αKG may bind to PA5072-LBD and the 15 ligands selected for further ITC studies are provided in Supp. Table 4. In analogy to the above results, we were unable to detect any binding and concluded that PA5072 binds exclusively αKG. The receptor was therefore named McpK (methyl-accepting chemotaxis protein K).

McpK-LBD dimer stabilization by αKG binding

The unexpected observation of binding with positive cooperativity indicates the presence of higher oligomeric states of the protein analyzed. To assess this issue, we carried out analytical ultracentrifugation studies of McpK-LBD in the absence and presence of αKG. Initial sedimentation velocity studies of ligand free protein revealed two species with standard sedimentation coefficients of $s_{20,w}$= 2.45 S and $s_{20,w}$= 3.18 S (Fig. 23; note: these values are standard values normalized for migration in water, whereas Fig. 23 shows the experimental data recorded in buffer). The frictional ratio (*fr*) for the peak at 2.45 S is 1.5, indicative of a rather elongated protein morphology, which agrees with the structure of HBM domains (Pineda-Molina *et al.*, 2012, Ortega & Krell, 2014). Based on this frictional ratio and using the diffusional scaling law of SEDFIT and the Svedberg equation, the average molar mass of the protein was determined 31.1kDa, which is very close to the sequence-derived mass of the monomer (30.5 kDa). The peak of the fast sedimenting species ($s_{20,w}$= 3.18 S) shows a similar *fr* corresponding to an elongated particle. The molar mass extracted was 45.8 kDa, which may point to a virtual intermediate species resulting from the fast equilibrium between the monomers and dimers. Such virtual species have been observed previously for the analysis of the homologous domain of the *P. putida* KT2440 McpQ chemoreceptor (Martin-Mora *et al.*, 2016b). When the experiment was conducted in the presence of 1 mM αKG a single peak with $s_{20,w}$= 3.58 S was observed that translates to a species with a molecular mass of 58.7 kDa, close to the sequence derived mass of the protein dimer (61 kDa).

The self-association behavior observed by sedimentation velocity was further demonstrated

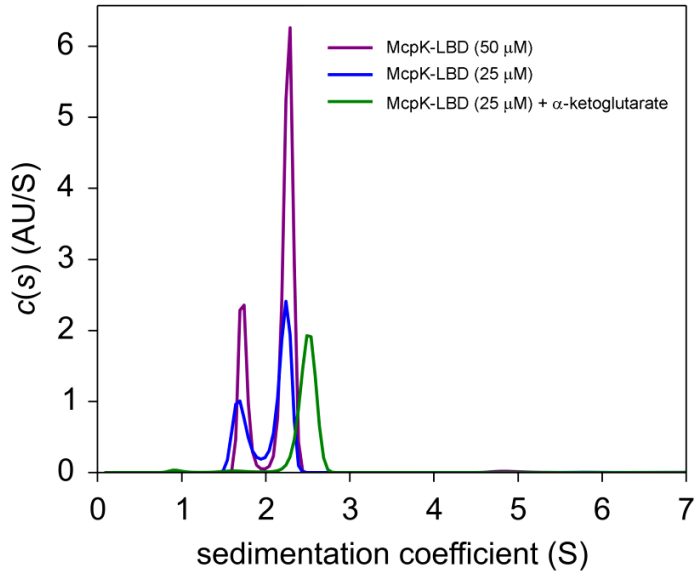

Figure 23. Determination of the oligomeric state of McpK-LBD by sedimentation velocity analytical ultracentrifugation. Shown are sedimentation coefficient distributions of McpK-LBD in the absence and presence of 1 mM α-ketoglutarate.

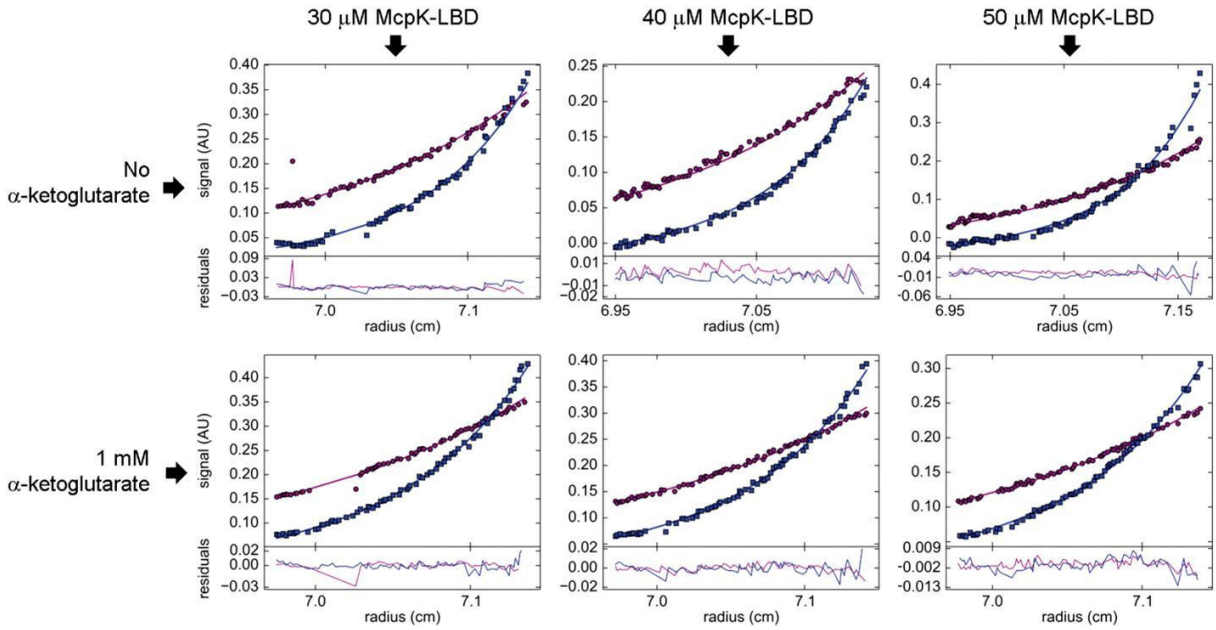

Figure 24. Study of McpK-LBD dimer association by sedimentation equilibrium analytical ultracentrifugation. Sedimentation equilibrium profiles of McpK-LBD at a speed of 9,740 (purple) and 20,606 x g (blue), at three different protein concentrations and in the absence and presence of 1 mM αKG. The best global fit is shown as a continuous line for both speeds along with the residuals of fitting in the lower part of the figure.

by multi-speed sedimentation equilibrium experiments. The sedimentation equilibrium of McpK at three different concentrations was analyzed by a global fit that confirmed the presence of both the monomeric and dimeric species at all concentrations (Fig. 24). For ligand-free McpK-LBD a dimer self-dissociation constant of 55.0 μM could be determined. When this experiment was repeated in the presence of 1mM αKG, a tighter association was observed, with an approximately 10-fold lower self-dissociation constant of 5.9 μM, confirming that αKG causes McpK-LBD dimer stabilization.

At the protein concentration used for ITC binding studies, McpK-LBD is thus partially present as dimer and the cooperativity observed is thus likely due to ligand binding to the different monomers of the dimer in a way that the initial binding to one monomer of the dimer enhances the affinity for the second monomer.

McpK mediates chemotaxis to αKG

Chemoreceptors can either mediate chemotaxis, have alternative cellular functions or are responsible for type IV pili mediated motility (Wuichet & Zhulin, 2010). To determine McpK function, we generated a *mcpK* deletion mutant and carried out quantitative capillary chemotaxis assays. Initially, control experiments were conducted to assess chemotaxis of the wt and mutant strain towards casamino acids. The choice of this chemoattractant was based on the fact that the chemotaxis towards amino acids is mediated by the three well-characterized chemoreceptors PctA, PctB and PctC (Taguchi *et al.*, 1997, Rico-Jimenez *et al.*, 2013a). As shown in Supp. Fig. 11, deletion of *mcpK* did not alter significantly chemotaxis to casamino acids, indicating that this mutation did not cause any general motility defect.

Subsequently, chemotaxis assays towards different αKG concentrations were performed. Experiments showed that the wt strain has significant taxis to αKG concentrations between 5 μM and 5mM, with an optimal response at 500 μM (Fig. 25). Importantly, the deletion of the *mcpK* gene resulted in a drop in the chemotactic response to close to baseline levels. Complementation of this

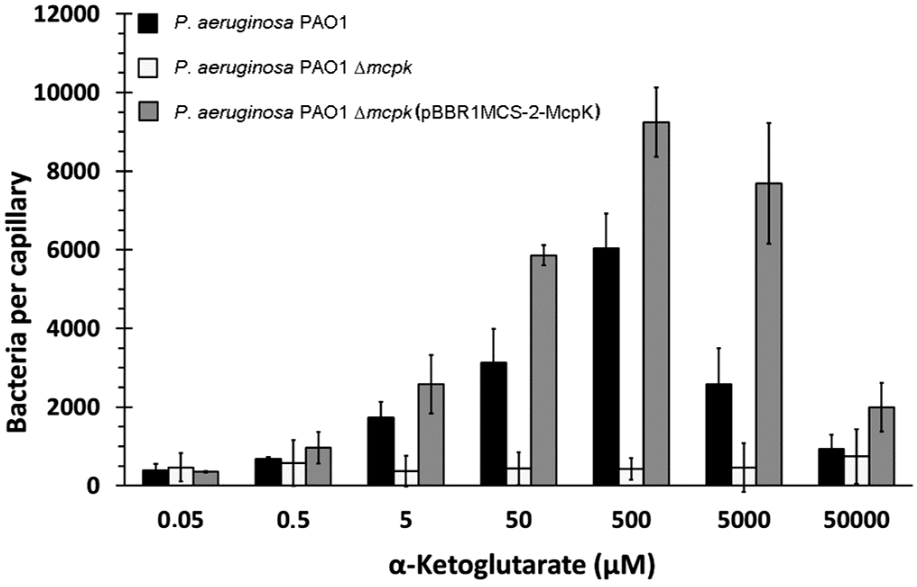

Figure 25. The effect of McpK on α-ketoglutarate chemotaxis. Quantitative capillary chemotaxis assays of *P. aeruginosa* PAO1, *P. aeruginosa* Δ*mcpK* and the complemented mutant *P. aeruginosa* Δ*mcpK* (pBBR1MCS-2-McpK) towards different αKG concentrations. Data were corrected with the number of cells that swam into buffer-containing capillaries (833 ± 106). Shown are means and standard errors from three independent experiments, each conducted in triplicate.

mutant by the *in trans* expression of the *mcpK* gene restored wild type like chemotaxis at all concentrations (Fig. 25). In order to determine whether the observed chemotaxis defect in the *mcpK* mutant is the result of an altered metabolism, we performed growth curves in M9 minimal medium supplemented with αKG and succinate as carbon sources. As shown in Supp. Fig. 10, there were no differences between the wt and mutant strain. Taken together, these data show that McpK is the primary chemoreceptor for αKG in *P. aeruginosa* PAO1.

Alpha-ketoglutarate does not regulate *mcpK* expression

We have recently assessed the effect of chemoeffectors on the gene expression of their cognate chemoreceptors in *P. putida* KT2440 (Lopez-Farfan *et al.*, 2017). We were able to show that the expression of a significant number of chemoreceptor genes is either up- or downregulated by the cognate chemoeffectors. However, this was not the case for genes encoding chemoreceptors that respond to TCA cycle intermediates, namely *mcpS*, *mcpQ* and *mcpR* that were expressed independently of the presence or absence of their cognate ligands.

To assess *mcpK* expression, we carried out real-time quantitative PCR measurements. Fig. 26A shows *mcpK* transcript levels of samples taken during mid-exponential phase in comparison to those of the housekeeping genes *gyrB* and *rpoD* as well as to genes encoding functionally characterized chemoreceptors such as the amino acid sensors PctA and PctC (Taguchi *et al.*, 1997), the Pi responsive CtpH (Wu *et al.*, 2000) or the TlpQ chemoreceptor that mediates taxis to ethylene (Kim & Tokura, 2007). Data show that *mcpK* transcript levels are low as compared to the housekeeping genes and in between most and less abundant chemoreceptor transcripts.

In subsequent experiments we assessed the effect of αKG on *mcpK* expression. However, the addition of αKG to *P. aeruginosa* cultures grown in M9 minimal medium supplemented with glucose did not alter *mcpK* expression (Fig. 26 B). Data thus show that, in analogy to the TCA cycle intermediate responsive chemoreceptors in *P. putida* KT2440, the cognate chemoeffector αKG does not modulate *mcpK* expression. Further experiments will show whether the constitutive expression

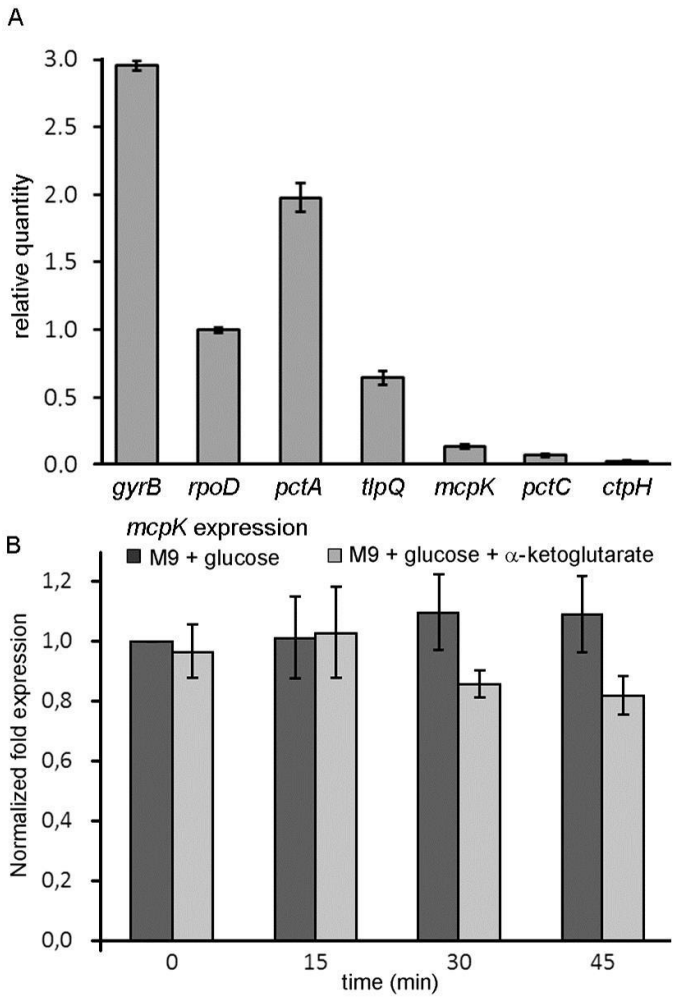

Figure 26. Expression of the *mcpK* gene in the absence and presence of α-ketoglutarate. A) RT-qPCR measurements of the relative transcript levels of *P. aeruginosa mcpK, pctA, tlpQ*, *pctC* and *ctpH* chemoreceptor genesas well as of the housekeeping genes *gyrB* and *rpoD*. Cells were grown in M9 minimal medium supplemented with 10mM glucose and samples taken at mid-exponential phase. B) Gene expression of *mcpK* in the absence and presence of 1 mMαKG. Cells were grown to mid-exponential phase in M9 supplemented with 10 mM glucose and samples were taken after 0, 15, 30 and 45 min. The results are expressed as the relative expression of *mcpK* normalized with the transcript level of the reference gene *rpoD* at time 0 in the absence of αKG. Data shown are the average of two independent experiments.

of TCA cycle intermediate responsive chemoreceptors, as observed in *P. putida* and *P. aeruginosa,* is a general feature.

McpK mediated chemotaxis does not affect plant root colonization

P. aeruginosa is a universal pathogen that is also able to colonize and infect different plants (Rahme *et al.*, 2000, Cao *et al.*, 2001, Walker *et al.*, 2004, Attila *et al.*, 2008). The web-based resource PIFAR allowed the identification of 175 gene products in *P. aeruginosa* putatively involved in the interaction with plants (Martinez-Garcia *et al.*, 2016) and the TlpQ chemoreceptor was found to mediate chemotaxis towards the plant hormone ethylene (Kim *et al.*, 2007). αKG is present at significant levels in plant root exudates (Tawaraya *et al.*, 2014, Ganie *et al.*, 2015) and chemotaxis to root exudate components was shown to be essential for efficient root colonization (de Weert *et al.*, 2002, Scharf *et al.*, 2016).

To determine the role of McpK in the colonization of the rhizosphere, we performed competitive colonization assays using maize as model plant. Initial experiments showed that *P. aeruginosa* colonizes the maize rhizosphere at a density of around 5 x 10^7 bacteria per gram of root. To distinguish between the wild type and the mutant strain, a kanamycin-resistant *P. aeruginosa* wild type strain was generated. This strain contains a kanamycin cassette inserted downstream of theglucosamine-6-phosphate synthetase encoding gene, *glmS*. This region was demonstrated to be neutral in multiple *Pseudomonas* strains, including *P. aeruginosa* (Koch *et al.*, 2001, Matilla *et al.*, 2007). The resulting strain, *P. aeruginosa* PAO1-Km, was shown to mediate chemotaxis to αKG (and

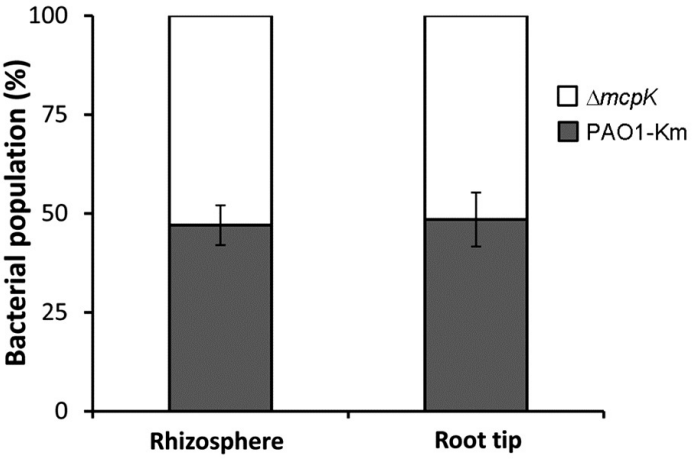

Figure 27. Competitive root colonization of *P. aeruginosa* PAO1-Km and *P. aeruginosa* Δ*mcpK*. The figure represents the percentage of bacteria recovered either from the rhizosphere or root tips of maize (*Zea mays*) plants. Data are the means and standard deviations of 6 plants.

other known chemoattractants) at the same levels as PAO1 (Supp. Fig. 12). Competitive colonization assays showed that the fitness of the mutant in *mcpK* in the rhizosphere was similar to the strain PAO1-Km (Fig. 27). Additionally, the strain Δ*mcpK* also colonized root tips at the wild type levels (Fig. 27).

DISCUSSION

Chemoreceptors can be classified according to their ligand spectrum into receptors that recognize various, structurally related chemoeffectors and those that appear to be specific for a single chemoeffector. Examples of the former group are receptors for different L-amino acids (Taguchi *et al.*, 1997, Glekas *et al.*, 2012, Oku *et al.*, 2012, Brennan *et al.*, 2013, Rico-Jimenez *et al.*, 2013a, Webb *et al.*, 2016), cyclic organic acids (Luu *et al.*, 2015), purines (Fernandez *et al.*, 2016), polyamines (Corral-Lugo *et al.*, 2016), aromatic hydrocarbons (Lacal *et al.*, 2011a), C4 to C6 organic acids (Lacal *et al.*, 2010a, Parales *et al.*, 2013) or C2- and C3-organic acids (Garcia *et al.*, 2015). Chemoreceptors that appear to respond to a single compound include the citrate specific chemoreceptors Tcp of *Salmonella typhimurium* (Yamamoto & Imae, 1993) and McpQ of *P. putida* KT2440 (Martin-Mora *et al.*, 2016b), the malate specific receptor PA2652 in *P. aeruginosa* or the GABA specific McpG of *P. putida* KT2440 (Reyes-Darias *et al.*, 2015b). Here we report with McpK another chemoreceptor that binds specifically a single compound, αKG. Interestingly, the ligands of these specific chemoreceptors are either part of or closely linked to the TCA cycle (note: GABA is part of the GABA shunt converting αKG into succinate). The evolution of specific chemoreceptors suggests that these compounds are of importance to the microorganism. The existence of a chemoreceptor dedicated to αKG may be linked to the central metabolic role of this compound (Fig. 28). Apart from being part of the TCA cycle, αKG also represents a branch point from which other important metabolic pathways depart such as the GABA shunt, biosynthetic pathways for several amino acids and coenzyme B or the purine and pyrimidine synthesis.

Several important chemoattractants have a dual function and exert metabolic as well as signaling roles. Examples are GABA, the only ligand of *P. putida* KT2440 McpG (Reyes-Darias *et al.*, 2015b), and putrescine, the high-affinity ligand of McpU of the same species (Corral-Lugo *et al.*, 2016). Both compounds serve as carbon and nitrogen sources and also exert functions as signaling molecules. Alpha-KG belongs to the same class of compound. Apart from being a carbon source it was shown to modulate the activity of the NtrB/NtrC TCS for the control of nitrogen utilization processes (Li & Lu, 2007). The activity of this TCS is regulated by the small protein PII that senses αKG as carbon signal and glutamine as nitrogen signals (Ninfa & Jiang, 2005). In addition, a model was proposed in which αKG regulates in *P. aeruginosa* the activity of another TCS, namely the

MifS/MifR system, which regulates genes that are involved in αKG transport and subsequent metabolism (Tatke *et al.*, 2015).

In contrast to the dCACHE domain that recognizes ligands in the monomeric state (Rico-Jimenez *et al.*, 2013a), the HBM and 4-HB domain need to be dimeric for ligand recognition (Milburn *et al.*, 1991, Lacal *et al.*, 2010a, Martin-Mora *et al.*, 2016b). This is due to the fact that the ligand binding sites are at the dimer interface and that amino acids from both monomers of the dimer are involved in ligand binding (Milburn *et al.*, 1991, Pineda-Molina *et al.*, 2012). Tsr (Lin *et al.*, 1994) and Tar (Milligan & Koshland, 1993, Biemann & Koshland, 1994, Danielson *et al.*, 1994) that both contain a 4HB domain, bind serine and aspartate, respectively, with a 1 per dimer stoichiometry, which is due to an extreme form of negative cooperativity in which ligand binding to the first monomer causes a dramatic reduction of affinity for the second monomer of the dimer. This negative cooperativity has been observed for the full-length receptor (Biemann & Koshland, 1994, Lin *et al.*, 1994) as well as for the individual, recombinant LBDs (Milligan & Koshland, 1993, Danielson *et al.*, 1994). In marked contrast, McpK-LBD bound its ligand with positive cooperativity. In contrast to the very strong negative cooperativity observed for Tar and Tsr, the positive cooperativity at McpK-LBD was more modest and ligand binding at the first monomer increased affinity of the second ligand by approximately 4-fold. To our knowledge, this is the first report on a chemoreceptor-LBD that recognizes its ligands in positively cooperative manner. The evolution of a receptor with positive cooperativity may be straight forward, since it was shown that the mutation of a single amino acid at the dimer interface of Tar converts its negative cooperativity into positive cooperativity (Kolodziej *et al.*, 1996). Further experiments will provide insight as to the functional or physiological reasons for ligand recognition with positive cooperativity.

Analytical ultracentrifugation studies show that αKG binding stabilizes the dimer. Equilibrium studies showed that αKG binding reduces the dimer self-dissociation constant from 55 μM to 5.9 μM. Chemoeffector mediated LBD dimer stabilization appears to be a general feature of 4HB and HBM domains since similar observations have been made for Tar-LBD (Milligan & Koshland, 1993, Yu *et al.*, 2015), McpQ (Martin-Mora *et al.*, 2016b), McpS (Lacal *et al.*, 2010a).

The expression of the genes of a significant number of *P. putida* chemoreceptors is modulated by their cognate ligands (Lopez-Farfan *et al.*, 2017). However, exceptions were the TCA cycle intermediate responsive chemoreceptor genes that are expressed constitutively. It was hypothesized that the omnipresence in natural habitats and metabolic importance of TCA cycle intermediates may be responsible for this constitutive expression (Lopez-Farfan *et al.*, 2017). The present finding that αKG does not modulate *mcpK* expression provides further support to this hypothesis.

Chemotaxis to plant root exudates was shown to promote bacterial colonization (de Weert *et al.*, 2002, Reyes-Darias *et al.*, 2015b, Scharf *et al.*, 2016). However, the deletion of the *mcpK* gene did not cause any significant differences in maize root colonization. Root exudates are complex mixtures of mainly sugars, amino acids and organic acids. A significant part of *P. aeruginosa* chemoreceptors is likely to respond to exudate components (like PctA, PctB and PctC) and therefore the effects caused by the elimination of a single chemoreceptor is compensated by other root exudate responsive receptors. We have shown that the elimination of the GABA specific McpG receptor did reduce root colonization (Reyes-Darias *et al.*, 2015b). However, GABA recognition at McpG-LBD (K_D=175 nM) was much tighter than αKG binding to McpK-LBD (K_{d1}=301 μM, $K_{d2=}$ 81 μM).

Chemoreceptors contain a variety of different LBD types (Lacal *et al.*, 2010b, Upadhyay *et al.*, 2016) and a central question in understanding this diversity is to elucidate whether there is a relationship between the LBD type and the structure of the chemoeffector recognized. In this aspect first tendencies have appeared and it was suggested that sCACHE domains may be linked to the recognition of C2- and C3-carboxylic acids (Garcia *et al.*, 2015), whereas the dCACHE domain may be

the dominant domain for the recognition of L-amino acids (Glekas *et al.*, 2012, Oku *et al.*, 2012, Liu *et al.*, 2015, Reyes-Darias *et al.*, 2015a). The alignment of all members of the HBM domain family revealed the conservation of amino acids of the ligand binding cavity (Ortega & Krell, 2014). Since C4 to C6 organic acids were found to bind to the first characterized member of this family, McpS, it was proposed that the HBM domain may be associated with the recognition of organic acids (Ortega & Krell, 2014). This hypothesis was supported by the identification of other HBM domain containing chemoreceptors that mediate taxis to this class of compound such as the citrate specific McpQ as well as McfS/McfQ (Parales *et al.*, 2013) and Pfl01_0728 that all respond to organic acids (Oku *et al.*, 2014). The identification of McpK as another HBM family member that binds to an organic acid lends further support to this hypothesis. Establishing LBD type – chemoeffector relationships will permit to orient experiments to a certain group of compounds, which in turn will accelerate the functional annotation of receptors.

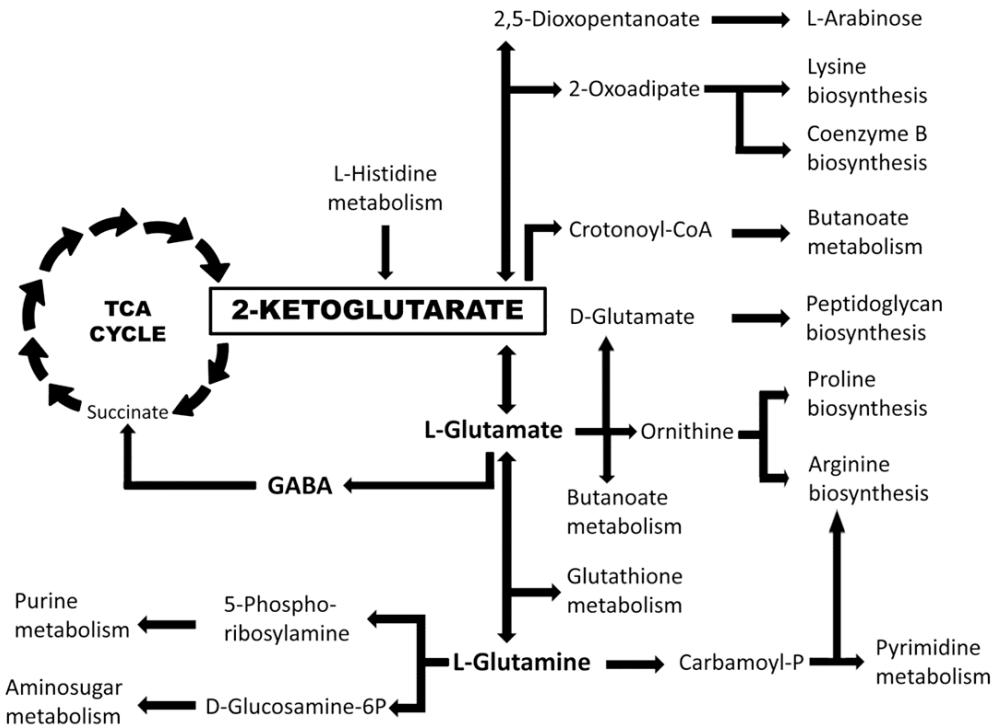

Figure 28. The central role of αKG in the metabolism of *P. aeruginosa* PAO1. Implication of αKG in key metabolic pathways as derived from the KEGG (Kanehisa *et al.*, 2016) map of *P. aeruginosa* PAO1.

SUPPLEMENTARY MATERIAL

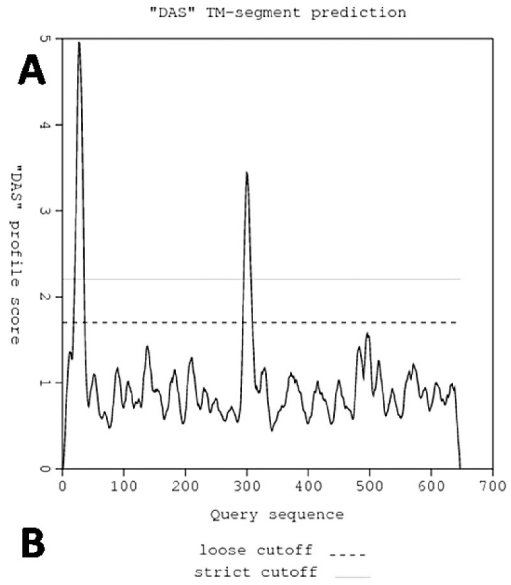

>PA5072/McpK.
MYDWWVLQLAKLSVSRKLMVGFGVLLALLLLVVISSNRTLTHQTALSEQLAEVASLMEQT
QQAEQGRLAFEAGSDPRQAEQVRQTLAGMLQRLQALRDSELDPAALAHQVEAIEAYRKAF
DDLAAADQQRSAARGVLVGTAQQALDSFARLEELMDASLAQQAGDPQALQRSRAVADLHQ
QLLMVRYQVRGYVFERSDKAEQAAFAAFDALRQAATTLRGQLPGEADAALEQAMGSLQGY
RGGIEQFRAGVIRTRQAQQAMQSSTQDMARAGRTLTEAGRQLRESTASRDRASLWLIAAL
ALAFGCVAGWAINRQIVRPLDEALAQAEAIAAGDLGKRPQNPLTLQRRDELGQLQRVMQR
MGDSLRELVGRISDGVSQLASSAEELSAVTEQTRAGVNSQKVETDQVATAMHEMAATVQD
VARNAELASQAARQADEEARQGDAVVDQAVTRIERLASEMDVSSEAMARLKNESEQIGSV
LDVIKSVAEQTNLLALNAAIEAARAGDAGRGFAVVADEVRGLAQRTQQSTAEIEGLIQRL
QQGAGEAAERLENSRSLTASTVELARRAGAALDSITRTVSDIQNMNLQIATAAEQQSTVA
EEINRSVLSVRDVAEQSAAASEQTAASSGELARLGTQLQAQVGRFRL

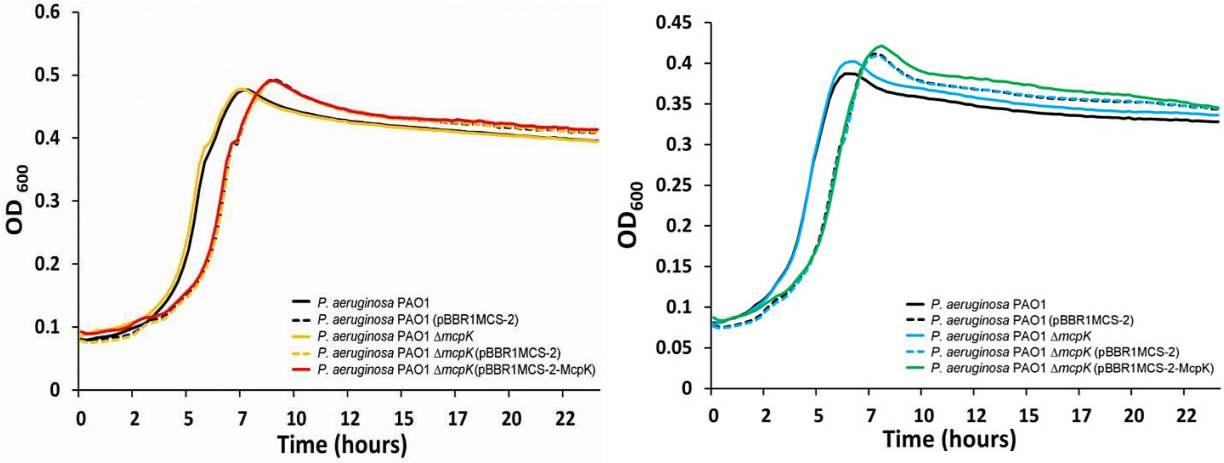

Supp. Fig 9. Prediction of transmembrane regions of chemoreceptor PA5072 from *P. aeruginosa* PAO1. A) Output from the DAS transmembrane prediction server (Cserzo *et al.*, 1997). B) Sequence of the PA5072/McpK chemoreceptor with the two transmembrane regions predicted highlighted in red.

Supp. Fig 10. Growth curve of different strains in M9 minimal medium supplemented with 10 mM α-ketoglutarate (left) or succinate (right).

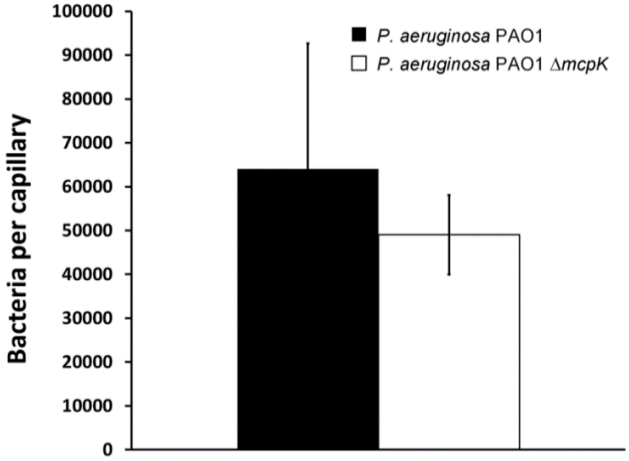

Supp. Fig 11. Quantitative capillary chemotaxis assays of *P. aeruginosa* towards 0.1 % (w/v) casamino acids. Shown are means and standard deviations from three independent experiments conducted in triplicate.

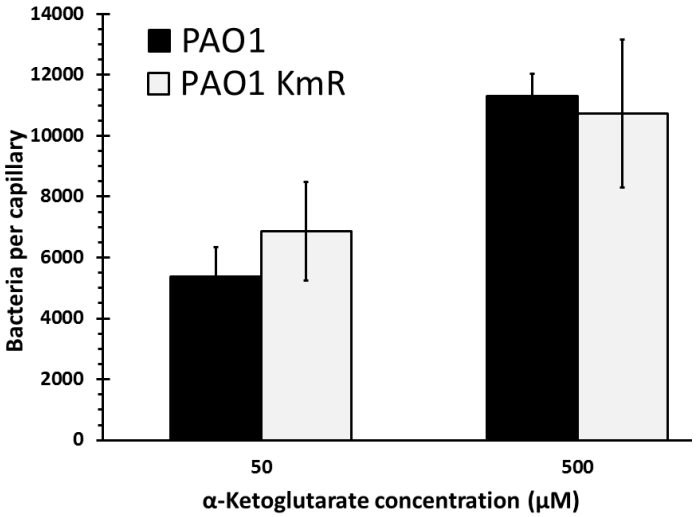

Supp. Fig 12. Chemotaxis of *P. aeruginosa* PAO1 and *P. aeruginosa* PAO1-Km to alpha-ketoglutarate. Shown are means and standard deviations from two experiments conducted in triplicates.

Supp. Table 3. Oligonucleotides used in this study

Name	Sequence (5'-3')	Purpose
McpK-LBD_fw	CATATGAGCAACCGCACCCTCACG	Cloning of McpK-LBD into expression vector
McpK-LBD_rv	GGATCCTTAGCTGGCGCGGTCG	Cloning of McpK-LBD into expression vector
PA5072UpF-HindIII	ATAAAGCTTAAAAACTCCGGTAAAAGACTGAAGGT	Generation of Δ*mcpK* mutant
PA5072UpR-XbaI	CTAGTCTAGACTAGCGTCATTACTCCAGGCAGTGCG	Generation of Δ*mcpK* mutant
PA5072DownF-XbaI	CTAGTCTAGACTAGGACATCCAGAACATGAACCTGCA	Generation of Δ*mcpK* mutant
PA5072DownR-EcoRI	AAGAATTCTGGCGTCATCTCCCAAAAGGC	Generation of Δ*mcpK* mutant
glmS-EcoRI_fw	TAATGAATTCGTGCGCGAATCCGACCTGAC	Generation of PAO1-Km strain
glmS-BamHI_rv	TAATGGATCCCGGCGTTACTCGACGGTGAC	Generation of PAO1-Km strain
glmS-BamHI_fw	TAATGGATCCGCTCGCTGTCAATCGCGCAAC	Generation of PAO1-Km strain
glmS-HindIII_rv	TAATAAGCTTGCTGGTCTTCCTGATGGCACG	Generation of PAO1-Km strain
McpK-comp_fw	TAATGGTACCGTGCTGCTGAACAGCTACCG	Generation of complementation plasmid
McpK-comp_rv	TAATTCTAGACCCAAAAGGCGAAAGCCTGA	Generation of complementation plasmid
mcpK_fw	TGCTTCTGCTGGTGGTGATC	qRT-PCR of the *mcpK* gene
mcpK_rv	TTGCTGGGTCTGTTCCATCAG	qRT-PCR of the *mcpK* gene
rpoD_fw	AGAAGAAAGCGACGACAGCA	qRT-PCR of the *rpoD* gene
rpoD_rv	CTTCTTGGCCTTGTCGAGCT	qRT-PCR of the *rpoD* gene
gyrB_fw	CTGAACACCAACAAGACCGC	qRT-PCR of the *gyrB* gene
gyrB_rv	TCGTTGAAGCTGTCGTTCCA	qRT-PCR of the *gyrB* gene
tlpQ_fw	TGAAAAGCGCCAGTACACAG	qRT-PCR of the *tlpQ* gene
tlpQ_rv	CCATGAAATAGCGCTGGATGC	qRT-PCR of the *tlpQ* gene
ctpH_fw	CGAAGACGTGATGGAAGAAACG	qRT-PCR of the *ctpH* gene
ctpH_rv	TTTCCAATTGGCGGATGACC	qRT-PCR of the *ctpH* gene
pctA_fw	TTCGCACTGTTCACCCTCTAC	qRT-PCR of the *pctA* gene
pctA_rv	ATGTTGCTGGAAGTCACGTC	qRT-PCR of the *pctA* gene
pctC_fw	TTTTCGCCTTCAGCTGCTTC	qRT-PCR of the *pctC* gene
pctC_rv	TTTCCCCGAGGTAGTTTTCCG	qRT-PCR of the *pctC* gene

Supp. Table 4. Binding studies of different ligands to recombinant McpK-LBD. The upper part shows compounds that altered the McpK-LBD Tm by at least 2 °C in a thermal shift assays screen of compounds listed in http://208.106.130.253/pdf/pm_lit/PM1-PM10.pdf. The last column indicates the outcome of ITC studies of these compounds to McpK-LBD. The lower part shows compounds with structural similarity to αKG that were analyzed for binding to McpK-LBD by ITC.

Ligand	Tm Shift (°C)	ITC binding to recombinant McpK-LBD
Compounds that caused Tm shifts of at least 2 °C		
α-ketoglutarate	+5.2	Yes
Uracil	+4.2	No
γ-aminobutyric acid	+4.1	No
5-aminovaleric acid	+3.9	No
Carbamyl phosphate	+3.5	No
Phenylethylamine	+3.5	No
D-glucosaminic acid	+3.5	No
Methyl pyruvate	+3.3	No
L-glutamic acid	+2.3	No
D-galacturonic acid	+2.3	No
L-glutamine	+2.2	No
D-galactonic acid-γ-lactone	+2	No
Itaconate	-2.2	No
Structurally related compounds		
Citrate	+0.8	No
Butyrate	+0.7	No
Malate	+0.5	No
Fumarate	+0.3	No
Tricarballylate	+0.3	No
Lactate	+0.2	No
Pyruvate	+0.1	No
Oxaloacetate	+0	No
Acetate	-0.2	No
Succinate	-0.3	No
cis-aconitate	Not tested	No
Isocitrate	Not tested	No
Valerate	Not tested	No
Glutarate	Not tested	No
2-aminoadipate	Not tested	No

CHAPTER 1.4: IDENTIFICATION OF A CHEMORECEPTOR IN *P. aeruginosa* PAO1 SPECIFIC FOR C4-DICARBOXYLIC ACIDS AND ASSESSMENT OF THE ROLE OF CHEMOEFFECTORS AND SIGNAL ANTAGONISTS

Published article

The activity of the C4-dicarboxylic acid chemoreceptor of Pseudomonas aeruginosa is controlled by chemoattractants and antagonists

David Martín-Mora, Álvaro Ortega, Francisco Pérez-Maldonado, Tino Krell, Miguel Ángel Matilla.

Dept. of Environmental Protection, Estación Experimental del Zaidín, Consejo Superior de Investigaciones Científicas

Scientific Reports (Published online 1 February2018); 8:2102.
doi: 10.1038/s41598-018-20283-7

ABSTRACT

Chemotaxis toward organic acids has been associated with colonization fitness and virulence and the opportunistic pathogen *P. aeruginosa* exhibits taxis toward several tricarboxylic acid intermediates. In this study, we used high-throughput ligand screening and isothermal titration calorimetry to demonstrate that the LBD of the chemoreceptor PA2652 directly recognizes five C4-dicarboxylic acids with K_D values ranging from 23 μM to 1.24 mM. *In vivo* experimentation showed that three of the identified ligands act as chemoattractants whereas two of them behave as antagonists by inhibiting the downstream chemotaxis signaling cascade. *In vitro* and *in vivo* competition assays showed that antagonists compete with chemoattractants for binding to PA2652-LBD, thereby decreasing the affinity for chemoattractants and the subsequent chemotactic response. Two chemosensory pathways encoded in the genome of *P. aeruginosa*, *che* and *che2*, have been associated to chemotaxis but we found that only the *che* pathway is involved in PA2652-mediated taxis. The receptor PA2652 is predicted to contain a sCACHE LBD and analytical ultracentrifugation analyses showed that PA2652-LBD is dimeric in the presence and the absence of ligands. Our results indicate the feasibility of using antagonists to interfere specifically with chemotaxis, which may be an alternative strategy to fight bacterial pathogens.

www.nature.com/scientificreports

SCIENTIFIC REPORTS

OPEN

The activity of the C4-dicarboxylic acid chemoreceptor of *Pseudomonas aeruginosa* is controlled by chemoattractants and antagonists

Received: 16 October 2017
Accepted: 15 January 2018
Published online: 01 February 2018

David Martín-Mora, Álvaro Ortega, Francisco J. Pérez-Maldonado, Tino Krell & Miguel A. Matilla

Chemotaxis toward organic acids has been associated with colonization fitness and virulence and the opportunistic pathogen *Pseudomonas aeruginosa* exhibits taxis toward several tricarboxylic acid intermediates. In this study, we used high-throughput ligand screening and isothermal titration calorimetry to demonstrate that the ligand binding domain (LBD) of the chemoreceptor PA2652 directly recognizes five C4-dicarboxylic acids with K_D values ranging from 23 µM to 1.24 mM. *In vivo* experimentation showed that three of the identified ligands act as chemoattractants whereas two of them behave as antagonists by inhibiting the downstream chemotaxis signalling cascade. *In vitro* and *in vivo* competition assays showed that antagonists compete with chemoattractants for binding to PA2652-LBD, thereby decreasing the affinity for chemoattractants and the subsequent chemotactic response. Two chemosensory pathways encoded in the genome of *P. aeruginosa*, *che* and *che2*, have been associated to chemotaxis but we found that only the *che* pathway is involved in PA2652-mediated taxis. The receptor PA2652 is predicted to contain a sCACHE LBD and analytical ultracentrifugation analyses showed that PA2652-LBD is dimeric in the presence and the absence of ligands. Our results indicate the feasibility of using antagonists to interfere specifically with chemotaxis, which may be an alternative strategy to fight bacterial pathogens.

A series of different signal transduction systems permit bacteria to sense changing environmental conditions and to generate adaptive responses. Next to one- and two-component systems, chemosensory pathways represent a major mechanism in bacterial signal transduction[1–3]. In these systems, the direct binding of chemoeffectors or chemoeffector-loaded periplasmic binding proteins to the ligand binding domain (LBD) of chemoreceptors[4] generates a molecular stimulus that alters the autophosphorylation of the histidine kinase CheA and consequently the transphosphorylation of the CheY response regulator, which represents the pathway output[2]. Chemosensory pathways were shown to mediate chemotaxis and type IV pili-based motility, or are involved in regulating alternative cellular processes[5–7].

The opportunistic pathogen *Pseudomonas aeruginosa* is an important model organism to investigate chemosensory pathways[8]. Its chemoreceptors feed into 4 different pathways. Two of these signalling cascades, *che* and *che2*, mediate flagellum-mediated taxis[9,10]. However, the *wsp* pathway controls c-di-GMP levels[5] whereas the fourth pathway, *chp*, is responsible for type IV pili-mediated motility[11,12] and the regulation of cAMP levels[13]. The function of most of the 26 *P. aeruginosa* chemoreceptors remains unknown but others have been characterized in depth, including the three paralogous receptors PctA, PctB and PctC for the chemotaxis to different amino acids[14–17] and the CtpH and CtpL[18,19] receptors that mediate chemoattraction to inorganic phosphate.

P. aeruginosa is a ubiquitous pathogen able to infect a broad range of different hosts such as human, animals, plants or fungi[20]. Part of our research interests consists in assessing how chemosensory signalling mechanisms compare in phylogenetically related species that have different lifestyles. To address this issue we study *P. putida*

Department of Environmental Protection, Estación Experimental del Zaidín, Consejo Superior de Investigaciones Científicas, Granada, Spain. Correspondence and requests for materials should be addressed to M.A.M. (email: miguel.matilla@eez.csic.es)

INTRODUCTION

A series of different signal transduction systems permit bacteria to sense changing environmental conditions and to generate adaptive responses. Next to one- and two-component systems, chemosensory pathways represent a major mechanism in bacterial signal transduction (Galperin, 2005, Laub & Goulian, 2007, Hazelbauer *et al.*, 2008). In these systems, the direct binding of chemoeffectors or chemoeffector-loaded periplasmic binding proteins to the LBD of chemoreceptors (Matilla & Krell, 2017) generates a molecular stimulus that alters the autophosphorylation of the histidine kinase CheA and consequently the transphosphorylation of the CheY response regulator, which represents the pathway output (Hazelbauer *et al.*, 2008). Chemosensory pathways were shown to mediate chemotaxis and type IV pili-based motility, or are involved in regulating alternative cellular processes (Hickman *et al.*, 2005, Zusman *et al.*, 2007, Wuichet & Zhulin, 2010).

The opportunistic pathogen *P. aeruginosa* is an important model organism to investigate chemosensory pathways (Kato *et al.*, 2008). Its chemoreceptors feed into 4 different pathways. Two of these signalling cascades, *che* and *che2*, mediate flagellum-mediated taxis (Ferrandez *et al.*, 2002, Guvener *et al.*, 2006). However, the *wsp* pathway controls c-di-GMP levels (Hickman *et al.*, 2005) whereas the fourth pathway, *chp*, is responsible for type IV pili-mediated motility (Darzins, 1994, Whitchurch *et al.*, 2004) and the regulation of cAMP levels (Fulcher *et al.*, 2010). The function of most of the 26 *P. aeruginosa* chemoreceptors remains unknown but others have been characterized in depth, including the three paralogous receptors PctA, PctB and PctC for the chemotaxis to different amino acids (Taguchi *et al.*, 1997, Rico-Jimenez *et al.*, 2013a, Reyes-Darias *et al.*, 2015b, Reyes-Darias *et al.*, 2015a) and the CtpH and CtpL (Wu *et al.*, 2000, Rico-Jimenez *et al.*, 2016) receptors that mediate chemoattraction to inorganic phosphate.

P. aeruginosa is a ubiquitous pathogen able to infect a broad range of different hosts such as human, animals, plants or fungi (Rahme *et al.*, 2000). Part of our research interests consists in assessing how chemosensory signalling mechanisms compare in phylogenetically related species that have different lifestyles. To address this issue we study *P. putida* KT2440, a non-pathogenic and nutritionally versatile soil bacterium with saprophytic lifestyle (Bagdasarian *et al.*, 1981, Espinosa-Urgel *et al.*, 2002, Regenhardt *et al.*, 2002). The genome of *P. putida* KT2440 encodes 3 chemosensory pathways (Garcia-Fontana *et al.*, 2013) and 27 chemoreceptors, which is very similar to the number of chemoreceptors in *P. aeruginosa* PAO1. However, sequence analyses and functional data appear to indicate that these are not sets of homologous proteins with homologous function. Initial evidence suggests that chemoreceptors that mediate responses to different compound classes are rather different. One such example are chemoreceptors of KT2440 and PAO1 for tricarboxylic acid cycle intermediates (TCA). In KT2440, three receptors, McpS, McpQ and McpR, have been shown to mediate responses to TCA cycle intermediates. McpS is a broad ligand range chemoreceptor that binds most of the TCA cycle intermediates (Lacal *et al.*, 2010a, Pineda-Molina *et al.*, 2012). Interestingly, McpS binds citrate, an abundant compound in plant tissues and root exudates, with only low affinity. However, McpS does not bind the metal ion complexed form of citrate (Lacal *et al.*, 2011b), which is the primary form of citrate in the environment. This may have been the reason for the evolution of the McpQ, a chemoreceptor that binds specifically citrate in both its metal-free and metal-complexed forms (Martin-Mora *et al.*, 2016b). In addition, McpR was found to mediate chemotaxis to malate and fumarate (Parales *et al.*, 2013). Remarkably, McpS and McpQ possess a HBM type LBD (Ortega & Krell, 2014) whereas McpR has a 4HB domain (Ulrich & Zhulin, 2005).

TCA cycle responsive chemoreceptors so far identified in *P. aeruginosa* are McpK, mediating specific responses to α-ketoglutarate (Martin-Mora *et al.*, 2016a), as well as the malate specific receptor, PA2652 (Alvarez-Ortega & Harwood, 2007). Whereas McpK has an HBM type LBD,

PA2652 possess a sCACHE domain. CACHE domains are abundant sensor domains in chemoreceptors and sensor kinases (Zhang & Hendrickson, 2010, Upadhyay *et al.*, 2016) and exist in two forms: (i) sCACHE (single CACHE), composed of a single structural module; and (ii) dCACHE (double CACHE), consisting of two CACHE modules in tandem. *P. aeruginosa* and *P. putida* contain a significant number of dCACHE containing chemoreceptors, namely 5 and 9, respectively. However, the genomes of both strains only encode a single sCACHE domain containing receptor. McpP, the sCACHE containing receptor of KT2440, was found to bind acetate, pyruvate, propionate and L-lactate (Garcia *et al.*, 2015). McpP and PA2652 share 37 % of sequence identity whereas the identity of their respective LBDs is only 23 % (Supp. Fig. 14), underling the important sequence divergence.

Here we report the characterization of the chemoreceptor PA2652 of *P. aeruginosa*. The study that reported its initial identification showed that a mutant in this gene did not respond to malate (Alvarez-Ortega & Harwood, 2007), but it is unknown whether it binds malate directly or via periplasmic binding proteins. This study also demonstrated that PA2652 is involved in the response of *P. aeruginosa* to malate but not to other organic acids such as succinate, 2-oxoglutarate, citrate or acetate (Alvarez-Ortega & Harwood, 2007). We used here high throughput approaches (Krell, 2015, McKellar *et al.*, 2015) to define more precisely the chemoeffector range of PA2652.

METHODOLOGY

Bacterial Strains, Culture Media, and Growth Conditions: Bacterial strains used in this study are listed in Supp. Table 7. *P aeruginosa* PAO1 and its derivative strains were routinely grown at 37 °C in LB (5 g yeast extract l^{-1}, 10 g Bacto tryptone l^{-1} and 5 g NaCl l^{-1}) or M9 medium supplemented with 1 mM MgSO4, 6 mg l^{-1} Fe-citrate, trace elements (Abril *et al.*, 1989) and 15 mM glucose as carbon source. For growth experiments to assess the capacity of PA2652-LBD ligands to support growth a sole C-source, PAO1 cells were pre-cultured overnight in M9 medium supplemented with 10 mM glucose and washed twice with M9 medium salts, prior to the inoculation of M9 medium containing10 mM of the different carbon sources. When necessary, the pH of the medium was adjusted to 7.0 prior to inoculation. Bacterial growth over the time was monitored using Bioscreen Microbiological Growth Analyser (Oy Growth Curves Ab Ltd, Helsinki, Finland). *E. coli* strains were grown at 37 °C in LB. *E. coli* DH5α was used as a host for gene cloning. When appropriate, antibiotics were used at the following final concentrations (in μg ml^{-1}): kanamycin, 25 (*E. coli* strains) and 100 (*Pseudomonas* strains); tetracycline, 40.

Construction of expression plasmid for PA2652-LBD: The DNA fragment encoding the LBD of PA2652 (Lys^{34}–Thr^{205}) was amplified from genomic DNA of *P. aeruginosa* PAO1 using primers 5'-TAATCATATGAAAAAACAGGCTGATGCCGA-3' and 5'-TAATGTCGACTCAGGTGCCGATACGCTCGTC-3' containing restriction sites for NdeI and SalI, respectively (underlined). The resulting PCR product was digested with NdeI and SalI and cloned into pET28b(+) using the same enzymes. The resulting plasmid, termed pET28b-PA2652LBD, was verified by DNA sequencing of the insert and flanking regions.

Overexpression and purification of PA2652-LBD: *E. coli* BL21 (DE3) containing pET28b-PA2652LBD was grown in 2 L Erlenmeyer flasks containing 400 ml LB medium supplemented with 50 μg ml^{-1} kanamycin at 30 °C. Once the culture reached an OD_{600} of 0.6, protein overexpression was induced by adding (IPTG) to a concentration of 0.1 mM. Growth was continued at 16 °C overnight prior to cell harvest by centrifugation at 10 000 x *g* for 30 min at 4 °C. Cell pellets were resuspended in buffer A (20 mM Tris/HCl, 0.1 mM EDTA, 300 mM NaCl, 10 mM imidazole, 5 % (v/v) glycerol, pH 8.0) and broken by French press treatment at 1000 psi. After centrifugation at 20 000 x *g* for 1 h, the supernatant was loaded onto a 5 ml HisTrap column (Amersham Bioscience), previously equilibrated with five column volumes of buffer A, washed with buffer A containing 35 mM of

imidazole and eluted with a 35–300 mM imidazole gradient in buffer A. Protein-containing fractions were pooled and dialyzed for immediate analysis.

Thermal Shift Assay based high-throughput ligand screening: Thermal shift assays were performed on a MyIQ2 Real-Time PCR instrument (BioRad). Ligands from the different compound arrays (Biolog, Hayward, CA, USA; the composition of these arrays is provided in http://208.106.130.253/pdf/pm_lit/PM1-PM10.pdf) were dissolved in 50 µl of MilliQ water, which, according to the manufacturer, corresponds to a concentration of 10-20 mM. Screening was performed using 96 wells plates. Each well contained 20 µM of protein dialyzed into TNG buffer (20 mM Tris/HCl, 150 mM NaCl, 10 % (v/v) glycerol, pH 6.7), 2.5 µl of the resuspended compounds and SYPRO Orange (Life Technologies) at 5 x concentration. In a single well (ligand free protein) the compound was substituted by water. Samples were heated from 23 °C to 85 °C at a scan rate of 1 °C/min. The protein unfolding curves were obtained by following the changes in SYPRO Orange fluorescence. Melting temperatures were determined using the first derivative values from the raw fluorescence data.

Isothermal titration calorimetry binding studies: Experiments were conducted on a VP-microcalorimeter (Microcal, Amherst, MA, USA) at 20 °C. PA2652-LBD was dialyzed overnight against TNG buffer, adjusted to a concentration of 20-35 µM and placed into the sample cell of the instrument. The protein was titrated by the injection of 9.6-14.4 µl aliquots of 1-20 mM ligand solutions that were prepared in TNG buffer (20 mM Tris/HCl, 150 mM NaCl, 10 % (v/v) glycerol, pH 6.8) immediately before use. The mean enthalpies measured from the injection of ligands into buffer were subtracted from raw titration data prior to data analysis with the MicroCal version of ORIGIN. Data were fitted with the "One binding site model".

Analytical ultracentrifugation studies: Experiments were performed on a Beckman Coulter Optima XL-A analytical ultracentrifuge (Beckman-Coulter, Palo Alto, CA, USA) equipped with UV-visible absorbance detection system, using an An50Ti 8-hole rotor and 12 mm path-length charcoal-filled epon double-sector centrepieces. The experiments were carried out at a rotor speed of 48 000 rpm and 7 °C using 400 µL samples of proteins dialyzed into in PIPES buffer (20 mM PIPES, pH 7.0). Protein was at 5-20 µM and L-malic acid (stock solution made up in dialysis buffer) was added at a final concentration of 1 mM. Dialysis buffer with and without ligand were used as reference. Light at a wavelength of 234 nm was recorded in the absorbance optics mode. A least squares boundary modelling of the data was used to calculate sedimentation coefficient distributions with the size-distribution c(s) method implemented in the SEDFIT v11.71 software (Schuck, 2000). The Svedberg equation allowed us to estimate the experimental molecular weight from the sedimentation and diffusion coefficients obtained. Buffer density (ρ = 1.0015 g/mL) and viscosity (η= 0.01449 Poise) at 7 °C were calculated from the buffer composition using SEDNTERP software (Laue *et al.*, 1992). This software was also used to calculate the partial specific volume (0.721 ml/g) and the molecular weight (21.5 kDa) of PA2652-LBD from its sequence.

Quantitative Capillary Chemotaxis Assays: Overnight cultures of *P. aeruginosa* strains were diluted to an OD_{660} of 0.05 in MS medium (30 mM Na_2HPO_4, 20 mMKH_2PO_4, 25 mM NH_4NO_3, 1 mM $MgSO_4$) supplemented with 6 mg l^{-1} Fe-citrate, trace elements (Abril *et al.*, 1989) and 15 mM glucose as carbon source, and grown at 37 ºC with orbital shaking (200 rpm). At an OD_{660} of 0.4 (early stationary phase of growth) cultures were centrifuged at 1,700 x *g* for 5 min and the resulting pellet was washed twice with chemotaxis buffer (50 mM potassium phosphate, 20 mM EDTA, 0.05 % (v/v) glycerol, pH 7.0). Subsequently, the cells were resuspended in the same buffer, adjusted to an OD_{660} of 0.1 and 230 µl aliquots of the bacterial cultures were placed into 96-well plates. For the quantitative assays, one-microliter capillary tubes (Microcaps, Drummond Scientific, Ref. P1424) were heat-sealed at one end and filled with either the chemotaxis buffer (negative control) or chemotaxis buffer containing the chemoeffectors to test. The capillaries were immersed into the bacterial suspensions at its open end. After 30 min at room temperature, capillaries were removed from the bacterial suspensions, rinsed with sterile water and the content expelled into 1 ml of M9

medium salts. Serial dilutions were plated onto M9 minimal medium (containing the appropriate antibiotics) supplemented with 15 mM glucose as carbon source. The number of colony forming units was determined after overnight incubation. In all cases, data were corrected with the number of cells that swam into buffer containing capillaries.

To determine the effect of antagonists in the chemotactic properties of PAO1, the assay was performed as previously described with two minor modifications: (i) Capillary tubes were filled with chemotaxis buffer containing 1 mM of the chemoattractants (L-malic acid or L-alanine) and 10-40 mM of the antagonists (methylsuccinic or citraconic acids); (ii) Bacterial cultures were washed with chemotaxis buffer and cells were finally resuspended in the same buffer but containing equimolar concentrations of methylsuccinic/citraconic acids to those present in the capillary tubes.

Competitive Root Colonization Assays: Sterilization and germination of maize seeds was carried out as described previously (Matilla *et al.*, 2007). Subsequently, 10 mL of M9 salts containing a 10^6 CFU/ml 1:1 mixture of PAO1-Km (wild type) and PAO-PA2652 (mutant) were added to 50 ml Sterilin tubes containing 40 g of sterile washed silica sand. Thereafter, one sterile seed was planted per Sterilin tube containing the inoculated silica sand. Plants were maintained at 24 °C with a daily light period of 16 h. After 6 days, bacterial cells were recovered from the rhizosphere and serial dilutions were plated on LB-agar medium supplemented with kanamycin or tetracycline to select PAO1-Km or the *PA2652* mutant strain, respectively

RESULTS

PA2652 binds several C2-substituted C4-dicarboxylic acids

To identify the LBD of PA2652, its sequence was analysed by the DAS transmembrane region prediction algorithm (Cserzo *et al.*, 1997). The receptor was found to possess two transmembrane regions (Supp. Fig. 13) and the DNA fragment encoding the section in between both regions was cloned into an expression vector. The resulting protein, PA2652-LBD, was expressed in *E. coli* and purified from the soluble fraction of the *E. coli* lysate by metal affinity chromatography.

To identify ligands that may bind to the LBD of PA2652, we conducted Differential Scanning Fluorimetry (DSF) based high throughput ligand screening assays as described previously (Krell,

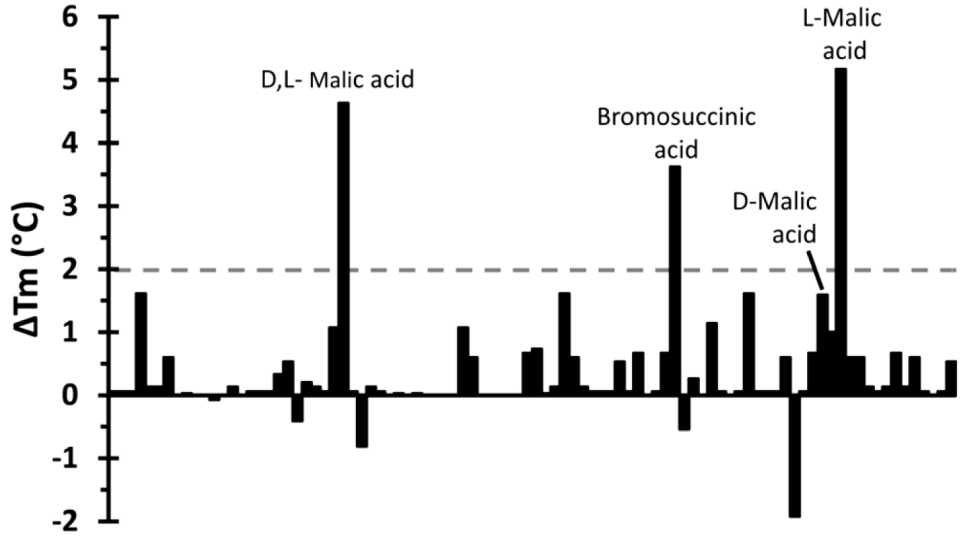

Figure 29. Differential Scanning Fluorimetry based high-throughput ligand screening of PA2652-LBD. Shown are Tm changes for each of the 95 compounds present in the Biolog PM1 compound array of carbon sources with respect to the Tm of the ligand-free protein of 45.5 °C. The dashed line indicates the threshold of 2 °C for significant hits.

2015, McKellar *et al.*, 2015). DSF analyses permit the determination of Tm values, which corresponds to the temperature at which half the protein is in its native conformation whereas the remaining half has undergone thermal unfolding. Since ligand binding typically enhances the thermal stability of proteins, increases in the Tm in the presence of ligands may be indicative of specific binding. We screened 450 different compounds available in five different ligand arrays from Biolog (http://208.106.130.253/pdf/pm_lit/PM1-PM10.pdf). The screened collection included different carbon and nitrogen sources, phosphorous and sulfurous compounds as well as different nutrient supplements. DSF assays evidenced a Tm of 45.5 °C for the ligand-free PA2652-LBD and Fig. 29 shows the Tm changes produced by the presence of each of the 95 compounds of the PM1 array of different carbon sources.

Tm increases of more than 2 °C, an accepted threshold for significant hits, were observed for a mixture of L- and D-malic acid, bromosuccinic acid as well as L-malic acid, whereas D-malic acid did not cause significant increases. Screening of other arrays also resulted in several hits, including citraconic and citramalic acids (Supp. Table 5).

Thermal shift assays indicate but do not constitute proof of binding (Krell, 2015, Martin-Mora *et al.*, 2016a). To unambiguously determine ligand binding, we have conducted Isothermal Titration Calorimetry (ITC)(Krell, 2008) binding studies with the purified protein. Fig. 30a shows the microcalorimetric titration of PA2652-LBD with the L- and D-isomers of malic acid. L-malic acid bound with a K_D value of 23 ± 1 µM, which is very similar to the affinities of ligands for McpP-LBD (Garcia *et al.*, 2015). Binding was driven by both favourable enthalpy (ΔH = -4.2 ± 1.2 kcal) and entropy changes ($T\Delta S$ = 2.1 ± 1 kcal/mol). In marked contrast, D-malic acid did not show binding

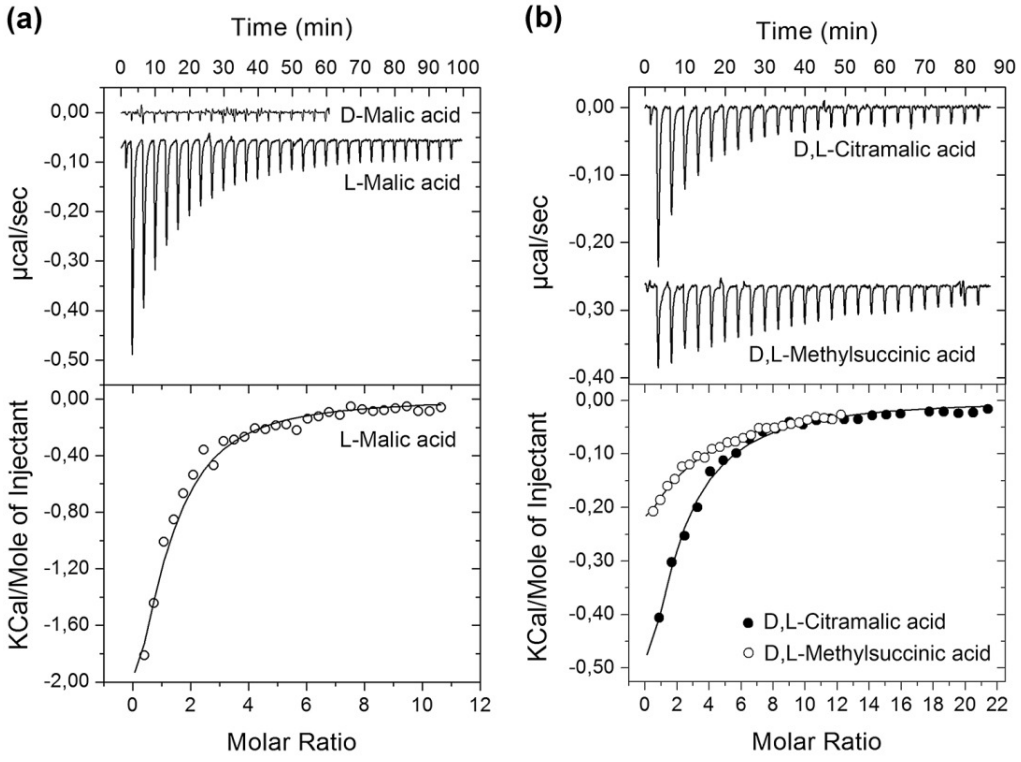

Figure 30. Isothermal titration calorimetry analysis of ligand binding to PA2652-LBD. (a) Titration with both malic acid isomers. (b) Titration with citramalic and methylsuccinic acids. The upper panels are the titration raw data for the injection of 9.6-14.4 µl aliquots of 1-2 mM ligand solution into 20-35 µM of protein. The lower panels are the integrated, dilution heat corrected and concentration normalized peak areas fitted with the "One binding site" model of ORIGIN.

(Fig. 30a) confirming the DSF data (Fig. 29).

We subsequently verified by ITC the binding of other compounds that caused Tm increases of at least 2 °C and detected binding for citramalic, citraconic and bromosuccinic acids with K_D values of 61 ± 4 µM, 210 ± 15 µM and 1.24 ± 0.7 mM, respectively (Figs. 30b and 31). As a result, it became clear that receptor PA2652 binds different C4-dicarboxylic acids and, in order to complete the ligand profile of this receptor, we analysed the binding of additional structurally related compounds.

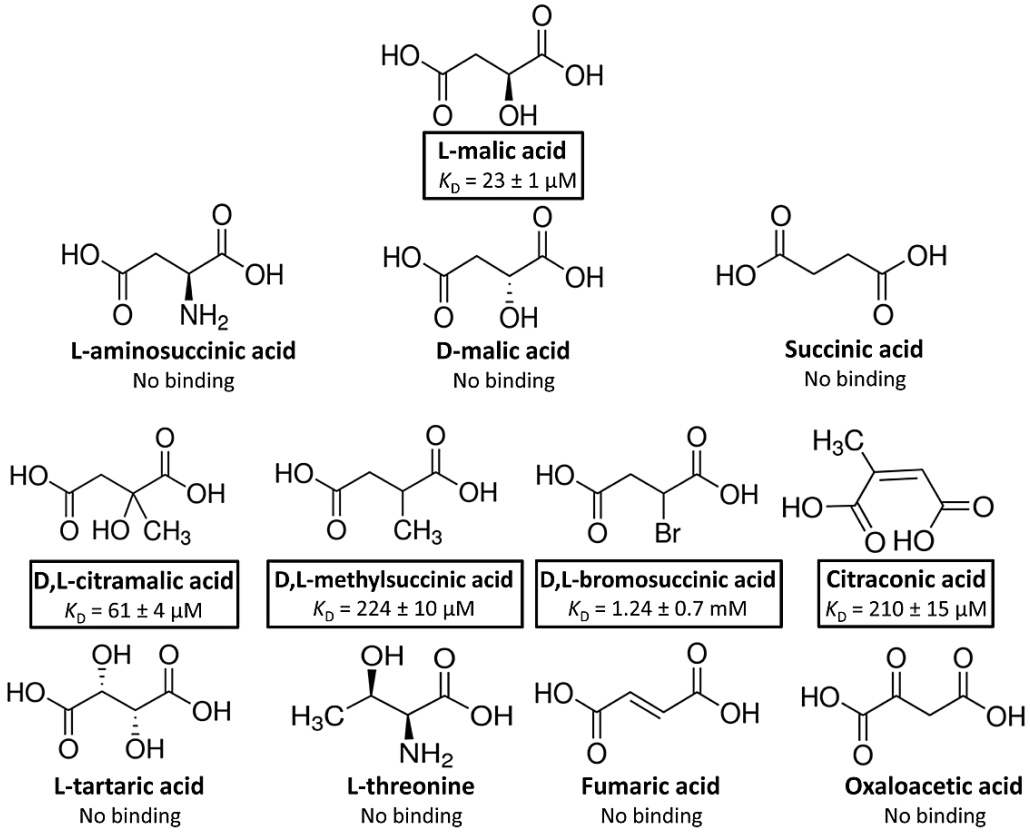

Figure 31. Summary of isothermal titration calorimetry studies. Shown are the structures of the five ligands that showed binding as well as of other compounds that were analysed but did not reveal binding. Dissociation constants are means and standard deviations from three experiments.

These experiments resulted in the detection of binding for methylsuccinic acid (not present in the compound arrays) whereas assays using other C4-dicarboxylates (Supp. Table 5) such as succinic, fumaric, oxalacetic, aminosuccinic or tartaric acids resulted in an absence of binding. Importantly, the five ligands recognized by PA2652 are thus C2-substituted C4-dicarboxylic acids (Fig. 31).

L-malic acid binding does not change the dimeric state of PA2652-LBD

Ligand-induced dimerization of the chemoreceptor ligand binding domain was proposed to be a necessary prerequisite for signaling (Stock, 1996). Chemoreceptors employ different types of LBD (Matilla & Krell, 2017) and previous studies have assessed the effect of ligand binding to the oligomeric state of individual LBDs. These experiments have resulted in two different scenarios. On one hand, individual 4HB or HBM domains are primarily monomeric in its ligand-free state and ligand binding induces dimerization (Milligan & Koshland, 1993, Lacal *et al.*, 2010a, Martin-Mora *et*

al., 2016a, Fernandez *et al.*, 2017). In contrast, dCACHE domains were found to be monomeric in the absence and presence of ligands (Rico-Jimenez *et al.*, 2013a). However, no information is available on the effect of ligand binding on the oligomeric state of sCACHE domains.

To address this issue, PA2652-LBD was analysed by sedimentation velocity analytical ultracentrifugation. Initial experiments were conducted using concentrations of ligand-free protein ranging from 5 to 20 μM. These assays showed no significant differences in the sedimentation coefficients calculated for the species identified, which rules out hydrodynamic non-ideality behaviour. The analysis of single species in the sedimentation profile resulted in a standard sedimentation coefficient of $s_{w,20}$ = 3.1 S and a frictional ratio of 1.4; the latter indicative of an elongated protein shape (Fig. 32). The molecular weight extracted from the sedimentation coefficient and the shape was of 41 kDa. Considering that the sequence-derived mass of the PA2652-LBD monomer is 21.5 kDa, the observed species is clearly a protein dimer. Since no shift to higher sedimentation coefficients was measured with increasing protein concentrations (data not shown), the dimer species can be considered stable over the protein concentration range analysed. The above experiments were also performed in the presence of saturating concentrations of L-malic acid. In these assays, the behaviour of PA2652-LBD was highly similar to that of the unliganded protein and data analysis resulted in the same sedimentation coefficient and frictional ratio as observed for the ligand-free protein (Fig. 32). It can therefore be concluded that PA2652-LBD forms stable dimers in the ligand-free state and that the binding of L-malic acid does not have any significant effects on the oligomerization state of the protein.

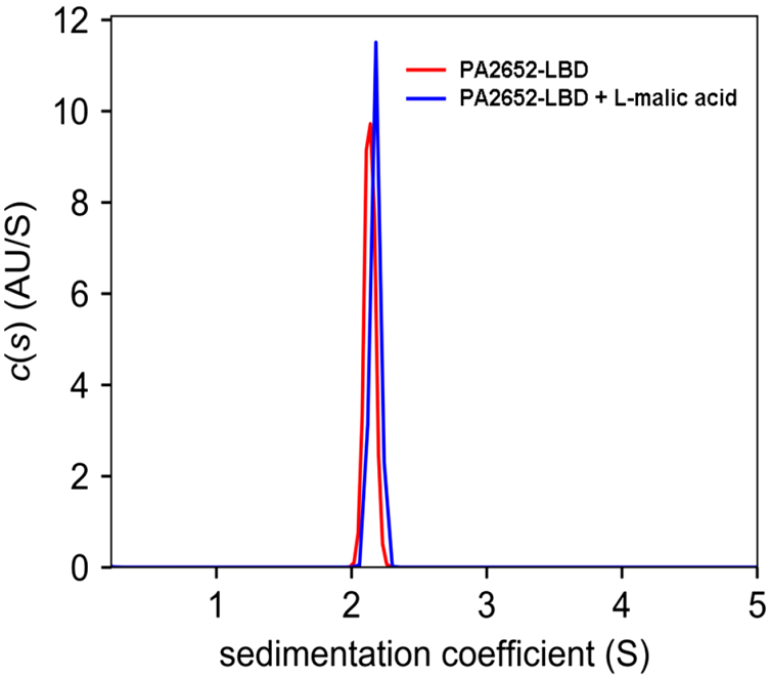

Figure 32. Sedimentation velocity analytical ultracentrifugation analysis of PA2652-LBD. The sedimentation coefficient profile is shown for the protein at 20 μM in the absence and in presence of 1 mM L-malic acid. Values shown are expressed at the conditions of the experiment, namely at a temperature of 7 ^{o}C and PIPES buffer.

PA2652 ligands act as attractants and antagonists

To evaluate the physiological relevance of the ligands identified, we first addressed the question of whether they could support bacterial growth as sole carbon source. To this end, we conducted growth experiments of the wild type (*wt*) strain and a mutant defective in *PA2652* in minimal medium supplemented with the different ligands as sole carbon sources. As shown in Supp. Fig. 16, L-malic, citramalic and methylsuccinic acids were able to efficiently sustain growth of both PAO1 strains. Alternatively, bromosuccinic acid poorly supported bacterial growth, whereas citraconic acid could not be used as sole carbon source (Supp. Fig. 16).

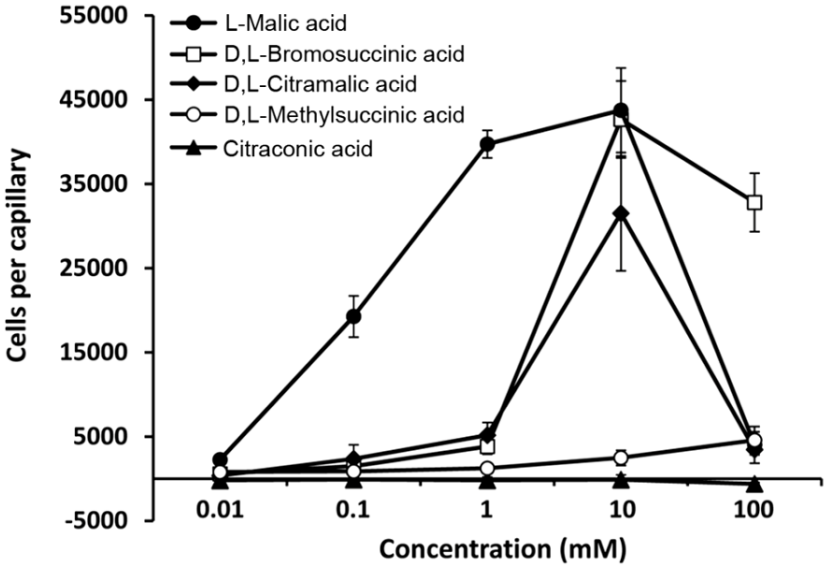

Figure 33. Quantitative capillary chemotaxis assays of *P. aeruginosa* PAO1 toward different organic acids. Data are means and standard deviations from three biological replicates conducted in triplicate. Data were corrected with the number of cells that swam into buffer containing capillaries (1713 ± 231).

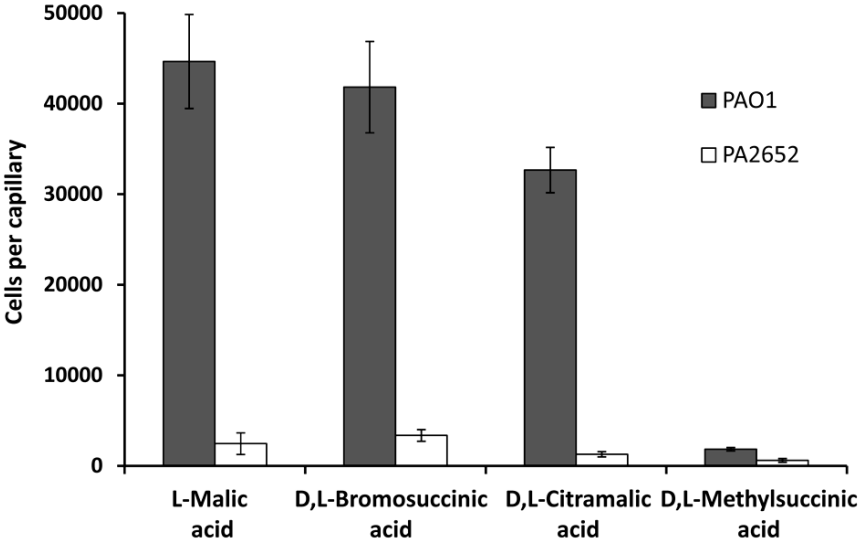

Figure 34. Quantitative capillary chemotaxis assays of *P. aeruginosa* PAO1 and its mutant defective in PA2652 to different PA2652 chemoeffectors. In all cases, chemoeffectors were used at a final concentration of 10 mM. Data were corrected with the number of cells that swam into buffer containing capillaries (1565 ± 327). Data are means and standard deviations from three biological replicates conducted in triplicate.

Secondly, we assessed the capacity of the ligands identified to induce chemotaxis. To this end, we carried out quantitative capillary chemotaxis assays using the wt strain and PA2652 ligands at concentrations ranging from 10 μM to 100 mM. Our results showed that L-malic acid induces strong chemotaxis responses over the concentration range of 100 μM to 10 mM (Fig. 33). Significant responses were also observed for bromosuccinic and citramalic acids, with a maximum chemotactic response at a concentration of 10 mM. Minor but statistically significant responses were also observed for methylsuccinic acid, whereas citraconic acid, the only ligand that did not support growth (Supp. Fig. 16), did not cause any chemotactic response (Fig. 33).

To determine the role of the PA2652 receptor in the observed tactic responses, we characterized phenotypically a mutant defective in the corresponding gene. Initial control experiments involved the measurement of chemotaxis of the wt and a *PA2652* mutant strain toward casamino acids, which is mediated by the three paralogous receptors PctA, PctB and PctC (Taguchi *et al.*, 1997, Rico-Jimenez *et al.*, 2013a). Both the wt and the mutant strain showed similar response to casamino acids (Supp. Fig. 17), indicating that the mutation of *PA2652* did not result in any

undesired secondary effects. Quantitative chemotaxis assays of the mutant strain toward 10 mM ligand solutions showed a dramatic reduction in chemotaxis for all ligands (Fig. 34), indicating that PA2652 is the primary receptor for these C4-dicarboxylic acids. The minor responses in the mutant strain may be potentially due to a secondary receptor. Importantly, *in trans* expression of PA2652 in a mutant defective in *PA2652* resulted in the complementation of the chemotaxis defect toward malate (Alvarez-Ortega & Harwood, 2007).

Attractants and antagonists compete for binding at PA2652-LBD *in vitro* and *in vivo*.

The above results suggest that chemoattractants (L-malic, bromosuccinic and citramalic acids) and antagonists (methylsuccinic and citraconic acids) may compete for binding to PA2652-LBD. In order to understand the mechanistic role of these antagonistics in the chemotaxis behaviour of *P. aeruginosa,* we first carried out ITC binding studies. In these assays, we measured the affinity of L-malic acid for PA2652-LBD in the presence of different concentrations of methylsuccinic and citraconic acids. Our data showed that heat released from the binding of L-malic acid was reduced as the antagonist concentration increased. The apparent affinity of L-malic acid decreased

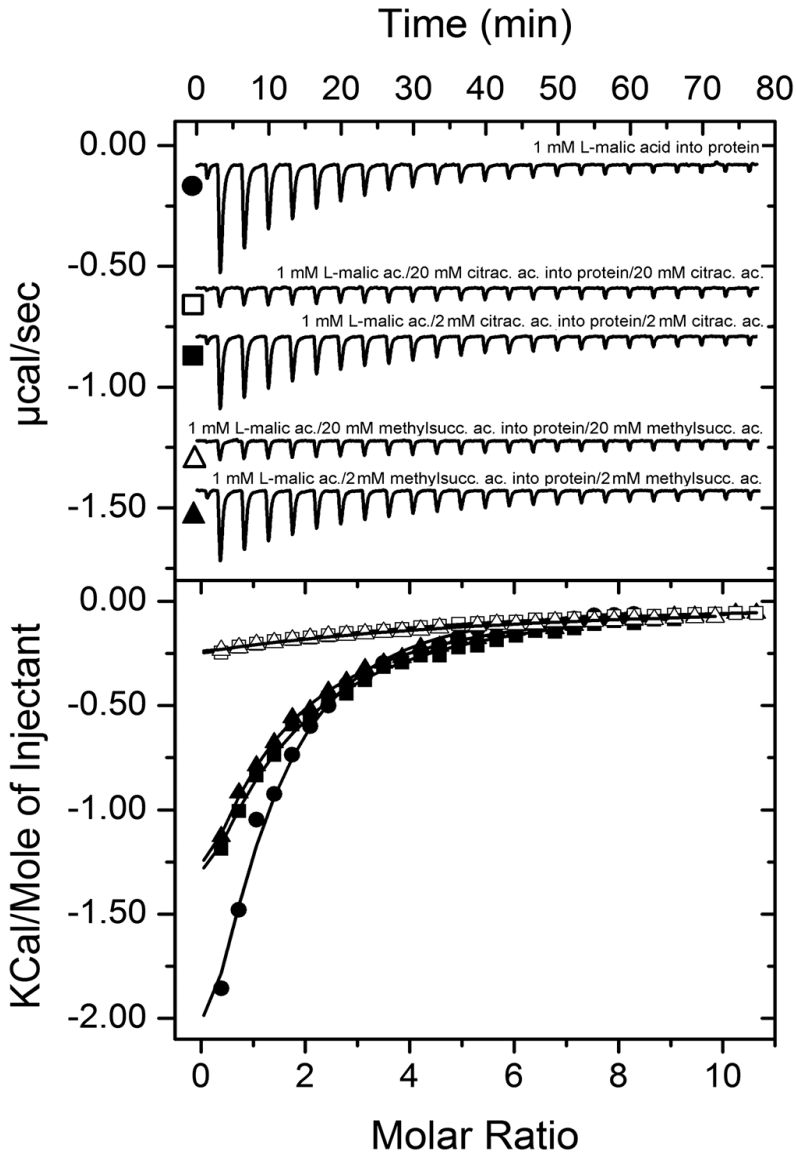

Figure 35. Attractants and antagonists compete for binding at PA2652-LBD *in vitro*. Isothermal titration calorimetry analysis of the binding of L-malic acid to PA2652-LBD in the absence and presence of 2 or 20 mM of the antagonists, citraconic and methylsuccinic acids. Upper panel: Titration raw data for the injection of 9.6 µl aliquots of 1 mM of L-malic acid into 20 µM of protein in the absence and presence of antagonists (present both in the injector syringe and sample cell). Lower panel: Integrated, dilution heat corrected and concentration normalized peak areas fitted with the "One binding site" model of ORIGIN. The apparent binding constants are listed in Supp. Table 2.

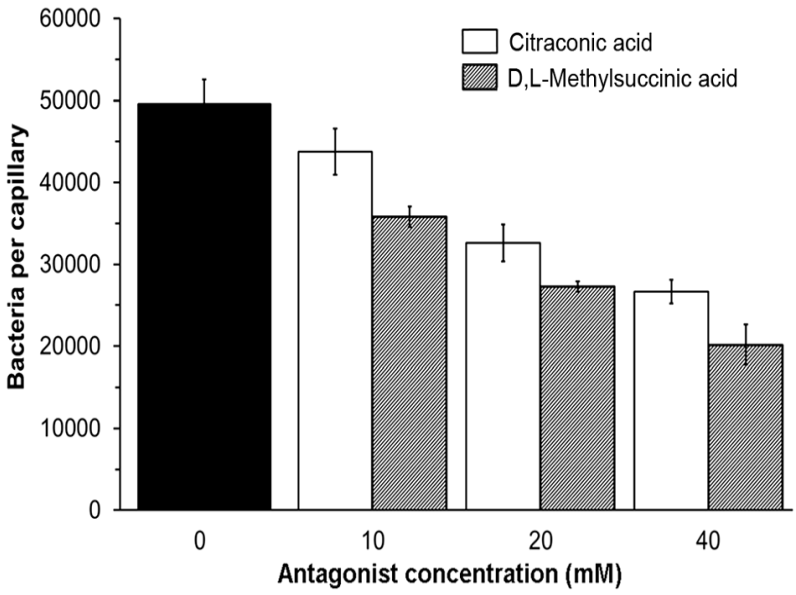

Figure 36. Antagonists reduce the magnitude of chemotaxis toward L-malic acid. Quantitative capillary chemotaxis assays of *P. aeruginosa* PAO1 toward 1 mM L-malic acid in the absence (black bars) and presence of different antagonist concentrations. Data are means and standard deviations from three biological replicates conducted in triplicate. Data were corrected with the number of cells that swam into buffer containing capillaries (4266 ± 1133).

approximately by a factor of two in the presence of 2 mM antagonists and increasing the concentration of antagonists to 20 mM led to a further reduction in the apparent affinity for L-malic acid (Fig. 35 and Supp. Table 5). Control assays titrating buffer or buffer/antagonist solutions in with L-malic acid or L-malic acid/antagonist solutions resulted in small and uniform peaks indicative of dilution heats (Supp. Fig. 18). Considering the close structural similarity of antagonists and L-malic acid (Fig. 31) it is likely that these compounds compete for binding at the same site at PA2652.

Following the demonstration of competition *in vitro* we have assessed the influence of antagonists on the chemotaxis toward L-malic acid. To this end we conducted chemotaxis assays toward L-malic acid in the absence or presence of 10, 20 and 40 mM of citraconic and methylsuccinic acids (that were added to both, the bacterial suspension and the chemoattractant solution). Our results showed that antagonists reduced the chemotaxis toward L-malic acid, with higher decreases in the chemotactic response as the concentration of the antagonist was increased, therefore indicating that citraconic and methylsuccinic acids are inhibiting the activation of the chemotaxis signalling cascade triggered by L-malic acid (Fig. 36). To verify whether the presence of antagonists may have a global inhibitory effect on the chemotactic properties of *P. aeruginosa* we performed assays toward L-alanine, a chemoattractant recognized by the receptors PctA and PctB (Rico-Jimenez *et al.*, 2013a), in the presence antagonists. As shown in Supp. Fig. 19, the presence of 20 or 40 mM citraconic and methylsuccinic acids did not significantly alter the chemotaxis toward 1 mM L-alanine.

The PA2652 chemoreceptor signals through the *che* chemosensory pathway

As mentioned in the introduction, *P. aeruginosa* has two chemosensory pathways that were found to be involved in chemotaxis, namely the *che* and the *che2* pathway (Ferrandez *et al.*, 2002, Guvener *et al.*, 2006). A recent bioinformatic study has predicted that PA2652 signals through the *che* pathway (I. B. Zhulin, unpublished data). To verify this prediction we conducted chemotaxis assays to L-malic acid using the wt strain as well as mutants in *cheA1* and *cheA2,* encoding respectively the histidine kinases of the *che* and *che2* pathways. As shown in Supp. Fig. 20, mutation of *cheA1* abolished chemotaxis to L-malic acid, whereas the response of the *cheA2* mutant was almost identical to that of wt strain, confirming bioinformatic predictions.

The effect of PA2652 in plant root colonization

P. aeruginosa is an ubiquitous pathogen and also able to colonize and infect different plants (Rahme *et al.*, 2000, Bais *et al.*, 2002, Attila *et al.*, 2008). Previous studies using a number of different bacterial species have shown that chemotaxis to root exudates is an important prerequisite for efficient plant root colonization (Bardy *et al.*, 2017). Taken together data from different plant species, malate and citrate are considered the most abundant organic acids in plant tissues and root exudates, and they can represent up to 25% of total photosynthate exuded by the plant (Johnson *et al.*, 1996, Jones, 1998). Therefore, considering the important concentrations of malate in root exudates and using maize as model plants, we carried out competitive root colonization assays of the kanamycin resistant *P. aeruginosa* strain PAO1-Km and a mutant defective in *PA2652*. The assays showed that the fitness of the mutant in *PA2652* was comparable to that of the wild type strain (Supp. Fig. 21).

DISCUSSION

Sensing of environmental signals by one- and two-component systems as well as chemotaxis signalling pathways occurs through sensor domains. Remarkably, the development of next generation sequencing technologies has allowed to determine that these three transduction mechanisms share a significant number of sensor domain types (Ulrich & Zhulin, 2010, Matilla & Krell, 2017). Additionally, the combination of computational and experimental approaches enabled the identification of inhibiting compounds, known as antagonists, that are sensed by one- and two-component systems. These molecules compete for binding to the sensor domains and block the agonist-induced response (Busch *et al.*, 2007, Swem *et al.*, 2009, Klein *et al.*, 2012, Silva-Jimenez *et al.*, 2012). Importantly, there is increasing evidence indicating that signal antagonists can also act on chemoreceptors. Thus, it was shown that the binding of several compounds to the 4HB type LBDs of the Tar and MCP2201 chemoreceptors, from *E. coli* and *C. testosteroni* respectively, did not cause any chemotactic responses (Bi *et al.*, 2013, Ni *et al.*, 2013, Yu *et al.*, 2015).

In this study we identified four new ligands for PA2652, which all occur naturally (Arun *et al.*, 2008, Khorassani *et al.*, 2011, Fuchs & Berg, 2014, Zhang *et al.*, 2016). However, significant chemotaxis was only observed for two of them, bromosuccinic and citramalic acids - to our knowledge the first report of bacterial chemotaxis to both of these compounds. In contrast, no or very minor responses were observed for citraconic and methylsuccinic acids, respectively (Fig. 33). Additional *in vivo* experimentation showed that citraconic and methylsuccinic acids bind to the sCACHE domain of PA2652 and act as antagonists by competing for binding with chemoattractants (Fig. 35). Consequently, taxis of *P. aeruginosa* toward chemoattractants was reduced in the presence of these two antagonists (Fig. 36), as observed previously for other chemoreceptor antagonists (Bi *et al.*, 2013, Ni *et al.*, 2013). Interestingly, malate was shown to be an antagonist of MCP2201 and its binding to the LBD of this chemoreceptor reduced the chemotactic behavior of *C. testosteroni* toward diverse aromatic compounds (Ni *et al.*, 2013). Taken together, our data illustrate that the action of antagonists is not only restricted to 4HB LBDs, but also occurs at chemoreceptors with a different LBD type. Could these findings be of applied interest? The increasing emergence of multidrug-resistant bacteria is challenging human health and new targets for the development of antibiotics are urgently needed (Brown & Wright, 2016). Chemotaxis has been shown to be required for the full virulence of multiple human pathogens (Stecher *et al.*, 2004, Keilberg & Ottemann, 2016, Schwarzer *et al.*, 2016, de Vries *et al.*, 2017) and drugs targeting chemosensory signalling pathways constitute promising approaches for the discovery of new antibiotics (Erhardt, 2016). Since many drugs are based on antagonists (Kenakin, 2005, Kenakin & Williams, 2014), the identification of compounds interfering with chemotactic transduction pathways may potentially enable the rational design of drugs inhibiting chemotaxis-associated processes.

Table 8. Summary of information available on malate responsive chemoreceptors.

Name	Species	Ligands	Binding mode	LBD type[a]	Predicted LBD location[b]	Ref.
PA2652	*P. aeruginosa* PAO1	L-malic, citramalic, citraconic, bromosuccinic and methylsuccinic acids	direct	sCACHE	periplasm	This work
McpS (PP4658)	*P. putida* KT2440	L-malic, oxalacetic, citric, isocitric, succinic, fumaric and butyric acids	direct	HBM	periplasm	(Lacal *et al.*, 2010a, Pineda-Molina *et al.*, 2012)
McpM (GenBank accession no. LC005239)	*R. pseudosolanacearum* Ps29	L-malic, D-malic, D-tartaric, succinic, and fumaric acids.	unknown	4HB	periplasm	(Hida *et al.*, 2015, Tunchai *et al.*, 2017)
McpT (GenBank accession no. LC005228)	*R. pseudosolanacearum* Ps29	D-malic acid, D-tartaric and L-tartaric acids.	unknown	4HB	periplasm	(Tunchai *et al.*, 2017)
McfS (Pput_4520)	*P. putida* F1	succinic, malic, citric and fumaric acids	unknown	HBM	periplasm	(Parales *et al.*, 2013)
McfR (Pput_0339)	*P. putida* F1	succinic, malic and fumaric acids	unknown	4HB	periplasm	(Parales *et al.*, 2013)
McpS (Pfl01_0728)	*P. fluorescens* Pf0-1	L-malic and succinic acids	unknown	HBM	periplasm	(Oku *et al.*, 2014)
McpT (Pfl01_3768)	*P. fluorescens* Pf0-1	L-malic and succinic acids	unknown	sCACHE	periplasm	(Oku *et al.*, 2014)
CcmL (Tlp3)	*C. jejuni* 11168-O	chemoattractants malic and fumaric acids, Ile, purine; chemorepellents Lys, Arg, glucosamine, succinic acid, thiamine	direct	dCACHE	periplasm	(Rahman *et al.*, 2014)
MCP2201 (CtCNB1_2201)	*C. testosteroni* CNB-1	malic acid (inhibitor of taxis to other organic acids), oxaloacetic, citric, isocitric, α-ketoglutaric, succinic and fumaric acids	direct	4HB	periplasm	(Ni *et al.*, 2013)

[a]Based on the Pfam database (Finn *et al.*, 2017)
[b]Based o the prediction of TM region using the DAS algorithm (Cserzo *et al.*, 1997).

CACHE domains are the most abundant sensor domains in chemoreceptors and sensor kinases (Zhang & Hendrickson, 2010, Upadhyay *et al.*, 2016). Whereas *P. aeruginosa* PAO1 and *P. putida* KT2440 have an elevated number of dCACHE containing chemoreceptors, both strains have a single sCACHE domain containing chemoreceptor. Although both receptors bind organic acids, their ligand profiles are different. Whereas McpP binds several C2- and C3 carboxylic acids (Garcia *et al.*, 2015), we show here that PA2652 binds several C2-substituted C4-dicarboxylic acids. Interestingly, the homologous chemoreceptor in the plant pathogen *P. syringae* pv. *actinidiae* was found to have a ligand profile that is very similar to that of *P. putida* KT2440 (Brewster *et al.*, 2016).

Several previous studies have shown that the affinity of ligands for the LBD correlate with the magnitude of the chemosensory output (Reyes-Darias *et al.*, 2015a, Fernandez *et al.*, 2017). However, this correlation was not observed
for the PA2652 ligands (Figs. 31 and 33). In the initial study of PA2652, chemotaxis assays were performed using malate samples containing both isomers (Alvarez-Ortega & Harwood, 2007). Here we show that PA2652 binds exclusively the L- but not the D-isomer of malic acid (Fig. 30a). In this respect, clear parallels exist to McpP that binds only L-lactate but not D-lactate (Garcia *et al.*, 2015). Many bacteria are able to synthesize D-malate (van der Werf *et al.*, 1992, Unden *et al.*, 2016) and *Pseudomonas* species were found to metabolize both isomers (Hopper *et al.*, 1970). However, L-malate is a common carboxylic acid whereas its D-isomer is less frequent (Scheu *et al.*, 2010). In the context of sensory mechanisms for the regulation of the metabolism of organic acids, it has been proposed that common carboxylic acids are sensed in the periplasm whereas uncommon acids are sensed in the cytosol (Scheu *et al.*, 2010, Unden *et al.*, 2016). For example the DcuS sensor kinase, comprising a periplasmic LBD, senses L-malate (Cheung & Hendrickson, 2008) whereas the cytosolic transcriptional regulator DmlR senses D-malate (Lukas *et al.*, 2010). This differentiation appears to also apply to L-malate chemoreceptors. Chemoreceptors can sense their ligands either in the cytosol or the extracytoplasmic space (Salah Ud-Din & Roujeinikova, 2017). A significant number of malate responsive chemoreceptors have been identified in a variety of different species and the corresponding information is summarized in Table 8. Whereas in some studies mixtures of D- and L-malate were used, other reports study the individual malate isomers. Interestingly, next to PA2652, the McpS receptor of *P. putida* KT2440 (Pineda-Molina *et al.*, 2012), McpM of *Ralstonia pseudosolanacearum* (Hida *et al.*, 2015) as well as thePfl01_0728 and Pfl01_3768 of *P. fluorescens* (Oku *et al.*, 2014) were found to mediate specifically L-malate chemotaxis. All these receptors are predicted to possess a LBD in the periplasmic space confirming the hypothesis of extracytoplasmic sensing of common organic acids. The response of *R. pseudosolanacearum* to D-malate has also been investigated and was attributed to a fortuitous response of L-malate sensing receptors (Tunchai *et al.*, 2017).

The inspection of information available on the different malate responsive chemoreceptors (Table 8) also shows that these receptors differ in their LBD type. In general, chemoreceptor LBDs can be classified according to their size into clusters I and II (Lacal *et al.*, 2010b). Interestingly, malate responsive receptors include cluster I (sCACHE, 4HB) as well as cluster II (dCACHE, HBM) LBDs, and direct malate binding has been observed for all 4 LBD types (Table 8). This diversity in the molecular architecture of malate responsive receptors underlines the important physiological relevance of this ligand. Thus, as an example, the importance of malate chemotaxis has been reflected in *R. pseudosolanacearum* since a mutant defective in *mcpM* exhibits reduced virulence as compared to the wt strain in tomato plants (Hida *et al.*, 2015). Additionally, taxis to organic acids has been shown to be important for the colonization of the gastrointestinal tract of chicken by *C. jejuni* (Chandrashekhar *et al.*, 2015).

Based on the hypothesis that ligand induced chemoreceptor dimerization is a prerequisite for signaling (Stock, 1996), the effect of ligands on the oligomeric state of different LBD types has been investigated in the past (Milligan & Koshland, 1993, Lacal *et al.*, 2010a, Rico-Jimenez *et al.*, 2013a, Martin-Mora *et al.*, 2016b, Rico-Jimenez *et al.*, 2016, Fernandez *et al.*, 2017). The individual

4HB domains of receptors Tar, CtpH and PcaY_PP (Milligan & Koshland, 1993, Rico-Jimenez *et al.*, 2016, Fernandez *et al.*, 2017) and HBM LBDs (receptors McpS and McpQ)(Lacal *et al.*, 2010a, Martin-Mora *et al.*, 2016a) were found to be largely monomeric in their ligand free state whereas in all cases the binding of the ligand induced complete LBD dimerization. This is due to the fact that ligands bind at the dimer interface and that amino acids from both monomers of the dimer establish contacts with the bound ligand (Milburn *et al.*, 1991, Pineda-Molina *et al.*, 2012). In marked contrast, dCACHE LBDs of the PctA and PctB chemoreceptors were entirely monomeric in the absence and presence of ligands. Importantly, no information was available on the oligomeric state of sCACHE domains and we show here that yet another scenario applies to PA2652-LBD. Thus, in the absence of ligand, PA2652-LBD was entirely dimeric over the concentration range tested and L-malic acid did not have any effect on its oligomeric state (Fig. 32).

P. aeruginosa has two chemosensory pathways involved in chemotaxis. Chemotaxis to L-malic acid in the *cheA2* mutant strain was indistinguishable from that of the wt, whereas no response was observed in a mutant defective in *cheA1*. These results confirm the bioinformatic prediction (I. B. Zhulin, unpublished data) but also demonstrate the exclusivity of the *che* pathway in mediating L-malic acid responses.

SUPPLEMENTARY MATERIAL

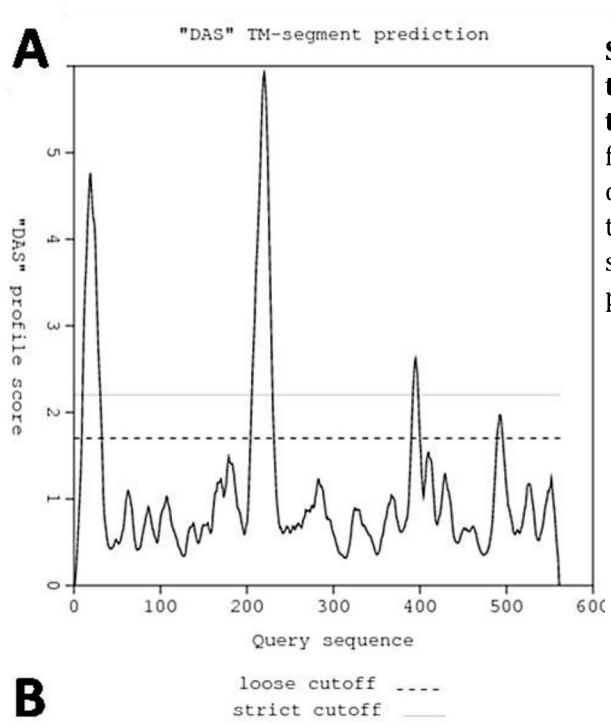

Supp. Fig 13. Prediction of transmembrane regions in PA2652 using the DAS algorithm. A, Graphical output from DAS (Cserzo *et al.*, 1997). B, Sequence of PA2652 showing in red the transmembrane regions and the LBD sequence cloned into the expression plasmid in blue.

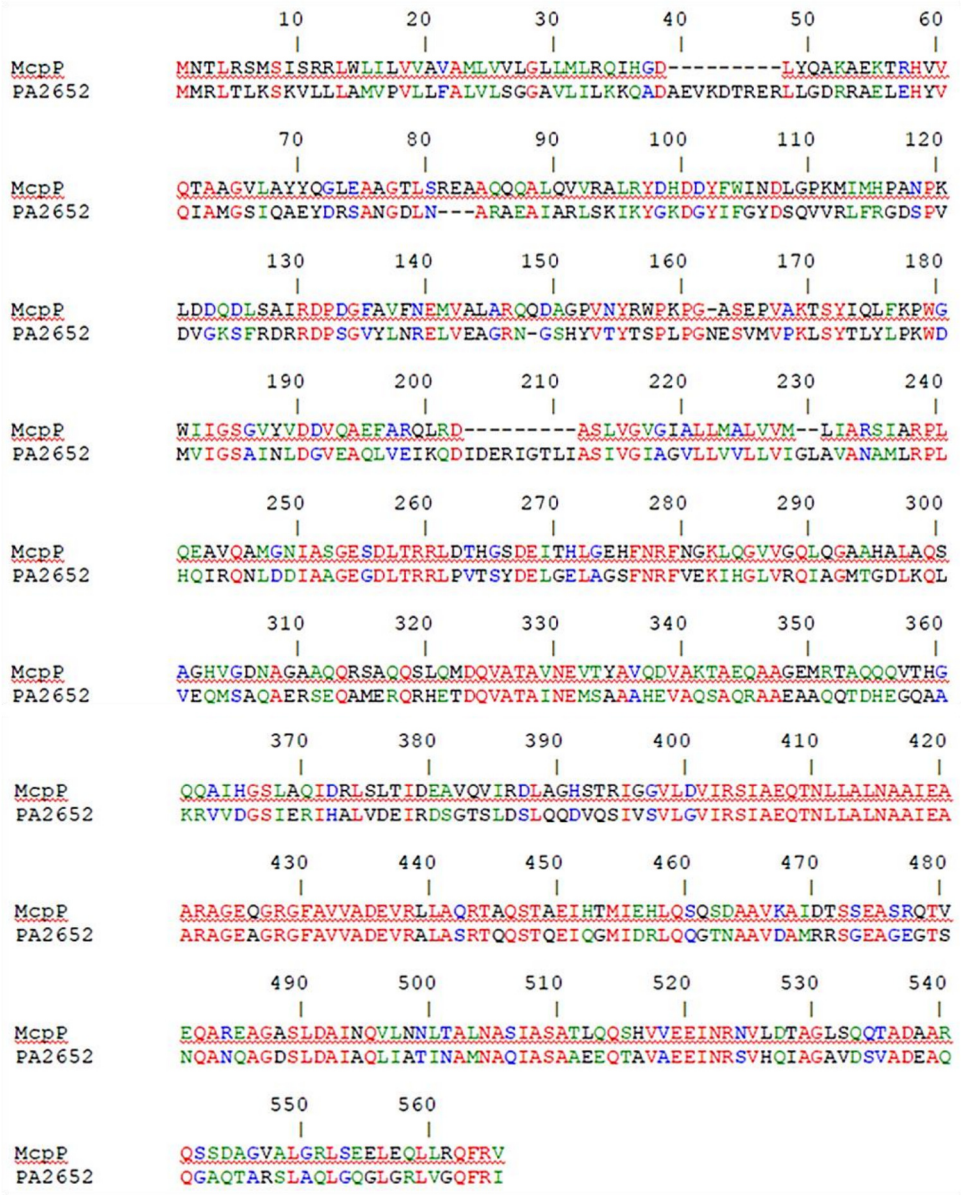

Supp. Fig 14. Sequence alignment of sCACHE LBD containing chemoreceptors in *P. putida* KT2440 (McpP) and *P. aeruginosa* PAO1 (PA2652). The alignment was performed in the slow mode using the CLUSTALW multiple alignment tool (Thompson *et al.*, 1994) of the NPS@ suite (Combet *et al.*, 2000). The GONNET protein weight matrix was used and gap opening and gap extension penalties of 10 and 0.1 were applied, respectively.

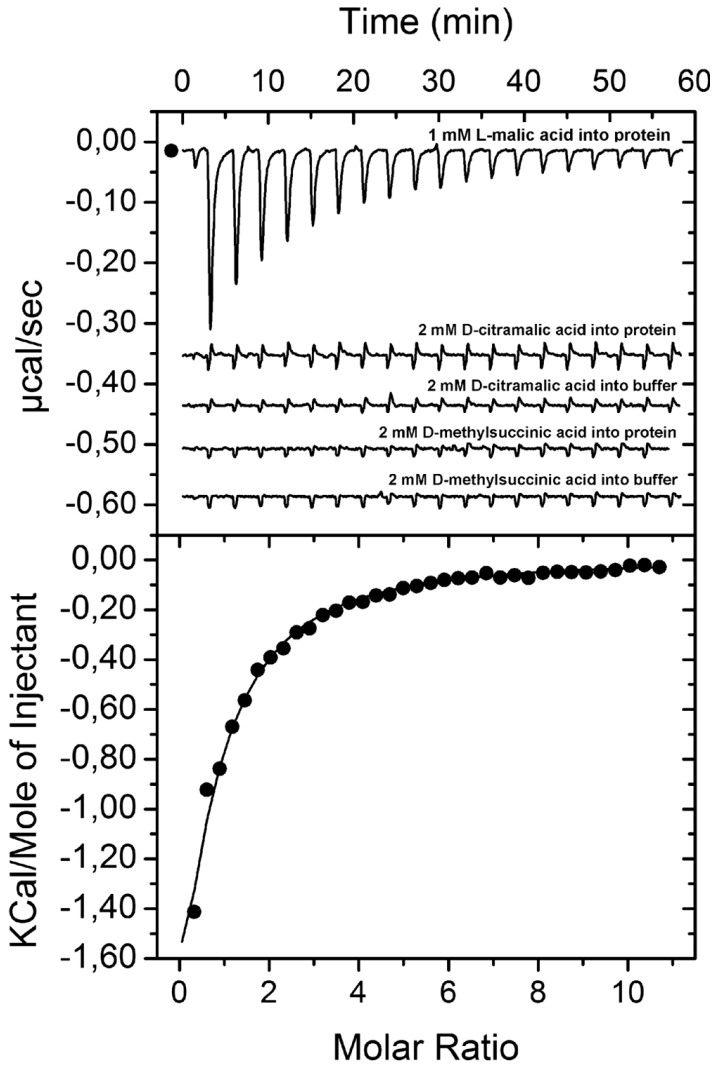

Supp. Fig 15. Microcalorimetric titrations of L- and D-enantiomers to PA2652-LBD. The upper panels are the titration raw data for the injection of 8-11.2 µl aliquots of 1–2 mM ligand solutions into 20 µM of protein. The lower panels are the integrated, dilution heat corrected and concentration normalized peak areas fitted with the "One binding site" model of ORIGIN. L-malic acid was used as positive control.

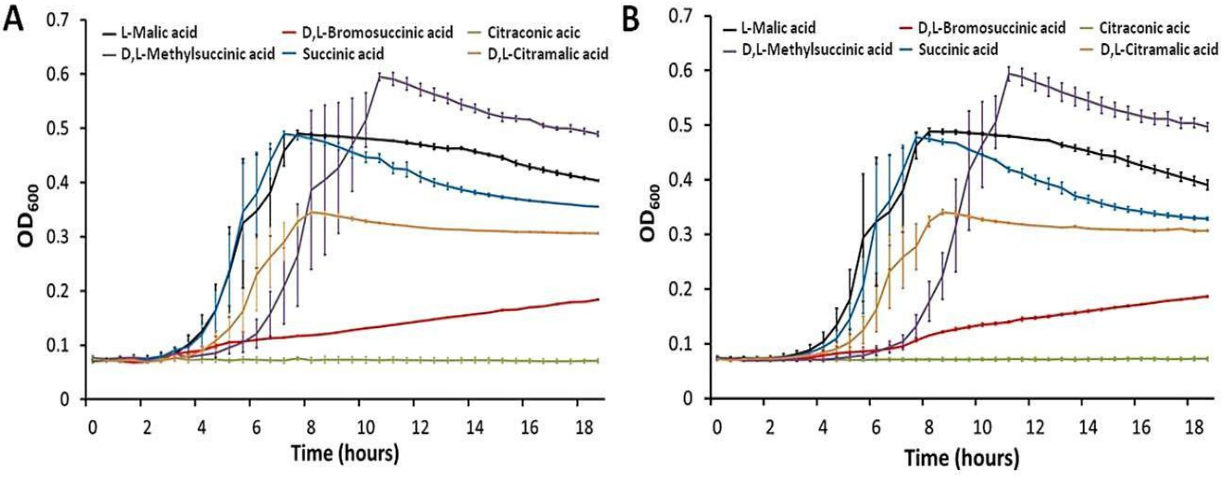

Supp. Fig 16. Growth curves of *P. aeruginosa* PAO1 (A) and a mutant deficient in PA2652 (B) in MS minimal medium supplemented with 5 mM of the different organic acids as sole carbon sources. Succinic acid was used an internal positive control. Data are means and standard deviations from three independent experiments.

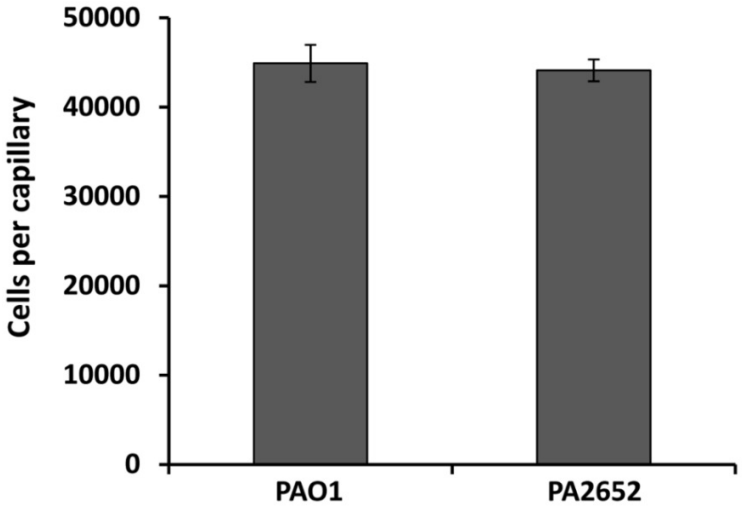

Supp. Fig 17. Quantitative capillary chemotaxis assays of *P. aeruginosa* PAO1 and its mutant in the PA2652 gene towards 0.1 % (w/v) casamino acids. Data were corrected with the number of cells that swam into buffer containing capillaries (2376 ± 272). Data are the means and standard deviations from three biological replicates conducted in triplicate.

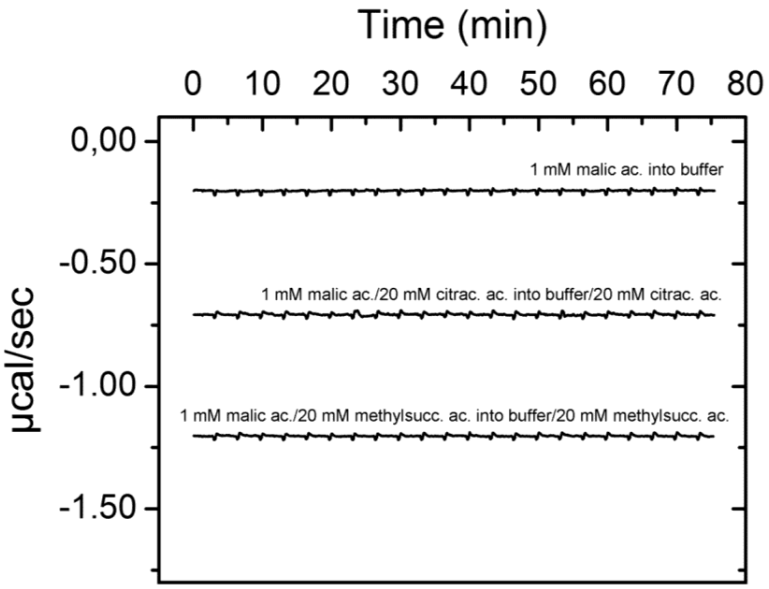

Supp. Fig 18. Microcalorimetric titrations of buffer or buffer/antagonist mixtures with L-malic acid or L-malic acid/antagonist mixtures. In all cases the injection volume was of 9.6 µl. Data are the corresponding controls to experiments shown in Fig. 7.

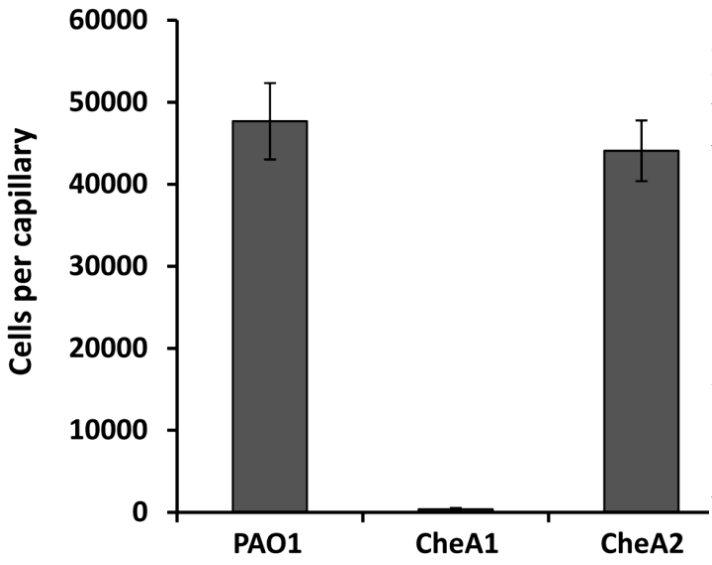

Supp. Fig 19. Implication of *che* and *che2* chemosensory pathways in the chemotactic behavior of *P. aeruginosa* PAO1 toward L-malic acid. Quantitative capillary chemotaxis assays were performed using L-malic acid at a final concentration of 10 mM. Data were corrected with the number of cells that swam into buffer containing capillaries (3115 ± 440). Data are the means and standard deviations from three biological replicates conducted in triplicate.

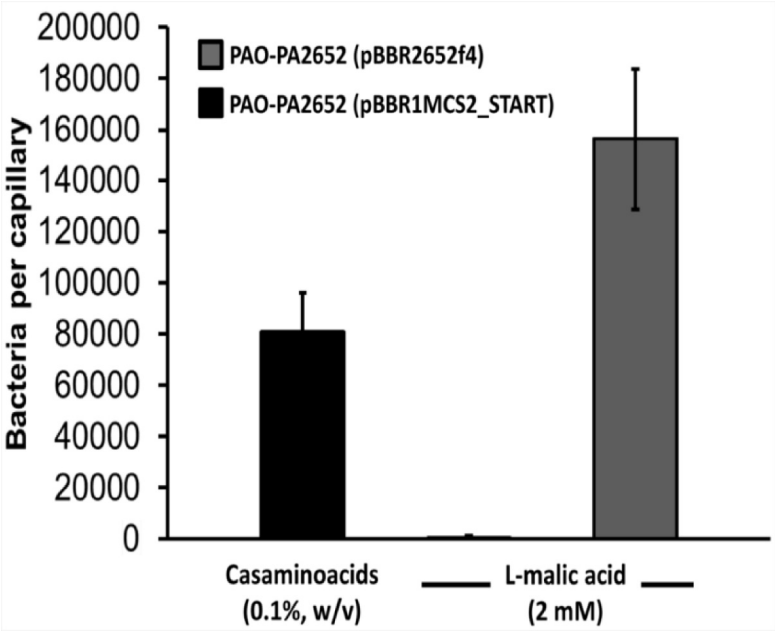

Supp. Fig 20. Quantitative capillary chemotaxis assays showing the genetic complementation of a *Pseudomonas aeruginosa* PAO1 mutant strain defective in PA2652. Complementation assays of the PA2652 mutant by the in trans expression of PA2652 using the pBBRMCS2-based vector, pBBR2652f4. As positive control, chemotaxis toward casaminoacids of the mutant strain harboring the empty plasmid pBBRMCS2_START was analyzed. Data were corrected with the number of cells that swam into buffer containing capillaries (from left to right, 1333 ± 500, 3481 ± 755 and 4962 ± 1003). Data are the means and standard deviations from three biological replicates conducted in triplicate.

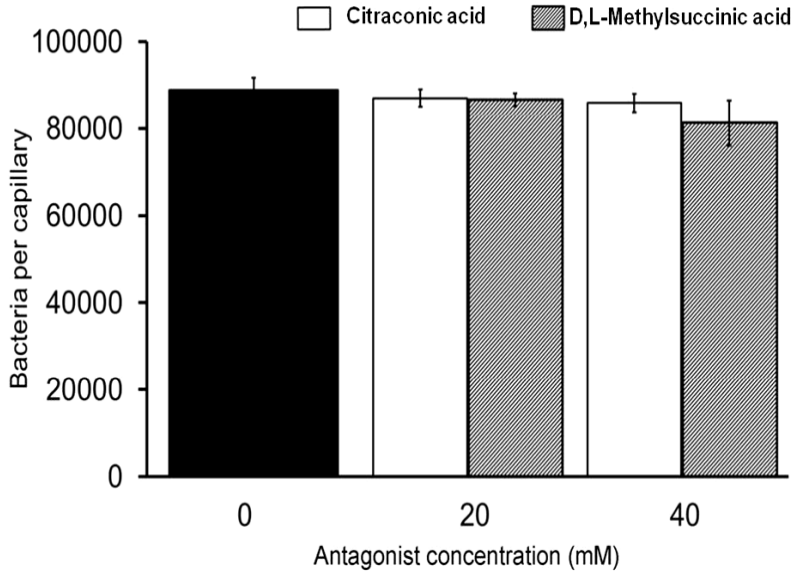

Supp. Fig 21. Effect of citraconic and D,L-methylsuccinic acids in the chemotaxis properties of *P. aeruginosa* toward L-alanine. Shown are number bacterial cells that migrate toward capillaries containing 1 mM of L-alanine (black bar) or 1 mM of L-alanine in the presence of different concentrations of citraconic and D,L-methylsuccinic acids. Data are means and standard deviations from three biological replicates conducted in triplicate. Data were corrected with the number of cells that swam into buffer containing capillaries (4400 ± 352).

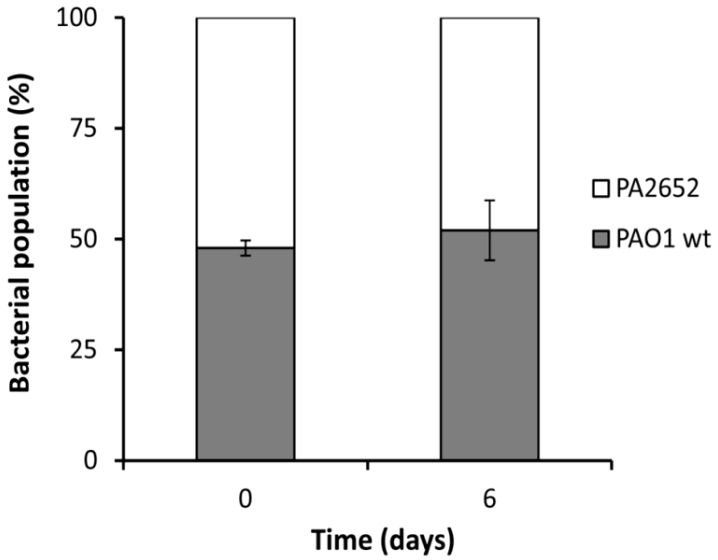

Supp. Fig 22. Competitive root colonization of *P. aeruginosa* PAO1-Km and a mutant defective in PA2652. The figure represents the percentage of bacteria recovered either from the rhizosphere or root tips of maize (*Zea mays*) plants. Data are the means and standard deviations of six plants.

Supp. Table 5. Tm shifts of at least 2 °C caused by the screening of compounds of Biolog arrays PM1, PM2A, PM3b, PM4a and PM5. The results of Isothermal Titration Calorimetry binding studies are also shown.

Compound	Tm Shift (°C)	Binding in ITC
L-malic acid	**+ 5.2**	**YES**
D,L-bromosuccinic acid	**+ 3.6**	**YES**
Citraconic acid	**+ 2.5**	**YES**
D,L-citramalic acid	**+ 2.1**	**YES**
D-lactic acid methyl ester	**+ 2.1**	commercially not available
L-pyroglutamic acid	**+ 2.0**	commercially not available
D,L-methylsuccinic acid	Not in Biolog arrays	**YES**
D-malic acid	No significant shift	NO
Succinic acid	No significant shift	NO
Fumaric acid	No significant shift	NO
Oxaloacetic acid	No significant shift	NO
L-tartaric acid	No significant shift	NO
Glutaric acid	No significant shift	NO
L-aspartic acid	No significant shift	NO
L-threonine	No significant shift	NO

Supp. Table 6. Apparent thermodynamic parameters derived from the microcalorimetric titrations of PA2652-LBD with L-malic acid in the absence and presence of the antagonists citraconic and methylsuccinic acids. Data were analysed using the "One binding site model" of the MicroCal version of ORIGIN. The corresponding data are shown in Fig. 35.

Antagonist	n	K_D(μM)	ΔH(kcal/mol)
none	1 ± 0.1	23 ± 1	-4.1 ± 0.6
2 mM citraconic acid	0.9 ± 0.2	53 ± 4	-5.1 ± 1
20 mM citraconic acid	1.1 ± 1	294 ± 58	-3.3 ± 5
2 mM D,L-methylsuccinic acid	0.6 ± 0.1	54 ± 5	-6.7 ± 1
20 mM D,L-methylsuccinic acid	1.1 ± 0.9	207 ± 31	-2.6 ± 2

Supp. Table 7. Bacterial strains and plasmids used in this study.

Strain or plasmid	Relevant characteristics[a]	Reference or source
Strains		
E. coli BL21 (DE3)	F-*ompT gal dcm lon hsd* S_B ($r_B^-m_B^-$) λ(DE3)	(Jeong *et al.*, 2009)
E. coli DH5α	*supE44 lacU169* (*Ø80lacZ*ΔM15) *hsdR17* ($r_k^-m_k^-$), *recA1 endA1 gyrA96 thi-1 relA1*	(Woodcock *et al.*, 1989)
P. aeruginosa PAO1	wild type	(Stover *et al.*, 2000)
PAO1-Km	wild type PAO1 with a Km cassette inserted in a neutral position downstream of *glmS*; Km^R	(Martin-Mora *et al.*, 2016a)
PAO-PA2652	*PA2652*::IS*phoA*/hah; Tc^R	(Jacobs *et al.*, 2003, Held *et al.*, 2012)
PCheA1	PAO1 transposon mutant *PA1458*::IS*phoA*/hah; Tc^R	(Jacobs *et al.*, 2003, Held *et al.*, 2012)
PCheA2	PAO1 transposon mutant *PA0178*::IS*lacZ*/hah; Tc^R	(Jacobs *et al.*, 2003, Held *et al.*, 2012)
Plasmids		
pET28b(+)	Km^R; Protein expression plasmid	Novagen
pET28-PA2652-LBD	Km^R; pET28b(+) derivative containing DNA fragment encoding PA2652-LBD	This study
pBBR1MCS2_START	Km^R; *oriRK2 mobRK2*	(Obranic *et al.*, 2013)
pBBR2652f4	Km^R; *PA2652* gene was cloned into NdeI and BamHI sites of pBBR1MCS-2_START	This study

[a]The following abbreviations were used for antibiotics: kanamycin, km; tetracycline, Tc.

CHAPTER 2
IDENTIFICATION OF CHEMORECEPTORS THAT MEDIATE CHEMOTAXIS TO POLYAMINES

CHAPTER 2.1: STRUCTURAL BASIS OF POLYAMINE RECOGNITION AT dCACHE-CONTAINING CHEMORECEPTOR IN *P. putida* KT2440

Published article

Structural Basis for Polyamine Binding at the dCACHE Domain of the McpU Chemoreceptor from *Pseudomonas putida*

José Antonio Gavira[1], Álvaro Ortega[2, 3], **David Martín-Mora**[2], María Teresa Conejero-Muriel[1], Andrés Corral-Lugo[2,4], Bertrand Morel[2,5], Miguel Ángel Matilla[2], Tino Krell T[2].

[1]Laboratory of Crystallographic Studies, IACT, (CSIC-UGR), Armilla, Granada, Spain.
[2]Dept of Environmental Protection, Estación Experimental del Zaidín, Consejo Superior de Investigaciones Científicas, Granada, Spain
[3] present address: Dept of Biochemistry and Molecular Biology and Immunology, Faculty of Chemistry, University of Murcia, Murcia, Spain.
[4] present address: Institut de Biologie Intégrative de la Cellule (I2BC), CNRS, Gif-Sur-Yvette, France.
[5] present address: Dept. de Física Química, Facultad de Ciencias, Universidad de Granada, Spain.

Journal of Molecular Biology (Published online 11 May 2018); 430(13):1950-1963.
Doi: 10.1016/j.jmb.2018.05.008

ABSTRACT

Many bacteria can move chemotactically to a variety of compounds and the recognition of chemoeffectors by the chemoreceptor ligand binding domain (LBD) defines the specificity of response. Many chemoreceptors were found to recognize different amino- and organic acids, but the McpU chemoreceptor from *Pseudomonas putida* was identified as the first chemoreceptor that bound specifically polyamines. We report here the three-dimensional structure of McpU-LBD in complex with putrescine at a resolution of 2.4 Å, which fitted well a solution structure generated by Small Angle X-ray Scattering. Putrescine bound to a negatively charged pocket in the membrane distal module of McpU-LBD. Similarities exist in the binding of putrescine to McpU-LBD and taurine to the LBD of the Mlp37 chemoreceptor of *Vibrio cholerae*. In both structures the primary amino group of the respective ligand is recognized by hydrogen bonds established by two aspartate and a tyrosine side chain. This feature may be used to predict the ligands of chemoreceptors with unknown function. Analytical ultracentrifugation revealed that McpU-LBD is monomeric in solution and that ligand binding does not alter this oligomeric state. This sensing mode thus differs from that of the well-characterised four-helix bundle domains where ligands bind to two sites at the LBD dimer interface. Although there appear to be different sensing modes, results are discussed in the context of data indicating that chemoreceptors employ the same mechanism of transmembrane signaling. This work enhances our understanding of CACHE domains, which are the most abundant sensor domains in bacterial chemoreceptors and sensor kinases.

Article

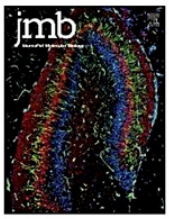

Structural Basis for Polyamine Binding at the dCACHE Domain of the McpU Chemoreceptor from *Pseudomonas putida*

José Antonio Gavira[1], Álvaro Ortega[2], David Martín-Mora[2], María Teresa Conejero-Muriel[1], Andrés Corral-Lugo[2], Bertrand Morel[2], Miguel A. Matilla[2] and Tino Krell[2]

1 - Laboratory of Crystallographic Studies, *IACT, (CSIC-UGR), Avenida de las Palmeras 4, 18100 Armilla, Granada, Spain*
2 - Department of Environmental Protection, *Estación Experimental del Zaidín, Consejo Superior de Investigaciones Científicas, Granada, Spain*

Correspondence to Tino Krell: *Estación Experimental del Zaidín, Consejo Superior de Investigaciones Científicas, C/ Prof. Albareda 1, 18008 Granada, Spain. tino.krell@eez.csic.es*
https://doi.org/10.1016/j.jmb.2018.05.008
Edited by I B. Holland

Abstract

Many bacteria can move chemotactically to a variety of compounds and the recognition of chemoeffectors by the chemoreceptor ligand binding domain (LBD) defines the specificity of response. Many chemoreceptors were found to recognize different amino and organic acids, but the McpU chemoreceptor from *Pseudomonas putida* was identified as the first chemoreceptor that bound specifically polyamines. We report here the three-dimensional structure of McpU-LBD in complex with putrescine at a resolution of 2.4 Å, which fitted well a solution structure generated by small-angle X-ray scattering. Putrescine bound to a negatively charged pocket in the membrane distal module of McpU-LBD. Similarities exist in the binding of putrescine to McpU-LBD and taurine to the LBD of the Mlp37 chemoreceptor of *Vibrio cholerae*. In both structures, the primary amino group of the respective ligand is recognized by hydrogen bonds established by two aspartate and a tyrosine side chain. This feature may be used to predict the ligands of chemoreceptors with unknown function. Analytical ultracentrifugation revealed that McpU-LBD is monomeric in solution and that ligand binding does not alter this oligomeric state. This sensing mode thus differs from that of the well-characterised four-helix bundle domains where ligands bind to two sites at the LBD dimer interface. Although there appear to be different sensing modes, results are discussed in the context of data, indicating that chemoreceptors employ the same mechanism of transmembrane signaling. This work enhances our understanding of CACHE domains, which are the most abundant sensor domains in bacterial chemoreceptors and sensor kinases.

Introduction

Bacteria possess an array of different signal transduction mechanisms that permit the adaptation of bacterial metabolism and behavior to a wide range of environmental signals. Most abundant are one- and two-component regulatory systems as well as chemosensory pathways [1,2]. Canonical signaling in chemosensory pathways is initiated by the direct binding of either chemoeffectors or chemoeffector-loaded periplasmic binding proteins to the ligand binding domain (LBD[1]) of chemoreceptors [3]. Chemoreceptor activation triggers a molecular stimulus that modulates CheA autophosphorylation and consequently transphosphorylation of the CheY response regulator, which generates the pathway output. Chemosensory pathways were shown to mediate chemotaxis and type IV pili-based motility, but are also involved in regulating alternative cellular processes [1].

Escherichia coli, the traditional model to study chemosensory pathway signaling, has five chemoreceptors [4]. On average, chemosensory pathway containing bacteria possess 14 chemoreceptor genes [5]. However, many other bacteria, particularly those that are metabolically versatile and that can

INTRODUCTION

Bacteria possess an array of different signal transduction mechanisms that permit the adaptation of bacterial metabolism and behaviour to a wide range of environmental signals. Most abundant are one-and two-component regulatory systems as well as chemosensory pathways (Ulrich *et al.*, 2005, Wuichet & Zhulin, 2010). Canonical signaling in chemosensory pathways is initiated by the direct binding of either chemoeffectors or chemoeffector-loaded periplasmic binding proteins to the LBD of chemoreceptors (Parkinson *et al.*, 2015). Chemoreceptor activation triggers a molecular stimulus that modulates CheA autophosphorylation and consequently transphosphorylation of the CheY response regulator, which generates the pathway output. Chemosensory pathways were shown to mediate chemotaxis and type IV pili-based motility, but are also involved in regulating alternative cellular processes (Wuichet & Zhulin, 2010).

E. coli, the traditional model to study chemosensory pathway signaling, has 5 chemoreceptors (Ortega *et al.*, 2017a). On average, chemosensory pathway containing bacteria possess 14 chemoreceptor genes (Lacal *et al.*, 2010b). However, many other bacteria, particularly those that are metabolically versatile and that can adapt to different ecological niches, have an elevated number of chemoreceptors (Alexandre *et al.*, 2004, Lacal *et al.*, 2010b). Typically, the function of chemoreceptors is determined by the specificity of signal recognition at the receptor LBD. However, the large majority of chemoreceptors are of unknown function and their identification is hampered by the significant sequence divergence of the receptor LBD, which does not allow the extrapolation of function to homologues in other species.

Over the last decade, research has turned to the study of diverse bacteria with different lifestyles (Bardy *et al.*, 2017). In order to understand the eco-physiological relevance of chemotaxis, it is indispensable to identify the function of their chemoreceptors and to define their ligand profile. This research has resulted in the functional annotation of many chemoreceptors of which many recognize amino- and organic acids (Ortega *et al.*, 2017a). Bioinformatics studies indicate that chemoreceptors employ more than eighty different LBD types for signal recognition (Ortega *et al.*, 2017a).

Due to its presence in *E. coli* chemoreceptors, the 4HB domain is the best characterized LBD (Parkinson *et al.*, 2015). These domains are present in a monomer-dimer equilibrium. Ligands bind to the dimer (Milligan & Koshland, 1993, Rico-Jimenez *et al.*, 2016), at a site close to the dimer interface and amino acids from both monomers participate in ligand binding (Milburn *et al.*, 1991). Ligand binding induces dimer stabilization shifting the equilibrium to the dimeric state (Milligan & Koshland, 1993, Rico-Jimenez *et al.*, 2016, Fernandez *et al.*, 2017). Binding causes translational and rotational movements of the final α-helix, which corresponds to the stimulus that is conveyed across the membrane changing ultimately the CheA activity (Ottemann *et al.*, 1999, Yu *et al.*, 2015).

Bioinformatics studies have shown that CACHE domains are the most common LBDs in chemoreceptors (Ortega *et al.*, 2017a) and sensor kinases (Zhang & Hendrickson, 2010). These domains are composed of a long N-terminal helix and either one (sCACHE) or two (dCACHE) globular modules (Zhang & Hendrickson, 2010). Recent studies have resulted in the identification of the ligand profile of several dCACHE containing chemoreceptors (Matilla & Krell, 2017). The dCACHE domain appears to be a universal domain that has served as chassis for the evolution of sensor domains for different compounds like amino acids (Glekas *et al.*, 2012), quaternary amines (Webb *et al.*, 2017b), galactose (Day *et al.*, 2016), taurine (Nishiyama *et al.*, 2016), purines (Fernandez *et al.*, 2016), polyamines (Corral-Lugo *et al.*, 2016), GABA (Reyes-Darias *et al.*, 2015a), organic acids (Rahman *et al.*, 2014) and thiamine (Rahman *et al.*, 2014). So far, the biochemical and structural information available indicates that most ligands bind to the membrane distal module of the dCACHE domain (Glekas *et al.*, 2010, Rico-Jimenez *et al.*, 2013a, Liu *et al.*, 2015, Nishiyama *et al.*, 2016). However, the structure of a dCACHE domain has recently been reported that contained the

ligand in the membrane proximal module (Machuca *et al.*, 2017). This makes it currently impossible to identify a general sensing mechanism for this domain family.

P. aeruginosa PAO1, *P. putida* KT2440 and *P. Fluorescens* Pf0-1 are important model organisms to study chemoreceptors (Ortega *et al.*, 2017a). These strains have numerous dCACHE LBD containing chemoreceptors, of which the majority have been annotated with a function (see legend to Supp. Fig. 23). However, sequence analyses have shown that their dCACHE domains form two groups (Ortega *et al.*, 2017a). Interestingly, these groups differ in size; whereas the first group has an average size of 330 ± 12 amino acids, group two domains are shorter with an average size of 253 ± 6 residues (Supp. Fig. 23). The structural differences and the functional relevance of the larger group 1 domains remain unclear.

We have identified previously McpU as the first chemoreceptor that binds and mediates chemoattraction to the polyamines putrescine, cadaverine and spermidine (Supp. Fig. 24)(Corral-Lugo *et al.*, 2016). McpU is from the *P. putida* KT2440 strain, which is a nutritionally versatile, saprophytic and plant root-colonizing Gram-negative soil bacterium. Putrescine, cadaverine, spermidine and spermine are the predominant polyamines in bacteria and are abundantly present in all kingdoms of life, where they exert a number of different metabolic and signaling functions (Miller-Fleming *et al.*, 2015). Apart from their role as bacterial growth substrates, there is increasing evidence for their central role as signal molecules in mediating plant-host interactions (Di Martino *et al.*, 2013). Interestingly, the McpU-LBD belongs to the larger group 1 (Supp. Fig. 23).

We present here an analysis of the McpU-LBD by different biophysical techniques and report structures determined by X-ray crystallography and Small Angle X-ray scattering (SAXS). The high resolution structural information also revealed amino acids involved in putrescine recognition, which has allowed to identify conserved features in other amine responsive dCACHE domains

METHODOLOGY

Protein expression and purification: McpU-LBD was expressed in *E. coli* and purified by affinity chromatography as described in (Corral-Lugo *et al.*, 2016). McpU-LBD comprises amino acids 33 to 334 of the McpU chemoreceptor (PP_1228). For the generation of the his-tag free form of McpU-LBD, protein was dialysed into analysis buffer (5 mM Tris, 5 mM Pipes, 5 mM Mes, 150 mM NaCl, pH 7.0) supplemented with 10 % (v/v) glycerol. Protein was adjusted to 100 µM and digested with thrombin (Sigma) at 15 °C on an orbital shaker for three hours. At the beginning and after 1 and 2 hours, 1 % (w/v) thrombin was added to the protein. Protein was then passed through a 5-ml HisTrap HP column (Amersham Biosciences) equilibrated with 20 mM Tris/HCl, 0.1 mM EDTA, 500 mM NaCl, 30 mM imidazole, 5 mM β-mercaptoethanol, 5% (v/v) glycerol, pH 7.8. The flow through was collected and the absence of the his-tag verified by SDS-PAGE.

Far UV circular dichroism (CD) spectroscopy: CD measurements were made with a Jasco J-715 spectropolarimeter (Tokyo, Japan) equipped with a thermostatized cell holder. Protein was dialysed into analysis buffer supplemented with 10 % (v/v) glycerol and measurements were made with a 1 mm path length quartz cuvette at a protein concentration of 18.5 µM. The ligands were prepared in the same buffer and were added at a final concentration of 200 µM. Spectra were recorded at a scan rate of 100 nm/min, 1 nm step resolution, 1 sec response and 1 nm bandwidth. The spectra shown are averages of 5 scans. Each spectrum was corrected by baseline subtraction using the buffer spectrum. The CD signal was normalized to mean residue molar ellipticity ([θ], in $deg.dmol^{-1}.cm^2$).

Differential Scanning Calorimetry: Experiments were carried out on a VP-DSC capillary-cell microcalorimeter from MicroCal (Northampton, MA) at a scan rate of 180 °C/h from 5 °C to 95 °C. Calorimetric cells (operating volume 0.134 ml) were kept under pressure (60 psi) to prevent sample degassing. Several buffer-buffer baselines were obtained before each protein run to ascertain proper equilibration of the instrument. Protein samples were exhaustively dialysed

against analysis buffer supplemented with 10 % (v/v) glycerol. The protein concentration was 37.8 µM. Ligands were prepared in dialysis buffer and added at a final concentration of 200 µM. The calorimetric enthalpies were estimated by integration of the transition peaks and the peak width at half-height was determined using Origin 7.5 (OriginLab Corporation, Northampton, MA).

Analytical Ultracentrifugation: Experiments were performed on a Beckman Coulter Optima XL-I analytical ultracentrifuge (Beckman-Coulter, Palo Alto, CA, USA) equipped with UV-visible absorbance and interference optics detection systems, using an An50Ti 8-hole rotor, 12 mm path-length charcoal-filled epon double-sector centrepieces. The experiments were carried out at 10 °C with a stabilizing period of at least 1 h once 10 °C were reached in the rotor chamber. His-tagged protein was in analysis buffer, whereas his-tag free protein in analysis buffer supplemented with 10 % (v/v) glycerol. Ligands were added at a final concentration of 100 µM. Laser at a wavelength of 280 nm was used in the absorbance optics mode. Sedimentation velocity runs were carried out at 48,000 rpm using 400 µl samples and dialysis buffer as reference. A series of 100 scans without time intervals between successive scans were acquired for each sample. A least squares boundary modelling of the data was used to calculate sedimentation coefficient distributions with the size-distribution *c(s)* method and the non-interacting discrete species model (Schuck, 2000) implemented in the SEDFIT v14.1 software. The molecular weight was extracted from the sedimentation profiles, via the Lamm equation included in the *c(s)* model of SEDFIT (Schuck, 2000). The best fit values obtained for the sedimentation coefficient (*s*, in S or Svedbergs) and diffusion were used to estimate the molar mass of the molecule using the Svedberg equation. Buffer density (ρ = 1.00684 g/mL) and viscosity (η = 0.013372 Poise) at 10 ^{0}C were estimated by SEDNTERP software (Laue *et al.*, 1992) from the buffer components.

Protein crystallization: Initial crystallization screening was done using the counter-diffusion technique and the commercially available kits GCB-CSK, PEG448-49 and AS-49 (Triana Science & Technology) with capillaries of 0.2 mm inner diameter and 50 mm length. Protein in analysis buffer supplemented with 10 % (v/v) glycerol was concentrated to 30 mg/ml using concentration units (Amicon). The protein was then incubated with a two-fold molar excess of putrescine. Unbound ligand was removed by buffer exchange with the same buffer. Capillaries were filled with protein, sealed with clay and inserted into pre-filled Granada Crystallization Box-Domino units through the top agarose layer. Experiments were incubated at 4 and 20 °C. For crystal improvement, agarose was added to the protein to a final concentration of 0.1 % or 0.05 % (w/v) prior to capillary loading. The best diffracting crystals were obtained with a PEG mixture (20 % PEG 400, 15 % PEG 4K, 10 % PEG 8K, pH 5.0 to 9.0) and in 30 % PEG 4K, 0.2 M NH_4-acetate, 0.1 M Na-acetate, pH 6.0. Crystals were extracted from the capillary and cryo-protected in mother liquid supplemented with 15 % (v/v) glycerol, cryo-cooled and stored until data collection. Crystals were diffracted at the European Synchrotron Radiation Facility (beam lines ID23-1 & 2, ID29 and ID30A-1) and the Spanish Synchrotron ALBA (Beamline XALOC). Data were indexed and integrated with XDS (Kabsch, 2010).

Structure determination and analysis: Attempts to solve the phase problem by molecular replacement techniques using all currently available dCACHE structures failed and therefore seleno-methionine containing protein was generated and crystallised following the protocol of the native protein. Several MAD data sets were collected but none gave a phase solution. We then tested several phasing methods available at the Auto-Rickshaw (Panjikar *et al.*, 2005) server and phases were obtained by the SAS method when eight data sets, collected at the Se-peak (0.97901Å), were used to increase data redundancy. Based on initial analyses, the resolution limit for substructure determination and initial phase calculation was set to 3.7 Å. Thirty two heavy atom positions, out of 38 possible, were identified by SHELXD (Schneider & Sheldrick, 2002) and the correct hand determined using SHELXE (Sheldrick, 2008). The occupancy of all substructure atoms was refined and initial phases were calculated using MLPHARE (Collaborative Computational Project, 1994). Map interpretation was initiated with ARP/wARP (Morris *et al.*, 2004) and finalized with BUCCANEER (Cowtan, 2006). Model building and ligand identification were performed with Coot. At

the last steps of refinement, Titration-Libration-Screw (TLS) was included and the model quality was verified using MolProbity (Chen *et al.*, 2010). Refinement statistics and quality indicators of the final model are summarized in Table 9.

Small Angle X-ray Scattering (SAXS): Experiments were performed at the BL-11 station of the ALBA Synchrotron Light Facility (Barcelona, Spain). Scattered radiation was recorded in a two-dimensional CCD detector. The sample-detector distance of 2.4 m covered the range of momentum transfer $0.003 < s < 0.45$ Å^{-1} and $\lambda = 1.28$ Å is the X-ray wavelength. For each sample, 20 spectra of 1 second were recorded in the sampler batch mode. Samples in analysis buffer were measured at concentrations of 62 mg/ml to 15.8 mg/ml. Buffer measurements were made before and after protein measurements and the average background scattering was subtracted from the protein scattering. The standard SAXS data reduction and analysis was done using PRIMUS (Konarev *et al.*, 2003). The pair distance distribution function *p(r)* and maximum size of the protein molecules D_{max} was calculated with the program GNOM (Svergun, 1992). The forward scattering *I(0)* and the radius of gyration *Rg* were computed using the Guinier approximation for $sRg < 1.3$. The molecular mass of the sample was estimated by comparing the extrapolated forward scattering *I(0)* to a bovine serum albumin reference solution.

Table 9. Data collection and refinement statistics of the three dimensional structure of McpU-LBD with putrescine (values in parentheses are for highest-resolution shell).

Data collection	
Beam line	ID23-1 (ESRF)
Space Group	C 2 2 2_1
Cell dimensions, a, b, c (Å)	133.98, 164.52, 123.61
ASU	5
Resolution (Å)	79.53 - 2.39 (2.47 - 2.39)
R_{merge} (%)	9.4 (59.8)
I/σ_I	8.80 (1.51)
Completeness (%)	96.31 (90.98)
Unique reflections	52459 (4922)
Multiplicity	3.0 (2.8)
CC(1/2)	0.99 (0.73)
Refinement	
Resolution (Å)	79.53 - 2.39
R_{work}/R_{free} (%)	19.4/23.4
No. atoms	11035
Protein	10670
Ligands	68
Water	297
B-factor (Å^2)	49.72
R.m.s deviations	
Bond lengths (Å)	0.003
Bond angles (^{0})	0.57
Ramachandran (%)	
Favoured	97.84
Outliers	0.23

Site-directed mutagenesis and Isothermal Titration Calorimetry: Derivatives of the McpU-LBD expression plasmid pET28b-LBDMcpU (Corral-Lugo *et al.*, 2016) containing the alanine substitution mutants were synthesized by GenScript (Piscataway, NJ). Mutant protein was purified following the protocol for the wt protein (Corral-Lugo *et al.*, 2016). Freshly purified protein was analysed by ITC. Experiments were conducted on a VP-microcalorimeter (Microcal, Amherst, MA) at 25 °C. McpU mutants (35 µM) were dialyzed overnight against analysis buffer supplemented with 10 % (v/v) glycerol and placed into the sample cell. Protein was titrated with 9.6-14.4 µl injections of 2-10 mM ligand solutions prepared in dialysis buffer. The mean enthalpies measured from the injection of ligands into buffer were subtracted from raw titration data prior to data analysis with the MicroCal version of ORIGIN. Data were fitted using the "One binding site model". Data are means and standard deviations from three experiments.

Construction of McpU-LBD_Δloop: An overlapping PCR approach was used to replace the loop between ß1 and ß2 in McpU-LBD (VFQPNALDQQDSHYLGQDAMGSNESGRFS) with its equivalent in PctA-LBD (GQQDG). Two amplicons were obtained using the primer pairs McpU-F-Up-NdeI (5´-TAATCATATGACCCAGGCCCATCGCAGCG-3´)/McpU-R-Up (5´-*GCCGTCCTGCTGGCC*CAGGTACAGGCCAATCACATC-3´) and McpU-F-down (5´-TACCTG*GGCCAGCAGGACGGC*CTGTACTGGTCCCAACCAAG-3´)/McpU-R-down-BamHI (5´-TAATGGATCCTCAGTTGGCGTTCTGGTTATGGGCA-3´). The sequence coding for GQQDG is shown in italics and restriction sites are underlined. Using a mixture of the two resulting PCR fragments as template, a 837 bp amplicon was obtained using primers McpU-F-Up-NdeI and McpU-R-down-BamHI. This PCR fragment was subsequently cloned into NdeI/BamHI sites of the expression vector pET28b(+) to generate pMAMV292. The replacement as well as the absence of further mutations were confirmed by DNA sequencing.

RESULTS

McpU-LBD unfolds in a single transition

McpU-LBD was purified as reported previously (Corral-Lugo *et al.*, 2016) and analysed by far UVCD spectroscopy in the absence and presence of ligands (Fig. 37A). Spectra were deconvoluted to determine the relative abundance of secondary structure elements (Supp. Table 8). Data show that ligand binding does not cause any significant alterations in the secondary structure content of the protein. The capacity of the protein analysed to bind polyamines has been verified by ITC (data not shown).

Differential Scanning Calorimetry was then used to follow protein unfolding in the absence and presence of ligands (Fig. 37B). Ligand-free McpU-LBD unfolded in a single event with a mid-point of unfolding (Tm) of 45.4 °C. The protein also unfolded in a single event in the presence of ligands that caused T_m increases between 3.3 to 5.4 °C (Supp. Table 9). However, the unfolding peak in the presence of ligands was narrower, as shown by a significant reduction in the peak width at half height (Supp. Table 9), indicating an increase in unfolding cooperativity in the presence of ligands.

Ligand binding does not alter the monomeric state of McpU-LBD

We conducted sedimentation velocity analytical ultracentrifugation experiments to assess the oligomeric state of McpU-LBD in the absence and presence of ligands. The analysis of ligand-free protein revealed that the sedimentation characteristics are independent of the protein concentration; therefore, non-ideality effects on the analysis could be discarded. A main species was observed characterized by a standard sedimentation coefficient (corrected for protein in water at

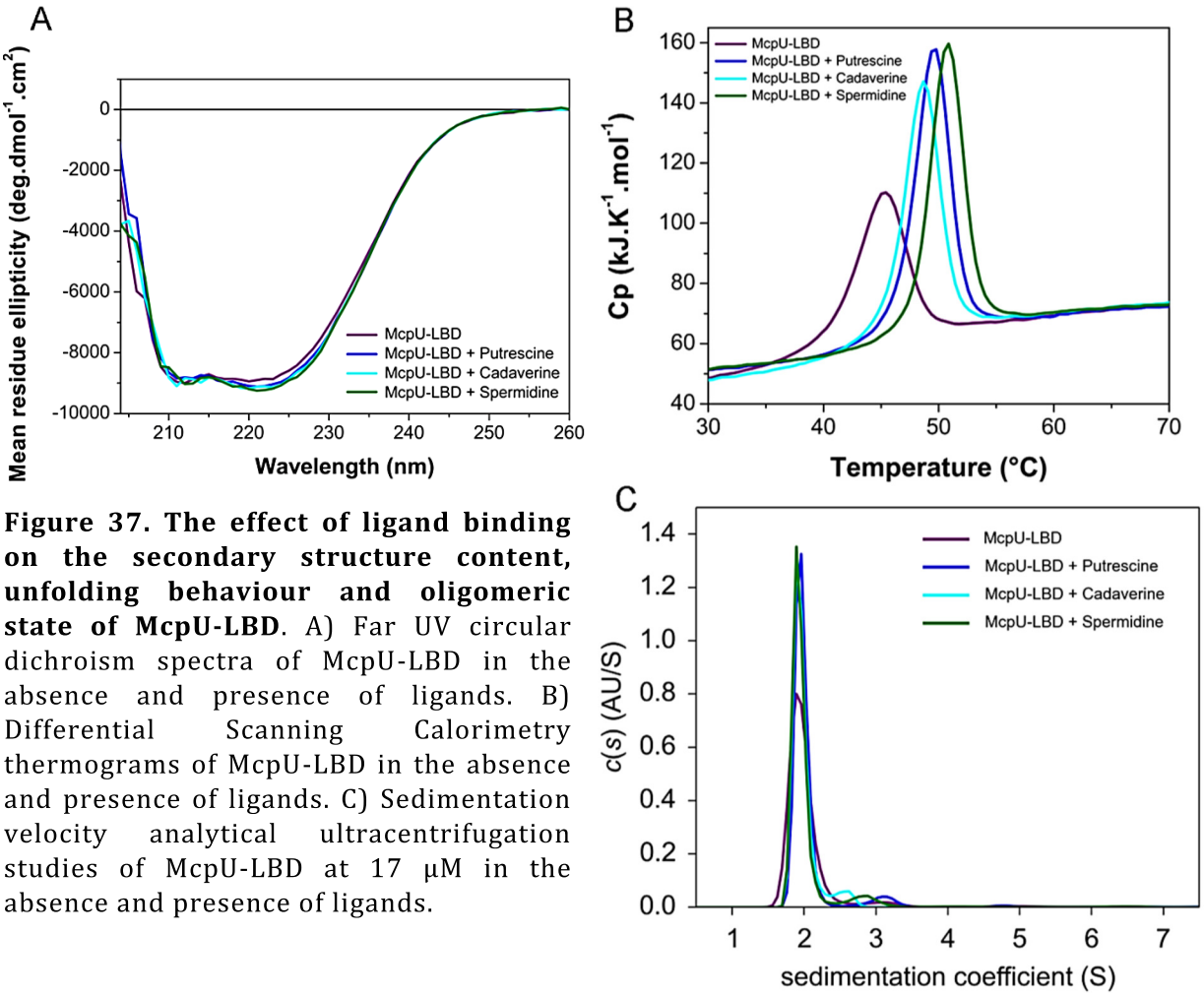

Figure 37. The effect of ligand binding on the secondary structure content, unfolding behaviour and oligomeric state of McpU-LBD. A) Far UV circular dichroism spectra of McpU-LBD in the absence and presence of ligands. B) Differential Scanning Calorimetry thermograms of McpU-LBD in the absence and presence of ligands. C) Sedimentation velocity analytical ultracentrifugation studies of McpU-LBD at 17 µM in the absence and presence of ligands.

20 C) of $s_{w,20}$ = 2.7 S and a frictional ratio (*fr*) of 1.5 (Fig. 37C). Based on the frictional ratio and using the diffusional scaling law implemented in SEDFIT and the Svedberg equation, the average molar mass of the McpU-LBD was determined to be 35.6 kDa, which is almost identical to the sequence-derived mass of the monomer (35.8 kDa). When the experiments were repeated in the presence of saturating concentrations of the three McpU ligands, no changes in the sedimentation coefficient distributions was observed (Fig. 37C). We have then generated a McpU-LBD batch from which the histidine tag had been removed. Isothermal titration experiments (Supp. Fig. 25) showed that the affinity of putrescine of the his-tag free protein (K_D=1.66 µM) was very similar to that of the his-tag containing form (K_D=2.0 µM)(Corral-Lugo *et al.*, 2016). We have then repeated the AUC experiments. Since the his-tag removal resulted in a slight reduction of protein solubility, experiments were conducted in analysis buffer supplemented with 10 % (v/v) glycerol (in contrast to the above studies that were carried out in the absence of glycerol). As shown in Supp. Fig. 26, a single peak was obtained for McpU-LBD in the presence and absence of ligands. Peaks had a standard sedimentation coefficient of 2.4 S, that corresponds to a species of 33 kDa. We therefore conclude that ligand binding does not induce self-association nor provokes major conformational changes of McpU-LBD.

The three dimensional structure of McpU-LBD

McpU-LBD in complex with putrescine was crystallised and the three dimensional structure was solved by X-ray crystallography to a resolution of 2.4 Å (Fig. 38). The unit cell contained five

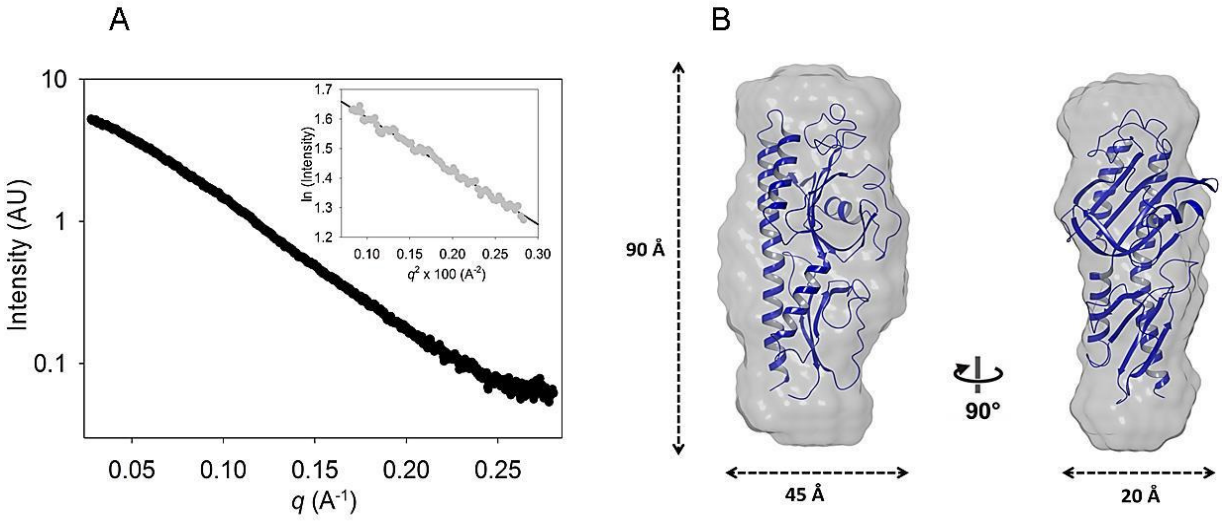

Figure 38. Small Angle X-ray Scattering studies of McpU-LBD. A) SAXS spectra, the inset shows the Guinier plot. B) Superimposition of the SAXS envelope obtained by averaging 20 SAXS models with the X-ray structure.

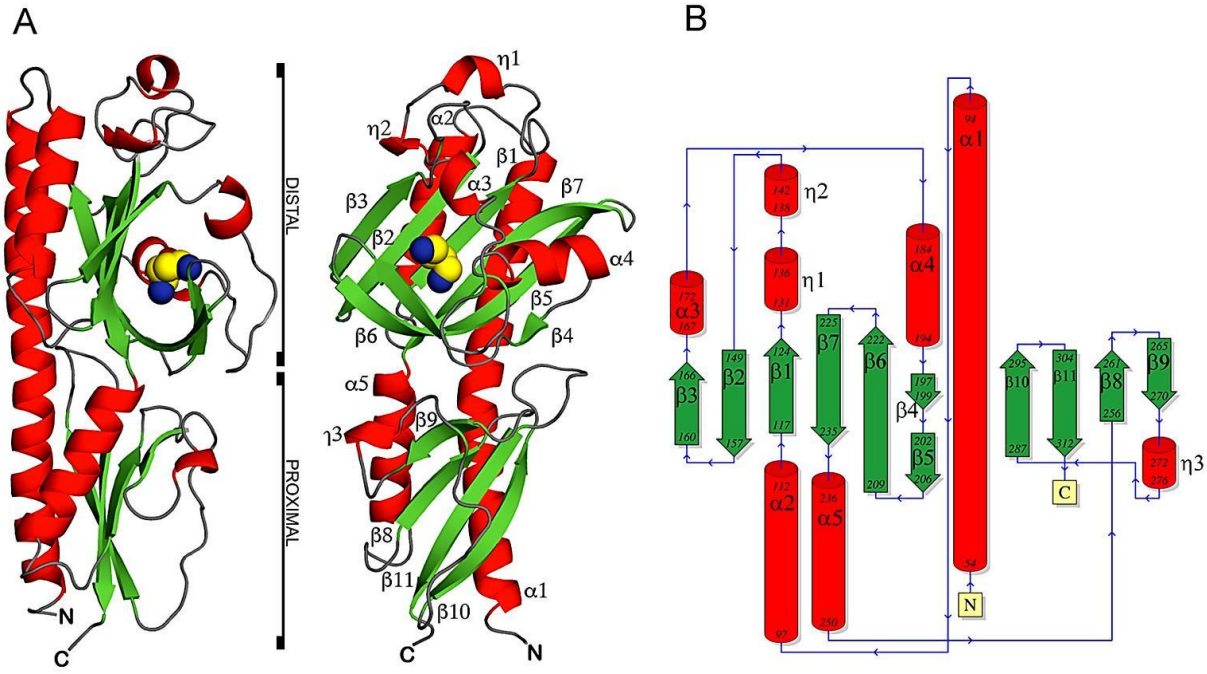

Figure 39. The three dimensional structure of McpU-LBD in complex with putrescine as determined by X-ray crystallography. A) Cartoon diagram with secondary structure elements annotated. Bound putrescine is shown in the spacefill mode. B) Schematic representation of the secondary structure elements.

protein chains, composed of two perpendicularly oriented dimers that contact with a protein monomer (Supp. Fig. 27). The McpU-LBD structure is composed of a long N-terminal α-helix followed by two α/ß containing modules that are referred to as membrane proximal and membrane distal modules. In all five chains putrescine was present in the distal module whereas no ligand other than water was present in the proximal module (Fig. 38).

In parallel, we analysed ligand free McpU-LBD by Small Angle X-ray Scattering (SAXS), which provides information on the oligomeric state of a protein and estimates its overall structure at low

resolution in solution. The scattering profile of McpU-LBD is shown in Fig. 39A and molecular envelopes of McpU-LBD were constructed from the SAXS data averaging 20 dummy-atom models (Fig. 39B). Its elongated shape has an axial ratio close to 3 which agrees with the information acquired from the frictional ratio of ~1.5 by AUC. The crystallographic structure of McpU-LBD could be well superimposed on the experimental molecular envelopes obtained by SAXS (Fig. 39B). Modelling by HYDROPRO (Ortega *et al.*, 2011) allows us to estimate the theoretical sedimentation coefficient (s), radius of gyration (R_g), intrinsic viscosity ([η]) and diffusion coefficient (D_t) from the SAXS and crystallographic models of McpU-LBD. The results (Supp. Table 10) indicate a close overlap between both structures, indicating a close resemblance of the sold-state and solution structures. When the SAXS experiments were repeated in the presence of putrescine no significant changes were noted neither in the overall structure nor in the oligomeric state, confirming above CD and AUC studies.

The electron density in the distal module of the X-ray structure has permitted the precise placement of the putrescine molecule (Fig. 40A). Fig. 40B highlights the amino acids that compose the ligand binding site. Ligand recognition appears to be mediated by hydrophobic interactions (mainly through W186) as well as electrostatic interactions. Putrescine is a polyamine with a pKa of 10.8, indicating that the amino groups are protonated at physiological pH. Two aspartate residues (D204 and D233) appear to play key roles in ligand recognition that establish together four hydrogen bonds with the bound ligand. In addition, another hydrogen bond is formed by Y202.

Key roles of aspartate residues in polyamine recognition

To assess the roles of the individual amino acids in ligand binding, we have created alanine substitution mutants in 6 residues located in vicinity of bound putrescine (shown in dark grey in Fig. 40B). Using ITC we have then assessed the binding of the three McpU ligands to the purified mutant proteins and the derived thermodynamic parameters are provided in Table 10. As a representative example the titration data with spermidine are shown in Fig. 41. Whereas W186A and Y202A showed approximately 100- and 20-fold reductions in affinity, the binding constant of M170A was unchanged. However, for the latter mutant the binding reaction was driven by favourable entropy changes as evidenced by the upwards going peaks representing endothermic reactions. In contrast, no binding heats were observed for mutants in aspartate residues 204 and 233.

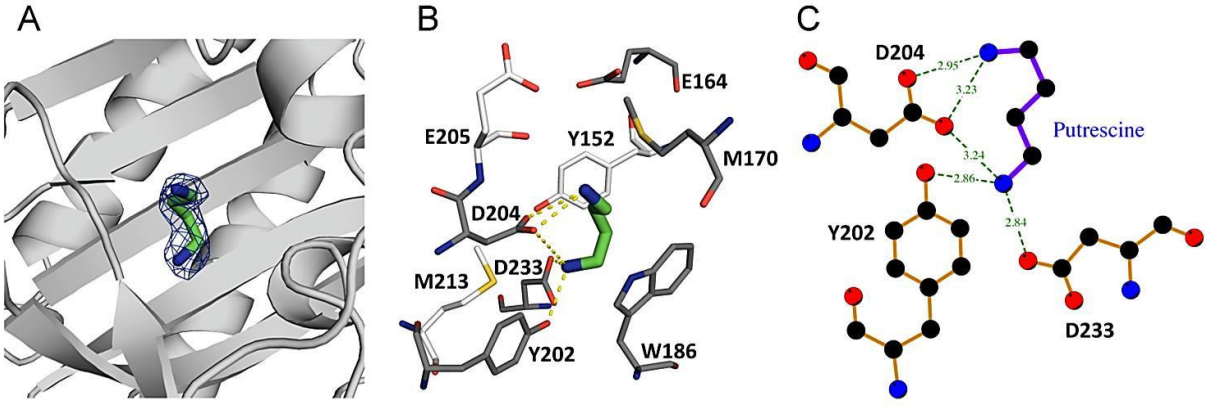

Figure 40. The ligand binding pocket of McpU-LBD. A) Zoom at the membrane distal module containing bound putrescine. The 2Fo-Fc electron density contoured at 1.5 σ is also shown. B) Amino acids that form the ligand binding site. Hydrogen bonds are indicated and amino acids that have been mutated are shown in dark grey. C) Schematic representation of the hydrogen bonding network of bound putrescine.

Table 10. Binding parameters derived from Isothermal Titration Calorimetry studies of McpU-LBD and site directed mutants.

Protein	Putrescine		Spermidine		Cadaverine	
	K_D (μM)	Δ*H* (kcal/mol)	K_D (μM)	Δ*H* (kcal/mol)	K_D (μM)	Δ*H* (kcal/mol)
McpU-LBD[1]	2 ± 1	-15 ± 0.1	4.5 ± 0.4	-4.3 ± 0.1	22 ± 2	-15.5 ± 0.5
E164A	44 ± 0.4	-2.1 ± 0.6	31 ± 4	-6.3 ± 0.6	9 ± 0.78	-32 ± 0.5
M170A	NO BINDING		4.7 ± 0.5	2.7 ± 0.1	65 ± 3	25 ± 8
W186A			463 ± 20	-5.2 ± 1.2	800 ± 300	-3.5 ± 5.9
Y202A			108 ± 7	-2.4 ± 0.2	369 ± 94	-1.3 ± 1
D204A			NO BINDING		275 ± 57	-2.1 ± 2
D233A					NO BINDING	

Data are means and standard deviation from three experiments
[1]reported previously in (Corral-Lugo *et al.*, 2016)

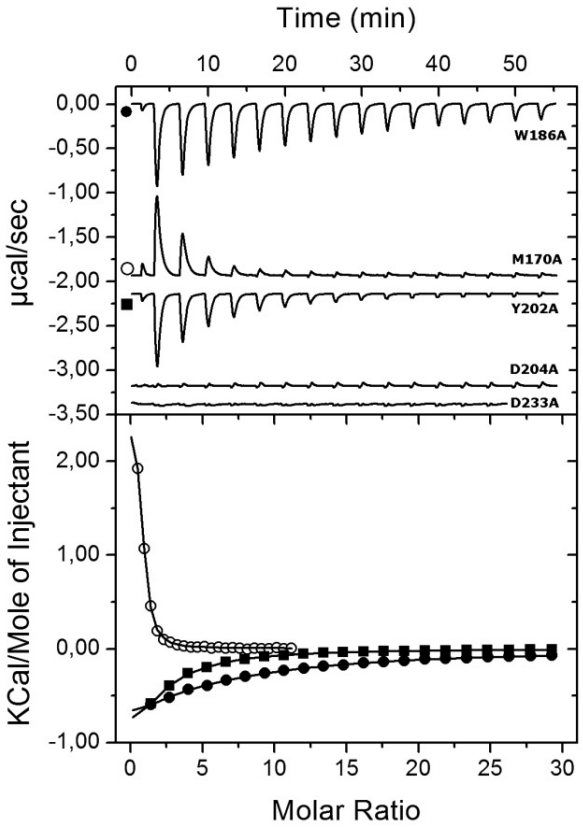

Figure 41. Isothermal titration calorimetry binding studies of different ligands to McpU-LBD site directed mutants. Upper panel: titration raw data for the injection of 11.2 to 12.8 μl aliquots of 2 mM or 5 mM (W186A and Y202A) spermidine into different mutant proteins (at 35 μM). Lower panel: integrated, dilution heat corrected and concentration normalized peak areas fitted with the "One binding site" model of ORIGIN.

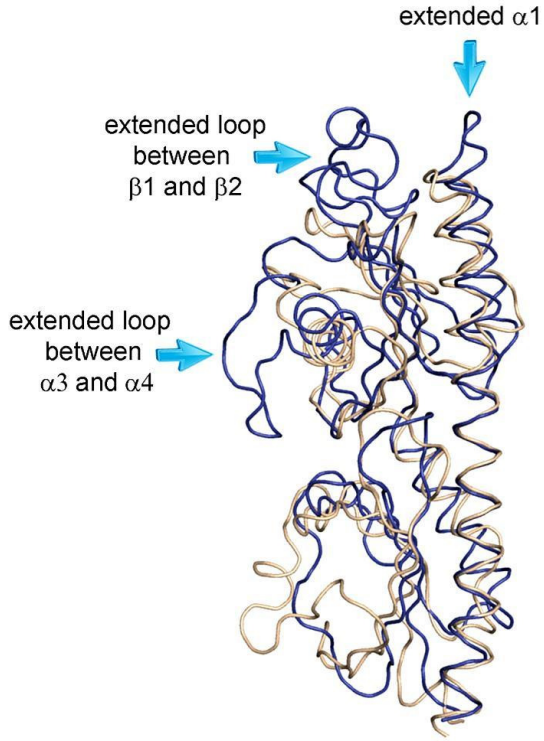

Figure 42. Structural extensions that account for the increased size of McpU-LBD. Structural alignment of the PctA-LBD (beige) and McpU-LBD (violet) structures. The different extensions in the McpU-LBD structure are shown.

The mutations had different effects on the binding of the remaining ligands. Whereas E164A was the only mutant that bound putrescine (with 20-fold reduced affinity), all but the D233A mutant bound cadaverine. Taken together, D204 and particularly D233 are key residues in ligand recognition. Hydrophobic contributions to binding through W186 as well as the hydrogen bond via Y202 are also very important since either no or strongly reduced binding was observed. In contrast, the contribution of E164 and M170 to polyamine binding is more modest (Table 10).

Extensions at three different sites explain the increased size of large LBD domain

The analysis of dCACHE domains in several *Pseudomonas* strains revealed the presence of two groups that differ in size (Supp. Fig. 23). Fig. 42 shows a structural alignment of McpU-LBD (group 1) with PctA-LBD (pdb ID: 5LTX), a representative member of group 2. The increased size of McpU-LBD is due to three extensions, which are all in the distal module. The N-terminal helix is slightly longer, a loop of significant size is inserted between ß1 and ß2 and the loop between α3 and α4 is also much longer than its equivalent in PctA-LBD.

The largest insertion was that in between ß1 and ß2 and to assess its relevance for ligand binding we generated a McpU mutant, McpU-LBD_Δloop, in which this loop (FQPNALDQQDSHYLGQDAMGSNESGRF) was replaced by its equivalent in PctA (GQQDG). However, this protein was insoluble which prevented all further analyses. Since two of the extensions are at the tip of the structure, we hypothesized that these regions may potentially be involved in the recognition of periplasmic binding proteins. To verify this hypothesis we have immobilized McpU-LBD and have conducted pull-down experiments, following the protocol reported in (Rico-Jimenez *et al.*, 2016) using different *P. putida* extracts. However, no evidence for the binding of other proteins to McpU-LBD was obtained.

Table 11. Structural alignment of the McpU-LBD with structures deposited in the Protein Data Bank.

PDB ID	Acronym	Z-score	Identity (%)	RMSD	LBD size[a]	Ligands	Protein/species	Reference
6f9g	McpU	-	-	-	302	Putrescine, cadaverine, spermidine	CR[b]/*P. putida*	This work
3lib	Z3	24.9	21	2.2	280	Unknown	HK[b]/*Methanosarcina mazei*	(Zhang & Hendrickson, 2010)
3li8	Z2	24.3	21	2.5	280	Unknown	HK/*M. mazei*	(Zhang & Hendrickson, 2010)
4wy9	CcaA/Tlp1	21.5	12	3.4	299	L-Asp?	CR/*C. jejuni*	(Machuca *et al.*, 2016)
3lic	Z6	19.3	19	3.3	281	Unknown	HK/*Sh. oneidensis*	(Zhang & Hendrickson, 2010)
5wbf	TlpC	18.3	16	2.8	272	Lactate	CR/*H. pylori*	(Machuca *et al.*, 2017)
5ave/5avf	Mlp37	18.1	15	2.8	253	L-Ser, taurine	CR/*V. cholerae*	(Nishiyama *et al.*, 2016)
5ltx	PctA	17.8	18	2.4	252	Proteinogenic amino acids	CR/*P. aeruginosa*	To be published
5ere	-	17.8	8	3.0	239[c]	Cytosine[d]	Substrate binding protein *Desulfohalobium retbaense*	To be published
5ltv	PctC	17.1	22	2.8	255	Proteinogenic amino acids /GABA	CR/*P. aeruginosa*	To be published
3lif	Z16	17.1	13	2.8	258	Unknown	HK/*Rhodopseudomonas palustris*	(Zhang & Hendrickson, 2010)
5lt9	PctB	16.9	16	3.1	251	Proteinogenic amino acids	CR/*P. aeruginosa*	To be published
3lid	Z8	16.1	7	3.8	293	Unknown	HK/*V. parahaemolyticus*	(Zhang & Hendrickson, 2010)
3t4k	AHK4	15.7	10	3.4	281	Cytokinins	HK/*Arabidopsis thaliana*	(Hothorn *et al.*, 2011)
4dbj	KinD	15.6	13	2.7	218	Butyrate, propionate, pyruvate, acetate	HK/*B. subtilis*	(Wu *et al.*, 2013b)
4xmq	Ccml/Tlp3	15.4	12	3.0	255	Amino acids, succinate, malate, fumarate, purine, thiamine	CR/*C. jejuni*	(Liu *et al.*, 2015)
2zbb	smDctB	15.2	10	3.2	280	Dicarboxylic acids	HK/*S. meliloti*	To be published

Shown are the structures with a Z-score above 15. Structures share less than 90 % of sequence similarity amongst each other.

[a] Size between tm regions

[b] HK: histidine kinase, CR: chemoreceptor

[c] part of cytosolic receptor, LBD size determined by structural alignment

[d] cytosine present in the binding pocket in the membrane distal module

DISCUSSION

The dCACHE domain is a very abundant LBD in sensor kinases and chemoreceptors (Zhang & Hendrickson, 2010, Upadhyay *et al.*, 2016). Previous studies have shown that dCACHE domains from *Pseudomonas* chemoreceptors form two groups which differ in size (Ortega *et al.*, 2017a). Comparing the PctA-LBD structure with that of McpU-LBD has revealed the reason for the increased size of group 1 domains, which consists in three different extensions that are all in the membrane distal module (Fig. 42). The significance of these extensions is unclear, but considering that the distal module has repeatedly been shown to bind the ligand (Wu *et al.*, 2013b, Liu *et al.*, 2015, Nishiyama *et al.*, 2016), these extensions may participate in some way in ligand recognition. Further research is needed to understand the relevance of these size differences in dCACHE domains.

Using the DALI algorithm we searched for structural homologues of McpU-LBD amongst all structures of the Protein Data Bank and the retrieved structures are listed in Table 11. Interestingly, the closest structural homologues of McpU-LBD were neither from chemoreceptors nor from bacteria, but from two histidine kinases of the archaea *Methanosarcina mazei*. The structurally most closely related dCACHE domain from a chemoreceptor was that of Tlp1 from the epsilon-protobacterium *Campylobacter jejuni*. Other close homologues are an ABC transporter substrate binding protein or a sensor domain from the plant *Arabidopsis thaliana*. These structural comparisons highlight the universality and omnipresence of dCACHE domains in sensing proteins.

A characteristic feature of sensor domains is their enormous sequence divergence, which hampers their functional annotation by sequence comparison with homologous proteins, since frequently the receptor function is not reflected in overall sequence similarity (Reyes-Darias *et al.*, 2015b). Therefore, the prediction of potential protein functions requires additional information on the amino acids that are involved in ligand binding. McpU is the first polyamine chemoreceptor identified and likely to exist in other species. Here we show that amino acids D204, D233, W186 and Y202 are essential for binding (Table 10). To assess their conservation we have aligned the sequences of the structural homologues listed in Table 11. This analysis showed a conservation of these amino acids in approximately half of the sequences (Supp. Fig. 28). We have subsequently analysed the ligand recognition by one of the receptors that showed partial conservation of binding site residues, namely the LBD of the Mlp37 of *Vibrio cholera* (Nishiyama *et al.*, 2016). This structure was solved in complex with taurine, a compound that contains a primary amino group. A structural alignment shows that the primary amino group in both structures is recognized in a similar way by three amino acids that establish three hydrogen bonds, namely residues Y202/142, D204/D144 and D233/173 (Fig. 43). McpU-LBD and Mlp37-LBD share 15 % of sequence identity (Supp. Fig. 29). Amino acids involved in binding the amino group of both ligands are conserved, whereas the remaining amino acids involved in ligand binding are, as expected, not conserved (Supp. Fig. 29). This conserved amino acid triad could thus correspond to a conserved structural feature for the recognition of amino groups. The ligands recognized by most bacterial sensor proteins are unknown and this amino acid triad could be a means to provide initial insight into receptor ligands. This is also consistent with the observation that many dCACHE domains recognize amines (Matilla & Krell, 2017).

To identify potential polyamine receptors in other species we have conducted a BLAST search using the McpU-LBD sequence, excluding strains of the genus *Pseudomonas*, in the NCBI data base of non-redundant sequences. The top 230 LBD sequences from this search form all part of chemoreceptors and shared 43 to 27 % sequence identity with McpU-LBD (Supp. Fig. 30). We have then assessed in these sequences the conservation of the four essential amino acids for binding (Supp. Fig. 30). D233 was absolutely conserved; W186 and Y202 were highly conserved and mostly substituted by other aromatic residues, whereas D204 was conserved in 60 % of the sequences. At

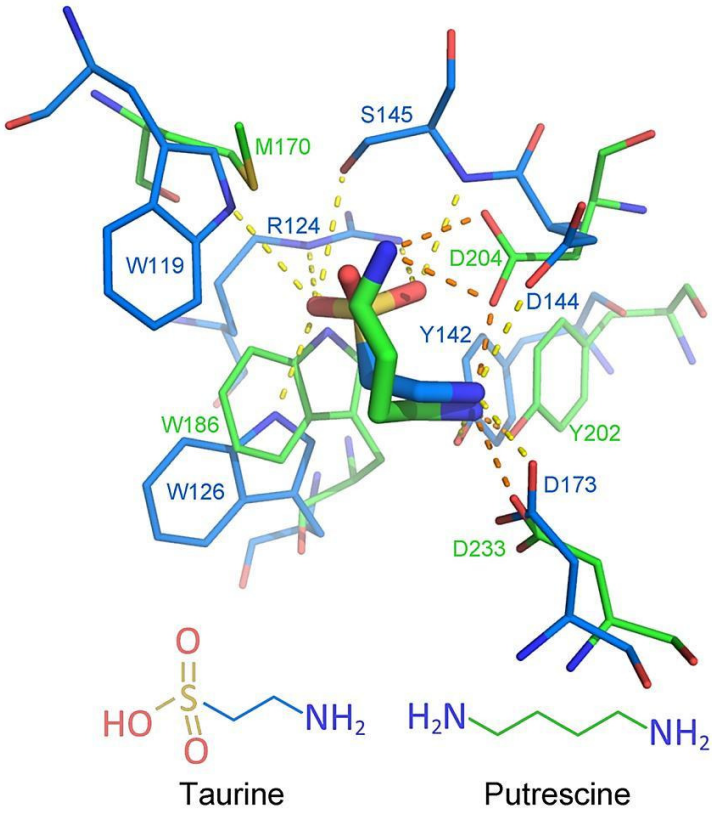

Figure 43. Similarities in the ligand recognition by McpU and the Mlp37 chemoreceptor of *Vibrio cholerae*. Zoom of the ligand binding pocket of a structural alignment of McpU-LBD (in green) with Mlp37-LBD (in blue, pdb ID: 5avf). Hydrogen bonds are indicated by dotted lines.

least three of these four amino acids were conserved in 71 % of the sequences, which can be considered as potential polyamine receptors. The corresponding species of these sequences are listed in Supp. Table 11 and the analysis of their lifestyles provides interesting insight. Almost all species have been isolated from either freshwater or seawater samples and most of these species are fish and shellfish pathogens. Almost two thirds of these species (Supp. Table 11) belong to the genus *Aeromonas* which are important disease-causing pathogens of fish and other coldblooded species (Janda & Abbott, 2010). Polyamines are widely distributed in life and were shown to modulate cell growth and proliferation, gene expression and stress resistance in eukaryotic and prokaryotic organisms (Miller-Fleming *et al.*, 2015). Additionally, polyamines were also found to promote the expression of virulence factors, modulate biofilm formation and enhance bacterial survival within hosts (Di Martino *et al.*, 2013). Chemotaxis towards host signals was shown to be crucial for the full virulence of a broad range of pathogens (Matilla & Krell, 2018) and in this context it can be hypothesized that chemotaxis to polyamines derived from fish and molluscs may be an important contribution to efficient infection.

CD, AUC and SAXS studies indicate that putrescine binding does neither cause major conformational changes nor alterations in the oligomeric state of the McpU-LBD. Clear tendencies now emerge as to the binding modes of effectors to the different LBD families. In a first mode, ligands bind to a site close to the LBD dimer interface. In those cases amino acids from both monomers of the dimer interact with the ligand (Milburn *et al.*, 1991, Pineda-Molina *et al.*, 2012). These LBDs are present in a dynamic monomer-dimer equilibrium and ligand binding shifts this equilibrium to the dimeric state (Milligan & Koshland, 1993, Lacal *et al.*, 2010a, Martin-Mora *et al.*, 2016a, Rico-Jimenez *et al.*, 2016, Fernandez *et al.*, 2017). Data so far available indicate that 4HB (Ulrich & Zhulin, 2005) and helical bimodular domains (HBM)(Ortega & Krell, 2014) employ this mechanism. Our data and those obtained in previous studies indicate that domains that belong to the CACHE family employ a different mechanism (Rico-Jimenez *et al.*, 2013a, Machuca *et al.*, 2017,

Martin-Mora *et al.*, 2018). The isolated domains are monomeric and ligand binding does not modulate this state. Although dimeric domain arrangements are sometimes observed in the crystal structures (Supp. Fig. 27 and (Liu *et al.*, 2015)), bound ligand only interacts with amino acids from a single monomer. The functional difference between both sensing modes may be related to the fact that ligand binding at dimers enables cooperativity and such cooperativity has been observed for 4HB as well as HBM domains (Milligan & Koshland, 1993, Biemann & Koshland, 1994, Martin-Mora *et al.*, 2016a). The mechanism of transmembrane signaling has been determined for 4HB domain containing chemoreceptors and consists in rotational and translation movements of the second transmembrane region (Ottemann *et al.*, 1999, Yu *et al.*, 2015). A number of chimeric receptors comprising dCACHE domains and the cytosolic fragment of Tar have been constructed, which were all found to be functional and to create signal output in response to the ligand recognised by the sensor domain (Reyes-Darias *et al.*, 2015b, Reyes-Darias *et al.*, 2015a, Bi *et al.*, 2016). Taken together, these data indicate that although dCACHE and 4HB/HBM domains differ in their sensing mechanisms, the corresponding receptors employ the same mechanism of transmembrane signalling.

Here we present the first study of a dCACHE domain using DSC. This technique permits the determination of the thermodynamic parameters of protein unfolding but can also provide insight into protein function. Many multidomain proteins are characterized by the consecutive unfolding of the individual domains giving rise to multiple events in a DSC thermogram (Johnson, 2013). McpU-LBD is also composed of two structural modules but unfolds cooperatively in a single event. Ligand binding increases the Tm value and the cooperativity of unfolding as evidenced by the lower peak width at half high in the presence of ligands (Supp. Table 9). Interesting parallels exist to a DSC study of another two-domain protein, the transcriptional regulator TtgV (Fillet *et al.*, 2011). Mechanistic studies revealed functional interaction between both domains, since ligand binding to its LBD modulated the properties of its DNA binding domain. In analogy to McpU-LBD, TtgV unfolded in a single event. However, preventing domain communication between both domains by site directed mutagenesis made that both domains unfolded consecutively in two different events. The authors concluded that functional domain interaction is reflected in cooperative unfolding, whereas functional domain uncoupling resulted in a consecutive unfolding of the individual domains (Fillet *et al.*, 2011). This may indicate that both McpU-LBD modules functionally communicate and that ligand binding to the distal module is efficiently conveyed to the proximal module. Further research will reveal the key amino acids that participate in this inter-module communication.

This study increases our knowledge on dCACHE domains and forms the basis for further investigations in the field of polyamine chemotaxis. Further research is needed to study homologous receptors in other species and to elucidate their potential roles in pathogenicity.

SUPPLEMENTARY MATERIAL

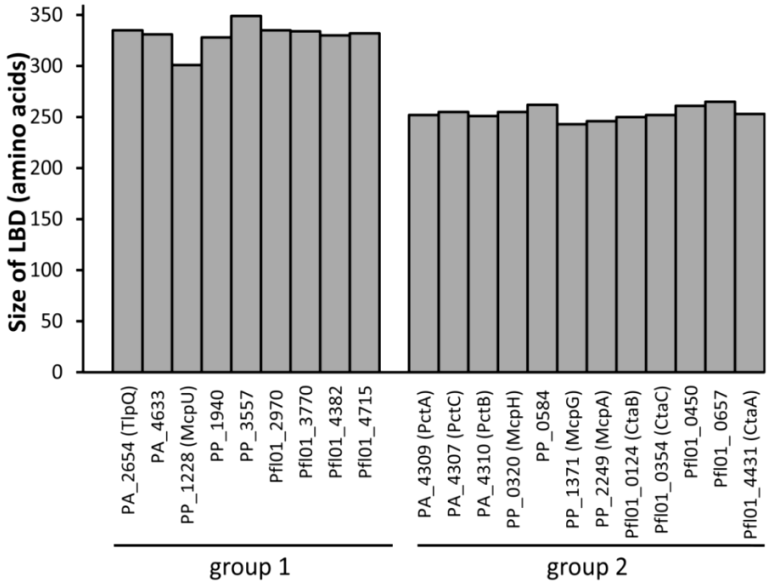

Supp. Fig 23. The two groups of dCACHE containing chemoreceptors in Pseudomonas strains differ in size. The definition of these groups was reported in (Ortega *et al.*, 2017a). The transmembrane regions of chemoreceptors from *P. putida* KT2440 (PP), *P. aeruginosa* (PA) and *P. fluorescens* Pf0-1 (Pfl01) were determined using the DAS algorithm (Cserzo *et al.*, 1997) and the length of the fragment between both transmembrane regions is plotted. The names of functionally annotated receptors are shown in brackets: TlpQ for ethylene (Kim & Tokura, 2007), McpU for polyamines (Corral-Lugo *et al.*, 2016), PctA, PctB and PctC for proteinogenic amino acids and GABA (Taguchi *et al.*, 1997, Rico-Jimenez *et al.*, 2013a, Reyes-Darias *et al.*, 2015b), McpH for purines (Fernandez *et al.*, 2016), McpG for GABA (Reyes-Darias *et al.*, 2015b), McpA, CtaA, CtaB and CtaC for amino acids (Oku *et al.*, 2012, Corral-Lugo *et al.*, 2016).

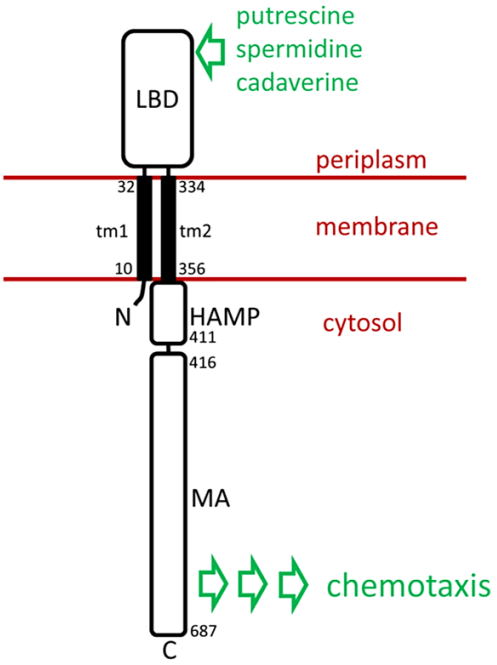

Supp. Fig 24. Schematic representation of the McpU chemoreceptor. Transmembrane regions (tm1 and tm2) were determined using the DAS algorithm (Cserzo *et al.*, 1997). Domain annotation and boundaries are according to the InterPro database (Finn *et al.*, 2017). LBD: Ligand Binding Domain; HAMP: domain found in found in Histidine kinases, Adenylcyclases, Methyl-accepting proteins and Phosphatases; MA: Methylaccepting signaling domain.

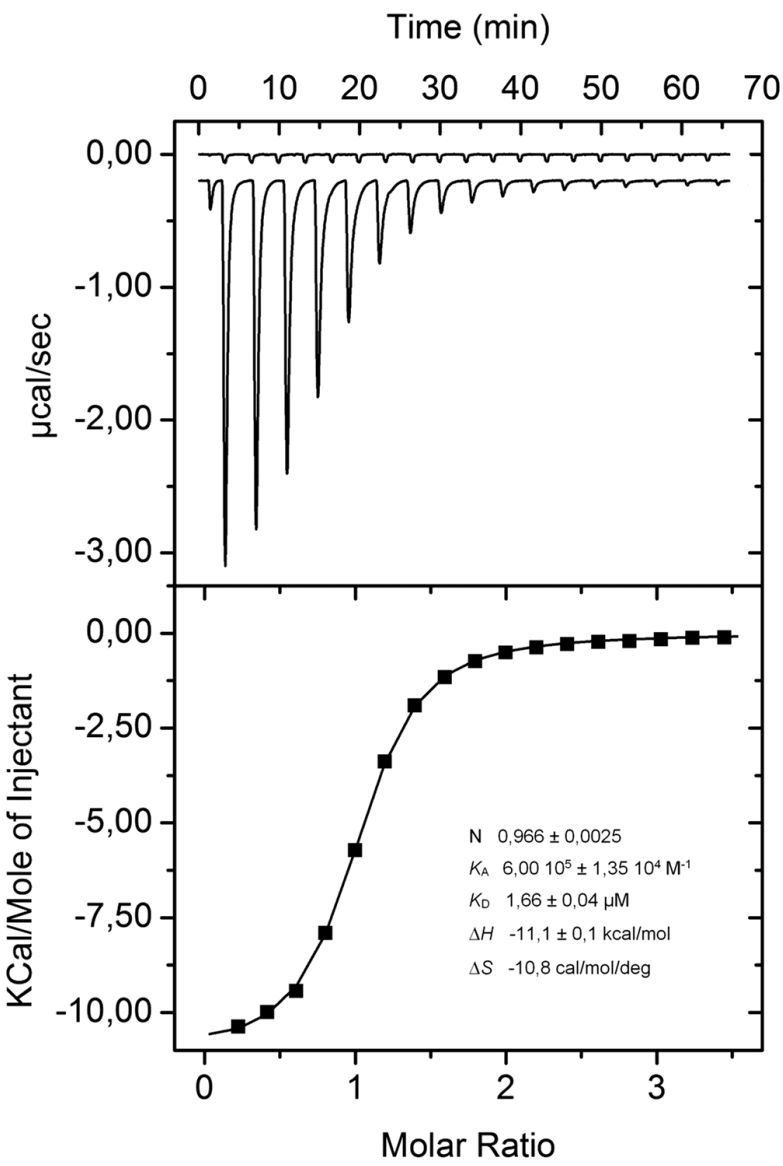

Supp. Fig 25. Microcalorimetric titration of buffer (upper trace) and 35 µM his-tag free McpU-LBD with aliquots of a 1 mM putrescine. The injection volume was of 9.6 µM. The lower panel shows the data fit with the "One binding site model" of the MicroCal version of ORIGIN. The derived thermodynamic parameters are shown.

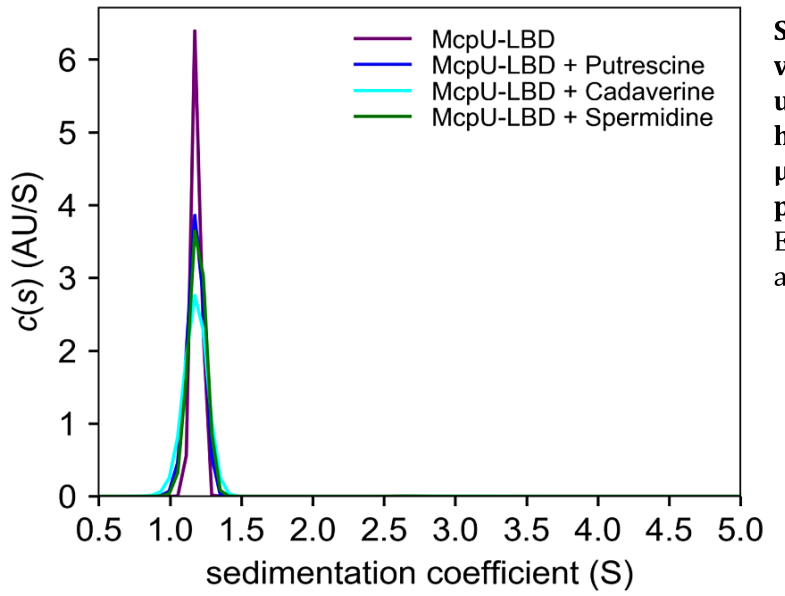

Supp. Fig 26. Sedimentation velocity analytical ultracentrifugation studies of his-tag free McpU-LBD at 17 µM in the absence and presence of 100 µM ligands. Experiments were conducted in analysis buffer.

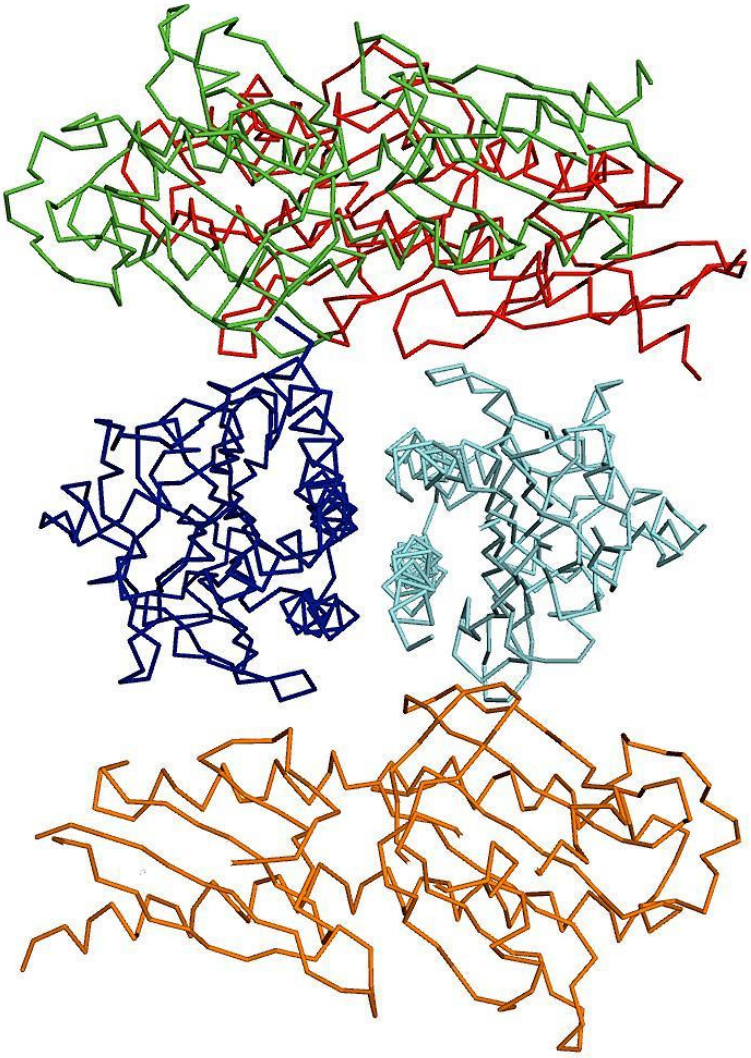

Supp. Fig 27. The content of the asymmetric unit of the McpU-LBD/putrescine crystal. Shown is the Cα trace of each of the 5 protein chains.

```
                  10        20        30        40        50        60
                   |         |         |         |         |         |
3lib      ----------------------------------------------------MES-TVTTQEE
3li8      ----------------------------------------------------MEIGTVTSQEE
5LTX      ----------------------------------------------------MNDYLQRNAIR
5LT9      ----------------------------------------------------MNDSLQRASIR
5LTV      ----------------------------------------------------MNDYRQREAVR
5AVE      ----------------------------------------------------GPLGSVRDEIR
3LIC      ----------------------------------------------------ENYLSIEKRLY
6f9g      ------------------------------------TQAHRSAALVNQANTAMLEDSAR
4WY9      ---------------------------------------------------TKQVSQNITKNTE
5WBF      ----------------------------------------------------GIDPFTESVLQ
4XMQ      ----------------------------------------------------GIDPFTKTSLY
4JGO      ----------------------------------------------------SNAEKEKDTIA
3LIF      ----------------------------------------------------KGYDSHKIAL
3LID      ---------------------------------------------------MEKYQALLANNV
2ZBB      ------------------------------MASMTGGEEMGRGSLLLARDYGRSQAL
5ERE      KPVVGVILPFSSAFEDIAVEQQRAVELALAESGSAFEIVFKDGGADVDTAVQAFQDLVRS
3T4K      ----------------------------------------------------MDDANKIRRE
```

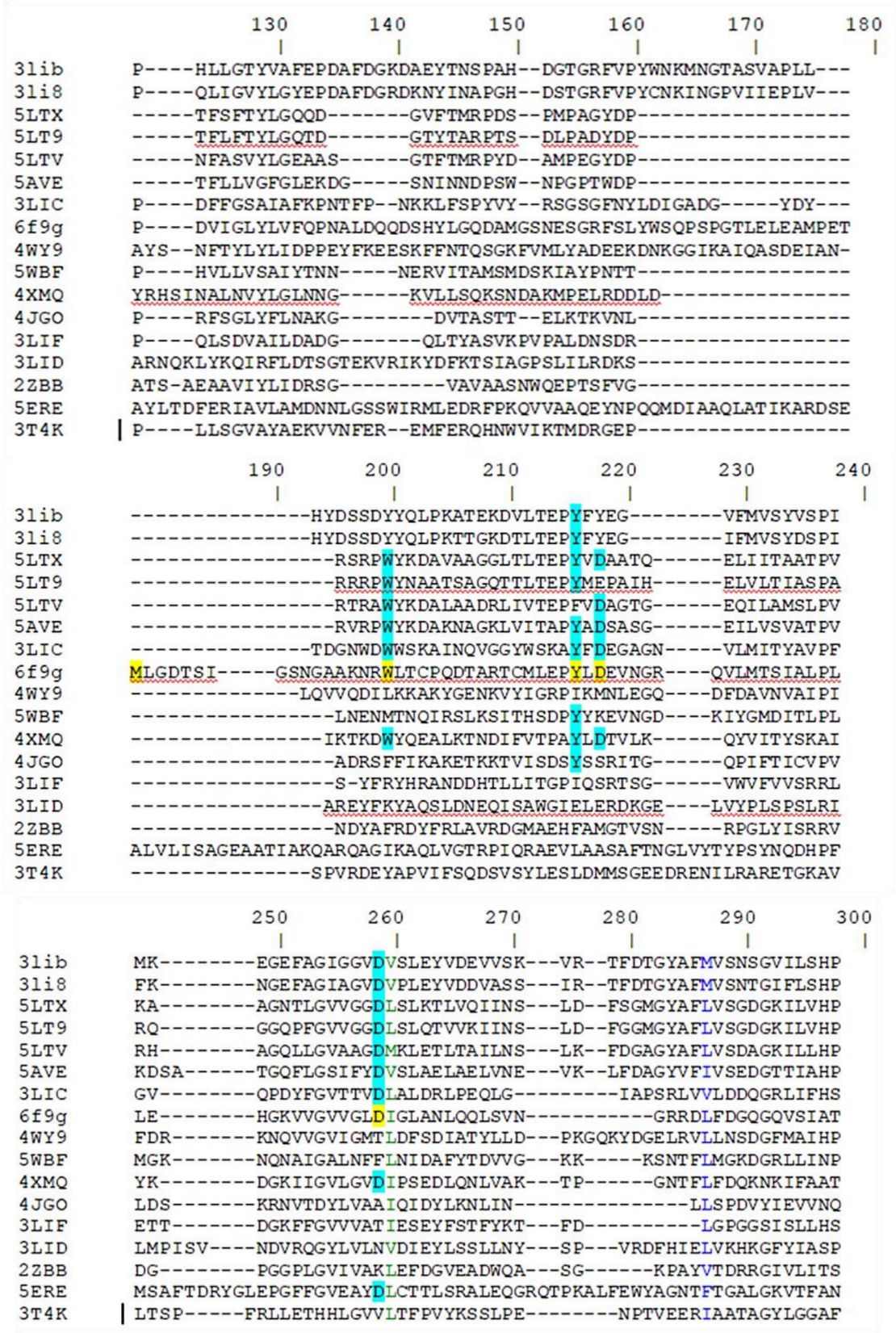
130 140 150 160 170 180
3lib P----HLLGTYVAFEPDAFDGKDAEYTNSPAH--DGTGRFVPYWNKMNGTASVAPLL---
3li8 P----QLIGVYLGYEPDAFDGRDKNYINAPGH--DSTGRFVPYCNKINGPVIIEPLV---
5LTX -----TFSFTYLGQQD-------GVFTMRPDS--PMPAGYDP----------
5LT9 -----TFLFTYLGQTD-------GTYTARPTS--DLPADYDP----------
5LTV -----NFASVYLGEAAS------GTFTMRPYD--AMPEGYDP----------
5AVE -----TFLLVGFGLEKDG-----SNINNDPSW--NPGPTWDP----------
3LIC P----DFFGSAIAFKPNTFP--NKKLFSPYVY--RSGSGFNYLDIGADG-----YDY---
6f9g P----DVIGLYLVFQPNALDQQDSHYLGQDAMGSNESGRFSLYWSQPSPGTLELEAMPET
4WY9 AYS--NFTYLYLIDPPEYFKEESKFFNTQSGKFVMLYADEEKDNKGGIKAIQASDEIAN-
5WBF P----HVLLVSAIYTNN-----NERVITAMSMDSKIAYPNTT----------
4XMQ YRHSINALNVYLGLNNG-----KVLLSQKSNDAKMPELRDDLD----------
4JGO P----RFSGLYFLNAKG-------DVTASTT--ELKTKVNL----------
3LIF P----QLSDVAILDADG-------QLTYASVKPVPALDNSDR----------
3LID ARNQKLYKQIRFLDTSGTEKVRIKYDFKTSIAGPSLILRDKS----------
2ZBB ATS-AEAAVIYLIDRSG---------VAVAASNWQEPTSFVG----------
5ERE AYLTDFERIAVLAMDNNLGSSWIRMLEDRFPKQVVAAQEYNPQQMDIAAQLATIKARDSE
3T4K P----LLSGVAYAEKVVNFER--EMFERQHNWVIKTMDRGEP----------
190 200 210 220 230 240
3lib ----------HYDSSDYYQLPKATEKDVLTEPYFYEG--------VFMVSYVSPI
3li8 ----------HYDSSDYYQLPKTTGKDTLTEPYFYEG--------IFMVSYDSPI
5LTX ----------RSRPWYKDAVAAGGLTLTEPYVDAATQ------ELIITAATPV
5LT9 ----------RRRPWYNAATSAGQTTLTEPYMEPAIH------ELVLTIASPA
5LTV ----------RTRAWYKDALAADRLIVTEPFVDAGTG------EQILAMSLPV
5AVE ----------RVRPWYKDAKNAGKLVITAPYADSASG------EILVSVATPV
3LIC ----------TDGNWDWWSKAINQVGGYWSKAYFDEGAGN-----VLMITYAVPF
6f9g MLGDTSI-----GSNGAAKNRWLTCPQDTARTCMLEPYLDEVNGR----QVLMTSIALPL
4WY9 ----------LQVVQDILKKAKYGENKVYIGRPIKMNLEGQ----DFDAVNVAIPI
5WBF ----------LNENMTNQIRSLKSITHSDPYYKEVNGD----KIYGMDITLPL
4XMQ ----------IKTKDWYQEALKTNDIFVTPAYLDTVLK------QYVITYSKAI
4JGO ----------ADRSFFIKAKETKKTVISDSYSSRITG------QPIFTICVPV
3LIF ----------S-YFRYHRANDDHTLLITGPIQSRTSG------VWVFVVSRRL
3LID ----------AREYFKYAQSLDNEQISAWGIELERDKGE----LVYPLSPSLRI
2ZBB ----------NDYAFRDYFRLAVRDGMAEHFAMGTVSN-----RPGLYISRRV
5ERE ALVLISAGEAATIAKQARQAGIKAQLVGTRPIQRAEVLAASAFTNGLVYTYPSYNQDHPF
3T4K ----------SPVRDEYAPVIFSQDSVSYLESLDMMSGEEDRENILRARETGKAV
250 260 270 280 290 300
3lib MK--------EGEFAGIGGVDVSLEYVDEVVSK---VR--TFDTGYAFMVSNSGVILSHP
3li8 FK--------NGEFAGIAGVDVPLEYVDDVASS---IR--TFDTGYAFMVSNTGIFLSHP
5LTX KA--------AGNTLGVVGGDLSLKTLVQIINS---LD--FSGMGYAFLVSGDGKILVHP
5LT9 RQ--------GGQPFGVVGGDLSLQTVVKIINS---LD--FGGMGYAFLVSGDGKILVHP
5LTV RH--------AGQLLGVAAGDMKLETLTAILNS---LK--FDGAGYAFLVSDAGKILLHP
5AVE KDSA------TGQFLGSIFYDVSLAELAELVNE---VK--LFDAGYVFIVSEDGTTIAHP
3LIC GV--------QPDYFGVTTVDLALDRLPEQLG---------IAPSRLVVLDDQGRLIFHS
6f9g LE--------HGKVVGVVGLDIGLANLQQLSVN----------GRRDLFDGQGQVSIAT
4WY9 FDR-------KNQVVGVIGMTLDFSDIATYLLD---PKGQKYDGELRVLLNSDGFMAIHP
5WBF MGK-------NQNAIGALNFFLNIDAFYTDVVG---KK-----KSNTFLMGKDGRLLINP
4XMQ YK--------DGKIIGVLGVDIPSEDLQNLVAK---TP------GNTFLFDQKNKIFAAT
4JGO LDS-------KRNVTDYLVAAIQIDYLKNLIN---------LLSPDVYIEVVNQ
3LIF ETT-------DGKFFGVVVATIESEYFSTFYKT---FD----------LGPGGSISLLHS
3LID LMPISV----NDVRQGYLVLNVDIEYLSSLLNY---SP---VRDFHIELVKHKGFYIASP
2ZBB DG--------PGGPLGVIVAKLEFDGVEADWQA---SG------KPAYVTDRRGIVLITS
5ERE MSAFTDRYGLEPGFFGVEAYDLCTTLSRALEQGRQTPKALFEWYAGNTFTGALGKVTFAN
3T4K LTSP-----FRLLETHHLGVVLTFPVYKSSLPE--------NPTVEERIAATAGYLGGAF

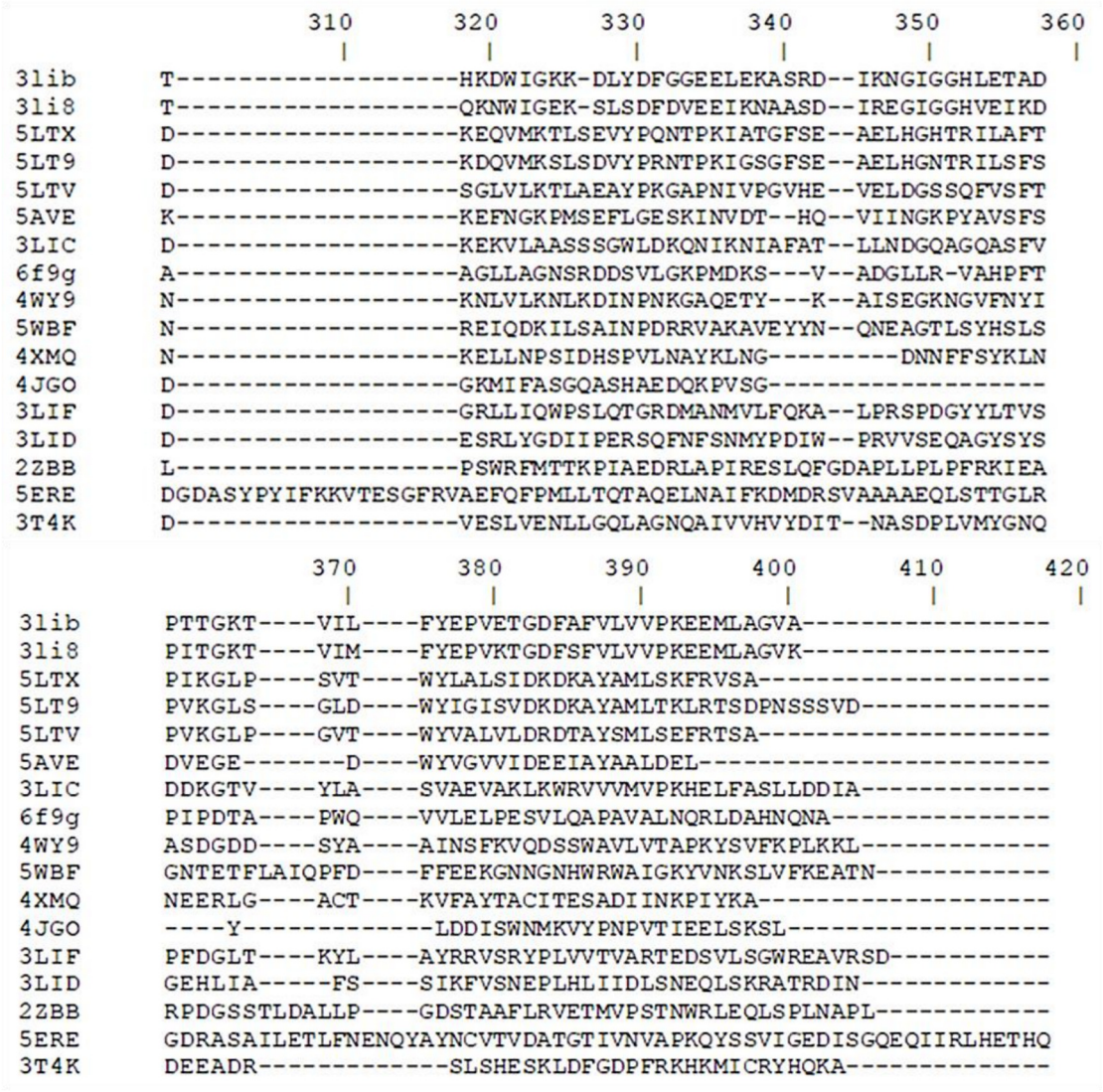

Supp. Fig 28. Sequence alignment of structural homologues of McpU-LBD listed in Table 11. The alignment was done using the CLUSTALW algorithm of the npsa software (Combet *et al.*, 2000). The Gonnet protein weight matrix was used; gap opening and gap extension penalties were 10.0 and 0.1, respectively. Residues in green are highly similar and blue weakly similar. Amino acids involved in putrescine binding to McpU-LBD are shaded in yellow and their conserved homologues in cyan.

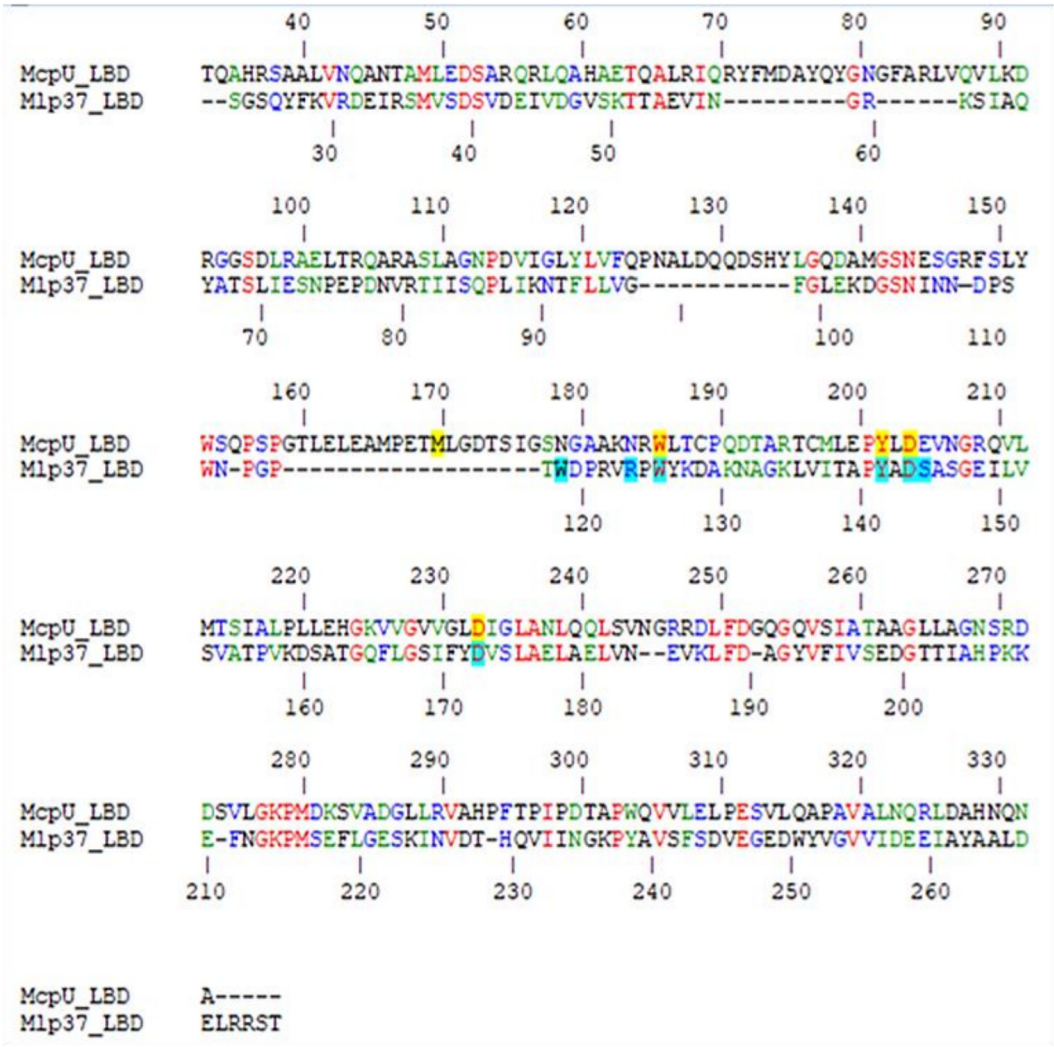

Supp. Fig 29. Sequence alignment of the ligand binding domains of the McpU and Mlp37 chemoreceptors from *P. putida* and *Vibrio cholerae*, respectively. Both sequences share 15 % of amino acid identity. McpU residues involved in putrescine recognition are shaded in yellow and amino acid involved in taturine binding by Mlp37 are shadedin cyan. The Mlp37-LBD structure had been reported in (Nishiyama *et al.*, 2016). The alignment was done using the CLUSTALW algorithm of the npsa software (Combet *et al.*, 2000). The Gonnet protein weight matrix was used; gap opening ang gap extension penalties were 10.0 and 0.1, respectively. Residues in red are identical, green highly similar and blue weakly similar.

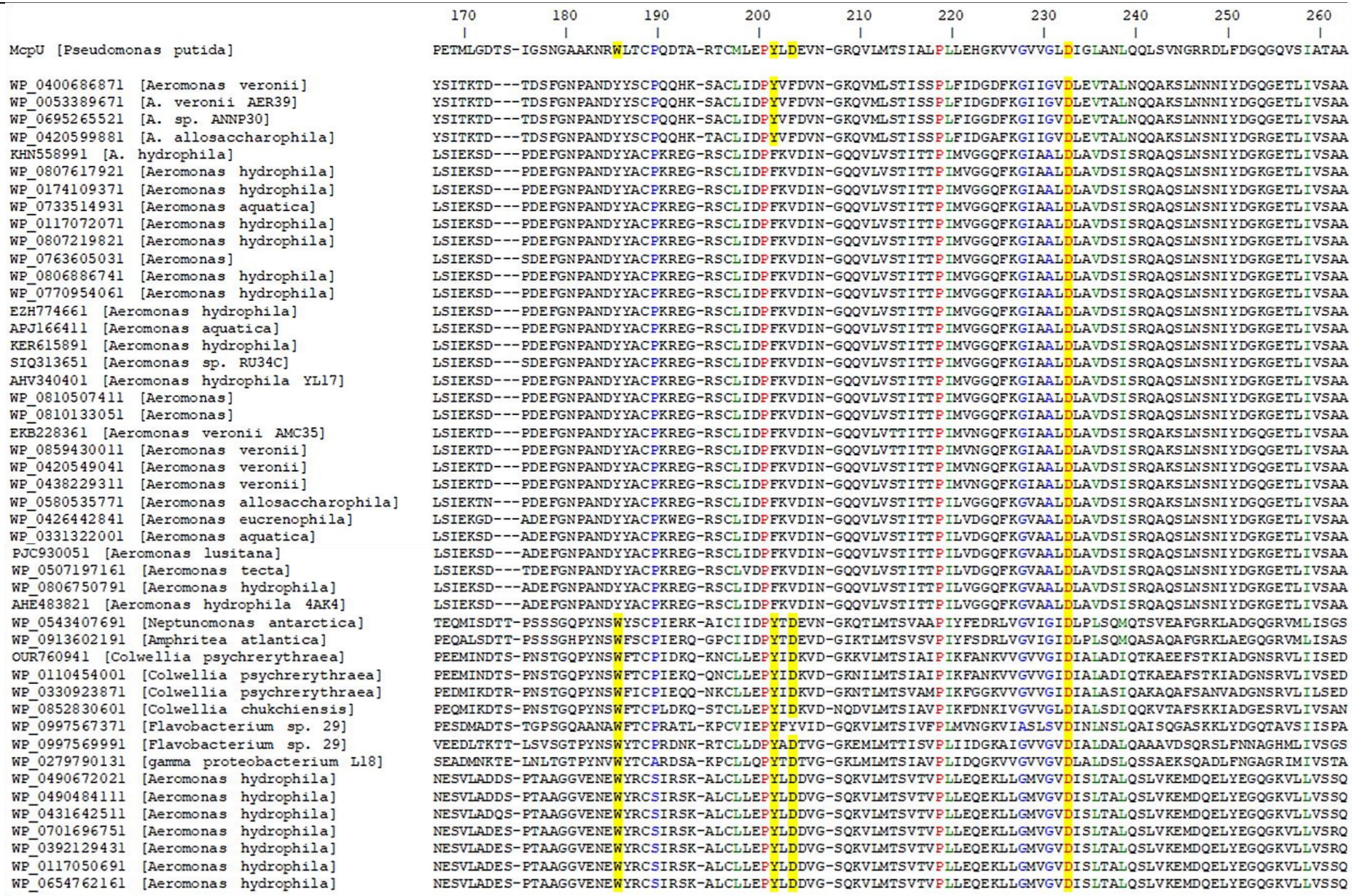
170 180 190 200 210 220 230 240 250 260
McpU [Pseudomonas putida] PETMLGDTS-IGSNGAAKNRWLTCPQDTA-RTCMLEPYLDEVN-GRQVLMTSIALPLLEHGKVVGVVGLDIGLANLQQLSVNGRRDLFDGQGQVSIATAA
WP_0400686871 [Aeromonas veronii] YSITKTD---TDSFGNPANDYYSCPQQHK-SACLIDPYVFDVN-GKQVMLSTISSPLFIDGDFKGIIGVDLEVTALNQQAKSLNNNIYDGQGETLIVSAA
WP_0053389671 [A. veronii AER39] YSITKTD---TDSFGNPANDYYSCPQQHK-SACLIDPYVFDVN-GKQVMLSTISSPLFIDGDFKGIIGVDLEVTALNQQAKSLNNNIYDGQGETLIVSAA
WP_0695265521 [A. sp. ANNP30] YSITKTD---TDSFGNPANDYYSCPQQHK-SACLIDPYVFDVN-GKQVMLSTISSPLFIGGDFKGIIGVDLEVTALNQQAKSLNNNIYDGQGETLIVSAA
WP_0420599881 [A. allosaccharophila] YSITKTD---TDSFGNPANDYYSCPQQHK-TACLIDPYVFDVN-GKQVMLSTISSPLFIDGAFKGIIGVDLEVTALNQQAKSLNSNIYDGRGETLIVSAA
KHN558991 [A. hydrophila] LSIEKSD---PDEFGNPANDYYACPKREG-RSCLIDPFKVDIN-GQQVLVSTITTPIMVGGQFKGIAALDLAVDSISRQAQSLNSNIYDGKGETLIVSAA
WP_0807617921 [Aeromonas hydrophila] LSIEKSD---PDEFGNPANDYYACPKREG-RSCLIDPFKVDIN-GQQVLVSTITTPIMVGGQFKGIAALDLAVDSISRQAQSLNSNIYDGKGETLIVSAA
WP_0174109371 [Aeromonas hydrophila] LSIEKSD---PDEFGNPANDYYACPKREG-RSCLIDPFKVDIN-GQQVLVSTITTPIMVGGQFKGIAALDLAVDSISRQAQSLNSNIYDGKGETLIVSAA
WP_0733514931 [Aeromonas aquatica] LSIEKSD---PDEFGNPANDYYACPKREG-RSCLIDPFKVDIN-GQQVLVSTITTPIMVGGQFKGIAALDLAVDSISRQAQSLNSNIYDGKGETLIVSAA
WP_0117072071 [Aeromonas hydrophila] LSIEKSD---PDEFGNPANDYYACPKREG-RSCLIDPFKVDIN-GQQVLVSTITTPIMVGGQFKGIAALDLAVDSISRQAQSLNSNIYDGKGETLIVSAA
WP_0807219821 [Aeromonas hydrophila] LSIEKSD---PDEFGNPANDYYACPKREG-RSCLIDPFKVDIN-GQQVLVSTITTPIMVGGQFKGIAALDLAVDSISRQAQSLNSNIYDGKGETLIVSAA
WP_0763605031 [Aeromonas] LSIEKSD---SDEFGNPANDYYACPKREG-RSCLIDPFKVDIN-GQQVLVSTITTPIMVGGQFKGIAALDLAVDSISRQAQSLNSNIYDGKGETLIVSAA
WP_0806886741 [Aeromonas hydrophila] LSIEKSD---PDEFGNPANDYYACPKREG-RSCLIDPFKVDIN-GQQVLVSTITTPIMVGGQFKGIAALDLAVDSISRQAQSLNSNIYDGKGETLIVSAA
WP_0770954061 [Aeromonas hydrophila] LSIEKSD---PDEFGNPANDYYACPKREG-RSCLIDPFKVDIN-GQQVLVSTITTPIMVGGQFKGIAALDLAVDSISRQAQSLNSNIYDGKGETLIVSAA
EZH774661 [Aeromonas hydrophila] LSIEKSD---PDEFGNPANDYYACPKREG-RSCLIDPFKVDIN-GQQVLVSTITTPIMVGGQFKGIAALDLAVDSISRQAQSLNSNIYDGKGETLIVSAA
APJ166411 [Aeromonas aquatica] LSIEKSD---PDEFGNPANDYYACPKREG-RSCLIDPFKVDIN-GQQVLVSTITTPIMVGGQFKGIAALDLAVDSISRQAQSLNSNIYDGKGETLIVSAA
KER615891 [Aeromonas hydrophila] LSIEKSD---PDEFGNPANDYYACPKREG-RSCLIDPFKVDIN-GQQVLVSTITTPIMVGGQFKGIAALDLAVDSISRQAQSLNSNIYDGKGETLIVSAA
SIQ313651 [Aeromonas sp. RU34C] LSIEKSD---SDEFGNPANDYYACPKREG-RSCLIDPFKVDIN-GQQVLVSTITTPIMVGGQFKGIAALDLAVDSISRQAQSLNSNIYDGKGETLIVSAA
AHV340401 [Aeromonas hydrophila YL17] LSIEKSD---PDEFGNPANDYYACPKREG-RSCLIDPFKVDIN-GQQVLVSTITTPIMVGGQFKGIAALDLAVDSISRQAQSLNSNIYDGKGETLIVSAA
WP_0810507411 [Aeromonas] LSIEKSD---PDEFGNPANDYYACPKREG-RSCLIDPFKVDIN-GQQVLVSTITTPIMVGGQFKGIAALDLAVDSISRQAQSLNSNIYDGKGETLIVSAA
WP_0810133051 [Aeromonas] LSIEKSD---PDEFGNPANDYYACPKREG-RSCLIDPFKVDIN-GQQVLVSTITTPIMVGGQFKGIAALDLAVDSISRQAQSLNSNIYDGKGETLIVSAA
EKB228361 [Aeromonas veronii AMC35] LSIEKTD---PDEFGNPANDYYACPKREG-RSCLIDPFKVDIN-GQQVLVTTITTPIMVNGQFKGIAALDLAVDSISRQAKSLNSNIYDGQGETLIVSAA
WP_0859430011 [Aeromonas veronii] LSIEKTD---PDEFGNPANDYYACPKREG-RSCLIDPFKVDIN-GQQVLVTTITTPIMVNGQFKGIAALDLAVDSISRQAKSLNSNIYDGQGETLIVSAA
WP_0420549041 [Aeromonas veronii] LSIEKTD---PDEFGNPANDYYACPKREG-RSCLIDPFKVDIN-GQQVLVSTITTPIMVNGQFKGIAALDLAVDSISRQAKSLNSNIYDGQGETLIVSAA
WP_0438229311 [Aeromonas veronii] LSIEKTD---PDEFGNPANDYYACPKREG-RSCLIDPFKVDIN-GQQVLVSTITTPIMVNGQFKGIAALDLAVDSISRQAKSLNSNIYDGQGETLIVSAA
WP_0580535771 [Aeromonas allosaccharophila] LSIEKTN---PDEFGNPANDYYACPKREG-RSCLIDPFKVDIN-GQQVLVSTITTPILVGGQFKGVAALDLAVDSISRQAKSLNSNIYDGQGETLIVSAA
WP_0426442841 [Aeromonas eucrenophila] LSIEKGD---ADEFGNPANDYYACPKWEG-RSCLIDPFKVDIN-GQQVLVSTITTPILVDGQFKGVAALDLAVDSISRQAQSLNSNIYDGKGETLIVSAA
WP_0331322001 [Aeromonas aquatica] LSIEKSD---ADEFGNPANDYYACPKREG-RSCLIDPFKVDIN-GQQVLVSTITTPILVDGQFKGVAALDLAVDSISRQAQSLNSNIYDGKGETLIVSAA
PJC930051 [Aeromonas lusitana] LSIEKSD---ADEFGNPANDYYACPKREG-RSCLIDPFKVDIN-GQQVLVSTITTPILVDGQFKGVAALDLAVDSISRQAQSLNSNIYDGKGETLIVSAA
WP_0507197161 [Aeromonas tecta] LSIEKSD---TDEFGNPANDYYACPKREG-RSCLVDPFKVDIN-GQQVLVSTITTPILVDGQFKGVAALDLAVDSISRQAQSLNSNIYDGKGETLIVSAA
WP_0806750791 [Aeromonas hydrophila] LSIEKSD---ADEFGNPANDYYACPKREG-RSCLIDPFKVDIN-GQQVLVSTITTPILVGGQFKGVAALDLAVDSISRQAQSLNSNIYDGKGETLIVSAA
AHE483821 [Aeromonas hydrophila 4AK4] LSIEKSD---ADEFGNPANDYYACPKREG-RSCLIDPFKVDIN-GQQVLVSTITTPILVGGQFKGVAALDLAVDSISRQAQSLNSNIYDGKGETLIVSAA
WP_0543407691 [Neptunomonas antarctica] TEQMISDTT-PSSSGQPYNSWYSCPIERK-AICIIDPYTDEVN-GKQTLMTSVAAPIYFEDRLVGVIGIDLPLSQMQTSVEAFGRKLADGQGRVMLISGS
WP_0913602191 [Amphritea atlantica] PEQALSDTT-PSSSGHPYNSWFSCPIERQ-GPCIIDPYTDEVD-GIKTLMTSVSVPIYFSDRLVGVIGIDLPLSQMQASAQAFGRKLAEGQGRVMLISAS
OUR760941 [Colwellia psychrerythraea] PEEMINDTS-PNSTGQPYNSWFTCPIDKQ-KNCLLEPYIDKVD-GKKVLMTSIAIPIKFANKVVGVVGIDIALADIQTKAEEFSTKIADGNSRVLIISED
WP_0110454001 [Colwellia psychrerythraea] PEEMINDTS-PNSTGQPYNSWFTCPIEKQ-QNCLLEPYIDKVD-GKNILMTSIAIPIKFANKVVGVVGIDIALADIQTKAEAFSTKIADGNSRVLIVSED
WP_0330923871 [Colwellia psychrerythraea] PEDMIKDTR-PNSTGQPYNSWFICPIEQQ-NKCLLEPYIDKVD-GKNTLMTSVAMPIKFGGKVVGVVGIDIALASIQAKAQAFSANVADGNSRVLILSED
WP_0852830601 [Colwellia chukchiensis] PEQMIKDTS-PNSTGQPYNSWFTCPLDKQ-STCLLEPYIDKVD-NQDVLMTSIAVPIKFDNKIVGVVGLDIALSDIQQKVTAFSKKIADGESRVLIVSAN
WP_0997567371 [Flavobacterium sp. 29] PESDMADTS-TGPSGQAANAWFTCPRATL-KPCVIEPYFYVID-GQKVLMTSIVFPLMVNGKVIASLSVDINLNSLQAISQGASKKLYDGQTAVSIISPA
WP_0997569991 [Flavobacterium sp. 29] VEEDLTKTT-LSVSGTPYNSWYTCPRDNK-RTCLLDPYADTVG-GKEMLMTTISVPLIIDGKAIGVVGVDIALDALQAAAVDSQRSLFNNAGHMLIVSGS
WP_0279790131 [gamma proteobacterium L18] SEADMNKTE-LNLTGTPYNVWYTCARDSA-KPCLLQPYTDTVG-GKLMLMTSIAVPLIDQGKVVGVVGVDLALDSLQSSAEKSQADLFNGAGRIMIVSTA
WP_0490672021 [Aeromonas hydrophila] NESVLADDS-PTAAGGVENEWYRCSIRSK-ALCLLEPYLDDVG-SQKVLMTSVTVPLLEQEKLLGMVGVDISLTALQSLVKEMDQELYEGQGKVLLVSSQ
WP_0490484111 [Aeromonas hydrophila] NESVLADDS-PTAAGGVENEWYRCSIRSK-ALCLLEPYLDDVG-SQKVLMTSVTVPLLEQEKLLGMVGVDISLTALQSLVKEMDQELYEGQGKVLLVSSQ
WP_0431642511 [Aeromonas hydrophila] NESVLADQS-PTAAGGVENEWYRCSIRSK-ALCLLEPYLDDVG-SQKVLMTSVTVPLLEQEKLLGMVGVDISLTALQSLVKEMDQELYEGQGKVLLVSSQ
WP_0701696751 [Aeromonas hydrophila] NESVLADES-PTAAGGVENEWYRCSIRSK-ALCLLEPYLDDVG-SQKVLMTSVTVPLLEQEKLLGMVGVDISLTALQSLVKEMDQELYEGQGKVLLVSRQ
WP_0392129431 [Aeromonas hydrophila] NESVLADES-PTAAGGVENEWYRCSIRSK-ALCLLEPYLDDVG-SQKVLMTSVTVPLLEQEKLLGMVGVDISLTALQSLVKEMDQELYEGQGKVLLVSRQ
WP_0117050691 [Aeromonas hydrophila] NESVLADES-PTAAGGVENEWYRCSIRSK-ALCLLEPYLDDVG-SQKVLMTSVTVPLLEQEKLLGMVGVDISLTALQSLVKEMDQELYEGQGKVLLVSSQ
WP_0654762161 [Aeromonas hydrophila] NESVLADES-PTAAGGVENEWYRCSIRSK-ALCLLEPYLDDVG-SQKVLMTSVTVPLLEQEKLLGMVGVDISLTALQSLVKEMDQELYEGQGKVLLVSSQ

```
WP_029301602.1 [Aeromonas hydrophila]          NESVLADES-PTAAGGVENEWYRCSIRSK-VLCLLEPYLDDVG-SQKVLMTSVTVPLLEQEKLLGMVGVDISLTALQSLVKEMDQELYEGQGKVLLVSSQ
WP_042067598.1 [Aeromonas hydrophila]          NESVLADES-PTAAGGVENEWYRCSIRSK-ALCLLEPYLDDVG-SQKVLMTSVTVPLLEQEKLLGMVGVDISLTALQSLVKEMDQELYEGQGKVLLVSSQ
WP_085734637.1 [Aeromonas hydrophila]          NESVLADES-PTAAGGVENEWYRCSIRSK-ALCLLEPYLDDVG-SQKVLMTSVTVPLLEQEKLLGMVGVDISLTALQSLVKEMDQELYEGQGKVLLVSSQ
WP_077095277.1 [Aeromonas hydrophila]          NESVLADES-PTAAGGVENEWYRCSIRSK-ALCLLEPYLDDVG-SQKVLMTSVTVPLLEQEKLLGMVGVDISLTALQSLVKEMDQELYEGQGKVLLVSSQ
WP_073349195.1 [Aeromonas aquatica]            NESVLADES-PTAAGGVENEWYRCSIRSK-ALCLLEPYLDDVG-SQKVLMTSVTVPLLEQEKLLGMVGVDISLTALQSLVKEMDQELYKGQGKVLLVSSQ
KGY50696.1 [Aeromonas hydrophila]              NESVLADES-PTAAGGVENEWYRCSIRSK-ALCLLEPYLDDVG-SQKVLMTSVTVPLLEQEKLLGMVGVDISLTALQSLVKEMDQELYEGQGKVLLVSSQ
WP_060388751.1 [Aeromonas hydrophila]          NESVLADES-PTAAGGVENEWYRCSIRSK-ALCLLEPYLDDVG-SQKVLMTSVTVPLLEQEKLLGMVGVDISLTALQSLVKEMDQELYEGQGKVLLVSSQ
WP_076361101.1 [Aeromonas]                     NESVLADES-PTAAGGVENEWYRCSIRSK-ALCLLEPYLDDVG-SQKVLMTSVTVPLLEQEKLLGMVGVDISLTALQSLVKEMDRELYEGQGKVLLVSSQ
WP_041217199.1 [Aeromonas hydrophila]          NESVLADES-PTAAGGVENEWYRCSIRSK-ALCLLEPYLDDVG-SQKVLMTSVTVPLLEQEKLLGMVGVDISLTALQSLVKEMDQELYEGQGKVLLVSSQ
AGM43006.1 [Aeromonas hydrophila ML09-119]     NESVLADES-PTAAGGVENEWYRCSIRSK-ALCLLEPYLDDVG-SQKVLMTSVTVPLLEQEKLLGMVGVDISLTALQSLVKEMDQELYEGQGKVLLVSSQ
WP_043118653.1 [Aeromonas hydrophila]          NESVLADES-PTAAGGVENEWYRCSIRSK-ALCLLEPYLDDVG-SQKVLMTSVTVPLLEQEKLLGMVGVDISLTALQSLVKEMDQELYEGQGKVLLVSSQ
WP_045790445.1 [Aeromonas hydrophila]          NESVLADES-PTAAGGVENEWYRCSIRSK-ALCLLEPYLDDVG-SQKVLMTSVTVPLLEQEKLLGMVGVDISLTALQSLVKEMDQELYEGQGKVLLVSSQ
WP_044799403.1 [Aeromonas hydrophila]          NESVLADES-PTAAGGVENEWYRCSIRSK-ALCLLEPYLDDVG-SQKVLMTSVTVPLLEQEKLLGMVGVDISLTALQSLVKEMDQELYEGQGKVLLVSSQ
WP_017408622.1 [Aeromonas hydrophila]          NESVLADES-PTAAGGVENEWYRCSIRSK-ALCLLEPYLDDVG-SQKVLMTSVTVPLLEQEKLLGMVGVDISLTALQSLVKEMDQELYEGQGKVLLVSSQ
WP_024945718.1 [Aeromonas hydrophila]          NESVLADES-PTAAGGVENEWYRCSIRSK-ALCLLEPYLDDVG-SQKVLMTSVTVPLLEQDKLLGMVGVDISLTALQSLVKEMDQELYEGQGKVLLVSSQ
WP_099359522.1 [Aeromonas dhakensis]           DESVLADES-PTAAGGVENEWYRCSIRSK-ALCLLEPYLDDVG-SQKVLMTSVTVPLLEQDKLLGMVGVDISLTALQSLVKEMDQELYEGQGKVLLVSSQ
WP_017781867.1 [Aeromonas hydrophila]          DESVLADD----AAGGVENEWYRCSIRSK-ALCLLEPYLDDVG-SQKVLMTSVTVPLLEQDKLLGMVGVDISLTALQSLVKEMDQELYEGQGKVLLVSSQ
WP_024943012.1 [Aeromonas hydrophila]          DESVLADES-PTAAGGVENEWYRCSIRSK-ALCLLEPYLDDVG-SQKVLMTSVTVPLLEQDKLLGMVGVDISLTALQSLVKEMDQELYEGQGKVLLVSSQ
WP_017779835.1 [Aeromonas dhakensis]           DESVLADES-PTAAGGVENEWYRCSIRSK-ALCLLEPYLDDVG-SQKVLMTSVTVPLLEQDKLLGMVGVDISLTALQSLVKEMDQELYEGQGKVLLVSSQ
WP_005303521.1 [Aeromonas hydrophila SSU]      DESVLADES-PTAAGGVENEWYRCSIRSK-ALCLLEPYLDDVG-SQKVLMTSVTVPLLEQDKLLGMVGVDISLTALQSLVKEMDQELYEGQGKVLLVSSQ
WP_017764096.1 [Aeromonas enteropelogenes]     DESVLADES-PTAAGGVENEWYRCSIRSK-ALCLLEPYLDDVG-SQKVLMTSVTVPLLEQDKLLGMVGVDISLTALQSLVKEMDQELYEGQGKVLLVSSQ
WP_043172570.1 [Aeromonas jandaei]             DESVLADES-PTAAGGVENEWYRCSIRSK-ALCLLEPYLDDVG-SQKVLMTSVTVPLLEQDKLLGMVGVDISLTALQSLVKEMDQELYEGQGKVLLVSSQ
WP_043171103.1 [Aeromonas hydrophila]          DESVLADES-PTAAGGVENEWYRCSIRSK-ALCLLEPYLDDVG-SQKVLMTSVTVPLLEQDKLLGMVGVDISLTALQSLVKEMDQELYEGQGKVLLVSSQ
WP_094696341.1 [Aeromonas sp. A35_P]           DESVLADES-PTAAGGVENEWYRCSIRSK-ALCLLEPYLDDVG-SQKVLMTSVTVPLLEQDKLLGMVGVDISLTALQSLVKEMDQELYEGQGKVLLVSSQ
WP_017784033.1 [Aeromonas]                     DESVLADES-PTAAGGVENEWYRCSIRSK-ALCLLEPYLDDVG-SQKVLMTSVTVPLLEQDKLLGMVGVDISLTALQSLVKEMDQELYEGQGKVLLVSSQ
WP_010634800.1 [Aeromonas dhakensis]           DESVLADES-PTAAGGVENEWYRCSIRSK-ALCLLEPYLDDVG-SQKVLMTSVTVPLLEQDKLLGMVGVDISLTALQSLVKEMDQELYEGQGKVLLVSSQ
WP_043134443.1 [Aeromonas salmonicida]         NESVLADES-PTAAGGVENEWYRCSIRSK-ALCLLEPYLDDVG-SQKVLMTSVTVPLLEQETLLGMVGVDISLATLQNLVKEMDKALYDGQGKVLLVSHE
WP_043554761.1 [Aeromonas bestiarum]           NESVLADES-PTAAGGVENEWYRCSIRSK-ALCLLEPYLDDVG-SQKVLMTSVTVPLLEQETLLGMVGVDISLATLQNLVKEMDKALYDGQGKVLLVSHE
WP_098984777.1 [Aeromonas sp. CA23]            NESVLADES-PTAAGGVENEWYRCSIRSK-ALCLLEPYLDDVG-SQKVLMTSVTVPLLEQETLLGMVGVDISLATLQNLVKEMDQALYDGQGKVLLVSHE
WP_065401479.1 [Aeromonas piscicola]           NESVLADES-PTAAGGVENEWYRCSIRSK-ALCLLEPYLDDVG-SQKVLMTSVTVPLLEQETLLGMVGVDISLATLQNLVKEMDKALYDGQGKVLLVSHE
WP_042867167.1 [Aeromonas piscicola]           NESVLADES-PTAAGGVENEWYRCSIRSK-ALCLLEPYLDDVG-SQKVLMTSVTVPLLEQETLLGMVGVDISLATLQNLVKEMDQALYDGQGKVLLVSHE
WP_042038095.1 [Aeromonas popoffii]            NESVLADES-PTAAGGVENEWYRCSIRSK-ALCLLEPYLDDVG-SQRVLMTSVTVPLLQQETLLGMVGVDISLATLQNLVKEMGQVLYDGQGKVLLVSHE
EHI53654.1 [Aeromonas salmonicida]             DESVLADES-PTAAGGVENDWYRCSIRSK-ALCLLEPYLDDVG-SQKVLMTSVTVPLLEQETLLGMVGVDISLATLQSLVKEMDQALYDGQGKVLLVSHE
EQC04590.1 [Aeromonas salmonicida]             DESVLADES-PTAAGGVENDWYRCSIRSK-ALCLLEPYLDDVG-SQKVLMTSVTVPLLEQETLLGMVGVDISLATLQSLVKEMDQALYDGQGKVLLVSHE
WP_034523767.1 [Aeromonas salmonicida]         DESVLADES-PTAAGGVENDWYRCSIRSK-ALCLLEPYLDDVG-SQKVLMTSVTVPLLEQETLLGMVGVDISLATLQSLVKEMDQALYDGQGKVLLVSHE
WP_099991888.1 [Aeromonas salmonicida]         DESVLVDES-PTAAGGVENDWYRCSIRSK-ALCLLEPYLDDVG-SQKVLMTSVTVPLLEQETLLGMVGVDISLATLQSLVKEMDQALYDGQGKVLLVSHE
WP_059112143.1 [Aeromonas salmonicida]         DESVLADES-PTAAGGVENDWYRCSIRSK-ALCLLEPYLDDVG-SQKVLMTSVTVPLLEQETLLGMVGVDISLATLQSLVKEMDQALYDGQGKVLLVSHE
WP_042467125.1 [Aeromonas salmonicida]         DESVLADES-PTAAGGVENDWYRCSIRSK-ALCLLEPYLDDVG-SQKVLMTSVTVPLLEQETLLGMVGVDISLATLQSLVKEMDQALYDGQGKVLLVSHE
WP_011898999.1 [Aeromonas]                     DESVLADES-PTAAGGVENDWYRCSIRSK-ALCLLEPYLDDVG-SQKVLMTSVTVPLLEQETLLGMVGVDISLATLQSLVKEMDQALYDGQGKVLLVSHE
WP_058393504.1 [Aeromonas salmonicida]         DESVLVDES-PTAAGGVENDWYRCSIRSK-ALCLLEPYLDDVG-SQKVLMTSVTVPLLEQENLLGMVGVDISLATLQSLVKEMDQALYDGQGKVLLVSHE
WP_059167951.1 [Aeromonas salmonicida]         DESVLADES-PTAAGGVENDWYRCSIRSK-ALCLLEPYLDDVG-SQKVLMTSVTVPLLEQETLLGMVGVDISLATLQSLVKEMDQALYDGQGKVLLVSHE
WP_042639553.1 [Aeromonas eucrenophila]        DEAMLADDK-PAANGGAKNDWYKCSIRTG-ALCLLEPYLDEVG-SQQVLMTSVTAPLLEQGKLLGMVGVDISLTRLQTLVLEMDKALYEGQGKVLLLSHE
WP_033132108.1 [Aeromonas aquatica]            DEATLADDK-PAANGGAKNDWYKCSIRTG-ALCLLEPYLDEVG-TQEVLMTSVTAPLLDQGKLLGMVGVDISLARLQTLVLEMDKALYGGQGKVLLLSHE
WP_050717971.1 [Aeromonas tecta]               NEAMLANKS-PTANGGVENFWYSCSIQSR-ALCLLEPYLDEVG-SQQVLMTSVTAPLLEQGNLLGMVGVDISLTTLQSLVEEMDKTLYDGQGKVLLLSHE
PJC95136.1 [Aeromonas lusitana]                NEAMLADKS-PTANGGVENFWYSCSIQSR-ALCLLEPYLDEVG-SEQVLMTSVTAPLLDQGTLLGMVGVDISLTTLQSLVEEMDKTLYNGQGKVLLLSHE
WP_042654092.1 [Aeromonas encheleia]           DEAVLADDK-PTANGGVENGWYSCSIRSR-ALCLLEPYLDEVG-TQEVLMTSVTAPLLEQGTLLGMVGVDISLTRLQSLVEEMDKTLYEGQGKVLLLSHE
WP_049636263.1 [Aeromonas caviae]              DEAMLANDK-PSGHGGLENDWYSCSIRSK-ALCLLEPYVDEVG-TQQVLMTSVTVPLLDQGSLLGMVGVDISLGTLQSLVEEMGRTLYKGQGKVLLLSSE
WP_043152488.1 [Aeromonas sp. HZM]             DEAMLANDK-PSGHGGLENDWYSCSIRSK-ALCLLEPYVDEVG-TQQVLMTSVTVPLLDQGSLLGMVGVDISLGTLQSLVEEMGRTLYKGQGKVLLLSSE
WP_039040706.1 [Aeromonas caviae]              DEAMLANDK-PSGHGGLENDWYSCSIRSK-ALCLLEPYVDEVG-TQQVLMTSVTVPLLDQGSLLGMVGVDISLGTLQSLVEEMGRTLYKGQGKVLLLSSE
KGY77484.1 [Aeromonas caviae]                  DEAMLANDK-PSGHGGLENDWYSCSIRSK-ALCLLEPYVDEVG-TQQVLMTSVTVPLLDQGSLLGMVGVDISLGTLQSLVEEMGRTLYKGQGKVLLLSSE
WP_042015878.1 [Aeromonas caviae]              DEAMLANDK-PSGHGGLENDWYSCSIRSK-ALCLLEPYVDEVG-TQQVLMTSVTVPLLDQGSLLGMVGVDISLGTLQSLVEEMGRTLYKGQGKVLLLSSE
```

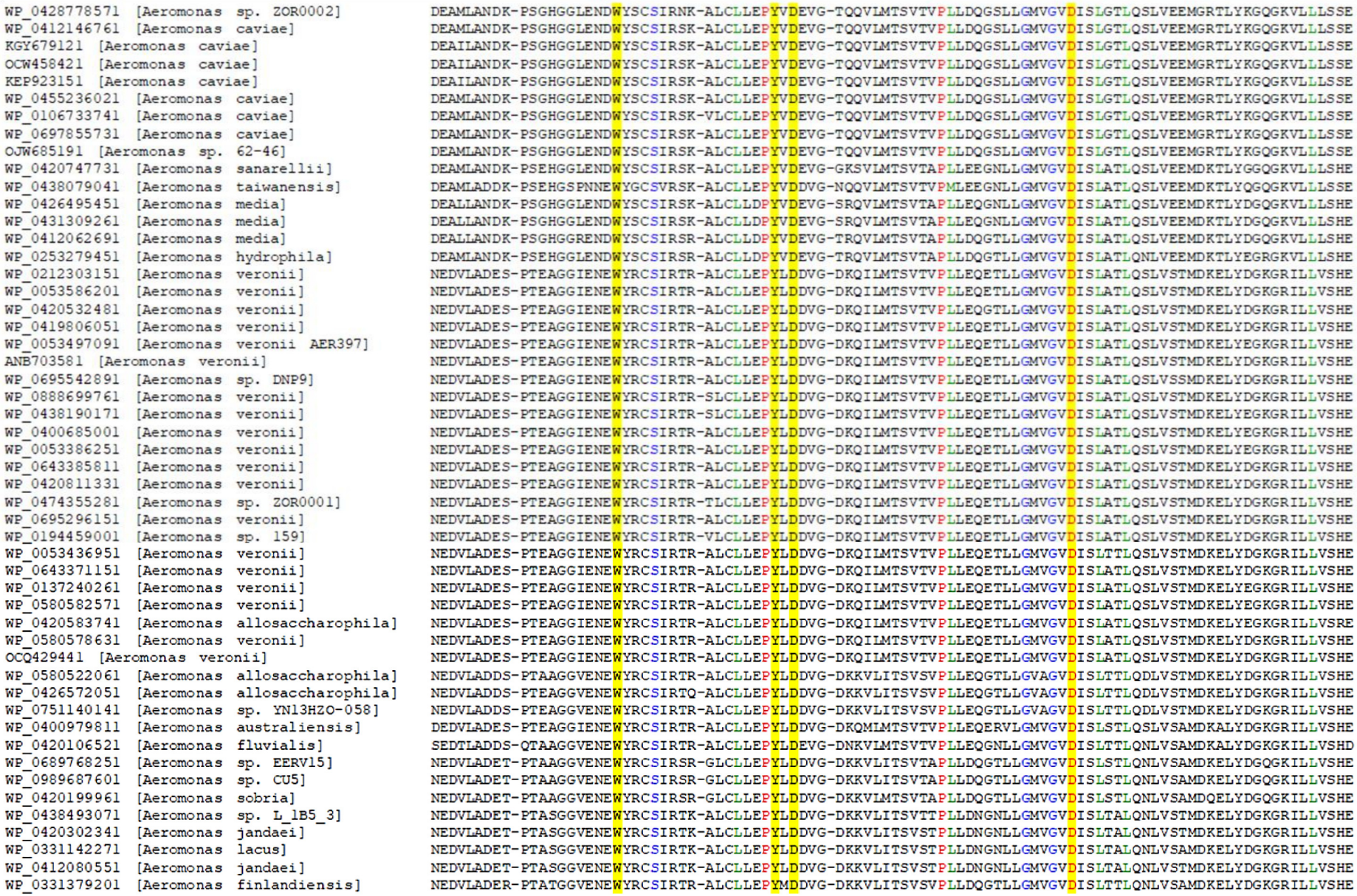
WP_0428778571 [Aeromonas sp. ZOR0002] DEAMLANDK-PSGHGGLENDWYSCSIRNK-ALCLLEPYVDEVG-TQQVLMTSVTVPLLDQGSLLGMVGVDISLGTLQSLVEEMGRTLYKGQGKVLLLSSE
WP_0412146761 [Aeromonas caviae] DEAMLANDK-PSGHGGLENDWYSCSIRSK-ALCLLEPYVDEVG-TQQVLMTSVTVPLLDQGSLLGMVGVDISLGTLQSLVEEMGRTLYKGQGKVLLLSSE
KGY679121 [Aeromonas caviae] DEAILANDK-PSGHGGLENDWYSCSIRSK-ALCLLEPYVDEVG-TQQVLMTSVTVPLLDQGSLLGMVGVDISLGTLQSLVEEMGRTLYKGQGKVLLLSSE
OCW458421 [Aeromonas caviae] DEAILANDK-PSGHGGLENDWYSCSIRSK-ALCLLEPYVDEVG-TQQVLMTSVTVPLLDQGSLLGMVGVDISLGTLQSLVEEMGRTLYKGQGKVLLLSSE
KEP923151 [Aeromonas caviae] DEAILANDK-PSGHGGLENDWYSCSIRSK-ALCLLEPYVDEVG-TQQVLMTSVTVPLLDQGSLLGMVGVDISLGTLQSLVEEMGRTLYKGQGKVLLLSSE
WP_0455236021 [Aeromonas caviae] DEAMLANDK-PSGHGGLENDWYSCSIRSK-ALCLLEPYVDEVG-TQQVLMTSVTVPLLDQGSLLGMVGVDISLGTLQSLVEEMGRTLYKGQGKVLLLSSE
WP_0106733741 [Aeromonas caviae] DEAMLANDK-PSGHGGLENDWYSCSIRSK-VLCLLEPYVDEVG-TQQVLMTSVTVPLLDQGSLLGMVGVDISLGTLQSLVEEMGRTLYKGQGKVLLLSSE
WP_0697855731 [Aeromonas caviae] DEAMLANDK-PSGHGGLENDWYSCSIRSK-ALCLLEPYVDEVG-TQQVLMTSVTVPLLDQGSLLGMVGVDISLGTLQSLVEEMGRTLYKGQGKVLLLSSE
OJW685191 [Aeromonas sp. 62-46] DEAMLANDK-PSGHGGLENDWYSCSIRSK-ALCLLEPYVDEVG-TQQVLMTSVTVPLLDQGSLLGMVGVDISLGTLQSLVEEMGRTLYKGQGKVLLLSSE
WP_0420747731 [Aeromonas sanarellii] DEAMLANDK-PSEHGGLENDWYSCSIRSK-ALCLLEPYVDEVG-GKSVLMTSVTAPLLEEGNLLGMVGVDISLATLQSLVEEMDKTLYGGQGKVLLLSHE
WP_0438079041 [Aeromonas taiwanensis] DEAMLADDK-PSEHGSPNNEWYGCSVRSK-ALCLLEPYVDDVG-NQQVLMTSVTVPMLEEGNLLGMVGVDISLATLQSLVEEMDKTLYQGQGKVLLLSSE
WP_0426495451 [Aeromonas media] DEALLANDK-PSGHGGLENDWYSCSIRSK-ALCLLDPYVDEVG-SRQVLMTSVTAPLLEQGNLLGMVGVDISLATLQSLVEEMDKTLYDGQGKVLLLSHE
WP_0431309261 [Aeromonas media] DEALLANDK-PSGHGGLENDWYSCSIRSK-ALCLLDPYVDEVG-SRQVLMTSVTAPLLEQGNLLGMVGVDISLATLQSLVEEMDKTLYDGQGKVLLLSHE
WP_0412062691 [Aeromonas media] DEALLANDK-PSGHGGRENDWYSCSIRSR-ALCLLDPYVDEVG-TRQVLMTSVTAPLLDQGTLLGMVGVDISLATLQSLVEEMDKTLYDGQGKVLLLSHE
WP_0253279451 [Aeromonas hydrophila] DEAMLANDK-PSEHGGLENDWYSCSIRSR-ALCLLDPYVDEVG-TRQVLMTSVTAPLLDQGTLLGMVGVDISLATLQNLVEEMDKTLYEGRGKVLLLSHE
WP_0212303151 [Aeromonas veronii] NEDVLADES-PTEAGGIENEWYRCSIRTR-ALCLLEPYLDDVG-DKQILMTSVTVPLLEQETLLGMVGVDISLATLQSLVSTMDKELYDGKGRILLVSHE
WP_0053586201 [Aeromonas veronii] NEDVLADES-PTEAGGIENEWYRCSIRTR-ALCLLEPYLDDVG-DKQILMTSVTVPLLEQETLLGMVGVDISLATLQSLVSTMDKELYDGKGRILLVSHE
WP_0420532481 [Aeromonas veronii] NEDVLADES-PTEAGGIENEWYRCSIRTR-ALCLLEPYLDDVG-DKQILMTSVTVPLLEQGTLLGMVGVDISLATLQSLVSTMDKELYDGKGRILLVSHE
WP_0419806051 [Aeromonas veronii] NEDVLADES-PTEAGGIENEWYRCSIRTR-ALCLLEPYLDDVG-DKQILMTSVTVPLLEQETLLGMVGVDISLATLQSLVSTMDKELYDGKGRILLVSHE
WP_0053497091 [Aeromonas veronii AER397] NEDVLADES-PTEAGGIENEWYRCSIRTR-ALCLLEPYLDDVG-DKQILMTSVTVPLLEQETLLGMVGVDISLATLQSLVSTMDKELYEGKGRILLVSHE
ANB703581 [Aeromonas veronii] NEDVLADES-PTEAGGIENEWYRCSIRTR-ALCLLEPYLDDVG-DKQILMTSVTVPLLEQETLLGMVGVDISLATLQSLVSTMDKELYDGKGRILLVSHE
WP_0695428911 [Aeromonas sp. DNP9] NEDVLADES-PTEAGGIENEWYRCSIRTR-ALCLLEPYLDDVG-DKQILMTSVTVPLLEQETLLGMVGVDISLATLQSLVSSMDKELYDGKGRILLVSHE
WP_0888699761 [Aeromonas veronii] NEDVLADES-PTEAGGIENEWYRCSIRTR-SLCLLEPYLDDVG-DKQILMTSVTVPLLEQETLLGMVGVDISLATLQSLVSTMDKELYDGKGRILLVSHE
WP_0438190171 [Aeromonas veronii] NEDVLADES-PTEAGGIENEWYRCSIRTR-SLCLLEPYLDDVG-DKQILMTSVTVPLLEQETLLGMVGVDISLATLQSLVSTMDKELYEGKGRILLVSHE
WP_0400685001 [Aeromonas veronii] NEDVLADES-PTEAGGIENEWYRCSIRTR-ALCLLEPYLDDVG-DKQILMTSVTVPLLEQETLLGMVGVDISLATLQSLVSTMDKELYEGKGRILLVSHE
WP_0053386251 [Aeromonas veronii] NEDVLADES-PTEAGGIENEWYRCSIRTR-ALCLLEPYLDDVG-DKQILMTSVTVPLLEQETLLGMVGVDISLATLQSLVSTMDKELYEGKGRILLVSHE
WP_0643385811 [Aeromonas veronii] NEDVLADES-PTEAGGIENEWYRCSIRTR-ALCLLEPYLDDVG-DKQILMTSVTVPLLEQETLLGMVGVDISLATLQSLVSTMDKELYDGKGRILLVSHE
WP_0420811331 [Aeromonas veronii] NEDVLADES-PTEAGGIENEWYRCSIRTR-ALCLLEPYLDDVG-DKQILMTSVTVPLLEQETLLGMVGVDISLATLQSLVSTMDKELYDGKGRILLVSHE
WP_0474355281 [Aeromonas sp. ZOR0001] NEDVLADES-PTEAGGIENEWYRCSIRTR-TLCLLEPYLDDVG-DKQILMTSVTVPLLEQETLLGMVGVDISLATLQSLVSTMDKELYDGKGRILLVSHE
WP_0695296151 [Aeromonas veronii] NEDVLADES-PTEAGGIENEWYRCSIRTR-ALCLLEPYLDDVG-DKQILMTSVTVPLLEQETLLGMVGVDISLATLQSLVSTMDKELYDGKGRILLVSHE
WP_0194459001 [Aeromonas sp. 159] NEDVLADES-PTEAGGIENEWYRCSIRTR-VLCLLEPYLDDVG-DKQILMTSVTVPLLEQETLLGMVGVDISLATLQSLVSTMDKELYDGKGRILLVSHE
WP_0053436951 [Aeromonas veronii] NEDVLADES-PTEAGGIENEWYRCSIRTR-ALCLLEPYLDDVG-DKQILMTSVTVPLLEQETLLGMVGVDISLTTLQSLVSTMDKELYDGKGRILLVSHE
WP_0643371151 [Aeromonas veronii] NEDVLADES-PTEAGGIENEWYRCSIRTR-ALCLLEPYLDDVG-DKQILMTSVTVPLLEQETLLGMVGVDISLATLQSLVSTMDKELYDGKGRILLVSHE
WP_0137240261 [Aeromonas veronii] NEDVLADES-PTEAGGIENEWYRCSIRTR-ALCLLEPYLDDVG-DKQILMTSVTVPLLEQETLLGMVGVDISLATLQSLVSTMDKELYEGKGRILLVSHE
WP_0580582571 [Aeromonas veronii] NEDVLADES-PTEAGGIENEWYRCSIRTR-ALCLLEPYLDDVG-DKQILMTSVTVPLLEQETLLGMVGVDISLATLQSLVSTMDKELYEGKGRILLVSHE
WP_0420583741 [Aeromonas allosaccharophila] NEDVLADES-PTEAGGIENEWYRCSIRTR-ALCLLEPYLDDVG-DKQILMTSVTVPLLEQETLLGMVGVDISLATLQSLVSTMDKELYEGKGRILLVSRE
WP_0580578631 [Aeromonas veronii] NEDVLADES-PTEAGGIENEWYRCSIRTR-ALCLLEPYLDDVG-DKQILMTSVTVPLLEQETLLGMVGVDISLATLQSLVSTMDKELYDGKGRILLVSHE
OCQ429441 [Aeromonas veronii] NEDVLADES-PTEAGGIENEWYRCSIRTR-ALCLLEPYLDDVG-DKQILMTSVTVPLLEQETLLGMVGVDISLATLQSLVSTMDKELYDGKGRILLVSHE
WP_0580522061 [Aeromonas allosaccharophila] NEDVLADDS-PTAAGGVENEWYRCSIRTR-ALCLLEPYLDDVG-DKKVLITSVSVPLLEQGTLLGVAGVDISLTTLQDLVSTMDKELYDGKGRILLVSHE
WP_0426572051 [Aeromonas allosaccharophila] NEDVLADDS-PTEAGGVENEWYRCSIRTQ-ALCLLEPYLDDVG-DKKVLITSVSVPLLEQGTLLGVAGVDISLTTLQDLVSTMDKELYDGKGRILLVSHE
WP_0751140141 [Aeromonas sp. YN13HZO-058] NEDVLADDS-PTEAGGVENEWYRCSIRTR-ALCLLEPYLDDVG-DKKVLITSVSVPLLEQGTLLGVAGVDISLTTLQDLVSTMDKELYDGKGRILLVSHE
WP_0400979811 [Aeromonas australiensis] DEDVLADES-PTEAGGIENEWYRCSIRTR-ALCLLEPYLDDVG-DKQMLMTSVTVPLLEQERVLGMVGVDISLSTLQSLVSAMDKALYDGKGRILLVSHE
WP_0420106521 [Aeromonas fluvialis] SEDTLADDS-QTAAGGVENEWYRCSIRTR-ALCLLEPYLDEVG-DNKVLMTSVTVPLLEQGNLLGMVGVDISLTTLQNLVSAMDKALYDGKGKILLVSHD
WP_0689768251 [Aeromonas sp. EERV15] NEDVLADET-PTAAGGVENEWYRCSIRSR-GLCLLEPYLDDVG-DKKVLITSVTAPLLDQGTLLGMVGVDISLSTLQNLVSAMDKELYDGQGKILLVSHE
WP_0989687601 [Aeromonas sp. CU5] NEDVLADET-PTAAGGVENEWYRCSIRSR-GLCLLEPYLDDVG-DKKVLITSVTAPLLDQGTLLGMVGVDISLSTLQNLVSAMDKELYDGQGKILLVSHE
WP_0420199961 [Aeromonas sobria] NEDVLADET-PTAAGGVENEWYRCSIRSR-GLCLLEPYLDDVG-DKKVLMTSVTAPLLDQGTLLGMVGVDISLSTLQNLVSAMDQELYDGQGKILLVSHE
WP_0438493071 [Aeromonas sp. L_1B5_3] NEDVLADET-PTASGGVENEWYRCSIRTK-ALCLLEPYLDDVG-DKKVLITSVTTPLLDNGNLLGMVGVDISLTALQNLVSTMDKELYDGKGRILLVSHE
WP_0420302341 [Aeromonas jandaei] NEDVLADET-PTASGGVENEWYRCSIRTK-ALCLLEPYLDDVG-DKKVLITSVSTPLLDNGNLLGMVGVDISLTALQNLVSTMDKELYDGKGRILLVSHE
WP_0331142271 [Aeromonas lacus] NEDVLADET-PTASGGVENEWYRCSIRTK-ALCLLEPYLDDVG-DKKVLITSVSTPLLDNGNLLGMVGVDISLTALQNLVSAMDKELYDGKGRILLVSHE
WP_0412080551 [Aeromonas jandaei] NEDVLADET-PTASGGVENEWYRCSIRTK-ALCLLEPYLDDVG-DKKVLITSVSTPLLDNGNLLGMVGVDISLTALQNLVSTMDKELYDGKGRILLVSHE
WP_0331379201 [Aeromonas finlandiensis] NEDVLADER-PTATGGVENEWYRCSIRTR-ALCLLEPYMDDVG-DKKVLITSVSVPLLDQGTLLGMVGVDISLTTLQNLVSAMDKELYDGKGRILLVSHE

```
WP_042027994.1 [Aeromonas enteropelogenes]      DEEVLADES-LTPTGGVENEWYRCSIRTR-ALCLLEPYLDEVG-GQQILMTSVTYPLQEEGALLGMVGVDVPLTSLQQLVNSMDQQLYSGKGKILLVSHE
WP_061475962.1 [Aeromonas enteropelogenes]      DEEVLADES-PTETGGVENEWYRCSIRTR-ALCLLEPYLDEVG-GQQILMTSVTYPLQEEGTLLGMVGVDVPLTSLQQLVSSMDQQLYSGKGKILLVSHE
WP_042073191.1 [Aeromonas enteropelogenes]      DEEVLADES-PTETGGVENEWYRCSIRTR-ALCLLEPYLDEVG-DQQILMTSVTYPLQEEGALLGMVGVDVPLTSLQQLVSSMDQQLYSGKGKILLVSHE
WP_042040786.1 [Aeromonas rivuli]              NEATLNDAS-PDESGTPKNEWYRCSLRDK-ALCLLEPYLDEVG-SEEVLMTSVTTPLLEEGKLLGMVGMDISLAKLQALVVEMDQTLYQGQGRILLLSHG
WP_005893348.1 [Aeromonas molluscorum]         NEATLNDAG-PDESGTPKNEWYRCSLREQ-SICLLEPYLDEVG-NQEVLMTSVTTPLLEEGKLLGMVGMDISLAKLQALVAEMDQTLYQGQGRILLLSHG
WP_041993285.1 [Aeromonas bivalvium]           DEATLKDAS-PDAFGTPQNEWYRCSLREQ-ALCLLEPYLDDVG-GEQVLMTSVTTPLREEGALLGMVGMDISLARLQTLVAEMDQTLYQGQGRILLLSQG
ALP42887.1 [Aeromonas schubertii]              SEEDLADSA-PDESGTPANYWYRCSLESR-SSCLLEPYLDEVE-GQSRLMTSVTVPLMEEGKVIGIVGVDLALDSLQQVVQGMDEDLYRGSGDVMLISQG
WP_050665801.1 [Aeromonas schubertii]          SEEDLADSA-PDESGTPANYWYRCSLESR-SSCLLEPYLDEVE-GQSRLMTSVTVPLMEEGKVIGIVGVDLALDSLQQVVQGMDEDLYRGSGDVMLISQG
WP_005349141.1 [Aeromonas diversa] >           SEEDLADVK-LDENGIPVNYWYSCSLKSG-RNCLLEPYLDEVE-GQNRLMTSVTAPLIDEGKVIGMVGVDLALDRLQQVVQSMDDALYGGSGDVMLLSQG
WP_076573363.1 [Aeromonas sp. RU39B]           NEANLADAS-TDANGMVRNQRYRCSMDKK-STCLLDPYLAERQ-GQTMLLTSVTVPMVSEGKVIGVVGVDLALAPMQQVVDQIDQALYQGAGDVLLVSQA
WP_081741476.1 [Tolumonas lignilytica]         TEKDIKDST-ANENGFAKNEWFNCSIRVH-GPCLLNPYKDTSN-KKELLMVTVTQPVVDGDNVLGVVGMDIALDSMQSAIKELDSQLFSGHGKAALISSE
EDM65417.1 [Moritella sp. PE36]                SEQQINNTS-LAVSGQASNFWYSCSTLNN-RTCVIEPYLYNEN-GTSQLISTITVPLRKDGDIIGVTGIDLKINVLQQYALRADQALFSGAGKVQIVSNN
WP_043994878.1 [Moritella sp. PE36]            SEQQINNTS-LAVSGQASNFWYSCSTLNN-RTCVIEPYLYNEN-GTSQLISTITVPLRKDGDIIGVTGIDLKINVLQQYALRADQALFSGAGKVQIVSNN
WP_017221500.1 [Moritella dasanensis]          TEQQINNSS-QAASGQADNFWYSCSTTNN-RTCVIEPYLYNES-GISQLISTITVPLRKDGEVIAVTGIDLKIDVLQQYALSADQALFSGAGKVQIVSNN
WP_075473447.1 [Moritella viscosa]             SEQQINNTT-QAISGQANNFWYSCSITNK-RMCVIEPYLYNEN-GATRLISPITVPLRKQGKIIGVTGIDLKIDVLQQYAQRADQALFAGAGKVRIVSNN
WP_045110875.1 [Moritella viscosa]             SEQQINNTT-QAISGQANNFWYSCSITNK-RMCVIEPYLYNEN-GATRLISPITVPLRKQGKIIGVTGIDLKIDVLQQYAQRADQALFAGAGKVRIVSNN
WP_075533361.1 [Moritella viscosa]             SEQQINNTT-QAISGQANNFWYSCSITNK-RMCVIEPYLYNEN-GATRLISPITVPLRKQGKIIGVTGIDLKIDVLQQYAQRADQALFAGAGKVRIVSNN
WP_075519028.1 [Moritella viscosa]             SEQQINNTT-QAISGQANNFWYSCSITNK-RMCVIEPYLYNEN-GATRLISPITVPLRKQGKIIGVTGIDLKIDVLQQYAQRADQALFAGAGKVRIVSNN
WP_075498083.1 [Moritella viscosa]             SEQQINNTT-QAISGQANNFWYSCSITNK-RMCVIEPYLYNEN-GATRLISPITVPLRKQGKIIGVTGIDLKIDVLQQYAQRADQALFAGAGKVRIVSNN
WP_075518437.1 [Moritella viscosa]             SEQQINNTT-QAISGQANNFWYSCSITNK-RMCVIEPYLYNEN-GATRLISPITVPLRKQGKIIGVTGIDLKIDVLQQYAQRADQALFAGAGKVRIVSNN
WP_075478528.1 [Moritella viscosa]             SEQQINNTT-QAISGQENNFWYSCSITNK-RMCVIEPYLYNEN-GATRLISPITVPLRKQGKIIGVTGIDLKIDVLQQYAQRADQALFAGAGKVRIVSNN
WP_067042685.1 [Moritella sp. JT01]            SEQQINNTT-QAMSGQANNFWYSCSITNK-RMCVIEPYLYNEN-GATRLISPITVPLRKEGKIIGVTGIDLKIDVLQQYAQRADQALFAGAGKVRIVSNN
WP_019441756.1 [Moritella marina]              TEQQINDTA-KAANGQANNFWYTCSITNK-RMCVIEPYLYKEN-GISHLVSTITVPVRKQGEIIGVTGIDLKIGVLQDFAQRADQALFTGAGTVKIVSNY
WP_065592991.1 [Aliivibrio sp. 1S165]           TEKELGNTT-VKSNGDATNYWFTCSLKES-RLCIMDPYYYESD-GITRLISSITAPLIKGDETIGMVGIDLDIARISGLITQADKAIFNGKGAIYVVNSK
WP_065601093.1 [Aliivibrio sp. 1S128]           TEKELGNTT-VKSNGDATNYWFTCSLKES-RLCIMDPYYYESD-GITRLISSITAPLIKGDETIGMVGIDLDIARISGLITQADKAIFNGKGAIYVVNSK
WP_048896962.1 [Photobacterium swingsii]        TESDI---------TAAQHHRFSCSIDQQ-TACVLRPEYSAN----QVLISSITTPLIVDGKAIGLLGLDINLSALQSVISDVDSNLFDGSGKVSLLSDD
WP_027252779.1 [Photobacterium halotolerans]    SEAKIG--------DKATNAWYTCSLNGR-ESCVQDPVFSTDN-GQKVLLSSITIPLIVKGEAVGVMGIDVKLDPLQSVINTVDDNLFNASGKVSLVSQN
WP_054961434.1 [Vibrio bivalvicida]             VEEDINDTE-LDETNTPFNEWYACPIRNQ-NACVLNPYLDTVG-NEEILMTSLTLPIVSKGQLVGMLGVDFGLNKIQTLITEADQNMFSGHGQVLLLSHG
WP_049846877.1 [Vibrio sp. VPAP30]              VEEDINDTE-LDETNTPFNEWYACSIRNQ-NACVLNPYLDTVG-NEEILMTSLTLPIVSKGQLVGMLGVDFGLNKIQTLITEADQNMFSGHGQVLLLSHG
WP_004745818.1 [Vibrio tubiashii]              LEEDINDTE-LDESNTPINEWYACSIRNR-NACVLNPYLDTVG-DEEILMTSLTLPIQSKGQLIGMLGVDFGLNKIQTLITQADQNMFSGHGQVLLLSHG
WP_007463501.1 [Photobacterium marinum]        LEEDLYDTE-LDDNQMSMNEWYACSMRNNGQACVLNPYLDTVD-GEEMLMTSLTLPLKENGRLIGMLGIDFSLADIQSMINQADRRIFDGDGEVILLSHG
WP_064609466.1 [Photobacterium sp. J15]         LEEDLYDTE-LDDNQMPMNEWYACSMRNNGQACVLNPYLDTVD-GEEMLMTSLTLPLKENGRLIGMLGIDFSLADIQSMINQADRRIFDGDGEVILLSHG
WP_090365441.1 [Ferrimonas sediminum]          DEAAIHNRQ-LNKQGVPENEWFDCPARTG-ELCVLNPYVDEVG-AGGNLITSVTLPLKADGKVIGVMGIDLSLATLQPLIESVDAEFVDGSGEVALISQD
WP_028114754.1 [Ferrimonas futtsuensis]        DEAAIHNRQ-LNKQGMPENEWFDCPARTG-DLCVLNPYVDEVG-AGGNLITSVTLPLKADGKVIGVMGIDLSLATLQPLIESVDAEFVGGNGEVALISQD
WP_028109598.1 [Ferrimonas futtsuensis]        NEQDVRNSS-PTKQGMPQNQWFSCPVERG-RACVLNPYVDEVG-SDQELITSVTLPLISQGEIIGVVGIDLSVAAMQPLIEQVDSKLVSGKGQVALVSQD
SDJ52060.1 [Ferrimonas sediminum]              AEEELSDTS-LNQYGIAESEWYTCAINSR-KACVLDPYLDDVG-TTELLMTSVTLPLLDEGQVIGMLGLDISLASLQPMIERVDGQFMEGAGEVALFSQA
WP_090365442.1 [Ferrimonas sediminum]          AEEELSDTS-LNQYGIAESEWYTCAINSR-KACVLDPYLDDVG-TTELLMTSVTLPLLDEGQVIGMLGLDISLASLQPMIERVDGQFMEGAGEVALFSQA
WP_035385330.1 [Ferrimonas futtsuensis]        LEEDLHDTA-LNDYGIPEVEWYQCAVRQR-KACVLDPYLDDVG-DNEMLMTSVTYPLLQGGELVGMLGIDISLAGLQPLIESVDSRLVDGEGEVALVSQA
WP_075766764.1 [Photobacterium proteolyticum]   EEEYITDTT-PGSFGRAKNEWYACSVRTR-QPCILNPFLDRAG-SEEVLMTAVTFPLLENGELLGTVGIDLSLQSLQVLIDAVDSSFYNGQGHAVLFGQD
WP_002538153.1 [Grimontia indica]              PLAGYADET-RTDGGARVGEYYLCSRDSR-RNCLLDPYVYPVN-GQNVLLTSVVSPVMVDGQFAGITGLDISLAALSHVAESLSQRLYQGQSHVMLVTDR
WP_046304191.1 [Grimontia sp. AD028]           PLAGYADET-RTDGGARVGEYYLCSRDSR-RNCLLDPYVYPVN-GQNVLLTSVVSPVMVDGQFAGITGLDISLAALSHVAESLSQRLYQGQSHVMLVTDR
WP_062665491.1 [Grimontia celer]               PLAGYADET-RTEGGARVGEYYLCSRDSR-RNCLLDPYVYPVN-GQNVLLTSVVSPILVNGRFAGITGLDISLAELSHVAESLSQRLYQGQSHVMLVTDR
WP_028021513.1 [Enterovibrio calviensis]       PLTGYADES-RSDGGARVGEYYLCSRDSN-RNCLLDPYVYPVN-GQNVLLTSVVSPITVNGQFVGITGLDISLQSLSQVAESLSQRLYSGQSHVMLVTDR
WP_067414762.1 [Enterovibrio coralii]          ALAGYNDES-RANNGARVGEYYLCSRDTR-QNCLLEPYVYPVN-GKSVLLTSVVSPIIVNGQFAGVTGLDISLSALSEVAESLSQRLYNGQSHVMLVTNQ
KZN50623.1 [Pseudoalteromonas luteoviolacea]    SSS-AKYSEALNRYGIREAEWYLCAKESK-LPCIMEPYLYEISKGNEMLMTSLTVPITQHGRFKGIIGVDVNLPSLQRLVQELSSQLYQGQGKVLLLSEL
WP_063361747.1 [Pseudoalt. luteoviolacea]       SSS-AKYSEALNRYGIREAEWYLCAKESK-LPCIMEPYLYEISKGNEMLMTSLTVPITQHGRFKGIIGVDVNLPSLQRLVQELSSQLYQGQGKVLLLSEL
KZN64463.1 [Pseudoalteromonas luteoviolacea]    SSS-AKYSEVLNRYGIREAEWYLCAKESK-LPCIMEPYLYEISKDNEMLMTSLTVPITQHGRFKGIIGVDVNLPNLQRLVQELSNQLYQGQGKVLLLSEL
KKE82938.1 [Pseudoalteromonas luteoviolacea]    SSS-AKYSEALNRYGIREAEWYLCAKESK-LPCIMEPYLYEISKGNEMLMTSLTVPITQHGRFKGIIGVDVNLPNLQRLVQELSSQLYQGQGKVLLLSEL
WP_076464155.1 [Marinobacterium stanieri]      ESTESKYDETINESGIRASEWYLCPLETA-QNCMVEPYLYEISEGNSILMTSLTVPIISNGKVVGVAGTDVNLPVLQEMTEAMAQELYQGQASITLLSEK
WP_010322463.1 [Marinobacterium stanieri]      ESTESKHDETINESGIRASEWYLCPLETA-QNCMVEPYLYEISEGNSILMTSLTVPIISNGEVVGVAGTDVNLPVLQEMTEAMAQELYQGQASITLLSEK
WP_067012339.1 [Marinomonas spartinae]         DPA-LKYVQDKDENGVRVSEWYLCPMDTK-KSCLLDPYLFELTSGQKVLMTTYSAPILADGKFVGMVGADINLSAIQKKLSQLTHNLFGGAGNITIVSEK
```

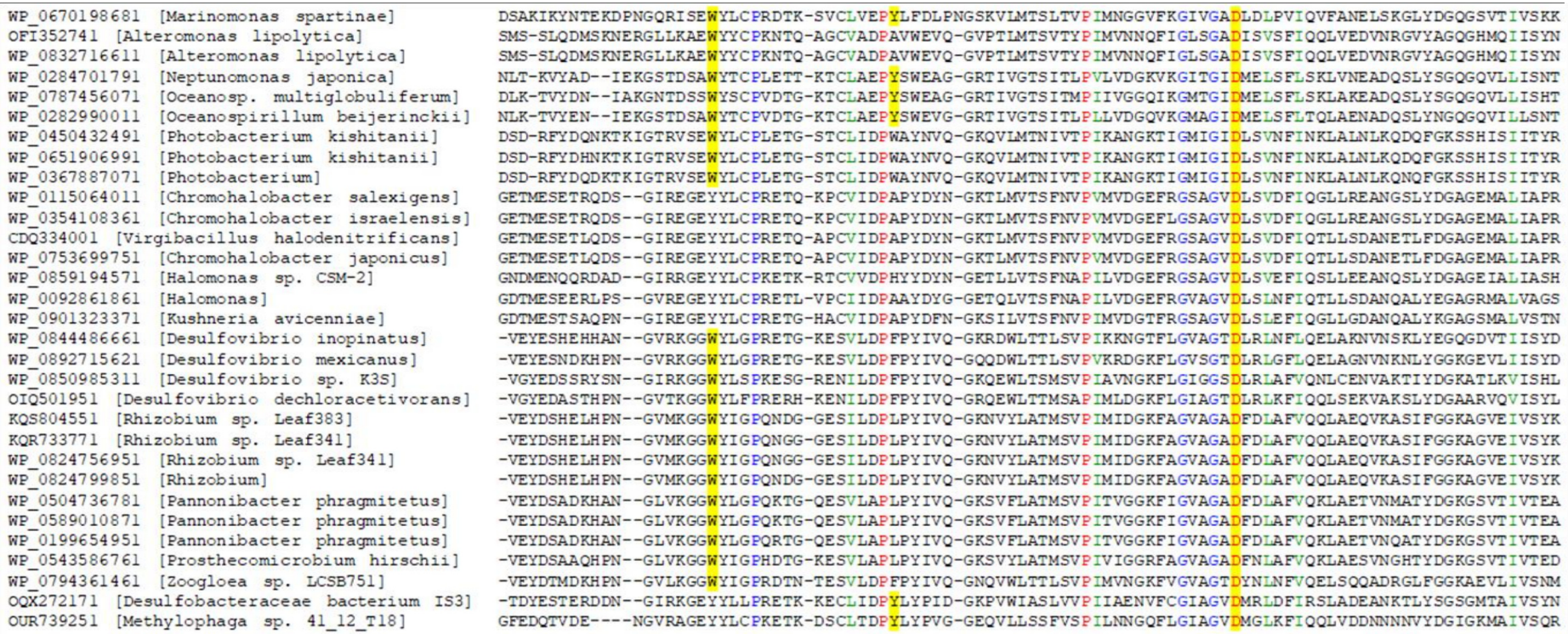

Supp. Fig 30. Fragment of the alignment of the top 230 sequences from a blastp search using the McpU-LBD sequence in the non-redundant protein sequence database of NCBI. Sequences from *Pseudomonas* strains were excluded in this search. The BLOSUM62 matrix was used and settings for gap costs were defined as: Existence: 11 and Extension: 1. The McpU-LBD sequence is shown on top of this alignment as a reference. The conservation of the four critical residues for ligand binding (D204, D233, W186 and Y202) is indicated by yellow shading.

Supp. Table 8. The relative abundance of McpU-LBD secondary structure elements in the absence and presence of ligands as derived from the deconvolution of far UVCD spectra. Protein was at 18.5 µM, ligands at 200 µM and deconvolution was made using the CDNN software package (Bohm *et al.*, 1992).

Ligand	Relative abundance of secondary structure elements (%)				
	α-helix	β-antiparallel	β-parallel	β-turn	Randomcoil
none	27.9	9.8	10.1	17.9	34.3
Putrescine	28.0	9.9	10.1	17.9	34.1
Cadaverine	28.3	9.7	10.0	17.8	34.2
Spermidine	28.2	9.7	10.0	17.8	34.3

Supp. Table 9. Thermodynamic parameters of the unfolding of McpU-LBD in the absence and presence of ligands. Protein was at 37.8 µM and ligands at 200 µM.

Ligand	T_m (°C)	ΔH_m (kcal/mol)	Peak width at half height (°C)
none	45.4	74	5.16
Putrescine	49.8	91	3.57
Cadaverine	48.7	88	3.56
Spermidine	50.8	92	3.17

Supp. Table 10. Hydrodynamic parameters calculated from the SAXS and the crystallographic structures of McpU-LBD. Shown is a comparison of some of the solution properties calculated by the HYDROPRO software from the crystallographic and the SAXS models of McpU-LBD using standard values for the primary atomic radius, at 20 °C and water solvent.

Parameter	X-ray crystallography	SAXS
Diffusion Coefficient x10^7 (cm^2/s)	8.3	8.0
Radius of Gyration (nm)	2.1	2.5
Intrinsic Viscosity (cm^3/g)	3.4	3.8
Sedimentation Coefficient (S)	3.2	3.1

Supp. Table 11. List of bacterial species from a sequence alignment with McpU-LBD (see Supp. Fig. 24) in which at least three of the four critical residues for ligand binding (Y202, D204, D233, W186) are conserved.

Species	Taxonomic phylum	Source/lifestyle/comments	References
Aeromonas allosaccharophila	Gammaproteobacteria	Bacterium firstly isolated from diseased elvers but later isolated from environmental freshwater, human and other mammals.	(Martinez-Murcia *et al.*, 1992, Saavedra *et al.*, 2007, Picao *et al.*, 2008, Janda & Abbott, 2010)
Aeromonas aquatica	Gammaproteobacteria	Bacterium whose main representative strain was isolated from a lake experiencing cyanobacterial blooms.	(Hossain *et al.*, 2014, Beaz-Hidalgo *et al.*, 2015)
Aeromonas australiensis	Gammaproteobacteria	Bacterium isolated from irrigation water.	(Aravena-Roman *et al.*, 2013)
Aeromonas bestiarum	Gammaproteobacteria	Bacterium isolated from fish and freshwater samples. Responsible for causing septicemia in fish.	(Minana-Galbis *et al.*, 2002, Kozinska & Guz, 2004, Beaz-

			Hidalgo *et al.*, 2010, Janda & Abbott, 2010)
Aeromonas bivalvium	Gammaproteobacteria	Bacterium whose main representative was isolated from bivalve molluscs.	(Minana-Galbis *et al.*, 2007, Janda & Abbott, 2010)
Aeromonas caviae	Gammaproteobacteria	Widely distributed bacterium that can be isolated from human, molluscs, fish, freshwater and seawater. Human and fish pathogen. Synonymous to *Aeromonas punctata.*	(Janda & Abbott, 2010, Silva *et al.*, 2017, Baldissera *et al.*, 2018)
Aeromonas dhakensis	Gammaproteobacteria	Bacterium isolated from human and fish samples. Emerging human and fish pathogen.	(Soto-Rodriguez *et al.*, 2013, Wu *et al.*, 2013a, Chen *et al.*, 2016)
Aeromonas diversa	Gammaproteobacteria	Bacterium whose main representative strain was isolated from human wounds.	(Minana-Galbis *et al.*, 2010, Farfan *et al.*, 2013)
Aeromonas encheleia	Gammaproteobacteria	Bacterium originally isolated from eels but also found in molluscs and freshwater samples.	(Esteve *et al.*, 1995, Novakova *et al.*, 2009, Janda & Abbott, 2010)
Aeromonas enteropelogenes	Gammaproteobacteria	Bacterium isolated from aquatic animals, human, environmental water and soils. Considered enterotoxic in animal models. Synonymous to *Aeromonastrota*.	(Singh & Sanyal, 1997, Janda & Abbott, 2010, Takahashi *et al.*, 2014, Silva *et al.*, 2017)
Aeromonas eucrenophila	Gammaproteobacteria	Bacterium mainly isolated from human (i.e. faecal samples, wounds), diseased fish and freshwater samples. Several strains were shown to produce different virulence factors.	(Singh & Sanyal, 1999, Demarta *et al.*, 2004, Janda & Abbott, 2010)
Aeromonas finlandiensis	Gammaproteobacteria	Bacterium whose main representative strain was isolated from a lake experiencing cyanobacterial blooms.	(Beaz-Hidalgo *et al.*, 2015)
Aeromonas fluvialis	Gammaproteobacteria	Aquatic bacterium whose main representative strain was isolated from river water.	(Alperi *et al.*, 2010a)
Aeromonas hydrophila	Gammaproteobacteria	Bacterium generally isolated from freshwater and human samples. Responsible for causing diseases in amphibians, birds, fishes, reptiles and humans. Its virulence is a multifactorial process that depends on the production of various virulence factors.	(Beaz-Hidalgo *et al.*, 2010, Janda & Abbott, 2010, Duarte *et al.*, 2015, Rasmussen-Ivey *et al.*, 2016, Silva *et al.*, 2017)
Aeromonas jandaei	Gammaproteobacteria	Bacterium generally isolated from human, fish and freshwater that causes disease in both human and	(Singh & Sanyal, 1997, Balsalobre *et al.*, 2009, Janda

		fish.	& Abbott, 2010, Dong *et al.*, 2017, Silva *et al.*, 2017)
Aeromonas lacus	Gammaproteobacteria	Bacterium whose main representative strain was isolated from a lake experiencing cyanobacterial blooms.	(Hossain *et al.*, 2014, Beaz-Hidalgo *et al.*, 2015)
Aeromonas lusitana	Gammaproteobacteria	Bacterium isolated from freshwater samples.	(Martinez-Murcia *et al.*, 2016)
Aeromonas media	Gammaproteobacteria	Opportunistic pathogen of human and fish *that can be isolated from* river freshwater, sewage water, animals and human.	(Beaz-Hidalgo *et al.*, 2010, Janda & Abbott, 2010, Talagrand-Reboul *et al.*, 2017)
Aeromonas molluscorum	Gammaproteobacteria	Marine bacterium generally isolated from bivalve molluscs and sediments. Potential bioremediator of the **organotin** biocide tributyltin.	(Minana-Galbis *et al.*, 2004, Janda & Abbott, 2010, Cruz *et al.*, 2013)
Aeromonas piscicola	Gammaproteobacteria	Bacterium that can be isolated from human and fish. Opportunistic pathogen of aquatic and terrestrial human and animals.	(Beaz-Hidalgo *et al.*, 2009, Duarte *et al.*, 2015)
Aeromonas popoffii	Gammaproteobacteria	Bacterium generally isolated from seawater and freshwater. Its genome encodes multiple virulence determinants and it has been shown to cause human infections.	(Soler *et al.*, 2002, Hua *et al.*, 2004, Janda & Abbott, 2010)
Aeromonas rivuli	Gammaproteobacteria	Freshwater bacterium whose main representative strain was isolated from a karst water rivulet.	(Figueras *et al.*, 2011)
Aeromonas salmonicida	Gammaproteobacteria	Fish pathogenic bacterium and the etiological agent of furunculosis. The bacterium possesses a worldwide distribution, with the exception of South America. Potential human pathogen. It can be isolated from both marine and freshwater environments, humans and fish.	(Janda & Abbott, 2010, Dallaire-Dufresne *et al.*, 2014, Menanteau-Ledouble *et al.*, 2016, Rouleau *et al.*, 2018)
Aeromonas sanarellii	Gammaproteobacteria	Bacterium isolated from human samples (i.e. wounds), water, and insect eggs. Its genome encodes several virulence determinants. Considered a pathogenic bacterium of both humans and fish.	(Alperi *et al.*, 2010b, Beaz-Hidalgo *et al.*, 2012)
Aeromonas schubertii	Gammaproteobacteria	Bacterium generally isolated from human, fish and molluscs. Pathogenic bacterium of fish, molluscs and human. Its genome encodes different virulence and antibiotic-resistance genes.	(Janda & Abbott, 2010, Latif-Eugenin *et al.*, 2016, Liu *et al.*, 2016)
Aeromonas sobria	Gammaproteobacteria	Mesophilic aeromonad considered as an opportunistic pathogen of	(Beaz-Hidalgo *et al.*, 2010, Janda &

		freshwater fish, amphibians and reptiles; although increasing evidence supports the existence of mutualistic interactions with fish.	Abbott, 2010, Gauthier *et al.*, 2017)
Aeromonas taiwanensis	Gammaproteobacteria	Bacterium isolated from human samples (i.e. wounds, faeces), water, and insect eggs. Its genome encodes several virulence determinants.	(Beaz-Hidalgo *et al.*, 2012, Wang *et al.*, 2014a)
Aeromonas tecta	Gammaproteobacteria	Bacterium isolated from human and water samples. Potential human pathogen.	(Demarta *et al.*, 2008, Janda & Abbott, 2010)
Aeromonas veronii	Gammaproteobacteria	Bacterium mainly isolated from fresh water, animals and humans samples. Considered an opportunistic human and fish pathogen. In aquaculture animals mainly causes hemorrhagic septicemia. Synonymous to *Aeromonas ichthiosmia.*	(Parras *et al.*, 1993, Janda & Abbott, 2010, Liu *et al.*, 2017, Silva *et al.*, 2017)
Amphritea atlantica	Gammaproteobacteria	Marine bacterium whose main representative was isolated from mussels in a hydrothermal vent field at the Mid-Atlantic Ridge.	(Gartner *et al.*, 2008)
Colwellia psychrerythraea	Gammaproteobacteria	Psychrotolerant marine bacterium whose most representative strain was isolated from Arctic marine sediments.	(Methe *et al.*, 2005)
Colwellia chukchiensis	Gammaproteobacteria	Psychrotolerant marine bacterium whose main representative strains was isolated from seawater samples of the Arctic Ocean.	(Yu *et al.*, 2011)
Ferrimonas futtsuensis	Gammaproteobacteria	Marine bacterium whose main representative was isolated from a marine sediment and it is able to use Fe(III)-oxyhydroxide, Fe(III)-citrate, selenate and selenite as electron acceptors.	(Nakagawa *et al.*, 2006)
Ferrimonas sediminum	Gammaproteobacteria	Marine bacterium whose main representative was isolated from a marine sediment and it is able to use Fe(III)-oxyhydroxide, Fe(III)-citrate, selenate and selenite as electron acceptors.	(Ji *et al.*, 2013)
Marinomonas spartinae	Gammaproteobacteria	Beneficial plant-associated bacterium whose main representative was isolated from the plant *Spartina maritima* in salt marshes in the south Atlantic Spanish coast.	(Lucena *et al.*, 2016)
Marinobacterium tanieri	Gammaproteobacteria	Marine bacterium previously classified as belonging to the *Pseudomonas* genus. One of its	(Satomi *et al.*, 2002, Choi *et al.*, 2012)

		representative stains was shown to exhibit xylanase activity.	
Moritella dasanensis	Gammaproteobacteria	Psychrophilic bacterium whose main representative strain was isolated from the Arctic ocean.	(Kim *et al.*, 2008)
Moritella marina	Gammaproteobacteria	Marine bacterium whose main representative, produces high levels of polyunsaturated fatty acids	(Urakawa *et al.*, 1998, Kautharapu & Jarboe, 2012)
Moritella viscosa	Gammaproteobacteria	Marine fish pathogen responsible for causing winter-ulcer disease.	(Karlsen *et al.*, 2017)
Neptunomonas antarctica	Gammaproteobacteria	Cryophylic marine bacterium whose main representative was isolated from a marine sediment.	(Zhang *et al.*, 2010)
Neptunomonas japonica	Gammaproteobacteria	Symbiont-like marine bacterium isolated from a marine sediment.	(Miyazaki *et al.*, 2008)
Oceanospirillum beijerinckii	Gammaproteobacteria	Marine spirillum often isolated from marine shellfishs.	(Satomi *et al.*, 2002)
Oceanospirillum multiglobuliferum	Gammaproteobacteria	Marine spirillum whose main representative strain was isolated from putrid infusions of a pacific oyster.	(Satomi *et al.*, 2002, Carney *et al.*, 2017)
Photobacterium marinum	Gammaproteobacteria	Marine bacterium whose main representative strain was isolated from sediments samples.	(Srinivas *et al.*, 2013)
Photobacterium proteolyticum	Gammaproteobacteria	Protease-producing marine bacterium. Its main representative strain was isolated from ocean sediments.	(Li *et al.*, 2017b)
Pseudoalteromonas luteoviolacea	Gammaproteobacteria	Marine bacterium commonly isolated as a sponges symbiont and characterized by its ability to produce the violacein (a pigment with strong antibacterial properties) and other bioactive secondary metabolites (i.e. indolmycin).	(Yang *et al.*, 2007, Thogersen *et al.*, 2016)
Tolumonas lignilytica	Gammaproteobacteria	Soil bacterium able to use lignin as sole carbon source.	(Billings *et al.*, 2015)
Vibrio bivalvicida	Gammaproteobacteria	Marine bacterium responsible for causing diseases in bivalve molluscs.	(Dubert *et al.*, 2016)
Vibrio tubiashii	Gammaproteobacteria	Marine bacterium responsible for causing diseases mainly in bivalve molluscs. More recent research showed that causes fish and coral diseases.	(Hada *et al.*, 1984, Austin *et al.*, 2005, Sere *et al.*, 2015)

CHAPTER 2.2: MOLECULAR BASIS OF *P. aeruginosa* PAO1 TAXIS TO HISTAMINE AND POLYAMINES.

Published article

High-Affinity Chemotaxis to Histamine Mediated by the TlpQ Chemoreceptor of the Human Pathogen *Pseudomonas aeruginosa*

Andrés Corral-Lugo[a,*], Miguel A. Matilla[a], **David Martín-Mora**[a], Hortencia Silva Jiménez[a,$], Noel Mesa Torres[a], Junichi Kato[b], Akiko Hida[b], Shota Oku[b], Mayte Conejero-Muriel[c], Jose Antonio Gavira[c#]and Tino Krell[a#]

[a]Dept. of Environmental Protection, Estación Experimental del Zaidín, Consejo Superior de Investigaciones Científicas, Granada, Spain.

[b]Dept, of Molecular Biotechnology, Graduate School of Advanced Sciences of Matter, Hiroshima University, Higashi-Hiroshima, Hiroshima, Japan.

[c]Laboratory of Crystallographic Studies, IACT, (CSIC-UGR), Armilla, Spain.

[*]present address: Institut de Biologie Intégrative de la Cellule (I2BC), CNRS, Gif-Sur-Yvette, France.

[$]present address: Instituto de Investigaciones Oceanológicas, Universidad Autónoma de Baja California, Ensenada, Baja California, México.

MBio (Published online 13 November 2018); 9(6).
Doi: 10.1128/mBio.01894-18

ABSTRACT

Histamine is a key biological signal molecule. It acts as a neurotransmitter in the central and peripheral nervous systems and coordinates local inflammatory responses by modulating the activity of different immune cells. During inflammatory processes, including bacterial infections, neutrophils stimulate the production and release of histamine. Here we report that the opportunistic human pathogen *Pseudomonas aeruginosa* exhibits chemotaxis towards histamine. This chemotactic response is mediated by the concerted action of the TlpQ, PctA and PctC chemoreceptors, which display differing sensitivities to histamine. Low concentrations of histamine were sufficient to activate TlpQ, which binds histamine with an affinity of 639 nM. To explore this binding, we resolved the high-resolution structure of the TlpQ ligand binding domain in complex with histamine. It has an unusually large dCACHE domain and binds histamine through a highly negatively charged pocket at its membrane distal module. Chemotaxis to histamine may play a role in the virulence of *P. aeruginosa* by recruiting cells at the infection site and consequently modulating the expression of quorum sensing-dependent virulence genes. TlpQ is the first bacterial histamine receptor to be described and greatly differs from human histamine receptors—indicating that eukaryotes and bacteria have pursued different strategies for histamine recognition.

AMERICAN SOCIETY FOR MICROBIOLOGY | mBio®

RESEARCH ARTICLE
Molecular Biology and Physiology

High-Affinity Chemotaxis to Histamine Mediated by the TlpQ Chemoreceptor of the Human Pathogen *Pseudomonas aeruginosa*

Andrés Corral-Lugo,[a]* Miguel A. Matilla,[a] David Martín-Mora,[a] Hortencia Silva Jiménez,[a]* Noel Mesa Torres,[a] Junichi Kato,[b] Akiko Hida,[b] Shota Oku,[b] Mayte Conejero-Muriel,[c] Jose A. Gavira,[c] Tino Krell[a]

[a]Department of Environmental Protection, Estación Experimental del Zaidín, Consejo Superior de Investigaciones Científicas, Granada, Spain
[b]Department of Molecular Biotechnology, Graduate School of Advanced Sciences of Matter, Hiroshima University, Higashi-Hiroshima, Hiroshima, Japan
[c]Laboratory of Crystallographic Studies, IACT, (CSIC-UGR), Armilla, Spain

ABSTRACT Histamine is a key biological signaling molecule. It acts as a neurotransmitter in the central and peripheral nervous systems and coordinates local inflammatory responses by modulating the activity of different immune cells. During inflammatory processes, including bacterial infections, neutrophils stimulate the production and release of histamine. Here, we report that the opportunistic human pathogen *Pseudomonas aeruginosa* exhibits chemotaxis toward histamine. This chemotactic response is mediated by the concerted action of the TlpQ, PctA, and PctC chemoreceptors, which display differing sensitivities to histamine. Low concentrations of histamine were sufficient to activate TlpQ, which binds histamine with an affinity of 639 nM. To explore this binding, we resolved the high-resolution structure of the TlpQ ligand binding domain in complex with histamine. It has an unusually large dCACHE domain and binds histamine through a highly negatively charged pocket at its membrane distal module. Chemotaxis to histamine may play a role in the virulence of *P. aeruginosa* by recruiting cells at the infection site and consequently modulating the expression of quorum-sensing-dependent virulence genes. TlpQ is the first bacterial histamine receptor to be described and greatly differs from human histamine receptors, indicating that eukaryotes and bacteria have pursued different strategies for histamine recognition.

IMPORTANCE Genome analyses indicate that many bacteria possess an elevated number of chemoreceptors, suggesting that these species are able to perform chemotaxis to a wide variety of compounds. The scientific community is now only beginning to explore this diversity and to elucidate the corresponding physiological relevance. The discovery of histamine chemotaxis in the human pathogen *Pseudomonas aeruginosa* provides insight into tactic movements that occur within the host. Since histamine is released in response to bacterial pathogens, histamine chemotaxis may permit bacterial migration and accumulation at infection sites, potentially modulating, in turn, quorum-sensing-mediated processes and the expression of virulence genes. As a consequence, the modulation of histamine chemotaxis by signal analogues may result in alterations of the bacterial virulence. As the first report of bacterial histamine chemotaxis, this study lays the foundation for the exploration of the physiological relevance of histamine chemotaxis and its role in pathogenicity.

KEYWORDS *Pseudomonas aeruginosa*, chemotaxis, histamine

Received 30 August 2018 **Accepted** 12 October 2018 **Published** 13 November 2018

Citation Corral-Lugo A, Matilla MA, Martín-Mora D, Silva Jiménez H, Mesa Torres N, Kato J, Hida A, Oku S, Conejero-Muriel M, Gavira JA, Krell T. 2018. High-affinity chemotaxis to histamine mediated by the TlpQ chemoreceptor of the human pathogen *Pseudomonas aeruginosa*. mBio 9:e01894-18. https://doi.org/10.1128/mBio.01894-18.

Invited Editor Gerald L. Hazelbauer, University of Missouri-Columbia

Editor Tarek Msadek, Institut Pasteur

Address correspondence to Jose A. Gavira, jgavira@iact.ugr-csic.es, or Tino Krell, tino.krell@eez.csic.es.

* Present address: Andrés Corral-Lugo, Institut de Biologie Intégrative de la Cellule (I2BC), CNRS, Gif-Sur-Yvette, France; Hortencia Silva Jiménez, Instituto de Investigaciones Oceanológicas, Universidad Autónoma de Baja California, Ensenada, Baja California, México.

INTRODUCTION

Bacteria possess different types of signal transduction systems that allow them to adapt to changes in environmental cues. In addition to one-and two-component signal transduction systems, chemosensory pathways play an important role in this process (Galperin, 2005, Laub & Goulian, 2007, Hazelbauer *et al.*, 2008). In a canonical chemosensory pathway, signaling is initiated by the binding of signal molecules to the chemoreceptor LBD, which in turn modulates the autophosphorylation activity of the CheA histidine kinase and the transphosphorylation of the CheY response regulator, which ultimately triggers pathway output (Hazelbauer *et al.*, 2008). While most chemoreceptors mediate chemotaxis, some also carry out alternative cellular functions, such as modulating c-di-GMP levels or type IV pili-based motility (Whitchurch *et al.*, 2004, Hickman *et al.*, 2005, Wuichet & Zhulin, 2010).

E. coli is the traditional model organism for the study of chemoreceptor-based signaling processes (Parkinson *et al.*, 2015). It has 5 chemoreceptors, of which 4 contain a periplasmic 4-helix bundle LBD. Importantly, these chemoreceptors bind signals either directly or in complex with a periplasmic ligand binding protein. *E. coli* has a single chemosensory cascade that mediates chemotaxis primarily towards sugars, amino acids or dipeptides (Parkinson *et al.*, 2015, Matilla & Krell, 2017).

More recently, chemoreceptor-based signaling has been studied in an array of bacteria with different lifestyles (Bardy *et al.*, 2017). Existing data suggests that the typical number of chemoreceptor genes in bacteria, which can reach as high as 80, is much higher than in *E. coli* (Alexandre *et al.*, 2004). Furthermore, sequence analyses indicate that chemoreceptors comprise more than eighty different LBD types (Ortega *et al.*, 2017a). The most abundant of these are CACHE type LBDs, which are present in either the mono-modular (sCACHE) or bimodular (dCACHE) form (Upadhyay *et al.*, 2016). The large number of chemoreceptor genes and the diversity of LBD types suggest that bacteria can respond to a wide variety of signal molecules. The scientific community is now beginning to explore this diversity and to elucidate the corresponding physiological relevance.

Pseudomonads are important model organisms for the study of chemoreceptor function (Kato *et al.*, 2008, Sampedro *et al.*, 2015), and the strains *P. putida* KT2440 and *P. aeruginosa* PAO1 have been well studied and characterized (Ortega *et al.*, 2017a). The former strain is a non-pathogenic soil bacterium with a saprophytic lifestyle (Belda *et al.*, 2016). In contrast, *P. aeruginosa* strains are amongst the most virulent opportunistic human pathogens and the leading cause of nosocomial infections, particularly in immunocompromised, cancer, burn and cystic fibrosis patients (Juhas, 2015).

Strains KT2440 and PAO1 have a similar number of chemoreceptor genes: 27 and 26, respectively. The function and the corresponding ligand profiles have been established for approximately ten receptors in each strain (Ortega *et al.*, 2017a, Ortega *et al.*, 2017b). Amongst the functionally annotated KT2440 chemotaxis receptors are several for different organic acids (Garcia *et al.*, 2015), purines (Fernandez *et al.*, 2016), proteinogenic amino acids (Corral-Lugo *et al.*, 2016) and GABA (Reyes-Darias *et al.*, 2015b). In addition, the McpU chemoreceptor of this strain was the first chemoreceptor identified that responded to the polyamines putrescine, spermidine and cadaverine (Corral-Lugo *et al.*, 2016, Gavira *et al.*, 2018). In contrast, PAO1 chemotaxis to proteinogenic amino acids and GABA is mediated by three paralogous receptors, namely PctA, PctB and PctC (Taguchi *et al.*, 1997, Rico-Jimenez *et al.*, 2013a). Additionally, this strain has two receptors for inorganic phosphate (Wu *et al.*, 2000, Rico-Jimenez *et al.*, 2016) as well as receptors for malate (Alvarez-Ortega & Harwood, 2007, Martin-Mora *et al.*, 2018), α-ketoglutarate (Martin-Mora *et al.*, 2016a) and chloroethylenes (Kim *et al.*, 2006). *P. aeruginosa* is also attracted to the plant hormone ethylene and it was shown that the deletion of the gene encoding the TlpQ chemoreceptor abolished ethylene chemotaxis (Kim *et al.*, 2007).

In this study, we provide the first report of bacterial chemotaxis towards histamine. This compound is produced by different animal tissues and is secreted by some bacteria (Barcik *et al.*, 2017). Histamine is a signal molecule with multiple functions. It is an aminergic neurotransmitter of the central and peripheral nervous system, and it is involved in numerous biological processes (De Benedetto *et al.*, 2015). It is also a key modulator of local immune responses by mediating effects on many cell types such as antigen-presenting cells, natural killer cells, epithelial cells as well as T and B lymphocytes (O'Mahony *et al.*, 2011).

Bacteria have been shown to impact histamine function. For example, bacterial respiratory tract infections stimulate neutrophils to release histamine (Xu *et al.*, 2006, Xu *et al.*, 2012). Also, it was shown that infection by PAO1 greatly increased neutrophil histamine content and secretion, but did not alter histamine production in mast cells, which are the classical histamine reservoirs (Xu *et al.*, 2012). Furthermore, it has been shown that histamine might play divergent roles in the immune response: it has been implicated in mediating defense against infection (Metz *et al.*, 2011), as well as increasing susceptibility to infection (Beghdadi *et al.*, 2008). While there has been preliminary evidence that histamine is a signal molecule for bacteria, the underlying mechanisms remain largely unknown (Kyriakidis *et al.*, 2012). The present study provides important insight into molecular mechanisms that permit bacteria to sense and respond to histamine.

METHODOLOGY

Bacterial strains and plasmids: Bacterial strains and plasmids used are listed in Table 12 and oligonucleotides in Supp. Table 13.

Construction of bacterial mutant strains and plasmids: The *pctA* and *tlpQ* genes were deleted in different mutant strains by unmarked gene deletion. Plasmids pK18*mobsacB-pctA* and pK18*mobsacB-tlpQ* were generated by amplifying 0.6 to 1.2-kb regions up- and downstream of the target gene. PCR products were digested with restriction enzymes listed in Supp. Table 13 and cloned into pK18*mobsacB*. The resulting plasmids were introduced into *E. coli* S17-1 *λpir* by electroporation. Plasmids were transferred to PAO1 by conjugation and cells were selected in Simmons citrate (BBL™, Becton Dickinson) agar plates supplemented with kanamycin. For plasmid excision, LB medium was inoculated with a kanamycin resistant colony and grown for 12 h, then spread on LB plates containing 20% (w/v) sucrose. To construct the triple deletion mutant in *pctA, pctC* and *tlpQ* in *P. aeruginosa* PA14, pK18*mobsacB-pctA* and pK18*mobsacB-tlpQ* were consecutively conjugated intoPA14 to generate the double mutant. Subsequently, plasmid pK18*mobsacB-pctC,* generated by amplifying regions up- and downstream of *pctC*, was conjugated into PA14 Δ*pctA* Δ*tlpQ.* Kanamycin resistant colonies were grown on LB-agar plates supplemented with 20% (w/v) sucrose for selection. For complementation purposes, the *pctC* gene was amplified by PCR and cloned into plasmid pUCP18 using restriction enzymes listed in Supp. Table 13. The ligation mixture was electroporated into *E. coli* JM109, and transformants were selected on carbenicillin containing LB plates. The resulting plasmid pPctC was transferred to PCTC1 and PCT2Q by electroporation.

Construction of the TlpQ-LBD expression plasmid: The DNA fragment encoding the LBD of TlpQ was amplified, digested with NdeI and BamHI and cloned into pET28b(+) linearized with the same enzymes.

Overexpression and purification of proteins: PctA-LBD and PctC-LBD were overexpressed and purified as described in (Rico-Jimenez *et al.*, 2013a). McpU-LBD and TlpQ-LBD were generated as reported in (Corral-Lugo *et al.*, 2016).

Thermal Shift Assay: Experiments were conducted as reported in (Fernandez *et al.*, 2018). McpU-LBD in polybuffer (5 mM Tris, 5 mM PIPES, 5 mM MES, 10% glycerol (v/v), 150 mM NaCl, pH 7.0) was used at a final concentration of 10 μM. Biolog (Hayward, CA, USA) compound arrays PM3B (nitrogen sources), PM4A (phosphorous and sulfur sources) and PM5 (nutrient supplements) were

used for screening. The composition of these arrays is provided in http://208.106.130.253/pdf/pm_lit/PM1-PM10.pdf.

Isothermal titration calorimetry: Titrations were carried out in a VP microcalorimeter (MicroCal, Northampton, MA, USA) at 25 °C. Proteins dialyzed into polybuffer were titrated with ligands in dialysis buffer. Typically, 15-30 µM of protein was titrated with 0.25 to 1 mM ligand solutions. For ethylene binding studies, TlpQ-LBD was titrated with 12 µl aliquots of a saturated ethylene solution in polybuffer, prepared as reported in (Kim *et al.*, 2007). The mean enthalpies from the injection of ligands into the buffer were subtracted from titration data prior to data fitting using the "One binding site model" of ORIGIN.

Table 12. Bacterial strains and plasmids used in this study.

Strains and plasmids	Characteristics	Reference
Strains		
E. coli BL21(DE3)	F– *ompI hsdS*$_B$(r^-_B m^-_B) *gal dam met*	(Jeong *et al.*, 2009)
DH5α	*supE44 lacU169*(*Ø80lacZΔ M15*) *hsdR17* (r$_K^-$m$_K^-$) *recA1 endA1 gyrA96 thi-1relA1*	(Woodcock *et al.*, 1989)
HB101	F$^-$Δ*(gpt-proA)62 leuB6 supE44 ara-14 galK2 lacY1* Δ*(mcrC-mrr) rpsL20* (Sm^r) *xyl-5 mtl-1 recA13 thi-1*	(Boyer & Roulland-Dussoix, 1969)
JM109	F′ *traD*36 *proA*$^+$B$^+$ *lacI*^{q}*Δ(lacZ)*M15/ *Δ(lac-proAB) glnV44* e14$^-$ gyrA96 recA1 relA1 endA1 thi hsdR17*]*	(Zylstra *et al.*, 1989)
S17-1 λ*pir*	Tp^R Sm^R(recA thi pro hsdR*)-M+RP4*: 2-Tc:Mu: Km Tn7 λ*pir*.	(Phornphisutthimas *et al.*, 2007)
R. pseudosolanacearum Ps29	Wildtype strain race 1, biovar 3, phylotype I	(Hida *et al.*, 2015)
P. putida KT2440	Wildtype	(Belda *et al.*, 2016)
KT2440R	Rifampicin-resistant derivative of KT2440	(Espinosa-Urgel & Ramos, 2004)
KT2440R-McpU	KT2440R transposon mutant *pp1228*::mini-tn*5*-Km;Rif^R, Km^R	(Duque *et al.*, 2007)
P. aeruginosa PAO1	Wildtype strain	(Holloway *et al.*, 1979)
PAO1 Δ*pctA*	PAO1 derivative, *pctA* gene deletion mutant	This study
PCTB1	PAO1 derivative,*pctB*::Km; Km^R	(Taguchi *et al.*, 1997)
PCTC1	PAO1 derivative,*pctC*::Km; Km^R	(Taguchi *et al.*, 1997)
PAO1 Δ*tlpQ*	PAO1 derivative, *pa2654* gene deletionmutant	This study
PCT2	PAO1 derivative; Δ*pctB-pctA-pa4308-pctC*::km; Km^{R1}	(Taguchi *et al.*, 1997)
PCTAQ	PAO1 derivative; Δ*pctA*, Δ*tlpQ*	This study
PCT2Q	PAO1 derivative;Δ*pctB-pctA-pa4308-pctC*::Km, Δ*tlpQ*; Km^R	This study
PCT2QP	PAO1 derivative;Δ*pctB-pctA-pa4308-pctC*::Km,Δ*tlpQ*,Δ*tlpP*; Km^R	J. Kato lab.
PCT2QART	PAO1 derivative;Δ*pctB-pctA-pa4308-pctC*,Δ*tlpQ*,Δ*tlpA* (*pa1646*), Δ*tlpR* (*pa2652*),Δ*tlpT*(*pa1930*); Km^R	J. Kato lab.
P. aeruginosa PA14	Wildtype strain. Human clinical isolate that elicits disease in plants, nematodes, insects and mice	(Rahme *et al.*, 1995)
PA14-ACQ	PA14 derivative;Δ*pctA*, Δ*pctC*, Δ*tlpQ,* Δ*pa4308*	This study

P. aeruginosa isolate 227	Isolated clinical strain from patients with urinary tract infections	(Oura *et al.*, 2015)
P. aeruginosa isolate 233	Isolated clinical strain from patients with urinary tract infections	(Oura *et al.*, 2015)
P. aeruginosa isolate 287	Isolated clinical strain from patients with urinary tract infections	(Oura *et al.*, 2015)
P. aeruginosa isolate 401	Isolated clinical strain from patients with urinary tract infections	(Oura *et al.*, 2015)
P. aeruginosa isolate 428	Isolated clinical strain from patients with urinary tract infections	(Oura *et al.*, 2015)
Plasmids		
pUCP18	*Escherichia-Pseudomonas* shuttle vector; Ap^R	(Schweizer, 1991)
pPctA	pUCP18 with a PCR fragment containing *pctA;* Ap^R	(Shitashiro *et al.*, 2005)
pPctB	pUCP18 with a PCR fragment containing *pctB;* Ap^R	(Shitashiro *et al.*, 2005)
pPctC	pUCP18 with a PCR fragment containing *pctC;*Ap^R	This study
pTlpQ	pUCP18 with a PCR fragment containing *tlpQ;* Ap^R	(27)
pK18*mobsacB*	plasmid for allelic exchange; pK18 *ori*$V_{E.c}$*lacZα mob sacB*; Km^R	(Schafer *et al.*, 1994)
pK18*mobsacB-pctA*	pK18*mobsacB* containing a deletion of the *pctA* gene; Km^R	This study
pK18*mobsacB-tlpQ*	pK18*mobsacB* containing a deletion of the *tlpQ* gene; Km^R	This study
pK18*mobsacB-pctABC*	pK18*mobsacB* containing a deletion of *pctB, pctA*, *pa4308*, *pctC*; Km^R	This study
pK18*mobsacB-pctC*	pK18*mobsacB* containing a deletion of *pctC* and *pa4308*; Km^R	This study
pET28b(+)	Protein expression plasmid; Km^R	Novagen
pET28b-McpU	pET28b derivative used to produce His-tagged McpU-LBD; Km^R	(Corral-Lugo *et al.*, 2016)
pET28b-TlpQ	pET28bderivative used to produce His-tagged TlpQ-LBD; Km^R	This study

[a]Ap, ampicillin; Km, kanamycin; Rif, rifampicin

[b]The *pa4308* gene (orf-1), which forms part of the *pctABC* operon, encodes a hypothetical protein that is not involved in chemotaxis (Taguchi *et al.*, 1997)

Chemotaxis assays: Soft agar plate assays:Strains were grown overnight in M9 minimal medium containing 0.1% glucose (w/v) and then diluted to an OD_{660} of 1 with fresh medium, washed twice with M9 medium and the pellet was resuspended in 1 ml M9 medium. 10 µl aliquots of 5 mM chemoattractant solutions were placed onto plates containing M9 medium, 2.5 mM glucose and 0.25% (w/v) agar. Two-microliter aliquots of bacterial suspensions were placed horizontally to each of the chemoattractant spots. Plates were incubated at 30°C for 16–20 h. Quantitative capillary chemotaxis assays: Two protocols were used that differed in the way cells were counted. The first protocol was used to generate data of Supp. Fig. 36, whereas the second protocol was used for the remaining chemotaxis experiments. In the *first protocol*, overnight cultures of strains were diluted to an OD_{660} of 0.05 in MS medium (Abril *et al.*, 1989) supplemented with 6 mg l^{-1} Fe-citrate, trace elements and 15 mM glucose and grown at 37 °C. At an OD_{660} of 0.4, cultures were centrifuged at 1,700 x *g* for 5 min and the pellet was washed twice with chemotaxis buffer (50 mM potassium

phosphate, 20 mM EDTA, 0.05 % (v/v) glycerol, pH 7.0). Cells were resuspended in this buffer, adjusted to an OD_{660} of 0.1 and 230 µl aliquots were placed into 96-well plates. Capillary tubes (Microcaps, Drummond Scientific, Ref. P1424) were heat-sealed at one end and filled with chemotaxis buffer or chemotaxis chemoattractant solution. The capillaries were then immersed into bacterial suspensions at their open ends. After 30 min at room temperature, capillaries were removed, rinsed with sterile water and the content expelled into 1 ml of M9 medium. Serial dilutions were plated onto LB medium and CFUs were determined. In all cases, data were corrected to the number of cells that swam into the buffer-containing capillaries. In the *second protocol* we used computer-assisted image analysis as reported previously (Nikata *et al.*, 1992). Briefly, capillaries were filled with chemoattractant solutions in 10 mM HEPES buffer, pH 7.0, containing 1% (w/v) agarose and heat sealed on one side. Cells were grown in 2xYT medium and 10 µl aliquots of the cell suspension were placed onto a microscope slide within the U-shaped spacer, which was then covered by a coverslip. The chemoattractant-filled capillaries were introduced into the chemotaxis chamber and cell movement was videotaped with images taken at the beginning and at different time intervals. If not otherwise stated, the contact time between cell and the chemoattractant was 2 minutes. The Bioinformatics Assistant Icy Sport detector software (de Chaumont *et al.*, 2012) was used to determine the number of cells per image. The magnitude of chemotaxis was expressed as the number of cells after a given time over the number of cells at the beginning of the experiment. Data shown are the means and standard deviation from three experiments conducted in triplicate.

Growth experiments: PAO1 was grown overnight in MS minimal medium (Martin-Mora *et al.*, 2016a) containing 20 mM D-glucose. Cultures were diluted to an OD_{600} of 0.02 into MS medium supplemented with 5 mM of a carbon or nitrogen source. The assays were performed in 100-well polystyrene plates and incubated at 30 °C (KT2440) or 37 °C (PAO1) in a Bioscreen Microbiological Growth Analyzer. Data represent means and standard deviations from three biological replicates conducted in triplicate.

Assessment of motility: To assess bacterial motility, PAO1 and KT2440 were used to inoculate LB and 2xYT medium to an OD_{600} of 0.01. Growth was carried out at 37°C (PAO1) or 30°C (KT2440) and bacteria were inspected microscopically. According to their motility, they were given different scores: score 1 = 25% of bacteria are motile;2 = 50%;3 = 75%; and 4 = 100%.

Crystallization and structure resolution: Crystallisation trials were carried out with TlpQ-LBD in the absence and presence of histamine. TlpQ-LBD in polybuffer was incubated with a two-fold molar excess of histamine on ice for 30 min. Unbound ligand was removed by buffer exchange using 10 kDa cut-off filters (Amicon) and polybuffer. The apo- (6 mg/ml) and ligand-bound protein (26 mg/ml) were loaded into 0.3 mm diameter capillaries for counter-diffusion crystallization using screen kits from Triana S & T (Granada, Spain). Only the LBD-TlpQ/histamine complex produced crystals in 1.5 M ammonium phosphate and 0.1 M sodium citrate pH 5.6. The same protocol was used to crystallize the Se-Met TlpQ-LBD. The capillaries were emptied into mother solution containing 10 to 25% (v/v) glycerol as cryo-protectant. Crystals were diffracted at the European Synchrotron Radiation Facility and the Spanish Synchrotron ALBA. Data were indexed and integrated with XDS (Kabsch, 2010) and scaled with SCALA (Evans, 2006). All attempts to obtain a molecular replacement solution failed. Phases were obtained from the Se-Methionine derivative by combining SAD data, at the selenium peak, with an initial model generated by Phyre2 (Kelley & Sternberg, 2009), as input files for Auto-Rickshaw (Panjikar *et al.*, 2005). All 26 expected heavy atoms positions were identified by SHELXD (Schneider & Sheldrick, 2002) using the data to 3.5 Å. The model generated was refined with phenix.refine (Afonine *et al.*, 2010). Further refinement was performed against the best data set (2.45 Å) with phenix.refine (Afonine *et al.*, 2010) using Coot (Emsley *et al.*, 2010). Model quality was checked using MolProbity (Chen *et al.*, 2010). Refinement statistics and quality indicators of the final model are summarized in Supp. Table 14. The structure was deposited at the protein databank with ID 6fu4.

RESULTS

Identification of histamine and additional polyamines as novel ligands for the *P. putida* KT2440 McpU chemoreceptor

By screening 190 compounds for binding to the purified McpU-LBD, we previously found that McpU binds to and mediates chemotaxis to putrescine, cadaverine and spermidine (Corral-Lugo *et al.*, 2016). In the present study we extended this screening to include 285 additional compounds. These compounds were mostly bacterial nitrogen, phosphorous and sulfur sources (see Materials and Methods). We used a thermal shift assay to monitor changes in the midpoint of protein unfolding (Tm) caused by ligand binding (Krell, 2015). In the absence of ligand, McpU-LBD had a Tm of 46.5°C. Of 95 nitrogen sources screened (Biolog plate PM3B), three additional compounds (agmatine, ethylenediamine and histamine) caused Tm increases greater than 2 °C (Fig. 44).

Using isothermal titration calorimetry (ITC), we found that all three compounds bind to McpU-LBD (Supp. Fig. 31A). Very tight binding was observed for agmatine with a K_D in the

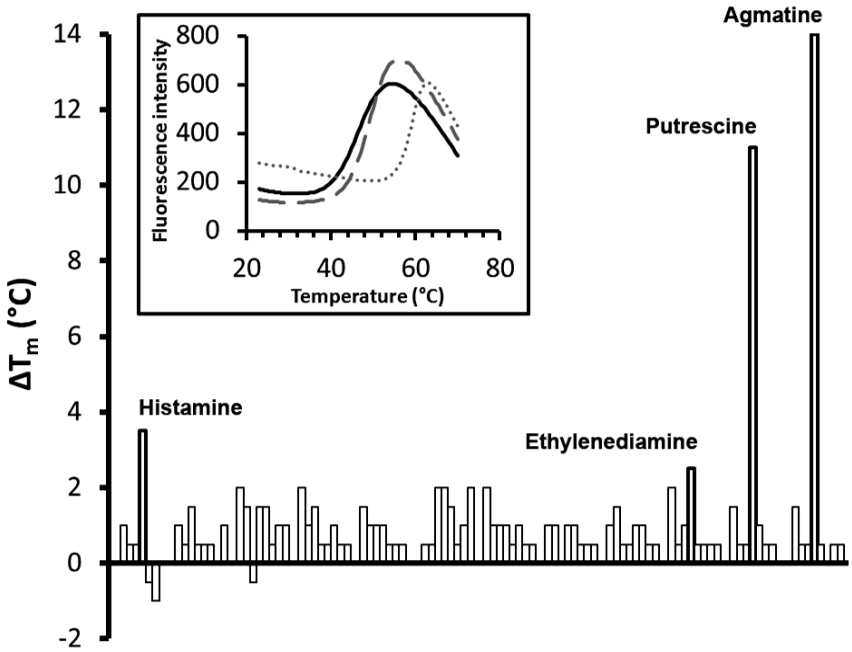

Figure 44. Thermal shift assays of *P. putida* KT2440 McpU-LBD against a library of ligands. Shown are the individual Tm changes caused by 95 compounds (Biolog array PM3B) that can serve as nitrogen sources. The insert shows the unfolding curves of McpU-LBD when free from ligand (continuous line) andin the presence of agmatine (dotted line) and histamine (dashed line).

Table 13. Thermodynamic parameters for the binding of ligands to McpU-LBD and TlpQ-LBD as derived from ITC experiments.

Compound	McpU-LBD		TlpQ-LBD		$K_{D\ McpU-LBD}/K_{D\ TlpQ-LBD}$
	K_D(μM)	Δ*H* (kcal mol^{-1})	K_D(nM)	Δ*H* (kcal mol^{-1})	
Putrescine	2 ± 0.1[b]	-15 ± 0.5	134 ± 12	-6.8 ± 0.3	15
Cadaverine	22 ± 2[b]	-15.5 ± 0.5	150 ± 4	-6.0 ± 0.1	147
Spermidine	4.5 ± 0.4[b]	-4.3 ± 0.3	56 ± 4	-4.6± 0.4	80
Agmatine	0.48 ± 0.02	-14.5 ± 0.2	150 ± 9	-5.4 ± 0.1	3
Ethylenediamine	39 ± 4	-9.7 ± 0.5	1710 ± 180	-6.3 ± 0.6	23
Histamine	26 ± 2	-2.6 ± 0.3	639 ± 27	-9.1 ± 0.3	41

[a] Means and standard deviations represent data from three independent experiments.
[b] Reported previously in reference (Corral-Lugo *et al.*, 2016).

nanomolar range, whereas histamine and ethylenediamine bound with much lower affinities (Table 13). It should be noted that of these three new McpU ligands and the previously identified ligands (i.e., putrescine, cadaverine and spermidine), all except for histamine are polyamines (Supp. Fig. 31B).

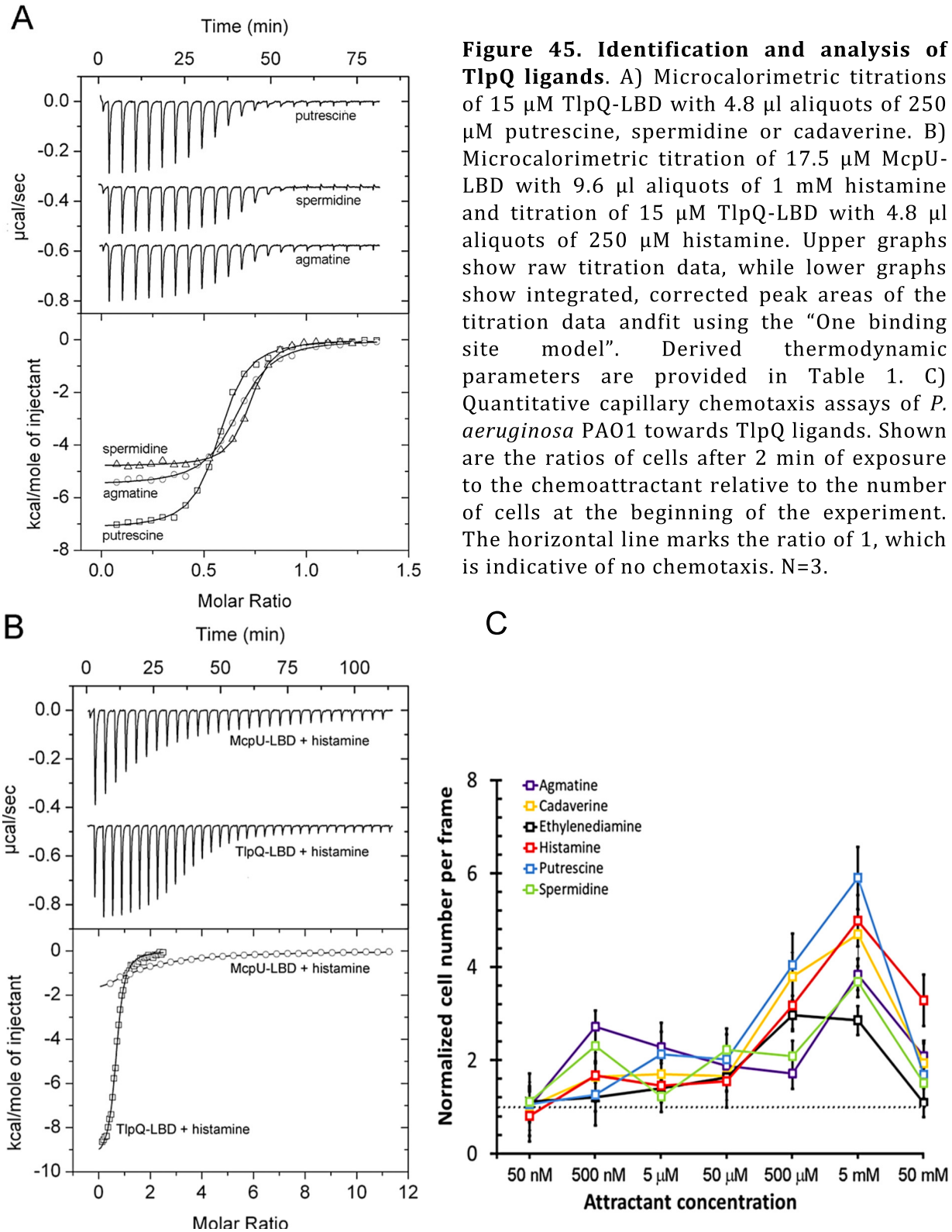

Figure 45. Identification and analysis of TlpQ ligands. A) Microcalorimetric titrations of 15 µM TlpQ-LBD with 4.8 µl aliquots of 250 µM putrescine, spermidine or cadaverine. B) Microcalorimetric titration of 17.5 µM McpU-LBD with 9.6 µl aliquots of 1 mM histamine and titration of 15 µM TlpQ-LBD with 4.8 µl aliquots of 250 µM histamine. Upper graphs show raw titration data, while lower graphs show integrated, corrected peak areas of the titration data andfit using the "One binding site model". Derived thermodynamic parameters are provided in Table 1. C) Quantitative capillary chemotaxis assays of *P. aeruginosa* PAO1 towards TlpQ ligands. Shown are the ratios of cells after 2 min of exposure to the chemoattractant relative to the number of cells at the beginning of the experiment. The horizontal line marks the ratio of 1, which is indicative of no chemotaxis. N=3.

Identification of TlpQ as a histamine receptor in *Pseudomonas aeruginosa*

Because histamine plays an important role in the immune response, we aimed at identifying McpU homologues in *P. aeruginosa* that may also sense and mediate chemotaxis to histamine. To this end, we carried out a sequence clustering analysis of all dCACHE containing chemoreceptors in PAO1 and KT2440 (Supp. Fig. 32A). This analysis revealed that the LBD of the TlpQ receptor shares 62% sequence identity with the McpU-LBD homologue (Supp. Fig. 32B). To verify TlpQ function, we purified TlpQ-Ledford ITC binding studies. Results showed that five McpU-LBD ligands bind to TlpQ-LBD with nanomolar affinities, whereas binding of ethylenediamine was slightly weaker (Fig. 45A, Table 13). Spermidine had a K_D of 56 nM, which is the highest ligand affinity ever observed for a chemoreceptor. Histamine had a K_D of 639 nM, which is an affinity 41 times higher than its affinity for McpU-LBD (Table 13, Fig. 45B).

Thus, the affinities of the ligands to TlpQ-LBD were 3 to 147 times higher than their affinities to the McpU-LBD (Table 13). Previous studies showed that TlpQ mediates chemotaxis to ethylene (Kim *et al.*, 2007), but the titration of TlpQ-LBD with a saturated ethylene solution did not show any binding (data not shown).

Characterization of histamine chemotaxis

KT2440 and PAO1 both contain a chemoreceptor that binds histamine. In initial experiments, we identified the optimal culture conditions for motility of both strains (Supp. Fig. 33). Using these conditions, we carried out capillary chemotaxis assays of PAO1 towards the six TlpQ ligands (Fig. 45C). All ligands caused chemotaxis, with significant responses observed for some ligands at concentrations as low as 500 nM, whereas optimal responses occurred at 5 mM. In subsequent experiments we compared the histamine dose response for KT2440 with that of PAO1 (Fig.46A). KT2440 showed only moderate chemotaxis over the entire concentration range tested, whereas PAO1 responses were much stronger. In accordance with the different binding affinities observed by ITC, the response onset between strains also differed. Thus, PAO1 required 500 nM histamine, while KT2440 required 5 µM.

To assess the metabolic value of these ligands, we conducted growth experiments with PAO1 and KT2440 in minimal medium containing each of the ligands as the sole carbon or nitrogen source. We found that most of the ligands supported growth either as carbon or nitrogen source (Supp. Fig. 34). Exceptions were spermidine and ethylenediamine that were either no or poor growth substrates for PAO1 and KT2440 (Supp. Fig. 34). Histamine permitted growth of both strains as sole C- and N-source.

Additional experiments were conducted to assess histamine chemotaxis in other bacteria. First, we assessed the motility of *P. aeruginosa* strains 227, 233, 287, 401 and 428, which have been isolated from patients with urinary tract infections (Oura *et al.*, 2015). Strains 233 and 401 exhibited motilities comparable to that of PAO1 and were therefore selected for further studies. *P. aeruginosa* PA14 as well as the plant pathogen *R. pseudosolanacearum* Ps29 were also included in these experiments. We found that all analyzed *P. aeruginosa* strains showed significant chemotaxis to 5 mM histamine and their chemotactic phenotype was significantly higher than that of KT2440. On the other hand, thestrainPs29 was not attracted to histamine (Fig. 46B). Growth experiments with Ps29 in minimal media containing histamine as sole carbon and nitrogen source revealed no significant growth (Supp. Fig. 34B), suggesting a link between chemotaxis and the capacity to use histamine for growth.

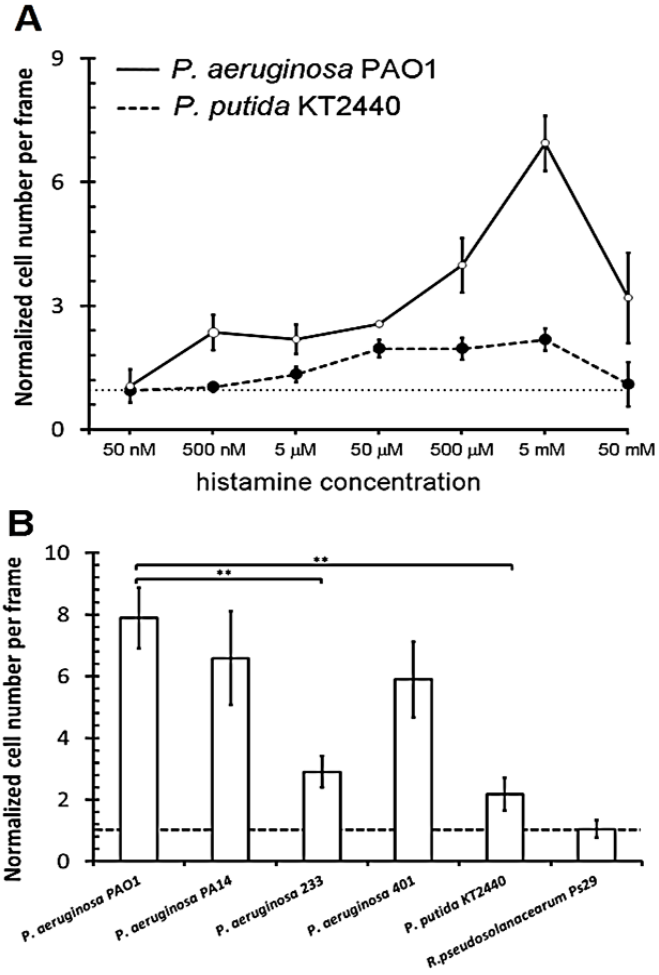

Figure 46. Histamine chemotaxis in different bacteria. A) Quantitative capillary chemotaxis assays of *P. aeruginosa* PAO1 and *P. putida* KT2440 to different histamine concentrations. B) Response of different strains to 5 mM histamine. N=3. **P<0.01 (by Student's t test).

The three-dimensional structure of TlpQ-LBD in complex with histamine

To determine the molecular determinants for histamine recognition by TlpQ, we solved the high-resolution structure of TlpQ-LBD in complex with histamine. There are four monomers in the asymmetric unit and the superimposition of their C_α atoms resulted in r.m.s.d. values of 0.4 to 0.8 Å, indicative of high similarity. Inspection of the structure reveals that it is a dCACHE domain (Upadhyay *et al.*, 2016) (Fig. 47). A long N-terminal helix is followed by two globular α/β modules, termed membrane-proximal and membrane-distal modules. The membrane-distal module contained bound histamine in all four monomers of the asymmetric unit (Fig. 47).

Structural alignments of TlpQ-LBD with entries in the protein data bank identified structural homologues (Supp. Table 12). Most of the homologues are categorized as dCACHE_1 Pfam domains (Upadhyay *et al.*, 2016). This domain is found in histidine kinases, chemoreceptors as well as in a novel cytosolic receptor protein (pdb ID 5ere), and are found in different bacteria as well as in *Arabidopsis*. The average size of the domains, while taking into account the segment in between both transmembrane regions, is 268 ± 17 amino acids (Supp. Table 12). Of all the homologous domains that we identified, TlpQ-LBD was the largest at 334 amino acids, namely due to particularly long inserts between β-strands 1 and 2, extended helices α1 and α2, and an extended loop between helices η3 and α3 (Supp. Fig. 35).

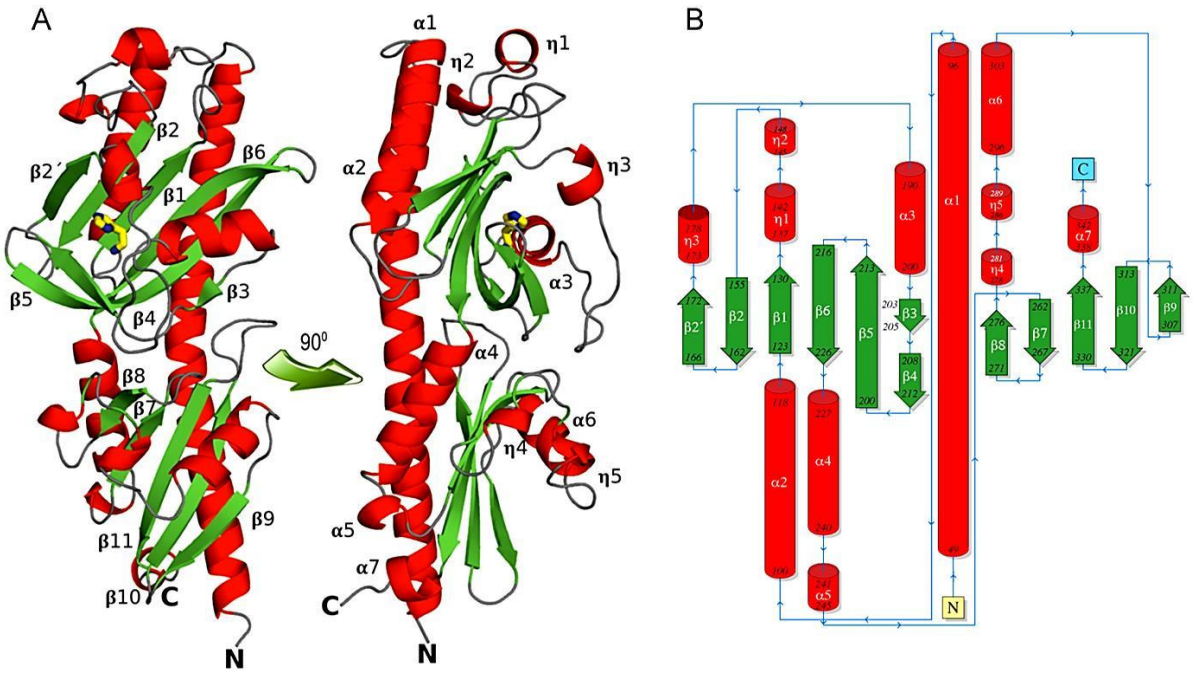

Figure 47. Structure of the TlpQ chemoreceptor ligand binding domain in complex with histamine. A) Ribbon diagram with annotated secondary structure elements. Bound histamine is shown as a stick structure. B) Schematic representation of the secondary structure elements.

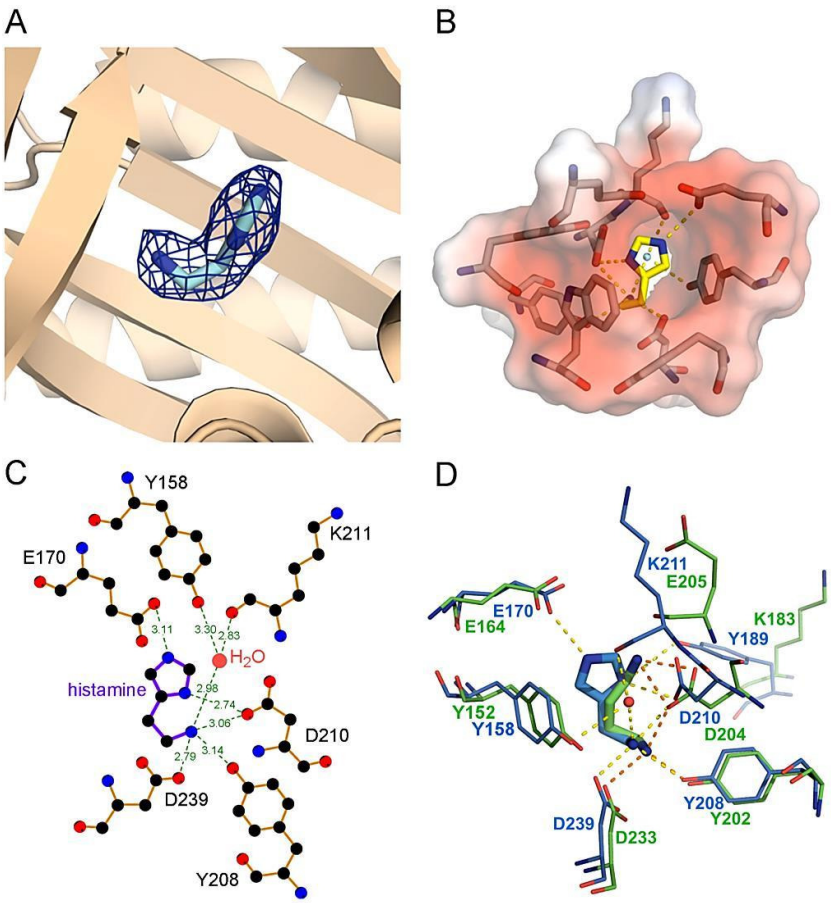

Figure 48. The ligand binding pocket of the TlpQ ligand binding domain. A) Close-up view of the ligand binding pocket. The electron density for histamine is shown. B) Surface charge representation of the histamine binding site, red and blue shading represents negative and positive charge, respectively. C) Schematic representation of amino acids involved in hydrogen bonds with histamine. D) Superimposition of the ligand binding pockets of McpU-LBD with bound putrescine (green, pdb ID: 6F9G) and TlpQ-LBD with bound histamine (blue).

Well-defined electron density for histamine was observed in all four monomers, enabling the ligand placement to be determined (Fig. 48A). TlpQ ligands are present as protonated polycations at neutral pH, which explains why the ligand binding pocket is highly negatively charged (Fig. 48B). All three histamine nitrogen atoms establish hydrogen bonds (Fig. 48C). TlpQ ligands contain at least one primary amino group and the primary amino group of histamine plays a central role in binding because it forms hydrogen bonds with the side chains of Tyr208, Asp210 and Asp239. In addition, this histamine amino group interacts with a water molecule coordinated by the main chain oxygen of Lys211 and the hydroxyl group of Tyr158. Each of the histamine imidazole nitrogen atoms form hydrogen bonds with Asp210 and Glu170. The LBDs of TlpQ and McpU of *P. putida* KT2440 share approximately 50% sequence identity (Supp. Fig. 32B). When their structures containing either histamine or putrescine are superimposed (Fig. 48D), it becomes apparent that the primary amino group of both ligands is coordinated in a similar manner via hydrogen bonds with Y208/D210/D239 of TlpQ-LBD or their equivalents in McpU-LBD.

Histamine chemotaxis is mediated by multiple chemoreceptors in PAO1

To assess the role of TlpQ in histamine chemotaxis, we generated a *tlpQ* mutant. Control experiments showed that its response to casamino acids was comparable to that of wildtype. However, the response of this mutant to 5 mM histamine was also similar to wildtype (Fig. 49A), indicating that additional chemoreceptors may be involved.

To identify these additional chemoreceptors, we screened a number of mutants, in which 3

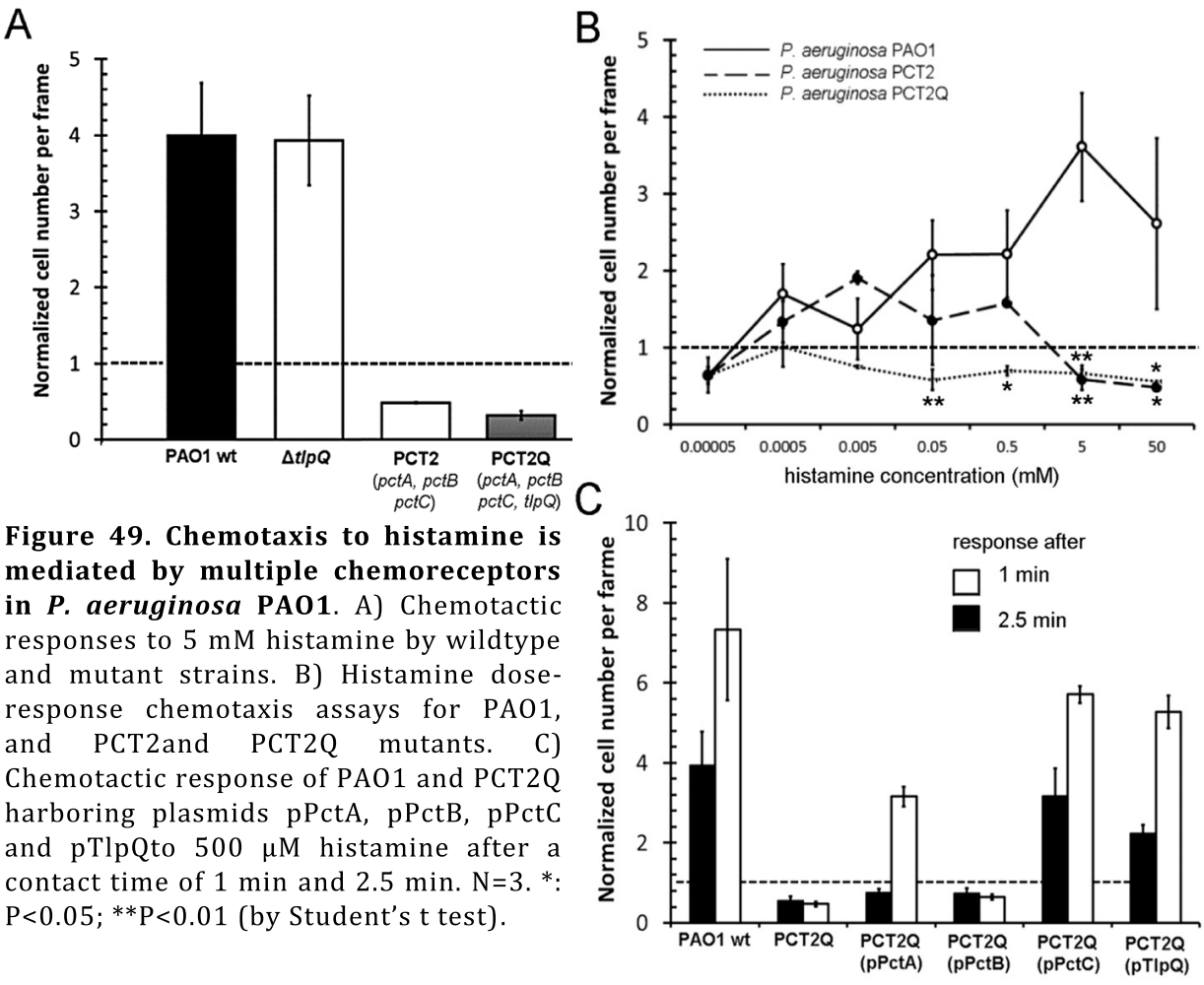

Figure 49. Chemotaxis to histamine is mediated by multiple chemoreceptors in *P. aeruginosa* PAO1. A) Chemotactic responses to 5 mM histamine by wildtype and mutant strains. B) Histamine dose-response chemotaxis assays for PAO1, and PCT2and PCT2Q mutants. C) Chemotactic response of PAO1 and PCT2Q harboring plasmids pPctA, pPctB, pPctC and pTlpQto 500 µM histamine after a contact time of 1 min and 2.5 min. N=3. *: P<0.05; **P<0.01 (by Student's t test).

to 7 chemoreceptor genes had been deleted. Our results showed that the deletion of the *pctA*, *pctB* and *pctC* chemoreceptor genes (strain PCT2) abolished chemotaxis to 5 mM histamine (Fig. 49A). PctA, PctB and PctC are chemoreceptors for L-amino acids (Taguchi *et al.*, 1997, Rico-Jimenez *et al.*, 2013a), while PctC also mediates chemotaxis towards GABA (Reyes-Darias *et al.*, 2015b). To clarify the role of PctA, PctB, PctC and TlpQ in histamine chemotaxis, we conducted dose-response experiments using wildtype, PCT2 as well as a mutant in which the *pctABC* as well as the *tlpQ* gene had been deleted, PCT2Q (Fig. 49B). The latter mutant was devoid of histamine chemotaxis over the entire concentration range (50 nM to 50 mM), whereas significant chemotaxis was observed for the PCT2mutant at a concentration range between 500 nM and500 µM. This indicates that TlpQ mediates chemotaxis to low histamine concentrations, which is in agreement with the very high affinity observed *in vitro*. In contrast, one or more of the PctA, PctB and PctC receptors mediate chemotaxis to elevated histamine concentrations.

To assess the role of the individual chemoreceptors, the PCT2Q mutant devoid of histamine chemotaxis was complemented with plasmids containing one of the four chemoreceptors—an approach that has previously proven effective to study complex chemotactic processes (Ni *et al.*, 2013). To confirm the phenotypes of these strains, chemotaxis was measured towards previously identified ligands, namely L-Ile (PctA), L-Arg (PctB) and GABA (PctC) (Taguchi *et al.*, 1997, Rico-Jimenez *et al.*, 2013a) and the three complemented strains responded to these ligands. Histamine chemotaxis measurements revealed that the *pctC* and *tlpQ* genes *in trans* recovered histamine chemotaxis using an exposure time of one minute. At 2.5 minutes, complementation with *pctA*, *pctC* and *tlpQ* resulted in significant chemotaxis (Fig. 49C). Thus, these data reveal that histamine chemotaxis is mediated by the concerted action of PctA, PctC and TlpQ. To assess the role of these receptors in another strain we have generated a triple mutant in the homologous receptors of *P. aeruginosa* PA14. As shown in Supp Fig. 36 the deletion of these receptors also abolished histamine chemotaxis.

TlpQ, PctA and PctC employ different mechanisms to mediate histamine chemotaxis

To determine the mechanism by which PctA and PctC respond to histamine, microcalorimetric binding studies with purified PctA-LBD and PctC-LBD were conducted. Whereas proteins bound L-Ala and L-Gln (Rico-Jimenez *et al.*, 2013a), respectively, histamine did not bind. Direct microcalorimetric titrations can only provide information on high affinity binding events due to the limitations presented by ligand dilution heats. To assess the possibility of low-affinity histamine binding, we conducted a competition assay. PctA-LBD was titrated with L-Ala in the presence and absence of 20 mM histamine. However, the resulting titration curves were almost identical (Supp. Fig. 37), confirming that histamine does not bind directly to PctA-LBD.

To assess whether PctA and PctC may be activated by histamine-containing periplasmic binding proteins, pull-down experiments with immobilized PctA-LBD and PctC-LBD as well as PAO1protein extracts were conducted using previously verified protocols (Rico-Jimenez *et al.*, 2016). However, our results provided no evidence for binding partners to either domain.

DISCUSSION

The elevated number of chemoreceptors in many bacteria suggests that this abundance confers chemotactic capabilities to many different stimuli, and the scientific community is only beginning to explore the diversity of these responses. In general, chemoeffectors can be classified into three groups according to their physiological role. First, the majority of chemoattractants are important nutritional sources, as evidenced by numerous receptors that respond to different

organic or amino acids (Ortega *et al.*, 2017a). Secondly, chemoattraction has been observed for signal molecules like plant hormones (Kim *et al.*, 2007, Antunez-Lamas *et al.*, 2009), neurotransmitters (Pasupuleti *et al.*, 2014) and quorum sensing signals (Laganenka *et al.*, 2016), which inform bacteria about their environment. Lastly, chemoreceptors can signal the presence of compounds that are involved in multiple functions, such as histamine.

What is thus the physiological relevance of chemotaxis towards histamine? One reason is certainly that, like most of the other McpU/TlpQ ligands, histamine supports growth as sole C- and N-source. However, chemotaxis to host signals has been shown for many different pathogens to be essential for efficient infection and virulence (Matilla & Krell, 2018). Importantly, *P. aeruginosa* PAO1 was shown to greatly increase neutrophil histamine content and secretionin mice models (Xu *et al.*, 2012), and chemotaxis to this host-derived signal will result in an accumulation of bacterial cells at the infection site. This increase in bacterial cell density is likely to alter the expression of quorum sensing-controlled genes, including those responsible for the production of virulence determinants and biofilm formation in *P. aeruginosa* (Azam & Khan, 2019). Nonetheless, the precise assessment of the role of histamine chemotaxis in the virulence of *P. aeruginosa* is technically a difficult undertaking since it is unfeasible to generate a mutant that is deficient in histamine chemotaxis without impairing taxis to the remaining identified ligands for PctA (17 amino acids), PctC (GABA and 2 amino acids) and TlpQ (5 polyamines) (Rico-Jimenez *et al.*, 2013a).

The interference with motility and chemotaxis is an alternative strategy to block bacterial pathogens (Erhardt, 2016). Previous work has shown that some chemoreceptors recognize chemoattractants and antagonists (Bi *et al.*, 2013, Yu *et al.*, 2015, Martin-Mora *et al.*, 2018) and the identification of antagonists that specifically interfere with histamine chemotaxis may thus be an alternative approach to modulate the virulence properties of *P. aeruginosa.* Remarkably, the identification of these antagonists may be facilitated by the resolution of the three-dimensional structure of TlpQ-LBD in complex with histamine (Figs. 47, 48).

High sensitivity histamine responses are mediated by the TlpQ chemoreceptor, which binds histamine directly. TlpQ is in many aspects an atypical chemoreceptor. Firstly, its LBD, which is of 334 amino acids, is larger than any other known chemoreceptor LBD (Ortega *et al.*, 2017a). Secondly, it has the highest affinity ever observed for the binding of a chemoattractant to the recombinant LBD of a chemoreceptor. Histamine binding occurred with an affinity of 639 nM, which is among the highest affinities observed for chemoattractants. This unusually high affinity permits responses to very low histamine concentrations and the onset of chemotactic response occurred at the unusually low concentration of 500 nM (Fig. 45C).

Frequently, the deletion of a chemoreceptor abolishes taxis to a given compound, indicating that there is a single receptor for a given chemoattractant (Garcia *et al.*, 2015, Martin-Mora *et al.*, 2016a). However, histamine chemotaxis is mediated by the concerted action of three receptors. What is thus the advantage of having multiple receptors for the same chemoattractant? In this context close similarities exist between histamine chemotaxis and the mechanisms by which *P. aeruginosa* is attracted to inorganic phosphate (Pi). Pi is a key signal molecule that controls the expression of many virulence genes (Zaborin *et al.*, 2009, Bains *et al.*, 2012). Chemotaxis to low Pi concentration is mediated by the CtpL receptor, whereas CtpH is responsible for responses to high concentrations (Wu *et al.*, 2000, Rico-Jimenez *et al.*, 2016). Whereas CtpH recognizes Pi directly at its LBD, CtpL is stimulated by the Pi loaded periplasmic binding protein PstS (Rico-Jimenez *et al.*, 2016). A chemoreceptor, either stimulated by direct or indirect signal recognition, is characterized by a response range (Neumann *et al.*, 2010). The combined action of multiple chemoreceptors with different sensing abilities permits the microorganism to expand its response range to a given chemoattractant. The presence of multiple receptors for a given chemoeffector may suggest that a compound is particularly physiologically relevant.

Four human histamine receptors have been described, termed H1, H2, H3 and H4 (Panula *et al.*, 2015). Histamine was shown to mediate chemotaxis of mast cells via the H4 receptor and this

mechanism might be responsible for mast cell accumulation in allergic tissues (Hofstra *et al.*, 2003). However, the topology of eukaryotic histamine receptors differs entirely from their bacterial counterparts. All four receptor types form a barrel composed of seven transmembrane helices (Panula *et al.*, 2015). The three-dimensional structure of the human H1 receptor has been solved (Shimamura *et al.*, 2011), which revealed that ligands bind within this transmembrane barrel. Therefore, the evolutionary strategies to sense histamine greatly differ between bacteria and humans.

Here we provide the first report of bacterial chemotaxis towards histamine. Histamine is vital to cellular processes in mammals and initial evidence suggests that histamine also functions as a bacterial signal molecule. This study expands the range of known bacterial chemoeffectors and lays the foundation for deciphering the molecular mechanisms underlying histamine chemotaxis and its role in bacterial virulence.

SUPPLEMENTARY MATERIAL

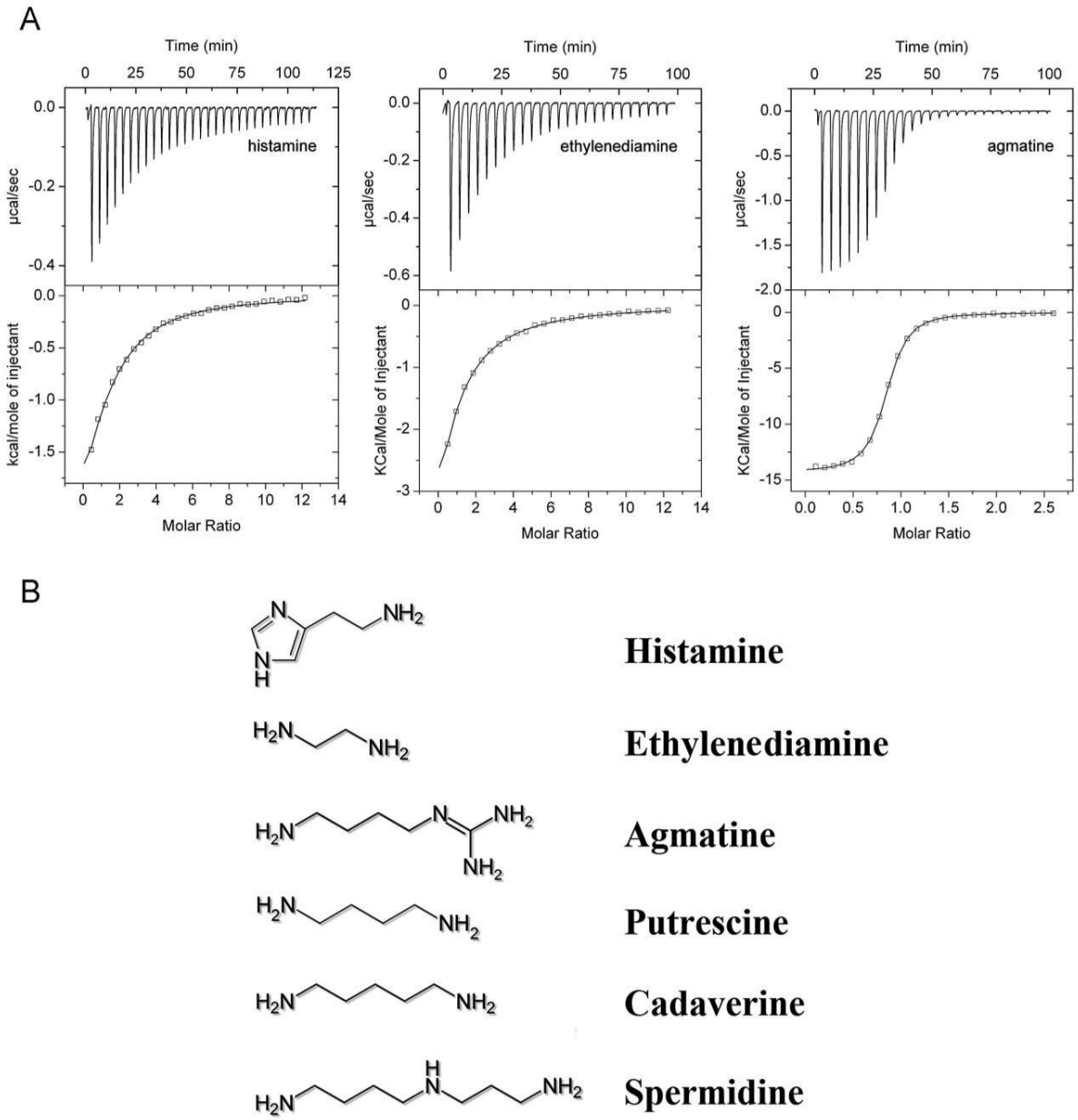

Supp. Fig 31. Microcalorimetric binding studies of McpU-LBD. A) Titrations of 17.5 µM McpU-LBD with 1 mM histamine and ethylenediamine and 30 µM McpU-LBD with 0.5 mM agmatine. B) Chemical structure of ligands recognized by the McpU and TlpQ chemoreceptors.

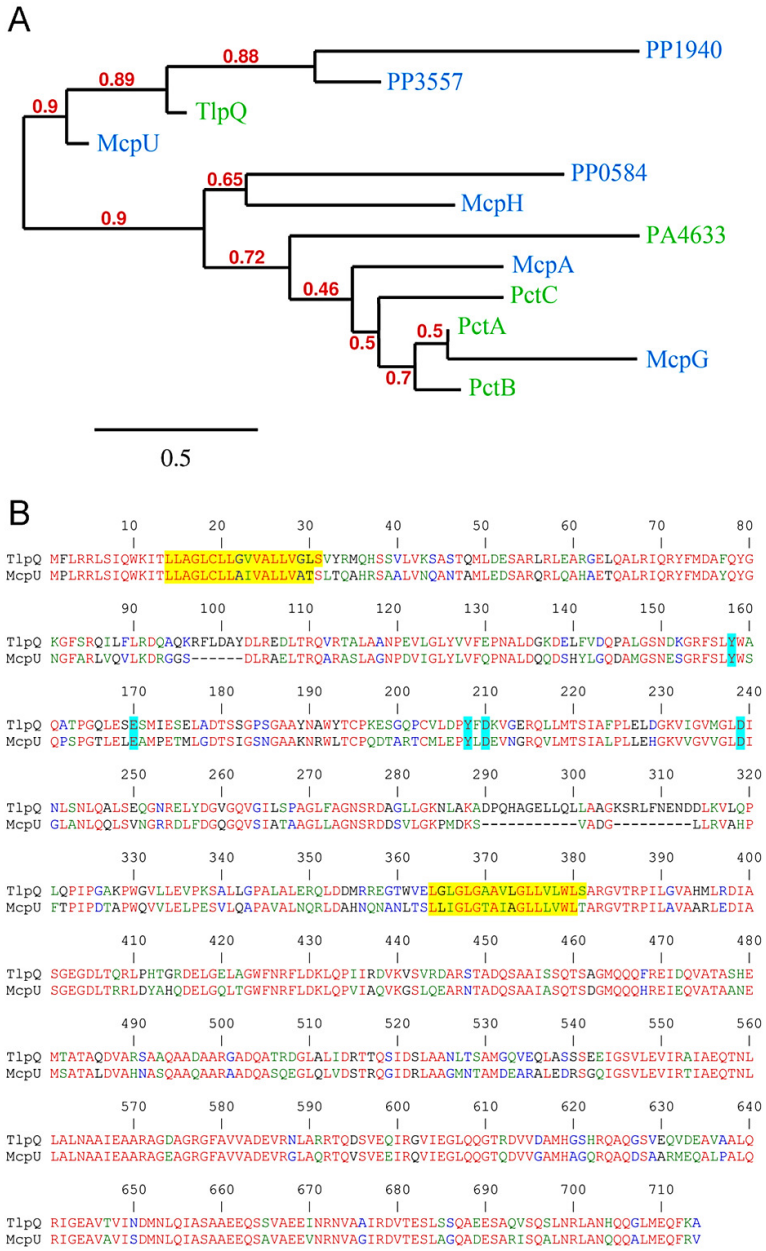

Supp. Fig 32. Identification of a McpU homologue. A) Sequence clustering of the ligand binding domains of dCACHE-containing chemoreceptors from *P. putida* KT2440 (blue) and *P. aeruginosa* PAO1 (green). The figure was produced using the Phylogeny.fr server. B) Sequence alignment of the TlpQ and McpU chemoreceptors. Sequence identity between the two receptors is 62%. The alignment was done in the slow mode using the CLUSTALW multiple alignment tool of the NPSA suite (https://npsa-prabi.ibcp.fr/cgi-bin/npsa_automat.pl?page=/NPSA/npsa_server.html). The GONNET protein weight matrix was used in the slow pairwise alignment mode using a gap opening penalty of 10 and a gap extension penalty of 0.1. Red = identical; green = highly similar; blue = weakly similar. The transmembrane regions flanking the ligand binding domain were predicted using the DAS algorithm (https://tmdas.bioinfo.se/DAS/index.html) and are highlighted in yellow. Cyan highlights amino acids that are involved in side-chain mediated interactions with bound histamine.

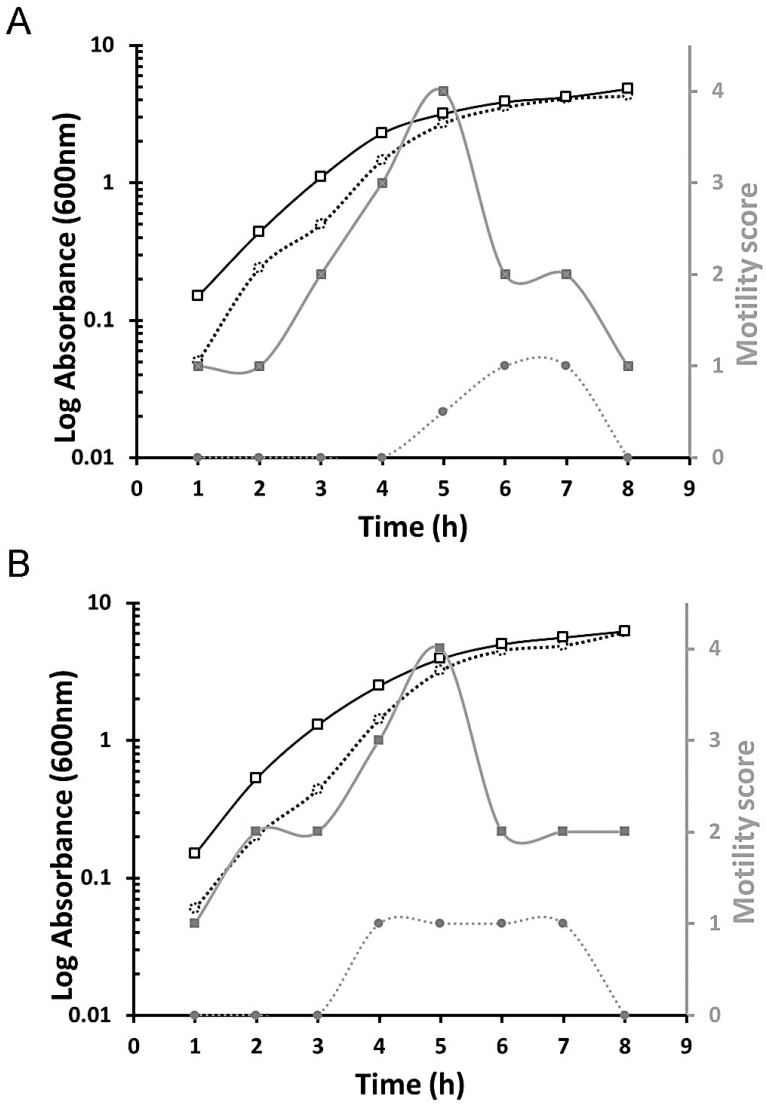

Supp. Fig 33. Assessment of motility during bacterial growth. Overnight cultures of *P. aeruginosa* PAO1 (continuous line) and *P. putida* KT2440 (dotted line) were used to inoculate LB (upper panel) and 2xYT medium (lower panel) to an OD_{600} of 0.01. Growth was carried out at 37°C (*P. aeruginosa* PAO1) or 30°C (P. putida KT2440) and bacteria were inspected microscopically. Motility scores were calculated: score 1 = 25% of bacteria are motile, 2 = 50%, 3 = 75% and 4 = 100%.

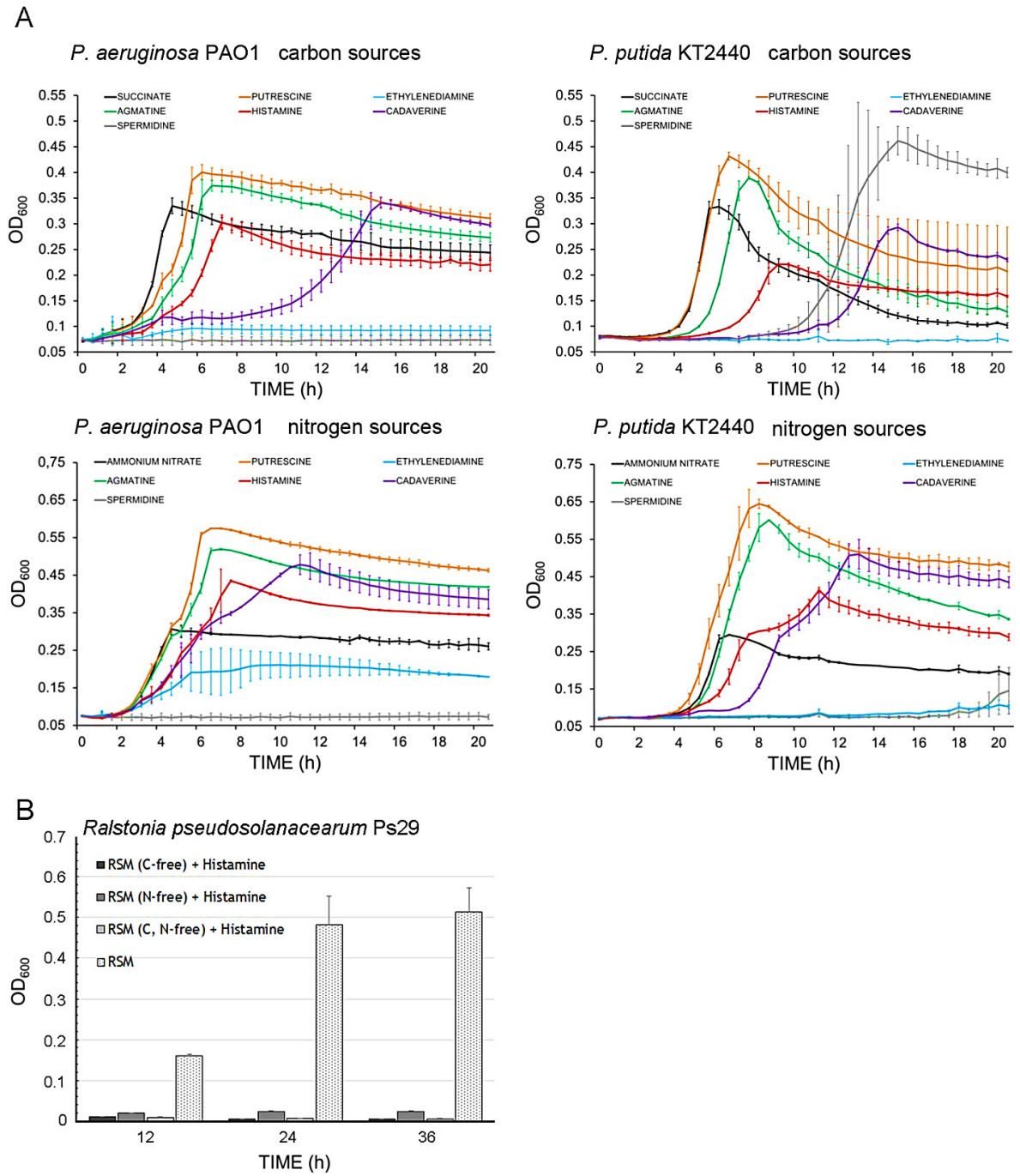

Supp. Fig 34. Growth experiments with McpU/TlpQ ligands as sole carbon or nitrogen source. A) Capacity of ligands to sustain growth of *P. aeruginosa* PAO1 and *P. putida* KT2440. Overnight cultures were used to inoculate MS minimal medium supplemented with the McpU/TlpQ ligands as either sole carbon or nitrogen source. As controls, succinate and ammonium nitrate were used. B) Growth of *Ralstonia pseudosolanacearum* Ps29 in media with histamine as sole carbon and nitrogen source. The initial OD_{660} was 0.005. The composition of the RSM medium is: 10 mM K_2HPO_3, 5.5 mM KH_2PO_4, 0.5 mM sodium citrate, 9.5 mM $(NH_4)_2SO_4$, 1 mM $MgSO_4$, 28 mM glucose. In all cases ligands were added at a concentration of 5 mM and shown are means and standard deviations from three biological replicates conducted in triplicate.

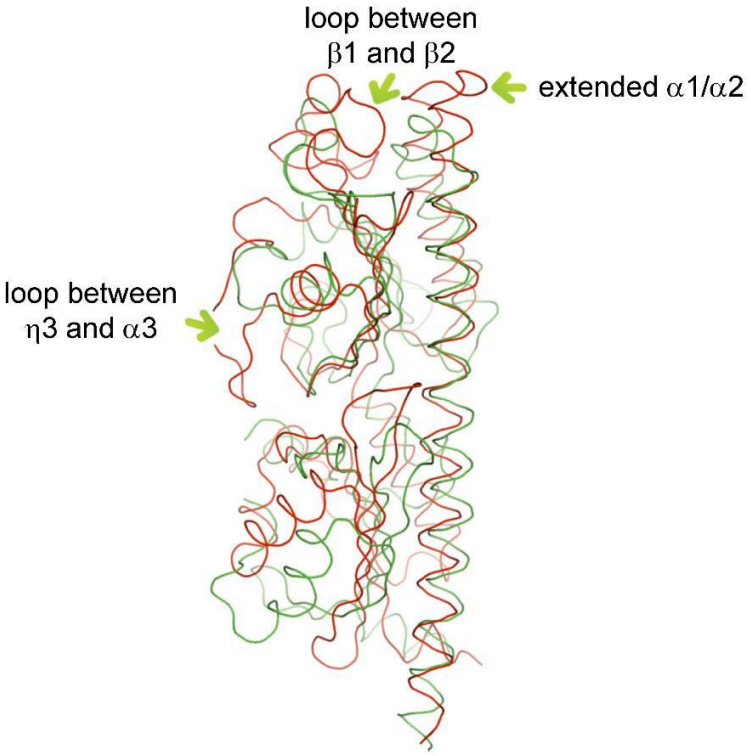

Supp. Fig 35. Structural alignment of the Cα chain of TlpQ-LBD (in red) with a homologous structure from a histidine kinase of *Shewanella oneidensis* (in green). This structure is deposited in the protein data bank with ID 3lic. The arrows indicate inserts and loops in the TlpQ-LBD structure that account for its elevated size.

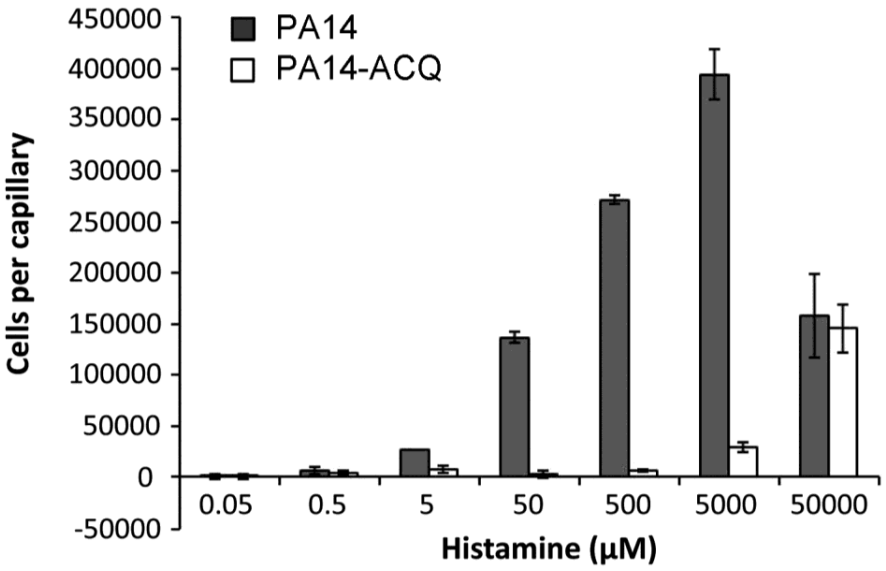

Supp. Fig 36. Quantitative capillary chemotaxis assays of *P. aeruginosa* PA14 and a mutant defective in the *pctA, pctC* and *tlpQ* genes towards histamine. Data have been corrected with the number of bacteria (6900 ± 142) that swam into buffer-containing capillaries. Shown are means and standard deviations from three individual experiments conducted in duplicate.

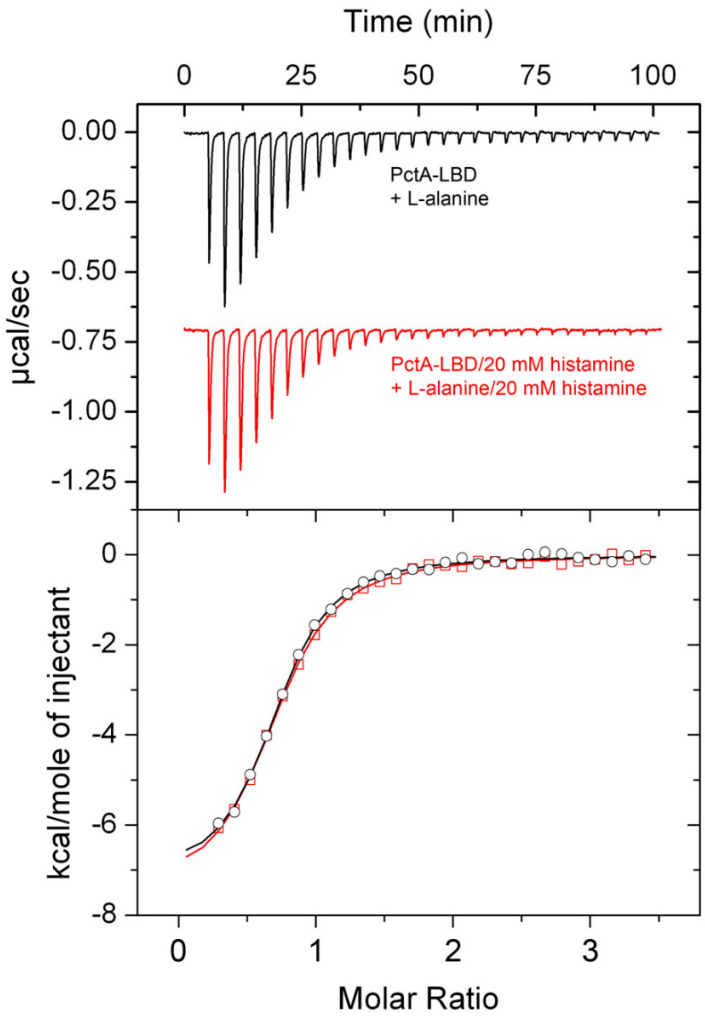

Supp. Fig 37. Assessment of potential low-affinity binding of histamine to PctA-LBD by microcalorimetric competition experiments. Shown are microcalorimetric titrations of 39 µM PctA-LBD with 1 mM L-alanine either in the absence or presence of 20 mM histamine. The resulting integrated peak areas are almost identical indicating that histamine does not compete with L-alanine for binding at PctA-LBD.

Supp. Table 12. Structural alignment of TlpQ-LBD with structures deposited in the protein data bank. Shown are the structures with a Z-score above 15. Id.: identity. Ref.: reference.

PDB ID	name	Z-score	Id. (%)	RMSD	LBD size[a]	Ligands	Protein/species	Loop between β1-β2 (size)	Extended α1/α2 (size)	Loop between η3-α3 (size)	Pfam signature	Ref.
6fu4	TlpQ	-	-	-	334	histamine, polyamines	CR[b]/*P. aeruginosa*	Yes (22)[c]	Yes (5/4)[c]	Yes (9)[c]	dCACHE_1	This work
6f9g	McpU	37.1	56	1.3	302	polyamines	CR/*P. putida*	Yes (22)	No	Yes (9)	dCACHE_1	(Gavira *et al.*, 2018)
3lib	Z3	28.0	21	2.2	280	unknown	HK[b]/*Methanosarcina mazei*	Yes (20)	No	No	dCACHE_1	(Zhang & Hendrickson, 2010)
3li8	Z2	27.2	21	2.3	280	unknown	HK/*M. mazei*	Yes (20)	No	No	dCACHE_1	(Zhang & Hendrickson, 2010)
4wy9	Tlp1	23.6	16	4.0	298	unknown	CR/*C. jejuni*	Yes (16)	Yes (2/-)	No	dCACHE_1	(Machuca *et al.*, 2016)
3lic	Z6	20.7	20	3.9	281	unknown	HK/*S. oneidensis*	Yes (7)	No	No	dCACHE_1	(Zhang & Hendrickson, 2010)
5ave	Mlp37	19.5	14	3.1	251	L-Ser, taurine	CR/*V. cholerae*	No	No	No	dCACHE_1	(Nishiyama *et al.*, 2016)
5ltx	PctA	19.3	18	2.7	252	amino acids	CR/*P. aeruginosa*	No	No	No	dCACHE_1	To be published
5ere		19.3	12	2.8	239[d]	cytosine[e]	Novel receptor/ *D. retbaense*	No	No	No	Peripla_BP (CL0144)	To be published
3lif	Z16	18.4	12	3.0	258	unknown	HK/*R. palustris*	No	No	No	dCACHE1	(Zhang & Hendrickson, 2010)
5ltv	PctC	18.3	22	2.8	255	amino acids/GABA	CR/*P. aeruginosa*	No	No	No	dCACHE_1	To be published
5lt9	PctB	18.1	18	3.4	251	amino acids	CR/*P. aeruginosa*	No	No	No	dCACHE_1	To be published
3lid	Z8	17.4	7	4.2	293	unknown	HK/*V. parahaemolyticus*	No	Yes (-/3)	No	dCACHE_1	(Zhang & Hendrickson, 2010)
4xmq	Tlp3/ Ccml	17.0	14	3.5	255	amino acids, succinate, malate, fumarate, purine,	CR/*C. jejuni*	No	Yes (-/3)	No	dCACHE_1	(Liu *et al.*, 2015)

						thiamine						
2zbb	smDctB	15.4	9	3.3	280	dicarboxylic acids	HK/*S. meliloti*	No	Yes (2/3)	No	none	To be published
3t4k	AHK4	15.3	11	3.5	281	cytokinins	HK/*A. thaliana*	Yes (7)	No	No	CACHE-like (CL0165)	(Hothorn *et al.*, 2011)
3by9	vcDctB	15.3	12	3.7	269	dicarboxylic acids	HK/*V. cholerae*	No	Yes (2/3)	No	dCACHE_1	(Cheung & Hendrickson, 2008)

[a] size between tm regions as determined by DAS (Cserzo *et al.*, 1997), [b] HK: histidine kinase, CR: chemoreceptor, [c] size in amino acids is shown in brackets, [d] part of cytosolic receptor, LBD size determined by structural alignment, [e] cytosine present in the binding pocket in the membrane distal module

Supp. Table 13. Oligonucleotides used in this study.

Plasmid	Primer Name	Sequence (5' to 3')[a]	Endonuclease
pK18*mobsacB-pctA*	NM-PctA-Up-F	AT**GAATTC**AACAGCCAGAGCAGGAAAG	EcoRI
	NM-PctA-Up-R	CAT**ACTAGT**CATGTTGTATTGCGTCCAGGAG	SpeI
	NM-PctA-Down-F	CAT**ACTAGT**CAGCTTCAAGATCTGAGACCG	SpeI
	NM-PctA-Down-R	ACAT**GTCGAC**TGACCGGAGAGAAACTGAG	SalI
pK18*mobsacB-tlpQ*	NM-TlpQ-Up-F	GGT**CTCGAG**TATCCTTGACTTCGGCATCAG	XhoI
	NM-TlpQ-Up-R	GAC **GAATTC** CCATTCTTGACGACGGTC	EcoRI
	NM-TlpQ-Down-F	GAA**GAATTC**GGCCTGATGGAACAGTTCAG	EcoRI
	NM-TlpQ-Down-R	ATG**GGATCC**GTGTGCAGTGGATGGGTCTG	BamHI
pK18*mobsacB-pctABC,orf1*	NM-PctABC-Orf1-Up-F	CTTTA**CTGCAG**AGACCCCTGCTATGCGTCC	PstI
	NM-PctABC-Orf1-Up-R	AGAAC**GGATCC**CCTGGCAAAAGCCTCAAGAG	BamHI
	NM-PctABC-Orf1-Down-F	GAACA**GGATCC**CAAGCTCAACGGAGGAAG	BamHI
	NM-PctABC-Orf1-Down-R	GAAGT**GAATTC**CGAGGATACGCTCAGGAAGAAG	EcoRI
pK18*mobsacB-orf1-pctC*	NM-Orf1-PctCUp-F	CGAT**GAATTC**GGTACGTTGG	EcoRI
	NM-Orf1-PctC-Up-R	AA**CTCGAG**TCCAATTCGACGGTGAAGAG	XhoI
	NM-Orf1-PctC-Down-F	AA**CTCGAG**TTGCGACATCCATTCATCCTC	XhoI
	NM-Orf1-PctC-Down-R	AA**GGATCC**GGCAAGTCCGGAAGCTTTAG	BamHI
pPctC	Comp-PctC-F	AA**GAATTC**GTGGCTCTGATTGCCGTATTG	EcoRI
	Comp-PctC-R	AA**GAGCTC**TGTCCAATTCGACGGTGAAGA	SacI
pET28-b-TlpQ	TlpQ-LBD-F	CTGGTCGGCCTTTCGGTCTAC**CATATG**	NdeI
	TlpQ-LBD-R	TGGGTCGAACT**GGATCC**CGGCCT	BamHI

[a]Sequences recognized by restriction enzymes are bolded.

Supp. Table 14. Data collection and refinement statistics of the three-dimensional structure of TlpQ-LBD (values in parentheses are for highest-resolution shell).

Protein **Ligand**	**TlpQ-LBD** **histamine**
PDB identifier	6fu4
Data collection	
Beam line	ID23-2 (ESRF)
Space Group	P 64
Cell dimensionsa, b, c (Å)	81.62, 103.98, 147.45
ASU	4
Resolution (Å)	84.98 - 2.45(2.54 - 2.45)
R_{merge} (%)	6.2 (36.9)
I/σ_I	12.5 (2.9)
Completeness (%)	98.12 (98.06)
Unique reflections	46027 (4544)
Multiplicity	3.9 (4.0)
CC(1/2)	99.8 (82.6)
Refinement	
Resolution (Å)	84.98 - 2.45
R_{work}/R_{free} (%)	19.3/23.7
No. atoms	10086
Protein	9711
Ligands	70
Water	305
B-factor (Å^2)	52.22
R.m.s deviations	
Bond lengths (Å)	0.005
Bond angles (^{0})	1.08
Ramachandran (%)	
Favored	97.86
Outliers	0.00

CHAPTER 3
IDENTIFICATION OF THE MOLECULAR MECHANISM FOR NITRATE CHEMOTAXIS IN *P. AERUGINOSA* PAO1

CHAPTER 3: IDENTIFICATION OF THE MOLECULAR MECHANISM FOR NITRATE CHEMOTAXIS IN *P. aeruginosa* PAO1

Published article

The molecular mechanism of nitrate chemotaxis via direct ligand binding to the PilJ domain of McpN

David Martín-Mora[a], Álvaro Ortega[a*], Miguel Ángel. Matilla[a], Sergio Martínez-Rodríguez[b, c], José A. Gavira[c#] and Tino Krell[1]

[a]Estación Experimental del Zaidín, Department of Environmental Protection, Consejo Superior de Investigaciones Científicas, Prof. Albareda 1, 18008 Granada, Spain
[b]Dept. de Bioquímica y Biología Molecular III e Inmunología. Universidad de Granada. Campus Universitario de Melilla. C/ Santander, 1. 52071 Melilla, Spain
[c]Laboratorio de Estudios Cristalográficos, IACT, (CSIC-UGR), Avd. las Palmeras 4, 18100 Armilla, Spain

MBio (Published online 19 February 2019); 10 (1).
doi: 10.1128/mBio.02334-18

ABSTRACT

Chemotaxis and energy taxis permit directed bacterial movements in gradients of environmental cues. Nitrate is a final electron acceptor for anaerobic respiration and can also serve as nitrogen source for aerobic growth. Previous studies indicated that bacterial nitrate taxis is mediated by energy tactic mechanisms, which are based on the cytosolic detection of consequences of nitrate metabolism. Here we show that *Pseudomonas aeruginosa* PAO1 mediates nitrate chemotaxis that is based on the specific nitrate sensing by the periplasmic PilJ domain of the PA2788/McpN chemoreceptor. Nitrate reduced *mcpN* transcript levels and McpN mediated taxis occurred only under nitrate starvation conditions. In contrast to the NarX and NarQ sensor kinases, McpN bound specifically nitrate and showed no affinity for other ligands such as nitrite. We report the three-dimensional structure of the McpN LBD at 1.3 Å resolution in complex with nitrate. Although structurally similar to 4-helix bundle domains, the ligand binding mode differs since a single nitrate molecule is bound to a site on the dimer symmetry axis. As for 4-helix bundle domains, ligand binding stabilized the McpN-LBD dimer. McpN homologues showed a wide phylogenetic distribution indicating that nitrate chemotaxis is a widespread phenotype. These homologues were particularly abundant in bacteria that couple sulfide/sulfur oxidation with nitrate reduction. This work expands the range of known chemotaxis effectors and forms the basis for the exploration of nitrate chemotaxis in other bacteria and to study its physiological role.

AMERICAN SOCIETY FOR MICROBIOLOGY | mBio®

RESEARCH ARTICLE
Molecular Biology and Physiology

The Molecular Mechanism of Nitrate Chemotaxis via Direct Ligand Binding to the PilJ Domain of McpN

David Martín-Mora,[a] Álvaro Ortega,[a]* Miguel A. Matilla,[a] Sergio Martínez-Rodríguez,[b,c] José A. Gavira,[c] Tino Krell[a]

[a]Estación Experimental del Zaidín, Department of Environmental Protection, Consejo Superior de Investigaciones Científicas, Granada, Spain
[b]Departamento de Bioquímica y Biología Molecular III e Inmunología, Universidad de Granada, Melilla, Spain
[c]Laboratorio de Estudios Cristalográficos, IACT, Superior de Investigaciones Científicas (CSIC) y la Universidad de Granada (UGR), Armilla, Spain

ABSTRACT Chemotaxis and energy taxis permit directed bacterial movements in gradients of environmental cues. Nitrate is a final electron acceptor for anaerobic respiration and can also serve as a nitrogen source for aerobic growth. Previous studies indicated that bacterial nitrate taxis is mediated by energy taxis mechanisms, which are based on the cytosolic detection of consequences of nitrate metabolism. Here we show that *Pseudomonas aeruginosa* PAO1 mediates nitrate chemotaxis on the basis of specific nitrate sensing by the periplasmic PilJ domain of the PA2788/McpN chemoreceptor. The presence of nitrate reduced *mcpN* transcript levels, and McpN-mediated taxis occurred only under nitrate starvation conditions. In contrast to the NarX and NarQ sensor kinases, McpN bound nitrate specifically and showed no affinity for other ligands such as nitrite. We report the three-dimensional structure of the McpN ligand binding domain (LBD) at 1.3-Å resolution in complex with nitrate. Although structurally similar to 4-helix bundle domains, the ligand binding mode differs since a single nitrate molecule is bound to a site on the dimer symmetry axis. As for 4-helix bundle domains, ligand binding stabilized the McpN-LBD dimer. McpN homologues showed a wide phylogenetic distribution, indicating that nitrate chemotaxis is a widespread phenotype. These homologues were particularly abundant in bacteria that couple sulfide/sulfur oxidation with nitrate reduction. This work expands the range of known chemotaxis effectors and forms the basis for the exploration of nitrate chemotaxis in other bacteria and for the study of its physiological role.

IMPORTANCE Nitrate is of central importance in bacterial physiology. Previous studies indicated that movements toward nitrate are due to energy taxis, which is based on the cytosolic sensing of consequences of nitrate metabolism. Here we present the first report on nitrate chemotaxis. This process is initiated by specific nitrate binding to the periplasmic ligand binding domain (LBD) of McpN. Nitrate chemotaxis is highly regulated and occurred only under nitrate starvation conditions, which is helpful information to explore nitrate chemotaxis in other bacteria. We present the three-dimensional structure of the McpN-LBD in complex with nitrate, which is the first structure of a chemoreceptor PilJ-type domain. This structure reveals striking similarities to that of the abundant 4-helix bundle domain but employs a different sensing mechanism. Since McpN homologues show a wide phylogenetic distribution, nitrate chemotaxis is likely a widespread phenomenon with importance for the life cycle of ecologically diverse bacteria.

KEYWORDS *Pseudomonas aeruginosa*, chemoreceptor, chemotaxis, nitrate

Many bacteria are capable of flagellum-driven tactic movements in stimulus gradients. Genome analyses have revealed that more than half of the bacterial genomes contain genes necessary for taxis (1). The canonical form of taxis is based on

Citation Martín-Mora D, Ortega Á, Matilla MA, Martínez-Rodríguez S, Gavira JA, Krell T. 2019. The molecular mechanism of nitrate chemotaxis via direct ligand binding to the PilJ domain of McpN. mBio 10:e02334-18. https://doi.org/10.1128/mBio.02334-18.

Editor Michael T. Laub, Massachusetts Institute of Technology

Address correspondence to José A. Gavira, jgavira@iact.ugr-csic.es, or Tino Krell, tino.krell@eez.csic.es.

* Present address: Álvaro Ortega, Department of Biochemistry and Molecular Biology 'B' and Immunology, Faculty of Chemistry, University of Murcia, Murcia, Spain.

Received 23 October 2018
Accepted 7 January 2019
Published 19 February 2019

INTRODUCTION

Many bacteria are able of flagellum-driven tactic movements in stimulus gradients. Genome analysis have revealed that more than half of the bacterial genomes contain genes necessary for taxis (Wuichet & Zhulin, 2010). The canonical form of taxis is based on stimulus reception by the chemoreceptor that leads to changes in the activity of the CheA autokinase, which subsequently modulates transphosphorylation to the CheY response regulator. The phosphorylated form of CheY binds to the flagellar motor causing ultimately taxis towards or away from the stimulus (Bi & Sourjik, 2018).

Many bacteria possess the capacity to perform chemotaxis and energy taxis. The typical chemotaxis mechanism is initiated by the recognition of specific chemoeffectors at periplasmic LBDs leading to receptor activation. Chemoreceptor function is largely determined by the nature of chemoeffectors recognized and chemoreceptors specific for different compound classes such as amino acids, TCA cycle intermediates, polyamines, purines or inorganic phosphate have been identified (Matilla & Krell, 2017). Alternatively, energy taxis is a metabolism-dependent form of taxis and is the directed movement in gradients of physico-chemical parameters that affect metabolism (Alexandre, 2010). In contrast to chemotaxis, not the chemoeffector *per se* is sensed but consequences of its metabolism. Energy taxis occurs to a very wide range of stimuli such as metabolizable substrates like sugars, organic acids and amino acids, electron acceptors like oxygen, nitrate, fumarate and dimethyl sulfoxide, or compounds that affect metabolism otherwise like light or metabolic inhibitors (Taylor *et al.*, 1999, Alexandre *et al.*, 2004, Schweinitzer & Josenhans, 2010).

E. coli, the traditional model organism to study chemotaxis, has 4 chemoreceptors with a periplasmic LBD that mediate chemotaxis primarily to amino acids, sugars or dipeptides (Parkinson *et al.*, 2015). In addition, it has an Aer chemoreceptor that mediates energy taxis by sensing redox changes via an FAD containing cytosolic PAS domain (Parkinson *et al.*, 2015). However, genome analyses indicate that many other bacteria have significantly more chemoreceptors, up to 80, than *E. coli* (Alexandre *et al.*, 2004). In addition, these chemoreceptors are characterized by a diversity in the LBD type since more than 80 different LBD types were found to form part of chemoreceptors (Ortega *et al.*, 2017a).

The elevated number of chemoreceptors and their diversity in the LBDs suggests that the chemosensory capacity of many bacteria is very extensive, but remains in general largely unexplored. The scientific community is now only at the beginning to identify the chemotactic spectra of many bacteria, to establish links between chemoeffectors and LBD types and to identify the physiological relevance of chemotaxis to newly identified chemoeffectors (Ortega *et al.*, 2017).

We have addressed this issue here using the opportunistic human pathogen *P. aeruginosa* PAO1 as model (Kato *et al.*, 2008, Ortega *et al.*, 2017a). This bacterium has 26 chemoreceptors that feed into four chemosensory pathways (Ortega *et al.*, 2017b). Two pathways, Che and Che2, were shown to play a role in chemotaxis. Whereas the Che pathway appears to be essential for chemotaxis (Masduki *et al.*, 1995, Kato *et al.*, 1999), the Che2 pathway was found to be required for optimal chemotactic responses (Ferrandez *et al.*, 2002). Alternatively, the Chp pathway was associated to twitching motility (Whitchurch *et al.*, 2004, Fulcher *et al.*, 2010, Persat *et al.*, 2015, Jansari *et al.*, 2016), whereas the Wsp pathway modulates c-di-GMP levels (Hickman *et al.*, 2005). *P. aeruginosa* chemoreceptors employ together eleven different LBD types for signal sensing (Ortega *et al.*, 2017a), with the 4HB (Ulrich & Zhulin, 2005), CACHE (Upadhyay *et al.*, 2016) and HBM (Ortega & Krell, 2014) domains being most abundant (Ortega *et al.*, 2017a). Several of these receptors have been functionally annotated and were all found to mediate chemoattraction. The 4HB domain containing receptor CtpH responded specifically to inorganic phosphate (Pi)(Wu *et al.*, 2000, Rico-Jimenez *et al.*, 2016), the HBM containing McpK and CtpL were respectively identified as α-ketoglutarate (Martin-Mora *et al.*, 2016a) and Pi specific receptors (Wu *et al.*, 2000, Rico-Jimenez

et al., 2016), the paralogous dCACHE domain containing receptors PctA, PctB and PctC mediate chemotaxis to amino acids (Taguchi *et al.*, 1997, Rico-Jimenez *et al.*, 2013a, Reyes-Darias *et al.*, 2015b, Reyes-Darias *et al.*, 2015a), whereas the sCACHE domain containing receptor PA2652 mediates taxis to different C4-carboxylic acids (Alvarez-Ortega & Harwood, 2007, Martin-Mora *et al.*, 2018).

P. aeruginosa has two chemoreceptors, PA2788 and PA0411/PilJ, that possess a PilJ type LBD (Pfam signature PF13675)(Ortega *et al.*, 2017a). This domain is annotated in the Pfam database (Finn *et al.*, 2016) as "Type IV pili methyl-accepting chemotaxis transducer N-ter". The PilJ receptor feeds into the Chp pathway and is not related to chemotaxis (Persat *et al.*, 2015), whereas PA2788 was predicted to feed into the Che pathway (Ortega *et al.*, 2017b). However, the ligands recognized by the PilJ and PA2788 are unknown. Bioinformatic analyses have shown that PilJ domains represent 2 % of all chemoreceptor LBDs (Ortega *et al.*, 2017a). In addition, a search in the Pfam database revealed that PilJ domains are also employed by other bacterial sensor proteins like sensor kinase, diguanylate cyclases or transcriptional regulators. In this study, we aimed at identifying the function of PilJ domain containing chemoreceptors in *P. aeruginosa*.

METHODOLOGY

Bacterial strains, culture media and growth conditions: Bacterial strains used are listed in Table 14. Bacteria were grown aerobically at 30 °C or 37 °C, unless specified, in LB, 2 x YT (10 g yeast extract l^{-1}, 16 g bactotryptone l^{-1} and 10 g NaCl l^{-1}) or MS medium (4.2 g/l Na_2HPO_4, 2.8 g/l KH_2PO_4, 2.0 g/l NH_4NO_3, 0.2 g/l $MgSO_4$ $7H_2O$, 17.0 mg/l $FeCl_3$ $6H_2O$, 0.8 mg/ $CoCl_2$ $6H_2O$, 0.6 mg/l $CaCl_2$ $2H_2O$, 0.3 mg/l Na_2MoO_4 $2H_2O$, 0.1 mg/l H_3BO_3, 0.2 mg/l $ZnSO_4$ $7H_2O$, 0.2 mg/l $CuSO_4$ $7H_2O$, 0.2 mg/l $MnSO_4$ $7H_2O$) supplemented with 20 mM D-glucose as carbon source. Alternatively, *Xanthomonas campestris* was grown in M9 minimal medium supplemented with 20 mM D-glucose, 5 mM $NaNO_3$ and 5 % (v/v) LB medium. *E. coli* DH5α was used as a host for gene cloning. When necessary, antibiotics were used at the following final concentrations (in µg/ml): ampicillin, 100; kanamycin, 50, tetracycline, 40.

Plasmid construction: Plasmids and oligonucleotides used are listed in Table 14 and Supp. Table 16, respectively. Protein expression plasmids were constructed by amplifying from genomic DNA of *P. aeruginosa* PAO1 the DNA fragments encoding the LBDs of PilJ (amino acids 36 to 315), McpN (amino acids 44 to 179) and PA4520 (amino acids 38 to 321). The resulting PCR products were cloned into pET28(+) to generate plasmids pPilJ-LBD, pMcpN-LBD and pET4520-LBD. In all cases, plasmids were verified by sequencing. For the construction of the complementing plasmid pBBRMcpN, the *mcpN* gene was amplified using primers listed in Supp. Table 16. The resulting PCR fragment was cloned into the NdeI and BamHI sites of pBBR1MCS2_STARTand the plasmid was transformed into *P. aeruginosa* PAO1-McpN by electroporation.

Protein overexpression and purification: *E. coli* BL21 (DE3) was transformed with the expression plasmids and resulting strains were grown in 2 l Erlenmeyer flasks containing 400 ml LB medium supplemented with kanamycin. Cultures were grown under continuous stirring (200 r.p.m.) at 30 °C. At an OD_{600} of 0.5, the growth temperature was lowered to 16 °C and after 30 min protein expression was induced by the addition of 0.1 mM IPTG. Cultures were grown for another 14 hours prior to cell harvest by centrifugation at 10 000 × g at 4 °C for 30 min. Cell pellets were resuspended in buffer A (20 mM Tris/HCl, 0.1 mM EDTA, 300 mM NaCl, 10 mM imidazole, 5 % (v/v) glycerol, pH 7.6) and broken by French press treatment at a gauge pressure of 62.5 psi. After centrifugation at 20 000 × *g* for 1 h, the supernatant was loaded onto a 5 ml HisTrap column (Amersham Bioscience), previously equilibrated with buffer A. After washing with buffer A containing 35 mM of imidazole, protein was eluted by a 35–500 mM imidazole gradient in buffer A. Proteins were dialyzed into the following buffers for analysis: PA2788-LBD: 20 mM Tris/HCl, pH

7.4; PA4520-LBD: 5 mM Tris/HCl, 5 mM MES, 5 mM PIPES, pH 7.5; PA0411-LBD: 50 mM HEPES, pH 7.5.

Table 14. Bacterial strains and plasmids used in this study.

Strains and plasmids	Genotype or relevant characteristics[a]	Reference
Strains		
E. coli BL21(DE3)	F⁻ *ompT gal dcm lon hsdS$_B$*($r_B^-m_B^-$) λ(DE3 [*lacI lacUV5-T7p07 ind1 sam7 nin5*]) [*malB*$^+$]$_{K\text{-}12}$(λ^S)	(Jeong *et al.*, 2009)
E. coli DH5α	F⁻ *endA1 glnV44 thi-1 recA1 relA1 gyrA96 deoR nupG purB20* φ80d*lacZ*ΔM15 Δ(*lacZYA-argF*)U169, hsdR17($r_K^-m_K^+$), λ⁻	(Woodcock *et al.*, 1989)
P putida KT2440	Wild type strain	(Belda *et al.*, 2016)
P. aeruginosa PAO1	Wild type strain	(Stover *et al.*, 2000)
PAO1-McpN	PAO1 transposon mutant *pa2788*::IS*lacZ*/hah; Tc^R	(Jacobs *et al.*, 2003)
PAO1-PilJ	PAO1 transposon mutant *pa0411*::IS*phoA*/hah; Tc^R	(Jacobs *et al.*, 2003)
PAO1-PA4520	PAO1 transposon mutant *pa4520*::IS*phoA*/hah; Tc^R	(Jacobs *et al.*, 2003)
PAO1-NarX	PAO1 transposon mutant *pa*3878::IS*phoA*/hah; Tc^R	(Jacobs *et al.*, 2003)
PAO1-CheA1	PAO1 transposon mutant *pa1458*::IS*phoA*/hah; Tc^R	(Jacobs *et al.*, 2003)
PAO1-CheA2	PAO1 transposon mutant *pa0178*::IS*lacZ*/hah; Tc^R	(Jacobs *et al.*, 2003)
P. fluorescens KU-7	Wild type strain	(Hasegawa *et al.*, 2000)
Pectobacterium atrosepticum SCRI1043	Wild type strain	(Bell *et al.*, 2004)
Xanthomonas campestris pv. *campestris*	Wild type strain	M. Milagros-Lopez (IVIA, Spain)
Plasmids		
pET28b(+)	Protein expression plasmid; Km^R	Novagen
pMcpN-LBD	pET28b(+) derivative containing a DNA fragment encoding McpN-LBD cloned into the NdeI/XhoI sites; N-terminal His6-tag; Km^R	This study
pPilJ-LBD	pET28b(+) derivative containing a DNA fragment encoding PilJ-LBD cloned into the NdeI/EcoRI sites; N-terminal His6-tag; Km^R	This study
pET4520-LBD	pET28b(+) derivative containing a DNA fragment encoding PA4520-LBD cloned into the NdeI/SalI sites; N-terminal His6-tag; Km^R	This study
pBBR1MCS2_START	*oriRK2 mobRK2*; Km^R	(Obranic *et al.*, 2013)
pBBRMcpN	pBBR1MCS2_START derivative containing *mcpN* gene; Km^R	This study
pCR2.1-TOPO	PCR cloning vector; *ori* pUC *ori* f1, *lacZα*; Ap^R, Km^R	Invitrogen
pCR-McpN-LBD	pTOPO derivative containing a DNA fragment encoding McpN-LBD; Ap^R, Km^R	This study
pCR-McpN-R61A	pTOPO derivative containing a DNA fragment encoding McpN-LBD (*R61A*); Ap^R, Km^R	This study
pMcpN-R61A	pET28b derivative containing a DNA fragment encoding His-tagged McpN-LBD (*R61A*); Km^R	This study

[a]Ap, ampicillin; Km, kanamycin; Tc, tetracycline.

Differential Scanning Fluorimetry: DSF assays were performed on a MyIQ2 Real-Time PCR instrument (Bio-Rad). Compounds from different arrays (Biolog, Hayward, CA, USA) were dissolved in 50 µl water, which, according to the manufacturer, corresponds to a concentration of 10–20 mM. The composition of these arrays is provided in http://208.106.130.253/pdf/pm_lit/PM1-PM10.pdf. Screening was performed using 96 well plates. Each well contained 2.5 µl of the dissolved compound, 20.5 µl protein and 2 µl SYPRO® Orange (Life Technologies). The control well contained protein without ligand. Samples were heated from 23 °C to 85 °C at a scan rate of 1 °C/min and fluorescence changes were monitored. Tm values correspond to the minima of the first derivatives of the raw data.

Isothermal Titration Calorimetry: Experiments were performed on a VP-microcalorimeter (Microcal, Amherst, MA, USA) at 25 °C. Proteins were placed into the sample cell (36 – 65 µM). Compound solutions (1 – 5 mM) were prepared in dialysis buffer and placed into the injector syringe. Titrations involved the injection of 9.6 – 19.2 µl aliquots of compound solution into the protein. In case no binding was observed, the experiment was repeated at an analysis temperature of 15 °C. The mean enthalpies from the titration of buffer with compounds were subtracted from raw titration data prior to data analysis with the "One binding site model" of the MicroCal version of ORIGIN.

Analytical ultracentrifugation: Experiments were performed on a Beckman Coulter Optima XL-I analytical ultracentrifuge (Beckman-Coulter, Palo Alto, CA, USA) equipped with UV-visible absorbance as well as interference optics detection systems, using an An50Ti 8-hole rotor, 12 mm path-length charcoal-filled epon double-sector centrepieces. The experiments were carried out at 10 °C, using 5 µM to 40 µM McpN-LBD in the absence and presence of 0.6 mM $NaNO_3$.

Sedimentation velocity (SV) runs were carried out at a rotor speed of 48 000 r.p.m. using 400 µl samples with the dialysis buffer as reference. Laser at a wavelength of 235 nm was used in the absorbance optics mode. A least squares boundary modeling of the SV data was used to calculate sedimentation coefficient distributions with the size-distribution *c(s)* method (Schuck, 2000) implemented in the SEDFIT v14.1 software. Buffer density, ρ= 1.003 g/ml (0.99989 g/ml in the presence of $NaNO_3$) and viscosity, η= 0.013137 Poise (0.01313 Poise in the presence of $NaNO_3$) at 10 °C were estimated by the SEDNTERP software (Laue *et al.*, 1992) from the buffer components. The partial specific volume used was 0.7192 ml/g as calculated from the amino acid sequence using the SEDNTERP software.

Intrinsic tryptophan fluorescence spectroscopy: McpN-LBD and McpN-LBD R61A mutant were dialyzed into20 mM Tris/HCl, pH 7.4 and adjusted to a concentration of 5 µM. Proteins were placed into a PTI QM-2003 fluorimeter (Photon Technology International, Lawrenceville, NJ) and emission spectra from 305 to 400 nm were recorded following excitation at 295 nm. Spectra were recorded at 20 °C using a slit width of 4 nm with a scan speed of 1 nm/s. Spectra were corrected with the buffer emission spectrum.

Quantitative capillary chemotaxis assays: Assays were conducted using two different protocols that differ in the cell culture conditions. Under nitrate abundant conditions, overnight cultures in MS minimal medium supplemented with 20 mM glucose as carbon source (note: this medium contains 25 mM NH_4NO_3) were used to inoculate fresh medium to an OD_{600} of 0.05. Cells were cultured at 30 °C or 37 °C until an OD_{600} of 0.4 – 0.5. Under nitrate limiting conditions, 150 µl of an overnight culture in rich 2 x YT medium was used to inoculate 20 ml of N0 medium (MS that lacks any nitrogen source). Growth was continued for 3 hours (*Pseudomonads*) or 4.5 hours (*P. atrosepticum*) at which point cells had reached an OD_{600} of 0.15 – 0.2. For *X. campestris*, M9 minimal medium supplemented with 20 mM D-glucose, 5 mM $NaNO_3$ and 5 % (v/v) LB was used for the nitrate abundant conditions, whereas M8 minimal medium (M9 without nitrogen source) supplemented with 20 mM D-glucose and 5 % (v/v) LB was used for nitrate limiting conditions. Cells were grown for 6 hours until the OD_{600} reached 0.25 – 0.3.

For both conditions, cells were washed twice by centrifugation (1 667 x g during 6 min at 4 °C) and resuspension in chemotaxis buffer (50 mM potassium phosphate, 20 µM EDTA, 0.05 % (v/v) glycerol, pH 7.0), and then resuspended in the same buffer to an OD_{600} of 0.1. Aliquots (230 µl) of the resulting cell suspension were placed into the wells of a 96-well microtiter plate. One-microliter capillaries (Microcaps, Drummond Scientific, Ref. P1424) were heat-sealed at one end and filled with buffer (control) or chemoeffector solution prepared in chemotaxis buffer. The capillaries were immersed into the bacterial suspensions at its open end. After 30 min, capillaries were removed from the wells, rinsed with sterile water and emptied into 1 ml of chemotaxis buffer. Serial dilutions were plated onto M9 minimal medium plates supplemented with 20 mM glucose and incubated overnight at 30 or 37 °C. The number of colony forming units was determined and corrected with the buffer control.

RT-qPCR gene expression analysis: Total RNA was extracted using the High Pure RNA Isolation Kit (Roche Diagnostics) and treated with Turbo DNase (Invitrogen). RNA quality was verified by agarose gel electrophoresis and quantified spectrophotometrically. Subsequently cDNA was synthesized from 500 ng RNA using the SuperScript™ II Reverse Transcriptase (Invitrogene) and 200 ng of random hexamer primers (Roche) following the manufacturer's instructions. Quantitative PCR was performed using the iQ™ SYBR® Green supermix (Bio-Rad) in a MyiQ2 thermal cycler (Bio-Rad). The following protocol was used: 95 °C (5 min), 35 cycles of 95 °C (10 s) and 61 °C (30 s), and melting curve analysis from 55 to 95 °C, with an increment of 0.5 °C/10 s. Gene expression data were normalized to the *rpoD* reference gene. The primers used are listed in Supp. Table 16.

McpN-LBD crystallization and structure resolution: Crystallization conditions were screened using the capillary counter-diffusion technique and the commercially available crystallization Kits GCB-CSK, PEG448-49 and AS-49 (Triana Science & Technology, Granada, Spain). The protein, at 1.5 mg/ml in 20 mM Tris/HCl, 200 mM NaCl, pH 7.5 was incubated at 4 °C with 1.7 mM $NaNO_3$ and the excess of $NaNO_3$ removed by centrifugation using Amicon concentrators (3 kDa cut-off). The protein-ligand complex was loaded into 0.2 mm inner diameter capillaries and crystals of sufficient size appeared in 0.82 M K/phosphate, 0.82 M Na/phosphate, 0.1 M Na/Hepes, pH 7.5. Crystals were extracted from the capillary, flash cooled in liquid nitrogen and stored until data collection. Crystals were diffracted at beam line ID23-1 of the European Synchrotron Radiation Facility (ESRF). Data were indexed and integrated with XDS (Kabsch, 2010) and scaled with SCALA (Evans, 2006). Molecular replacement using homology models generated using the NarX (PDB ID 3EZI) and NarQ sensor domains (PDB ID 5IJI), was unsuccessful. Phases were obtained using Arcimboldo (Sammito *et al.*, 2015) and searching for two helices of 30 amino acids length. Initial refinement was initiated with Refmac (Murshudov *et al.*, 2011) and finalized with phenix.refine (Afonine *et al.*, 2012) tracking the quality with MolProbity (Chen *et al.*, 2010). Refinement statistics and quality indicators are summarized in Supp. Table 17.

Site-directed mutagenesis: An overlapping PCR mutagenesis approach was used to construct the alanine substitution mutant McpN-LBD R61A. First, a NdeI/XhoI DNA fragment of pMcpN-LBD was cloned into the same sites of pCR2.1-TOPO and transformed into *E. coli* DH5α (*dam*$^+$). Next, the resulting pCR-McpN-LBD plasmid was fully amplified by PCR using a complementary primer pair carrying the mutation. The parental plasmid was cleaved using DpnI and plasmids with the desired mutation were recirculated with T4 DNA ligase (Roche). The presence of the mutation in the resulting plasmid, pCR-McpN-R61A, was confirmed by sequencing prior to cloning into the NdeI/XhoI sites of pET28(+) to generate pMcpN-R61A (Table 14).

RESULTS

Nitrate is a specific ligand for PA2788-LBD

To identify ligands that bind to PA2788 we have cloned the DNA sequence encoding the LBD of PA2788 into an expression vector. Protein was expressed in *E. coli* and purified by affinity chromatography. High-throughput ligand screening assays using the thermal shift method (Krell, 2015) were then conducted. In this assay changes in the melting temperature (Tm) of a protein, representing the midpoint of thermal protein unfolding, are recorded. The binding of ligands typically increases the Tm and shifts superior to 2 °C are considered significant. We screened480 ligands from Biolog compound arraysPM1, PM2A, PM3B, PM4A and PM5 that serve as bacterial carbon, nitrogen, phosphorous and sulfur sources.

In the absence of ligand the Tm of PA2788-LBD was 43.5 °C. Fig. 50A shows the changes in Tm caused by each of the 95 compounds of array PM3B comprising nitrogen sources. In the presence of $NaNO_3$ the Tm was increased by 3.5 °C, whereas $NaNO_2$caused only a minor increase of 0.5 °C. No significant Tm shifts were obtained for the compounds in arrays PM1, PM2A, PM4A and PM5.

To verify ligand binding, isothermal titration calorimetry experiments were conducted. In an initial control experiment the heat changes derived from the injection of 2 mM $NaNO_3$ into buffer were recorded (Fig. 50B) showing that dilution heats were small and uniform. The titration of PA2788-LBD with the same ligand caused endothermic heat changes (ΔH=0.38 ± 0.1 kcal/mol) indicative of an entropy driven binding process ($T\Delta S$=6.4 kcal/mol) characterized by a dissociation constant of 47 ± 8 μM. The same protein was also titrated with $NaNO_2$, ammonia and uric acid (Fig. 50B), but in all cases an absence of binding was noted confirming the thermal shift assays. We were intrigued by the failure of PA2788-LBD to sense nitrite since other sensor proteins were found to sense nitrate as well as nitrite (Williams & Stewart, 1997, Lee *et al.*, 1999, Stewart, 2003). ITC titrations with ligands only provide information on higher-affinity binding events. To confirm that PA2788-LBD does not bind nitrite with low affinity, we titrated PA2788-LBD with nitrate in the absence and presence of 20 mM nitrite. In case of nitrite binding, this would alter nitrate recognition. However, this was not the case (Supp. Fig. 38A) confirming that PA2788-LBD is a nitrate-specific receptor. Following the demonstration that PA2788 binds specifically nitrate, this chemoreceptor was named McpN.

Nitrate is not recognized by the LBDs of the PilJ and PA4520 chemoreceptors

The inspection of the chemoreceptor repertoire of *P. aeruginosa* (Ortega *et al.*, 2017a) suggests that two other chemoreceptors may also bind nitrate. Firstly, the LBD of the PilJ (PA0411) receptor is composed of two consecutive PilJ domains (Ortega *et al.*, 2017a). Secondly, chemoreceptor PA4520 was predicted to contain a NIT LBD (Pfam PF08376). This domain, representing approximately 3 % of all extracellular prokaryotic LBDs (Upadhyay *et al.*, 2016), was predicted to recognize nitrate and nitrite (Shu *et al.*, 2003).

To verify whether these receptors also bind nitrate, we generated the purified individual LBDs of both receptors for thermal shift assay ligand screening using the PM3B array. In the absence of ligand, PilJ-LBD and PA4520-LBD unfolded with Tm values of 41.8 and 34.4 °C, respectively. However, in both cases no significant ligand induced Tm shifts were noted (Supp. Fig. 39 A, B) and microcalorimetric titrations confirmed the absence of $NaNO_3$ and $NaNO_2$ binding (Supp. Fig. 39C). To exclude the possibility that endothermic and exothermic contributions to binding cancel out each other at a given analysis temperature, experiments were repeated at 15 °C, which, however, produced the same result confirming the absence of nitrate/nitrite binding to PilJ-LBD and PA4520-LBD.

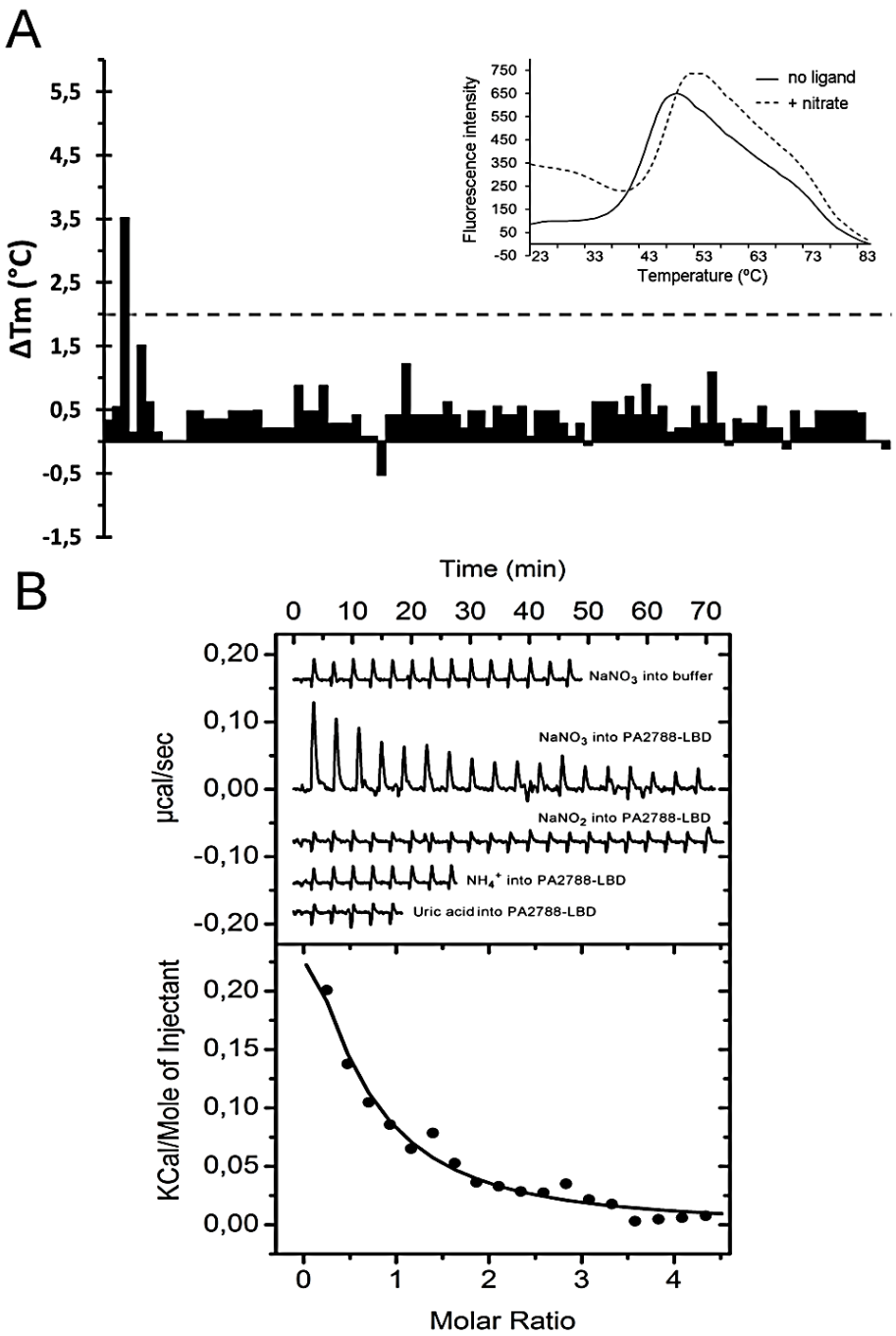

Figure 50. Identification of nitrate as PA2788-LBD ligand. A) Thermal shift assay using compounds of Biolog compound array PM3B. Shown are the Tm changes with respect to the ligand-free protein. The insert shows the thermal unfolding curves of ligand-free PA2788-LBD and in the presence of nitrate. B) Microcalorimetric binding studies of PA2788-LBD. The upper panel shows the heat changes caused by the injection of 2 mM (12.8 µl aliquots) $NaNO_3$ into buffer and 36 µM PA2788-LBD as well as the titration of PA2788-LBD with 2 mM $NaNO_2$, 2 mM ammonia and 1 mM uric acid. The lower panel depicts the concentration-normalized and dilution heat-corrected integrated peak areas of the PA2788-LBD titration data with $NaNO_3$. The line corresponds to the best fit using the "One binding site model" of the MicroCal version of ORIGIN.

McpN mediates nitrate chemotaxis under nitrate starvation conditions

To assess the function of McpN, we have conducted quantitative capillary chemotaxis assays to $NaNO_3$ using the wild type strain as well as a mutant deficient in the *mcpN* gene. These assays were conducted using the standard condition that we routinely employ to study *P. aeruginosa* chemotaxis. This assay involves cell culture in MS minimal medium supplemented with glucose (note: this medium also contains 25 mM NH_4NO_3 as N-source). However, only very minor, non-significant responses were detected over the entire nitrate concentration range (Supp. Fig. 40).

Previous studies have shown that chemotaxis to Pi in PAO1 was not observed in rich medium containing significant amounts of Pi, but was induced by Pi starvation (Wu *et al.*, 2000). We hypothesized that this may also be the case for nitrate chemotaxis and have followed a similar approach as Wu *et al.* (Wu *et al.*, 2000). Thus, cells were pre-cultured in the rich 2xYT medium, then diluted 133-fold into the N0 medium that lacks nitrogen sources and continued to grow for another 3 h. Under these conditions strong chemotactic responses towards $NaNO_3$ were obtained. Initial significant responses were obtained at a $NaNO_3$ concentration of 5 μM, whereas maximal responses were observed at 500 μM (Fig. 51). No nitrate chemotaxis was observed for the *mcpN* mutant, suggesting that it is the sole nitrate chemotaxis receptor. The complementation of this mutant with a plasmid harboring the *mcpN* gene restored nitrate chemotaxis (Fig. 51).

To identify the possible role of the PilJ receptor and the NIT domain containing PA4520 chemoreceptor in nitrate chemotaxis, the single mutants of the corresponding genes were also analyzed. As shown in Fig. 51A, their responses to nitrate were similar to the *wt* strain confirming that the observed nitrate chemotaxis is solely mediated by McpN.

Nitrate reduces *mcpN* transcript levels

To explain the absence of taxis in nitrate abundant conditions we hypothesized that nitrate may repress the expression of the *mcpN* gene. To verify this hypothesis, we have quantified *mcpN* transcript levels by reverse transcription quantitative PCR (RT-qPCR). These assays were carried out using RNA from cells grown using the same protocol used for the chemotaxis assays under nitrate abundant and limiting conditions. As shown in Fig. 51B, *mcpN* transcript levels were approximately 16 times higher in nitrate-limiting conditions as compared to nitrate-abundant conditions. To verify that the absence or presence of nitrate is the cause for these differences, $NaNO_3$ to a final concentration of 1 mM was added to these cultures and samples for RT-qPCR experiments were taken after another 20 and 40 min of growth. The results show that the addition of nitrate to cells grown under nitrate-limiting conditions reduced *mcpN* transcript levels to those seen under nitrate-abundant conditions, indicating that nitrate reduces *mcpN* expression (Fig. 51B).

The NarX/NarL TCS senses nitrate and regulates genes involved in nitrate metabolism (Van Alst *et al.*, 2009). To identify a potential role of this TCS in *mcpN* expression, we quantified *mcpN* transcript levels in a mutant defective in the gene encoding the NarX sensor kinase. However, RT-qPCR data revealed no statistical differences in the transcript levels of *mcpN* (Fig. 51B).

McpN signals through the Che pathway

The twenty six PAO1 chemoreceptor signal through four different chemosensory pathways and McpN was predicted to signal through the Che pathway (Ortega *et al.*, 2017b). To verify this prediction, we have conducted chemotaxis assays to $NaNO_3$ using mutants defective in the genes encoding the CheA paralogues of the Che ($CheA_1$) and Che2 ($CheA_2$) pathways. As shown in Supp. Fig. 41, no nitrate chemotaxis was observed in the *cheA1* mutant, whereas responses of the *cheA2* mutant were comparable to wt levels. These results thus confirm that McpN signals through the Che pathway (Ortega *et al.*, 2017b).

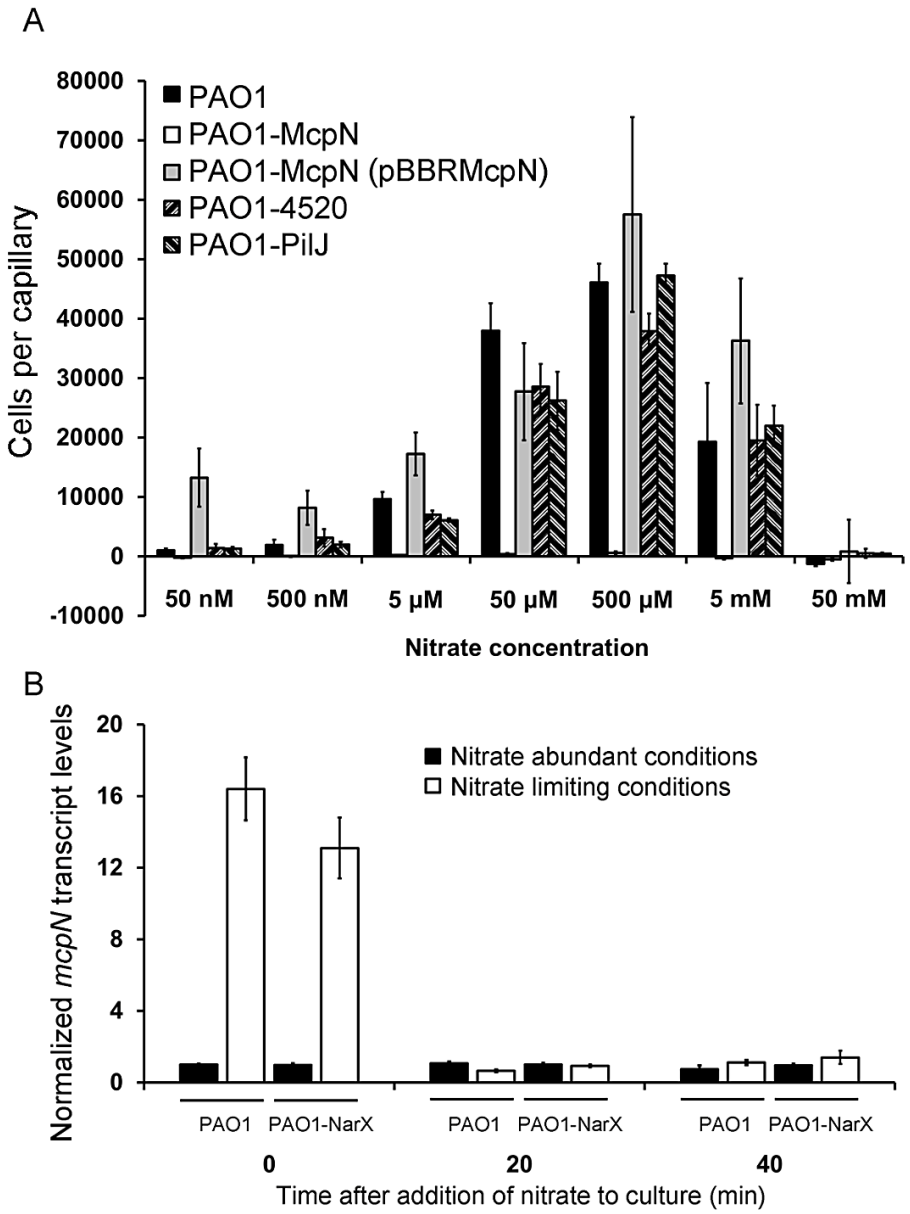

Figure 51. The McpN chemoreceptor of *P. aeruginosa* mediates nitrate chemotaxis. A) Quantitative capillary chemotaxis assays of different *P. aeruginosa* PAO1 strains to different $NaNO_3$ concentrations. Cells were grown in rich 2 x YT medium and then diluted 133-fold into the N0 medium, deficient in nitrogen sources. Data are means of three biological replicates conducted in triplicate. B) RT-qPCR analysis of the mcpN transcript in the wild type strain and a mutant defective in the NarX sensor kinase. Cells were gown in MS medium supplemented with glucose (containing 25 mM NH_4NO_3) or in nitrate deficient medium N0 (inoculated using a culture grown in 2xYT medium) until an $OD_{600}$of 0.15 at which point (time 0) $NaNO_3$ to a final concentration of 1 mM was added. Further samples were taken after 20 and 40 min. Shown are mcpN transcript levels normalized with respect to the transcript levels of the reference gene rpoD at time 0 in nitrate abundant conditions. Data are means and standard deviation from three biological replicates conducted in triplicate.

The three dimensional structure of McpN-LBD

McpN-LBD in complex with nitrate was crystallized in a buffer at pH 7.5 and its structure was resolved by X-ray crystallography to a resolution of 1.3 Å. According to the Matthews coefficient, the unit cell accommodates three chains. A structural alignment of these three chains resulted in RMSD below 0.5, indicating that these chains can be considered as identical. Chains A and B of the unit cell form a dimer (Fig. 52A), whereas chain C forms another dimer with a symmetry related chain. The McpN-LBD monomer is composed of 4 α-helices that pack into a 4-helix bundle. Dimerization is achieved through the interaction of 22 residues of chains A and B that establish 16 hydrogen bonds and occlude a surface of approximately 1100 $Å^2$ in each monomer.

A single molecule of nitrate is bound to a site with positive surface charge at the dimer interface. The binding site is situated on the dimer symmetry axis and consequently the same amino acids from both monomers establish interactions with bound nitrate. Whereas G58, A59 and M62 establish non-bonded contacts, R61 played a key role in recognition since it forms two hydrogen bonds with nitrate (Fig. 52B). To verify the role of R61 we have generated the McpN-LBD R61A mutant. The intrinsic tryptophan fluorescence emission spectrum (Supp. Fig. 42A) and the thermal unfolding properties of the mutant protein (Fig. 50, Supp. Fig. 42B) were comparable to that of the native protein indicating that this amino acid replacement did not cause major changes to the overall protein structure. Analysis of this protein by the thermal shift assay and ITC showed that this protein is unable to recognize nitrate (Supp. Fig. 42B, C).

The McpN-LBD structure was aligned to all structures currently deposited in the protein data bank using the DALI algorithm and closest structural homologues are listed in Table 15. Surprisingly, the closest structure was a LBD of a histidine kinase that belonged to a different family, namely CHASE3. The closeness of the structural similarity between this domain and McpN-LBD is illustrated in Fig. 53A. The only chemoreceptor LBD with significant structural similarity was the HBM domain of the McpS chemoreceptor that is composed of two 4-helix bundles (Pineda-Molina *et al.*, 2012).

Nitrate binding promotes McpN-LBD dimerization

Analytical ultracentrifugation experiments were conducted to assess the oligomeric state of McpN-LBD. Initially, we used the three dimensional structure of McpN-LBD to calculate the expected sedimentation coefficients using the HYDROPRO (Ortega *et al.*, 2011) software. This analysis resulted in $s_{20,w}$ values of 1.7 S and 2.8 S (at 20 degrees and water) for the monomeric and dimeric species, respectively.

Sedimentation velocity experiments were performed on 5 μM to 40 μM McpN-LBD in the absence of ligand and data obtained with 10 and 20 μM protein are shown in Fig. 52D. At 10 μM two peaks could be identified with $s_{20,w}$ values of 1.85 S and $s_{20,w}$ = 2.69 S, that fit well with the values for the monomer and dimer, respectively. At 20 μM and 40 μM, only protein dimers were observed indicating that the equilibrium has shifted completely to this oligomeric state. To assess the effect of nitrate binding on the oligomeric state, the above experiments were repeated in the presence of saturating nitrate concentrations. No changes in oligomeric state occurred at the 20 and 40 μM concentrations, whereas at 10 μM protein a single peak with $s_{20,w}$ = 2.79 S (Fig. 52D) was obtained indicating that nitrate binding has shifted the equilibrium entirely to the dimeric state. Taken together, data indicate that McpN-LBD is present in a monomer-dimer equilibrium and that nitrate binding stabilizes the dimeric state.

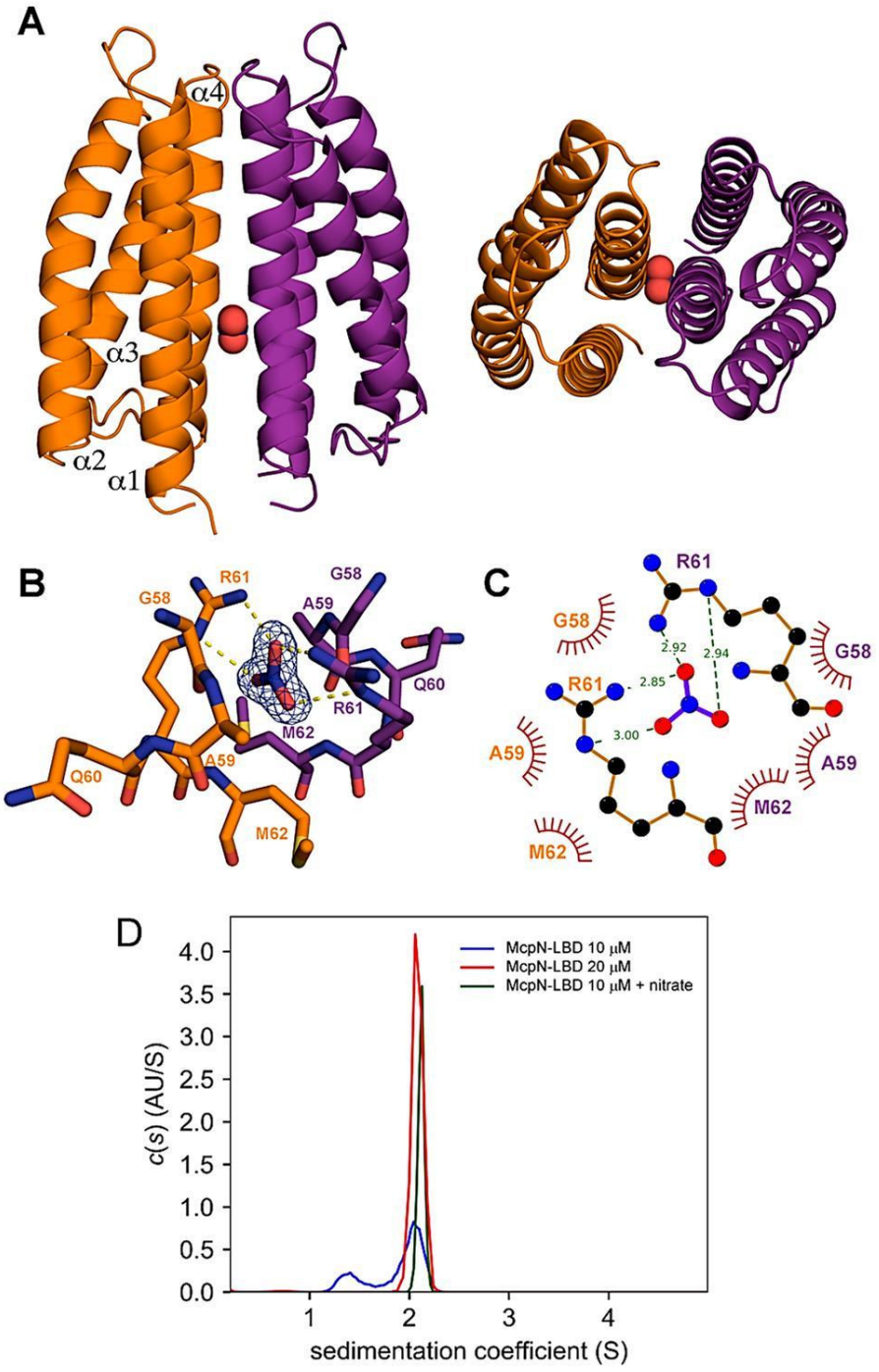

Figure 52. The three-dimensional structure of McpN-LBD in complex with nitrate. A) Side and tope view of the overall structure. Nitrate is shown in red. B) The nitrate binding pocket. Shown are amino acids from both chains that interact with nitrate. The |2Fo-Fc| electron density of nitrate is contoured at 1.5 sigma. C) Schematic representation of amino acids involved in hydrogen bonding to nitrate, shown as dotted lines, while the spoked arcs represent residues that make non-bonded contacts. D) Analysis of the oligomeric state of McpN-LBD using sedimentation velocity analytical ultracentrifugation. Shown are the sedimentation velocity c(s) profiles of ligand-free McpN-LBD at different concentrations and protein in complex with nitrate.

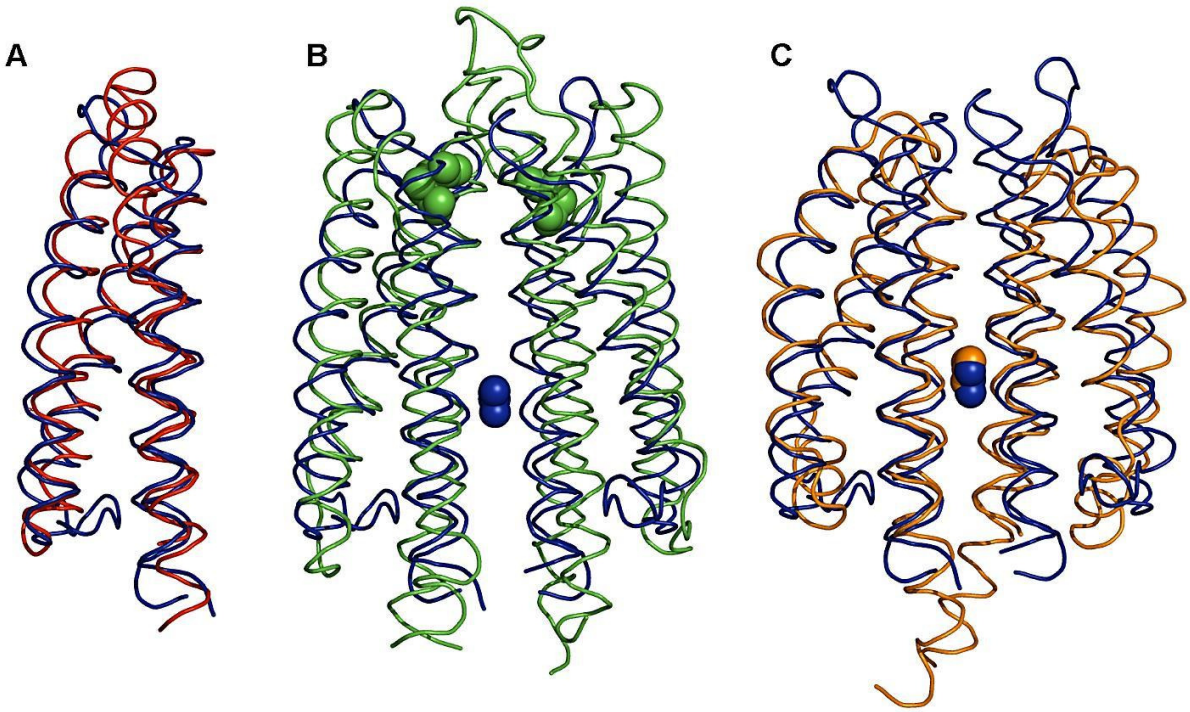

Figure 53. Structural alignment of the McpN-LBD C_α chain with structural homologues. In all cases McpN-LBD is shown in blue. A) Alignment with a CHASE3 domain of an uncharacterized histidine kinase of *Rhodopseudomonas palustris* (PDB ID 3VA9), the closest structural homologue in a DALI search (Table 1). B) Alignment with Tar-LBD (PDB ID 1VLT); bound aspartate (Tar) is shown in green, whereas bound nitrate (McpN) is shown in blue. C) Alignment with the sensor domain of the NarX histidine kinase (PDB ID 3EZH). Bound nitrate overlap and are shown in blue (McpN) and orange (NarX).

Definition of the N-box

To identify potential McpN homologues in other species we have conducted a BLAST-P search of McpN-LBD in the NCBI database of non-redundant protein sequences excluding members of the *Pseudomonas* genus. An alignment of the top 87 sequences is shown in Supp. Fig. 43. All sequences belong to the PilJ family and form part of chemoreceptors. Most of the corresponding species were marine bacteria and a significant part of them are able to oxidize elemental sulfur or sulfite (Supp. Table 15). Furthermore, a number of human pathogens such as *Enterobacter cloacae*, *Streptococcus pneumoniae* or *Eggerthia catenaformis* were among the species that harbor McpN homologues (Supp. Table 15).

The sequence alignment of McpN-LBD homologues revealed only a very modest overall sequence identity of approximately 5 %. However, the zone around the nitrate binding site, which we have termed N-box, was highly conserved and the corresponding sequence logo is shown in Fig. 54A. We have shown above that not all PilJ domains bind nitrate, since no binding was observed for the PilJ-LBD that is composed of two PilJ domains (Supp. Fig. 38). As shown in Supp. Fig. 44, the N-box was not conserved in neither of the PilJ domains of the PilJ chemoreceptor. Using PROSITE (Sigrist *et al.*, 2013) we have then scanned the TrEMBL database using consensus pattern for the N-box,[IVL]-[ND]-x-A-G-x-Q-R-M-L-[ST]-Q. The random statistical probability of a match was well below 1 sequence.

Table 15. Structural alignment of McpN-LBD with structures deposited in the Protein Data Bank. Shown are the structures with a Z-score above 10. Structures share less than 90 % of sequence similarity amongst each other.

Pdb ID	Protein type	Species	Ligands	Pfam/ InterPro	Z score	Aligned residues	Seq. Id. %	Ref.
3va9	LBD of HK9 SK[1]	*Rhodopseudomonas palustris*	-	CHASE3 (PF05227)	13.6	114	13	UP[1]
5xsj	LBD of LytS SK	*Clostridium beijerinckii*	XylFII ligand binding protein	Un-annotated	13.3	112	6	(Li *et al.*, 2017a)
4k0d	LBD of Adeh_2942 SK	*Anaeromyxobacter dehalogenans*	-	Un-annotated	12.3	117	17	(Pokkuluri *et al.*, 2013)
2yfb	LBD of McpS CR[1]	*P. putida*	TCA cycle intermediates	HBM (PF16591)	12.0	113	12	(Pineda-Molina *et al.*, 2012)
3ezh	LBD of NarX SK	*E. coli*	Nitrate/ nitrite	PilJ (PF13675)	11.9	104	21	(Cheung & Hendrickson, 2009)
3o1j	LBD of TorS SK	*Vibrio parahaemolyticus*	TorT periplasmic binding protein	TorS-like (IPR038188)	11.2	111	14	(Moore & Hendrickson, 2012)
4igg	α-catenin	*Homo sapiens*	β-catenin	VINCULIN (PF01044)	10.7	114	5	(Rangarajan & Izard, 2013)
5jeq	LBD of NarQ SK	*E. coli*	Nitrate/ nitrite	PilJ (PF13675)	10.6	103	15	(Gushchin *et al.*, 2017)
5xa5	α-catenin	*Caenorhabditis elegans*	β-catenin	VINCULIN (PF01044)	10.4	110	7	(Rangarajan & Izard, 2013)
5xfl	α-catenin	*Mus musculus*	β-catenin	VINCULIN (PF01044)	10.3	114	5	(Rangarajan & Izard, 2013)

[1] SK: sensor kinase, CR: chemoreceptor, UP: unpublished, Seq. Id.: sequence identity

However, 941 sequences containing PilJ domains were retrieved, which are likely to be nitrate binding domains. Retrieved sequences form part of all major families of signal transduction systems, namely transcriptional regulators, sensor kinases, chemoreceptors and diguanylate cyclases. At the time of search there were 1135 protein sequences with at least one PilJ domain in Pfam and the N-box may be a means to identify PilJ domains that are able to bind nitrate.

Nitrate chemotaxis in other bacterial species

Subsequent work was aimed at assessing nitrate chemotaxis in other species. To this end we have conducted quantitative capillary chemotaxis assays using different strains grown under nitrate abundant and limiting conditions. *P. putida* KT2440 and *P. fluorescens* KU-7 do not have a McpN homologue, but contain, as *P. aeruginosa,* a NIT domain containing chemoreceptor. Our experimentsshow that *P. putida* KT2440was devoid of nitrate chemotaxis whereas *P. fluorescens* showed only some minor responses to 50 mM nitrate (Fig. 55).

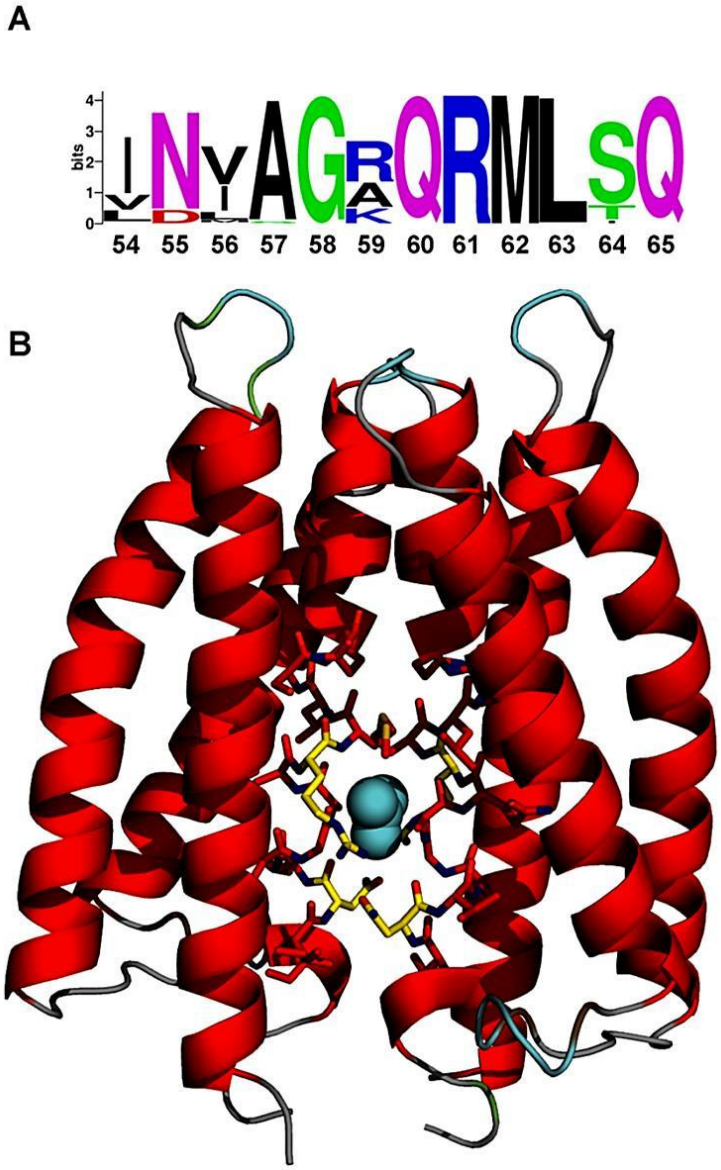

Figure 54. Definition of the N-box of PilJ domains. A) The sequence logo of the N-box as derived from the alignment shown in Fig. S6. B) Structure of McpN-LBD in which the 12 amino-acids of the N-box are shown as sticks together with bound nitrate.

We then studied two bacterial species that are among the top 10 plant pathogenic bacteria (Mansfield *et al.*, 2012), namely *Pectobacterium atrosepticum* and *Xanthomonas campestris* pv. *campestris*. Interestingly, responses of *P. atrosepticum* were very similar to that of PAO1, since only very minor responses were observed in nitrate-abundance, but strong responses under nitrate-starvation (Fig. 55). Among the 36 chemoreceptors of this strain there is no McpN homologue, but a single receptor with a NIT domain. *X. campestris* pv. *campestris* showed also significant chemotaxis under nitrate-limiting conditions and only minor responses in nitrate-abundance (Fig. 55). Altogether, these data suggest that the induction of nitrate chemotaxis by nitrate-limitation is common to other bacteria.

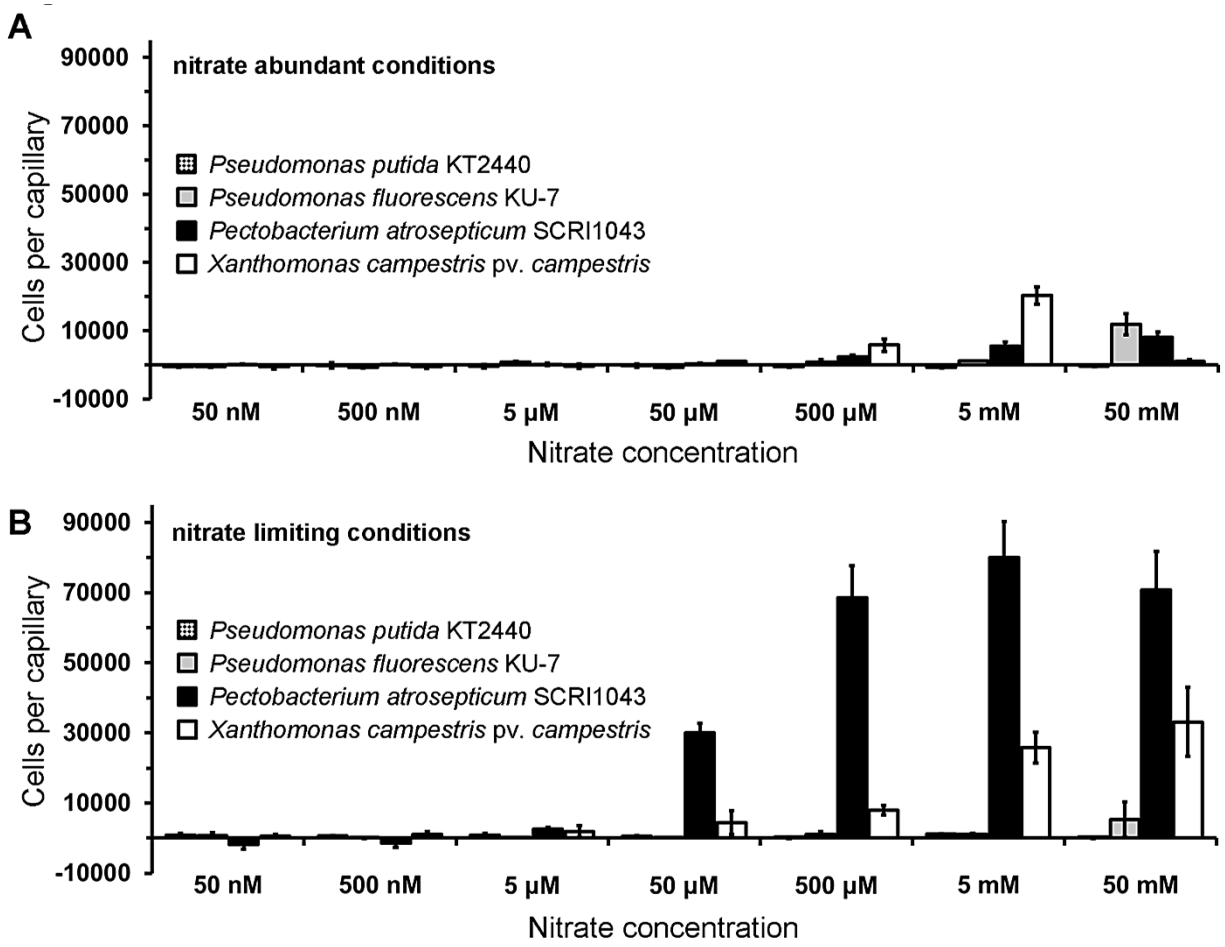

Figure 55. Quantitative capillary chemotaxis assays of different strains to $NaNO_3$. A) Cells grown in nitrate abundant conditions. B) Cells grown in nitrate limiting conditions. Data are means and standard deviations from three biological replicates conducted in triplicate.

DISCUSSION

Nitrate is a final electron acceptor for anaerobic respiration and also serves as nitrogen source for aerobic growth. Taxis to nitrate has been observed for a significant number of bacteria such as *E. coli, S. typhimurium* (Taylor *et al.*, 1979, Rivera-Chavez *et al.*, 2016), *Pseudomonas* spp. (Kennedy & Lawless, 1985, Emerson, 1999, Roush *et al.*, 2006, Dennis *et al.*, 2013), *Shewanella* spp. (Nealson *et al.*, 1995, Baraquet *et al.*, 2009), *Azospirillum brasilense* (Greer-Phillips *et al.*, 2004), *Rhodobacter sphaeroides, Agrobacterium tumefaciens* (Lee *et al.*, 2002), *Thioploca* spp. (Zopfi *et al.*, 2001) or *Synechococcus* spp. (Willey & Waterbury, 1989). The three major bacterial pathways for nitrate metabolism include respiratory, assimilatory and dissimilatory nitrate reduction (Sparacino-Watkins *et al.*, 2014) and any type of metabolism can lead to energy taxis. In some of the cases it has been demonstrated that bacterial nitrate taxis is based on energy taxis (Lee *et al.*, 2002, Greer-Phillips *et al.*, 2004, Baraquet *et al.*, 2009, Rivera-Chavez *et al.*, 2016). For example, the deletion or inhibition of enzymes that participate in nitrate metabolism abolished nitrate taxis (Baraquet *et al.*, 2009). In other reports the molecular mechanism of nitrate taxis is unclear such as for example in the case of lake water bacteria (Dennis *et al.*, 2013) or different denitrifying strains (Kennedy &

Lawless, 1985, Roush *et al.*, 2006). It is possible that these observations are based on chemotaxis. Here we identify the molecular mechanism of nitrate-specific chemotaxis that is initiated by the specific recognition of nitrate at a periplasmic chemoreceptor LBD. McpN homologues show a broad phylogenetic distribution including archaea and bacteria belonging to the Firmicutes and Proteobacteria phyla (Supp. Table 15), as an indication that nitrate chemotaxis may be a widespread mechanism.

Interestingly, among the species that harbor McpN homologues were a significant number of bacteria isolated form marine sediments that are able to oxidize sulfide or elemental sulfur (Supp. Table 15). In these bacteria there is evidence that the oxidation of reduced sulfur compounds is coupled to the reduction of electron acceptors such as nitrate (Xie *et al.*, 2011). As a consequence some sulfide oxidizers were found to store nitrate in vacuoles (Schulz *et al.*, 1999) up to a concentration of 370 mM (McHatton *et al.*, 1996, Ahmad *et al.*, 1999). This intracellular nitrate is used to oxidize sulfide in deeper anoxic zones of sediments. This process has been particularly well studied in *Beggiatoa* spp. (Preisler *et al.*, 2007), which are also among the species that contain an McpN homologue (Supp. Table 15). Based on experiments with nitrate reducing/sulfide oxidizing shelf sediment bacteria belonging to the *Thioploca* genus, a functional model was proposed (Zopfi *et al.*, 2001). The authors show that the nitrate concentration in the sediment is lower than that of the flume water and nitrate chemotaxis was shown to direct bacteria to the sediment surface, where they fill their vacuoles with nitrate. They then migrate back into deeper sediment layers where they oxidize sulfide to sulfate until nitrate is depleted that induces the upward movement. Taken together, data thus suggest a particular importance of nitrate chemotaxis in marine sulfide/sulfur oxidizing bacteria.

Nitrate serves PAO1 as sole nitrogen source for growth and the anaerobic growth of this strain is accomplished through the denitrification enzyme pathway that catalyzes the sequential reduction of nitrate to nitrogen gas (Van Alst *et al.*, 2007). Nitrate chemotaxis was observed in pathogenic *P. aeruginosa* but not in the non-pathogenic *P. putida* and *P. fluorescens*, suggesting that it may be related to virulence. Previous studies have shown a link between virulence and nitrate metabolism for anaerobically grown PAO1 since a mutant in the nitrate reductase was avirulent in *C. elegans* (Van Alst *et al.*, 2007). PAO1 causes airway infections in cystic fibrosis patients and the sputum nitrate/nitrite concentration was with 774 μM in cystic fibrosis patients well above the healthy control group (421 μM)(Linnane *et al.*, 1998). Importantly, these concentrations are in the range of optimal chemotaxis responses measured (Fig. 51) indicating that nitrate chemotaxis may be related to pathogenicity, like in *S. typhimurium,* where taxis to host-derived nitrate is required for efficient host infection (Rivera-Chavez *et al.*, 2016).

PAO1 nitrate chemotaxis was only observed under nitrate starvation conditions (Fig. 51A), whereas no taxis was observed in nitrate abundance (Supp. Fig. 40), and similar observation have been made for *P. atrosepticum* (Fig. 55). This is unusual since chemotactic behaviors are typically either constitutive or inducible by the chemoeffector (Parales, 2004, Shi *et al.*, 2017). However, striking similarities exist between Pi and nitrate chemotaxis in PAO1. Pi taxis was only observed under Pi starvation and not in Pi abundance (Wu *et al.*, 2000, Rico-Jimenez *et al.*, 2016). As in the case of *mcpN,* Pi was shown to decrease the transcript levels of both Pi chemoreceptor genes, *ctpL* and *ctpH* (Bains *et al.*, 2012). Pi was identified as a key signal molecule that controls the expression of many virulence genes and features in PAO1 (Zaborin *et al.*, 2009, Bains *et al.*, 2012). Pi and nitrate are both inorganic anions and it is tempting to speculate that chemotaxis repression by chemoeffector abundance is a feature of this compound family.

Almost one third of all chemoreceptor LBDs are recognized by the Pfam 4HB domain signature (Ortega *et al.*, 2017a). Signaling of chemoreceptors with this domain has been extensively studied and the 3D structure reveals a 4-helix antiparallel bundle (Milburn *et al.*, 1991, Ottemann *et al.*, 1999). Although the McpN-LBD sequence is not recognized by the Pfam 4HB signature, its structure superimposes very well with that of the 4HB Tar-LBD (Fig. 53B). This, together with the

fact that the closest structural McpN-LBD homologue is a CHASE3 domain (Table 15), demonstrates that the4-helix bundle is a conserved structural motif for ligand sensing formed by members of different LBD families. Although conserved in structure, the mode of ligand binding for McpN-LBD and Tar-LBD is different. The Tar-LBD dimer recognizes with high negative cooperativity two signal molecules that bind to the dimer interface at two sites that are not on the dimer symmetry axis (Milburn *et al.*, 1991, Milligan & Koshland, 1993). In contrast, a single molecule of nitrate binds to a single site located at the dimer symmetry axis of McpN-LBD (Fig. 52A). However, 4HB domains and McpN-LBD (Fig. 52D) have in common that the individual domains are present in a monomer-dimer equilibrium and that ligand binding shifts this equilibrium to the dimeric state (Milligan & Koshland, 1993, Fernandez *et al.*, 2017).

The NarX/NarL and NarQ/NarP two-component systems control transcriptional responses to nitrate and nitrite that are the preferred anaerobic electron acceptors in *E. coli* (Noriega *et al.*, 2010). The LBDs of the NarX and NarQ sensor kinases are structural homologs of McpN-LBD (Table 15) and their 3D structures have been solved in complex with nitrate (Cheung & Hendrickson, 2009, Gushchin *et al.*, 2017). Although McpN-LBD and NarX-LBD share only 21 % sequence identify, their structures align very well and the nitrate binding site is conserved (Fig. 53C). McpN-LBD differs from NarX-LBD in several aspects. Our AUC studies show that McpN-LBD has an intrinsic propensity to dimerize which is enhanced in the presence of nitrate. In contrast, NarX-LBD is monomeric even at a concentration of 10 mM and in the presence of nitrate (Cheung & Hendrickson, 2009). NarX and NarQ are characterized by a certain plasticity in ligand recognition since they bind to nitrate, nitrite and sulfite (Williams & Stewart, 1997, Lee *et al.*, 1999, Stewart, 2003). In contrast, McpN-LBD recognizes exclusively nitrate and has no physiologically relevant affinity for nitrite (Fig. 50, Supp. Fig. 38A). The superimposition of the ligand binding pockets of NarX-LBD and McpN-LBD (Supp. Fig. 38B) does not provide any obvious reason for this difference in ligand specificity.

The NIT domain is present in different signal transduction protein families and was proposed to be a sensor domain for nitrate and nitrite (Shu *et al.*, 2003). However, the recombinant NIT domain of PA4520 did not bind nitrate or nitrite (Supp. Fig. 39) and a mutant defective in this receptor was not affected in nitrate chemotaxis (Fig. 51). In addition, *P. putida* and *P. fluorescens* both possess a NIT domain containing chemoreceptor, which, however, did not mediate nitrate chemotaxis under the experimental conditions tested (Fig. 55). The NIT domain may thus be a superfamily that contains subfamilies with different ligand binding properties and biological functions.

The demonstration of specific nitrate chemotaxis as reported here widens the range of known chemoeffectors and provides the basis for an assessment of this phenotype in other bacteria and for the elucidation of its physiological relevance.

SUPPLEMENTARY MATERIAL

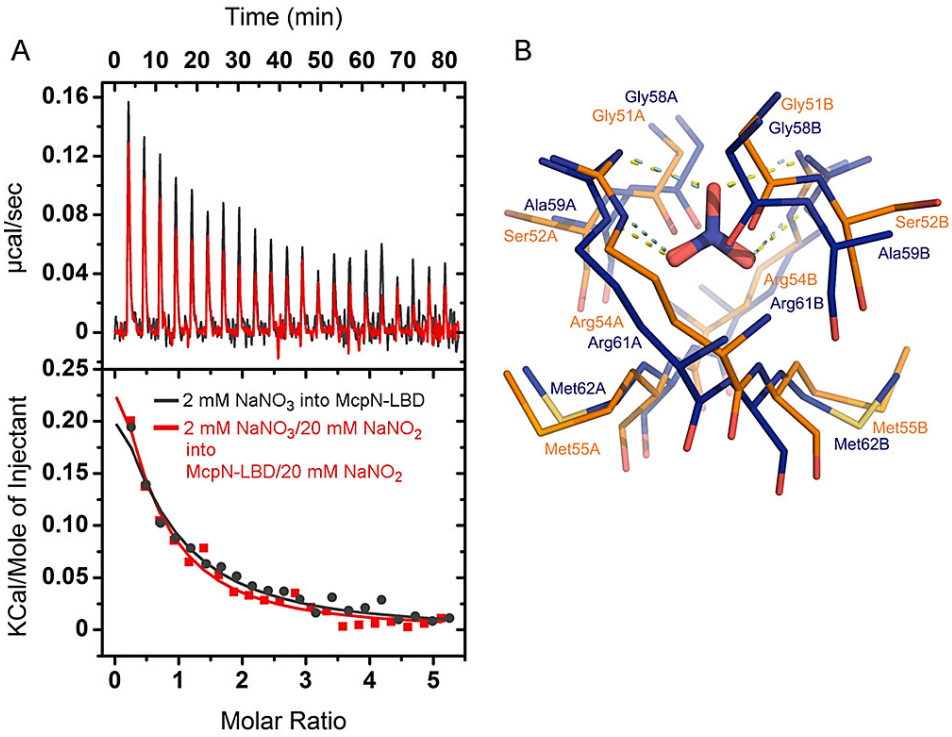

Supp. Fig 38. Specificity of nitrate recognition at McpN-LBD. A) Microcalorimetric titration of McpN-LBD with $NaNO_3$ in the absence and presence of 20 mM $NaNO_2$. Upper panel: In black: raw data for the titration of 36 µM McpN-LBD with 12,8 µl aliquots of 2 mM $NaNO_3$. In red: repetition of the experiment with both ligands containing in addition 20 mM $NaNO_2$. Lower panel: Concentration normalized and dilution heat corrected integrated peak areas of raw data. The continuous lines are the curve fits using the "One binding site model" of ORIGIN. B) Superimposition of the nitrate molecule in the structures of McpN-LBD (in blue) and NarX-LBD (in orange, pdb ID 3EZH). Shown are the amino acid residues in the vicinity of bound nitrate. Hydrogen bonds are indicated by dotted lines.

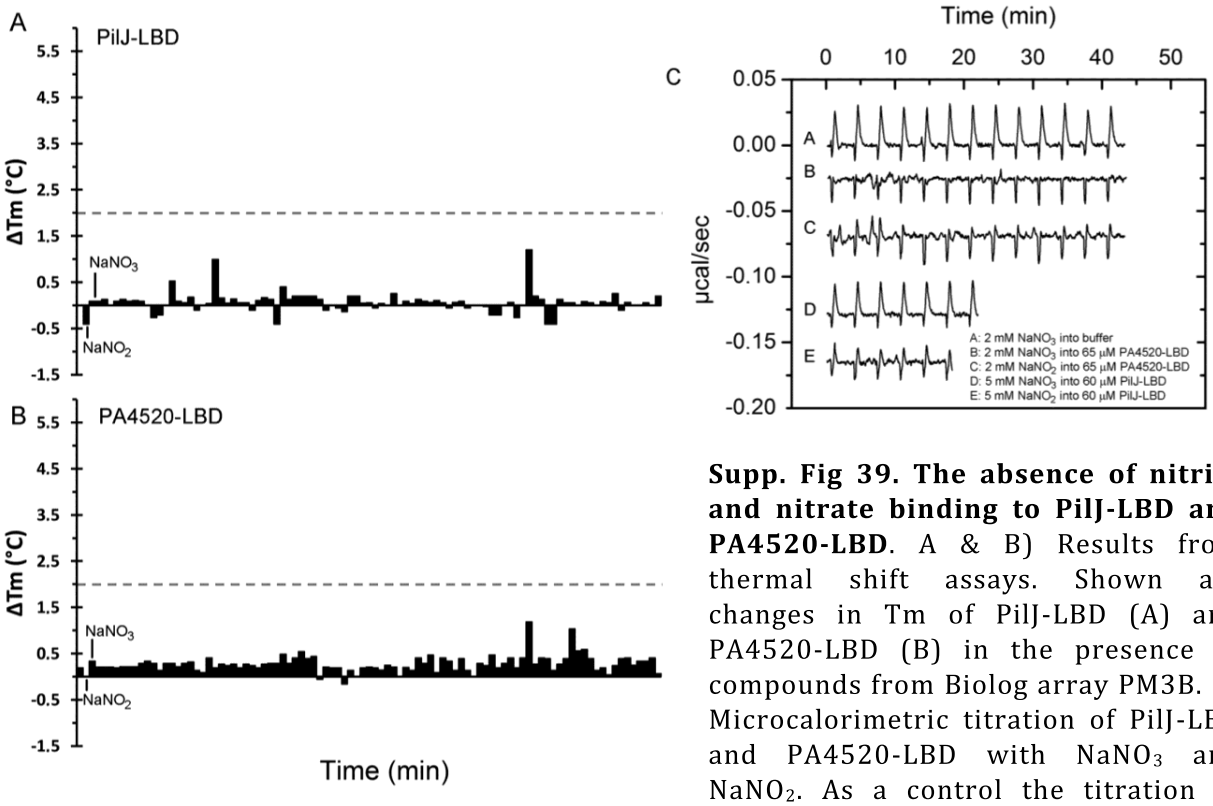

Supp. Fig 39. The absence of nitrite and nitrate binding to PilJ-LBD and PA4520-LBD. A & B) Results from thermal shift assays. Shown are changes in Tm of PilJ-LBD (A) and PA4520-LBD (B) in the presence of compounds from Biolog array PM3B. C) Microcalorimetric titration of PilJ-LBD and PA4520-LBD with $NaNO_3$ and $NaNO_2$. As a control the titration of buffer with $NaNO_3$ is shown. The injection volume was 19.2 µl.

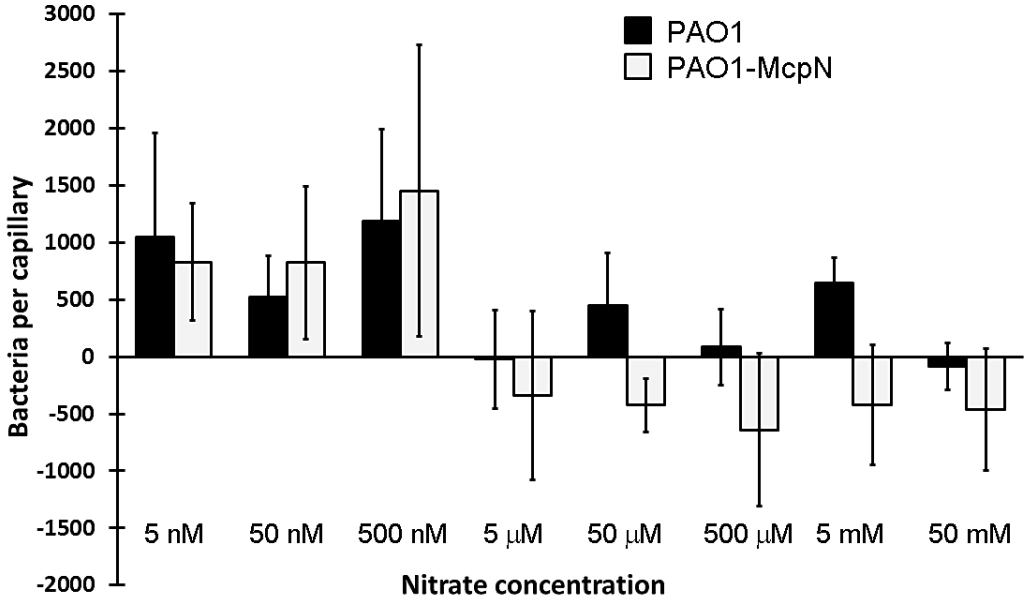

Supp. Fig 40. Quantitative capillary chemotaxis assays of *P. aeruginosa* PAO1 and the *mcpN* mutant under nitrate abundant conditions. Cells were grown in M9 minimal medium supplemented with glucose as carbon source. This medium contains 25 mM ammonium nitrate as nitrogen source. Data were corrected using the number of cells that swam into buffer containing capillaries (1992 ± 298).

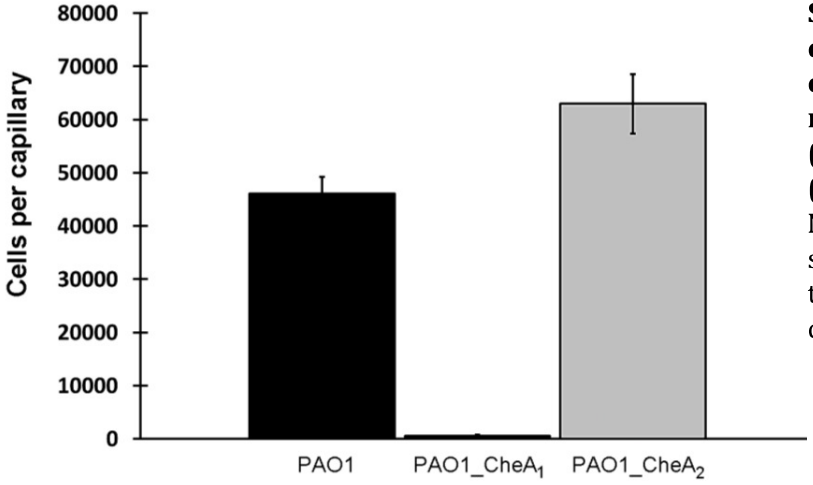

Supp. Fig 41. Quantitative capillary chemotaxis assays of *P. aeruginosa* PAO1 and mutants deficient in *cheA1* (*PA1458*) and *cheA2* (*PA0178*) towards 500 µM $NaNO_3$. Data are means and standard deviations from three biological replicates conducted in triplicate.

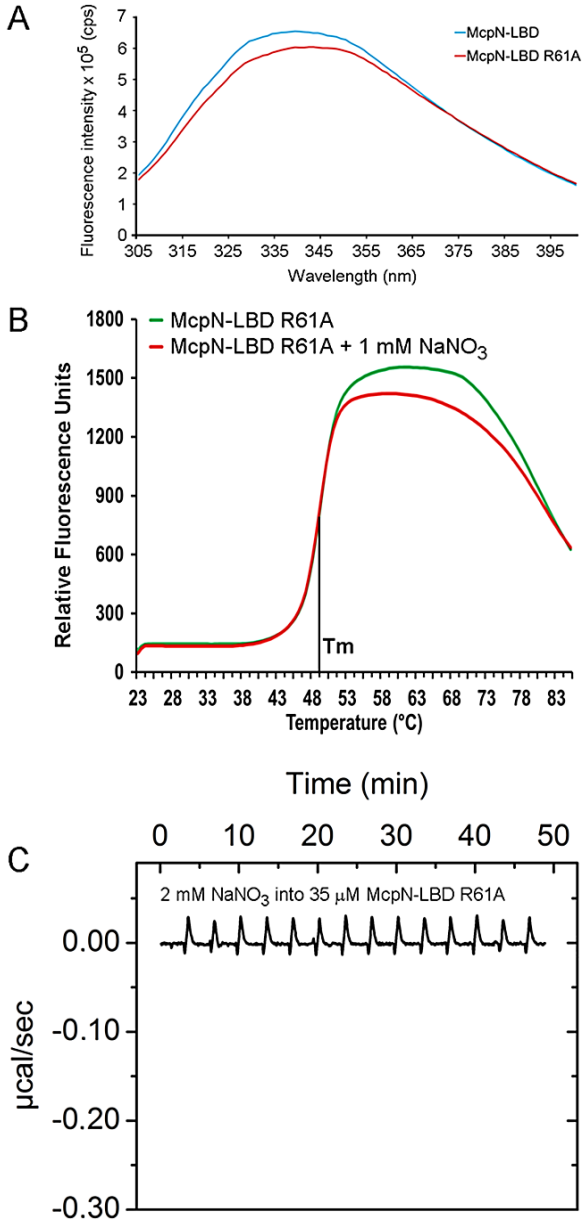

Supp. Fig 42. Analysis of the McpN-LBD R61A mutant. A) Intrinsic tryptophan fluorescence emission spectra of McpN-LBD and McpN-LBD R61A. B) Thermal shift assay of McpN-LBD R61A in the absence and presence of $NaNO_3$. C) Microcalorimetric titration of McpN-LBD R61A with $NaNO_3$.

```
                                                          120       130       140       150       160
                                                           |         |         |         |         |
WP_083651730 [Photobacterium proteolyticum]               GIIYYGMEA-DAATINVAGRQRMLSQRVAKEVLLVQSGMEQ----QEGVNKTIKL
OLQ80001 [Photobacterium proteolyticum]                   GIIYYGMEA-DAATINVAGRQRMLSQRVAKEVLLVQSGMEQ----QEGVNKTIKL
EDQ01086 [Shewanella benthica KT99]                       AIIYNDMQA-DAATINIAGRQRMLSQLVAKEVLLLQFGVGR----DTGVKKAIEL
WP_040571760 [Shewanella benthica]                        AIIYNDMQA-DAATINIAGRQRMLSQLVAKEVLLLQFGVGR----DTGVKKAIEL
WP_022940319 [Psychromonas hadalis]                       SIIYSSMEA-DATTINVAGKQRMLSQRIAKEVLLVQFSSLE----KQQVQQTITQ
WP_104417027 [Marinobacter persicus]                      SFLYFSTDPGEARSLNVAGAQRMLSQRVAKEVQMVAAGVEE----PAQAQKTIEQ
KXS52579 [Marinobacter sp. T13-3]                         SFLYFSTDPGEARSLNVAGAQRMLSQRVAMEVQMVAAGVED----PAQAQKTIEQ
KXS51160 [Marinobacter sp. T13-3]                         SFLYFSTDPGEARSLNVAGAQRMLSQRVAKEVQMVAAGVEE----PAQAQKTIEQ
WP_104425587 [Marinobacter persicus]                      SFLYFSTDPGEAKSLNVAGAQRMLSQRVAKEVQMVAAGVEE----SSQAQQTIDQ
WP_104416353 [Marinobacter persicus]                      SFLYFSTDPGEAKSLNVAGAQRMLSQRVAKEVQMVAAGVEE----SSQAQQTIDQ
PKM00178 [Gammaproteobacteria bacterium HGW]              -----SSK--DASQIDMAGAQRMLSQKMMKEALLAAQGIGS----PADVDRTIQR
PKM12203 [Gammaproteobacteria bacterium HGW]              AVLFMSAK--DASQIDMAGAQRMLSQKMMKEALLAAQGVGD----KAAVDKTIQR
CJK46151 [Streptococcus pneumoniae]                       GVLFMSSK--DASQIDMAGAQRMLSQKMMKEALLAAQGIGS----PADVDKTIQR
McpN [P. aeruginosa PAO1]                                 VALYLSMSI-SPETINVAGAQRMLSQKMAREALQLRLGAGD----PKALAATIAQ
OUC50533 [Eggerthia catenaformis]                         VALYLSMSI-SPETINVAGAQRMLSQKMAREALQLRLGAGD----PKALAATIAQ
SAJ26551 [Enterobacter cloacae]                           VALYLSMSI-SPETINVAGAQRMLSQKMAREALQLRLGAGD----PKALAATIAQ
PKM29122 [Gammaproteobacteria-12]                         VALYLSMSV-SPETINIAGAQRMLSQKMTKEALLQREGVLP----AATLEATMAQ
WP_027848104 [Marinospirillum minutulum]                  VSLYMSLSV-SPETINVAGAQRMLSQKMTKEALLITQGVEE----RKVLDSTINS
WP_027850591 [Marinospirillum insulare]                   ISLYMSLSV-SPETINVAGAQRMLSQKMTKEALLIIGKVEN----KTVLDKTVAS
WP_072325584 [Marinospirillum alkaliphilum]               VSLYMSLSV-SPETINVAGAQRMLSQKMTKEALLITQGASD----RGTLDATMRQ
WP_091963700 [Marinospirillum celere]                     ASLFMSLSV-SPETINVAGAQRMLSQKMTKEALLLTQGVGD----QATLNATQRQ
WP_068999334 [Terasakiispira papahanaumokuakeensis]       VSLFLSMSV-SPQTINVAGAQRMLSQKMTKEVLLLEVGAVD----QQTLQTTMQR
SFX75036 [Marinospirillum alkaliphilum DSM 21637]         ISLYLSMSV-SPETINVAGAQRMLSQKITRDVLLVVQGAEQ----QQVLNRTIQR
WP_084662276 [Marinospirillum alkaliphilum]               ISLYLSMSV-SPETINVAGAQRMLSQKITRDVLLVVQGAEQ----QQVLNRTIQR
WP_086481606 [Oceanospirillum sanctuarii]                 VSLYLSMAI-DPQTINIAGRQRMLSQKMAKEALLVAAQVEN----KSTLQKTMQL
WP_078320434 [Oceanospirillales]                          IFLYLSMAI-DPQTINIAGRQRMLSQKMAKEALLVASQVEN----KSTLQKTMQL
WP_102043389 [Oceanospirillum maris]                      VSLYLSMAI-DPQTINIAGRQRMLSQKMAKEALLVAAQVEN----KTTLQKTMQL
WP_028300494 [Oceanospirillum beijerinckii]               VSLYLSMAI-NPQTINIAGRQRMLSQKIAKEALLVAAQVEN----QNTLQKTMQL
WP_078743715 [Oceanospirillum multiglobuliferum]          VALYMSMAI-NPQTINVAGRQRMLSQKIAKEALLVAAKIEN----EAVLRKTMQL
EAR59890 [Oceanospirillum sp. MED92]                      ISLYFSMAI-NPQTINMAGRQRMLSQKIAKEALLVAAQVEQ----QSTLKKTMEL
WP_083774892 [Neptuniibacter caesariensis]                ISLYFSMAI-NPQTINMAGRQRMLSQKIAKEALLVAAQVEQ----QSTLKKTMEL
WP_093308400 [Pseudospirillum japonicum]                  IALYLSMSI-NPQTINIAGRQRMLSQKMAKEALLVAVNIEN----TSNLQATMQM
WP_051252630 [Ferrimonas kyonanensis]                     VMLYATSGN-SAEMINVAGAQRMLSQRYAKEALLVVQGGVD----HAALDKTVAR
WP_075186461 [Alteromonadales bacterium BS08]             LSLYISMSV-SANTVDIAGRQRMLSQRLAKEAFLVVNGAEQ----MEAVRSTIGL
WP_045855660 [Alteromonadaceae bacterium Bs12]            GSMYLTLDI-TADTVDVAGRQRMLTQRLAKEAFLVANEAEP----QSVVQETITE
WP_018274184 [Teredinibacter turnerae]                    FSLYMTMQA-SADTVNIAGRQRMLSQRLAKEALLVGQQAMD----KSALEQTIEL
WP_019606173 [Teredinibacter turnerae]                    FSLYMTMQA-SADTVNIAGRQRMLSQRLAKEALLVGQQAMD----KSALEQTIEL
WP_045827023 [Teredinibacter sp. 991H.S.0a.06]            FSLYMTMQA-SADTVNIAGRQRMLSQRLAKEALLVAQQAMD----KSALEQTIEL
WP_028885168 [Teredinibacter turnerae]                    FSLYMTMQA-SADTVNIAGRQRMLSQRLAKEALLVGQQAMD----KSALEQTIEL
WP_028881853 [Teredinibacter turnerae]                    FSLYMTMQA-SADTVNIAGRQRMLSQRLAKEALLVAQQAMD----KSALEQTIEL
WP_018415357 [Teredinibacter turnerae]                    FSLYMTMQA-SADTVNIAGRQRMLSQRLAKEALLVAQQAMD----KSALEQTIEL
WP_015819270 [Teredinibacter turnerae]                    FSLYMTMQA-SADTVNIAGRQRMLSQRLAKEALLVTQQAMD----KSALEQTIEL
WP_028876398 [Teredinibacter turnerae]                    FSLYMTMQA-SADTVNIAGRQRMLSQRLAKEALLVTQQAMD----KSALEQTIEL
WP_019602011 [Teredinibacter turnerae]                    FSLYMTMQA-SADTVNIAGRQRMLSQRLAKEALLVTQQAMD----KSALEQTIEL
WP_011467154 [Saccharophagus degradans]                   ISLYLSMSS-SANTVDVAGRQRMLSQRLAKEALLVGAGVES----RATMQSTIDL
WP_082067039 [Teredinibacter sp. 1162T.S.0a.05]           GSLYLTMSA-SAETVNIAGRQRMLSQRLAKEALLIRTGAEN----EAIAQQTIAL
WP_027328238 [Marinimicrobium agarilyticum]               GVSYLSLSA-TAETVDVAGRQRMLIQRLAKEAMLTEQGALD----ASGLNATIEL
WP_076717438 [Motiliproteus sp.MSK22-1]                   GSLYLTMSA-SAETINVAGRQRMLSQRLAKETLMVVQGVEQ----KVAVEKTMQL
WP_076714176 [Motiliproteus sp.MSK22-1]                   VSLYFSLSN-DAATINEAGRQRMLSQRLAKEAMMVVQGVEE----KAVLEKTIKL
WP_081475260 [Marinobacterium stanieri]                   VSVWMTGSD-DATAINVAGKQRMLSQRLAKETLLIQQGAVD----TGLAQATIRS
WP_076462706 [Marinobacterium stanieri]                   VSVWMTGSD-DATAINVAGKQRMLSQRLAKETLLIQQGAVD----TGLAQATIRS
WP_091825072 [Marinobacterium georgiense]                 AAVYLSDNT-DASAINVAGAQRMLSQKMAKEVLLLSQDVGD----RSGVTKTMNA
PKM43282 [Gammaproteobacteria bacterium HGW]              ASLFYGFGT-DATSINVAGAQRMLSQKVAKEALLAGQGGES----RETVYATLAQ
PKM45884 [Gammaproteobacteria bacterium HGW]              ASLYFSIST-DATSINVAGAQRMLSQKVAKEALLAGQGVES----RDTVLATIRQ
OOZ41054 [Solemya velesiana gill symbiont]                ASLYFSLGS-DATSINVAGRQRMLSQKVAKEAMLAAQKVES----LQAVEKTIAL
WP_078483146 [Solemya velesiana gill symbiont]            ASLYFSLGS-DATSINVAGRQRMLSQKVAKEAMLAAQKVES----LQAVEKTIAL
WP_083220704 [Candidatus Thiodiazotropha endolucinida]    VSLFTSLGS-DATAINVAGRQRMLSQKVAKEALLAAQSIES----RDTVNNTIAL
ODJ87354 [Candidatus Thiodiazotropha endolucinida]        VSLFTSLGS-DATAINVAGRQRMLSQKVAKEALLAAQSIES----RDTVNNTIAL
WP_084594071 [Arhodomonas aquaeolei]                      ASLYFSLGS-SATAVDIAGRQRMLSQRVAKEAVMAVQGVGS----REDVEKTIAL
WP_029132713 [Sedimenticola selenatireducens]             ITIYLSLGV-NSNSIDVAGRQRMLSQRLAKEAMLVAQQAES----REVMEKTINL
PLX63594 [Sedimenticola selenatireducens]                 ITIYLSLGV-NSNSIDVAGRQRMLSQRLAKEAMLVAQQAES----REVMEKTINL
WP_057957096 [endosymbiont of Ridgeia piscesae]           ASIYWSLDS-DAAAINIAGRQRMLSQRVAKEALMVVQGVES----PAVVQKTLAL
WP_067616512 [Dissulfuribacter thermophilus]              LKTVYGQRG-DAVAINIAGRQRMLTQKMTKEALFFNSTQNDK--WKSSLDATIVL
WP_083779049 [Desulfarculus baarsii]                      IVLLGLQET-DGQVVNIAGRQRMLSQRMTKEALILASGDRAAAKN---LAATLEL
ADK86400 [Desulfarculus baarsii DSM 2075]                 IVLLGLQET-DGQVVNIAGRQRMLSQRMTKEALILASGDRAAAKN---LAATLEL
WP_053111464 [Desulfocarbo indianensis]                   IILLGMQEA-DGVVVDIAGRQRMLSQKMTKEALLLLSSGGNTEKDRKELKATADL
WP_072909408 [Malonomonas rubra]                          VFVLNGQKD-DSTVVNIAGRQRMLSQKMSKEALSIAAGLEVSSNR-DSLKQTADL
ENN95934 [Methanocaldococcus villosus KIN24-T80]          TILLKDMEH-DANIINIAGKQRMLIQKMSKEAFMIALGNL---EMKKELIKTAQE
WP_017981124 [Methanocaldococcus villosus]                TILLKDMEH-DANIINIAGKQRMLIQKMSKEAFMIALGNL---EMKKELIKTAQE
WP_079710389 [Paraliobacillus ryukyuensis]                NMFLTEQET-DATIINVAGKQRMLIQKMSKEALIVSDGN----GSADDLVETINL
```

```
ODS31255 [Candidatus Scalindua rubra]                ---MLEKKASDPVKINLAGKQRMLTQKMSKEAIALSQG----IGSTESLEKTANL
ODS31259 [Candidatus Scalindua rubra]                TISFLNKQKADGVVINLAGKQRMLTQKMSKEALAVSQG----TGSKESLEKTADL
ODS31256 [Candidatus Scalindua rubra]                VIVLMNSQKDDGAVINLAGKQRMLTQKMSKEAIALSQG----IGSKQSLVKTINL
DAB34330 [Sulfurospirillum sp. UBA12182]             NVIMNDKSKKDSLIINIAGKQRMLTQKMSKEIFYLKQKD---SIDFRELNSAVDE
DAB32648 [Sulfurospirillum sp. UBA11407]             NVIMNDKSKKDSLIINIAGKQRMLTQKMSKEIFYLKQKD---SIDFRELNSAVDE
OQY52690 [Beggiatoa sp. 4572_84]                     ACGGGVTKQEMGVIMDLAGKQRMFTQKMTKEILLIAKGINV-AENKKKLRQTAIL
OAD20060 [Candidatus Thiomargarita nelsonii]         ------------MSIDLAGKQRMLTQKMSKEILLIAKNIDR-DDNKKNLCETAAL
KHD07211 [Candidatus Thiomargarita nelsonii]         AY--AATQQEMATTINLAGKQRMLTQKMSKEILLIAKGINV-AANKKNLQKTAAL
WP_083760414 [Sulfurovum sp. NBC37-1]                AV--AQTKQQSGVVINLAGKQRMLTQKMSKEALYIAKGIDA-EANTENLKKTAAL
BAF71977 [Sulfurovum sp. NBC37-1]                    AV--AQTKQQSGVVINLAGKQRMLTQKMSKEALYIAKGIDA-EANTENLKKTAAL
WP_103922382 [Thiotrichales bacterium HS_08]         AQ--ASSKTEMGKVINLAGKQRMLTQKMSKEALFIAKGVDA-TGNQGNLKKTANL
WP_038034074 [Thermopetrobacter sp. TC1]             NAIVEQSSAELAVQINLSGRQRMLTQKMSKEAFLVALGVDP-EENRQNAARTAAL
OQX74572 [Campylobacteraceae bacterium 4484_4]       SF--ALTTKQLAVSINLAGKQRMLTQKMTKEALLIKAGVEK-EQNLKKLEATSTL
OGX22015 [Omnitrophica WOR_2 bacterium GWF2_43_52]   GFC-APTPEQWGIIMNISGRQRMLSQKMSKEALLAIAGINP-DENLKKLAESMKL
OGR47178 [Elusimicrobia bacterium GWA2_66_18]        SS--AASEKEFAKVINVAGRQRMLSQKMAAEFLLMKLGIAA-EDNKKKMDADIST
OGR71769 [Elusimicrobia bacterium GWC2_65_9]         SS--AASEKEFAKVINVAGRQRMLSQKMAAEFLLMKLGIAA-EDNKKKMDADIST
PIQ95337 [Nitrospinae bacterium CG11]                TVFTLENQKLDGNVINLAGKQRMLTQKLSKSIMELQLG--D-LSKTGEIGQIKTE
WP_037929253 [Sulfitobacter pseudonitzschiae]        TAQVAASGSAVVVRVDISGRQRMLSQRMAMASCFVMGDVETEKN-IKNAHQAYDL
```

```
                          175       185       195       205       215
                            |         |         |         |         |
WP_083651730    FESSMNLLRNGDKEQGISAPKTPEIEAQLSKVNELWLEYRAGIQKLLQIDESQLR
OLQ80001        FESSMNLLRNGDKEQGISAPKTPEIEAQLSKVNELWLEYRAGIQKLLQIDESQLR
EDQ01086        FESSMNMLLNGDTKRGISAPMTPEIKSRLGKVNKLWSKYREGIQALLLLGDKDQH
WP_040571760    FESSMNMLLNGDTKRGISAPMTPEIKSRLGKVNKLWSKYREGIQALLLLGDKDQH
WP_022940319    FESSMNKLINGDESAGIHAFSDVAIKTQLLKVKDTWQEYRINIEQILQLSPFDLA
WP_104417027    WERAHGWLLNGSEEAGVPAVKDPEIRAQLESVFALWQEYRPALVDYMNAPDT---
KXS52579        WERAHGWLLNGSEEAGVPAVKDPDIRAQLESVFALWQKYRPALVDYMNAPDT---
KXS51160        WERAHGWLLNGSEEAGVPAVKDPEIRAQLEHVLTLWQKYRPALVDYMNAPDT---
WP_104425587    WERAHGWLLNGSEEAGVPAVTDTAIRAQLEHVLTLWQDYRPALVEYMEAPDT---
WP_104416353    WERAHGWLLNGSEEAGVPAVTDTAIRAQLEHVLTLWQDYRPALVEYMEAPDT---
PKM00178        FEQSHRLLLNGDRAQGIAPVELASAKPHLQRVDQIWQRYRPA-VQALAAGQS---
PKM12203        FEQSHRLLLNGDRAQGIAPVELTSAQPHLQRVDQIWQRYRPA-VQALAAGQS---
CJK46151        FEQSHRLLLNGDSAQGIVRVELASAQPYLQRVDQIWQRYRPA-VQALAAGQS---
McpN_LBD        YERSAADLDAGNAERNVSRMGAPEIAAQRQKVAQIWGRYRAMLDQVAQPAS----
OUC50533        YERSAADLDAGNAERNVSRMGAPEIAAQRQKVAQIWGRYRAMLDQVAQPAS----
SAJ26551        YERSAADLDAGNAERNVSRMGAPEIAAQRQKVAQIWGRYRAMLDQVAQPAS----
PKM29122        FDAAHRDLLSGNAVRNISAIAEPGIQAQMNKVGGLWQGFRTQLQRVVA-GD----
WP_027848104    FERAHQDLLVGNRERNITAFDDEEIHQQMQQVDQLWQQMKARLEQAVNKQD----
WP_027850591    FETAHKDLIAGNRDRDITAFDDSEIQQQMQQVDQLWQQMKVRLDQALVQQD----
WP_072325584    FEQAHRDLLQGNRERNITAFDDPAIRQQMQRVDQLWQQMKTRLDATLTNPG----
WP_091963700    FEQAHQDLIQGNPERNISAIDDPEIQQQMQRVDDLWQQIQDSLQEVVNNPN----
WP_068999334    FETAHRDLMAGNPAKNIAVFDDPVIQRQMQTVDQLWQQMASLINRQLQDPQ----
SFX75036        FDAAHRDLVQGNPERSISRINDPVVQQQLQQVEVSWQEFQGVIQNYLKQPL----
WP_084662276    FDAAHRDLVQGNPERSISRINDPVVQQQLQQVEVSWQEFQGVIQNYLKQPL----
WP_086481606    FESSHKDIINGNKAQGMNPITDKEILGQMQKVESLWKDYSKTLLQYADNPT----
WP_078320434    FERSHKDIINGNKAQGMNPTTDPSILSQMQIVENLWSGYSKILLQYTDSPS----
WP_102043389    FEQSHDHILNGNKSLSMNPIEDPEIVAQMQRVQDLWRSYSITLLEYAERPD----
WP_028300494    FERSHKDIIHGNTELGMNPINDKAILAQMQKVEGLWQSYKGMINRYASTPT----
WP_078743715    FEQSHRDIVNGNVEQGMNPITNPAVLSQMQKVEGLWRDYSALVERYIANPN----
EAR59890        FESSHKKIMLGNEELGMNAIKDSEILKQMQHVETLWATYKGVIESHITQPS----
WP_083774892    FESSHKKIMLGNEELGMNAIKDSEILKQMQHVETLWATYKGVIESHITQPS----
WP_093308400    FDRSHQDIIQGNTQQGMNPITDEDILQQMAVVGRLWQDYRELLLAYVQAPS----
WP_051252630    FERAHRLLLEGDANRGLPPVSEPAIVQQLNRVGEFWSSYRQQVDAYLMAPS----
WP_075186461    FENSHRDLLAGNRNADIQPPATKAIESQLKKVEGVWNGYQQSVTRYINSQQ----
WP_045855660    FERSHRDLMMGNKRAGIAIP-TSEVLAQLKEVERVWRQYKLTVAAYIRSKN----
WP_018274184    FEQSHNRLLYGSPENGILAPQTVKIFDKLKVVGGMWENYKIAIRTYATTQD----
WP_019606173    FEQSHNRLLYGSPENGILAPQTVKIFDKLKVVGGMWENYKIAIRTYASTQD----
WP_045827023    FEQSHNRLLYGSPENGILAPQTVKIFDKLKVVGGMWENYKIAIRTYAATQD----
WP_028885168    FEQSHNRLLYGSPENGILAPQTVKIFDKLKVVGGMWENYKIAIRTYATTQD----
WP_028881853    FEQSHNRLLYGSPENGILAPQTVKISDKLKAVGGMWENYKIAIRTYVATKD----
WP_018415357    FEQSHNRLLYGSPENGILAPQTVKISDKLKAVGGMWENYKIAIRTYVASKD----
WP_015819270    FEQSHNRLLYGSPENGILAPQTVKIFDQLKVVDGLWENYKIAIRTYVASKD----
WP_028876398    FEQSHNRLLYGSPENGILAPQTVKIFDQLKVVDGLWENYKIAIRTYVASKD----
WP_019602011    FEQSHNRLLYGSPENGILAPQTVKIFDQLKVVDGLWENYKIAIRTYVASKD----
WP_011467154    FERSHRKLISGDQSDDIHPPATQEIKQALVTVEKQWAEYKRLVNHYVSAKD----
WP_082067039    FESSHQALMNGDKDKGIHAPESAEIKQQLQKVEALWLEYKKGIASLIAGED----
WP_027328238    FEQSHQNLLNGNESAGIQPPQTAEINQSLLNVLQEWNQYKAIIFDYIGADP----
WP_076717438    FESSHQDLINGNPSTGIVAPATPQISQQLEHVGSLWTDYKQTINNYLVDAS----
WP_076714176    FSDSHLHLINGNPESGISAPANAEIRKQLEHVGQLWQHYQSAISNYLENPN----
WP_081475260    FEAAHKALLNGNADMGIKAASEVDIRKQLEHVGTLWRDYRATVEQLVSGTDGN--
WP_076462706    FETAHRALLNGNAGLGIKAASEVDIRKQLEHVGTLWRDYRATVEQLVSGSDGN--
WP_091825072    FESAHQALLNGSAEQGIKAAEDAEIRSRLEQVGTLWNSYRATLNQYLQQPD----
```

```
PKM43282        FESVHQALLQGDAQRDIAVVTDTAVRAQLQKVGQVWKEYRQEIVAYVEQPA----
PKM45884        FEGAHRALLEGDAQRGMRAVKDAAVRTQLQKVEQLWQAYKQDILAYIEQPD----
OOZ41054        FESSHNALLQGDKKQKIDAVKAKPIIDQLKHVEQLWGKYKVHILSYSNNPT----
WP_078483146    FESSHNALLQGDKKQKIDAVKAKPIIDQLKHVEQLWGKYKVHILSYSNNPT----
WP_083220704    FESSHQNLLNGDQNAGIQAVDDPVVRGQLNKVEGLWITYRESIDAYLENPS----
ODJ87354        FESSHQNLLNGDQNAGIQAVDDPVVRGQLNKVEGLWITYRESIDAYLENPS----
WP_084594071    FESSHRKLLQGDPGMGIEPVQDPAIRDQLREVQSLWQRYRGDIQAYLDEPT----
WP_029132713    FESSHKALFEGDEAQNILPVKDALILEQLKLVEQLWSGYKQVITQYAASPD----
PLX63594        FESSHKALFEGDEAQNILPVKDALILEQLKLVEQLWSGYKQVITQYAASPD----
WP_057957096    FEDSQHRLLLGDPEAGITPPMNEAIRQQLAKTSQLWSAYRRHLEAYLATPS----
WP_067616512    FEKSLNGLAVGDAELGLSGTTDKGVQEELNKLQQMWIPFKKALYIITDTSSSK--
WP_083779049    FDASLRGLIEGDAAMGLPPTDDSRIAAQMQKVAALWGPFRQSAEIVLRAGGSADP
ADK86400        FDASLRGLIEGDAAMGLPPTDDSRIAAQMQKVAALWGPFRQSAEIVLRAGGSADP
WP_053111464    FDRSLQGLIGGDAAMGLPPTTNPDILAQMKTVSELWKPFHANLTGVTITTDINSP
WP_072909408    FASSLNSLINGDEKLNLPPTQNPQILSQMRQVEVLWDNFSPHIDTFVNP-ASTEA
ENN95934        FDKNLNDLINGNEERGITPAPP-IVKAQLLKVKSMWSEFYKNILIIYEK-DPSDP
WP_017981124    FDKNLNDLINGNEERGITPAPP-IVKAQLLKVKSMWSEFYKNILIIYEK-DPSDP
WP_079710389    FDEAIEGLMGGSKSLGLPKMPSEEVANQLQSVELLWQPFKENLQMIAN--DNGN-
ODS31255        FDKTLRGLISGDEELRLSPTKDPKIISQLNHIQGLWQDFRANLNAVLANPTGA--
ODS31259        FDKTLKGLISGDKELGLPATKNIEILSQLNQVQKLWKDLHANLDVVLANSDVT--
ODS31256        FDKTLKGLVSGDSELNLPATSNPEILGQLNHVQKLWKDLHANLSIVLANSDVT--
DAB34330        FSENLKDLLEGNSVKGIYHPQDEKIEAKLQKVQKIWFPFKEKIEALKKLIQEN--
DAB32648        FSENLKDLLEGNSVKGIYHPQDEKIEAKLQKVQKIWFPFKEKIEALKKLIQEN--
OQY52690        FNKTLIGLFDGDSELGLVKVENPHIVQQLNKVADLWREFRNNVDAVLRG-NTS--
OAD20060        FNQTLIGLIEGDSELGLVETEKPAIKQQLYKVVELWNKFRINVDAVLMG-NTS--
KHD07211        FERTLKGLLNGDARLGLVKTENAAIVKQLKKVGRLWGKFRQNVKAVLAG-NTS--
WP_083760414    FDKTLKGLIGGDSSLNLPKTDNKEILAQLQKVTDLWVPFKANIDKVIAG-KAD--
BAF71977        FDKTLKGLIGGDSSLNLPKTDNKEILAQLQKVTDLWVPFKANIDKVIAG-KAD--
WP_103922382    FDRTLKGLKDGDADLGLPKTTDAGILAQLDVVAKLWITFKGNIDAVLAG-KTS--
WP_038034074    FERTLKGLMQGDEALKLAPAPNEKILAQLKKVEGLWRRFKPLIEKVAAG-DVS--
OQX74572        FDRTLKGLIKGDEGLKLKPCQNAEVQKQLGVVQQLWKPFRQNIMRVIQG-KAD--
OGX22015        FETSHHALTEGDAAMNIPACEFPDISEQLEKVSILYAELDKIFDKMVEGEKAD--
OGR47178        FDKSLASLSNGDGEAGIPAPPNEQISRQFAQVKLLWGSYVRALQSAGTS------
OGR71769        FDKSLASLSNGDGEAGIPAPPNEQISRQFAQVKLLWGSYVRALQSAGTS------
PIQ95337        FEGVLSGLKRGDTEKGLVAAETPEIMAMLEATEKLWLPFAERVDKVASLWPGI--
WP_037929253    FSQTQGVLRHGGTRDNLEPERDPQVLALLDQSDEIFDTYGRAVLQVTHQDLQ---
```

Supp. Fig 43. Alignment of the McpN-LBD sequences with homologues from other species. The alignment is based on a BLAST-P search of McpN-LBD in the NCBI database of non-redundant sequences, excluding species of the genus *Pseudomonas*. The alignment was done using the CLUSTALW algorithm of the npsa software (Combet et al. (2000) Trends Biochem Sci. 25, 147-150). The BLOSUM62 matrix was used and settings for gap costs were defined as: Existence: 11 and Extension: 1. The McpN-LBD sequence is shaded in yellow.

```
                          50         60         70         80          90
                           |          |          |          |          |
McpN_LBD        ---YLSMS--ISPETINVAGAQRMLSQKMAREALQLRLGAGDP----KALAATIAQYERS
PilJ_pilJ1      NFAYLNTQSNHDKQYIGHAGELRVLSQRIAKNATEAAAGKGEAF---KLLKDARNDFEKR
PilJ_pilJ2      -VVDILLENGAPADQVAVAQRQSLLAERILGSVNKVLAGDENSVQAADSFGRDASLFGRV

                     100        110        120        130             140
                      |          |          |          |               |
McpN_LBD        AADLDAGNAERNVSRMGAPEIAAQRQKVAQIWGRYRAMLDQVAQP-----ASQVDLRGFS
PilJ_pilJ1      WNILVNGDESTSLPPS-PEAVKPQMDVVQQDWDGLRKNADSIL-------ASEQTVLSLH
PilJ_pilJ2      LKGMQEGNAAMSISKVTNAEAVDRLNEIAELFEFVSGSVDEILETSPDLFQVREAANNIF

                150        160          170        180
                 |          |           |          |
McpN_LBD        QYSTELLGELNNLVSLMS--ARADSVQHTQMWI
PilJ_pilJ1      QVASTLAETIPQLQ-----------VEYEE---
PilJ_pilJ2      SVSQTLLDKASQLADGFENLAGGRSINLFAGY-
```

Supp. Fig 44. Sequence alignment of the PilJ domains of the McpN and PilJ chemoreceptors of *P. aeruginosa* PAO1. PilJ-pilJ1 corresponds to the N-terminal PilJ domain (amino acids 36-163), which is followed in sequence by the PilJ-pilJ2 domain (amino acids 164-314). The N-box in McpN is shaded in yellow. Red: identical residues, green: highly similar residues, blue: weakly similar residues. The alignment was done using the CLUSTALW algorithm of the npsa software Combet et al. (2000) Trends Biochem Sci. 25, 147-150. The BLOSUM62 matrix was used and settings for gap costs were defined as: Existence: 11 and Extension: 1.

Supp. Table 15. Characteristics of species that contain McpN homologues. A BLAST-P search was conducted in the NCBI database of non-redundant protein sequences (excluding species of the genus *Pseudomonas*) and the top 87 sequences are listed in Supp. Fig. 43. This Table shows the characteristics of the corresponding bacterial species. Human pathogens are highlighted in green and bacteria that oxidize sulfurous compounds are highlighted in yellow. R/S: reference or source.

Species	Taxonomic group (Phylum/Class/Order)	Source/lifestyle/comments	R/S
Photobacterium proteolyticum	Proteobacteria/Gammaproteobacteria/ Vibrionales	Isolated from the ocean sediment of Laizhou Bay, PR China, optimal growth in 2-3 % (w/v) NaCl	(Li *et al.*, 2017b)
Shewanella benthica	Proteobacteria/Gammaproteobacteria/ Alteromonodales	Isolated from the abyssal South Pacific Ocean, piezophilic	(Lauro *et al.*, 2013)
Psychromonas hadalis	Proteobacteria/Gammaproteobacteria/ Alteromonodales	Collected from the bottom of the Japan Trench, piezophilic	(Nogi *et al.*, 2007)
Marinobacter persicus	Proteobacteria/Gammaproteobacteria/ Alteromonodales	Isolated from the hypersaline lake Aran-Bidgol in Iran, halophilic	(Bagheri *et al.*, 2013)
Streptococcus pneumoniae	Firmicutes/Bacilli/Lactobacillales	Human pathogen, particularly upper airways infections	(Weiser *et al.*, 2018)
Eggerthia catenaformis	Firmicutes/Erysipelotrichia/ Erysipelotrichales	Isolated from human dental abscess, causes bacteremia	(Kordjian *et al.*, 2015)
Enterobacter cloacae	Proteobacteria/Gammaproteobacteria/ Enterobacterales	Human pathogen, urinary tract infections, nosocomial infections	(Davin-Regli & Pages, 2015)
Marinospirillum minutulum	Proteobacteria/Gammaproteobacteria/ Oceanospirillales	Isolated from Japanese fermented brine, halophilic	(Satomi *et al.*, 1998)
Marinospirillum insulare	Proteobacteria/Gammaproteobacteria/ Oceanospirillales	Isolated from fermented fish brine in Japan, halophilic	(Satomi *et al.*, 2004)
Marinospirillum alkaliphilum	Proteobacteria/Gammaproteobacteria/ Oceanospirillales	Isolated from Haoji soda lake in China, halophilic, alkaliphilic	(Zhang *et al.*, 2002)
Marinospirillum celere	Proteobacteria/Gammaproteobacteria/ Oceanospirillales	Isolated from Mono Lake (USA), halophilic, alkaliphilic	(Namsaraev *et al.*, 2009)
Ferrimonas kyonanensis	Proteobacteria/Gammaproteobacteria/ Alteromonadales	Isolated from the Tokyo Bay,	(Nakagawa *et al.*, 2006)
Oceanospirillum sanctuarii	Proteobacteria/Gammaproteobacteria/ Oceanospirillales	Sediment sample collected at the Coringa Wildlife Sanctuary, Indian Ocean	(Sidhu *et al.*, 2017)
Oceanospirillum maris	Proteobacteria/Gammaproteobacteria/ Oceanospirillales	Marine bacterium	(Satomi *et al.*, 2002)
Oceanospirillum	Proteobacteria/Gammaproteobacteria/	Marine bacterium	(Satomi *et al.*, 2002)

beijerinckii	Oceanospirillales		
Oceanospirillum multiglobuliferum	Proteobacteria/Gammaproteobacteria/ Oceanospirillales	Marine bacterium	(Satomi *et al.*, 2002)
Neptuniibacter caesariensis	Proteobacteria/Gammaproteobacteria/ Oceanospirillales	Isolated from a surface water sample from the eastern Mediterranean Sea, slightly halophilic	(Arahal *et al.*, 2007)
Pseudospirillum japonicum	Proteobacteria/Gammaproteobacteria/ Oceanospirillales	Marine bacterium	(Satomi *et al.*, 2002)
Terasakiispira papahanaumokuakeensis	Proteobacteria/Gammaproteobacteria/ Oceanospirillales	Isolated from an anchialine pool on Hawaiian Islands, halophilic	(Zepeda *et al.*, 2015)
Alteromonadales bacterium BS08	Proteobacteria/Gammaproteobacteria/ Alteromonadales	Marine bacteria	GenBankNZ_MRUG01000000
Teredinibacter turnerae	Proteobacteria/Gammaproteobacteria/ Cellvibrionales	Isolated from the gill tissue of a wood-boring mollusc (shipworm), marine isolate, cellulytic	(Distel *et al.*, 2002)
Saccharophagus degradans	Proteobacteria/Gammaproteobacteria/ Alteromonadales	Carbohydrate degrading marine bacteria	(Ekborg *et al.*, 2005)
Marinimicrobium agarilyticum	Proteobacteria/Gammaproteobacteria/ Cellvibrionales	Isolated from tidal flat sediment of the South Sea in Korea, halotolerant	(Lim *et al.*, 2006)
Motiliproteussp. MSK22-1	Proteobacteria/Gammaproteobacteria/ Oceanospirillales	Marine bacteria, isolated from Pacific Ocean island	GenBank NZ_MIEQ01000000
Marinobacterium stanieri	Proteobacteria/Gammaproteobacteria/ Oceanospirillales	Marine bacterium	(Satomi *et al.*, 2002)
Paraliobacillus ryukyuensis	Firmicutes/Bacilli/Bacillales	Isolated from a decomposing marine alga collected in Okinawa, Japan, halophilic, extremely halotolerant, alkaliphilic	(Ishikawa *et al.*, 2002)
Candidatus thiodiazotropha endolucinida	Proteobacteria/Gammaproteobacteria/ unclassified	Endosymbiont of the mollusk *Codakia orbicularis*, sulfur oxidizing, nitrogen fixation	(Konig *et al.*, 2016)
Arhodomonas aquaeolei	Proteobacteria/Gammaproteobacteria/ Chromatiales	Isolated from subterranean brine, halophilic	(Adkins *et al.*, 1993)
Sedimenticola selenatireducens	Proteobacteria/Gammaproteobacteria/ unclassified	Isolated from sediment samples of inter-tidal regions, selenate respiring	(Narasingarao & Haggblom, 2006)
Dissulfuribacter thermophilus	Proteobacteria/Deltaproteobacteria/ unclassified	Isolated from a deep-sea hydrothermal vent chimney in the Pacific Ocean, uses elemental sulfur as the only energy source	(Slobodkin *et al.*, 2013)
Desulfarculus baarsii	Proteobacteria/Deltaproteobacteria/ Desulfarculales	Sulfate reducing bacterium, isolated from ditch sediment near Konstanz University	(Sun *et al.*, 2010)
Desulfocarbo	Proteobacteria/Deltaproteobacteria/	Sulfate-reducing, isolated from water extracted from a coal	(An & Picardal,

indianensis	Desulfarculales	bed in Indiana, USA	2014)
Malonomonas rubra	Proteobacteria/Deltaproteobacteria/ Desulfuromonadales	Isolated from anoxic marine sediment samples, grows on malonate	(Dehning & Schink, 1989)
Methanocaldococcus villosus	Euryarchaeota (Archaea)/Methanococci/ Methanococcales	Isolated from a submarine hydrothermal system at the Kolbeinsey Ridge, north of Iceland, heavily flagellated	(Bellack *et al.*, 2011)
Marinobacterium georgiense	Proteobacteria/Gammaproteobacteria/ Oceanospirillales	Isolated from marine pulp mill effluent, cellulytic	(Gonzalez *et al.*, 1997)
Candidatus scalinduarubra	Planctomycetes/Planctomycetia/ Candidatus Brocadiales	Interface Above the Discovery Deep Brine in the Red Sea,	(Speth *et al.*, 2017)
Sulfurospirillum sp. UBA12182	Proteobacteria/Epsilonprotobacteria/ Campylobacterales	Able to oxidize elemental sulfur	(Schubert, 2017)
Beggiatoa sp. 4572_84	Proteobacteria/Gammaproteobacteria/ Thiotrichales	Sulfide oxidizers, found in coastal sediments, can store nitrate	(Preisler *et al.*, 2007)
Candidatus thiomargaritanelsonii	Proteobacteria/Gammaproteobacteria/ Thiotrichales	Sulfur and sulfide oxidizers	(Flood *et al.*, 2016)
Sulfurovum sp. NBC37-1	Proteobacteria/Epsilonprotobacteria/ Unclassified	Sulfur oxidizing bacteria, isolated from sediment of the Iheya North hydrothermal system in the mid-Okinawa Trough, Japan	(Inagaki *et al.*, 2004)
Thiotrichalesbacterium HS_08	Proteobacteria/Gammaproteobacteria/ Thiotrichales	Sulfur oxidizing bacteria	GenBank NZ_FMSV02000000
Thermopetrobacter sp. TC1	Proteobacteria/Alphaproteobacteria/ unclassified	Probably sulfur oxidizing bacterium	(Watanabe *et al.*, 2016)
Campylobacteraceae bacterium 4484_4	Proteobacteria/Epsilonprotobacteria/ Campylobacteriales	Multiple lifestyles	GenBankNZ_JQKX01 000000
Sulfitobacter pseudonitzschiae	Proteobacteria/Alphaproteobacteria/ Rhodobacterales	Isolated from the toxic marine diatom *Pseudo-nitzschia multiseries*, able to reduce nitrate and oxidize sulfite	(Hong *et al.*, 2015)
Elusimicrobiabacterium GWA2_66_18	Elusimicrobia/Elusimicrobia/ Elusimicrobiales	Isolated from the hindgut of the termite *Reticulitermes speratus*, but widespread in the environment	(Herlemann *et al.*, 2007)

Supp. Table 16. Oligonucleotides used in this study.

Oligonucleotide	Sequence (5'-3')[a]	Purpose
PA2788-NdeI-F	GGAATTCCATATGTACCTGAGCATGTCGATCTC	Generation of pMcpN-LBD
PA2788-XhoI-R	CCGCTCGAGTCACCACATCTGGGTGTGCTG	
PA4520-NdeI-F	GGAATTCCATATGTATCTGGTGCGCGATGCCTA	Generation of pET4520-LBD
PA4520-SalI-R	TAATGTCGACTCACATCTGCGTGCGCACCT	
PA0411-NdeI-F	GGAATTCCATATGAACTTTGCCTACCTCAACACC	Generation of pPilJ-LBD
PA0411-EcoRIR	GGAATTCTCAGGCGTAACCGGCGAACA	
q2788-F	AGGGGTTGATCGAGCAGTTG	RT-qPCR of the *mcpN* gene
q2788-R	TTGAGGCCGTCCAGTTCTTC	
qrpoD-F	AGAAGAAAGCGACGACAGCA	RT-qPCR of the *rpoD* gene
qrpoD-R	CTTCTTGGCCTTGTCGAGCT	
PA2788R61A-F	CGTGGCCGGCGCGCAGGCCATGCTCAGCCAGAAGATGGC	Generation of pMcpN-R61A, overlapping PCR primers.
PA2788R61A-R	CTTCTGGCTGAGCATGGCCTGCGCGCCGGCCACGTTGATG	
2788c_NdeI-F	TAATCATATGAACGAAAGCGTCGCCAG	Generation of pBBRMcpN
2788c_BamHI-R	TAATGGATCCTCAGGTACGGAAGCGGCC	

Supp. Table 17. Data collection and refinement statistics of the 3D structure of the McpN-LBD-nitrate complex. Values in parentheses are for the highest-resolution shell.

Protein	**McpN-LBD**
Ligand	nitrate
PDB identifier	6GCV
Data collection	
Beam line	ID23-1 (ESRF)
Space Group	C 1 2 1
Cell dimensions	
a, b, c (Å)	92.78, 87.95, 52.89
β (°)	93.05
ASU	2
Resolution (Å)	46.32 - 1.30 (1.35 - 1.30)
R_{merge} (%)	3.2 (37.4)
I/σ_I	14.98 (2.38)
Completeness (%)	85.43 (92.43)
Unique reflections	88758 (9541)
Multiplicity	2.7 (2.7)
CC(1/2)	0.999 (0.837)
CC*	1 (0.955)
Refinement	
Resolution (Å)	46.32 - 1.30
R_{work}/R_{free} (%)	12.53 / 15.32
CC(wok)/CC(free) (%)	97.2 / 96.1
No. atoms	3683
Protein	3217
Ligands	36
Water	430
B-factor (Å^2)	17.09
R.m.s deviations	
Bond lengths (Å)	0.013
Bond angles (°)	1.41
Ramachandran (%)	
Favored	100
Outliers	0
Average B-factor	24.51
macromolecules	22.96
ligands	32.60
solvent	35.42

GENERAL DISCUSSION

GENERAL DISCUSSION

The species *Pseudomonas putida* and *Pseudomonas aeruginosa* are characterized by metabolic and lifestyle versatility (Timmis, 2002, Kato *et al.*, 2008), which is related to the complexity and number of their signaling systems (Alexandre *et al.*, 2004). The number of chemoreceptors in *P. putida* KT2440 and *P. aeruginosa* PAO1 strains is similar (27 and 26 chemoreceptors, respectively) and as such superior to the bacterial average of 14 (Lacal *et al.*, 2010b). The diversity of the LBD type (Ortega *et al.*, 2017a) of Pseudomonas chemoreceptors may indicate the ability to sense and respond to a variety of different signals. At the beginning of this thesis, the function and ligand profile of most of the *P. putida* KT2440 and *P. aeruginosa* PAO1 LBDs were unknown, and 3D structural information was only available for a single chemoreceptor (Pineda-Molina *et al.*, 2012). The main purpose of this thesis was to start closing this gap of knowledge using interdisciplinary methodologies. As a result we have functionally annotated the receptors McpP, McpQ, McpK, PA2652 (CtpM), McpU, TlpQ and McpN, and have resolved the 3D structure of the LBDs of McpU, TlpQ and McpN in complex with their cognate ligands. This work has not only provided experimental data about sensing and signaling, but has also enhanced our understanding of the forces that have shaped the evolution of chemosensory pathways and chemotactic mechanisms.

Initial relationships between LBD type and ligand type

In contrast to the conserved MA domain of chemoreceptors, the LBDs show a high variability, with more than 80 LBD types being detected at chemoreceptors (Ortega *et al.*, 2017a). Due to the high degree of sequence variability of LBDs from homologous receptors, it is very difficult to extrapolate and predict the function of chemoreceptors that share sequence homology. Frequently, similarities in the chemoreceptor ligand profile are poorly reflected in overall LBD sequence homology. However, as a result of this thesis initial assumptions can be made on the relationship between LBD type and the ligands recognized.

- HBM LBD containing chemoreceptors: Our laboratory has identified the ligand profile, function and structure of McpS from *P. putida* KT2440, the first chemoreceptor with an HBM type LBD (Pineda-Molina *et al.*, 2012). McpS recognized directly and mediates chemotaxis toward TCA cycle intermediates and other organic acids, most of them recognized in the membrane proximal module (malate, fumarate, oxalacetate, succinate, citrate, isocitrate, and butyrate) (Lacal *et al.*, 2010a, Pineda-Molina *et al.*, 2012). We have determined the ligand profile of the McpS homologues McpQ (Martin-Mora *et al.*, 2016b) and McpK (Martin-Mora *et al.*, 2016a) from *P. putida* KT2440 and *P. aeruginosa* PAO1, respectively. Since these receptors recognize the TCA cycle intermediates citrate and αKG, respectively (Martin-Mora *et al.*, 2016a, Martin-Mora *et al.*, 2016b), it can be suggested that this receptor family recognizes primarily TCA cycle intermediates.
- CACHE LBD containing chemoreceptors: This LBD type can be subdivided into the monomodular sCACHE and bimodular dCACHE LBDs. On one hand, McpP and PA2652 recognize C_2, C_3 and C_4 carboxylic acids and are predicted to have sCACHE LBDs (Garcia *et al.*, 2015, Martin-Mora *et al.*, 2018). In addition, other related sCACHE LBDs structures have been solved in complex with this kind of organic acids (structures with protein database identifications 4K08 and 4EXO of *A. dehalogenans* and of *V. parahaemolyticus*, respectively), suggesting that sCACHE domains bind frequently C2 to C4 carboxylic acids. On the other hand, examples of dCACHE LBDs are *P. aeruginosa* PctA, PctB and PctC (Rico-Jimenez *et al.*, 2013a, Reyes-Darias *et al.*, 2015b), their

homologues in *P. putida* (Reyes-Darias *et al.*, 2015b), McpB and McpC of *B. subtilis* (Glekas *et al.*, 2010) and McpX and Mlp37 of *V. cholerae* (Nishiyama *et al.*, 2012, Nishiyama *et al.*, 2016). These receptors have in common that they sense different amines. In this thesis, we also report the structure and ligand profile of McpU (Gavira *et al.*, 2018) and TlpQ (Corral-Lugo *et al.*, 2018) from *P. putida* KT2440 and *P. aeruginosa* PAO1, respectively, which were also found to sense amines, namely different polyamines and histamine. Interestingly, the structural super-imposition of different dCACHE LBDs have revealed the presence of a conserved Y-X-D-X(n)-D motif that established a conserved hydrogen bonding network with the amino group of their cognate ligands. It thus appears that dCACHE domains bind frequently amines and the detection of the above sequence motif in chemoreceptors of unknown ligand profile can consolidate such hypotheses.

- PilJ- and NIT- LBD containing chemoreceptors: PilJ and NIT type LBDs were predicted to sense nitrate and nitrite (Ortega *et al.*, 2017a). However, only the PilJ domain of McpN and not the PilJ receptor bound nitrate and the NIT domain containing chemoreceptor PA4520 (all of *P. aeruginosa*) (Martin-Mora *et al.*, 2019) was also unable to bind nitrate. These data combined with other recent data from our laboratory suggest that both domains can be further subdivided into receptor families that bind nitrate and those that do not. The 3D structure of McpN-LBD has led to the identification of a conserved sequence motif necessary for nitrate recognition (Martin-Mora *et al.*, 2019), which can be used to predict whether a given NIT domain binds nitrate. Currently, the ligands recognized by PilJ and PA4520 are unknown and their identification requires further experimentation.

LBDs differ in their oligomeric properties

The biophysical characterization of LBDs indicate clear differences in the oligomerization state of antiparallel α-helix bundles LBDs (4HB, PilJ, HBM, NIT) and PAS-like *α/β* folds LBDs (PAS, CACHE, GAF) as well as in the effect of ligand binding on the LBD oligomeric state. 4HB and HBM domains were found to be present in a dynamic equilibrium between the monomeric and dimeric state and ligand binding was shown to promote dimerization. This is due to the fact that the ligand binding pockets are at the dimer interface where amino acids form both monomers establish contacts with the bound ligand (Park *et al.*, 2011, Pineda-Molina *et al.*, 2012). On the contrary, sCACHE and dCACHE LBDs were found to be exclusively monomeric and ligand binding did not later their oligomeric state. The inspection of sCACHE and dCACHE 3D structures (Garcia *et al.*, 2015, Brewster *et al.*, 2016, Nishiyama *et al.*, 2016, Gavira *et al.*, 2018, Sweeney *et al.*, 2018) has shown that ligand bind to a pocket that is formed exclusively by the monomer. In addition, binding at the Tar-LBD (4HB) and McpK-LBD (HBM) occurs in a cooperative manner where the initial binding of the ligand either reduces or increase the affinity for the second ligand molecule, respectively (Biemann & Koshland, 1994, Martin-Mora *et al.*, 2016a). There are no reports of binding cooperativity in dCACHE LBDs, which is explained by their monomeric state in solution. However, the ligand affinities of dCACHE LBDs are generally higher than those for 4HB and HBM domains, as exemplified by TlpQ which has the highest ligand affinity ever measured for a chemoreceptor (Corral-Lugo *et al.*, 2018). Taken together, it can be hypothesized that the cooperative binding mode of 4HB and HBM domains may have evolved to mediate fine tuning of the response, whereas the binding mode at dCACHE LBDs permits high sensitivity responses.

Evolution of broad range and narrow ligand range chemoreceptors

Gene duplication and their subsequent divergence drives the evolution of paralogous genes (Innan & Kondrashov, 2010), which permits the appearance and evolution of novel gene functions (Innan & Kondrashov, 2010). Genome and sequence analysis have shown the existence of

chemoreceptor paralogues in bacterial chemosensory pathways. Ligand recognition is always a trade-off between affinity and specificity. The HBM LBD of McpS of *P. putida* KT2440 recognizes TCA cycle intermediates, but does not recognize citrate/metal complexes and free citrate with only low affinity (Lacal *et al.*, 2010a). Citrate is among the most abundant compounds in root exudates and is present primarily in complex with metal cations (Kamilova *et al.*, 2006). However, the McpS (Lipton *et al.*, 1987, Qin *et al.*, 2007) paralogue McpQ has evolved to recognize specifically citrate and citrate/metal complexes and mediates chemoattraction (Martin-Mora *et al.*, 2016b), which in turn complements functionally McpS. The same evolutionary feature occurs in other species. In *P. aeruginosa* PAO1, the broad range chemoreceptor PctA mediates chemotaxis toward most of the proteinogenic amino acids except L-Gln (Rico-Jimenez *et al.*, 2013a), that is sensed specifically by PctB chemoreceptor. *B. subtilis* is other example, where McpC is the broad range chemoreceptor for amino acids except for L-Asn, that is recognized specifically by its paralogue McpB (Glekas *et al.*, 2010, Glekas *et al.*, 2012).

Importantly, this correlates with the "specialization or escape from adaptive conflict" evolutionary model, which suggests that, after duplication, the two copies of the original gene can suffer specialization by positive selection (Hughes, 1994). This evolutionary process permits the improvement of one of the main functions with respect to the original key gene, that may drive the appearance of new functions (Piatigorsky *et al.*, 1988, Hughes, 1994). Consequently, the two paralogues contribute to the adaptive advantage of the species, that should favor its fitness with respect to those of unduplicated orthologues in closely related species (Innan & Kondrashov, 2010). These data suggest the existence of an evolutionary tendency for paralogues evolution, in which probably the original broad range chemoreceptor has maintained its function while the duplicated narrow range paralogue has evolved to close the "ligand gaps".

Physiological relevance of ligand specificity

In contrast to the plasticity of ligand recognition present in broad range chemoreceptors, many chemoreceptors are specific for the recognition of a single chemoeffector. The existence of this specificity may indicate that these signals are important for the bacteria and that may be of particular physiological relevance.

- In *P. aeruginosa* PAO1, McpK and PctB recognize specifically αKG and L-Gln (Rico-Jimenez *et al.*, 2013a, Martin-Mora *et al.*, 2016a), which are not only a carbon source (αKG) or carbon and nitrogen source (L-Gln), but are central metabolic molecules. Moreover, among this key metabolic role, both molecules have an important signaling function. They modulate the activity of the NtrB/NtrC TCS and its regulator PII, by which the bacteria regulate the C : N balance by sensing the content of cytoplasmic L-Gln and αKG (Ninfa & Jiang, 2005, Li & Lu, 2007). The McpN chemoreceptor is another example. McpN recognizes specifically nitrate and mediates chemotaxis only under nitrogen starving conditions (Martin-Mora *et al.*, 2019). Nitrate is not only an important nitrogen source, but is also an electron acceptor for anaerobic respiration, as *P. aeruginosa* PAO1 has the respiratory, assimilatory and dissimilatory nitrate reduction pathways (Sparacino-Watkins *et al.*, 2014). Mutants in these pathways are less virulent and are affected in their capacity for form biofilm (Van Alst *et al.*, 2007). The nitrate concentration in the lungs of healthy people and patients with cystic fibrosis are in the sensing range of McpN, suggesting that specific nitrate chemotaxis may be related to pathogenicity, since host-derived nitrate appears to be required for efficient infection (Rivera-Chavez *et al.*, 2016).
- In *P. putida* KT2440, McpQ shows specificity for citrate and citrate/metal complexes. The analysis of root exudates from many plants has shown that citrate is frequently the most abundant compound (Lipton *et al.*, 1987, Kuiper *et al.*, 2002, Kravchenko *et al.*, 2003, Kamilova *et al.*, 2006, Liao *et al.*, 2006). *P. putida* KT2440 is a soil bacterium and able to efficiently colonize plant roots (Molina *et al.*, 2006, Matilla *et al.*, 2010). In this context it is not astonishing to

observe a chemoreceptor that responds specifically to a very abundant compound in root exudates.

Chemoattraction appears to be the predominant form of chemotaxis

Chemotactic behaviour can be sub-classified into chemoattraction and chemorepellence (Ng *et al.*, 2010, Sampedro *et al.*, 2015). In this thesis we have conducted an un-biased screening for ligands that interact with chemoreceptors LBDs. However, the subsequent phenotypic characterization of all chemoreceptors reported in this thesis (McpP, McpQ, MpcK, PA2652, McpU, TlpQ and McpN), along with all the other chemoreceptors characterized by our laboratory (Ortega *et al.*, 2017a), showed exclusively chemoattractant responses. Moreover, most of the chemoreceptors reported in other model species (*B. subtilis, E. coli, S, typhimurium, H. pylori, C. jejuni*)(Ortega *et al.*, 2017a) showed chemoattraction. Chemorepellence has been observed in a number of cases (Yamamoto & Imae, 1993, Pham & Parkinson, 2011, Rader *et al.*, 2011) and was interpreted as a strategy to escape from toxic compounds. However, data appear to indicate that chemorepellence is not a primary strategy to cope with toxic compounds or that its molecular mechanism is different to that of chemoattraction.

Chemoreceptor function can be modulated by antagonists

There are numerous reports on signal antagonists that interfere with the signaling of OCS and TCS (Ortega-Calvo *et al.*, 2003, Busch *et al.*, 2007, Swem *et al.*, 2009, Klein *et al.*, 2012, Bi *et al.*, 2013). In this thesis we show that signal antagonists can also modulate chemoreceptor function. Chemoreceptor PA2652 was found to recognize L-malic acid and other structurally related compounds like citraconic acid and methylsuccinic acid. These latter compounds act as antagonists and compete with PA2652 chemoattractants for binding leading to a reduction in the chemotactic response (Martin-Mora *et al.*, 2018). Other examples for the action of antagonists on chemoreceptors have been reported for *E. coli* (Bi *et al.*, 2013) and *C. testosteroni* (Ni *et al.*, 2013). Chemotaxis is necessary for tissue colonization and virulence (Matilla & Krell, 2018), and the rational design of antagonists may thus be a strategy to interfere with chemoreceptor signaling, leading potentially to an attenuation of virulence (Erhardt, 2016).

Differential impact of chemoeffectors on the transcript levels of their cognate chemoreceptor genes

One main issue that our laboratory is studying is the cellular abundance of the different chemoreceptors. Chemoreceptors that mediate chemotaxis signal all into a single pathway leading ultimately to changes in the phosphorylation state of CheY. The cellular abundance of chemoreceptors is thus a key element that defines the bacterial response bias towards a given chemoeffector. Previous reports have revealed that the culture media have strong influence on the chemoreceptor transcript levels (Li & Hazelbauer, 2004, Lopez-Farfan *et al.*, 2017). Transcript levels of *P. putida* KT2440 cultures grown in minimal media were superior to those in rich media. Further studies revealed that the cognate chemoeffectors can also alter transcript levels (Lopez-Farfan *et al.*, 2017). Taken all experimental data together, the cognate ligands can have the following three different effects on the transcript levels of cognate chemoreceptors.

- 1. Chemoeffectors increase transcript levels. Putrescine is a cognate ligand of McpU, and its addition to a *P. putida* KT2440 culture grown in M9 minimal medium, increase McpU transcript levels 25 fold (Lopez-Farfan *et al.*, 2017). This appears to be a putrescine specific effect since the addition of the remaining McpU ligands did not change *mcpU* transcript levels (Lopez-Farfan *et al.*, 2017). Similar increases in transcript levels were reported for the McpP ligand acetate, the

PcaY_PP ligand 4-hydroxybenzoate and the McpH ligands guanine, xanthine and uric acid (Lopez-Farfan *et al.*, 2017). Notably, all compounds serve as carbon and or nitrogen source for growth.

- 2. Chemoeffectors reduce transcript levels. The presence of nitrate and inorganic phosphate was found to repress the transcript levels of their cognate chemoreceptors McpN (Martin-Mora *et al.*, 2019) and CtpL/CtpH (Lopez-Farfan *et al.*, 2017), respectively. The abundance of these chemoreceptors is kept at a very low basal levels until nitrate or inorganic phosphate scarceness increases transcript levels enabling chemotaxis. As a consequence neither inorganic phosphate nor nitrate chemotaxis occurs in rich culture media. This corresponds to an alternative evolutionary strategy and it remains to be elucidated whether it is limited to the response to inorganic anions like phosphate and nitrate.
- 3. Chemoeffectors do not alter transcript levels. It has been shown that the cognate ligands do not alter the transcript levels of the McpS, McpQ (*P. putida* KT2440), McpK (*P. aeruginosa* PAO1) and McpR (*P. putida* F1) chemoreceptors (Parales *et al.*, 2013, Martin-Mora *et al.*, 2016b, Lopez-Farfan *et al.*, 2017). These receptors have in common that they mediate chemotaxis to different TCA cycle intermediates. Data suggest that the central metabolic role of these compounds may be associated with the constitutive expression of chemoreceptor genes.

These data show that there are clearly different evolutionary strategies and experimentation with other bacterial models is required to determine to what extent these observations are of general nature.

Future outlook on chemotaxis research

The flagellum-mediated chemotactic response has been using typically pure chemoeffector solutions (Kalinin *et al.*, 2010, Darias *et al.*, 2014). However, in their physiological habitats bacteria are exposed to complex mixtures of chemoeffectors. Future work is required to elucidate the molecular mechanisms that permit the priorization of responses to a given chemoattractant. Certainly, one factor is the affinity by which chemoeffectors are recognized which defines the magnitude of signaling output (Reyes-Darias *et al.*, 2015a). As mentioned above, another parameter that defines the magnitude of signaling output is the chemoreceptor abundance. Experiments using reconstituted core chemosensory complexes embedded into nanodiscs (2 x (trimer of dimers + CheW + CheA)), have shown that the Tar and Tsr homodimer ratios in the core complexes correlate with the ratio of CheA inhibition in the presence of saturating concentrations of L-aspartate or L-serine (Parkinson *et al.*, 2015)(Fig. 56), providing clear evidence that chemoreceptor abundance correlates with signaling output.

Currently there is a scarceness of information available on the regulatory mechanisms that regulate chemoreceptor expression and a major research need in this field consists in closing this gap of knowledge.

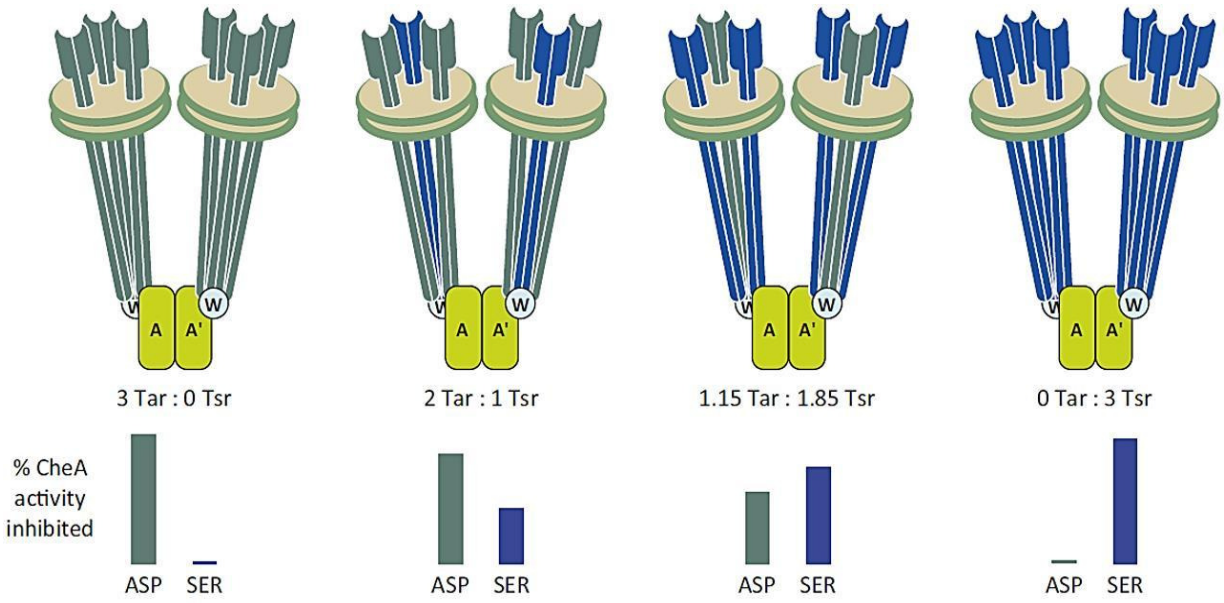

Figure 56. CheA inhibition in mixed-receptor core signaling complexes. Shown are representations of the Tar (green) and Tsr (blue) soluble core signaling complexes assembled using Nanodisc. The Tar : Tsr chemoreceptor dimer ratios are indicated for each core complex. Bars show the extent of CheA inhibition at saturation with the Tar ligand aspartate (ASP, green) and the Tsr ligand serine (SER, blue), respectively. A and A': CheA. W: Che W. Modified from Parkinson *et al.,* (2015).

CONCLUSIONS

CONCLUSIONS

1. Chemoreceptors McpP, McpQ and McpU of *P. putida* KT2440 and McpK, PA2652 (CtpM), TlpQ and McpN of *P. aeruginosa* PAO1 signal through the *che* pathway mediating chemotaxis.
2. The McpP chemoreceptor is responsible for *P. putida* KT2440 chemotaxis toward acetate, propionate, pyruvate and L-lactate. These ligands stimulate McpP by direct binding to its LBD.
3. McpQ is the main chemoreceptor for citrate and citrate/metal complexes in *P. putida* KT2440.
4. The McpQ chemoreceptor recognizes citrate/metal complexes with higher affinity than citrate that may be attributed to the fact that citrate is predominantly present as metal complex in the environment.
5. McpK of *P. aeruginosa* PAO1 recognizes and mediates specifically chemotaxis toward α-ketoglutarate. The binding of α-ketoglutarate occurs with positive cooperativity and corresponds to the first report of ligand recognition by chemoreceptors with positive cooperativity.
6. Chemotaxis of *P. aeruginosa* PAO1 towards L-malate and the structurally related bromosuccinate and citramalate is mediated by CtpM chemoreceptor.
7. Methylsuccinate and citraconate are antagonists that compete with the above chemoeffectors for the binding at CtpM-LBD.
8. The three dimensional structure of McpU-LBD shows that ligands bind to the membrane distal module and identifies structural extensions that account for it increased size.
9. The superimposition of the McpU-LBD and TlpQ-LBD structure with those of other members of the dCACHE family has led to the identification of a conserved Y-X-D-X(n)-D sequence motif for the binding of amino groups.
10. Histamine chemotaxis of *P. aeruginosa* PAO1 is mediated by the concerted action of the TlpQ, PctA and PctC chemoreceptors. TlpQ binds histamine and other polyamines directly. TlpQ-LBD binds spermidine with an affinity of 56 nM, which is the highest affinity ever measured for ligand binding at chemoreceptors.
11. Chemoreceptor McpN but not the NIT domain containing receptor PA4520 is responsible for *P. aeruginosa* PAO1 chemotaxis toward nitrate.
12. The three-dimensional structure of McpN LBD shows that a single molecule of nitrate binds to the domain dimer interface, which is a binding mode different to that of the well-studied Tar chemoreceptor.
13. The sequence alignment of McpN-LBD homologues from other species identifies conserved consensus pattern around the binding site, termed N-box, which can be used to identify nitrate binding PilJ domains.
14. Nitrate chemotaxis occurs only under nitrate starvation conditions, which is likely to be due to the nitrate mediated reduction of *mcpN* transcript levels.
15. Binding of ligands to the sCACHE type domains of McpP and CtpM and dCACHE domains McpU and TlpQ do not cause any alteration in their oligomeric state. In contrast, ligand binding to domains composed of parallel helices (McpQ, McpK and McpN) causes dimer stabilization, indicating the existence of different sensing mechanisms.
16. The use of protein-based high-throughput screening using differential scanning fluorimetry is a powerful tool to identify ligands and can be used to study other signal transduction systems.

REFERENCES

Abril, M.A., Michan, C., Timmis, K.N. *et al.* (1989) Regulator and enzyme specificities of the TOL plasmid-encoded upper pathway for degradation of aromatic hydrocarbons and expansion of the substrate range of the pathway. *J Bacteriol* 171: 6782-90

Adase, C.A., Draheim, R.R., Manson, M.D. (2012) The residue composition of the aromatic anchor of the second transmembrane helix determines the signaling properties of the aspartate/maltose chemoreceptor Tar of *Escherichia coli*. *Biochemistry* 51: 1925-32

Adkins, J.P., Madigan, M.T., Mandelco, L. *et al.* (1993) *Arhodomonas aquaeolei* gen. nov., sp. nov., an aerobic, halophilic bacterium isolated from a subterranean brine. *Int J Syst Bacteriol* 43: 514-20

Adler, J. (1966) Chemotaxis in bacteria. *Science* 153: 708-16

Adler, J., Hazelbauer, G.L., Dahl, M.M. (1973) Chemotaxis toward sugars in *Escherichia coli*. *J Bacteriol* 115: 824-47

Adler, J. (1973) A method for measuring chemotaxis and use of the method to determine optimum conditions for chemotaxis by *Escherichia coli*. *J Gen Microbiol* 74: 77-91

Afonine, P.V., Mustyakimov, M., Grosse-Kunstleve, R.W. *et al.* (2010) Joint X-ray and neutron refinement with phenix.refine. *Acta Crystallogr D Biol Crystallogr* 66: 1153-63

Afonine, P.V., Grosse-Kunstleve, R.W., Echols, N. *et al.* (2012) Towards automated crystallographic structure refinement with phenix.refine. *Acta Crystallogr D Biol Crystallogr* 68: 352-67

Aguilar, P.S., Hernandez-Arriaga, A.M., Cybulski, L.E. *et al.* (2001) Molecular basis of thermosensing: a two-component signal transduction thermometer in *Bacillus subtilis*. *EMBO J* 20: 1681-91

Ahmad, A., Barry, J.P., Nelson, D.C. (1999) Phylogenetic affinity of a wide, vacuolate, nitrate-accumulating *Beggiatoa* sp. from Monterey Canyon, California, with *Thioploca* spp. *Appl Environ Microbiol* 65: 270-7

Airola, M.V., Watts, K.J., Bilwes, A.M. *et al.* (2010) Structure of concatenated HAMP domains provides a mechanism for signal transduction. *Structure* 18: 436-48

Airola, M.V., Huh, D., Sukomon, N. *et al.* (2013a) Architecture of the soluble receptor Aer2 indicates an in-line mechanism for PAS and HAMP domain signaling. *J Mol Biol* 425: 886-901

Airola, M.V., Sukomon, N., Samanta, D. *et al.* (2013b) HAMP domain conformers that propagate opposite signals in bacterial chemoreceptors. *PLoS Biol* 11: e1001479

Alexander, R.P., Zhulin, I.B. (2007) Evolutionary genomics reveals conserved structural determinants of signaling and adaptation in microbial chemoreceptors. *Proc Natl Acad Sci U S A* 104: 2885-90

Alexander, R.P., Lowenthal, A.C., Harshey, R.M. *et al.* (2010) CheV: CheW-like coupling proteins at the core of the chemotaxis signaling network. *Trends Microbiol* 18: 494-503

Alexandre, G., Greer-Phillips, S., Zhulin, I.B. (2004) Ecological role of energy taxis in microorganisms. *FEMS Microbiol Rev* 28: 113-26

Alexandre, G. (2010) Coupling metabolism and chemotaxis-dependent behaviours by energy taxis receptors. *Microbiology* 156: 2283-93

Alexandre, G. (2015) Chemotaxis control of transient cell aggregation. *J Bacteriol* 197: 3230-7

Alperi, A., Martinez-Murcia, A.J., Monera, A. *et al.* (2010a) *Aeromonas fluvialis* sp. nov., isolated from a Spanish river. *Int J Syst Evol Microbiol* 60: 72-7

Alperi, A., Martinez-Murcia, A.J., Ko, W.C. *et al.* (2010b) *Aeromonas taiwanensis* sp. nov. and *Aeromonas sanarellii* sp. nov., clinical species from Taiwan. *Int J Syst Evol Microbiol* 60: 2048-55

Alvarez-Ortega, C., Harwood, C.S. (2007) Identification of a malate chemoreceptor in *Pseudomonas aeruginosa* by screening for chemotaxis defects in an energy taxis-deficient mutant. *Appl Environ Microbiol* 73: 7793-5

Ames, P., Zhou, Q., Parkinson, J.S. (2014) HAMP domain structural determinants for signalling and sensory adaptation in Tsr, the *Escherichia coli* serine chemoreceptor. *Mol Microbiol* 91: 875-86

An, T.T., Picardal, F.W. (2014) *Desulfocarbo indianensis* gen. nov., sp. nov., a benzoate-oxidizing, sulfate-reducing bacterium isolated from water extracted from a coal bed. *Int J Syst Evol Microbiol* 64: 2907-14

Anand, G.S., Goudreau, P.N., Stock, A.M. (1998) Activation of methylesterase CheB: evidence of a dual role for the regulatory domain. *Biochemistry* 37: 14038-47

Anantharaman, V., Aravind, L. (2000) Cache - a signaling domain common to animal Ca(2+)-channel subunits and a class of prokaryotic chemotaxis receptors. *Trends Biochem Sci* 25: 535-7

Anderson, J.K., Huang, J.Y., Wreden, C. *et al.* (2015) Chemorepulsion from the quorum signal autoinducer-2 promotes *Helicobacter pylori* biofilm dispersal. *MBio* 6: e00379

Antunez-Lamas, M., Cabrera, E., Lopez-Solanilla, E. *et al.* (2009) Bacterial chemoattraction towards jasmonate plays a role in the entry of *Dickeya dadantii* through wounded tissues. *Mol Microbiol* 74: 662-71

Arahal, D.R., Lekunberri, I., Gonzalez, J.M. *et al.* (2007) *Neptuniibacter caesariensis* gen. nov., sp. nov., a novel marine genome-sequenced gammaproteobacterium. *Int J Syst Evol Microbiol* 57: 1000-6

Aravena-Roman, M., Beaz-Hidalgo, R., Inglis, T.J. *et al.* (2013) *Aeromonas australiensis* sp. nov., isolated from irrigation water. *Int J Syst Evol Microbiol* 63: 2270-6

Arun, A.B., Schumann, P., Chu, H.I. *et al.* (2008) *Pseudoxanthobacter soli* gen. nov., sp. nov., a nitrogen-fixing alphaproteobacterium isolated from soil. *Int J Syst Evol Microbiol* 58: 1571-5

Attila, C., Ueda, A., Cirillo, S.L. *et al.* (2008) *Pseudomonas aeruginosa* PAO1 virulence factors and poplar tree response in the rhizosphere. *Microb Biotechnol* 1: 17-29

Austin, B., Austin, D., Sutherland, R. *et al.* (2005) Pathogenicity of vibrios to rainbow trout (*Oncorhynchus mykiss*, Walbaum) and *Artemia nauplii*. *Environ Microbiol* 7: 1488-95

Azam, M.W., Khan, A.U. (2019) Updates on the pathogenicity status of *Pseudomonas aeruginosa*. *Drug Discov Today* 24: 350-359

Bader, M.W., Sanowar, S., Daley, M.E. *et al.* (2005) Recognition of antimicrobial peptides by a bacterial sensor kinase. *Cell* 122: 461-72

Bagdasarian, M., Lurz, R., Ruckert, B. *et al.* (1981) Specific-purpose plasmid cloning vectors. II. Broad host range, high copy number, RSF1010-derived vectors, and a host-vector system for gene cloning in *Pseudomonas*. *Gene* 16: 237-47

Bagheri, M., Amoozegar, M.A., Didari, M. *et al.* (2013) *Marinobacter persicus* sp. nov., a moderately halophilic bacterium from a saline lake in Iran. *Antonie Van Leeuwenhoek* 104: 47-54

Bains, M., Fernandez, L., Hancock, R.E. (2012) Phosphate starvation promotes swarming motility and cytotoxicity of *Pseudomonas aeruginosa*. *Appl Environ Microbiol* 78: 6762-8

Bais, H.P., Park, S.W., Stermitz, F.R. *et al.* (2002) Exudation of fluorescent beta-carbolines from *Oxalis tuberosa* L roots. *Phytochemistry* 61: 539-43

Baldissera, M.D., Souza, C.F., Bottari, N.B. *et al.* (2018) Purinergic signalling displays an anti-inflammatory profile in the spleen of fish experimentally infected with *Aeromonas caviae*: Modulation of the immune response. *J Fish Dis* 41: 683-687

Balsalobre, L.C., Dropa, M., Matte, G.R. *et al.* (2009) Molecular detection of enterotoxins in environmental strains of *Aeromonas hydrophila* and *Aeromonas jandaei*. *J Water Health* 7: 685-91

Bansal, T., Englert, D., Lee, J. *et al.* (2007) Differential effects of epinephrine, norepinephrine, and indole on *Escherichia coli* O157:H7 chemotaxis, colonization, and gene expression. *Infect Immun* 75: 4597-607

Bar-On, Y.M., Phillips, R., Milo, R. (2018) The biomass distribution on Earth. *Proc Natl Acad Sci U S A* 115: 6506-6511

Baraquet, C., Theraulaz, L., Iobbi-Nivol, C. *et al.* (2009) Unexpected chemoreceptors mediate energy taxis towards electron acceptors in *Shewanella oneidensis*. *Mol Microbiol* 73: 278-90

Barcik, W., Wawrzyniak, M., Akdis, C.A. *et al.* (2017) Immune regulation by histamine and histamine-secreting bacteria. *Curr Opin Immunol* 48: 108-113

Bardy, S.L., Briegel, A., Rainville, S. *et al.* (2017) Recent advances and future prospects in bacterial and archaeal locomotion and signal transduction. *J Bacteriol* 199: e00203-17

Beaz-Hidalgo, R., Alperi, A., Figueras, M.J. *et al.* (2009) *Aeromonas piscicola* sp. nov., isolated from diseased fish. *Syst Appl Microbiol* 32: 471-9

Beaz-Hidalgo, R., Alperi, A., Bujan, N. *et al.* (2010) Comparison of phenotypical and genetic identification of *Aeromonas* strains isolated from diseased fish. *Syst Appl Microbiol* 33: 149-53

Beaz-Hidalgo, R., Shaked, T., Laviad, S. *et al.* (2012) Chironomid egg masses harbour the clinical species *Aeromonas taiwanensis* and *Aeromonas sanarellii*. *FEMS Microbiol Lett* 337: 48-54

Beaz-Hidalgo, R., Latif-Eugenin, F., Hossain, M.J. *et al.* (2015) *Aeromonas aquatica* sp. nov., *Aeromonas finlandiensis* sp. nov. and *Aeromonas lacus* sp. nov. isolated from Finnish waters associated with cyanobacterial blooms. *Syst Appl Microbiol* 38: 161-8

Beghdadi, W., Porcherie, A., Schneider, B.S. *et al.* (2008) Inhibition of histamine-mediated signaling confers significant protection against severe malaria in mouse models of disease. *J Exp Med* 205: 395-408

Belda, E., van Heck, R.G., Jose Lopez-Sanchez, M. *et al.* (2016) The revisited genome of *Pseudomonas putida* KT2440 enlightens its value as a robust metabolic chassis. *Environ Microbiol* 18: 3403-3424

Bell, K.S., Sebaihia, M., Pritchard, L. *et al.* (2004) Genome sequence of the enterobacterial phytopathogen *Erwinia carotovora* subsp. atroseptica and characterization of virulence factors. *Proc Natl Acad Sci U S A* 101: 11105-10

Bellack, A., Huber, H., Rachel, R. *et al.* (2011) *Methanocaldococcus villosus* sp. nov., a heavily flagellated archaeon that adheres to surfaces and forms cell-cell contacts. *Int J Syst Evol Microbiol* 61: 1239-45

Berleman, J.E., Bauer, C.E. (2005) Involvement of a Che-like signal transduction cascade in regulating cyst cell development in *Rhodospirillum centenum*. *Mol Microbiol* 56: 1457-66

Bi, S., Yu, D., Si, G. *et al.* (2013) Discovery of novel chemoeffectors and rational design of *Escherichia coli* chemoreceptor specificity. *Proc Natl Acad Sci U S A* 110: 16814-9

Bi, S., Lai, L. (2015) Bacterial chemoreceptors and chemoeffectors. *Cell Mol Life Sci* 72: 691-708

Bi, S., Pollard, A.M., Yang, Y. *et al.* (2016) Engineering hybrid chemotaxis receptors in bacteria. *ACS Synth Biol* 5: 989-1001

Bi, S., Sourjik, V. (2018) Stimulus sensing and signal processing in bacterial chemotaxis. *Curr Opin Microbiol* 45: 22-29

Bibikov, S.I., Biran, R., Rudd, K.E. *et al.* (1997) A signal transducer for aerotaxis in *Escherichia coli*. *J Bacteriol* 179: 4075-9

Biemann, H.P., Koshland, D.E., Jr. (1994) Aspartate receptors of *Escherichia coli* and *Salmonella typhimurium* bind ligand with negative and half-of-the-sites cooperativity. *Biochemistry* 33: 629-34

Billings, A.F., Fortney, J.L., Hazen, T.C. *et al.* (2015) Genome sequence and description of the anaerobic lignin-degrading bacterium *Tolumonas lignolytica* sp. nov. *Stand Genomic Sci* 10: 106

Bilwes, A.M., Alex, L.A., Crane, B.R. *et al.* (1999) Structure of CheA, a signal-transducing histidine kinase. *Cell* 96: 131-41

Bohm, G., Muhr, R., Jaenicke, R. (1992) Quantitative analysis of protein far UV circular dichroism spectra by neural networks. *Protein Eng* 5: 191-5

Boldog, T., Grimme, S., Li, M. *et al.* (2006) Nanodiscs separate chemoreceptor oligomeric states and reveal their signaling properties. *Proc Natl Acad Sci U S A* 103: 11509-14

Boyer, H.W., Roulland-Dussoix, D. (1969) A complementation analysis of the restriction and modification of DNA in *Escherichia coli*. *J Mol Biol* 41: 459-72

Brennan, C.A., DeLoney-Marino, C.R., Mandel, M.J. (2013) Chemoreceptor VfcA mediates amino acid chemotaxis in *Vibrio fischeri*. *Appl Environ Microbiol* 79: 1889-96

Brewster, J.L., McKellar, J.L., Finn, T.J. *et al.* (2016) Structural basis for ligand recognition by a Cache chemosensory domain that mediates carboxylate sensing in *Pseudomonas syringae*. *Sci Rep* 6: 35198

Briegel, A., Ortega, D.R., Tocheva, E.I. *et al.* (2009) Universal architecture of bacterial chemoreceptor arrays. *Proc Natl Acad Sci U S A* 106: 17181-6

Briegel, A., Li, X., Bilwes, A.M. *et al.* (2012) Bacterial chemoreceptor arrays are hexagonally packed trimers of receptor dimers networked by rings of kinase and coupling proteins. *Proc Natl Acad Sci U S A* 109: 3766-71

Briegel, A., Ames, P., Gumbart, J.C. *et al.* (2013) The mobility of two kinase domains in the *Escherichia coli* chemoreceptor array varies with signalling state. *Mol Microbiol* 89: 831-41

Briegel, A., Wong, M.L., Hodges, H.L. *et al.* (2014a) New insights into bacterial chemoreceptor array structure and assembly from electron cryotomography. *Biochemistry* 53: 1575-85

Briegel, A., Ladinsky, M.S., Oikonomou, C. *et al.* (2014b) Structure of bacterial cytoplasmic chemoreceptor arrays and implications for chemotactic signaling. *Elife* 3: e02151

Briegel, A., Ortega, D.R., Huang, A.N. *et al.* (2015) Structural conservation of chemotaxis machinery across Archaea and Bacteria. *Environ Microbiol Rep* 7: 414-9

Brown, E.D., Wright, G.D. (2016) Antibacterial drug discovery in the resistance era. *Nature* 529: 336-43

Busch, A., Lacal, J., Martos, A. *et al.* (2007) Bacterial sensor kinase TodS interacts with agonistic and antagonistic signals. *Proc Natl Acad Sci U S A* 104: 13774-9

Busch, A., Guazzaroni, M.E., Lacal, J. *et al.* (2009) The sensor kinase TodS operates by a multiple step phosphorelay mechanism involving two autokinase domains. *J Biol Chem* 284: 10353-60

Cao, H., Baldini, R.L., Rahme, L.G. (2001) Common mechanisms for pathogens of plants and animals. *Annu Rev Phytopathol* 39: 259-84

Carney, J.G., Trachtenberg, A.M., Rheaume, B.A. *et al.* (2017) Genome sequence of a marine *Spirillum*, *Oceanospirillum multiglobuliferum* ATCC 33336(T), isolated from Japan. *Genome Announc* 5

Chandrashekhar, K., Gangaiah, D., Pina-Mimbela, R. *et al.* (2015) Transducer like proteins of *Campylobacter jejuni* 81-176: role in chemotaxis and colonization of the chicken gastrointestinal tract. *Front Cell Infect Microbiol* 5: 46

Chantranupong, L., Wolfson, R.L., Sabatini, D.M. (2015) Nutrient-sensing mechanisms across evolution. *Cell* 161: 67-83

Chao, X., Muff, T.J., Park, S.Y. *et al.* (2006) A receptor-modifying deamidase in complex with a signaling phosphatase reveals reciprocal regulation. *Cell* 124: 561-71

Chen, A.I., Dolben, E.F., Okegbe, C. *et al.* (2014) *Candida albicans* ethanol stimulates *Pseudomonas aeruginosa* WspR-controlled biofilm formation as part of a cyclic relationship involving phenazines. *PLoS Pathog* 10: e1004480

Chen, P.L., Lamy, B., Ko, W.C. (2016) *Aeromonas dhakensis*, an increasingly recognized human pathogen. *Front Microbiol* 7: 793

Chen, V.B., Arendall, W.B., 3rd, Headd, J.J. *et al.* (2010) MolProbity: all-atom structure validation for macromolecular crystallography. *Acta Crystallogr D Biol Crystallogr* 66: 12-21

Cheung, J., Hendrickson, W.A. (2008) Crystal structures of C4-dicarboxylate ligand complexes with sensor domains of histidine kinases DcuS and DctB. *J Biol Chem* 283: 30256-65

Cheung, J., Hendrickson, W.A. (2009) Structural analysis of ligand stimulation of the histidine kinase NarX. *Structure* 17: 190-201

Chi, Y.I., Yokota, H., Kim, S.H. (1997) Apo structure of the ligand-binding domain of aspartate receptor from *Escherichia coli* and its comparison with ligand-bound or pseudoligand-bound structures. *FEBS Lett* 414: 327-32

Choi, Y.U., Kwon, Y.K., Ye, B.R. *et al.* (2012) Draft genome sequence of *Marinobacterium stanieri* S30, a strain isolated from a coastal lagoon in Chuuk state in Micronesia. *J Bacteriol* 194: 1260

Colauto, N.B., Fermor, T.R., Eira, A.F. *et al.* (2016) *Pseudomonas putida* stimulates primordia on *Agaricus bitorquis*. *Curr Microbiol* 72: 482-8

Coleman, M.D., Bass, R.B., Mehan, R.S. *et al.* (2005) Conserved glycine residues in the cytoplasmic domain of the aspartate receptor play essential roles in kinase coupling and on-off switching. *Biochemistry* 44: 7687-95

Colin, R., Sourjik, V. (2017) Emergent properties of bacterial chemotaxis pathway. *Curr Opin Microbiol* 39: 24-33

Collaborative Computational Project, N. (1994) The CCP4 suite: programs for protein crystallography. *Acta Crystallogr D Biol Crystallogr* 50: 760-3

Collins, J.C., Reilly, E.J. (1968) Chemical composition of the exudate from excised maize roots. *Planta* 83: 218-22

Combet, C., Blanchet, C., Geourjon, C. *et al.* (2000) NPS@: network protein sequence analysis. *Trends Biochem Sci* 25: 147-50

Corral-Lugo, A., De la Torre, J., Matilla, M.A. *et al.* (2016) Assessment of the contribution of chemoreceptor-based signalling to biofilm formation. *Environ Microbiol* 18: 3355-3372

Corral-Lugo, A., Matilla, M.A., Martin-Mora, D. *et al.* (2018) High-affinity chemotaxis to histamine mediated by the TlpQ chemoreceptor of the human pathogen *Pseudomonas aeruginosa*. *MBio* 9: e01894-18

Cowtan, K. (2006) The Buccaneer software for automated model building. 1. Tracing protein chains. *Acta Crystallogr D Biol Crystallogr* 62: 1002-11

Croset, V., Rytz, R., Cummins, S.F. *et al.* (2010) Ancient protostome origin of chemosensory ionotropic glutamate receptors and the evolution of insect taste and olfaction. *PLoS Genet* 6: e1001064

Cruz, A., Areias, D., Duarte, A. *et al.* (2013) *Aeromonas molluscorum* Av27 is a potential tributyltin (TBT) bioremediator: phenotypic and genotypic characterization indicates its safe application. *Antonie Van Leeuwenhoek* 104: 385-96

Cserzo, M., Wallin, E., Simon, I. *et al.* (1997) Prediction of transmembrane alpha-helices in prokaryotic membrane proteins: the dense alignment surface method. *Protein Eng* 10: 673-6

Cuppels, D.A. (1988) Chemotaxis by *Pseudomonas syringae* pv. tomato. *Appl Environ Microbiol* 54: 629-632

Dallaire-Dufresne, S., Tanaka, K.H., Trudel, M.V. *et al.* (2014) Virulence, genomic features, and plasticity of *Aeromonas salmonicida* subsp. *salmonicida*, the causative agent of fish furunculosis. *Vet Microbiol* 169: 1-7

Danielson, M.A., Biemann, H.P., Koshland, D.E., Jr. *et al.* (1994) Attractant- and disulfide-induced conformational changes in the ligand binding domain of the chemotaxis aspartate receptor: a 19F NMR study. *Biochemistry* 33: 6100-9

Danielson, M.A., Bass, R.B., Falke, J.J. (1997) Cysteine and disulfide scanning reveals a regulatory alpha-helix in the cytoplasmic domain of the aspartate receptor. *J Biol Chem* 272: 32878-88

Darias, J.A., Garcia-Fontana, C., Lugo, A.C. *et al.* (2014) Qualitative and quantitative assays for flagellum-mediated chemotaxis. *Methods Mol Biol* 1149: 87-97

Darzins, A. (1994) Characterization of a *Pseudomonas aeruginosa* gene cluster involved in pilus biosynthesis and twitching motility: sequence similarity to the chemotaxis proteins of enterics and the gliding bacterium *Myxococcus xanthus*. *Mol Microbiol* 11: 137-53

Davin-Regli, A., Pages, J.M. (2015) *Enterobacter aerogenes* and *Enterobacter cloacae*; versatile bacterial pathogens confronting antibiotic treatment. *Front Microbiol* 6: 392

Day, C.J., King, R.M., Shewell, L.K. *et al.* (2016) A direct-sensing galactose chemoreceptor recently evolved in invasive strains of *Campylobacter jejuni*. *Nat Commun* 7: 13206

De Benedetto, A., Yoshida, T., Fridy, S. *et al.* (2015) Histamine and skin barrier: are histamine antagonists useful for the prevention or treatment of atopic dermatitis? *J Clin Med* 4: 741-55

de Chaumont, F., Dallongeville, S., Chenouard, N. *et al.* (2012) Icy: an open bioimage informatics platform for extended reproducible research. *Nat Methods* 9: 690-6

de Lorenzo, V., Herrero, M., Jakubzik, U. *et al.* (1990) Mini-Tn5 transposon derivatives for insertion mutagenesis, promoter probing, and chromosomal insertion of cloned DNA in gram-negative eubacteria. *J Bacteriol* 172: 6568-72

de Vries, S.P., Linn, A., Macleod, K. *et al.* (2017) Analysis of *Campylobacter jejuni* infection in the gnotobiotic piglet and genome-wide identification of bacterial factors required for infection. *Sci Rep* 7: 44283

de Weert, S., Vermeiren, H., Mulders, I.H. *et al.* (2002) Flagella-driven chemotaxis towards exudate components is an important trait for tomato root colonization by *Pseudomonas fluorescens*. *Mol Plant Microbe Interact* 15: 1173-80

Dehning, I., Schink, B. (1989) *Malonomonas rubra* gen. nov. sp. nov., a microaerotolerant anaerobic bacterium growing by decarboxylation of malonate. *Archives of Microbiology* 151: 427-433

Deleage, G., Blanchet, C., Geourjon, C. (1997) Protein structure prediction. Implications for the biologist. *Biochimie* 79: 681-6

Demarta, A., Huys, G., Tonolla, M. *et al.* (2004) Polyphasic taxonomic study of "*Aeromonas eucrenophila*-like" isolates from clinical and environmental sources. *Syst Appl Microbiol* 27: 343-9

Demarta, A., Kupfer, M., Riegel, P. *et al.* (2008) *Aeromonas tecta* sp. nov., isolated from clinical and environmental sources. *Syst Appl Microbiol* 31: 278-86

Dennis, J.J., Zylstra, G.J. (1998) Plasposons: modular self-cloning minitransposon derivatives for rapid genetic analysis of gram-negative bacterial genomes. *Appl Environ Microbiol* 64: 2710-5

Dennis, P.G., Seymour, J., Kumbun, K. *et al.* (2013) Diverse populations of lake water bacteria exhibit chemotaxis towards inorganic nutrients. *ISME J* 7: 1661-4

Di Martino, M.L., Campilongo, R., Casalino, M. *et al.* (2013) Polyamines: emerging players in bacteria-host interactions. *Int J Med Microbiol* 303: 484-91

Distel, D.L., Morrill, W., MacLaren-Toussaint, N. *et al.* (2002) *Teredinibacter turnerae* gen. nov., sp. nov., a dinitrogen-fixing, cellulolytic, endosymbiotic gamma-proteobacterium isolated from the gills of wood-boring molluscs (Bivalvia: *Teredinidae*). *Int J Syst Evol Microbiol* 52: 2261-9

Djordjevic, S., Goudreau, P.N., Xu, Q. *et al.* (1998) Structural basis for methylesterase CheB regulation by a phosphorylation-activated domain. *Proc Natl Acad Sci U S A* 95: 1381-6

Doebber, M., Bordignon, E., Klare, J.P. *et al.* (2008) Salt-driven equilibrium between two conformations in the HAMP domain from *Natronomonas pharaonis*: the language of signal transfer? *J Biol Chem* 283: 28691-701

Doi, R., Ranamukhaarachchi, S.L. (2009) Soil dehydrogenase in a land degradation-rehabilitation gradient: observations from a savanna site with a wet/dry seasonal cycle. *Rev Biol Trop* 57: 223-34

Dong, H.T., Techatanakitarnan, C., Jindakittikul, P. *et al.* (2017) *Aeromonas jandaei* and *Aeromonas veronii* caused disease and mortality in Nile tilapia, *Oreochromis niloticus* (L.). *J Fish Dis* 40: 1395-1403

Dorotkiewicz-Jach, A., Augustyniak, D., Olszak, T. *et al.* (2015) Modern therapeutic approaches against *Pseudomonas aeruginosa* infections. *Curr Med Chem* 22: 1642-64

Dos Santos, V.A., Heim, S., Moore, E.R. *et al.* (2004) Insights into the genomic basis of niche specificity of *Pseudomonas putida* KT2440. *Environ Microbiol* 6: 1264-86

Draheim, R.R., Bormans, A.F., Lai, R.Z. *et al.* (2005) Tryptophan residues flanking the second transmembrane helix (TM2) set the signaling state of the Tar chemoreceptor. *Biochemistry* 44: 1268-77

Driscoll, J.A., Brody, S.L., Kollef, M.H. (2007) The epidemiology, pathogenesis and treatment of *Pseudomonas aeruginosa* infections. *Drugs* 67: 351-68

Duarte, A.S., Cavaleiro, E., Pereira, C. *et al.* (2015) *Aeromonas piscicola* AH-3 expresses an extracellular collagenase with cytotoxic properties. *Lett Appl Microbiol* 60: 288-97

Dubert, J., Spinard, E.J., Nelson, D.R. *et al.* (2016) Draft genome sequence of the new pathogen for bivalve larvae *Vibrio bivalvicida*. *Genome Announc* 4

Duque, E., Rodriguez-Herva, J.J., de la Torre, J. *et al.* (2007) The RpoT regulon of *Pseudomonas putida* DOT-T1E and its role in stress endurance against solvents. *J Bacteriol* 189: 207-19

Ekborg, N.A., Gonzalez, J.M., Howard, M.B. *et al.* (2005) *Saccharophagus degradans* gen. nov., sp. nov., a versatile marine degrader of complex polysaccharides. *Int J Syst Evol Microbiol* 55: 1545-9

Elliott, K.T., Dirita, V.J. (2008) Characterization of CetA and CetB, a bipartite energy taxis system in *Campylobacter jejuni*. *Mol Microbiol* 69: 1091-103

Elliott, K.T., Zhulin, I.B., Stuckey, J.A. *et al.* (2009) Conserved residues in the HAMP domain define a new family of proposed bipartite energy taxis receptors. *J Bacteriol* 191: 375-87

Emerson, D. (1999) Complex pattern formation by *Pseudomonas* strain KC in response to nitrate and nitrite. *Microbiology* 145 (Pt 3): 633-41

Emsley, P., Lohkamp, B., Scott, W.G. *et al.* (2010) Features and development of Coot. *Acta Crystallogr D Biol Crystallogr* 66: 486-501

Erhardt, M. (2016) Strategies to block bacterial pathogenesis by interference with motility and chemotaxis. *Curr Top Microbiol Immunol* 398: 185-205

Escobar, M.A., Dandekar, A.M. (2003) *Agrobacterium tumefaciens* as an agent of disease. *Trends Plant Sci* 8: 380-6

Espinosa-Urgel, M., Kolter, R., Ramos, J.L. (2002) Root colonization by *Pseudomonas putida*: love at first sight. *Microbiology* 148: 341-343

Espinosa-Urgel, M., Ramos, J.L. (2004) Cell density-dependent gene contributes to efficient seed colonization by *Pseudomonas putida* KT2440. *Appl Environ Microbiol* 70: 5190-8

Esteve, C., Gutierrez, M.C., Ventosa, A. (1995) *Aeromonas encheleia* sp. nov., isolated from European eels. *Int J Syst Bacteriol* 45: 462-6

Evans, P. (2006) Scaling and assessment of data quality. *Acta Crystallogr D Biol Crystallogr* 62: 72-82

Falke, J.J., Erbse, A.H. (2009) The piston rises again. *Structure* 17: 1149-51

Falke, J.J. (2014) Piston versus scissors: chemotaxis receptors versus sensor His-kinase receptors in two-component signaling pathways. *Structure* 22: 1219-1220

Farfan, M., Spataro, N., Sanglas, A. *et al.* (2013) Draft genome sequence of the *Aeromonas diversa* type strain. *Genome Announc* 1

Fernandez, M., Morel, B., Corral-Lugo, A. *et al.* (2016) Identification of a chemoreceptor that specifically mediates chemotaxis toward metabolizable purine derivatives. *Mol Microbiol* 99: 34-42

Fernandez, M., Matilla, M.A., Ortega, A. *et al.* (2017) Metabolic value chemoattractants are preferentially recognized at broad ligand range chemoreceptor of *Pseudomonas putida* KT2440. *Front Microbiol* 8: 990

Fernandez, M., Ortega, A., Rico-Jimenez, M. *et al.* (2018) High-throughput screening to identify chemoreceptor ligands. *Methods Mol Biol* 1729: 291-301

Ferrandez, A., Hawkins, A.C., Summerfield, D.T. *et al.* (2002) Cluster II *che* genes from *Pseudomonas aeruginosa* are required for an optimal chemotactic response. *J Bacteriol* 184: 4374-83

Figueras, M.J., Alperi, A., Beaz-Hidalgo, R. *et al.* (2011) *Aeromonas rivuli* sp. nov., isolated from the upstream region of a karst water rivulet. *Int J Syst Evol Microbiol* 61: 242-8

Fillet, S., Krell, T., Morel, B. *et al.* (2011) Intramolecular signal transmission in a tetrameric repressor of the IclR family. *Proc Natl Acad Sci U S A* 108: 15372-7

Finan, T.M., Kunkel, B., De Vos, G.F. *et al.* (1986) Second symbiotic megaplasmid in *Rhizobium meliloti* carrying exopolysaccharide and thiamine synthesis genes. *J Bacteriol* 167: 66-72

Finn, R.D., Coggill, P., Eberhardt, R.Y. *et al.* (2016) The Pfam protein families database: towards a more sustainable future. *Nucleic Acids Res* 44: D279-85

Finn, R.D., Attwood, T.K., Babbitt, P.C. *et al.* (2017) InterPro in 2017-beyond protein family and domain annotations. *Nucleic Acids Res* 45: D190-D199

Flemming, H.C., Wuertz, S. (2019) Bacteria and archaea on Earth and their abundance in biofilms. *Nat Rev Microbiol* 17: 247-260

Flood, B.E., Fliss, P., Jones, D.S. *et al.* (2016) Single-cell (meta-)genomics of a dimorphic candidatus *Thiomargarita nelsonii* reveals genomic plasticity. *Front Microbiol* 7: 603

Frank, V., Vaknin, A. (2013) Prolonged stimuli alter the bacterial chemosensory clusters. *Mol Microbiol* 88: 634-44

Fuchs, G., Berg, I.A. (2014) Unfamiliar metabolic links in the central carbon metabolism. *J Biotechnol* 192 Pt B: 314-22

Fulcher, N.B., Holliday, P.M., Klem, E. *et al.* (2010) The *Pseudomonas aeruginosa* Chp chemosensory system regulates intracellular cAMP levels by modulating adenylate cyclase activity. *Mol Microbiol* 76: 889-904

Galperin, M.Y. (2005) A census of membrane-bound and intracellular signal transduction proteins in bacteria: bacterial IQ, extroverts and introverts. *BMC Microbiol* 5: 35

Galperin, M.Y. (2018) What bacteria want. *Environ Microbiol* 20: 4221-4229

Ganie, A.H., Ahmad, A., Pandey, R. *et al.* (2015) Metabolite profiling of low-P tolerant and low-P sensitive maize genotypes under phosphorus starvation and restoration conditions. *PLoS One* 10: e0129520

Garcia-Fontana, C., Reyes-Darias, J.A., Munoz-Martinez, F. *et al.* (2013) High specificity in CheR methyltransferase function: CheR2 of *Pseudomonas putida* is essential for chemotaxis, whereas CheR1 is involved in biofilm formation. *J Biol Chem* 288: 18987-99

Garcia-Fontana, C., Corral Lugo, A., Krell, T. (2014) Specificity of the CheR2 methyltransferase in *Pseudomonas aeruginosa* is directed by a C-terminal pentapeptide in the McpB chemoreceptor. *Sci Signal* 7: ra34

Garcia, D., Watts, K.J., Johnson, M.S. *et al.* (2016) Delineating PAS-HAMP interaction surfaces and signalling-associated changes in the aerotaxis receptor Aer. *Mol Microbiol* 100: 156-72

Garcia, V., Reyes-Darias, J.A., Martin-Mora, D. *et al.* (2015) Identification of a chemoreceptor for C2 and C3 carboxylic acids. *Appl Environ Microbiol* 81: 5449-57

Garrity, L.F., Schiel, S.L., Merrill, R. *et al.* (1998) Unique regulation of carbohydrate chemotaxis in *Bacillus subtilis* by the phosphoenolpyruvate-dependent phosphotransferase system and the methyl-accepting chemotaxis protein McpC. *J Bacteriol* 180: 4475-80

Gartner, A., Wiese, J., Imhoff, J.F. (2008) *Amphritea atlantica* gen. nov., sp. nov., a gammaproteobacterium from the Logatchev hydrothermal vent field. *Int J Syst Evol Microbiol* 58: 34-9

Garvis, S., Munder, A., Ball, G. *et al.* (2009) *Caenorhabditis elegans* semi-automated liquid screen reveals a specialized role for the chemotaxis gene *cheB2* in *Pseudomonas aeruginosa* virulence. *PLoS Pathog* 5: e1000540

Gauthier, J., Vincent, A.T., Charette, S.J. *et al.* (2017) Strong genomic and phenotypic heterogeneity in the *Aeromonas sobria* species complex. *Front Microbiol* 8: 2434

Gavira, J.A., Lacal, J., Ramos, J.L. *et al.* (2012) Crystallization and crystallographic analysis of the ligand-binding domain of the *Pseudomonas putida* chemoreceptor McpS in complex with malate and succinate. *Acta Crystallogr Sect F Struct Biol Cryst Commun* 68: 428-31

Gavira, J.A., Ortega, A., Martin-Mora, D. *et al.* (2018) Structural basis for polyamine binding at the dCACHE domain of the McpU chemoreceptor from *Pseudomonas putida*. *J Mol Biol* 430: 1950-1963

Gellatly, S.L., Hancock, R.E. (2013) *Pseudomonas aeruginosa*: new insights into pathogenesis and host defenses. *Pathog Dis* 67: 159-73

Glekas, G.D., Foster, R.M., Cates, J.R. *et al.* (2010) A PAS domain binds asparagine in the chemotaxis receptor McpB in *Bacillus subtilis*. *J Biol Chem* 285: 1870-8

Glekas, G.D., Mulhern, B.J., Kroc, A. *et al.* (2012) The *Bacillus subtilis* chemoreceptor McpC senses multiple ligands using two discrete mechanisms. *J Biol Chem* 287: 39412-8

Glusker, J.P., Minkin, J.A., Patterson, A.L. (1969) X-ray crystal analysis of the substrates of aconitase. IX. A refinement of the structure of anhydrous citric acid. *Acta Crystallogr B* 25: 1066-72

Goers Sweeney, E., Henderson, J.N., Goers, J. *et al.* (2012) Structure and proposed mechanism for the pH-sensing *Helicobacter pylori* chemoreceptor TlpB. *Structure* 20: 1177-88

Goldman, J.P., Levin, M.D., Bray, D. (2009) Signal amplification in a lattice of coupled protein kinases. *Mol Biosyst* 5: 1853-9

Gonzalez, J.M., Mayer, F., Moran, M.A. *et al.* (1997) Microbulbifer hydrolyticus gen. nov., sp. nov., and *Marinobacterium georgiense* gen. nov., sp. nov., two marine bacteria from a lignin-rich pulp mill waste enrichment community. *Int J Syst Bacteriol* 47: 369-76

Greer-Phillips, S.E., Alexandre, G., Taylor, B.L. *et al.* (2003) Aer and Tsr guide *Escherichia coli* in spatial gradients of oxidizable substrates. *Microbiology* 149: 2661-7

Greer-Phillips, S.E., Stephens, B.B., Alexandre, G. (2004) An energy taxis transducer promotes root colonization by *Azospirillum brasilense*. *J Bacteriol* 186: 6595-604

Gushchin, I., Melnikov, I., Polovinkin, V. *et al.* (2017) Mechanism of transmembrane signaling by sensor histidine kinases. *Science* 356

Guvener, Z.T., Tifrea, D.F., Harwood, C.S. (2006) Two different *Pseudomonas aeruginosa* chemosensory signal transduction complexes localize to cell poles and form and remould in stationary phase. *Mol Microbiol* 61: 106-18

Hada, H.S., West, P.A., Lee, J.V. *et al.* (1984) *Vibrio tubiashii* s p . nov., a pathogen of bivalve mollusks. *Int J Syst Bacteriol* 34: 1-4

Hall, B.A., Armitage, J.P., Sansom, M.S. (2011) Transmembrane helix dynamics of bacterial chemoreceptors supports a piston model of signalling. *PLoS Comput Biol* 7: e1002204

Hamer, R., Chen, P.Y., Armitage, J.P. *et al.* (2010) Deciphering chemotaxis pathways using cross species comparisons. *BMC Syst Biol* 4: 3

Hanlon, D.W., Ordal, G.W. (1994) Cloning and characterization of genes encoding methyl-accepting chemotaxis proteins in *Bacillus subtilis*. *J Biol Chem* 269: 14038-46

Harayama, S., Palva, E.T., Hazelbauer, G.L. (1979) Transposon-insertion mutants of *Escherichia coli* K12 defective in a component common to galactose and ribose chemotaxis. *Mol Gen Genet* 171: 193-203

Harwood, C.S., Rivelli, M., Ornston, L.N. (1984) Aromatic acids are chemoattractants for *Pseudomonas putida*. *J Bacteriol* 160: 622-8

Harwood, C.S. (1989) A methyl-accepting protein is involved in benzoate taxis in *Pseudomonas putida*. *J Bacteriol* 171: 4603-8

Hasegawa, Y., Muraki, T., Tokuyama, T. *et al.* (2000) A novel degradative pathway of 2-nitrobenzoate via 3-hydroxyanthranilate in *Pseudomonas fluorescens* strain KU-7. *FEMS Microbiol Lett* 190: 185-90

Hazelbauer, G.L., Falke, J.J., Parkinson, J.S. (2008) Bacterial chemoreceptors: high-performance signaling in networked arrays. *Trends Biochem Sci* 33: 9-19

Hegde, M., Englert, D.L., Schrock, S. *et al.* (2011) Chemotaxis to the quorum-sensing signal AI-2 requires the Tsr chemoreceptor and the periplasmic LsrB AI-2-binding protein. *J Bacteriol* 193: 768-73

Held, K., Ramage, E., Jacobs, M. *et al.* (2012) Sequence-verified two-allele transposon mutant library for *Pseudomonas aeruginosa* PAO1. *J Bacteriol* 194: 6387-9

Henry, J.T., Crosson, S. (2011) Ligand-binding PAS domains in a genomic, cellular, and structural context. *Annu Rev Microbiol* 65: 261-86

Herlemann, D.P., Geissinger, O., Brune, A. (2007) The termite group I phylum is highly diverse and widespread in the environment. *Appl Environ Microbiol* 73: 6682-5

Herrero, M., de Lorenzo, V., Timmis, K.N. (1990) Transposon vectors containing non-antibiotic resistance selection markers for cloning and stable chromosomal insertion of foreign genes in gram-negative bacteria. *J Bacteriol* 172: 6557-67

Hickman, J.W., Tifrea, D.F., Harwood, C.S. (2005) A chemosensory system that regulates biofilm formation through modulation of cyclic diguanylate levels. *Proc Natl Acad Sci U S A* 102: 14422-7

Hida, A., Oku, S., Kawasaki, T. *et al.* (2015) Identification of the *mcpA* and *mcpM* genes, encoding methyl-accepting proteins involved in amino acid and l-malate chemotaxis, and involvement of McpM-mediated chemotaxis in plant infection by *Ralstonia pseudosolanacearum* (formerly *Ralstonia solanacearum* phylotypes I and III). *Appl Environ Microbiol* 81: 7420-30

Ho, S.N., Hunt, H.D., Horton, R.M. *et al.* (1989) Site-directed mutagenesis by overlap extension using the polymerase chain reaction. *Gene* 77: 51-9

Hofstra, C.L., Desai, P.J., Thurmond, R.L. *et al.* (2003) Histamine H4 receptor mediates chemotaxis and calcium mobilization of mast cells. *J Pharmacol Exp Ther* 305: 1212-21

Holloway, B.W., Krishnapillai, V., Morgan, A.F. (1979) Chromosomal genetics of *Pseudomonas*. *Microbiol Rev* 43: 73-102

Hong, C.S., Kuroda, A., Ikeda, T. *et al.* (2004a) The aerotaxis transducer gene *aer*, but not *aer-2*, is transcriptionally regulated by the anaerobic regulator ANR in *Pseudomonas aeruginosa*. *J Biosci Bioeng* 97: 184-90

Hong, C.S., Shitashiro, M., Kuroda, A. *et al.* (2004b) Chemotaxis proteins and transducers for aerotaxis in *Pseudomonas aeruginosa*. *FEMS Microbiol Lett* 231: 247-52

Hong, Z., Lai, Q., Luo, Q. *et al.* (2015) *Sulfitobacter pseudonitzschiae* sp. nov., isolated from the toxic marine diatom *Pseudo-nitzschia* multiseries. *Int J Syst Evol Microbiol* 65: 95-100

Hopper, D.J., Chapman, P.J., Dagley, S. (1970) Metabolism of L-malate and D-malate by a species of *Pseudomonas*. *J Bacteriol* 104: 1197-202

Hossain, M.J., Beaz-Hidalgo, R., Figueras, M.J. *et al.* (2014) Draft genome sequences of two novel *Aeromonas* species recovered in association with cyanobacterial blooms. *Genome Announc* 2

Hothorn, M., Dabi, T., Chory, J. (2011) Structural basis for cytokinin recognition by *Arabidopsis thaliana* histidine kinase 4. *Nat Chem Biol* 7: 766-8

Houtman, J.C., Brown, P.H., Bowden, B. *et al.* (2007) Studying multisite binary and ternary protein interactions by global analysis of isothermal titration calorimetry data in SEDPHAT: application to adaptor protein complexes in cell signaling. *Protein Sci* 16: 30-42

Hua, H.T., Bollet, C., Tercian, S. *et al.* (2004) *Aeromonas popoffii* urinary tract infection. *J Clin Microbiol* 42: 5427-8

Huang, Z., Wang, Y.H., Zhu, H.Z. *et al.* (2019) Cross talk between chemosensory pathways that modulate chemotaxis and biofilm formation. *MBio* 10

Hugdahl, M.B., Beery, J.T., Doyle, M.P. (1988) Chemotactic behavior of *Campylobacter jejuni*. *Infect Immun* 56: 1560-6

Hughes, A.L. (1994) The evolution of functionally novel proteins after gene duplication. *Proc Biol Sci* 256: 119-24

Hulko, M., Berndt, F., Gruber, M. *et al.* (2006) The HAMP domain structure implies helix rotation in transmembrane signaling. *Cell* 126: 929-40

Inagaki, F., Takai, K., Nealson, K.H. *et al.* (2004) *Sulfurovum lithotrophicum* gen. nov., sp. nov., a novel sulfur-oxidizing chemolithoautotroph within the epsilon-Proteobacteria isolated from Okinawa trough hydrothermal sediments. *Int J Syst Evol Microbiol* 54: 1477-82

Inda, M.E., Vandenbranden, M., Fernandez, A. *et al.* (2014) A lipid-mediated conformational switch modulates the thermosensing activity of DesK. *Proc Natl Acad Sci U S A* 111: 3579-84

Ingolia, T.D., Koshland, D.E., Jr. (1979) Response to a metal ion-citrate complex in bacterial sensing. *J Bacteriol* 140: 798-804

Innan, H., Kondrashov, F. (2010) The evolution of gene duplications: classifying and distinguishing between models. *Nat Rev Genet* 11: 97-108

Ishikawa, M., Ishizaki, S., Yamamoto, Y. *et al.* (2002) *Paraliobacillus ryukyuensis* gen. nov., sp. nov., a new Gram-positive, slightly halophilic, extremely halotolerant, facultative anaerobe isolated from a decomposing marine alga. *J Gen Appl Microbiol* 48: 269-79

Iwaki, H., Muraki, T., Ishihara, S. *et al.* (2007) Characterization of a pseudomonad 2-nitrobenzoate nitroreductase and its catabolic pathway-associated 2-hydroxylaminobenzoate mutase and a chemoreceptor involved in 2-nitrobenzoate chemotaxis. *J Bacteriol* 189: 3502-14

Iwama, T., Nakao, K.I., Nakazato, H. *et al.* (2000) Mutational analysis of ligand recognition by Tcp, the citrate chemoreceptor of *Salmonella enterica* serovar *typhimurium*. *J Bacteriol* 182: 1437-41

Iwama, T., Ito, Y., Aoki, H. *et al.* (2006) Differential recognition of citrate and a metal-citrate complex by the bacterial chemoreceptor Tcp. *J Biol Chem* 281: 17727-35

Jacobs, M.A., Alwood, A., Thaipisuttikul, I. *et al.* (2003) Comprehensive transposon mutant library of *Pseudomonas aeruginosa*. *Proc Natl Acad Sci U S A* 100: 14339-44

Janda, J.M., Abbott, S.L. (2010) The genus *Aeromonas*: taxonomy, pathogenicity, and infection. *Clin Microbiol Rev* 23: 35-73

Jansari, V.H., Potharla, V.Y., Riddell, G.T. *et al.* (2016) Twitching motility and cAMP levels: signal transduction through a single methyl-accepting chemotaxis protein. *FEMS Microbiol Lett* 363

Jeong, H., Barbe, V., Lee, C.H. *et al.* (2009) Genome sequences of *Escherichia coli* B strains REL606 and BL21(DE3). *J Mol Biol* 394: 644-52

Ji, S., Zhao, R., Li, Z. *et al.* (2013) *Ferrimonas sediminum* sp. nov., isolated from coastal sediment of an amphioxus breeding zone. *Int J Syst Evol Microbiol* 63: 977-81

Johnson, C.K. (1965) X-Ray crystal analysis of the substrates of aconitase. V. Magnesium citrate decahydrate (Mg(H2o)6)(Mgc6h5o7(H2o))2. 2h2o. *Acta Crystallogr* 18: 1004-18

Johnson, C.M. (2013) Differential scanning calorimetry as a tool for protein folding and stability. *Arch Biochem Biophys* 531: 100-9

Johnson, J.F., Allan, D.L., Vance, C.P. *et al.* (1996) Root carbon dioxide fixation by phosphorus-deficient *Lupinus albus* (contribution to organic acid exudation by proteoid roots). *Plant Physiol* 112: 19-30

Johnson, K.S., Ottemann, K.M. (2018) Colonization, localization, and inflammation: the roles of *H. pylori* chemotaxis in vivo. *Curr Opin Microbiol* 41: 51-57

Jones, D.L. (1998) Orgaic acids in the rhizosphere - a critical review. *Plant and Soil* 205: 25-44

Juhas, M. (2015) *Pseudomonas aeruginosa* essentials: an update on investigation of essential genes. *Microbiology* 161: 2053-60

Kabsch, W. (2010) Xds. *Acta Crystallogr D Biol Crystallogr* 66: 125-32

Kalinin, Y., Neumann, S., Sourjik, V. *et al.* (2010) Responses of *Escherichia coli* bacteria to two opposing chemoattractant gradients depend on the chemoreceptor ratio. *J Bacteriol* 192: 1796-800

Kamath, K.S., Pascovici, D., Penesyan, A. *et al.* (2016) *Pseudomonas aeruginosa* cell membrane protein expression from phenotypically diverse cystic fibrosis isolates demonstrates host-specific adaptations. *J Proteome Res* 15: 2152-63

Kamilova, F., Kravchenko, L.V., Shaposhnikov, A.I. *et al.* (2006) Organic acids, sugars, and L-tryptophane in exudates of vegetables growing on stonewool and their effects on activities of rhizosphere bacteria. *Mol Plant Microbe Interact* 19: 250-6

Kanehisa, M., Sato, Y., Kawashima, M. *et al.* (2016) KEGG as a reference resource for gene and protein annotation. *Nucleic Acids Res* 44: D457-62

Kaniga, K., Delor, I., Cornelis, G.R. (1991) A wide-host-range suicide vector for improving reverse genetics in gram-negative bacteria: inactivation of the *blaA* gene of *Yersinia enterocolitica*. *Gene* 109: 137-41

Karlsen, C., Hjerde, E., Klemetsen, T. *et al.* (2017) Pan genome and CRISPR analyses of the bacterial fish pathogen *Moritella viscosa*. *BMC Genomics* 18: 313

Kato, J., Nakamura, T., Kuroda, A. *et al.* (1999) Cloning and characterization of chemotaxis genes in *Pseudomonas aeruginosa*. *Biosci Biotechnol Biochem* 63: 155-61

Kato, J., Kim, H.E., Takiguchi, N. *et al.* (2008) *Pseudomonas aeruginosa* as a model microorganism for investigation of chemotactic behaviors in ecosystem. *J Biosci Bioeng* 106: 1-7

Kautharapu, K.B., Jarboe, L.R. (2012) Genome sequence of the psychrophilic deep-sea bacterium *Moritella marina* MP-1 (ATCC 15381). *J Bacteriol* 194: 6296-7

Kearns, D.B., Robinson, J., Shimkets, L.J. (2001) *Pseudomonas aeruginosa* exhibits directed twitching motility up phosphatidylethanolamine gradients. *J Bacteriol* 183: 763-7

Keilberg, D., Ottemann, K.M. (2016) How *Helicobacter pylori* senses, targets and interacts with the gastric epithelium. *Environ Microbiol* 18: 791-806

Keller, S., Vargas, C., Zhao, H. *et al.* (2012) High-precision isothermal titration calorimetry with automated peak-shape analysis. *Anal Chem* 84: 5066-73

Kelley, L.A., Sternberg, M.J. (2009) Protein structure prediction on the Web: a case study using the Phyre server. *Nat Protoc* 4: 363-71

Kenakin, T. (2005) New concepts in drug discovery: collateral efficacy and permissive antagonism. *Nat Rev Drug Discov* 4: 919-27

Kenakin, T., Williams, M. (2014) Defining and characterizing drug/compound function. *Biochem Pharmacol* 87: 40-63

Kennedy, M.J., Lawless, J.G. (1985) Role of chemotaxis in the ecology of denitrifiers. *Appl Environ Microbiol* 49: 109-14

Kercher, M.A., Lu, P., Lewis, M. (1997) Lac repressor-operator complex. *Curr Opin Struct Biol* 7: 76-85

Kertesz, M.A., Mirleau, P. (2004) The role of soil microbes in plant sulphur nutrition. *J Exp Bot* 55: 1939-45

Kessler, B., de Lorenzo, V., Timmis, K.N. (1992) A general system to integrate *lacZ* fusions into the chromosomes of gram-negative eubacteria: regulation of the Pm promoter of the TOL plasmid studied with all controlling elements in monocopy. *Mol Gen Genet* 233: 293-301

Khorassani, R., Hettwer, U., Ratzinger, A. *et al.* (2011) Citramalic acid and salicylic acid in sugar beet root exudates solubilize soil phosphorus. *BMC Plant Biol* 11: 121

Kim, H.-E., Shitashiro, M., Kuroda, A. *et al.* (2007) Ethylene chemotaxis in *Pseudomonas aeruginosa* and other *Pseudomonas* species. *Microbes and Environments* 22: 186-189

Kim, H.E., Shitashiro, M., Kuroda, A. *et al.* (2006) Identification and characterization of the chemotactic transducer in *Pseudomonas aeruginosa* PAO1 for positive chemotaxis to trichloroethylene. *J Bacteriol* 188: 6700-2

Kim, H.E., Tokura, H. (2007) Influence of two different light intensities from 16:00 to 20:30 hours on evening dressing behavior in the cold. *Coll Antropol* 31: 145-51

Kim, H.J., Park, S., Lee, J.M. *et al.* (2008) *Moritella dasanensis* sp. nov., a psychrophilic bacterium isolated from the Arctic ocean. *Int J Syst Evol Microbiol* 58: 817-20

Kim, K.K., Yokota, H., Kim, S.H. (1999) Four-helical-bundle structure of the cytoplasmic domain of a serine chemotaxis receptor. *Nature* 400: 787-92

Kim, S.H. (1994) "Frozen" dynamic dimer model for transmembrane signaling in bacterial chemotaxis receptors. *Protein Sci* 3: 159-65

Kirby, J.R., Zusman, D.R. (2003) Chemosensory regulation of developmental gene expression in *Myxococcus xanthus*. *Proc Natl Acad Sci U S A* 100: 2008-13

Kirby, J.R. (2009) Chemotaxis-like regulatory systems: unique roles in diverse bacteria. *Annu Rev Microbiol* 63: 45-59

Kitanovic, S., Ames, P., Parkinson, J.S. (2011) Mutational analysis of the control cable that mediates transmembrane signaling in the *Escherichia coli* serine chemoreceptor. *J Bacteriol* 193: 5062-72

Klare, J.P., Bordignon, E., Engelhard, M. *et al.* (2011) Transmembrane signal transduction in archaeal phototaxis: the sensory rhodopsin II-transducer complex studied by electron paramagnetic resonance spectroscopy. *Eur J Cell Biol* 90: 731-9

Klein, T., Henn, C., de Jong, J.C. *et al.* (2012) Identification of small-molecule antagonists of the *Pseudomonas aeruginosa* transcriptional regulator PqsR: biophysically guided hit discovery and optimization. *ACS Chem Biol* 7: 1496-501

Klockgether, J., Munder, A., Neugebauer, J. *et al.* (2010) Genome diversity of *Pseudomonas aeruginosa* PAO1 laboratory strains. *J Bacteriol* 192: 1113-21

Koch, B., Jensen, L.E., Nybroe, O. (2001) A panel of Tn7-based vectors for insertion of the *gfp* marker gene or for delivery of cloned DNA into Gram-negative bacteria at a neutral chromosomal site. *J Microbiol Methods* 45: 187-95

Kofoid, E.C., Parkinson, J.S. (1988) Transmitter and receiver modules in bacterial signaling proteins. *Proc Natl Acad Sci U S A* 85: 4981-5

Kolb, A., Busby, S., Buc, H. *et al.* (1993) Transcriptional regulation by cAMP and its receptor protein. *Annu Rev Biochem* 62: 749-95

Kolodziej, A.F., Tan, T., Koshland, D.E., Jr. (1996) Producing positive, negative, and no cooperativity by mutations at a single residue located at the subunit interface in the aspartate receptor of *Salmonella typhimurium*. *Biochemistry* 35: 14782-92

Konarev, P.V., Volkov, V.V., Sokolova, A.V. *et al.* (2003) PRIMUS: a Windows PC-based system for small-angle scattering data analysis. *J. Appl. Crystallogr* 36: 1277-1282

Konig, S., Gros, O., Heiden, S.E. *et al.* (2016) Nitrogen fixation in a chemoautotrophic lucinid symbiosis. *Nat Microbiol* 2: 16193

Kordjian, H.H., Schultz, J.D., Rosenvinge, F.S. *et al.* (2015) First clinical description of *Eggerthia catenaformis* bacteremia in a patient with dental abscess. *Anaerobe* 35: 38-40

Kovach, M.E., Elzer, P.H., Hill, D.S. *et al.* (1995) Four new derivatives of the broad-host-range cloning vector pBBR1MCS, carrying different antibiotic-resistance cassettes. *Gene* 166: 175-6

Kozakov, D., Beglov, D., Bohnuud, T. *et al.* (2013) How good is automated protein docking? *Proteins* 81: 2159-66

Kozinska, A., Guz, L. (2004) The effect of various *Aeromonas bestiarum* vaccines on non-specific immune parameters and protection of carp (*Cyprinus carpio* L.). *Fish Shellfish Immunol* 16: 437-45

Kravchenko, L.V., Azarova, T.S., Leonova-Erko, E.I. *et al.* (2003) Tomato root exudates and their effect on the growth and antifungal activity of *Pseudomonas* strains. *Mikrobiologiia* 72: 48-53

Krell, T. (2008) Microcalorimetry: a response to challenges in modern biotechnology. *Microb Biotechnol* 1: 126-36

Krell, T., Lacal, J., Busch, A. *et al.* (2010) Bacterial sensor kinases: diversity in the recognition of environmental signals. *Annu Rev Microbiol* 64: 539-59

Krell, T. (2015) Tackling the bottleneck in bacterial signal transduction research: high-throughput identification of signal molecules. *Mol Microbiol* 96: 685-8

Krembel, A., Colin, R., Sourjik, V. (2015) Importance of multiple methylation sites in *Escherichia coli* chemotaxis. *PLoS One* 10: e0145582

Kristich, C.J., Ordal, G.W. (2002) *Bacillus subtilis* CheD is a chemoreceptor modification enzyme required for chemotaxis. *J Biol Chem* 277: 25356-62

Kristich, C.J., Glekas, G.D., Ordal, G.W. (2003) The conserved cytoplasmic module of the transmembrane chemoreceptor McpC mediates carbohydrate chemotaxis in *Bacillus subtilis*. *Mol Microbiol* 47: 1353-66

Kuiper, I., Kravchenko, L.V., Bloemberg, G.V. *et al.* (2002) *Pseudomonas putida* strain PCL1444, selected for efficient root colonization and naphthalene degradation, effectively utilizes root exudate components. *Mol Plant Microbe Interact* 15: 734-41

Kuroda, A., Kumano, T., Taguchi, K. *et al.* (1995) Molecular cloning and characterization of a chemotactic transducer gene in *Pseudomonas aeruginosa*. *J Bacteriol* 177: 7019-25

Kyriakidis, D.A., Theodorou, M.C., Tiligada, E. (2012) Histamine in two component system-mediated bacterial signaling. *Front Biosci (Landmark Ed)* 17: 1108-19

Lacal, J., Alfonso, C., Liu, X. *et al.* (2010a) Identification of a chemoreceptor for tricarboxylic acid cycle intermediates: differential chemotactic response towards receptor ligands. *J Biol Chem* 285: 23126-36

Lacal, J., Garcia-Fontana, C., Munoz-Martinez, F. *et al.* (2010b) Sensing of environmental signals: classification of chemoreceptors according to the size of their ligand binding regions. *Environ Microbiol* 12: 2873-84

Lacal, J., Munoz-Martinez, F., Reyes-Darias, J.A. *et al.* (2011a) Bacterial chemotaxis towards aromatic hydrocarbons in *Pseudomonas*. *Environ Microbiol* 13: 1733-44

Lacal, J., Garcia-Fontana, C., Callejo-Garcia, C. *et al.* (2011b) Physiologically relevant divalent cations modulate citrate recognition by the McpS chemoreceptor. *J Mol Recognit* 24: 378-85

Lacal, J., Reyes-Darias, J.A., Garcia-Fontana, C. *et al.* (2013) Tactic responses to pollutants and their potential to increase biodegradation efficiency. *J Appl Microbiol* 114: 923-33

Laganenka, L., Colin, R., Sourjik, V. (2016) Chemotaxis towards autoinducer 2 mediates autoaggregation in *Escherichia coli*. *Nat Commun* 7: 12984

Laganenka, L., Sourjik, V. (2018) Autoinducer 2-dependent *Escherichia coli* biofilm formation is enhanced in a dual-species coculture. *Appl Environ Microbiol* 84

Lai, R.Z., Parkinson, J.S. (2014) Functional suppression of HAMP domain signaling defects in the *E. coli* serine chemoreceptor. *J Mol Biol* 426: 3642-55

Lai, W.C., Beel, B.D., Hazelbauer, G.L. (2006a) Adaptational modification and ligand occupancy have opposite effects on positioning of the transmembrane signalling helix of a chemoreceptor. *Mol Microbiol* 61: 1081-90

Lai, W.C., Barnakova, L.A., Barnakov, A.N. *et al.* (2006b) Similarities and differences in interactions of the activity-enhancing chemoreceptor pentapeptide with the two enzymes of adaptational modification. *J Bacteriol* 188: 5646-9

Lambert, A., Takahashi, N., Charon, N.W. *et al.* (2012) Chemotactic behavior of pathogenic and nonpathogenic *Leptospira* species. *Appl Environ Microbiol* 78: 8467-9

Laskowski, R.A., Swindells, M.B. (2011) LigPlot+: multiple ligand-protein interaction diagrams for drug discovery. *J Chem Inf Model* 51: 2778-86

Latif-Eugenin, F., Beaz-Hidalgo, R., Figueras, M.J. (2016) First record of the rare species *Aeromonas schubertii* from mussels: phenotypic and genetic reevaluation of the species and a review of the literature. *Arch Microbiol* 198: 333-45

Laub, M.T., Goulian, M. (2007) Specificity in two-component signal transduction pathways. *Annu Rev Genet* 41: 121-45

Laue, T.M., Shah, B.D., Ridgeway, T.M. *et al.* (1992) Computer-aided interpretation of analytical sedimentation data for proteins. In *Analytical Ultracentrifugation in Biochemistry and Polymer Science*, E. HS, J. RA, C HJ (eds) pp 90–125. Cambridge, UK: Royal Society of Chemistry

Lauro, F.M., Chastain, R.A., Ferriera, S. *et al.* (2013) Draft genome sequence of the deep-sea bacterium *Shewanella benthica* strain KT99. *Genome Announc* 1

Lee, A.I., Delgado, A., Gunsalus, R.P. (1999) Signal-dependent phosphorylation of the membrane-bound NarX two-component sensor-transmitter protein of *Escherichia coli*: nitrate elicits a superior anion ligand response compared to nitrite. *J Bacteriol* 181: 5309-16

Lee, D.Y., Ramos, A., Macomber, L. *et al.* (2002) Taxis response of various denitrifying bacteria to nitrate and nitrite. *Appl Environ Microbiol* 68: 2140-7

Li, J., Wang, C., Yang, G. *et al.* (2017a) Molecular mechanism of environmental D-xylose perception by a XylFII-LytS complex in bacteria. *Proc Natl Acad Sci U S A* 114: 8235-8240

Li, M., Hazelbauer, G.L. (2004) Cellular stoichiometry of the components of the chemotaxis signaling complex. *J Bacteriol* 186: 3687-94

Li, M., Khursigara, C.M., Subramaniam, S. *et al.* (2011) Chemotaxis kinase CheA is activated by three neighbouring chemoreceptor dimers as effectively as by receptor clusters. *Mol Microbiol* 79: 677-85

Li, M., Hazelbauer, G.L. (2011) Core unit of chemotaxis signaling complexes. *Proc Natl Acad Sci U S A* 108: 9390-5

Li, W., Lu, C.D. (2007) Regulation of carbon and nitrogen utilization by CbrAB and NtrBC two-component systems in *Pseudomonas aeruginosa*. *J Bacteriol* 189: 5413-20

Li, X.G., Zhang, T.L., Wang, X.X. *et al.* (2013) The composition of root exudates from two different resistant peanut cultivars and their effects on the growth of soil-borne pathogen. *Int J Biol Sci* 9: 164-73

Li, Y., Zhou, M., Wang, F. *et al.* (2017b) *Photobacterium proteolyticum* sp. nov., a protease-producing bacterium isolated from ocean sediments of Laizhou Bay. *Int J Syst Evol Microbiol* 67: 1835-1840

Liao, H., Wan, H., Shaff, J. *et al.* (2006) Phosphorus and aluminum interactions in soybean in relation to aluminum tolerance. Exudation of specific organic acids from different regions of the intact root system. *Plant Physiol* 141: 674-84

Lim, J.M., Jeon, C.O., Lee, J.C. *et al.* (2006) *Marinimicrobium koreense* gen. nov., sp. nov. and *Marinimicrobium agarilyticum* sp. nov., novel moderately halotolerant bacteria isolated from tidal flat sediment in Korea. *Int J Syst Evol Microbiol* 56: 653-7

Lin, L.N., Li, J., Brandts, J.F. *et al.* (1994) The serine receptor of bacterial chemotaxis exhibits half-site saturation for serine binding. *Biochemistry* 33: 6564-70

Linnane, S.J., Keatings, V.M., Costello, C.M. *et al.* (1998) Total sputum nitrate plus nitrite is raised during acute pulmonary infection in cystic fibrosis. *Am J Respir Crit Care Med* 158: 207-12

Lipton, D.S., Blanchar, R.W., Blevins, D.G. (1987) Citrate, malate, and succinate concentration in exudates from P-sufficient and P-stressed *Medicago sativa* L. seedlings. *Plant Physiol* 85: 315-7

Liu, J., Hu, B., Morado, D.R. *et al.* (2012) Molecular architecture of chemoreceptor arrays revealed by cryoelectron tomography of *Escherichia coli* minicells. *Proc Natl Acad Sci U S A* 109: E1481-8

Liu, L., Li, N., Zhang, D. *et al.* (2016) Complete genome sequence of the highly virulent *Aeromonas schubertii* strain WL1483, isolated from diseased snakehead fish (*Channa argus*) in China. *Genome Announc* 4

Liu, P., Huang, D., Hu, X. *et al.* (2017) Targeting inhibition of SmpB by peptide aptamer attenuates the virulence to protect Zebrafish against *Aeromonas veronii* infection. *Front Microbiol* 8: 1766

Liu, X., Parales, R.E. (2008) Chemotaxis of *Escherichia coli* to pyrimidines: a new role for the signal transducer tap. *J Bacteriol* 190: 972-9

Liu, Y.C., Machuca, M.A., Beckham, S.A. *et al.* (2015) Structural basis for amino-acid recognition and transmembrane signalling by tandem Per-Arnt-Sim (tandem PAS) chemoreceptor sensory domains. *Acta Crystallogr D Biol Crystallogr* 71: 2127-36

Lopez-Farfan, D., Reyes-Darias, J.A., Krell, T. (2017) The expression of many chemoreceptor genes depends on the cognate chemoeffector as well as on the growth medium and phase. *Curr Genet* 63: 457-470

Lowe, E.C., Basle, A., Czjzek, M. *et al.* (2012) A scissor blade-like closing mechanism implicated in transmembrane signaling in a Bacteroides hybrid two-component system. *Proc Natl Acad Sci U S A* 109: 7298-303

Lucena, T., Mesa, J., Rodriguez-Llorente, I.D. *et al.* (2016) *Marinomonas spartinae* sp. nov., a novel species with plant-beneficial properties. *Int J Syst Evol Microbiol* 66: 1686-91

Lukas, H., Reimann, J., Kim, O.B. *et al.* (2010) Regulation of aerobic and anaerobic D-malate metabolism of *Escherichia coli* by the LysR-type regulator DmlR (YeaT). *J Bacteriol* 192: 2503-11

Luu, R.A., Schneider, B.J., Ho, C.C. *et al.* (2013) Taxis of *Pseudomonas putida* F1 toward phenylacetic acid is mediated by the energy taxis receptor Aer2. *Appl Environ Microbiol* 79: 2416-23

Luu, R.A., Kootstra, J.D., Nesteryuk, V. *et al.* (2015) Integration of chemotaxis, transport and catabolism in *Pseudomonas putida* and identification of the aromatic acid chemoreceptor PcaY. *Mol Microbiol* 96: 134-47

Machuca, M.A., Liu, Y.C., Beckham, S.A. *et al.* (2016) The crystal structure of the tandem-PAS sensing domain of *Campylobacter jejuni* chemoreceptor Tlp1 suggests indirect mechanism of ligand recognition. *J Struct Biol* 194: 205-13

Machuca, M.A., Johnson, K.S., Liu, Y.C. *et al.* (2017) *Helicobacter pylori* chemoreceptor TlpC mediates chemotaxis to lactate. *Sci Rep* 7: 14089

Mansfield, J., Genin, S., Magori, S. *et al.* (2012) Top 10 plant pathogenic bacteria in molecular plant pathology. *Mol Plant Pathol* 13: 614-29

Manson, M.D., Blank, V., Brade, G. *et al.* (1986) Peptide chemotaxis in *E. coli* involves the Tap signal transducer and the dipeptide permease. *Nature* 321: 253-6

Martin-Mora, D., Ortega, A., Reyes-Darias, J.A. *et al.* (2016a) Identification of a chemoreceptor in *Pseudomonas aeruginosa* that specifically mediates chemotaxis toward alpha-ketoglutarate. *Front Microbiol* 7: 1937

Martin-Mora, D., Reyes-Darias, J.A., Ortega, A. *et al.* (2016b) McpQ is a specific citrate chemoreceptor that responds preferentially to citrate/metal ion complexes. *Environ Microbiol* 18: 3284-3295

Martin-Mora, D., Ortega, A., Perez-Maldonado, F.J. *et al.* (2018) The activity of the C4-dicarboxylic acid chemoreceptor of *Pseudomonas aeruginosa* is controlled by chemoattractants and antagonists. *Sci Rep* 8: 2102

Martin-Mora, D., Ortega, A., Matilla, M.A. *et al.* (2019) The molecular mechanism of nitrate chemotaxis via direct ligand binding to the PilJ domain of McpN. *MBio* 10: e02334-18

Martín-Mora, D., Fernández, M., Velando, F. *et al.* (2018) Functional annotation of bacterial signal transduction systems: progress and challenges. *Int J Mol Sci* 19

Martinez-Garcia, P.M., Lopez-Solanilla, E., Ramos, C. *et al.* (2016) Prediction of bacterial associations with plants using a supervised machine-learning approach. *Environ Microbiol* 18: 4847-4861

Martinez-Murcia, A., Beaz-Hidalgo, R., Navarro, A. *et al.* (2016) *Aeromonas lusitana* sp. nov., isolated from untreated water and vegetables. *Curr Microbiol* 72: 795-803

Martinez-Murcia, A.J., Esteve, C., Garay, E. *et al.* (1992) *Aeromonas allosaccharophila* sp. nov., a new mesophilic member of the genus *Aeromonas*. *FEMS Microbiol Lett* 70: 199-205

Martinez, S.E., Beavo, J.A., Hol, W.G. (2002) GAF domains: two-billion-year-old molecular switches that bind cyclic nucleotides. *Mol Interv* 2: 317-23

Maruyama, I.N., Mikawa, Y.G., Maruyama, H.I. (1995) A model for transmembrane signalling by the aspartate receptor based on random-cassette mutagenesis and site-directed disulfide cross-linking. *J Mol Biol* 253: 530-46

Masduki, A., Nakamura, J., Ohga, T. *et al.* (1995) Isolation and characterization of chemotaxis mutants and genes of *Pseudomonas aeruginosa*. *J Bacteriol* 177: 948-52

Matilla, M.A., Espinosa-Urgel, M., Rodriguez-Herva, J.J. *et al.* (2007) Genomic analysis reveals the major driving forces of bacterial life in the rhizosphere. *Genome Biol* 8: R179

Matilla, M.A., Ramos, J.L., Bakker, P.A. *et al.* (2010) *Pseudomonas putida* KT2440 causes induced systemic resistance and changes in *Arabidopsis* root exudation. *Environ Microbiol Rep* 2: 381-8

Matilla, M.A., Krell, T. (2017) Chemoreceptor-based signal sensing. *Curr Opin Biotechnol* 45: 8-14

Matilla, M.A., Krell, T. (2018) The effect of bacterial chemotaxis on host infection and pathogenicity. *FEMS Microbiol Rev* 42

Matsunaga, T., Okamura, Y., Fukuda, Y. *et al.* (2005) Complete genome sequence of the facultative anaerobic magnetotactic bacterium *Magnetospirillum* sp. strain AMB-1. *DNA Res* 12: 157-66

McEvoy, M.M., Bren, A., Eisenbach, M. *et al.* (1999) Identification of the binding interfaces on CheY for two of its targets, the phosphatase CheZ and the flagellar switch protein fliM. *J Mol Biol* 289: 1423-33

McHatton, S.C., Barry, J.P., Jannasch, H.W. *et al.* (1996) High nitrate concentrations in vacuolate, autotrophic marine *Beggiatoa* spp. *Appl Environ Microbiol* 62: 954-8

McKellar, J.L., Minnell, J.J., Gerth, M.L. (2015) A high-throughput screen for ligand binding reveals the specificities of three amino acid chemoreceptors from *Pseudomonas syringae* pv. *actinidiae*. *Mol Microbiol* 96: 694-707

McLaughlin, H.P., Caly, D.L., McCarthy, Y. *et al.* (2012) An orphan chemotaxis sensor regulates virulence and antibiotic tolerance in the human pathogen *Pseudomonas aeruginosa*. *PLoS One* 7: e42205

Menanteau-Ledouble, S., Kumar, G., Saleh, M. *et al.* (2016) *Aeromonas salmonicida*: updates on an old acquaintance. *Dis Aquat Organ* 120: 49-68

Merritt, P.M., Danhorn, T., Fuqua, C. (2007) Motility and chemotaxis in *Agrobacterium tumefaciens* surface attachment and biofilm formation. *J Bacteriol* 189: 8005-14

Mesibov, R., Adler, J. (1972) Chemotaxis toward amino acids in *Escherichia coli*. *J Bacteriol* 112: 315-26

Methe, B.A., Nelson, K.E., Deming, J.W. *et al.* (2005) The psychrophilic lifestyle as revealed by the genome sequence of *Colwellia psychrerythraea* 34H through genomic and proteomic analyses. *Proc Natl Acad Sci U S A* 102: 10913-8

Metz, M., Doyle, E., Bindslev-Jensen, C. *et al.* (2011) Effects of antihistamines on innate immune responses to severe bacterial infection in mice. *Int Arch Allergy Immunol* 155: 355-60

Milburn, M.V., Prive, G.G., Milligan, D.L. *et al.* (1991) Three-dimensional structures of the ligand-binding domain of the bacterial aspartate receptor with and without a ligand. *Science* 254: 1342-7

Miller-Fleming, L., Olin-Sandoval, V., Campbell, K. *et al.* (2015) Remaining mysteries of molecular biology: the role of polyamines in the cell. *J Mol Biol* 427: 3389-406

Miller, A.S., Falke, J.J. (2004) Side chains at the membrane-water interface modulate the signaling state of a transmembrane receptor. *Biochemistry* 43: 1763-70

Milligan, D.L., Koshland, D.E., Jr. (1993) Purification and characterization of the periplasmic domain of the aspartate chemoreceptor. *J Biol Chem* 268: 19991-7

Millikan, D.S., Ruby, E.G. (2003) FlrA, a sigma54-dependent transcriptional activator in *Vibrio fischeri,* is required for motility and symbiotic light-organ colonization. *J Bacteriol* 185: 3547-57

Minana-Galbis, D., Farfan, M., Loren, J.G. *et al.* (2002) Biochemical identification and numerical taxonomy of *Aeromonas* spp. isolated from environmental and clinical samples in Spain. *J Appl Microbiol* 93: 420-30

Minana-Galbis, D., Farfan, M., Fuste, M.C. *et al.* (2004) *Aeromonas molluscorum* sp. nov., isolated from bivalve molluscs. *Int J Syst Evol Microbiol* 54: 2073-8

Minana-Galbis, D., Farfan, M., Fuste, M.C. *et al.* (2007) *Aeromonas bivalvium* sp. nov., isolated from bivalve molluscs. *Int J Syst Evol Microbiol* 57: 582-7

Minana-Galbis, D., Farfan, M., Gaspar Loren, J. *et al.* (2010) Proposal to assign *Aeromonas diversa* sp. nov. as a novel species designation for *Aeromonas* group 501. *Syst Appl Microbiol* 33: 15-9

Miyazaki, M., Nogi, Y., Fujiwara, Y. *et al.* (2008) *Neptunomonas japonica* sp. nov., an *Osedax japonicus* symbiont-like bacterium isolated from sediment adjacent to sperm whale carcasses off Kagoshima, Japan. *Int J Syst Evol Microbiol* 58: 866-71

Moglich, A., Ayers, R.A., Moffat, K. (2009) Structure and signaling mechanism of Per-ARNT-Sim domains. *Structure* 17: 1282-94

Molina, M.A., Ramos, J.L., Espinosa-Urgel, M. (2006) A two-partner secretion system is involved in seed and root colonization and iron uptake by *Pseudomonas putida* KT2440. *Environ Microbiol* 8: 639-47

Moore, J.O., Hendrickson, W.A. (2012) An asymmetry-to-symmetry switch in signal transmission by the histidine kinase receptor for TMAO. *Structure* 20: 729-41

Moradali, M.F., Ghods, S., Rehm, B.H. (2017) *Pseudomonas aeruginosa* lifestyle: A paradigm for adaptation, survival, and persistence. *Front Cell Infect Microbiol* 7: 39

Moreno, R., Rojo, F. (2013) The contribution of proteomics to the unveiling of the survival strategies used by *Pseudomonas putida* in changing and hostile environments. *Proteomics* 13: 2822-30

Morgan, R., Kohn, S., Hwang, S.H. *et al.* (2006) BdlA, a chemotaxis regulator essential for biofilm dispersion in *Pseudomonas aeruginosa*. *J Bacteriol* 188: 7335-43

Morris, R.J., Zwart, P.H., Cohen, S. *et al.* (2004) Breaking good resolutions with ARP/wARP. *J Synchrotron Radiat* 11: 56-9

Mougel, C., Zhulin, I.B. (2001) CHASE: an extracellular sensing domain common to transmembrane receptors from prokaryotes, lower eukaryotes and plants. *Trends Biochem Sci* 26: 582-4

Moukhametzianov, R., Klare, J.P., Efremov, R. *et al.* (2006) Development of the signal in sensory rhodopsin and its transfer to the cognate transducer. *Nature* 440: 115-9

Moulton, R.C., Montie, T.C. (1979) Chemotaxis by *Pseudomonas aeruginosa*. *J Bacteriol* 137: 274-80

Mowery, P., Ostler, J.B., Parkinson, J.S. (2008) Different signaling roles of two conserved residues in the cytoplasmic hairpin tip of Tsr, the *Escherichia coli* serine chemoreceptor. *J Bacteriol* 190: 8065-74

Muller, J., Schiel, S., Ordal, G.W. *et al.* (1997) Functional and genetic characterization of *mcpC*, which encodes a third methyl-accepting chemotaxis protein in *Bacillus subtilis*. *Microbiology* 143 (Pt 10): 3231-40

Muraki, T., Taki, M., Hasegawa, Y. *et al.* (2003) Prokaryotic homologs of the eukaryotic 3-hydroxyanthranilate 3,4-dioxygenase and 2-amino-3-carboxymuconate-6-semialdehyde decarboxylase in the 2-nitrobenzoate degradation pathway of *Pseudomonas fluorescens* strain KU-7. *Appl Environ Microbiol* 69: 1564-72

Murshudov, G.N., Skubak, P., Lebedev, A.A. *et al.* (2011) REFMAC5 for the refinement of macromolecular crystal structures. *Acta Crystallogr D Biol Crystallogr* 67: 355-67

Nakagawa, T., Iino, T., Suzuki, K. *et al.* (2006) *Ferrimonas futtsuensis* sp. nov. and *Ferrimonas kyonanensis* sp. nov., selenate-reducing bacteria belonging to the Gammaproteobacteria isolated from Tokyo Bay. *Int J Syst Evol Microbiol* 56: 2639-45

Nakazawa, T. (2002) Travels of a Pseudomonas, from Japan around the world. *Environ Microbiol* 4: 782-6

Namsaraev, Z., Akimov, V., Tsapin, A. *et al.* (2009) *Marinospirillum celere* sp. nov., a novel haloalkaliphilic, helical bacterium isolated from Mono Lake. *Int J Syst Evol Microbiol* 59: 2329-32

Narasingarao, P., Haggblom, M.M. (2006) *Sedimenticola selenatireducens*, gen. nov., sp. nov., an anaerobic selenate-respiring bacterium isolated from estuarine sediment. *Syst Appl Microbiol* 29: 382-8

Nealson, K.H., Moser, D.P., Saffarini, D.A. (1995) Anaerobic electron acceptor chemotaxis in *Shewanella putrefaciens*. *Appl Environ Microbiol* 61: 1551-4

Neumann, S., Hansen, C.H., Wingreen, N.S. *et al.* (2010) Differences in signalling by directly and indirectly binding ligands in bacterial chemotaxis. *EMBO J* 29: 3484-95

Neumann, S., Grosse, K., Sourjik, V. (2012) Chemotactic signaling via carbohydrate phosphotransferase systems in *Escherichia coli*. *Proc Natl Acad Sci U S A* 109: 12159-64

Ng, W.L., Wei, Y., Perez, L.J. *et al.* (2010) Probing bacterial transmembrane histidine kinase receptor-ligand interactions with natural and synthetic molecules. *Proc Natl Acad Sci U S A* 107: 5575-80

Ni, B., Huang, Z., Fan, Z. *et al.* (2013) *Comamonas testosteroni* uses a chemoreceptor for tricarboxylic acid cycle intermediates to trigger chemotactic responses towards aromatic compounds. *Mol Microbiol* 90: 813-23

Nichols, N.N., Harwood, C.S. (2000) An aerotaxis transducer gene from *Pseudomonas putida*. *FEMS Microbiol Lett* 182: 177-83

Nikata, T., Sumida, K., Kato, J. *et al.* (1992) Rapid method for analyzing bacterial behavioral responses to chemical stimuli. *Appl Environ Microbiol* 58: 2250-4

Nikel, P.I., Silva-Rocha, R., Benedetti, I. *et al.* (2014) The private life of environmental bacteria: pollutant biodegradation at the single cell level. *Environ Microbiol* 16: 628-42

Nikel, P.I., de Lorenzo, V. (2014) Robustness of *Pseudomonas putida* KT2440 as a host for ethanol biosynthesis. *N Biotechnol* 31: 562-71

Ninfa, A.J., Jiang, P. (2005) PII signal transduction proteins: sensors of alpha-ketoglutarate that regulate nitrogen metabolism. *Curr Opin Microbiol* 8: 168-73

Nishiyama, S., Suzuki, D., Itoh, Y. *et al.* (2012) Mlp24 (McpX) of *Vibrio cholerae* implicated in pathogenicity functions as a chemoreceptor for multiple amino acids. *Infect Immun* 80: 3170-8

Nishiyama, S., Garzon, A., Parkinson, J.S. (2014) Mutational analysis of the P1 phosphorylation domain in *Escherichia coli* CheA, the signaling kinase for chemotaxis. *J Bacteriol* 196: 257-64

Nishiyama, S., Takahashi, Y., Yamamoto, K. *et al.* (2016) Identification of a *Vibrio cholerae* chemoreceptor that senses taurine and amino acids as attractants. *Sci Rep* 6: 20866

Nogi, Y., Hosoya, S., Kato, C. *et al.* (2007) *Psychromonas hadalis* sp. nov., a novel piezophilic bacterium isolated from the bottom of the Japan Trench. *Int J Syst Evol Microbiol* 57: 1360-4

Noriega, C.E., Lin, H.Y., Chen, L.L. *et al.* (2010) Asymmetric cross-regulation between the nitrate-responsive NarX-NarL and NarQ-NarP two-component regulatory systems from *Escherichia coli* K-12. *Mol Microbiol* 75: 394-412

Norsworthy, A.N., Visick, K.L. (2013) Gimme shelter: how *Vibrio fischeri* successfully navigates an animal's multiple environments. *Front Microbiol* 4: 356

Novakova, D., Svec, P., Sedlacek, I. (2009) Characterization of *Aeromonas encheleia* strains isolated from aquatic environments in the Czech Republic. *Lett Appl Microbiol* 48: 289-94

O'Connor, J.R., Kuwada, N.J., Huangyutitham, V. *et al.* (2012) Surface sensing and lateral subcellular localization of WspA, the receptor in a chemosensory-like system leading to c-di-GMP production. *Mol Microbiol* 86: 720-9

O'Mahony, L., Akdis, M., Akdis, C.A. (2011) Regulation of the immune response and inflammation by histamine and histamine receptors. *J Allergy Clin Immunol* 128: 1153-62

Obranic, S., Babic, F., Maravic-Vlahovicek, G. (2013) Improvement of pBBR1MCS plasmids, a very useful series of broad-host-range cloning vectors. *Plasmid* 70: 263-7

Oku, S., Komatsu, A., Tajima, T. *et al.* (2012) Identification of chemotaxis sensory proteins for amino acids in *Pseudomonas fluorescens Pf0-1* and their involvement in chemotaxis to tomato root exudate and root colonization. *Microbes Environ* 27: 462-9

Oku, S., Komatsu, A., Nakashimada, Y. *et al.* (2014) Identification of *Pseudomonas fluorescens* chemotaxis sensory proteins for malate, succinate, and fumarate, and their involvement in root colonization. *Microbes Environ* 29: 413-9

Ortega-Calvo, J.J., Marchenko, A.I., Vorobyov, A.V. *et al.* (2003) Chemotaxis in polycyclic aromatic hydrocarbon-degrading bacteria isolated from coal-tar- and oil-polluted rhizospheres. *FEMS Microbiol Ecol* 44: 373-81

Ortega, A., Amoros, D., Garcia de la Torre, J. (2011) Prediction of hydrodynamic and other solution properties of rigid proteins from atomic- and residue-level models. *Biophys J* 101: 892-8

Ortega, A., Krell, T. (2014) The HBM domain: introducing bimodularity to bacterial sensing. *Protein Sci* 23: 332-6

Ortega, A., Zhulin, I.B., Krell, T. (2017a) Sensory repertoire of bacterial chemoreceptors. *Microbiol Mol Biol Rev* 81

Ortega, D.R., Zhulin, I.B. (2016) Evolutionary genomics suggests that CheV Is an additional adaptor for accommodating specific chemoreceptors within the chemotaxis signaling complex. *PLoS Comput Biol* 12: e1004723

Ortega, D.R., Fleetwood, A.D., Krell, T. *et al.* (2017b) Assigning chemoreceptors to chemosensory pathways in *Pseudomonas aeruginosa*. *Proc Natl Acad Sci U S A* 114: 12809-12814

Ottemann, K.M., Xiao, W., Shin, Y.K. *et al.* (1999) A piston model for transmembrane signaling of the aspartate receptor. *Science* 285: 1751-4

Oura, H., Tashiro, Y., Toyofuku, M. *et al.* (2015) Inhibition of *Pseudomonas aeruginosa* swarming motility by 1-naphthol and other bicyclic compounds bearing hydroxyl groups. *Appl Environ Microbiol* 81: 2808-18

Panjikar, S., Parthasarathy, V., Lamzin, V.S. *et al.* (2005) Auto-rickshaw: an automated crystal structure determination platform as an efficient tool for the validation of an X-ray diffraction experiment. *Acta Crystallogr D Biol Crystallogr* 61: 449-57

Panula, P., Chazot, P.L., Cowart, M. *et al.* (2015) International union of casic and clinical pharmacology. XCVIII. Histamine receptors. *Pharmacol Rev* 67: 601-55

Parales, R.E. (2004) Nitrobenzoates and aminobenzoates are chemoattractants for *Pseudomonas strains*. *Appl Environ Microbiol* 70: 285-92

Parales, R.E., Luu, R.A., Chen, G.Y. *et al.* (2013) *Pseudomonas putida* F1 has multiple chemoreceptors with overlapping specificity for organic acids. *Microbiology* 159: 1086-96

Park, H., Im, W., Seok, C. (2011) Transmembrane signaling of chemotaxis receptor tar: insights from molecular dynamics simulation studies. *Biophys J* 100: 2955-63

Park, S.Y., Chao, X., Gonzalez-Bonet, G. *et al.* (2004a) Structure and function of an unusual family of protein phosphatases: the bacterial chemotaxis proteins CheC and CheX. *Mol Cell* 16: 563-74

Park, S.Y., Quezada, C.M., Bilwes, A.M. *et al.* (2004b) Subunit exchange by CheA histidine kinases from the mesophile *Escherichia coli* and the thermophile *Thermotoga maritima*. *Biochemistry* 43: 2228-40

Parkinson, J.S. (2010) Signaling mechanisms of HAMP domains in chemoreceptors and sensor kinases. *Annu Rev Microbiol* 64: 101-22

Parkinson, J.S., Hazelbauer, G.L., Falke, J.J. (2015) Signaling and sensory adaptation in *Escherichia coli* chemoreceptors: 2015 update. *Trends Microbiol* 23: 257-66

Parras, F., Diaz, M.D., Reina, J. *et al.* (1993) Meningitis due to *Aeromonas* species: case report and review. *Clin Infect Dis* 17: 1058-60

Pasupuleti, S., Sule, N., Cohn, W.B. *et al.* (2014) Chemotaxis of *Escherichia coli* to norepinephrine (NE) requires conversion of NE to 3,4-dihydroxymandelic acid. *J Bacteriol* 196: 3992-4000

Pedetta, A., Parkinson, J.S., Studdert, C.A. (2014) Signalling-dependent interactions between the kinase-coupling protein CheW and chemoreceptors in living cells. *Mol Microbiol* 93: 1144-55

Penaloza, E., Gutierrez, A., Martinez, J. *et al.* (2002) Differential gene expression in proteoid root clusters of white lupin (*Lupinus albus*). *Physiol Plant* 116: 28-36

Persat, A., Inclan, Y.F., Engel, J.N. *et al.* (2015) Type IV pili mechanochemically regulate virulence factors in *Pseudomonas aeruginosa*. *Proc Natl Acad Sci U S A* 112: 7563-8

Pestana, M.N., Gomes, A.A. (2014) The effect of soil on cork quality. *Front Chem* 2: 80

Petrova, O.E., Sauer, K. (2012) Dispersion by *Pseudomonas aeruginosa* requires an unusual posttranslational modification of BdlA. *Proc Natl Acad Sci U S A* 109: 16690-5

Pham, H.T., Parkinson, J.S. (2011) Phenol sensing by *Escherichia coli* chemoreceptors: a nonclassical mechanism. *J Bacteriol* 193: 6597-604

Phornphisutthimas, S., Thamchaipenet, A., Panijpan, B. (2007) Conjugation in *Escherichia coli:* A laboratory exercise. *Biochem Mol Biol Educ* 35: 440-5

Piasta, K.N., Ulliman, C.J., Slivka, P.F. *et al.* (2013) Defining a key receptor-CheA kinase contact and elucidating its function in the membrane-bound bacterial chemosensory array: a disulfide mapping and TAM-IDS Study. *Biochemistry* 52: 3866-80

Piatigorsky, J., O'Brien, W.E., Norman, B.L. *et al.* (1988) Gene sharing by delta-crystallin and argininosuccinate lyase. *Proc Natl Acad Sci U S A* 85: 3479-83

Picao, R.C., Poirel, L., Demarta, A. *et al.* (2008) Plasmid-mediated quinolone resistance in *Aeromonas allosaccharophila* recovered from a Swiss lake. *J Antimicrob Chemother* 62: 948-50

Pineda-Molina, E., Reyes-Darias, J.A., Lacal, J. *et al.* (2012) Evidence for chemoreceptors with bimodular ligand-binding regions harboring two signal-binding sites. *Proc Natl Acad Sci U S A* 109: 18926-31

Pokkuluri, P.R., Dwulit-Smith, J., Duke, N.E. *et al.* (2013) Analysis of periplasmic sensor domains from *Anaeromyxobacter dehalogenans* 2CP-C: structure of one sensor domain from a histidine kinase and another from a chemotaxis protein. *Microbiologyopen* 2: 766-77

Poole, P.S., Armitage, J.P. (1988) Motility response of *Rhodobacter sphaeroides* to chemotactic stimulation. *J Bacteriol* 170: 5673-9

Popova, T.N., Pinheiro de Carvalho, M.A. (1998) Citrate and isocitrate in plant metabolism. *Biochim Biophys Acta* 1364: 307-25

Porter, S.L., Wadhams, G.H., Armitage, J.P. (2011) Signal processing in complex chemotaxis pathways. *Nat Rev Microbiol* 9: 153-65

Preisler, A., de Beer, D., Lichtschlag, A. *et al.* (2007) Biological and chemical sulfide oxidation in a *Beggiatoa* inhabited marine sediment. *ISME J* 1: 341-53

Qin, R., Hirano, Y., Brunner, I. (2007) Exudation of organic acid anions from poplar roots after exposure to Al, Cu and Zn. *Tree Physiol* 27: 313-20

Rader, B.A., Wreden, C., Hicks, K.G. *et al.* (2011) *Helicobacter pylori* perceives the quorum-sensing molecule AI-2 as a chemorepellent via the chemoreceptor TlpB. *Microbiology* 157: 2445-55

Rahman, H., King, R.M., Shewell, L.K. *et al.* (2014) Characterisation of a multi-ligand binding chemoreceptor CcmL (Tlp3) of *Campylobacter jejuni*. *PLoS Pathog* 10: e1003822

Rahme, L.G., Stevens, E.J., Wolfort, S.F. *et al.* (1995) Common virulence factors for bacterial pathogenicity in plants and animals. *Science* 268: 1899-902

Rahme, L.G., Ausubel, F.M., Cao, H. *et al.* (2000) Plants and animals share functionally common bacterial virulence factors. *Proc Natl Acad Sci U S A* 97: 8815-21

Ramos-Gonzalez, M.I., Molin, S. (1998) Cloning, sequencing, and phenotypic characterization of the *rpoS* gene from *Pseudomonas putida* KT2440. *J Bacteriol* 180: 3421-31

Rangarajan, E.S., Izard, T. (2013) Dimer asymmetry defines alpha-catenin interactions. *Nat Struct Mol Biol* 20: 188-93

Rao, C.V., Glekas, G.D., Ordal, G.W. (2008) The three adaptation systems of *Bacillus subtilis* chemotaxis. *Trends Microbiol* 16: 480-7

Rasmussen-Ivey, C.R., Figueras, M.J., McGarey, D. *et al.* (2016) Virulence factors of *Aeromonas hydrophila*: in the wake of reclassification. *Front Microbiol* 7: 1337

Regenhardt, D., Heuer, H., Heim, S. *et al.* (2002) Pedigree and taxonomic credentials of *Pseudomonas putida* strain KT2440. *Environ Microbiol* 4: 912-5

Reyes-Darias, J.A., Yang, Y., Sourjik, V. *et al.* (2015a) Correlation between signal input and output in PctA and PctB amino acid chemoreceptor of *Pseudomonas aeruginosa*. *Mol Microbiol* 96: 513-25

Reyes-Darias, J.A., Garcia, V., Rico-Jimenez, M. *et al.* (2015b) Specific gamma-aminobutyrate chemotaxis in pseudomonads with different lifestyle. *Mol Microbiol* 97: 488-501

Rico-Jimenez, M., Munoz-Martinez, F., Garcia-Fontana, C. *et al.* (2013a) Paralogous chemoreceptors mediate chemotaxis towards protein amino acids and the non-protein amino acid gamma-aminobutyrate (GABA). *Mol Microbiol* 88: 1230-43

Rico-Jimenez, M., Munoz-Martinez, F., Krell, T. *et al.* (2013b) Purification, crystallization and preliminary crystallographic analysis of the ligand-binding regions of the PctA and PctB chemoreceptors from *Pseudomonas aeruginosa* in complex with amino acids. *Acta Crystallogr Sect F Struct Biol Cryst Commun* 69: 1431-5

Rico-Jimenez, M., Reyes-Darias, J.A., Ortega, A. *et al.* (2016) Two different mechanisms mediate chemotaxis to inorganic phosphate in *Pseudomonas aeruginosa*. *Sci Rep* 6: 28967

Righetti, P.G., Verzola, B. (2001) Folding/unfolding/refolding of proteins: present methodologies in comparison with capillary zone electrophoresis. *Electrophoresis* 22: 2359-74

Rivera-Chavez, F., Lopez, C.A., Zhang, L.F. *et al.* (2016) Energy taxis toward host-derived nitrate supports a *Salmonella* pathogenicity island 1-independent mechanism of invasion. *MBio* 7: e00960-16

Rouleau, F.D., Vincent, A.T., Charette, S.J. (2018) Genomic and phenotypic characterization of an atypical *Aeromonas salmonicida* strain isolated from a lumpfish and producing unusual granular structures. *J Fish Dis* 41: 673-681

Roush, C.J., Lastoskie, C.M., Worden, R.M. (2006) Denitrification and chemotaxis of *Pseudomonas stutzeri* KC in porous media. *J Environ Sci Health A Tox Hazard Subst Environ Eng* 41: 967-83

Saavedra, M.J., Perea, V., Fontes, M.C. *et al.* (2007) Phylogenetic identification of *Aeromonas* strains isolated from carcasses of pig as new members of the species *Aeromonas allosaccharophila*. *Antonie Van Leeuwenhoek* 91: 159-67

Salah Ud-Din, A.I.M., Roujeinikova, A. (2017) Methyl-accepting chemotaxis proteins: a core sensing element in prokaryotes and archaea. *Cell Mol Life Sci* 74: 3293-3303

Sammito, M., Millan, C., Frieske, D. *et al.* (2015) ARCIMBOLDO_LITE: single-workstation implementation and use. *Acta Crystallogr D Biol Crystallogr* 71: 1921-30

Sampedro, I., Parales, R.E., Krell, T. *et al.* (2015) Pseudomonas chemotaxis. *FEMS Microbiol Rev* 39: 17-46

Saragosti, J., Calvez, V., Bournaveas, N. *et al.* (2011) Directional persistence of chemotactic bacteria in a traveling concentration wave. *Proc Natl Acad Sci U S A* 108: 16235-40

Sarand, I., Osterberg, S., Holmqvist, S. *et al.* (2008) Metabolism-dependent taxis towards (methyl)phenols is coupled through the most abundant of three polar localized Aer-like proteins of *Pseudomonas putida*. *Environ Microbiol* 10: 1320-34

Satomi, M., Kimura, B., Hayashi, M. *et al.* (1998) *Marinospirillum* gen. nov., with descriptions of *Marinospirillum megaterium* sp. nov., isolated from kusaya gravy, and transfer of *Oceanospirillum minutulum* to *Marinospirillum minutulum* comb. nov. *Int J Syst Bacteriol* 48 Pt 4: 1341-8

Satomi, M., Kimura, B., Hamada, T. *et al.* (2002) Phylogenetic study of the genus *Oceanospirillum* based on 16S rRNA and gyrB genes: emended description of the genus *Oceanospirillum*, description of *Pseudospirillum* gen. nov., *Oceanobacter* gen. nov. and *Terasakiella* gen. nov. and transfer of *Oceanospirillum jannaschii* and *Pseudomonas stanieri* to *Marinobacterium* as

Marinobacterium jannaschii comb. nov. and *Marinobacterium stanieri* comb. no. *Int J Syst Evol Microbiol* 52: 739-47

Satomi, M., Kimura, B., Hayashi, M. *et al.* (2004) *Marinospirillum* insulare sp. nov., a novel halophilic helical bacterium isolated from kusaya gravy. *Int J Syst Evol Microbiol* 54: 163-7

Sawai, H., Sugimoto, H., Shiro, Y. *et al.* (2012) Structural basis for oxygen sensing and signal transduction of the heme-based sensor protein Aer2 from *Pseudomonas aeruginosa*. *Chem Commun (Camb)* 48: 6523-5

Schafer, A., Tauch, A., Jager, W. *et al.* (1994) Small mobilizable multi-purpose cloning vectors derived from the *Escherichia coli* plasmids pK18 and pK19: selection of defined deletions in the chromosome of *Corynebacterium glutamicum*. *Gene* 145: 69-73

Scharf, B.E., Hynes, M.F., Alexandre, G.M. (2016) Chemotaxis signaling systems in model beneficial plant-bacteria associations. *Plant Mol Biol* 90: 549-59

Scheu, P.D., Kim, O.B., Griesinger, C. *et al.* (2010) Sensing by the membrane-bound sensor kinase DcuS: exogenous versus endogenous sensing of C(4)-dicarboxylates in bacteria. *Future Microbiol* 5: 1383-402

Schloss, P.D., Handelsman, J. (2004) Status of the microbial census. *Microbiol Mol Biol Rev* 68: 686-91

Schneider, T.R., Sheldrick, G.M. (2002) Substructure solution with SHELXD. *Acta Crystallogr D Biol Crystallogr* 58: 1772-9

Schubert, T. (2017) The organohalide-respiring bacterium *Sulfurospirillum multivorans:* a natural source for unusual cobamides. *World J Microbiol Biotechnol* 33: 93

Schuck, P. (2000) Size-distribution analysis of macromolecules by sedimentation velocity ultracentrifugation and lamm equation modeling. *Biophys J* 78: 1606-19

Schulz, H.N., Brinkhoff, T., Ferdelman, T.G. *et al.* (1999) Dense populations of a giant sulfur bacterium in Namibian shelf sediments. *Science* 284: 493-5

Schwarzer, C., Fischer, H., Machen, T.E. (2016) Chemotaxis and binding of *Pseudomonas aeruginosa* to scratch-wounded human cystic fibrosis airway epithelial cells. *PLoS One* 11: e0150109

Schweinitzer, T., Josenhans, C. (2010) Bacterial energy taxis: a global strategy? *Arch Microbiol* 192: 507-20

Schweizer, H.P. (1991) *Escherichia-Pseudomonas* shuttle vectors derived from pUC18/19. *Gene* 97: 109-21

Schweizer, H.P. (1992) Allelic exchange in *Pseudomonas aeruginosa* using novel ColE1-type vectors and a family of cassettes containing a portable *oriT* and the counter-selectable *Bacillus subtilis sacB* marker. *Mol Microbiol* 6: 1195-204

Sere, M.G., Tortosa, P., Chabanet, P. *et al.* (2015) Identification of a bacterial pathogen associated with *Porites* white patch syndrome in the Western Indian Ocean. *Mol Ecol* 24: 4570-81

Seymour, F.W., Doetsch, R.N. (1973) Chemotactic responses by motile bacteria. *J Gen Microbiol* 78: 287-96

Sheldrick, G.M. (2008) A short history of SHELX. *Acta Crystallogr A* 64: 112-22

Shi, K., Fan, X., Qiao, Z. *et al.* (2017) Arsenite oxidation regulator AioR regulates bacterial chemotaxis towards arsenite in *Agrobacterium tumefaciens* GW4. *Sci Rep* 7: 43252

Shimamura, T., Shiroishi, M., Weyand, S. *et al.* (2011) Structure of the human histamine H1 receptor complex with doxepin. *Nature* 475: 65-70

Shitashiro, M., Tanaka, H., Hong, C.S. *et al.* (2005) Identification of chemosensory proteins for trichloroethylene in *Pseudomonas aeruginosa*. *J Biosci Bioeng* 99: 396-402

Shu, C.J., Ulrich, L.E., Zhulin, I.B. (2003) The NIT domain: a predicted nitrate-responsive module in bacterial sensory receptors. *Trends Biochem Sci* 28: 121-4

Sidhu, C., Thakur, S., Sharma, G. *et al.* (2017) *Oceanospirillum sanctuarii* sp. nov., isolated from a sediment sample. *Int J Syst Evol Microbiol* 67: 3428-3434

Sigrist, C.J., de Castro, E., Cerutti, L. *et al.* (2013) New and continuing developments at PROSITE. *Nucleic Acids Res* 41: D344-7

Silva-Jimenez, H., Garcia-Fontana, C., Cadirci, B.H. *et al.* (2012) Study of the TmoS/TmoT two-component system: towards the functional characterization of the family of TodS/TodT like systems. *Microb Biotechnol* 5: 489-500

Silva, L., Leal-Balbino, T.C., Melo, B.S.T. *et al.* (2017) Genetic diversity and virulence potential of clinical and environmental *Aeromonas* spp. isolates from a diarrhea outbreak. *BMC Microbiol* 17: 179

Singh, D.V., Sanyal, S.C. (1997) Enteropathogenicity of *Aeromonas jandaei* and *A. trota*. *FEMS Immunol Med Microbiol* 17: 243-50

Singh, D.V., Sanyal, S.C. (1999) Virulence patterns of *Aeromonas eucrenophila* isolated from water and infected fish. *J Diarrhoeal Dis Res* 17: 37-42

Slobodkin, A.I., Reysenbach, A.L., Slobodkina, G.B. *et al.* (2013) *Dissulfuribacter thermophilus* gen. nov., sp. nov., a thermophilic, autotrophic, sulfur-disproportionating, deeply branching deltaproteobacterium from a deep-sea hydrothermal vent. *Int J Syst Evol Microbiol* 63: 1967-71

Soler, L., Figueras, M.J., Chacon, M.R. *et al.* (2002) Potential virulence and antimicrobial susceptibility of *Aeromonas popoffii* recovered from freshwater and seawater. *FEMS Immunol Med Microbiol* 32: 243-7

Somavanshi, R., Ghosh, B., Sourjik, V. (2016) Sugar influx sensing by the phosphotransferase system of *Escherichia coli*. *PLoS Biol* 14: e2000074

Soto-Rodriguez, S.A., Cabanillas-Ramos, J., Alcaraz, U. *et al.* (2013) Identification and virulence of *Aeromonas dhakensis, Pseudomonas mosselii* and *Microbacterium paraoxydans* isolated from Nile tilapia, *Oreochromis niloticus*, cultivated in Mexico. *J Appl Microbiol* 115: 654-62

Sourjik, V., Berg, H.C. (2002) Receptor sensitivity in bacterial chemotaxis. *Proc Natl Acad Sci U S A* 99: 123-7

Sourjik, V., Wingreen, N.S. (2012) Responding to chemical gradients: bacterial chemotaxis. *Curr Opin Cell Biol* 24: 262-8

Souza, R., Ambrosini, A., Passaglia, L.M. (2015) Plant growth-promoting bacteria as inoculants in agricultural soils. *Genet Mol Biol* 38: 401-19

Sparacino-Watkins, C., Stolz, J.F., Basu, P. (2014) Nitrate and periplasmic nitrate reductases. *Chem Soc Rev* 43: 676-706

Speth, D.R., Lagkouvardos, I., Wang, Y. *et al.* (2017) Draft genome of *Scalindua rubra,* obtained from the interface above the discovery deep brine in the Red Sea, sheds light on potential salt adaptation strategies in *Anammox* bacteria. *Microb Ecol* 74: 1-5

Springer, M.S., Goy, M.F., Adler, J. (1977) Sensory transduction in *Escherichia coli*: two complementary pathways of information processing that involve methylated proteins. *Proc Natl Acad Sci U S A* 74: 3312-6

Srinivas, T.N., Vijaya Bhaskar, Y., Bhumika, V. *et al.* (2013) *Photobacterium marinum* sp. nov., a marine bacterium isolated from a sediment sample from Palk Bay, India. *Syst Appl Microbiol* 36: 160-5

Starrett, D.J., Falke, J.J. (2005) Adaptation mechanism of the aspartate receptor: electrostatics of the adaptation subdomain play a key role in modulating kinase activity. *Biochemistry* 44: 1550-60

Stecher, B., Hapfelmeier, S., Muller, C. *et al.* (2004) Flagella and chemotaxis are required for efficient induction of *Salmonella enterica* serovar *Typhimurium* colitis in streptomycin-pretreated mice. *Infect Immun* 72: 4138-50

Stewart, V. (2003) Biochemical Society Special Lecture. Nitrate- and nitrite-responsive sensors NarX and NarQ of proteobacteria. *Biochem Soc Trans* 31: 1-10

Stewart, V., Chen, L.L. (2010) The S helix mediates signal transmission as a HAMP domain coiled-coil extension in the NarX nitrate sensor from *Escherichia coli* K-12. *J Bacteriol* 192: 734-45

Stewart, V. (2014) The HAMP signal-conversion domain: static two-state or dynamic three-state? *Mol Microbiol* 91: 853-7

Stock, A.M., Robinson, V.L., Goudreau, P.N. (2000) Two-component signal transduction. *Annu Rev Biochem* 69: 183-215

Stock, J. (1996) Receptor signaling: dimerization and beyond. *Curr Biol* 6: 825-7

Stover, C.K., Pham, X.Q., Erwin, A.L. *et al.* (2000) Complete genome sequence of *Pseudomonas aeruginosa PAO1*, an opportunistic pathogen. *Nature* 406: 959-64

Studier, F.W., Moffatt, B.A. (1986) Use of bacteriophage T7 RNA polymerase to direct selective high-level expression of cloned genes. *J Mol Biol* 189: 113-30

Sun, H., Spring, S., Lapidus, A. *et al.* (2010) Complete genome sequence of *Desulfarculus baarsii* type strain (2st14). *Stand Genomic Sci* 3: 276-84

Svergun, D.I. (1992) Determination of the regularization parameter in indirect-transform methods using perceptual criteria. *J. Appl. Crystallogr* 25: 495-503

Swain, K.E., Falke, J.J. (2007) Structure of the conserved HAMP domain in an intact, membrane-bound chemoreceptor: a disulfide mapping study. *Biochemistry* 46: 13684-95

Swain, K.E., Gonzalez, M.A., Falke, J.J. (2009) Engineered socket study of signaling through a four-helix bundle: evidence for a yin-yang mechanism in the kinase control module of the aspartate receptor. *Biochemistry* 48: 9266-77

Sweeney, E.G., Perkins, A., Kallio, K. *et al.* (2018) Structures of the ligand-binding domain of *Helicobacter pylori* chemoreceptor TlpA. *Protein Sci* 27: 1961-1968

Swem, L.R., Swem, D.L., O'Loughlin, C.T. *et al.* (2009) A quorum-sensing antagonist targets both membrane-bound and cytoplasmic receptors and controls bacterial pathogenicity. *Mol Cell* 35: 143-53

Sze, C.W., Zhang, K., Kariu, T. *et al.* (2012) *Borrelia burgdorferi* needs chemotaxis to establish infection in mammals and to accomplish its enzootic cycle. *Infect Immun* 80: 2485-92

Szurmant, H., Muff, T.J., Ordal, G.W. (2004a) *Bacillus subtilis* CheC and FliY are members of a novel class of CheY-P-hydrolyzing proteins in the chemotactic signal transduction cascade. *J Biol Chem* 279: 21787-92

Szurmant, H., Bunn, M.W., Cho, S.H. *et al.* (2004b) Ligand-induced conformational changes in the *Bacillus subtilis* chemoreceptor McpB determined by disulfide crosslinking in vivo. *J Mol Biol* 344: 919-28

Taguchi, K., Fukutomi, H., Kuroda, A. *et al.* (1997) Genetic identification of chemotactic transducers for amino acids in *Pseudomonas aeruginosa*. *Microbiology* 143 (Pt 10): 3223-9

Takahashi, E., Ozaki, H., Fujii, Y. *et al.* (2014) Properties of hemolysin and protease produced by *Aeromonas trota*. *PLoS One* 9: e91149

Talagrand-Reboul, E., Roger, F., Kimper, J.L. *et al.* (2017) Delineation of taxonomic species within complex of species: *Aeromonas media* and related species as a test case. *Front Microbiol* 8: 621

Tareen, A.M., Dasti, J.I., Zautner, A.E. *et al.* (2010) *Campylobacter jejuni* proteins Cj0952c and Cj0951c affect chemotactic behaviour towards formic acid and are important for invasion of host cells. *Microbiology* 156: 3123-35

Tatke, G., Kumari, H., Silva-Herzog, E. *et al.* (2015) *Pseudomonas aeruginosa* MifS-MifR Two-Component System Is Specific for alpha-Ketoglutarate Utilization. *PLoS One* 10: e0129629

Tawaraya, K., Horie, R., Saito, S. *et al.* (2014) Metabolite profiling of root exudates of common bean under phosphorus deficiency. *Metabolites* 4: 599-611

Taylor, B.L., Miller, J.B., Warrick, H.M. *et al.* (1979) Electron acceptor taxis and blue light effect on bacterial chemotaxis. *J Bacteriol* 140: 567-73

Taylor, B.L., Zhulin, I.B., Johnson, M.S. (1999) *Aerotaxis* and other energy-sensing behavior in bacteria. *Annu Rev Microbiol* 53: 103-28

Taylor, B.L., Zhulin, I.B. (1999) PAS domains: internal sensors of oxygen, redox potential, and light. *Microbiol Mol Biol Rev* 63: 479-506

Thogersen, M.S., Delpin, M.W., Melchiorsen, J. *et al.* (2016) Production of the bioactive compounds violacein and indolmycin is conditional in a *maeA* mutant of *Pseudoalteromonas luteoviolacea* S4054 lacking the malic enzyme. *Front Microbiol* 7: 1461

Thompson, J.D., Higgins, D.G., Gibson, T.J. (1994) CLUSTAL W: improving the sensitivity of progressive multiple sequence alignment through sequence weighting, position-specific gap penalties and weight matrix choice. *Nucleic Acids Res* 22: 4673-80

Thompson, J.D., Gibson, T.J., Plewniak, F. *et al.* (1997) The CLUSTAL_X windows interface: flexible strategies for multiple sequence alignment aided by quality analysis tools. *Nucleic Acids Res* 25: 4876-82

Timmis, K.N. (2002) *Pseudomonas putida*: a cosmopolitan opportunist par excellence. *Environ Microbiol* 4: 779-81

Toker, A.S., Macnab, R.M. (1997) Distinct regions of bacterial flagellar switch protein FliM interact with FliG, FliN and CheY. *J Mol Biol* 273: 623-34

Tso, W.W., Adler, J. (1974) Negative chemotaxis in *Escherichia coli*. *J Bacteriol* 118: 560-76

Tunchai, M., Hida, A., Oku, S. *et al.* (2017) Identification and characterization of chemosensors for D-malate, unnatural enantiomer of malate, in *Ralstonia pseudosolanacearum*. *Microbiology* 163: 233-242

Turner, L., Ryu, W.S., Berg, H.C. (2000) Real-time imaging of fluorescent flagellar filaments. *J Bacteriol* 182: 2793-801

Ulrich, L.E., Zhulin, I.B. (2005) Four-helix bundle: a ubiquitous sensory module in prokaryotic signal transduction. *Bioinformatics* 21 Suppl 3: iii45-8

Ulrich, L.E., Koonin, E.V., Zhulin, I.B. (2005) One-component systems dominate signal transduction in prokaryotes. *Trends Microbiol* 13: 52-6

Ulrich, L.E., Zhulin, I.B. (2010) The MiST2 database: a comprehensive genomics resource on microbial signal transduction. *Nucleic Acids Res* 38: D401-7

Unden, G., Strecker, A., Kleefeld, A. *et al.* (2016) C4-dicarboxylate utilization in aerobic and anaerobic growth. *EcoSal Plus* 7

Upadhyay, A.A., Fleetwood, A.D., Adebali, O. *et al.* (2016) Cache domains that are homologous to, but different from PAS domains comprise the largest superfamily of extracellular sensors in Prokaryotes. *PLoS Comput Biol* 12: e1004862

Urakawa, H., Kita-Tsukamoto, K., Steven, S.E. *et al.* (1998) A proposal to transfer *Vibrio marinus* (Russell 1891) to a new genus *Moritella* gen. nov. as *Moritella marina* comb. nov. *FEMS Microbiol Lett* 165: 373-8

Vaknin, A., Berg, H.C. (2006) Osmotic stress mechanically perturbs chemoreceptors in *Escherichia coli*. *Proc Natl Acad Sci U S A* 103: 592-6

Van Alst, N.E., Picardo, K.F., Iglewski, B.H. *et al.* (2007) Nitrate sensing and metabolism modulate motility, biofilm formation, and virulence in *Pseudomonas aeruginosa*. *Infect Immun* 75: 3780-90

Van Alst, N.E., Sherrill, L.A., Iglewski, B.H. *et al.* (2009) Compensatory periplasmic nitrate reductase activity supports anaerobic growth of *Pseudomonas aeruginosa* PAO1 in the absence of membrane nitrate reductase. *Can J Microbiol* 55: 1133-44

van der Werf, M.J., van den Tweel, W.J., Hartmans, S. (1992) Screening for microorganisms producing D-malate from maleate. *Appl Environ Microbiol* 58: 2854-60

Vangnai, A.S., Takeuchi, K., Oku, S. *et al.* (2013) Identification of CtpL as a chromosomally encoded chemoreceptor for 4-chloroaniline and catechol in *Pseudomonas aeruginosa* PAO1. *Appl Environ Microbiol* 79: 7241-8

Vistica, J., Dam, J., Balbo, A. *et al.* (2004) Sedimentation equilibrium analysis of protein interactions with global implicit mass conservation constraints and systematic noise decomposition. *Anal Biochem* 326: 234-56

Vladimirov, N., Lebiedz, D., Sourjik, V. (2010) Predicted auxiliary navigation mechanism of peritrichously flagellated chemotactic bacteria. *PLoS Comput Biol* 6: e1000717

Wadhams, G.H., Armitage, J.P. (2004) Making sense of it all: bacterial chemotaxis. *Nat Rev Mol Cell Biol* 5: 1024-37

Walker, T.S., Bais, H.P., Deziel, E. *et al.* (2004) *Pseudomonas aeruginosa*-plant root interactions. Pathogenicity, biofilm formation, and root exudation. *Plant Physiol* 134: 320-31

Wang, H.C., Ko, W.C., Shu, H.Y. *et al.* (2014a) Genome sequence of *Aeromonas taiwanensis* LMG 24683T, a clinical wound isolate from Taiwan. *Genome Announc* 2

Wang, X., Wu, C., Vu, A. *et al.* (2012) Computational and experimental analyses reveal the essential roles of interdomain linkers in the biological function of chemotaxis histidine kinase CheA. *J Am Chem Soc* 134: 16107-10

Wang, X., Vallurupalli, P., Vu, A. *et al.* (2014b) The linker between the dimerization and catalytic domains of the CheA histidine kinase propagates changes in structure and dynamics that are important for enzymatic activity. *Biochemistry* 53: 855-61

Watanabe, T., Kojima, H., Fukui, M. (2016) Identity of major sulfur-cycle prokaryotes in freshwater lake ecosystems revealed by a comprehensive phylogenetic study of the dissimilatory adenylylsulfate reductase. *Sci Rep* 6: 36262

Watts, K.J., Taylor, B.L., Johnson, M.S. (2011) PAS/poly-HAMP signalling in Aer-2, a soluble haem-based sensor. *Mol Microbiol* 79: 686-99

Webb, B.A., Hildreth, S., Helm, R.F. *et al.* (2014) *Sinorhizobium meliloti* chemoreceptor McpU mediates chemotaxis toward host plant exudates through direct proline sensing. *Appl Environ Microbiol* 80: 3404-15

Webb, B.A., Helm, R.F., Scharf, B.E. (2016) Contribution of individual chemoreceptors to *Sinorhizobium meliloti* chemotaxis towards amino acids of host and nonhost seed exudates. *Mol Plant Microbe Interact* 29: 231-9

Webb, B.A., Compton, K.K., Del Campo, J.S.M. *et al.* (2017a) *Sinorhizobium meliloti* chemotaxis to multiple amino acids is mediated by the chemoreceptor McpU. *Mol Plant Microbe Interact* 30: 770-777

Webb, B.A., Karl Compton, K., Castaneda Saldana, R. *et al.* (2017b) *Sinorhizobium meliloti* chemotaxis to quaternary ammonium compounds is mediated by the chemoreceptor McpX. *Mol Microbiol* 103: 333-346

Weis, R.M., Hirai, T., Chalah, A. *et al.* (2003) Electron microscopic analysis of membrane assemblies formed by the bacterial chemotaxis receptor Tsr. *J Bacteriol* 185: 3636-43

Weiser, J.N., Ferreira, D.M., Paton, J.C. (2018) *Streptococcus pneumoniae*: transmission, colonization and invasion. *Nat Rev Microbiol* 16: 355-367

Welch, M., Oosawa, K., Aizawa, S. *et al.* (1993) Phosphorylation-dependent binding of a signal molecule to the flagellar switch of bacteria. *Proc Natl Acad Sci U S A* 90: 8787-91

Whitchurch, C.B., Leech, A.J., Young, M.D. *et al.* (2004) Characterization of a complex chemosensory signal transduction system which controls twitching motility in *Pseudomonas aeruginosa*. *Mol Microbiol* 52: 873-93

WHO (2017) Global priority list of antibiotic-resistant bacteria to guide research, discovery, and development of new antibiotics. *https://wwwwhoint/medicines/publications/global-priority-list-antibiotic-resistant-bacteria/en/*

Wicher, D. (2012) Functional and evolutionary aspects of chemoreceptors. *Front Cell Neurosci* 6: 48

Willey, J.M., Waterbury, J.B. (1989) Chemotaxis toward nitrogenous compounds by swimming strains of marine *Synechococcus* spp. *Appl Environ Microbiol* 55: 1888-1894

Williams, S.B., Stewart, V. (1997) Discrimination between structurally related ligands nitrate and nitrite controls autokinase activity of the NarX transmembrane signal transducer of *Escherichia coli* K-12. *Mol Microbiol* 26: 911-25

Woodcock, D.M., Crowther, P.J., Doherty, J. *et al.* (1989) Quantitative evaluation of *Escherichia coli* host strains for tolerance to cytosine methylation in plasmid and phage recombinants. *Nucleic Acids Res* 17: 3469-78

Wright, G.A., Crowder, R.L., Draheim, R.R. *et al.* (2011) Mutational analysis of the transmembrane helix 2-HAMP domain connection in the *Escherichia coli* aspartate chemoreceptor tar. *J Bacteriol* 193: 82-90

Wu, C.J., Wang, H.C., Chen, P.L. *et al.* (2013a) AQU-1, a chromosomal class C beta-lactamase, among clinical *Aeromonas dhakensis* isolates: distribution and clinical significance. *Int J Antimicrob Agents* 42: 456-61

Wu, H., Kato, J., Kuroda, A. *et al.* (2000) Identification and characterization of two chemotactic transducers for inorganic phosphate in *Pseudomonas aeruginosa*. *J Bacteriol* 182: 3400-4

Wu, R., Gu, M., Wilton, R. *et al.* (2013b) Insight into the sporulation phosphorelay: crystal structure of the sensor domain of *Bacillus subtilis* histidine kinase, KinD. *Protein Sci* 22: 564-76

Wuichet, K., Alexander, R.P., Zhulin, I.B. (2007) Comparative genomic and protein sequence analyses of a complex system controlling bacterial chemotaxis. *Methods Enzymol* 422: 1-31

Wuichet, K., Zhulin, I.B. (2010) Origins and diversification of a complex signal transduction system in prokaryotes. *Sci Signal* 3: ra50

Xie, W., Wang, F., Guo, L. *et al.* (2011) Comparative metagenomics of microbial communities inhabiting deep-sea hydrothermal vent chimneys with contrasting chemistries. *ISME J* 5: 414-26

Xu, X., Zhang, D., Zhang, H. *et al.* (2006) Neutrophil histamine contributes to inflammation in mycoplasma pneumonia. *J Exp Med* 203: 2907-17

Xu, X., Zhang, H., Song, Y. *et al.* (2012) Strain-dependent induction of neutrophil histamine production and cell death by *Pseudomonas aeruginosa*. *J Leukoc Biol* 91: 275-84

Yamamoto, K., Imae, Y. (1993) Cloning and characterization of the *Salmonella typhimurium*-specific chemoreceptor Tcp for taxis to citrate and from phenol. *Proc Natl Acad Sci U S A* 90: 217-21

Yang, L.H., Xiong, H., Lee, O.O. *et al.* (2007) Effect of agitation on violacein production in *Pseudoalteromonas luteoviolacea* isolated from a marine sponge. *Lett Appl Microbiol* 44: 625-30

Yarza, P., Yilmaz, P., Pruesse, E. *et al.* (2014) Uniting the classification of cultured and uncultured bacteria and archaea using 16S rRNA gene sequences. *Nat Rev Microbiol* 12: 635-45

Yu, D., Ma, X., Tu, Y. *et al.* (2015) Both piston-like and rotational motions are present in bacterial chemoreceptor signaling. *Sci Rep* 5: 8640

Yu, Y., Li, H.R., Zeng, Y.X. (2011) *Colwellia chukchiensis* sp. nov., a psychrotolerant bacterium isolated from the Arctic Ocean. *Int J Syst Evol Microbiol* 61: 850-3

Zaborin, A., Romanowski, K., Gerdes, S. *et al.* (2009) Red death in *Caenorhabditis elegans* caused by *Pseudomonas aeruginosa* PAO1. *Proc Natl Acad Sci U S A* 106: 6327-32

Zepeda, V.K., Busse, H.J., Golke, J. *et al.* (2015) *Terasakiispira papahanaumokuakeensis* gen. nov., sp. nov., a gammaproteobacterium from Pearl and Hermes Atoll, Northwestern Hawaiian Islands. *Int J Syst Evol Microbiol* 65: 3609-17

Zhang, J., Yang, D., Li, M. *et al.* (2016) Metabolic profiles reveal changes in wild and cultivated soybean seedling leaves under salt stress. *PLoS One* 11: e0159622

Zhang, W., Xue, Y., Ma, Y. *et al.* (2002) *Marinospirillum alkaliphilum* sp. nov., a new alkaliphilic helical bacterium from Haoji soda lake in Inner Mongolia Autonomous Region of China. *Extremophiles* 6: 33-7

Zhang, X.Y., Zhang, Y.J., Yu, Y. *et al.* (2010) *Neptunomonas antarctica* sp. nov., isolated from marine sediment. *Int J Syst Evol Microbiol* 60: 1958-61

Zhang, Y., Gardina, P.J., Kuebler, A.S. *et al.* (1999) Model of maltose-binding protein/chemoreceptor complex supports intrasubunit signaling mechanism. *Proc Natl Acad Sci U S A* 96: 939-44

Zhang, Z., Hendrickson, W.A. (2010) Structural characterization of the predominant family of histidine kinase sensor domains. *J Mol Biol* 400: 335-53

Zhou, Q., Ames, P., Parkinson, J.S. (2009) Mutational analyses of HAMP helices suggest a dynamic bundle model of input-output signalling in chemoreceptors. *Mol Microbiol* 73: 801-14

Zhou, Q., Ames, P., Parkinson, J.S. (2011) Biphasic control logic of HAMP domain signalling in the *Escherichia coli* serine chemoreceptor. *Mol Microbiol* 80: 596-611

Zopfi, J., Kjaer, T., Nielsen, L.P. *et al.* (2001) Ecology of *Thioploca* spp.: nitrate and sulfur storage in relation to chemical microgradients and influence of *Thioploca* spp. on the sedimentary nitrogen cycle. *Appl Environ Microbiol* 67: 5530-7

Zusman, D.R., Scott, A.E., Yang, Z. *et al.* (2007) Chemosensory pathways, motility and development in *Myxococcus xanthus*. *Nat Rev Microbiol* 5: 862-72

Zwir, I., Latifi, T., Perez, J.C. *et al.* (2012) The promoter architectural landscape of the *Salmonella* PhoP regulon. *Mol Microbiol* 84: 463-85

Zylstra, G.J., Wackett, L.P., Gibson, D.T. (1989) Trichloroethylene degradation by *Escherichia coli* containing the cloned *Pseudomonas putida* F1 toluene dioxygenase genes. *Appl Environ Microbiol* 55: 3162-6